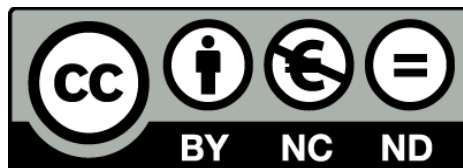


Volcanic hazard assessment in monogenetic volcanic fields

Stefania Bartolini



Aquesta tesi doctoral està subjecta a la llicència **Reconeixement- NoComercial – SenseObraDerivada 3.0. Espanya de Creative Commons.**

Esta tesis doctoral está sujeta a la licencia **Reconocimiento - NoComercial – SinObraDerivada 3.0. España de Creative Commons.**

This doctoral thesis is licensed under the **Creative Commons Attribution-NonCommercial-NoDerivs 3.0. Spain License.**

A thesis submitted for the degree of
Doctor of Philosophy



UB - Department of Geodynamics and Geophysics
CSIC - Institute of Earth Sciences Jaume Almera

Research in: Geohazards and Geomorphology

Volcanic hazard assessment in monogenetic volcanic fields

AUTHOR : Stefania Bartolini

Supervisor DR. JOAN MARTÍ, Professor of Research (CSIC)

Tutor Dr. Joan Manuel Vilaplana, Professor (UB)

Barcelona 2014

Acknowledgements

First of all, I offer my sincerest gratitude to my supervisor, Dr. Joan Martí, for introducing me to the interesting field of volcanic hazard assessment, for his constant encouragement and valuable advice during my Ph.D., which have permitted to take this work to its final completion.

I am indebted to CSIC for providing generous financial support throughout the Ph.D. Thesis with a predoctoral grant JAE-predoc, and to the European Commission (FP7 Theme: ENV.2011.1.3.3-1; Grant 282759: VUELCO).

Thanks are also extended to Dr. Christopher Kilburn (University College of London) for allowing me the opportunity to collaborate with the Aon Benfield UCL Hazard Centre during my short-stay in UK.

I would also like to thank Dr. Rosa Sobradelo and Dr. Adelina Geyer, for their support and guidance, kind advice, for patiently helping me during these years, and for their scientific expertise.

Many thanks also to Dr. Ramón Ortiz, Dr. Alicia Felpeto, Dr. Carmen López, for introduce me in the world of programming. Dr. Gerardo Aguirre-Díaz as travel companion and for teaching me volcanology during our volcanic field trips. I also want to thank Dr. Annalisa Cappello, Dr. Roberto Carniel, Sophie Mossoux, Dr. Ciro del Negro, to collaborate with me in different stages of this thesis.

I also wish to thank my friends and colleagues at the Jaume Almera and in Barcelona: David for his congeniality and kindness, Beatriz & Aloña for their dear friendship, Xevi with whom I shared many good times in our office, Erika a friend always present, Dario & Antonella for the good times spent together, Lavinia, JP, Silvia, Stephanie. Also thanks to my friends of the GIS Master: my dear friend Jordi, Anna, and Edu. Thanks are also given to my italian friends that have supported me: Paola, Marina & Giuliano with their fantastic children Ivan & Melissa, and Serena, Massi, Alessio, Luciano, Annalisa.

My greatest thanks go to my best overseas friends Silvina & Leandro.

I would also like to thank the people who have been close and have represented my little family when I was away from home. Thanks to Ariadna, Ona, Alfredo, Viviana, Chiara. Thanks to Jamila and Lalit for welcoming me in London and for the wonderful friendship that binds us.

A special thanks to Laura, a workmate but most of all a dear friend, for the moments we spent together and for facing this adventure helping each other.

Also thanks to my dearest friends Osvaldo and Dorina for the joy and the love that gave me over this years.

Finally, my special thanks go to my Mom Anna & my Dad Ruggero for believing in me, my great brother Daniele, and also to my whole family: Irene & Mario, Elisa, Claudia, Fabio, and the little ones Riccardo & Massimo, all of whom have given me encouragement, love and support throughout.

My last but the most important special thanks go to Mauro for his constant support throughout these years of my Ph.D. project, and for giving me all his patience and affection in every moment.



A MAURO

Contents

Abstract	xi
Resumen	xiii
I	1
1 Introduction	3
1.1 Motivation	3
1.2 State of the art	4
1.2.1 Monogenetic volcanic fields	4
1.2.2 Volcanic hazard assessment	5
1.3 Aims of dissertation	8
1.4 Thesis structure	9
2 QVAST: a new Quantum GIS plugin for estimating volcanic susceptibility	13
2.1 Abstract	14
2.2 Introduction	14
2.3 Optimal bandwidth in kernel density estimation	16
2.3.1 Least square cross-validation (Cappello et al., 2012)	18
2.3.2 The h_{opt} score (Silverman, 1986)	18
2.3.3 The sum of asymptotic mean squared error selector (Connor et al., 2012)	19
2.4 Kernel density estimation	20
2.5 Interface and tools of QVAST	20
2.6 Applying QVAST: Lanzarote (Canary Islands, Spain) and La Garrotxa (NE Spain)	24
2.6.1 Lanzarote: geological context	24
2.6.2 La Garrotxa: geological context	25

2.6.3	Data sets and bandwidth estimation	26
2.6.4	Susceptibility map	32
2.7	Conclusions	35
3	HASSET: a probability event tree tool to evaluate future volcanic scenarios using Bayesian Inference. Presented as a plug-in for QGIS	41
3.1	Abstract	42
3.2	Introduction	42
3.3	HASSET: Hazard Assessment Event Tree	45
3.3.1	Event Tree Structure	47
3.3.2	Probability Estimates	51
3.3.3	How precise are the probability estimates?	52
3.4	HASSET software: a QGIS plug-in to perform hazard assessment using Bayesian event tree methodology	53
3.5	HASSET applied to Teide-Pico Viejo volcanic complex	56
3.6	Discussion and Conclusions	64
4	Long-term volcanic hazard assessment on El Hierro (Canary Islands)	71
4.1	Abstract	72
4.2	Introduction	72
4.3	Geological setting	75
4.4	Methods	78
4.5	How: characterisation of the eruptions	78
4.6	Where: spatial analysis	80
4.7	When: temporal analysis	82
4.8	Input data for HASSET	84
4.8.1	Node 1: unrest	84
4.8.2	Node 2: origin	85
4.8.3	Node 3: outcome	85
4.8.4	Node 4: location	86
4.8.5	Node 5: composition	87
4.8.6	Node 6: size	88
4.8.7	Node 7: hazard	88

4.8.8	Node 8: extent	89
4.9	Results	91
4.10	Eruptive scenarios	93
4.11	Lava flow scenarios	93
4.12	Scenarios for pyroclastic density currents (PDCs)	94
4.13	Fallout	95
4.14	Total hazard map	98
4.15	Discussion and conclusions	100
5	Volcanic hazard on Deception Island (South Shetland Islands, Antarctica)	111
5.1	Abstract	112
5.2	Introduction	112
5.3	Geological setting	118
5.4	Recent Volcanic Activity & Volcanic Hazards	119
5.5	Threat Analysis	126
5.5.1	Hazard factors	126
5.5.2	Exposure factor	128
5.6	Volcanic hazard assessment: spatial and temporal analysis	129
5.6.1	Susceptibility analysis	131
5.6.2	Temporal analysis	133
5.6.3	Eruptive scenarios	142
5.6.4	Hazard map	147
5.7	Discussion	149
5.8	Conclusions	151
6	Hazard assessment at the Quaternary La Garrotxa Volcanic Field (NE Iberia)	171
6.1	Abstract	172
6.2	Introduction	172
6.3	General features of the GVF	174
6.4	Methods	176
6.5	Characterisation of past eruptive activity	177
6.6	Volcanic susceptibility	179

6.7	Temporal recurrence rate	180
6.8	Eruptive scenarios	183
6.8.1	Lava flow	183
6.8.2	Pyroclastic density current	185
6.8.3	Ash fall	185
6.9	Discussion and conclusions	188
7	VERDI: a new Volcanic managEment Risk Database desIgn	197
7.1	Abstract	198
7.2	Introduction	198
7.3	VERDI architecture	202
7.3.1	GroupCore	202
7.3.2	GroupVolcano	203
7.3.3	GroupSusceptibility	205
7.3.4	GroupHazard	206
7.3.5	GroupMeteorology	207
7.3.6	GroupLaboratory	207
7.3.7	GroupDevice	207
7.3.8	GroupVulnerability	209
7.3.9	GroupCosts	210
7.3.10	GroupManagement	211
7.3.11	GroupReferences	212
7.3.12	GroupModels	213
7.4	VERDI usefulness: case study of El Hierro	213
7.4.1	Emergency planning phase	214
7.4.2	Unrest phase	216
7.5	Conclusions and final remarks	219
8	Summary of results & Discussion	231
9	Conclusions	237
	References	239

II	245
Appendix 1	247
Appendix 2	251
Appendix 3	265
Appendix 4	281
Appendix 5	299
Appendix 6	321
Appendix 7	351
9.1 Submission decision	390

Abstract

One of the most important tasks of modern volcanology, which represents a significant socio-economic implication, is to conduct hazard assessment in active volcanic systems. These volcanological studies are aimed at hazard that allows to constructing hazard maps and simulating different eruptive scenarios, and are mainly addressed to contribute to territorial planning, definition of emergency plans or managing volcanic crisis.

Volcanic hazard is defined as the probability of any particular area being affected by a destructive volcanic event within a given period of time. The impact of a natural event, as a volcanic eruption, can significantly affect human life, property, infrastructures, and the environment. Long periods of quiescence are quite common in many volcanic areas and this often leads to a fall in the alert. The consequence is lack of preparation to deal with a volcanic crisis. Volcanic hazard assessment is an important scientific, economic, and political issue, especially in densely populated areas threatened by volcanoes, and to be effective should be conducted well in advance to any possible eruption.

The present Ph.D. Thesis is focused on the development and application of different tools for the spatial and temporal analyses to assess volcanic hazard in monogenetic volcanic fields. Monogenetic volcanic fields are commonly not regarded as potentially dangerous and only a few studies concerning hazard assessment have been conducted in such environments. This is probably due to the relative small size of their eruptions and their episodic recurrence. In the long-term hazard assessment, we assume that the future eruptive behaviour in the volcanic field could be similar to the last eruptive activity. First, we have developed a new tool, QVAST (QGIS for VolcAnic SuscepTibility), designed to carry out the spatial analysis. This tool allows to calculate the volcanic susceptibility of the area, i.e. the probability of new vent opening, using direct and indirect structural data. Second, we have developed a new tool, HASSET (Hazard Assessment Event Tree), to conduct temporal analysis. Combining both tools and the previous one, VORIS 2.0.1 (Felpeto et al., 2007), that uses simulation models to predict the most probable eruptive scenarios

and which areas could be affected by a future eruptive event, we can evaluate in a probabilistic way long-term hazard represented by a qualitative hazard map that allows us to identify different levels of hazard in the study area, or when dealing with short-term hazard, possible outcomes of volcanic unrest within a specific time frame. In this thesis we present different case studies. The first example was carried out at El Hierro Island (Canary Islands), an island essentially characterized by basaltic volcanism with both Strombolian and Hawaiian activity. Recent volcanic activity on El Hierro is largely characterised by monogenetic mafic volcanism. The last eruption on El Hierro occurred in 2011–2012 demonstrates the importance of reliable data and tools that can enable scientific advisors and decision-makers to consider possible future eruptive scenarios. The second case study was Deception Island (Southern Shetland Archipelago, Antarctica), which is the most active volcano in the South Shetland Islands and has been the scene of more than twenty eruptions over the past two centuries. We identified a number of significant scenarios using our GIS (Geographic Information System)-based tools and evaluated the potential extent of the main volcanic hazards to be expected on the island. The last case study presented is La Garrotxa Volcanic Field (NE of Spain), which is a quaternary volcanic field, located in the Northeast of the Iberian Peninsula, and includes more than 50 well preserved volcanoes. The volcanic activity varies from Hawaiian to Violent Strombolian, showing numerous episodes of phreatomagmatic activity.

Finally, considering the importance of both quantity and quality of the available volcanic data and an optimum storage mechanism and as complement to the e-tools we have developed, we describe the design of a new spatial database structure, VERDI (**V**olcanic manag**E**ment **R**isk **D**atabase des**I**gn), which allows different types of data to be manipulated, organized and managed. The design of purpose-built databases should facilitate spatial and temporal analysis that will produce probabilistic hazard models for future vent opening, simulate volcanic hazards and assess their socio-economic impact, avoiding any duplication of information.

The methodologies described in this Ph.D. Thesis establish the general guidelines of a procedure that facilitates undertaking volcanic hazard assessment in a systematic way, which can be easily applied to any volcanic area or system, and in particular to any monogenetic volcanic field.

Resumen

Una de las tareas más importantes de la vulcanología moderna, que representa una implicación socio-económica significativa, es llevar a cabo la evaluación de la peligrosidad en los sistemas volcánicos activos. Estos estudios vulcanológicos están enfocados a la elaboración de mapas de peligro y la simulación de diferentes escenarios eruptivos, y están dirigidas principalmente para contribuir a la planificación territorial, a la definición de los planes de emergencia o la gestión de crisis volcánicas.

El peligro volcánico se define como la probabilidad de que una área en particular se vea afectada por un evento volcánico destructivo dentro de un período de tiempo determinado. El impacto de un evento natural, como una erupción volcánica, puede afectar significativamente la vida humana, los bienes, las infraestructuras y el medio ambiente. Los largos períodos de inactividad son muy comunes en muchas zonas volcánicas y esto frecuentemente conduce a una disminución de la alerta. La consecuencia es una falta de preparación para hacer frente a una crisis volcánica. La evaluación del peligro volcánico es una importante cuestión científica, económica, y política, especialmente en zonas densamente pobladas amenazadas por los volcanes, y para que sea eficaz debe llevarse a cabo con suficiente antelación antes de cualquier posible erupción.

La presente Tesis doctoral está enfocada al desarrollo y aplicación de diferentes herramientas informáticas para los análisis espacial y temporal del peligro volcánico en campos volcánicos monogenéticos. Los campos volcánicos monogenéticos comúnmente no se consideran como potencialmente peligrosos y sólo unos pocos estudios relativos a la evaluación del peligro se han llevado a cabo en este tipo de entornos. Esto es probablemente debido al tamaño pequeño de las erupciones y sus recurrencia episódica. En la evaluación del peligro a largo plazo, se considera que el futuro comportamiento eruptivo en el campo volcánico podría ser similar a la última actividad eruptiva. En primer lugar, hemos desarrollado una nueva herramienta, QVAST (QGIS for VolcAnic SuscepTibility), diseñada para llevar a cabo el análisis espacial. Esta herramienta permite calcular la susceptibilidad volcánica de la zona de estudio, es decir, la probabilidad de apertura de un nuevo centro emisor, utilizando datos

estructurales directos e indirectos. En segundo lugar, hemos desarrollado una nueva herramienta, HASSET (Hazard Assessment Event Tree), para llevar a cabo el análisis temporal. La combinación de ambos instrumentos y una herramienta anterior, VORIS 2.0.1 (Felpeto et al., 2007), que utiliza modelos de simulación para predecir los escenarios eruptivos más probables y aquellas áreas que podrían verse afectadas por un futuro evento eruptivo, nos permite evaluar de forma probabilística el peligro a largo plazo, representado por un mapa cualitativo que nos permite identificar los diferentes niveles de peligro en el área de estudio, o cuando se trata de peligro a corto plazo, los posibles resultados de la actividad volcánica dentro de un marco de tiempo específico. En esta tesis se presentan diferentes casos de estudio. El primer ejemplo se llevó a cabo en la isla de El Hierro (Islas Canarias), una isla esencialmente caracterizada por un vulcanismo basáltico con una actividad tanto estromboliana como hawaiana. La actividad volcánica reciente en El Hierro se caracteriza en gran medida por un vulcanismo máfico monogenético. La última erupción en El Hierro en 2011-2012 demuestra la importancia de disponer de datos fiables y herramientas que pueda permitir a los asesores científicos y tomadores de decisiones considerar posibles futuros escenarios eruptivos. El segundo estudio se llevó a cabo en la isla Decepción (archipiélago de las Shetland del Sur, Antártida), que es el volcán más activo de las islas Shetland del Sur y ha sido escenario de más de una veintena de erupciones en los últimos dos siglos. Se identificaron una serie de escenarios significativos utilizando nuestras herramientas dentro de un SIG (Sistema de Información Geográfica) y evaluamos el grado potencial de los principales peligros volcánicos que se pueden esperar en la isla. El último caso de estudio presentado es el campo volcánico de La Garrotxa (NE de España), que es un campo volcánico cuaternario, que se encuentra en el noreste de la Península Ibérica, e incluye más de 50 volcanes bien conservados. La actividad volcánica varía de hawaiana a estromboliana violenta, mostrando numerosos episodios de actividad freatomagmática.

Por último, teniendo en cuenta la importancia de la cantidad y la calidad de los datos volcánológicos disponibles y un mecanismo de almacenamiento óptimo como complemento de las herramientas que hemos desarrollado, se describe el diseño de una nueva estructura de base de datos espaciales, VERDI (**V**olcanic manag**E**ment **R**isk **D**atabase des**I**gn), que permite manipular, organizar y gestionar diferentes tipos de datos. El diseño específico de unas bases de datos debería facilitar el análisis espacial y temporal para obtener modelos probabilísticos de apertura de un futuro

centro emisor, simular los peligros volcánicos y evaluar su impacto socio-económico, evitando la duplicación de información.

Las metodologías descritas en esta Tesis doctoral establecen líneas guía generales de un procedimiento que facilita la realización de la evaluación del peligro volcánico de forma sistemática, los cuales se pueden aplicar fácilmente a cualquier zona volcánica o sistema, y en particular, a cualquier campo volcánico monogenético.

RESUMEN

PART I



Introduction

1.1 Motivation

The impact of a natural event, such as a volcanic eruption, can affect considerably human life and the environment. It is clear that a volcanic eruption, although it can be at the same time fascinating and impressive, presents similar or even more problems than more frequent natural events. Volcanic activity can cause damage not only during an eruption, but also can have consequences in subsequent periods. It is possible to live near a volcanic area if we consider the benefits that volcanoes can give us, but it is important to be aware of the existing threat and to know how to minimize the risk. Quantifying volcanic hazard is one of the most important tasks of modern volcanology.

To know the potential hazard and the probability of occurrence of a volcanic phenomenon imply to study the process and monitorize it. Nowadays, the way in which we assess volcanic hazard has been progressively changing thanks to the development of computer science. In recent years, the use of GIS (Geographic Information System) and the improvement of the modelling of volcanic processes have become useful tools in volcanic hazard and risk assessment. This allows now to obtain quantitative hazard maps from numerical simulations of possible eruptions effects. In fact, susceptibility, hazard, vulnerability and risk maps have been built using GIS tools and can be represented in a GIS environment as a support for spatial decision-making. Until now most of the models that contribute to the evaluation of the hazard are limited to the scientific groups that have developed them, but today it is necessary to manage volcanic risk in a rapid way and containing costs. Therefore, an important step in the hazard assessment is to develop and use free tools that allow their dissemination and to exchange information.

In order to minimise risk it is necessary to identify and simulate different eruptive scenarios based on past activity. The most problematic situations use to come from

volcanoes with long quiescent periods that suddenly enter into an unrest phase and subsequent eruption. Long periods of quiescence are quite common in many volcanic areas and this often leads to a fall in the alert, because the lack of emergency plans, correct territorial planning, and volcano monitoring. This is common in many monogenetic volcanic fields around the World, which are characterised by long quiescence periods, and in many cases by the lack of historical volcanism. In this case, it is essential to develop an appropriate territorial planning, to identify those areas that could be affected by an eruption, and to establish emergency plans. It involves to assess volcanic hazard based on the analysis of the past history of the volcano and on the volcano-structural data.

In order to improve volcanic hazard assessment in monogenetic fields, this Ph.D. Thesis provides the development of a series of e-tools aimed at facilitating susceptibility and hazard analysis of these areas, generating the necessary hazard maps and the spatial and temporal analysis of the most probable eruptive scenarios, and applies them to the study of different examples (El Hierro Island, Deception Island, La Garrotxa Volcanic Field) a mode of test cases. The results obtained demonstrate the suitability of these tools and methodology for hazard assessment and will permit to export them to the characterization of volcanic hazards in other areas of similar characteristics, thus helping to reduce volcanic risk.

1.2 State of the art

1.2.1 Monogenetic volcanic fields

Most of the hazard assessment studies conducted during last years refer to composite or stratovolcanoes located close to populated areas, for which volcanic threat is always present (e.g.: Somma-Vesuvio, Italy (Lirer et al., 2001); Campi Flegrei and Somma-Vesuvio (Alberico et al., 2011); Teide-Pico Viejo, Canary Islands (Martí et al., 2008; 2012); Popocatépetl, Mexico (Siebe and Macías, 2006); Mt. Cameroon, Africa (Favalli et al., 2012); Etna, Italy (Cappello et al., 2011)). However, monogenetic volcanic fields are commonly not regarded as potentially dangerous and only a few studies concerning hazard assessment have been conducted in such environments (e.g.: Auckland volcanic field, New Zealand (Bebbington and Cronin, 2011), El Hierro, Canary Islands (Becerril et al., 2014); Tohoku volcanic arc, Japan (Mar-

tin et al., 2004)). This is probably due to the relative small size of their eruptions (0.01–0.2 km³ of mafic magma) and their episodic recurrence, sometimes separated by inter eruptive periods of thousands to tens of thousands years (Fiske and Jackson, 1972; Walker, 1999). Nevertheless, numerous monogenetic volcanic fields exist around the World, covering periods of activity from several millions of years to present, sometimes with high potentiality to erupt in the near future (Wood, 1980; Cas and Wright, 1987; Kereszturi and Németh, 2012). Examples of monogenetic eruptions occurred in recent times after long periods of quiescence are not uncommon (e.g.: Jorullo, Mexico (Guilbaud et al., 2011), Parícutin, Mexico (Scandone, 1979), El Hierro, Canary Islands (Becerril et al., 2014)).

The distribution of the monogenetic volcanoes depends in each case on their regional and local tectonic controls and for this reason they are commonly clustered within volcanic fields and are present in any geotectonic and environmental setting (Connor and Conway, 2000; Valentine and Gregg, 2008; Kereszturi and Németh, 2012). Eruptions in monogenetic volcanic fields are difficult to forecast because the factors controlling the precursory activity are still poorly understood.

This implies that undertaking hazard assessment in monogenetic volcanism is necessary as a precautionary measure to reduce volcanic risk, even if no signals of volcanic activity are now present.

1.2.2 Volcanic hazard assessment

The volcanic hazard of a given area is the probability that it will be affected by a process of a certain volcanic magnitude within a specific time interval (Fournier d'Albe, 1979). The main steps in volcanic hazard assessment can be divided into long- and short-term analyses (Blong, 2000). Long-term hazard assessment is based on the past history of the volcano and requires information from the geological record. This analysis enables us to determine the eruption recurrence and the possible nature of a forthcoming eruption. Short-term hazard assessment, on the other hand, provides complementary information resulting from the combination of a long-term analysis with real-time monitoring data gathered during a crisis or an unrest episode, and helps forecast where and when the eruption might take place and the most likely eruptive scenarios. To quantify volcanic hazard, we need to estimate probabilities of occurrence of a particular eruptive scenario in time and space, in order to evaluate possible outcomes of volcanic unrest within a specific time frame and to predict

the most probable eruptive scenarios and which areas could be affected by a future eruptive event.

One of the first steps in the assessment of volcanic hazard is the evaluation of the volcano susceptibility, defined as the spatial probability of vent opening (Martí and Felpeto, 2010). The susceptibility analysis enables us to identify which areas have the greatest likelihood of hosting new vents. Furthermore, in monogenetic volcanism each new eruption creates a different vent, suggesting that volcanic susceptibility contains a high degree of randomness and that accurate spatial forecasting is highly uncertain.

Published works in this field (Connor and Hill, 1995; Felpeto et al., 2007; Jaquet et al., 2008; Martí and Felpeto, 2010; Favalli et al., 2011; Connor et al., 2012; Cappello et al., 2012, 2013) report the use of kernel density functions to evaluate susceptibility. However, this technique is based mainly on the assumption that new vents will not form far from existing ones (Martin et al., 2004; Jaquet et al., 2008). This is *a priori* hypothesis for long-term hazard assessment, in which the use of volcano structural alignments (eruptive fissures, fractures, dykes) and the location of past emission centers assumes implicitly that the general stress field has not changed significantly since the formation of these structures. Conversely, when dealing with short-term hazard assessment, monitoring data (Martí and Felpeto, 2010), which provide important information regarding magma migration and its ascent to the surface plays a major role in determining volcanic susceptibility.

One of the most important aspect in calculating volcanic susceptibility is the estimation of the kernel function and the associated bandwidth, which provide a measure of the degree of randomness (or structural control) presented by the distribution of past vents and how this will affect the location of the new ones. The smoothness and the modelling ability of the kernel function is controlled by the smoothing parameter or bandwidth h , which determines how the probabilities spread out from the volcanic structures or vents (Diggle, 1985; Connor and Hill, 1995; Lutz and Gutmann, 1995; Cappello et al., 2012). Thus, for small h values, the kernel function gives high probability estimates in the vicinity of the existing volcanic structures. Conversely, when high bandwidth values are assigned, the probability estimates are distributed in a more homogeneous way throughout the entire area under study. One chapter of this thesis presents a new tool to evaluate volcanic susceptibility, allowing the selection of an appropriate method for evaluating the bandwidth for

the kernel function.

As for temporal analysis, long-term forecasting is based on historical and geological data, as well as on theoretical models, and refers to the time window available before an unrest episode occurs in the volcanic system. Some authors use probabilistic statistical methods based on the Bayesian event tree for long-term volcanic hazard assessment (Newhall and Hoblitt, 2002; Marzocchi et al., 2008; Sobradelo and Martí, 2010), while some others use a deterministic approach (Voight and Cornelius, 1991; Kilburn, 2003; see also Hill et al., 2001). The first approach proposes a general event tree scheme to estimate the probability of all the relevant possible scenarios of a volcanic crisis and, in general, to quantify the volcanic hazard and risk (Sobradelo et al., 2010). Marzocchi et al. (2008, 2010) developed probabilistic tools for long- and short-term eruption forecasting based on Bayesian methodology and using event tree structure. In this thesis a new tool is presented with the advantage to be integrated in a GIS platform and evaluates the hazard associated with eruptive and non-eruptive volcanic scenarios and looks at the hazard for different types of magma composition and different vent locations, together with the geological hazard and its extent.

Once spatial and temporal probabilities have been estimated, the next step forward consists of computing several scenarios as a means of evaluating the potential extent of the main expected volcanic and associated hazards. Most of these studies allow volcanic hazards such as lava flows, PDCs and ash fallout to be modelled and visualised on a GIS framework (Pareschi et al., 2000; Felpeto et al., 2007; Toyos et al., 2007; Crisci et al., 2008; Cappello et al., 2012; Martí et al., 2012; Alcorn et al., 2013). Similar approaches have been applied in volcanic areas such as Auckland, New Zealand (Bebbington and Cronin, 2011); Etna, Sicily (Cappello et al., 2013); and Tenerife, Spain (Martí et al., 2012); Peru (Sandri et al., 2014). Nevertheless, other procedures have also been applied in order to assess volcanic hazards in Campi Flegrei, Italy (Lirer et al., 2001); Furnas (São Miguel, Azores) Vesuvius in Italy (Chester et al., 2002); and Auckland, New Zealand (Sandri et al., 2012). Compared with these previous approaches, the methodology presented in this thesis offers a procedure that facilitates undertaking volcanic hazard assessment in a systematic way, which can be easily applied to other volcanic areas around the world.

Another important aspect in risk assessment is the management and exchange of information, due largely to the nature, variety and availability of the data we need

to handle (De la Cruz-Reyna, 1996). The quality of the data will determine the evaluation of the volcanic risk, which is an essential part of risk-based decision-making in land-use planning and emergency management. Some of the most relevant issues include how and where to store the data, in which format should it be made available, and how to facilitate its use and exchange. To date, the databases used in volcanology have been created to store and analyze different types of information and have been employed to analyze, for example, (1) the impacts of volcanic phenomena on people (Witham, 2005); (2) potentially active volcanoes situated in regions of high geodynamic unrest (Gogu et al., 2006); (3) collapse calderas (Geyer and Martí, 2008); (4) volcano monitoring data that include instrumentally and visually recorded changes in seismicity, ground deformation, gas emission and other parameters (WOVOdat (Venezky and Newhall, 2007)); (5) global volcanic unrest (Phillipson et al., 2013); and (6) active faults on Mt. Etna (Barreca et al., 2013). In particular, efforts have been made to construct a Global Volcanic Risk database of large magnitude explosive volcanic eruptions (LaMEVE (Croweller et al., 2012)). However, none of the existing databases is based on a simple architecture that contains all the necessary information for volcanic risk analysis and management. Thus, it is essential to design an appropriate database that is specifically adapted to the task of evaluating and managing volcanic risk. In the last chapter of this thesis, we present an architecture for a geodatabase for volcanic risk assessment and management. The rationale behind constructing this database is the need to create a comprehensive structure including all known or identified fields that might contribute to the assessment of volcanic risk. The database also aims to make the task of volcanic risk management easier for decision makers.

1.3 Aims of dissertation

The aim of this thesis is to supply new tools and a systematic method to assess long-term volcanic hazard in monogenetic volcanic fields. Here, we propose and test different statistical methodologies to interpret volcanic data and assess volcanic hazard. The use of free tools based on statistical techniques to determine where next eruptive vents could be and the eruption recurrence for an area is crucial to reduce the potential volcanic risk. Frequently, the information about past eruptive history and present state of activity is incomplete. For this reason, we need to build

the strategies that are required to successfully face up to and minimise the impact of future volcanic activity and reduce in a quantitative way decision-makers under uncertainty.

Particular attention has been paid to integrate the volcanological insights with statistical modelling into e-tools to the study of volcanology and volcanic hazard. Therefore, the main overall objective has been to establish general guidelines to evaluate long-term volcanic hazard on monogenetic volcanism, thus contributing to improve their understanding. This has been achieved by constructing free tools that are easy to use and allow to update results whenever new information becomes available.

The specific aims of this Ph.D. Thesis are: (a) to elaborate susceptibility map based on the quantification of objective geological and geophysical data through QVAST tool, (b) to estimate a probability of occurrence for possible future volcanic scenarios through HASSET tool, (c) to simulate different eruptive scenarios that allow to construct final hazard map, (d) to test these tools and the methodology in different monogenetic volcanic fields, and (e) to create a database design that permits the exchange of information and the updating of data in order to prevent redundancy and repetitiveness. The selected case studies have been El Hierro (Canary Islands, Spain), Deception Island (South Shetland Islands, Antarctica), La Garrotxa (NE of Spain), which offer as a whole a wide range of eruption styles and behaviors.

The specific results obtained from this multidisciplinary work represent an essential tool to lead a correct and systematic volcanic hazard assessment in monogenetic volcanic fields, but also a step forward in the development and application of free tools in the scientific community.

1.4 Thesis structure

This thesis is structured into 9 chapters, being the first chapter this Introduction, the following six different research papers and the results/discussion and conclusions chapters. Each of the studies contributes to achieve the main objectives of the Ph.D. Thesis and describes in a logical sequence the different methodologies and different applications in monogenetic volcanic fields. All these chapters represent a coherent conceptual methodology and a step forward in the evaluation of volcanic hazard

potentially useful for long-term emergency planning.

Chapter 2 proposes and describes a new tool, QVAST (**Q**GIS for **VolcAnic SuscepTibility**), which is designed to create user-friendly quantitative assessments of volcanic susceptibility, allowing the selection of an appropriate method for evaluating the bandwidth for the kernel function and the evaluation of the probability density function. It was performed in order to obtain a quantitative assessment of volcanic hazards, based on the development of susceptibility maps (i.e., the spatial probability of a future vent opening given the past eruptive activity of a volcano). The potential of QVAST, developed in a free and user-friendly environment, is shown through its application in the volcanic fields of Lanzarote (Canary Islands) and La Garrotxa (NE Spain). This methodology has been published in *Natural Hazards and Earth System Sciences* and constitutes the body of chapter two and the appendix 2.

Chapter 3 presents a new tool based on an alternative methodology to assess volcanic hazard that uses Bayesian Inference to assign the probabilities of occurrence to each eruptive scenario. Compared to previously existing tools (e.g., BET_EF and BET_VH (Marzocchi et al., 2008, 2010)), HASSET (Hazard Assessment Event Tree) uses a more complex and complete event tree to assign the probabilities of occurrence to each eruptive scenario and allows to compute the long-term probability of each and all of the mutually exclusive and exhaustive events. HASSET estimates the probability of occurrence of a future volcanic scenario and evaluates the most relevant sources of uncertainty from the corresponding volcanic system. This methodology has been published in *Bulletin of Volcanology* and constitutes the body of chapter three and the appendix 3.

Chapter 4 performs a long-term hazard evaluation carried out at El Hierro Island (Canary Islands), an island essentially characterized by basaltic volcanism with both Strombolian and Hawaiian activity. Recent volcanic activity on El Hierro is largely characterised by monogenetic mafic volcanism. The last eruption on El Hierro occurred in 2011–2012 demonstrates how reliable data and tools can enable scientific advisors and decision-makers to consider possible future eruptive scenarios. The main objective of the work was to analyse the past eruptive activity in order to determine the spatial and temporal probability and likely style of a future eruption on the island. The results obtained, through the combination of the most probable scenarios, is the first qualitative integrated volcanic hazard map of El Hierro. This methodology has been published in *Natural Hazards and Earth System Sciences* and

constitutes the body of chapter four and the appendix 4.

Chapter 5 presents and describes a methodology to assess volcanic hazard assessment at Deception Island (Southern Shetland Archipelago, Antarctica), which is the most active volcano in the South Shetland Islands and has been the scene of more than twenty identified eruptions over the past two centuries. The research is based on the use of probabilistic methods and statistical techniques to estimate volcanic susceptibility, eruption recurrence and the most likely future eruptive scenarios. The Bayesian event tree statistical method HASSET is applied to calculate eruption recurrence, while the QVAST tool is used to analyse past activity and to calculate the possibility that new vents will open (volcanic susceptibility). On the basis of these calculations, we identify a number of significant scenarios using the GIS-based VORIS 2.0.1 and LAHARZ software and evaluate the potential extent of the main volcanic hazards to be expected on the island. This study represents a step forward in the evaluation of volcanic hazard on Deception Island and the results obtained are potentially useful for long-term emergency planning. This methodology has been accepted for publication to the Journal of Volcanology and Geothermal Research and constitutes the body of chapter four and the appendix 5.

Chapter 6 is the last case study presented in this Thesis and applies to La Garrotxa Volcanic Field (NE of Spain), which is a Quaternary volcanic field, located in the Northeast of the Iberian Peninsula, and includes more than 50 well preserved volcanoes. The volcanic activity varies from Hawaiian to Violent Strombolian, showing numerous episodes of phreatomagmatic activity. Although the potentiality for future eruptions and high demographic and industrial development of the area, no study of its volcanic hazard has been made yet. We present an evaluation of different volcanic hazards through an analysis of the susceptibility, temporal recurrence rate, simulation of different eruptive scenarios, such as lava flow, pyroclastic density current (PDC), and ashfall, and a final hazard map. The final hazard map shows La Garrotxa volcanic field subdivided into four different levels of hazards and aims at becoming a reference for land use management planning. This methodology has been submitted to the Journal of Quaternary Science in August 2014, and constitutes the body of chapter four and the appendix 6.

Finally, Chapter 7 describes the design of a new spatial database structure, VERDI (**V**olcanic **m**anag**E**ment **R**isk **D**atabase des**I**gn), considering the importance of both the quantity and quality of the available volcanic data and an optimum

storage mechanism. This database allows to manipulate, organize and manage different types of data, including geological, volcanological, meteorological, monitoring and socio-economic information. The design of purpose-built databases that take into account data format and availability and afford easy data storage and sharing, should facilitate spatial and temporal analysis that will produce probabilistic hazard models for future vent opening, simulate volcanic hazards and assess their socio-economic impact, avoiding any duplication of information. The potential of the VERDI structure is shown through its application on El Hierro (Canary Islands) and the possibilities it offers in regard to data organization. This methodology has been submitted to the *Journal of Volcanology and Geothermal Research* in May 2014, and constitutes the body of chapter four and the appendix 7.

The last chapters (Chapters 8 and 9) summarise the results and the general conclusions of the whole work presented in this thesis and talks about future research.

QVAST: a new Quantum GIS plugin for estimating volcanic susceptibility

Published in:

Natural Hazards and Earth System Sciences

Authors:

Stefania Bartolini^a

Annalisa Cappello^b

Joan Martí^a

Ciro Del Negro^b

a) Group of volcanology, (SIMGEO-UB), Institute of Earth Sciences Jaume Almera, ICTJA-CSIC, Barcelona, Spain

b) Istituto Nazionale di Geofisica e Vulcanologia, Sezione di Catania, Osservatorio Etneo, Catania, Italy

2.1 Abstract

One of the most important tasks of modern volcanology is the construction of hazard maps simulating different eruptive scenarios that can be used in risk-based decision making in land-use planning and emergency management. The first step in the quantitative assessment of volcanic hazards is the development of susceptibility maps (i.e., the spatial probability of a future vent opening given the past eruptive activity of a volcano). This challenging issue is generally tackled using probabilistic methods that use the calculation of a kernel function at each data location to estimate probability density functions (PDFs). The smoothness and the modeling ability of the kernel function are controlled by the smoothing parameter, also known as the bandwidth. Here we present a new tool, QVAST, part of the open-source geographic information system Quantum GIS, which is designed to create user-friendly quantitative assessments of volcanic susceptibility. QVAST allows the selection of an appropriate method for evaluating the bandwidth for the kernel function on the basis of the input parameters and the shapefile geometry, and can also evaluate the PDF with the Gaussian kernel. When different input data sets are available for the area, the total susceptibility map is obtained by assigning different weights to each of the PDFs, which are then combined via a weighted summation and modeled in a non-homogeneous Poisson process. The potential of QVAST, developed in a free and user-friendly environment, is here shown through its application in the volcanic fields of Lanzarote (Canary Islands) and La Garrotxa (NE Spain).

2.2 Introduction

Volcano susceptibility is defined as the spatial probability of vent opening (Martí and Felpeto, 2010) and constitutes one of the first steps in the assessment of volcanic hazards and the construction of hazard maps of eruptive products (e.g., lava flows, ash, and pyroclastic density currents). The exact site of a new eruption - a central vent or a vent located on the flanks of a stratovolcano, or at any other apparently randomly distributed point in a larger monogenetic volcanic field - is of critical importance in determining the potential outcome of an eruption. For the same eruption, different eruption scenarios and, consequently, different potential impacts are to be expected depending on the exact location of the vent and on the geographic

and demographic characteristics of the area. Hence, evaluating where future eruptive vents are most likely to open greatly influences volcanic hazard assessment (Cappello et al., 2011a, b).

The exact path that the over-pressurized magma will take from its accumulation site to the earth's surface - and hence the site of any new vent - will be determined by geological structure and stress distribution inside the crust. We know that the energetic investment by the magma on this path will be the minimum and that it will be parallel to the trajectory of the main principal stress and normal to the minimum principal stress (Gudmundsson, 2008, 2012). However, we do not have any direct criteria that enable us to determine this route *a priori* since we lack detailed 3-D knowledge of the stress field of the area. In the long term it is possible to base some approaches on the location of previous eruptions and on the structural characteristics of the volcano or the volcanic area. On the other hand, in the short term it is also possible to take into account monitoring data from the volcanic field. Therefore, the estimation of the most probable vent site is not an impossible task and can be undertaken as part of volcanic hazard assessment. This is a less difficult task in stratovolcanoes for which good knowledge of past eruptive history exists and where real-time volcano monitoring is currently being performed. However, volcano susceptibility assessment is more complex in monogenetic volcanic fields, as has been shown by the recent eruption at El Hierro (Martí et al., 2013), where stress conditions may change from one eruption to another.

Published works in this field (Connor and Hill, 1995; Felpeto et al., 2007; Jaquet et al., 2008; Martí and Felpeto, 2010; Favalli et al., 2011; Connor et al., 2012; Cappello et al., 2012, 2013) report the use of kernel density functions to evaluate susceptibility. However, this technique is based mainly on the assumption that new vents will not form far from existing ones (Martin et al., 2004; Jaquet et al., 2008). This is an *a priori* hypothesis for long-term hazard assessment, in which the use of volcano structural alignments (eruptive fissures, fractures, dykes) and the location of past centers of emission assumes implicitly that the general stress field has not changed significantly since the formation of these structures. Conversely, when dealing with short-term hazard assessment, monitoring data (Martí and Felpeto, 2010) - which provide important information regarding the evolution of magma migration and its ascent to the surface - play a major role in determining volcanic susceptibility.

A kernel function is a density function used to obtain the intensity of volcanic events. It is based on the distance from nearby volcanoes and a smoothing constant h (Martin et al., 2004), which indicates the spatial probability that a new eruptive vent will form. A Gaussian kernel is a kernel function describing a normal distribution that is used in volcanology to estimate local volcanic event densities in volcanic fields (Martin et al., 2004; Connor et al., 2012; Cappello et al., 2012).

The aim of this work is to (i) analyze different approaches to evaluate the smoothing parameter h (also known as the bandwidth), (ii) estimate for each approach the corresponding probability density function (PDF) and (iii) assess long-term spatial susceptibility in monogenetic volcanic fields. We describe here a new user-friendly plugin known as QVAST (**Q**GIS for **V**olc**A**nic **S**uscep**T**ibility) for the free geographic information system Quantum GIS (QGIS), which can make these calculations and help users to choose the best option in each particular case (Fig. 2.1). We describe the QVAST interface step by step via two different applications: the first in Lanzarote (Canary Islands, Spain) and the second in La Garrotxa (NE Spain). These two case studies show QVAST's great flexibility and its ability to identify the most likely zones to host new eruptions in monogenetic volcanic fields.

2.3 Optimal bandwidth in kernel density estimation

The probability distribution in a kernel technique is strongly influenced by a smoothing parameter or bandwidth, which determines how probabilities are distributed in terms of the distance from the volcanic structures or vents. The smoothness of the kernel density estimate is evident compared to the discreteness of the histogram, as bin width of a histogram, for continuous random variables (Scott, 1979). An optimal smoothing bandwidth is based on the clustering behavior of the volcanic structures and varies proportionally with the volcanic field size and vent density. Indeed, narrow bandwidths accentuate densities near the locations of past events. Conversely, broad bandwidths may oversmooth the density estimate, resulting in unreasonably low density estimates near clusters of past events, or overestimate densities at greater distances from past events. In a Gaussian kernel function, the bandwidth is equivalent to the variance of the kernel (Connor et al., 2012).

In volcanic hazard applications, the choice of the optimal bandwidth is difficult

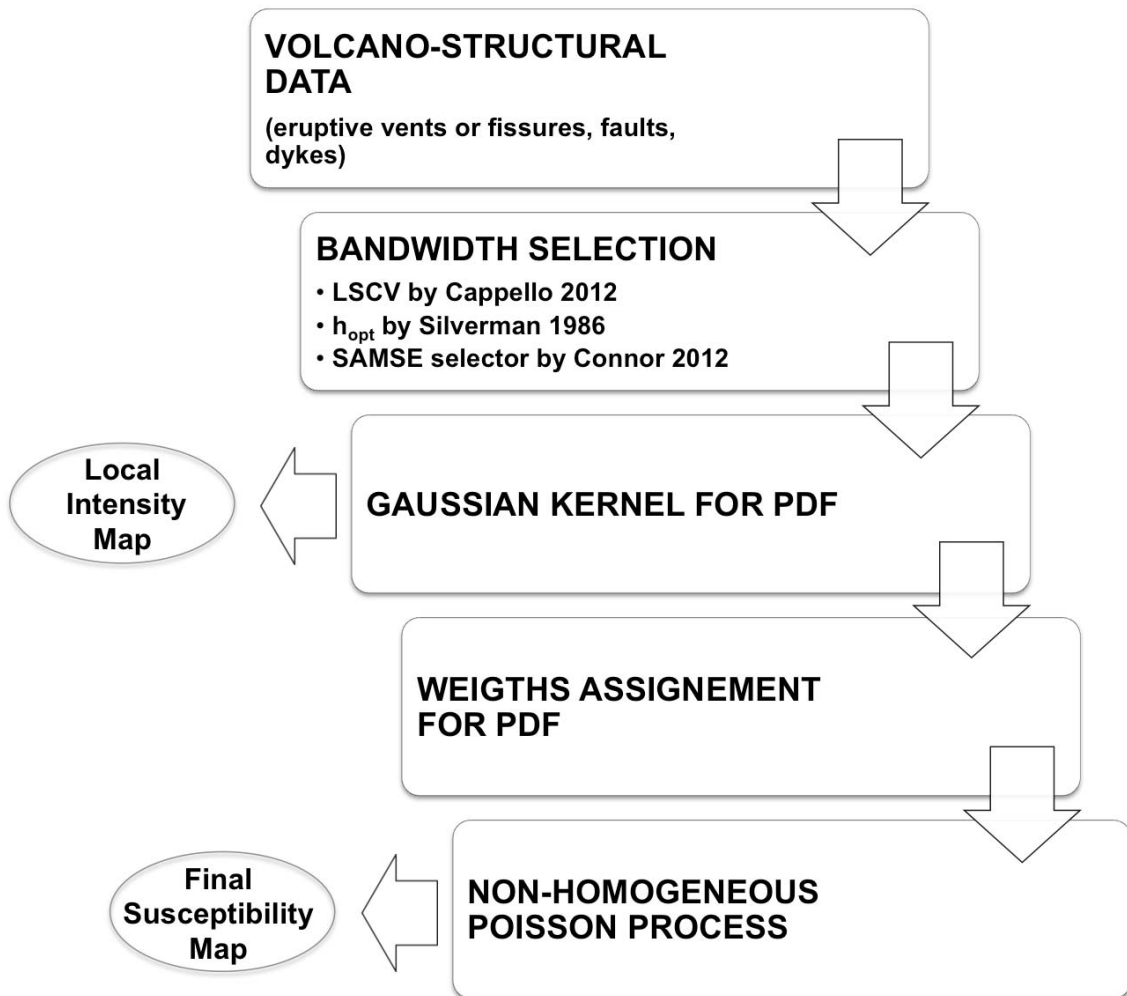


Figure 2.1: Flowchart showing the main steps available in QVAST

and depends on the field size and degree of cluster determining the probability distribution at distance from volcanic structures or eruptive vents.

QVAST provides a number of different methods for estimating the optimal bandwidths. The least square cross-validation (LSCV - Cappello et al., 2012) is made available for the volcanic structures with linear geometries (e.g., dykes, eruptive fissures, faults), and three methods are provided for the eruptive vents: the LSCV, the \hat{h} score (Silverman, 1986) and the sum of asymptotic mean squared error (SAMSE) selector H (Connor et al., 2012).

An exhaustive description of each of these methods is hereinafter provided.

2.3.1 Least square cross-validation (Cappello et al., 2012)

Least square cross-validation (LSCV) is a procedure that uses an iterative approach to determine the optimal bandwidth for fixed kernel functions. Initially proposed by Rudemo (1982) and Bowman (1984), the LSCV uses the minimization of the integrated square error between the estimated distribution and the true distribution.

In our QGIS plugin, we used the version proposed by Worton (1995), defined as

$$\begin{aligned} \text{LSCV}_h &= \frac{1}{\pi h^2 n} + \frac{1}{4\pi h^2 n^2} \\ &\times \sum_{i=1}^n \sum_{j=1}^n \left(\exp \left[\frac{-d_{ij}^2}{4h^2} \right] - 4 \exp \left[\frac{-d_{ij}^2}{2h^2} \right] \right), \end{aligned} \quad (2.1)$$

where h is the smoothing factor, n the total number of historical data and d_{ij} the Euclidean distance between the i th and the j th points, when dealing with eruptive vents.

Conversely, if historical data consist of broken lines containing a number of linear segments, QVAST uses a modified version of LSCV (Cappello et al., 2012; Becerril et al., 2013; Cappello et al., 2013), where d_{ij} is the “minimax distance” (i.e., the minimum value of the maximum distances between each end point of the i th volcanic structure and all the end points of the j th volcanic structure).

2.3.2 The h_{opt} score (Silverman, 1986)

The Silverman method determines the optimal bandwidth h based on the assumption that the location of the vent opening is a random variable. The generalization

of the Silverman's rule of thumb (Silverman, 1986) in the multivariate case is as follows (Scott, 1992; Härdle et al., 2004):

$$\hat{h} = n^{1/(d+4)} \hat{\sigma}. \quad (2.2)$$

In the bivariate case $d = 2$, n is the length of the samples (x and y are the Cartesian coordinates), and $\hat{\sigma}$ is the standard deviation. Thus, we obtain

$$\hat{h} = n^{1/6} \sqrt{\frac{\sigma_x^2 + \sigma_y^2}{2}}, \quad (2.3)$$

where σ_x and σ_y are the standard deviations of the x and y coordinates, respectively.

2.3.3 The sum of asymptotic mean squared error selector (Connor et al., 2012)

The pilot bandwidth selector is a modified asymptotic mean integrated squared error (AMISE) method developed by Duong and Hazelton (2003) to evaluate the optimal bandwidth in kernel density estimation.

Despite their mathematical complexity, SAMSE bivariate bandwidth selectors can help find optimal bandwidths using actual data locations, and so remove subjectivity from the process (Connor et al., 2012). In Duong and Hazelton (2003), the bivariate kernel density is defined by

$$\hat{f}(\vec{x}; \mathbf{H}) = n^{-1} \sum_{i=1}^n K_{\mathbf{H}}(\mathbf{x} - \mathbf{X}_i), \quad (2.4)$$

where n is the sample size, $\vec{x} = (x_1, x_2)^T$, $\mathbf{X}_i = (X_{i1}, X_{i2})^T$, for $i = 1, 2, \dots, n$, and K is the bivariate kernel that depends on \mathbf{H} , the bandwidth matrix that is symmetric and positive definite. To measure the performance of \hat{f} , a SAMSE pilot selector is used, which is simpler and more parsimonious than the AMISE selectors.

The SAMSE selector is freely available within the “ks” package of the R Project for Statistical Computing (Duong, 2007; Hornik, 2009) and can be expressed as follows:

$$H = Hpi(\mathbf{x}, nstage, pilot = 'samse', pre = 'sphere'), \quad (2.5)$$

where \mathbf{x} is a vector or matrix of data (vents), $nstage$ is the number of stages in the plugin bandwidth selector, $pilot$ is the pilot estimation, and “pre” concerns the pre-transformations.

The spatial density estimates are based on the distribution of past events within a volcanic field and the time period under consideration, and can be used as the basis for estimating the probability of the opening of new vents within a region. Connor et al. (2012) define an event as the opening of a new vent at a new location during a new episode of volcanic activity.

The optimal bandwidth matrix obtained using Eq. (2.5) represents smoothing in E-W and N-S directions, the upper left and lower right diagonal elements, respectively.

2.4 Kernel density estimation

Kernel density estimation is a well-known, non-parametric approach to the estimation of probability density functions using a finite number of samples. The shape of kernel function - be it Cauchy kernel (Martin et al., 2004), Epanechnikov kernel (Lutz and Gutmann, 1995) or Gaussian kernel (Connor and Hill, 1995) - is important in probability calculations, even if it is less relevant than other parameters (Connor and Hill, 1995; Lutz and Gutmann, 1995).

In the general case, if \mathbf{X}_i denotes samples of size n , then the kernel density estimate of λ in the point x is given by

$$\lambda(x) = \frac{1}{n} \sum_{i=1}^n K_h(x, \mathbf{X}_i), \quad (2.6)$$

where K_h is a kernel function with bandwidth h , satisfying the condition that $\int K_h(x, \cdot) dx = 1$ to ensure that $\lambda(x)$ is a density. In the Gaussian formulation,

$$\lambda(x) = \frac{1}{2\pi nh^2} \sum_{i=1}^n \exp\left(-\frac{d_i^2}{2h^2}\right). \quad (2.7)$$

2.5 Interface and tools of QVAST

Available open-source desktop GIS have notable differences in quality and performance (Sherman, 2008; Chen et al., 2010). Quantum GIS (QGIS) is a free, open-

source and cross-platform software, distributed at www.QGIS.org. It includes all of the common GIS functions and features and possesses an intuitive and user-friendly interface. One of the great advantages of QGIS is the availability of plugins from official and third-party repositories that provide a large number of additional functions. These features make QGIS the most suitable software for our plugin.

QVAST is developed in Python script, an interpreted, general-purpose, high-level programming language, whose codes can be packaged into stand-alone executable programs (using sub-process calls to R) and C++ codes. A graphical user interface (GUI) is available to provide users with a dynamic graphical window in QGIS.

QVAST includes different methods for choosing the optimal value for the bandwidth, which depends on the size of the volcanic field and the degree of clustering in the available data. The PDF is constructed using a kernel density estimator, which is a function centered at each data sample location that exerts an influence on the surrounding region (Diggle, 1985). It is employed to estimate how the density of new vent openings varies across a study area in accordance with the distribution of past eruptions and the bandwidth. Different types of kernels can be used to describe the spatial density, e.g., the Cauchy (Martin et al., 2004), Epanechnikov (Lutz and Gutmann, 1995), Gaussian (Connor and Hill, 1995), or elliptical (Kiyosugi et al., 2010) kernels. Here we use the Gaussian kernel, which responds well to the clustering phenomena commonly observed in volcanic distributions (Weller et al., 2006).

Long-term spatial susceptibility is obtained through a non-homogeneous Poisson process (NHPP), where the PDFs and their relative weights are combined through a weighted sum. QVAST allows users to assign different weights to each of the PDFs depending on the relevance and reliability of data sets. Once the user has installed the plugin in the QGIS plugins folder, a new option called “Volcano” appears in the QGIS menu bar where the QVAST model is installed.

The QVAST structure consists of three main modules (Fig. 2.2):

1. Estimation of the optimal bandwidth starting from different geometric layers (points and polylines);
2. Evaluation of the Gaussian kernel and generation of the PDF in the volcanic area under study;
3. Calculation of the susceptibility map from one or more PDFs. In this latter case, QVAST allows users to assign different weights to each layer.

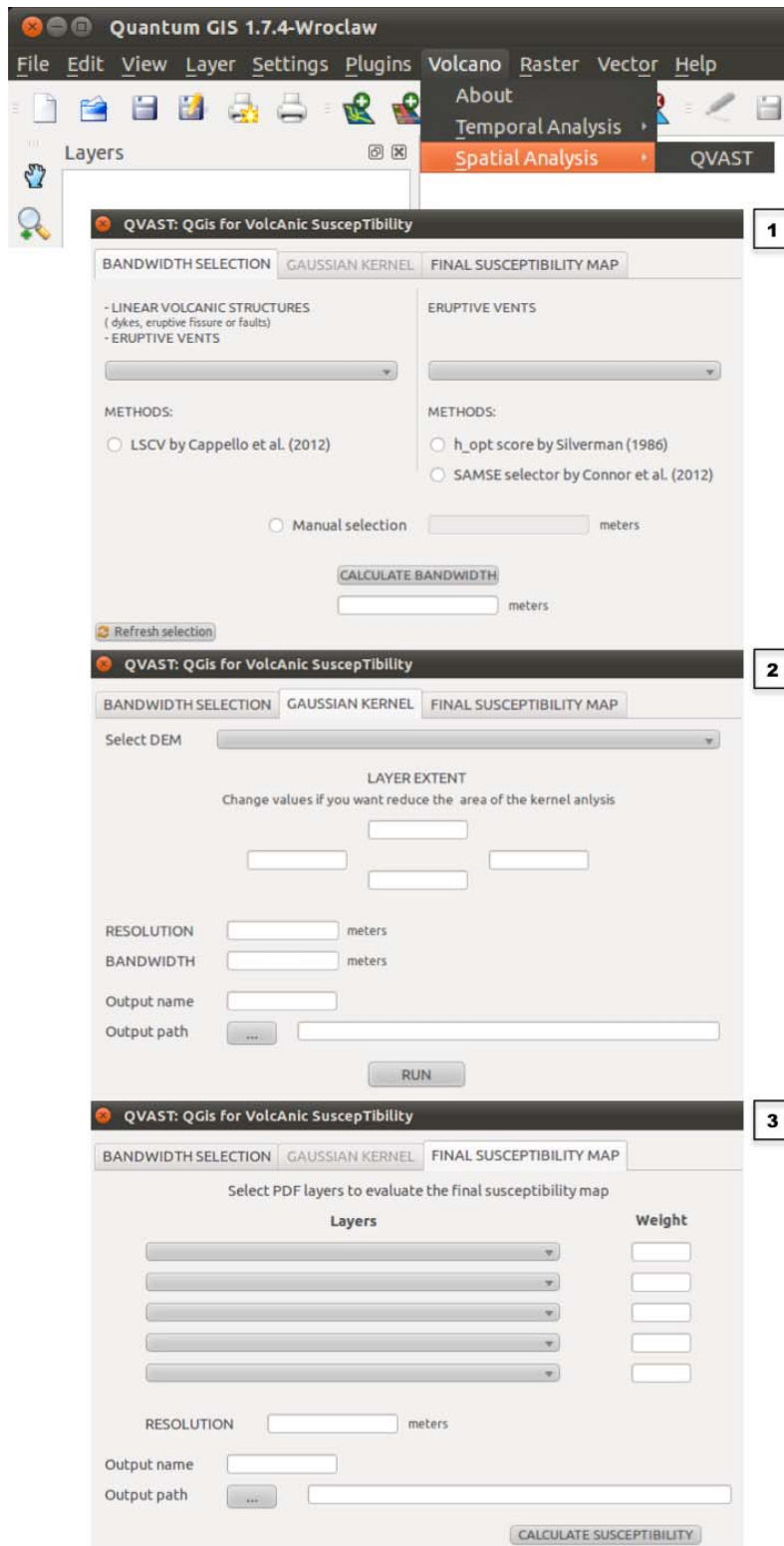


Figure 2.2: QVAST main interface: screenshots of the optimal bandwidth selection (1), for the parameter needed by the Gaussian kernel (2) and for the assignment of weights to the different PDFs (3)

The first window that appears after launching the plugin is the evaluation of the bandwidth. A drop-down menu contains the shapefile layers added in the “Layers” menu in the QGIS project. To estimate the optimal bandwidth in case of a group of sample points (e.g., eruptive vents), QVAST offers three different methods: LSCV, the \hat{h} score and the SAMSE selector H . If the GIS layer consists of linear volcanic structures (e.g., dykes, eruptive fissures, or faults), only the LSCV score can be used. Otherwise, the plugin allows the user to introduce the optimal value for the bandwidth by hand (if known) and continue directly to the construction of the PDF.

Once the layer and the method for evaluating the bandwidth have been selected, the value of the smoothing parameter is calculated using the “CALCULATE BANDWIDTH” button.

The second window enables the PDF with the Gaussian kernel to be evaluated using the calculated optimal bandwidth. To evaluate the Gaussian kernel on the selected layer, QVAST needs the following input parameters: the surface area on which the calculation is to be performed (raster layer), the grid resolution (which should be clearly smaller than the size of the volcanic area under study), the bandwidth value, the output name, and the output path where the results are to be saved. The surface area can be less than the entire digital elevation model (DEM) if the user is only interested in a particular area. The result of the Gaussian kernel is a PDF in GeoTIFF raster format, which is automatically added as a new layer to the active QGIS project. The results show the distribution of the PDF in the volcanic area related to the input layer selected.

The third window enables simultaneously considering different layers to which different weights can be assigned and thus calculate the final susceptibility map. Once the grid size and the weight for each PDF have been defined, QVAST calculates the weighted sum and evaluates the final raster map that represents the spatial susceptibility. The map is presented in a GeoTIFF raster format and is added to the layer.

Hence, the steps needed to obtain the final susceptibility can be summarized as follows (Fig. 2.1):

1. Gathering of all volcano structural data available;
2. Optimal bandwidth selection using different methods;
3. Application of the Gaussian kernel to obtain the PDF;

4. Assignment of a relative weight to each PDF;
5. Creation of the susceptibility map with an NHPP.

The functionality and flexibility provided by QVAST have been demonstrated in Lanzarote and La Garrotxa volcanic fields. Different methods were used to identify the optimal bandwidth, and different results were obtained when different weights to the PDFs were assigned.

2.6 Applying QVAST: Lanzarote (Canary Islands, Spain) and La Garrotxa (NE Spain)

2.6.1 Lanzarote: geological context

Lanzarote lies in the northeast of the Canary Islands archipelago (Fig. 2.3). It forms the emergent part of the so-called East Canary Ridge (ECR), a NNE-SSW linear volcanic structure located on atypical oceanic crust, at least 11 km thick (Banda et al., 1981), lying between the continental rise and the Canary Basin.

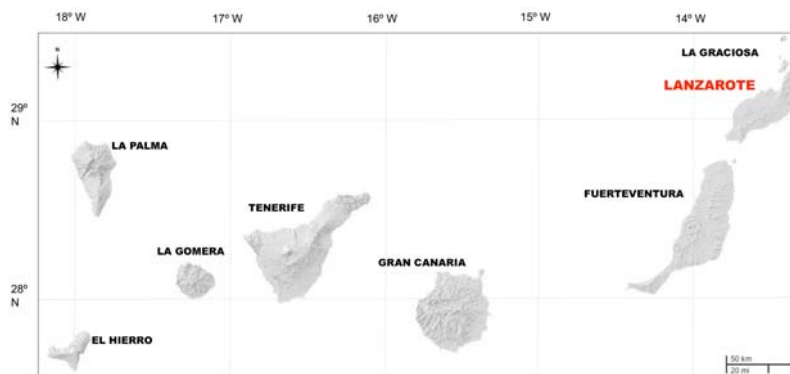


Figure 2.3: Geographical setting of the Canary Islands

The geological evolution of Lanzarote involves two main stages: the first pre-erosional during the Miocene-Pliocene and the second - divided into two periods of volcanic activity - post-erosional during the Quaternary (Marinoni and Pasquaré, 1994).

Sub-aerial volcanic activity has been almost continuous during the past 20 Myr and reveals that these islands are part of a sector of the lithosphere in which the

thermal and dynamic anomalies that lead to the production and ascent of alkaline basaltic magmas have persisted for an exceptionally long period (Coello et al., 1992; Blanco-Montenegro et al., 2005).

In historical times eruptions on Lanzarote took place during the 18th and 19th centuries. The eruption between 1730 and 1736 was one of the earth's biggest ever historical eruptions. A large number of volcanic cones were formed along an around 15 km long fissure. During the eruption 3-5 km³ of lava were emitted, covering an area of approximately 200 km² (Carracedo et al., 1992; Felpeto et al., 2001).

The structural evolution results from a complex interaction between the magmatism and both the regional stress field and the local stress field generated during the growth of the island itself. Hence, the present structural architecture is the result of a complex magmatic and tectonic evolution characterized by variations in the stress field that have been at work from the Miocene to the present day (Camacho et al., 1991).

2.6.2 La Garrotxa: geological context

The Catalan Volcanic Zone (CVZ, NE Iberian Peninsula) is one of the alkaline Quaternary volcanic provinces that form part of the European rift system (Fig. 2.4). The age of its volcanism has not yet been fully defined. Available data indicate that volcanic activity started over 12 Ma ago and continued up to the beginning of the Holocene. Despite being significant in both extension and volume, this volcanism whose eruptions continued up to the Holocene is poorly known in comparison to the contemporaneous alkaline volcanism in other parts of western and central Europe. Volcanism in the CVZ lies predominantly in a NW-SE direction corresponding to the graben system present in the area. Various vents in the area can be aligned in the same NW-SE direction in parallel to the local fault systems. The volcanism younger than 0.5 Ma is mostly concentrated in an area of about 100 km² located between the cities of Olot and Girona. This basaltic volcanic field exhibits scoria cones, lava flows, tuff rings, and maars. Magmatic eruptions range from Hawaiian to violent Strombolian. Phreatomagmatism is also common and has contributed to the construction of more than half of the region's volcanic edifices. It is frequently associated with Strombolian activity but has also acted independently, thereby giving rise to a large variety of different types of eruptive sequences (Martí et al., 2011).

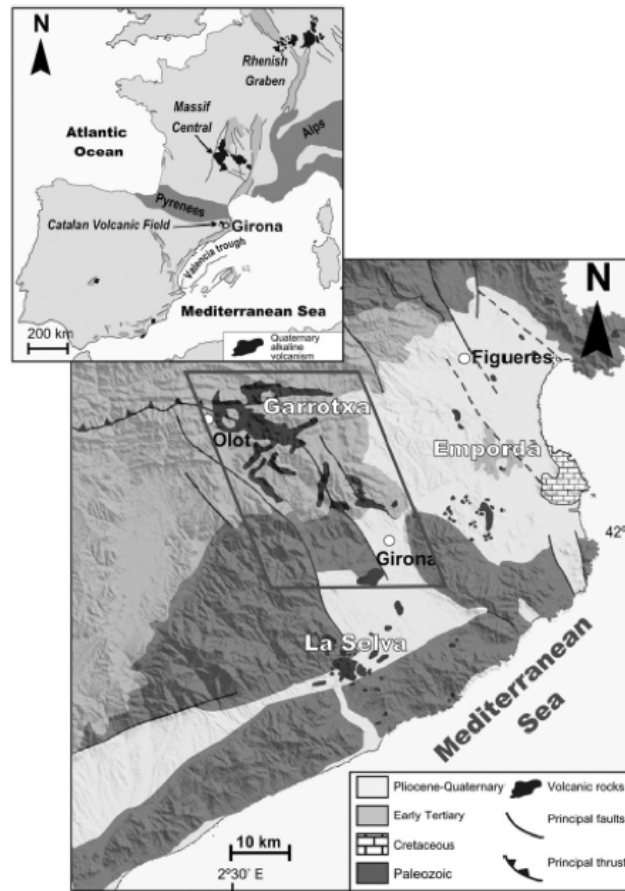


Figure 2.4: Geographical and geological settings of the La Garrotxa volcanic field (Martí et al., 2011)

2.6.3 Data sets and bandwidth estimation

DEMs created by the Instituto Geográfico Nacional (IGN) for Lanzarote and by the Institut Cartogràfic de Catalunya (ICC) for La Garrotxa with a cell size of 25×25 m were used in these analyses. Volcano structural data were retrieved by the Instituto Geológico y Minero de España (IGME, 1988) for Lanzarote and by the Institut Geològic de Catalunya (IGC, 2007) for la Garrotxa.

Volcanic susceptibility was estimated by studying separately all structural data in order to identify different data sets that could be used for the probabilistic analysis. Using the available literature and geological maps, we were able to identify vent locations, vent alignments, and dykes.

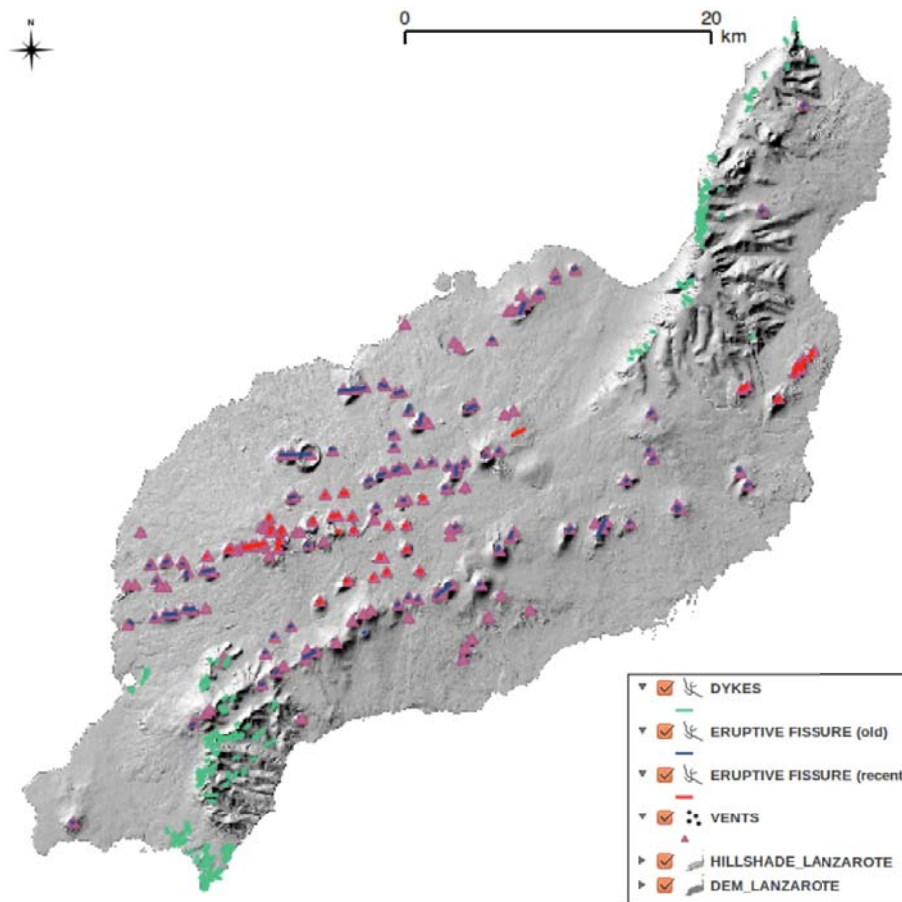


Figure 2.5: Main volcano structural data (dykes, vent alignments and emission centers) used to build the susceptibility map of Lanzarote. The topographic base is 25 m resolution DEM

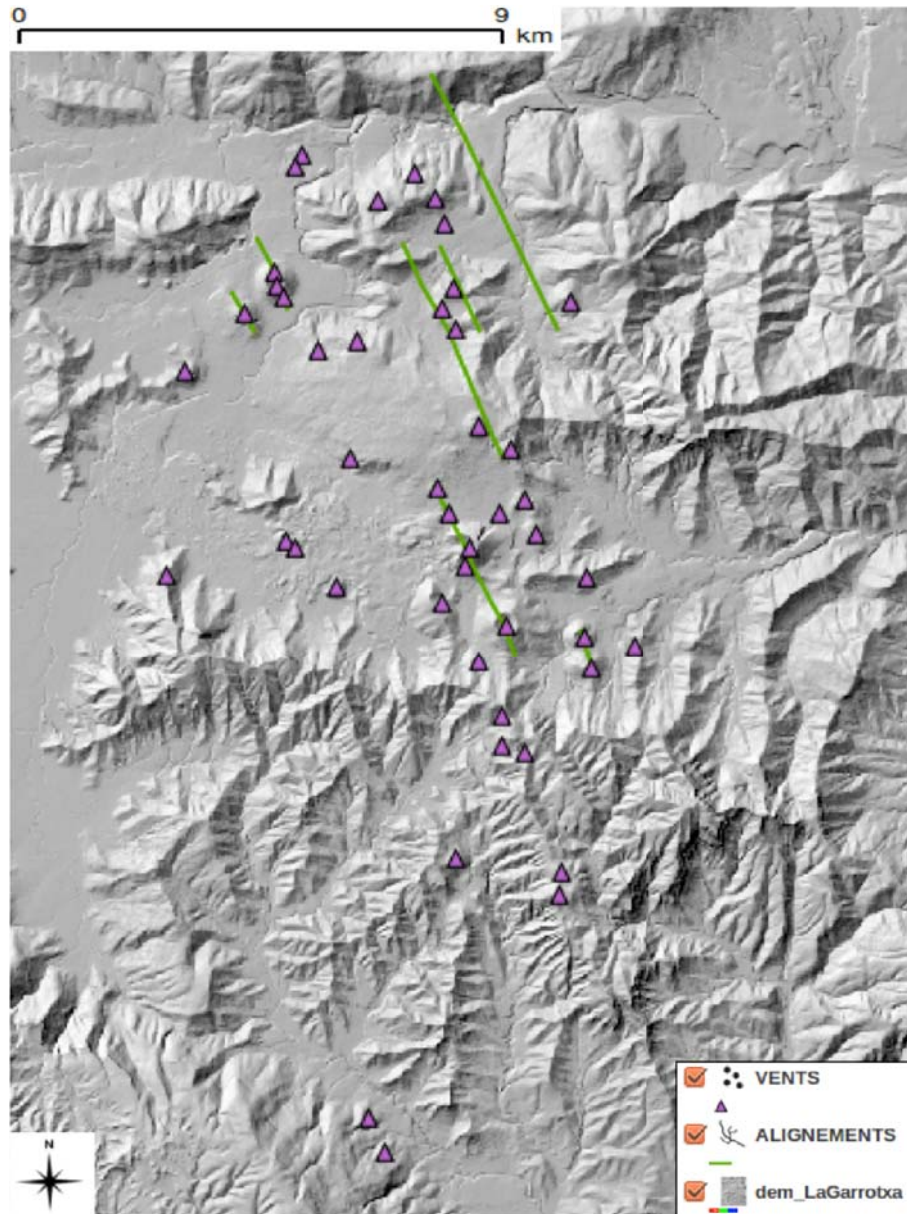


Figure 2.6: Main volcano structural data (dykes, vent alignments and emission centers) used to build the susceptibility map of La Garrotxa. The topographic base is 25 m resolution DEM

Application to Lanzarote

Volcanic structures on Lanzarote are shown in Fig. 2.5. Specifically, we considered 256 dykes and two layers of vent alignments containing 75 older vent alignments and 30 more recent vent alignments, formed during the Holocene. Since both dykes and vent alignments can be represented as polyline shapefiles, QVAST used the LSCV method to calculate the optimal values for the bandwidth, which were found to be the following:

- 351 m for dykes,
- 3000 m for the oldest vent alignments,
- 2304 m for the most recent vent alignments.

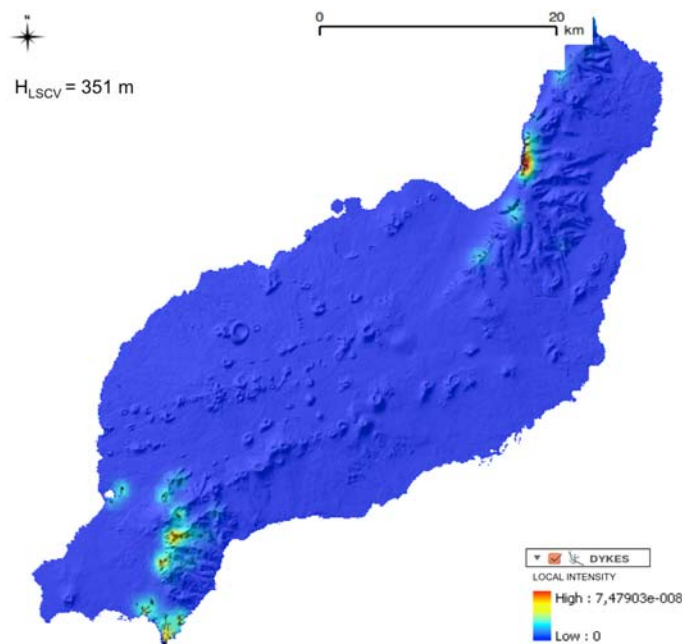


Figure 2.7: PDF of Lanzarote dykes calculated with the Gaussian kernel using a bandwidth of 351 m

As well, we identified a total of 187 emission centers (Quaternary pyroclastic cones and eruptive vents), most of which are distributed in the central part of the island in a NE-SW direction (Marinoni and Pasquaré, 1994).

The evaluation of the bandwidth for the vent locations was performed using the three methods available in QVAST and the following results were obtained: (i) 333 m

with the LSCV method, (ii) 3844 m with Silverman’s method, and (iii) 3934 m with the SAMSE selector.

The PDFs for each layer evaluated using the Gaussian kernel and a 500 m spaced grid are shown for dykes in Fig. 2.7, for vent alignments in Fig. 2.8, and for emission centers in Fig. 2.9.

Given that the PDF generated using the bandwidth obtained with the LSCV seems to provide the best reflection of the current clustering of the emission centers observed, we decided to use this method for the final susceptibility map.

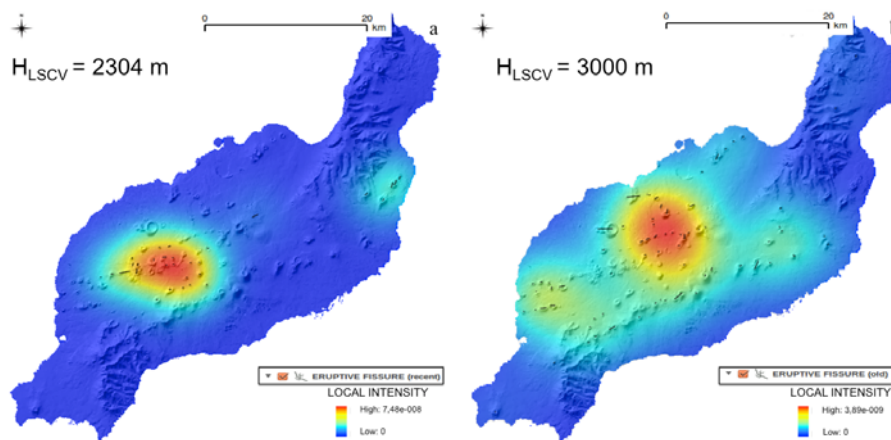


Figure 2.8: PDFs calculated with the Gaussian kernel for the most recent (a) and the oldest (b) vent alignments of Lanzarote

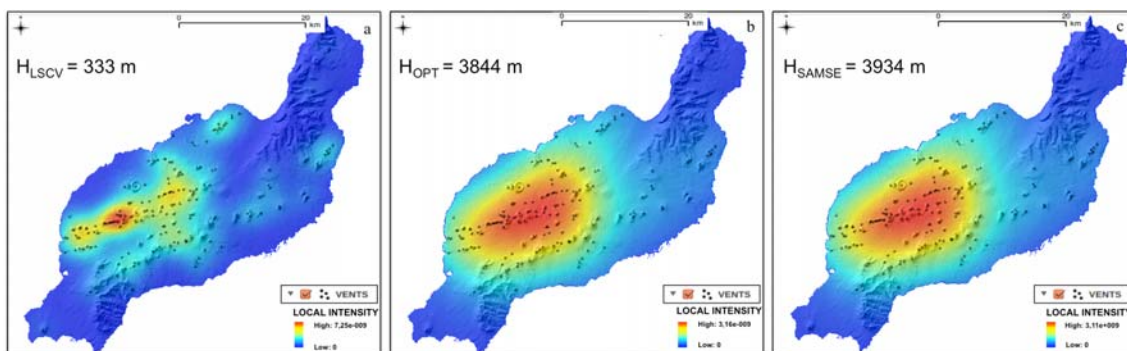


Figure 2.9: PDFs of Lanzarote emission centers calculated with the Gaussian kernel using different bandwidths: 333 m as computed by the LSCV method (a), 3844 m as by the h_{opt} score (b), and 3934 m as by the SAMSE selector (c)

Application to La Garrotxa

Volcanic structures in La Garrotxa are shown in Fig. 2.6. Specifically, we considered vent alignments and emission centers.

Given that the vent alignments can be represented as polyline shapefiles, QVAST used the LSCV method to calculate the optimal value for the bandwidth, which was found to be 4012 m.

In addition, we identified a total of 45 emission centers aligned in a NW-SE direction, parallel to the fault systems (Martí et al., 2011).

As on Lanzarote, the evaluation of the bandwidth for the vent locations was performed using the three methods available in QVAST, which gave the following results: (i) 2002 m with the LSCV method, (ii) 1774 m with Silverman's method, and (iii) 1567 m with the SAMSE selector.

The PDFs for each layer evaluated using the Gaussian kernel and a 500 m spaced grid are shown for vent alignments in Fig. 2.10 and for emission centers in Fig. 2.11.

The PDFs obtained for the vent locations using different bandwidth values generate similar local intensity results. Taking into account isolated vents, we decided to use Silverman's method for the final susceptibility map since it seems to provide the best reflection of the degree of clustering currently observed.

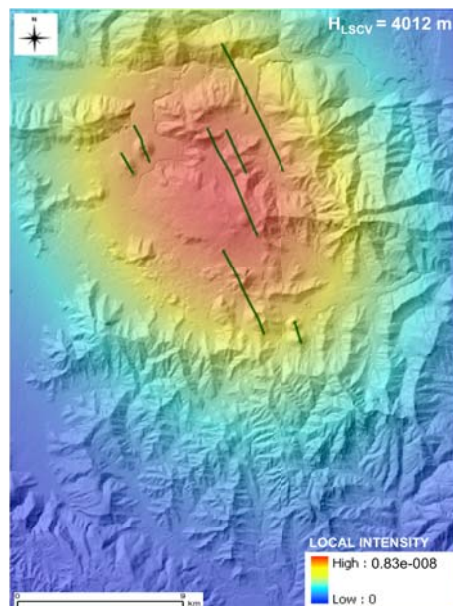


Figure 2.10: PDFs calculated with the Gaussian kernel for the vent alignments of La Garrotxa

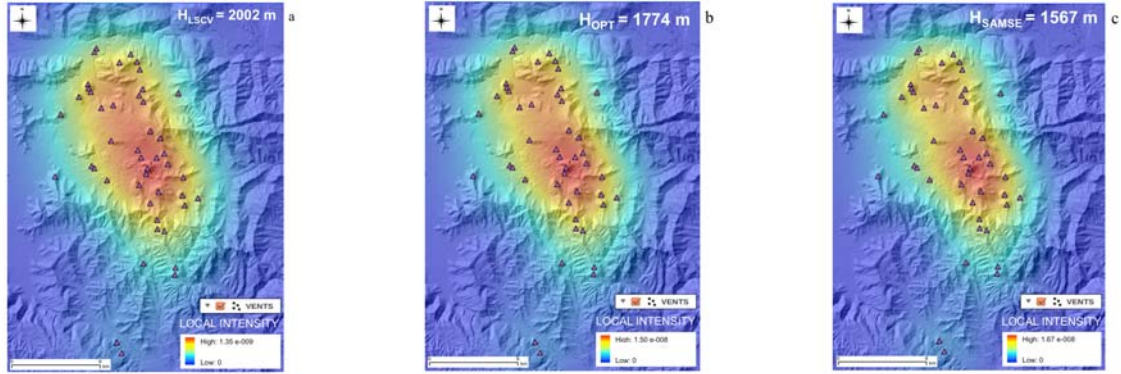


Figure 2.11: PDFs of La Garrotxa emission centers calculated with the Gaussian kernel using different bandwidths: 2002 m as computed by the LSCV method (a), 1774 m as by the h_{opt} score (b), and 1567 m as by the SAMSE selector (c)

2.6.4 Susceptibility map

The spatial probability of future vent openings is obtained by applying an NHPP to each potential vent (x, y) as follows:

$$\text{susc}(x, y) = 1 - \exp(-\Lambda(x, y)\Delta x\Delta y), \quad (2.8)$$

where $\Delta x\Delta y$ is the size of the grid cell ($500 \text{ m} \times 500 \text{ m}$) and $\Lambda(x, y)$ is the weighted sum of the four PDFs and their relative weights.

QVAST provides two opportunities for assigning the weights that reflect the importance and reliability of each input data set. In the first, the user does not assign any specific individual weight and so QVAST defines the same constant value for all PDFs in the computation of the final probability map. In the second case, weights are assigned using expert judgment on the basis of structural criteria (Aspinall, 2006; Neri et al., 2008; Martí and Felpeto, 2010), which provides initial indicative probability distributions to be associated with each PDF.

In this case study, we demonstrated the flexibility of QVAST by generating two different susceptibility maps.

In the first map, the same weight (i.e., 0.25) was assigned to each PDF under the assumption that the probability of all future vent openings is influenced equally by all volcano structural data.

In the second case, we assigned to each of the PDFs the following weights for Lanzarote:

- 0.05 for dykes,
- 0.15 for the oldest vent alignments,
- 0.3 for the most recent vent alignments,
- 0.5 for the emission centers;

and for La Garrotxa, the following weights:

- 0.3 for the vent alignments,
- 0.7 for the emission centers.

On Lanzarote, the highest weight (50 %) was assigned to the emission centers in the center of the island, where eruptions occurred in historical times. This means that new eruptions are given the greatest likelihood of occurring close to the most recent eruptions. Decreasing importance was awarded to the most recent vent alignments, the oldest vent, alignments and dykes. Obviously, the total sum of weights is equal to 1. In La Garrotxa, the highest weight (70 %) was assigned to the emission centers.

The two final susceptibility maps for Lanzarote are shown in Fig. 2.12 and for La Garrotxa in Fig. 2.13.

As it is obvious, on Lanzarote the susceptibility obtained using the same weight for all PDFs (Fig. 2.12a) provides a very homogeneous probability distribution, with the highest values corresponding to exposed dykes. This is disputable, since these dykes are volcanic structures that are clustered as a wide swarm chiefly at the headwalls of the main landslide and have probably been buried by recent volcanic products in other areas. Hence it is not clear whether they have acted as feeders or not (Becerril et al., 2013).

Conversely, the susceptibility map obtained using different weights (Fig. 2.12b) would appear to be more accurate and reliable, and reflects coherently the recent distribution of alignments located in the central part of the island in a NE-SW direction.

If we change the assigned weights, results differ for Lanzarote but not for La Garrotxa. In fact, in this latter volcanic field, the susceptibility maps obtained using the same (Fig. 2.13a) and different weights (Fig. 2.13b) for the PDFs are both coherent. The choice of the final technique for constructing hazard maps depends on the reliability of the method used to assign the weights.

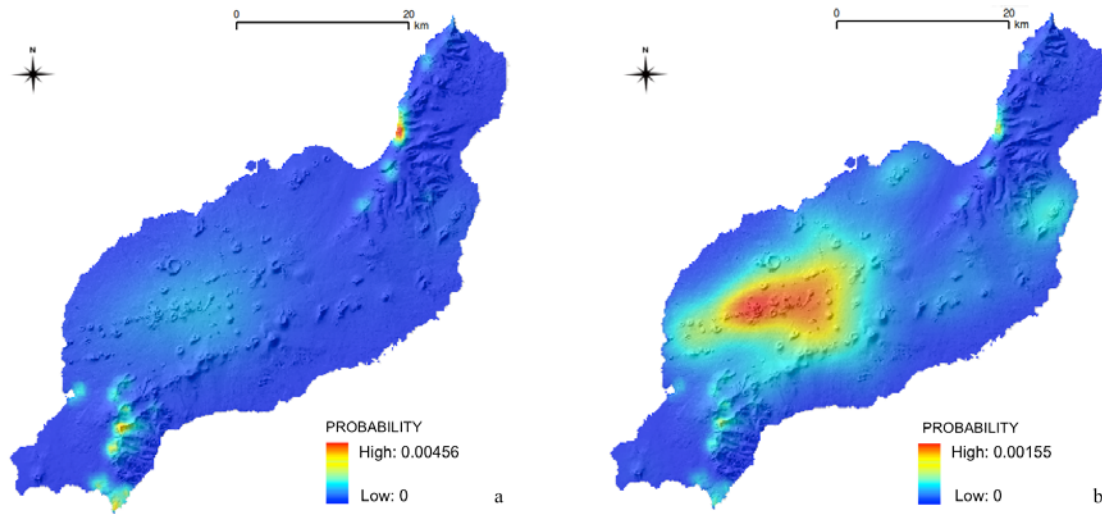


Figure 2.12: Lanzarote susceptibility maps calculated assigning the same weights to all PDFs (a) and variable weights, i.e., 0.05 for dykes, 0.15 for the oldest vent alignments, 0.3 for the most recent vent alignments and 0.5 for the emission centers (b)

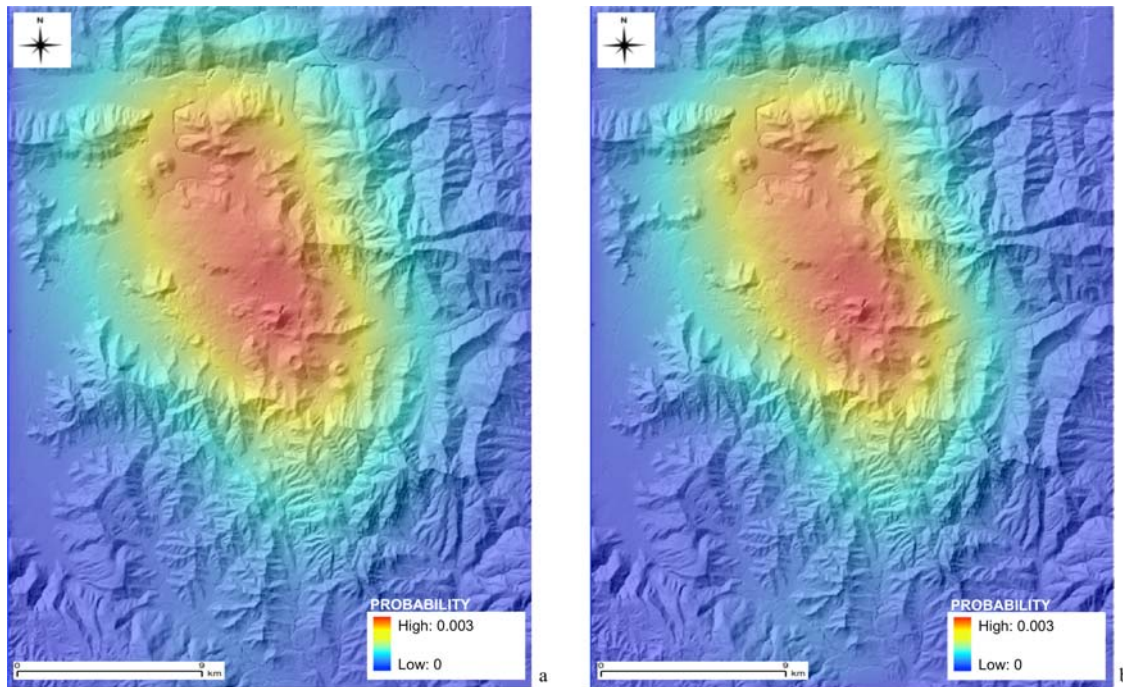


Figure 2.13: La Garrotxa susceptibility maps calculated assigning the same weights to all PDFs (a) and variable weights, i.e., 0.03 for alignments and 0.7 for the emission centers (b)

2.7 Conclusions

The elaboration of a susceptibility map based on the quantification of objective geological and geophysical data is the first and most important step in the quantitative assessment of volcanic hazard and risk. Here we have presented QVAST, the new tool for calculating volcanic susceptibility that works under QGIS, a free and user-friendly GIS environment.

QVAST is built to evaluate volcanic susceptibility, that is, the spatial probability of the appearance of a future vent opening, based on the activity of the volcanic area under study. The main steps involved are as follows: (i) calculation of the bandwidth using different methods, (ii) evaluation of the PDF using a Gaussian kernel, (iii) assignment of the weights to each PDF, and (iv) evaluation of the susceptibility map using an NHPP.

The comparison of different volcanic fields shows the importance of choosing the optimal bandwidth parameters. The strength of QVAST lies in the possibility of selecting various methods for evaluating the bandwidth parameter and for obtaining the final susceptibility map. The volcanic fields of Lanzarote and La Garrotxa are excellent case studies for learning how to use this interface and for comparing the different results generated using different bandwidths for the kernel; this thus allows an optimal bandwidth for the volcanic field to be chosen.

QVAST is part of a larger project consisting of several modules (implemented in QGIS) that will interact and will analyze the current situation of volcano fields as part of the task of generating hazard maps.

In the cases of Lanzarote and La Garrotxa, although data availability is somewhat restricted, the preliminary results obtained are good enough to be used as a starting point for generating eruptive scenarios that can aid local territorial planning and risk-mitigation programs. Thus, we propose that this tool should be used as a common way for determining the susceptibility of future volcanic eruptions in active regions and as a necessary tool in the reduction of volcanic risks.

Future work will include the spatio-temporal analysis of future vent openings and the construction of volcanic hazard maps, all of which will be of great help to the governmental bodies in charge of territorial planning and the development of mitigation plans.

Acknowledgements

This work was supported by the European Commission (FP7 Theme: ENV.2011.1.3.3-1; grant 282759: VUELCO) and developed in the frame of TecnoLab, the Laboratory for the Technological Advance in Volcano Geophysics organized by INGV-CT and UNICT. The authors thank Rosa Sobradelo, Erika Ronchin, and Elisabeth Riera Pedra for improving the paper. The English text was corrected by Michael Lockwood. We thank Olivier Jaquet and an anonymous reviewer for the supportive comments that helped to improve the manuscript, and the Editor Antonio Costa for his efficient handling.

Edited by: A. Costa

Reviewed by: O. Jaquet and one anonymous referee

References

Aspinall, W. P.: Structured elicitation of expert judgment for probabilistic hazard and risk assessment in volcanic eruptions, in: *Statistics in Volcanology*, edited by: Mader, H. M., Coles, S. G., Connor, C. B., and Connor, L. J., Geological Society of London, Special Publication of IAVCEI, 1, 15–30, 2006.

Banda, E., Dafiobeitia, J. J., Surifiach, E., and Ansorge, J.: Features of crustal structure under the Canary Islands, *Earth Planet. Sci.Lett.*, 55, 11–24, 1981.

Becerril, L., Cappello, A., Galindo, I., Neri, M., and Del Negro, C.: Spatial probability distribution of future volcanic eruptions at El Hierro Island (Canary Islands, Spain), *J. Volcanol. Geoth. Res.*, 257, 21–30, doi:10.1016/j.jvolgeores.2013.03.005, 2013.

Blanco-Montenegro, I., Montesinos, F. G., García, A., Vieira, R., and Vilalain, J. J.: Paleomagnetic determinations on Lanzarote from magnetic and gravity anomalies: Implications for the early history of the Canary Islands, *J. Geophys. Res. Solid Earth*, 110, 1–12, doi:10.1029/2005JB003668, 2005.

Bowman, A. W.: An alternative Method of Cross Validation for the Smoothing of Density Estimates, *Biometrika*, 71, 353–360, 1984.

Camacho, A.G., Vieira, R., and Toro, C.: Microgravimetric model of the Las

Cañadas caldera (Tenerife), *J. Volcanol. Geother. Res.*, 47, 75–80, 1991.

Cappello, A., Vicari, A., and Del Negro, C.: Assessment and modeling of lava flow hazard on Etna volcano, *Boll. Geofis. Teor. Appl.*, 52, 299–308, 2011a.

Cappello, A., Vicari, A., and Del Negro, C.: Retrospective validation of a lava flow hazard map for Mount Etna volcano, *Ann. Geophys.*, 54, 634–640, 2011b.

Cappello, A., Neri, M., Acocella, V., Gallo, G., Vicari, A., and Del Negro, C.: Spatial vent opening probability map of Etna volcano (Sicily, Italy), *Bull. Volcanol.*, 74, 2083–2094, doi:10.1007/s00445-012-0647-4, 2012.

Cappello, A., Bilotta, G., Neri, M., and Del Negro, C.: Probabilistic modeling of future volcanic eruptions at Mount Etna, *J. Geophys. Res. Solid Earth*, 118, 1–11, doi:10.1002/jgrb.50190, 2013.

Carracedo, J. C., Rodríguez Badiola, E., and Soler, V.: The 1730–1736 eruption of Lanzarote, Canary Islands: a long, high-magnitude basaltic fissure eruption, *J. Volcanol. Geotherm. Res.*, 53, 239–250, 1992.

Chen, D., Shams, S., Carmona-Moreno, C., and Leone, A.: Assessment of open source gis software for water resources management in developing countries, *J. Hydro-environ. Res.*, 4, 253–264, 2010.

Coello, J., Cantagrel, J. M., Hernán, F., Fúster, J. M., Ibarrola, E., Ancochea, E., Casquet, C., Jamond, C., Díaz de Terán, J. R., and Cendrero, A.: Evolution of the eastern volcanic ridge of the Canary Islands based on new K-Ar data, *J. Volcanol. Geotherm. Res.*, 53, 251–274, 1992.

Connor, C. B. and Hill, B. E.: Three nonhomogenous Poisson models for the probability of basaltic volcanism: application to the Yucca Mountain region, Nevada, *J. Geophys. Res.*, 100, 10107–10125, 1995.

Connor, L. J., Connor, C. B., Meliksetian, K., and Savov, I.: Probabilistic approach to modeling lava flow inundation: a lava flow hazard assessment for a nuclear facility in Armenia, *J. Appl. Volcanol.*, 1, 1–19, doi:10.1186/2191-5040-1-3, 2012.

Diggle, P. J.: A kernel method for smoothing point process data, *Applied Statistics*, *J. R. Stat. Soc. Ser. C*, 34, 138–147, 1985.

Duong, T.: ks: Kernel Density Estimation and Kernel Discriminant Analysis for Multivariate Data in R, *J. Stat. Soft.*, 21, 1–16, 2007.

Duong, T. and Hazelton, M.: Plug-in bandwidth matrices for bivariate kernel density estimation, *J. Nonparametr. Stat.*, 15, 17–30, 2003.

Favalli, M., Tarquini, S., Papale, P., Fornaciai, A., and Boschi, E.: Lava flow haz-

ard and risk at Mt. Cameroon volcano, *Bull. Volcanol.*, 74, 423–439, doi:10.1007/s00445-011-0540-6, 2011.

Felpeto, A., Araña, V., Ortiz, R., Astiz, M., and García, A.: Assessment and modelling of lava flow hazard on Lanzarote (Canary Islands), *Nat. Hazards*, 23, 247–257, 2001.

Felpeto, A., Martí, J., and Ortiz, R.: Automatic GIS-based system for volcanic hazard assessment, *J. Volcanol. Geotherm. Res.*, 166, 106–116, 2007.

Gudmundsson, A.: Magma-chamber geometry, fluid transport, local stresses and rock behavior during collapse caldera formation, in: *Caldera Volcanism*, edited by: Gottsmann, J. and Martí, J., *Developments in Volcanology*, 10, Elsevier, Amsterdam, 313–349, 2008.

Gudmundsson, A.: Strengths and strain energies of volcanic edifices: implications for eruptions, collapse calderas, and landslides, *Nat. Hazards Earth Syst. Sci.*, 12, 2241–2258, doi:10.5194/nhess-12-2241-2012, 2012.

Härdle, W., Müller, M., Sperlich, S., and Werwatz, A.: *Nonparametric and Semiparametric Models, An Introduction*, Springer Series in Statistics, Springer, Berlin, 2004.

Hornik, K.: The R FAQ, available at: <http://CRAN.R-project.org/doc/FAQ/R-FAQ.html>, ISBN 3-900051-08-9, 2009.

Jaquet, O., Connor, C. B., and Connor, L.: *Probabilistic Methodology for Long Term Assessment of Volcanic Hazards*, IHLRMW, Las Vegas, USA, 2008.

Kiyosugi, K., Connor, C. B., Zhao, D., Connor, L. J., and Tanaka, K.: Relationships between temporal-spatial distribution of monogenetic volcanoes, crustal structure, and mantle velocity anomalies: An example from the Abu monogenetic volcano group, southwest Japan, *Bull. Volcanol.*, 72, 331–340, doi:10.1007/s00445-009-0316-4, 2010.

Lutz, T. M. and Gutmann, J. T.: An improved method for determining and characterizing alignments of point-like features and its implications for the Pinacate volcanic field, Sonoran, Mexico, *J. Geophys. Res.*, 100, 17659–17670, 1995.

Marinoni, L. B., and Pasquaré, G.: Tectonic evolution of the emergent part of a volcanic ocean island: Lanzarote, Canary Islands, *Tectonophysics*, 239, 111–135, 1994.

Martí, J. and Felpeto, A.: Methodology for the computation of volcanic susceptibility: Application to Tenerife Island (Canary Islands), *J. Volcanol. Geother.*

Res., 195, 69–77, 2010.

Martí, J., Planagumà, L., Geyer, A., Canal, E., and Pedrazzi, D.: Complex interaction between Strombolian and phreatomagmatic eruptions in the Quaternary monogenetic volcanism of the Catalan Volcanic Zone (NE of Spain), *J. Volcanol. Geotherm. Res.*, 201, 178–193, doi:10.1016/j.jvolgeores.2010.12.009, 2011.

Martí, J., Castro, A., Rodríguez, C., Costa, F., Carrasquilla, S., Pedreira, R., and Bolos, X.: Correlation of Magma Evolution and Geophysical Monitoring during the 2011–2012 El Hierro (Canary Islands) Submarine Eruption, *J. Petrology*, 54, 1349–1373, doi:10.1093/petrology/egt014, 2013.

Martin, A. J., Umeda, K., Connor, C. B., Weller, J. N., Zhao, D., and Takahashi, M.: Modeling long-term volcanic hazards through Bayesian inference: an example from the Tohoku volcanic arc Japan, *J. Geophys. Res.*, 109, B10208, doi:10.1029/2004JB003201, 2004.

Neri, A., Aspinall, W. P., Cioni, R., Bertagnini, A., Baxter, P. J., Zuccaro, G., Andronico, D., Barsotti, S., Cole, P. D., Esposti Ongaro, T., Hincks, T. K., Macedonio, G., Papale, P., Rosi, M., Santacroce, R., and Woo, G.: Developing an Event Tree for probabilistic hazard and risk assessment at Vesuvius, *J. Volcanol. Geotherm. Res.*, 178, 397–415, doi:10.1016/j.jvolgeores.2008.05.014, 2008.

Rudemo, M.: Empirical choice of histograms and kernel density estimators, *Scandinavian J. Stat.*, 9, 65–78, 1982.

Scott, D. W.: On optimal and data-based histograms, *Biometrika*, 66, 605–610, 1979.

Scott, D. W.: *Multivariate Density Estimation: Theory, Practice, and Visualization* (Wiley Series in Probability and Statistics), Wiley Interscience Publications, ISBN-13: 978-0471547709, 1992.

Sherman, G. E.: *Desktop GIS. Mapping our Planet with Open Source Tools*, The Pragmatic Bookshelf, Raleigh, North Carolina, USA, 2008.

Silverman, B. W.: *Density Estimation for Statistics and Data Analysis*, Chapman & Hall, London, 1986.

Weller, J. N., Martin, A. J., Connor, C. B., Connor, L. J., and Karakhanian, A.: Modelling the spatial distribution of volcanoes: an example from Armenia, in: *Statistics in volcanology*, edited by: Mader, H. M., Coles, S. G., Connor, C. B., and Connor, L. J., Spec. Pub. IAVCEI, Geol. Soc. London, 77–88, 2006.

Worton, B. J.: Using Monte Carlo simulation to evaluate kernel-based home

range estimators, *J. Wild. Manag.*, 59, 794–800, 1995.

HASSET: a probability event tree tool to evaluate future volcanic scenarios using Bayesian Inference. Presented as a plug-in for QGIS

Published in:

Bulletin of Volcanology

Authors:

Rosa Sobradelo^{a,b}

Stefania Bartolini^a

Joan Martí^a

a) Group of Volcanology, (SIMGEO-UB) CSIC Institute of Earth Sciences “Jaume Almera”. Lluís Sole i Sabaris s/n, 08028 Barcelona, Spain. Phone: +34934095410. Fax: +34934110012.

b) Aon Benfield UCL Hazard Centre. Department of Earth Sciences. University College London. Gower Street, London, WC1E 6BT, UK.

3.1 Abstract

Event tree structures constitute one of the most useful and necessary tools in modern volcanology for assessment of hazards from future volcanic scenarios (those that culminate in an eruptive event as well as those that do not). They are particularly relevant for evaluation of long- and short-term probabilities of occurrence of possible volcanic scenarios and their potential impacts on urbanized areas. In this paper, we introduce Hazard Assessment Event Tree (HASSET), a probability tool, built on an event tree structure that uses Bayesian inference to estimate the probability of occurrence of a future volcanic scenario and to evaluate the most relevant sources of uncertainty from the corresponding volcanic system. HASSET includes hazard assessment of noneruptive and nonmagmatic volcanic scenarios, that is, episodes of unrest that do not evolve into volcanic eruption but have an associated volcanic hazard (e.g., sector collapse and phreatic explosion), as well as unrest episodes triggered by external triggers rather than the magmatic system alone. Additionally, HASSET introduces the Delta method to assess precision of the probability estimates, by reporting a 1 standard deviation variability interval around the expected value for each scenario. HASSET is presented as a free software package in the form of a plug-in for the open source geographic information system Quantum Gis (QGIS), providing a graphically supported computation of the event tree structure in an interactive and user-friendly way. We also include further in-depth explanations for each node together with an application of HASSET to Teide-Pico Viejo volcanic complex (Spain).

Keywords

Volcanic hazard · Event tree · Probability estimation · Bayesian inference · QGIS

3.2 Introduction

Volcanic systems near urbanized areas require sound risk evaluation to support decision makers during the critical times of emergency management, as well as before the onset of volcanic unrest, to build preparedness plans and define land use manage-

ment. Assessment of volcanic hazard from future eruptive scenarios in probabilistic ways has become a widely used technique for risk evaluation in recent years (Newhall and Hoblitt, 2002; Marzocchi et al., 2004, 2006, 2008, 2010; Aspinall, 2006; Neri et al., 2008; Martí et al., 2008a, 2011; Sobradelo and Martí, 2010; Sobradelo et al., 2011). Volcanic hazard is the probability of any particular area being affected by a destructive volcanic event within a given period of time (Blong, 2000). So, to quantify volcanic hazard, we need to estimate probabilities of occurrence of a particular eruptive scenario in time and space. Despite the limitations in the construction of an event tree usually imposed by the lack of knowledge about the past and present behavior of active volcanoes, it is clear from the works previously cited and experiences from volcanic crises (Aspinall and Cook, 1998) that construction of an event tree is extremely useful for hazard assessment.

Future probabilities of occurrence of an eruptive scenario can be analyzed for both the short term and long term. Short- and long-term forecasts of eruption are defined based on the expected time interval over which the volcanic system enters unrest and/or shows significant variations. For the purpose of our analysis, long-term volcanic hazard refers to the time window before the volcanic system goes into unrest, and short-term volcanic hazard refers to the unrest phase. Consequently, long-term forecasting is mainly based on geological, historical and geochronological data, and theoretical models, while short-term forecasting is complemented with information from continuous monitoring.

The complexity of any volcanic system and its associated eruptive processes, together with the lack of data that characterize many active volcanoes, particularly those with long intervals between events, make volcanic hazard quantification very challenging, as there is often not enough observational data to build a robust statistical model. However, it is important to find a way to summarize the uncertainty of a volcanic scenario in a structured and systematic way, so that when new evidence arrives, we can update these uncertainties in a consistent and rigorous way. This will allow paths to decisions to be documented and later tracked, rather than being based on intuition or gut feelings.

Bayesian inference is based on the principle that every state of uncertainty can be modeled with a probability distribution. It provides a numerical instrument, based on rigorous mathematical modeling, to define and interpret uncertainties. As more data arrives, the method incorporates the new evidences in order to progressively

reduce uncertainty. The precision of the probability estimates for each possible eruptive scenario will depend heavily on the available data. We begin with the state of total ignorance and use noninformative priors to quantify our uncertainty before observing the data, and later update these with the arrival of new evidence from geochronological and geophysical data, to get the posterior probabilities, which provide an estimate of the uncertainty after observing the data. Due to the poor and incomplete data catalogue often used when doing eruption estimates, aleatoric (stochastic) and epistemic (data or knowledge limited) uncertainties are significant, and we need to find a way to correctly evaluate them.

The aleatoric (stochastic) uncertainty is a consequence of the intrinsic complexity of a system, hence a limitation to our ability to predict the evolution of the system in a deterministic way. The aleatoric uncertainty introduces a component of randomness in the outcomes, regardless of our physical knowledge of the system. The epistemic uncertainty is directly related to our knowledge of the system and the quality and quantity of data we have about the system. The more data we have, the better we know the system and the lower the epistemic uncertainty (Woo, 1999).

In this paper, we present Hazard Assessment Event Tree (HASSET), a probability tool that uses Bayesian inference in an event tree structure to assess volcanic hazard of future volcanic scenarios. It evaluates the most relevant sources of uncertainty in estimating the probability of occurrence of a future volcanic event. HASSET is presented as a free software package in the form of a plug-in for the open source geographic information system Quantum Gis (QGIS), providing a graphically supported computation of the event tree structure in an interactive and user-friendly way. It is built on the Bayesian event tree model proposed by Sobradelo and Martí (2010) and expanded further to include two additional and important nodes to account for the type and extension of the hazard phenomena. Additionally, HASSET introduces the Delta method to approximate the precision in the probability estimates, by constructing a 1 standard deviation variability interval around the expected probability value for each scenario.

It is important to mention that some parts of our tool overlap with the BET_EF and BET_VH tools presented by Marzocchi et al. (2008, 2010). These tools use Bayesian theory in an event tree structure. HASSET is built on QGIS platform, taking advantage of additional features of this geographic information system, and BET_EF and BET_VH are presented in the form of an independent software. The

main differences are that HASSET evaluates the hazard associated with magmatic and nonmagmatic unrest episodes, by accounting for unrest induced by external triggers (geothermal, seismic), as opposed to internal triggers alone (magmatic) (this will be further described in the next section). HASSET evaluates the hazard associated with eruptive and noneruptive volcanic scenarios (e.g., phreatic explosion and sector failure) and looks at the hazard for different types of magma composition and different vent locations, together with the geological hazard and its extent. This allows for identification of important eruptive scenarios which otherwise would go unnoticed. In this respect, HASSET overcomes the limitations of previous event tree models by allowing a larger set of future volcanic scenarios in their probability estimation, and thus extending their use to a wider range of volcanic systems, accounting for aleatoric and epistemic uncertainties, and reducing the additional bias that the human decision component adds to the use of alternative techniques for estimating event tree probabilities (Aspinall, 2006; Loughlin et al., 2002). In this paper, we will focus on the long-term volcanic hazard assessment of the system, so we will base our analysis on the past behavior of the volcano.

3.3 HASSET: Hazard Assessment Event Tree

An event tree is a tree graph representation of events in the form of nodes and branches and it was first introduced to volcanology by Newhall and Hoblitt (2002) as a tool for volcanic hazard assessment. Each node represents a step and contains a set of possible branches (outcomes for that particular category). The nodes are alternative steps from a general prior event, state, or condition through increasingly specific subsequent events to final outcomes. The objective is to outline all relevant possible outcomes of volcanic unrest, at progressively higher degrees of detail, and assess the probability of each hazard scenario occurring within a specified future time interval. HASSET uses this event tree structure (Fig. 3.1a) to make these estimations based on a statistical methodology, further described below, called Bayesian inference (Rice, 2007) (Fig. 3.1b, c). All nodes are independent and the corresponding branches are mutually exclusive and exhaustive. That is, they cannot happen simultaneously and they sum up to 1. These are initial conditions set for simplicity and practical application of the Bayesian inference methodology. In general, an event tree can have any form or shape and the nodes need not be independent or

mutually exclusive, in which case a different mathematical approach is needed. Future work is needed to address this issue and eliminate the dependency and mutually exclusive restrictions to make a free form event tree structure. However, it remains to be proven whether the presumed accuracy increase in the probability estimates would justify the additional complexity that dependency and nonmutually exclusive assumptions would introduce in the model settings and calculations.

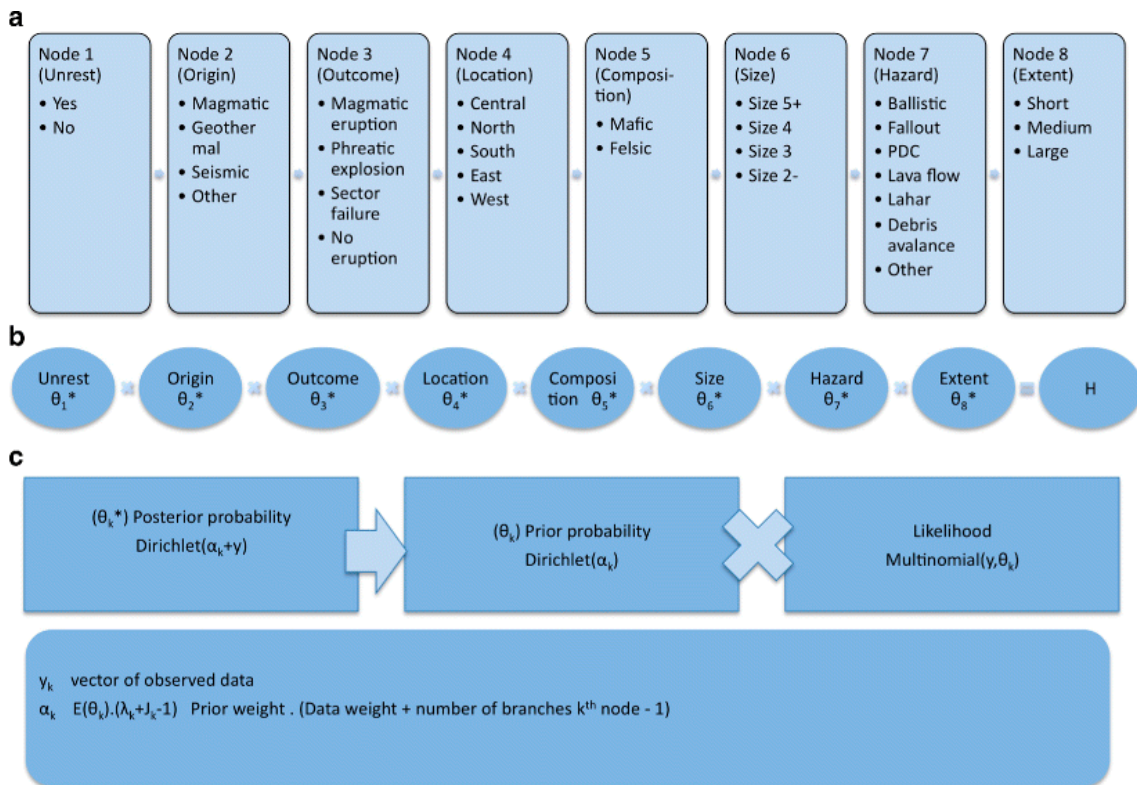


Figure 3.1: HASSET event tree structure (a) formed by eight nodes and corresponding mutually exclusive and exhaustive branches to account for all possible scenarios likely to occur in a volcanic system. By the condition of independence of the nodes, the probability of a particular eruptive scenario, as a combination of branches across nodes, is the product of the individual probabilities of occurrence of each branch in that scenario (b). These probabilities are calculated using a Bayesian inference approach (c). (See text for further details)

HASSET accounts for the possibility of flank vent eruptions (as opposed to only central), making it also useful for monogenetic volcanism. A novelty of HASSET is that it accounts for nonmagmatic unrest (geothermal or seismic), as opposed to only magmatic, and for noneruptive scenarios (phreatic explosions or sector failure), as opposed to volcanic eruptions only. Also, it accounts for felsic or mafic composition,

and their associated volcanic hazards as possible outputs of an eruption, together with the extent reached by each hazard.

3.3.1 Event Tree Structure

Each possible volcanic scenario is a combination of one branch per node evolving from a more general node of unrest (yes or no) to the more specific node of the extent of the hazard. Below is a detailed explanation of each node and corresponding branches (see Sobradelo and Martí (2010) for further details on the event tree methodology). It is possible to stop at a particular node if we want to evaluate the hazard at a more general level. Each possible volcanic scenario is made up from the following nodes:

Node 1, Unrest: Yes or No. Given that we have the capacity to differentiate the origin of the precursory signals, we define unrest in a particular time window τ as any modification of the background activity of the volcano or volcanic area recorded by the monitoring network, and which may or may not be followed by an eruption of any kind.

Node 2, Origin: We define four possible sources of unrest, which comprises events (above background) recorded by the network, that are likely to happen, magmatic, geothermal, seismic, and other. Assuming we can define the precursors that identify the source of the unrest, it is crucial in a complex volcanic system to differentiate between unrest caused by internal triggers or caused by external triggers, which ultimately may condition the outcome and further development of the system. Every eruption type, including a phreatic episode, requires the presence of fresh magma at shallow depths in the volcanoes. However, we do not discard the possibility of starting an eruption process from an unrest directly associated with the hydrothermal system or even due to external triggers, such as regional tectonics, if eruptible magma is already present in the system. It is also important to mention that the interior of a volcanic system may react to changes in the regional stress field or regional tectonics, so a seismic trigger for unrest cannot be ruled out.

Node 3, Outcome: We consider here the outcome of the unrest being of four different types, magmatic eruption, sector failure, phreatic explosion (triggered by unrest of any type, where no magma is expelled in the eruption), no eruption (there is unrest but no further outcome develops). It is important to address the hazard associated with noneruptive scenarios in the event of unrest. That is, the hazard

could arise in response to internal or external triggers that do not evolve into a magmatic eruption but rather originate a sector failure or a phreatic episode. These volcanic scenarios should not be left out when assessing volcanic hazard, especially for a volcano with a hydrothermal system or a shallow aquifer.

Magmatic eruptions can be preceded directly by magmatic unrest, which may or may not itself be preceded by sector failure. A magmatic eruption can also be triggered indirectly by geothermal or seismic unrest, in which case, externally driven decompression of the shallow volcanic system would be required. This could be achieved by sector failure or tectonic fracture opening. When the unrest is geothermal or seismic, for a magmatic eruption to occur, an initial sector collapse or fracture opening is needed to decompress the whole system. In discussing a magmatic eruption which was originated by geothermal or seismic unrest, we assume that a sector failure or a tectonically induced fracture opening has previously occurred.

Sector failure alone, triggered by magmatic, geothermal, or seismic unrest, corresponds with the sector collapse itself, not being followed by an eruption. A sector failure followed by a magmatic eruption is considered in the previous branch (magmatic eruption), caused indirectly by a magmatic unrest triggering a sector collapse (see Sobradelo and Martí (2010)).

Node 4, Location: We segment possible locations for an imminent eruption into five different areas, which can be customized and named accordingly. By default, we have named them as *central*, *north*, *south*, *east*, and *west*, and the coverage area for each location would vary for each volcanic system according to topography, surroundings, and/or important topographic barriers which may impose a different level of hazard and risk depending on what side of the volcano the eruption occurs.

Node 5, Composition: Mafic or felsic. The magma composition will determine two main types of eruptions associated with different hazard implications, as felsic magmas are generally associated with more violent eruptions than mafic magmas. The importance in distinguishing these two outcomes for node 5 is the different level of hazard associated with each one (Martí et al., 2008b). For simplicity in the model, we will assume the two branches are exclusive, and thus a branch for mixed composition is left out. We are aware some compositions can be a mix of both mafic and felsic magmas, but for the purpose of the hazard estimation, we will assume that a magma with felsic composition will fall in the category of *felsic*, regardless of the proportion.

Node 6, Size: This node represents the size of the eruption, assigned to one of four categories, *size* ≥ 5 , *size* 4, *size* 3, *size* ≤ 2 . The size can be expressed in terms of either the volcanic explosive index (VEI), or simply the magnitude of the eruption, as a function of the erupted volume. Also, the four category groups can be modified to better fit a particular volcanic system. For instance, one may be interested in merging *size* ≤ 2 and *size* 3 into one group *size* ≤ 3 and segmenting group *size* ≥ 5 into two additional categories, say *size* 5 and *size* ≥ 6 . Similarly, as VEI is not necessarily an integer, the branches could be defined as bins, e.g., VEI 5 could correspond to $3.5 < VEI \leq 4.5$. The only condition is that the groups are mutually exclusive and exhaustive.

Node 7, Hazard: This node and the following are a new contribution of this paper to the event tree structure from (Sobradelo and Martí, 2010). Here, we list the most relevant hazardous phenomena originating from a volcanic eruption, *ballistic*, *fall-out*, *PDC*, *lava flows*, *lahars*, *debris avalanche*, and include a seventh branch called *other* to account for the remaining hazards, like *direct blast*, to make the branches exhaustive (this is another difference with BET_VH (Marzocchi et al., 2010) where Node 6 phenomena is left open without an upper bound). We assume, without loss of generality, that any two hazards do not happen at exactly the same time (this is, $P(A_1 \cap A_2) = 0$, where hazard A_1 could be ballistic and hazard A_2 could be Fallout), but with a time interval in between, so that the condition of mutual exclusivity still holds, and so does the condition of exhaustivity of the branches, where $P(A_1 \cup A_2 \cup \dots \cup A_7) = P(A_1) + P(A_2) + \dots + P(A_7) = 1$, A_1, A_2, \dots, A_7 are the different branches in the node. This is a conservative assumption, as we may be overestimating the total probability of two hazard events by not subtracting the probability of the intersection (by definition $P(A_1 \cup A_2) = P(A_1) + P(A_2) - P(A_1 \cap A_2)$). With this in mind, we compute the probability of more than one hazard associated with the same eruption by adding the individual probabilities of each scenario alone. The issue of possible dependency of the branches does not affect us here as we are analyzing scenarios with primary hazards alone, as opposed to scenarios with secondary hazards. This should be assessed in future work, as during a volcanic eruption with multiple phases, the probability of a second hazard being triggered after a primary one has happened is strongly determined by the dependency of the hazards. In this case, the issues of correlation and multicollinearity of the different hazards should be addressed (Rice, 2007).

Ballistic: We consider here blocks and bombs that are sent ballistically and can happen in any eruption with explosive phases, including phreatic phases (without fresh magma), dome explosions, strombolian, plinian, etc.

Fallout: Here, we include ashfall originating from pyroclasts in strombolian eruptions as fire fountains, to ash fall from an eruption column.

Pyroclastic density current (PDC): This includes the spectrum of currents from dense to dilute. Dense flows will only have a runout since they are mostly small volume confined to the valleys, but the diluted ones and large pyroclastic flows can have an important lateral extension. In some cases, as frequently occurs with dome collapse PDCs, the only measurable parameter is runout, as they are mostly confined to the valleys, but sometimes there are PDCs that have an important extension so we must consider both.

Lava flows: All types of lava flows of any composition or rheology.

Lahar: Debris flows and mudflows, related to ice melting, rain, etc.

Debris avalanche: We include here collapse of nonexplosive lava domes or sector collapses of the volcanic edifice, regardless of their origin.

Other: So far, we have included what we consider to be the six most likely hazards. There are additional phenomena that could also occur (direct blast, gas emissions, etc.), but they are not so likely to happen as to justify their own branch, so we grouped them all together. However, the branches in this node could be easily renamed if there is evidence that alternative hazards should be included instead.

Node 8, Extent: This node refers exclusively to the maximum distance and areal extent reached by a volcanic hazard regardless of the nature and potential impact it may cause. It is a measure of the expected zone that will be affected by a particular hazard but it does not estimate any degree of vulnerability. The extent has to be estimated separately for each volcano or volcanic zone by comparing the maximum and minimum extent of each volcano or volcanic area, and should not be compared among different volcanoes even when these might show similar characteristics. This is an important node for completion of a thorough hazard assessment because the area affected by a particular eruptive scenario refers to the spatial part of the definition of hazard. We consider three types of mutually exclusive and exhaustive extents, *short*, *medium*, and *large*, with respect to the eruptive vent.

Each option will fall inside an area previously defined by the user for that particular volcanic system, based on different levels of exposure. For each analysis, the

area covered (and maximum distance reached) by each type of hazard will be previously defined, so that a *short*, *medium*, or *large* extent will refer, respectively, to the distance and area from the source regardless of what type of hazard reaches there. In the case of single vents, the application is straightforward, but in volcanic systems with an option for multiple vents, we will consider the largest volcanic susceptibility values (i.e., maximum probability of vent opening) and proceed in the same way as with a single vent, assuming a larger area. Obviously, the interpretation of the results will be different if there is a large lava flow versus a large PDC, for example, and this should be reflected on the conditional probabilities computed later.

3.3.2 Probability Estimates

We will use Bayesian Inference to compute the probability of occurrence for each scenario. The fundamental principle of Bayesian statistics is that what is known about anything that is incomplete or imperfectly known can be described as a probability distribution. See Sobradelo and Martí (2010) and references within for further details on how the Bayesian methodology is applied to the event tree. Our knowledge about a random variable θ given the observed data is expressed through its posterior distribution $p(\theta|y) \propto p(\theta) \times p(y|\theta)$. That is, the posterior distribution is proportional to the prior distribution times the likelihood. The prior distribution, $p(\theta)$, expresses our uncertainty about θ before seeing the data. The posterior distribution, $p(\theta|y)$, expresses our uncertainty about θ after seeing the data. The likelihood function allows us to use the past data (y_k) at node k to modify the a priori beliefs or priori distribution.

By the condition of independence of the nodes, the probability of a particular eruptive scenario, as a combination of branches across nodes, is the product of the individual probabilities of occurrence of each branch in that scenario (Fig. 3.1b). For example scenario j , the probability of having a magmatic unrest that evolves into a central vent basaltic eruption of VEI 4, generating a lava flow of short runout, in the time interval $(t_0, t_0 + \tau)$ is:

$$\begin{aligned}
 H_j = & \theta_1^*(\text{unrest}) \times \theta_2^*(\text{magmatic}) \times \theta_3^*(\text{eruption}) \\
 & \times \theta_4^*(\text{central}) \times \theta_5^*(\text{basaltic}) \times \theta_6^*(\text{VEI 4}) \\
 & \times \theta_7^*(\text{lavas}) \times \theta_8^*(\text{short})
 \end{aligned}
 \tag{3.1}$$

Where the posterior probability for a specific branch in node k , denoted θ_k^* for simplicity, is the expected value of a random variable that follows a Dirichlet distribution of parameters $(\alpha_k + y_k)$ (Figure 3.1c). The parameter $\alpha_k = E[\theta_k] (\lambda_k + J_k - 1)$, where $E[\theta_k]$ is computed from alternative physical models and a priori beliefs, and accounts for the aleatoric uncertainty. J_k is the number of branches in node k and λ_k is the data weight, also input to the model, and controls the confidence at which $E[\theta_k]$ is considered a reliable estimate. λ_k accounts for the epistemic uncertainty. The choice of the Dirichlet (Beta) distribution is itself rather subjective. In general, theoretical models, a priori beliefs, and/or expert elicitation provide estimations of the expected average of the prior distribution that represents the “best guess”. Further details on this choice can be found in Marzocchi et al. (2004).

3.3.3 How precise are the probability estimates?

The probability estimate we assign to each scenario is, as explained in the previous section, the product of the individual probabilities for each branch. This property is attributed to the condition of independence of the nodes, which allows us to write the expected value of the product as the product of the individual expected values. The expected value (mean) is a measure of central tendency used to describe a probability distribution (Dirichlet in this case), together with the variance (or standard deviation). Unfortunately, the same property does not apply to the variance, the measure of dispersion around the mean, used to estimate the precision. Since the variance of the product cannot be written as the product of the variance of each individual variable, we have to use alternative methods to estimate or approximate this. One way is using the Delta method (Rice, 2007). Hence, to assess the precision in the probability estimate for eruptive scenario \hat{H}_j , we use the Delta method to estimate the variance $\hat{\sigma}_j^2$ and corresponding standard deviation $\hat{\sigma}_j = \sqrt{\hat{\sigma}_j^2}$.

Using the Delta method to determine the asymptotic distribution of $\hat{\sigma}_j^2$, we get:

$$\hat{\sigma}_j^2 = E(H)^2 \sum_{k=1}^m \frac{Var(\theta_{kn}^*)}{[E(\theta_{kn}^*)]^2} \quad (3.2)$$

Where,

$$E(\theta_{kn}^*) = \frac{\alpha_{kn} + y_{kn}}{\sum_{i=1}^{J_k} (\alpha_{ki} + y_{ki})} \quad (3.3)$$

and

$$Var(\theta_{kn}^*) = \frac{E[\theta_{kn}^*](1 - E[\theta_{kn}^*])}{\lambda_k + J_k} \quad (3.4)$$

are the expected value and variance from the posterior distribution for θ_{kn}^* in branch n and node k , and where J_k is the number of branches in node k . See Appendix for details on how to derive Eq. 3.2. Hence, we have written the variance for an eruptive scenario H_j as a function of the expected value and variances of the individual random variables, θ_{kn}^* , involved in that scenario. See Sobradelo and Martí (2010) Eq. (4)-(10) for further details on how to derive Eqs. 3.3 and 3.4.

3.4 HASSET software: a QGIS plug-in to perform hazard assessment using Bayesian event tree methodology

Geographic information systems (GIS) are increasingly being used in environmental management as a powerful tool to store, visualize, and model environmental processes in support of management decisions (Longley et al., 2001; Renschler, 2005; Chen et al., 2010). Open source desktop GIS have been developed in different countries, with some differences in performance (Sherman, 2008; Chen et al., 2010). We have decided to use the QGIS (www.qgis.org) for its functionalities and the ability to run it on Linux, Mac OSX, and Windows, as well as the open possibility of connecting HASSET with a mapping format structure. Currently, the software has been developed for Mac OS (tested on version 10.7.4 and above) and Linux (tested on Ubuntu 10.10 and above). The version for Windows OS is under development. HASSET is available upon request to the authors or it can be downloaded online at the website of the CSIC Group of Volcanology of Barcelona (<http://www.gvb-csic.es>) on the “Software & Databases” tab.

The original R code for the Bayesian model was adapted to a Python script, and the HASSET program was developed and implemented in QGIS as an accessible and dynamic graphical user interface (GUI) plug-in, which, once properly installed following a few easy steps, creates a new option in the QGIS menu bar called “volcano,” where the HASSET model is installed. Along with HASSET, an html manual (HASSET_MANUAL) with step-by-step explanations on how to use it is also pro-

vided.

HASSET implements the Bayesian event tree method described earlier, where the user previously defines a forecasting time interval. The user provides all volcanological data for the analysis, which HASSET then merges using the Bayesian event tree approach described above and in the Appendix. To do that, a user-friendly interface will guide the user through all the steps. The first step, and most important, is to enter all the data for the analysis. The second step is to compute the probability estimates for each branch in the event tree and corresponding variability. The third step computes the total probability estimate for different scenarios. It is important to highlight the advantages of having a simple GUI that makes it easy for the user to input the data parameters and generate results with the correct interpretations. HASSET also allows the user to edit and save the output in various formats (more details in the manual).

In the next section, we describe the tool using an example. In summary, HASSET allows the user to easily:

- Browse the csv file and select input data or enter data manually.
- Enter the dataset time window and decide the forecasting time interval.
- Identify five different locations and size values relevant to a particular volcanic system.
- Evaluate probability at each branch (RUN button).
- Calculate total probability for any particular scenario and compare up to 5 different scenarios.
- Sum the total probability of the scenarios selected.
- Visualize the five most likely scenarios out of all the possibilities for the selected nodes.
- Access the information in each step and locate where we are in the event tree for each node.

Table 3.1: Volcanic data used for the Teide-Pico Viejo case study (see Sobrado and Martí (2010) and references within for in-depth explanation of the catalogue and corresponding source)

Eruption name	Year	Node 1 Unrest	Node 2 Origin	Node 3 Outcome	Node 4 Location	Node 5 Composition	Node 6 Size (VEI)	Node 7 Hazard	Node 8 Extent
Chahorra	1798	Yes	Magmatic	Erupt M	West	Mafic	≤ 2	Lava flows Fallout	Short Medium
Mta Reventada	895 bp	Yes	Magmatic	Erupt M	North	Mafic	≤ 2	Lava flows Fallout	Short Short
Lavas Negras	1150 bp	Yes	Magmatic	Erupt M	Central	Felsic	≤ 2	Lava flows	Large
Roques Blancos	1714 bp	Yes	Magmatic	Erupt M	North	Felsic	4	Lava flows	Large
Mta Blanca	2000 bp	Yes	Magmatic	Erupt M	East	Felsic	3	Lava flows Fallout	Short Medium
PV surges	(2528-2000) bp	Yes	Magmatic	Erupt M	Central	Mafic	≤ 2	PDCs Ballistic Fallout	Short Short Medium
Hoya del Cedro	(2528-2000) bp	Yes	Magmatic	Erupt M	North	Felsic	4	Fallout	Short
Mta Majua	(2528-2000) bp	Yes	Magmatic	Erupt M	South	Felsic	≤ 2	Fallout	Short
Mta de la Cruz	(2528-2000) bp	Yes	Magmatic	Erupt M	East	Mafic	≤ 2	Lava flows Fallout	Short Short
Arenas Blancas	(2528-2000) bp	Yes	Magmatic	Erupt M	East	Felsic	≤ 2	Lava flows	Medium
Mta Los Conejos	(2528-2000) bp	Yes	Magmatic	Erupt M	East	Mafic	≤ 2	Lava flows Fallout	Short Short
Bocas de Maria	(2528-2000) bp	Yes	Magmatic	Erupt M	East	Mafic	≤ 2	Lava flows Fallout	Short Short
Mta Las Lajas	(2528-2000) bp	Yes	Magmatic	Erupt M	East	Felsic	≤ 2	Lava flows Fallout	Short Short
El Boqueron	2528 bp	Yes	Magmatic	Erupt M	North	Felsic	4	Fallout	Large
Cañada Blanca	(5911-2528) bp	Yes	Magmatic	Erupt M	Central	Felsic	3	Lava flows	Medium
Abejera Baja	5911 bp	Yes	Magmatic	Erupt M	North	Felsic	4	Lava flows	Medium
Abejera Alta	5486 bp	Yes	Magmatic	Erupt M	North	Felsic	4	Lava flows	Medium
Pico Cabras	(7900-5486) bp	Yes	Magmatic	Erupt M	North	Felsic	4	Lava flows	Large

3.5 HASSET applied to Teide-Pico Viejo volcanic complex

Here, we use the existing data catalogue for Teide-Pico Viejo (TPV) as shown in Table 3.1. More in-depth explanation of the data can be found in Sobradelo and Martí (2010) and references within.

In this example, we want to assess the long-term volcanic hazard of TPV for the next 100 years, so we set $\tau = 100$. For node 4, we consider five different locations: central, north, south, east, and west, and for Node 6, we use VEI to define four different sizes: $\text{VEI} \leq 2$, VEI 3, VEI 4, $\text{VEI} \geq 5$ (see Sobradelo and Martí (2010)). All of the volcanic data input for HASSET, as well as the prior distribution and model beliefs, input as data and prior weights, are reported in Table 3.2. Note that even if there are no records of unrest with geothermal or seismic origin, we do not rule out this as a possible future scenario, because in our example, there is a hydrothermal system underneath the volcanic complex. We account for these additional sources of volcanic hazard by assigning positive weights to the corresponding branches, and assume the lack of records in the dataset could be due to incompleteness in the data catalogue. Not accounting for these scenarios could underestimate the volcanic hazard. The same applies to the noneruptive volcanic scenarios (sector failure and phreatic explosion) despite no records in the data catalogue. In this example, we assumed that every unrest episode results in an eruption, as we do not have records otherwise. Alternative models and expert elicitation are used to adjust the input data and assign weights to the priors and the data. Here, we assume maximum epistemic uncertainty (i.e., the minimum data weight value of 1) and proportional prior weights (refer to Sobradelo and Martí (2010) for further details).

A crucial determinant of the reliability of the results is the data used in the study, and so it is the first step of introduction of the input parameters. The user has the possibility of manually entering the data shown in Table 3.1 or uploading it from a comma-separated (csv) file (Table 3.2), where the input data for past events, priori weight, and data weight are selected from a drop-down menu. Figure 3.2 shows a screenshot of the first window where the data are uploaded into the HASSET GUI.

As mentioned earlier, the extent of a volcanic hazard is a relative measure of the maximum distance reached, or the area covered by a particular event. It has to be estimated separately for each volcano or volcanic zone by comparing the maximum

Table 3.2: .csv file with volcanic data formatted and ready to upload into HASSET

Node #	Node	Branch	Past events	Prior weight	Data weight
1	Unrest	Yes	18	0.5	1
1	Unrest	No	62	0.5	1
2	Origin	Magmatic	18	0.25	1
2	Origin	Geothermal	0	0.25	1
2	Origin	Seismic	0	0.25	1
2	Origin	Other	0	0.25	1
3	Outcome	Magmatic eruption	18	0.25	1
3	Outcome	Sector failure	0	0.25	1
3	Outcome	Phreatic explosion	0	0.25	1
3	Outcome	No eruption	0	0.25	1
4	Location	Central	3	0.2	1
4	Location	North	7	0.2	1
4	Location	South	1	0.2	1
4	Location	East	6	0.2	1
4	Location	West	1	0.2	1
5	Composition	Mafic	3	0.5	1
5	Composition	Felsic	15	0.5	1
6	Size	VEI \geq 5	0	0.25	1
6	Size	VEI4	6	0.25	1
6	Size	VEI3	3	0.25	1
6	Size	VEI \leq 2	9	0.25	1
7	Hazard	Ballistic	1	0.14	1
7	Hazard	Fallout	10	0.15	1
7	Hazard	PDC	1	0.14	1
7	Hazard	Lava flow	14	0.15	1
7	Hazard	Lahars	0	0.14	1
7	Hazard	Debris avalanche	0	0.14	1
7	Hazard	Other	0	0.14	1
8	Extent	Short	15	0.4	1
8	Extent	Medium	7	0.3	1
8	Extent	Large	4	0.3	1

and minimum extent of each hazard in particular.

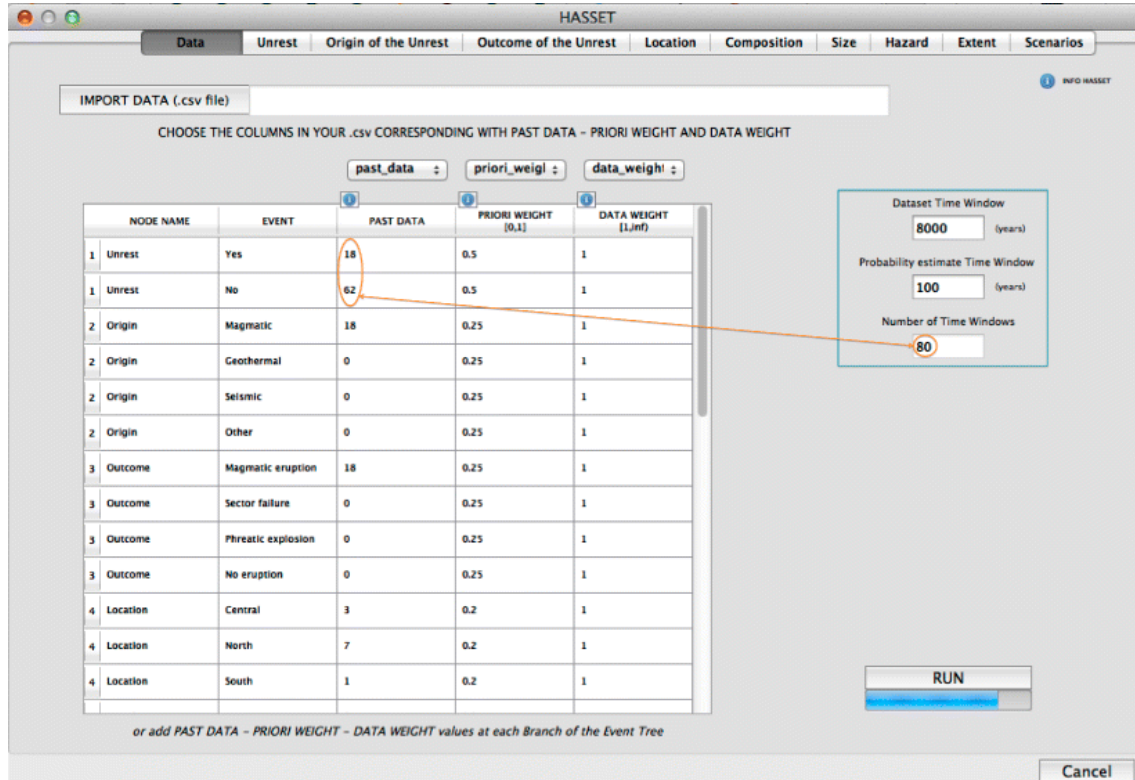


Figure 3.2: This is the main window of HASSET, where the user has to define the input parameters of the model. A “Browser .csv file” button allows the user to visualize only the *.csv files in the user computer in order to import the data. The three drop-down menus allow the user to import the information for past events, prior and data weights directly from the *.csv. The information can also be entered manually. The location names and the size bins need to be defined. The “Dataset” total time and “Probability estimate Time Windows” need to be defined. The “Number of Time Windows” has to be the same as the sum of “unrest” and “no unrest” episodes entered

In the case of Teide-Pico Viejo, regardless of the type of hazard reaching the area, we consider short extent any area within 3 km of the volcanic region of study, medium extent would be the area between 3 and 15 km, and large extent any area further than 15 km. Impact may be assessed by comparing a combination of hazard and extent, for instance the hazard from a lava flow of medium extent compared to a PDC of large extent.

As the time over which eruptions in our dataset took place is 8,000 years and we want to estimate the probability of at least one eruption in the next 100 years, we have 80 time intervals of data for the study. For each branch, we count the number

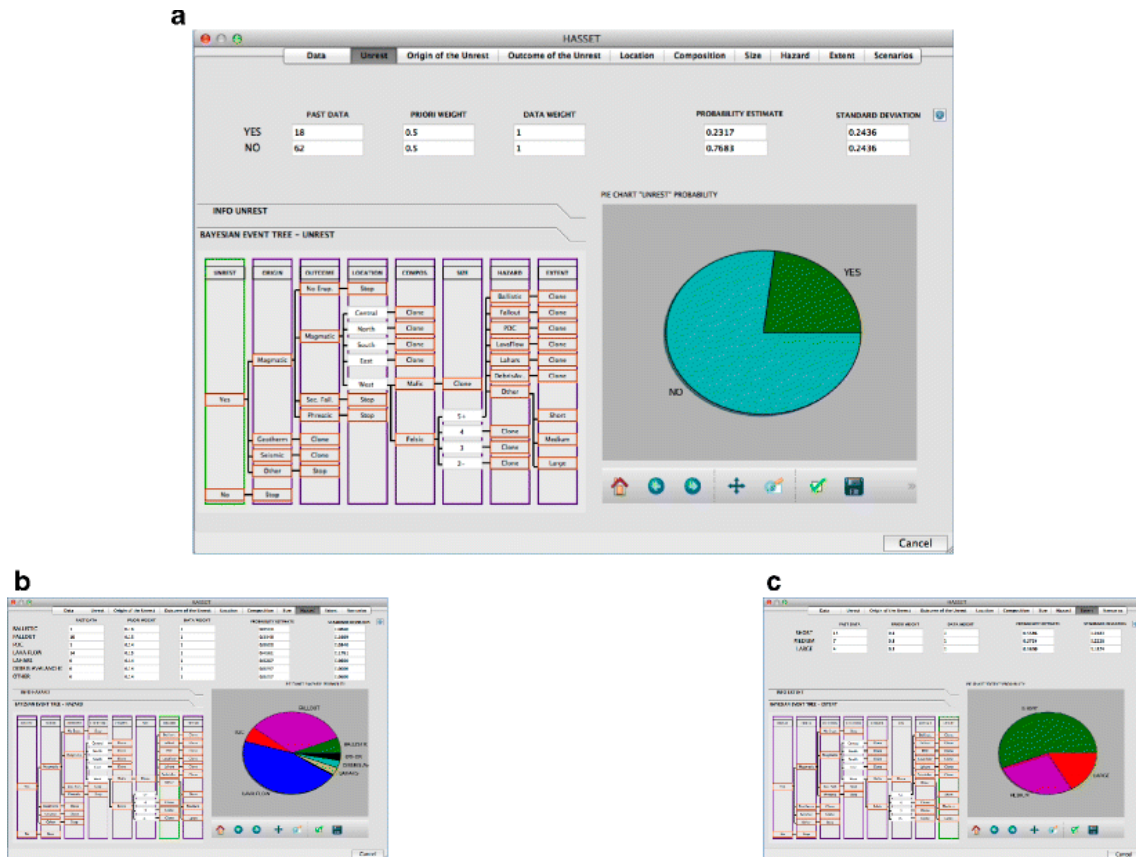


Figure 3.3: The first result is represented by the probability estimated at each node and by the corresponding precision. All nodes are visualized with the individual results for each branch. In this example, we show the results for nodes **a** unrest, **b** hazard, and **c** extent. The results are displayed as a numeric value, but also in a pie chart that can be zoomed in, saved to a file or used to show a graphical view of the probability. The node tabs contain an information button with further details and the current node is highlighted on the event tree scheme

of intervals where at least one event of that type has occurred. For example, out of 80 time intervals, 18 observed an episode of unrest and 62 did not.

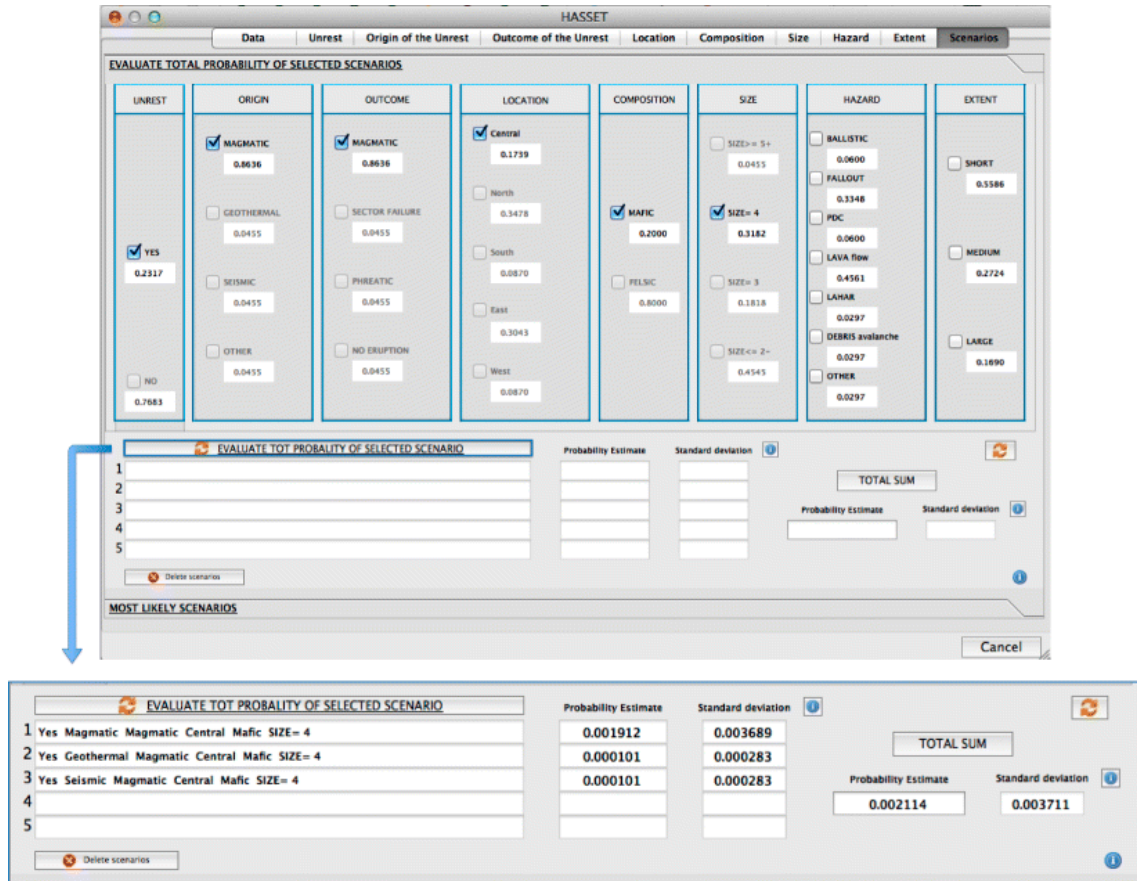


Figure 3.4: The “*Scenarios*” window represents the Event Tree structure with all the nodes and branches. The results obtained in the first analysis of HASSET, i.e., the probability values at each node, are also showed. Here, the user has the possibility to evaluate the probability of different volcanic scenarios by choosing different combinations of branches

Once the data is entered, HASSET computes a probability estimate and corresponding standard deviation for each branch of all the eight nodes, and displays them in table and graphical format for simplicity. Figure 3.3a shows an example of how the unrest tab displays the output on HASSET. The initial beliefs are entered for this node in columns for prior and data weight. We can see the 80 time windows of which 18 had an episode of unrest and 62 did not. With these data, the probability estimate of having at least one unrest episode in the next time window of 100 years is 23.17 %, versus the complement 76.83 % of no unrest. The pie chart in Fig. 3.3

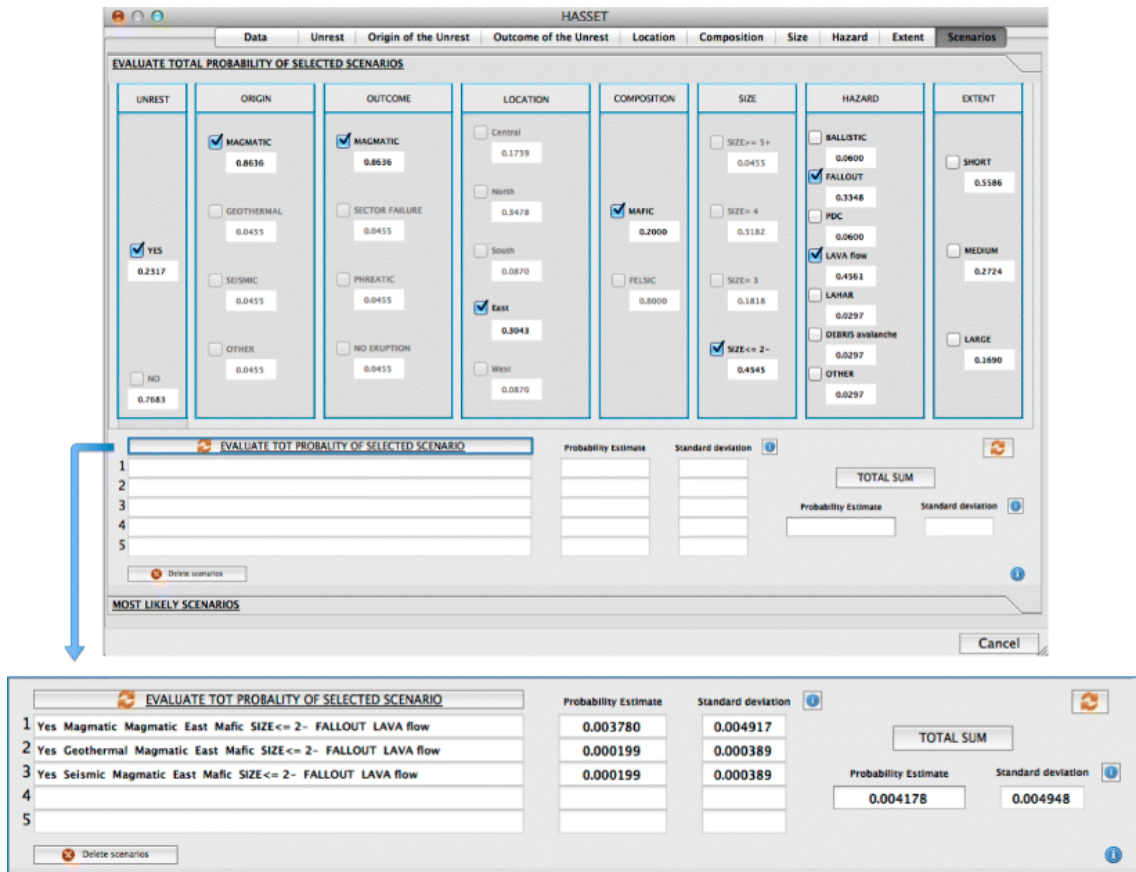


Figure 3.5: The probability estimate for various volcanic scenarios can be compared and visualized with the “*EVALUATE TOTAL PROBABILITY OF SELECTED SCENARIOS*” button. Only five scenarios can be visualized at the same time and the “*Delete scenarios*” button is used to erase the selected scenarios and perform a new scenario analysis

displays graphically these probabilities. On the event tree graph (Fig. 3.3), we see the node of unrest highlighted in green to show the user at what point of the event tree are we. The same applies for all of the remaining seven nodes. Figure 3.3b and c show the results for the hazards and extent node, where after observing the data, we compute that fallout and lava flows account for nearly 80 % of the total probability estimate of the occurrence of these particular hazards in the next 100 years, while the possibility of any of this hazard affecting a medium/large area is not far from 50 % (22.26 and 18.74 %, respectively). Note that the variability interval for each estimate is very wide, as we are assuming maximum epistemic uncertainty and noninformative priors. Figures 3.4 and 3.5 show the scenario selection tab, where the entire event tree is displayed with all the nodes and corresponding probability estimates for each branch. From this window, we can now evaluate all scenarios of interest by clicking on the desired branch. Note that some eruptive scenarios are formed of different combinations, as shown in the bottom part of the figures, where a magmatic eruption can be triggered by different types of unrest, and so HASSET allows for computation and summing of all cases. Also note that the *hazards* node allows the user to select more than one option (Fig. 3.5), since the same eruption could produce different hazards.

When studying a particular volcanic system, it could be the case that we are not interested in a particular eruptive scenario but more so knowing what the most likely eruptive scenarios are. One of the prime features of HASSET is that it includes an option to identify the five most likely scenarios to occur up to a particular node. In Fig. 3.6, we see that the most likely scenarios to occur are magmatic eruptions, mainly of VEI 2 or less, on the north or east sides of the volcano producing lava flows and fallout of short extent.

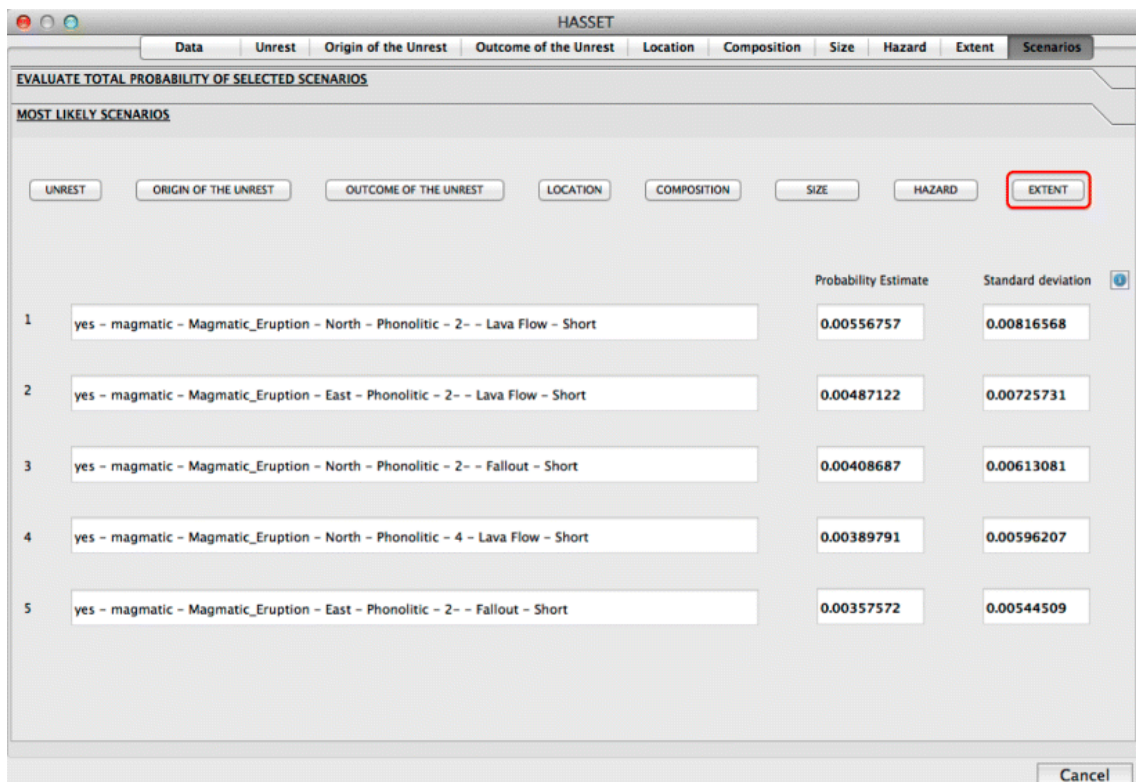


Figure 3.6: This window shows at each node (e.g., Extent) the five most likely scenarios, i.e., the ones with the highest probability estimates. See text for explanations

3.6 Discussion and Conclusions

HASSET is a probability tool built on an event tree structure of possibilities that outlines possible future volcanic scenarios, eruptive and noneruptive, originated by internal or external triggers, and then uses Bayesian theory to estimate a probability of occurrence for each scenario. Further, it determines the five most likely scenarios based on the information given. The main goal of this tool is to focus discussion and draw attention to possible scenarios that otherwise would go unnoticed or underestimated. The reliability of the results will strongly depend on the reliability of the volcanological information provided. With HASSET, we wanted to create a realistic, simple, and practical tool that brings a particular hazard assessment technique closer to the decision maker or the monitoring expert, to help structure and focus discussion on the main aspects of the volcanic hazard. This tool could be useful for land use planning and preparedness actions.

The interpretation of the individual probability estimates for each scenario is subjective. The absolute value of the estimate will strongly depend on the accuracy and completeness of the data, as mentioned earlier, but also on the starting assumptions of independence of the nodes and the choice of mathematical technique to model the uncertainty surrounding the corresponding volcanic system. We turn to probability models when we want to make inferences and decisions about the future in view of uncertainty. We observe the past history of a volcanic system and assume that the future behavior will be similar, and then, based on the data provided, extract a probability model that may guide decisions and make inferences about future scenarios. The model selection is an additional source of uncertainty. HASSET provides a systematic and structured way of using all of the available information such as models, state of the volcano, geochronological and historical data, expert opinion and theoretical beliefs, to analyze the uncertainty surrounding a volcano, based on robust and well-established mathematical theory, that will enable us to rapidly update our estimates when new evidence arrives.

HASSET is a probabilistic approach that accounts for the epistemic (data or knowledge limited) and aleatory (stochastic) uncertainties (given reliable input information), providing a more realistic assessment of the probability estimates.

HASSET can be used to identify the relative importance of several scenarios by comparing their probabilities of occurrence, providing an important tool for the

decision maker to redirect resources and prioritize emergency plans, based on what is most likely to occur. Note that the five most likely scenarios, identified through HASSET, may very well not be the five most threatening, in terms of the risk they pose, because the model does not consider what is exposed to the hazards. The relative interpretation of the probability estimates will depend on the decision maker, his or her perception of risk, and the level of loss considered acceptable.

HASSET is part of a larger project to build an architecture for decision making during volcanic crises, incorporating information from other relevant sources like cost, loss, vulnerability, spatial hazards, etc. It represents the first of several modules, temporal and spatial, that will also be implemented in QGIS and will interact with each other to elaborate an analysis report on the current situation of the volcano. The next step of HASSET is to add monitoring data to perform short-term volcanic hazard assessment.

Acknowledgments

This work was supported by the European Commission (FP7 Theme: ENV.2011.1.3.3-1; grant 282759: VUELCO). The authors are grateful to Henry Odbert and an anonymous reviewer for their insightful comments and thorough review of the manuscript, which has helped us improve considerably this work. We also thank the Associate Editor Eliza Calder for handling this paper and for her editing and scientific corrections.

References

Aspinall, W. and Cook, R.: Expert judgement and the Montserrat volcano eruption. In: Mosleh A et al. (eds) Proceedings of the 4th international conference on Probabilistic Safety Assessment and Management PSAM4, 13–14 September. Springer, New York, pp 2113–2118, 1998.

Aspinall, W.P.: Structured elicitation of expert judgment for probabilistic hazard and risk assessment in volcanic eruptions. In: Mader HM et al. (eds) Statistics in volcanology. Special Publication of IAVCEI, Geological Society of London, 2006.

Blong, R.: Volcanic hazards and risk management. In: Sigurdsson H et al. (eds) Encyclopedia of volcanoes. Academic, San Diego, pp 1215–1227, 2000.

Chen, D., Shams, S., Carmona-Moreno, C., and Leone, A.: Assessment of open source gis software for water resources management in developing countries. *J Hydro Environ Res* 4(3):253–264, 2010.

Longley, P.A., Goodchild, M.F., Maguire, D.J., and Rhin, D.W.: *Geographic information, systems and science*. Wiley, Chischester, 2001.

Loughlin, S., Baxter, P., Aspinnall, W., Darroux, B., Harford, C., and Miller, A.D.: Eyewitness accounts of the 25 June 1997 pyroclastic flows and surges at Soufriere Hills Volcano, Montserrat, and implications for disaster mitigation. *Geol Soc Lond Mem* 2002(21):211– 230, 2002.

Martí, J., Aspinnall, W., Sobradelo, R., Felpeto, A., Geyer, A., Ortiz, R., Baxter, P., Cole, P., Pacheco, J., Blanco, M., and Lopez, C.: A long-term volcanic hazard event tree for Teide-Pico Viejo stratovolcanoes (Tenerife, Canary Islands). *J Volcanol Geotherm Res* 178(3):543– 552, 2008a.

Martí, J., Geyer, A., Andújar, J., Teixidó, F., and Costa, F.: Assessing the potential for future explosive activity from Teide-Pico Viejo stratovolcanoes (Tenerife, Canary Islands). *J Volcanol Geotherm Res* 178(3):529–542. *Evaluating Explosive Eruption Risk at European Volcanoes - Contribution from the EXPLORIS Project*, 2008b.

Martí, J., Sobradelo, R., Felpeto, A., and García, O.: Eruptive scenarios of phonolitic volcanism at Teide-Pico Viejo volcanic complex (Tenerife, Canary Islands). *Bull Volcanol* 74:767–782, 2011.

Marzocchi, W., Sandri, L., Gasparini, P., Newhall, C., and Boschi, E.: Quantifying probabilities of volcanic events: the example of volcanic hazard at Mount Vesuvius. *J Geophys Res* 109. doi:10.1029/2004JB003155, 2004.

Marzocchi, W., Sandri, L., and Furlan, C.: A quantitative model for volcanic hazard assessment. In: Mader HM, et al. (eds) *Statistics in volcanology*. Special Publication of IAVCEI, Geological Society of London, 2006.

Marzocchi, W., Sandri, L., and Selva, J.: BET_EF: a probabilistic tool for long- and short-term eruption forecasting. *Bull Volcanol* 70(5):623–632, 2008.

Marzocchi, W., Sandri, L., and Selva, J.: BET_VH: a probabilistic tool for long-term volcanic hazard assessment. *Bull Volcanol* 72:705– 716, 2010.

Neri, A., Aspinnall, W., Cioni, R., Bertagnini, A., Baxter, P., Zuccaro, G., Andronico, D., Barsotti, S., Cole, P., Ongaro, T.E., Hincks, T., Macedonio, G., Papale, P., Rosi, M., Santacroce, R., and Woo, G.: Developing an event tree for probabilistic

hazard and risk assessment at vesuvius. *J Volcanol Geotherm Res* 178(3):397–415, 2008.

Newhall, C.G. and Hoblitt, R.P.: Constructing event trees for volcanic crisis. *Bull Volcanol* 64:3–20, 2002.

Renschler, C.S.: Scales and uncertainties in using models and gis for volcano hazard prediction. *J Volcanol Geotherm Res* 139(1– 2):73–87, 2005.

Rice, J.A.: *Mathematical statistics and data analysis*. Duxbury, Belmont, 2007.

Sherman, G.E.: *Desktop GIS. Mapping our planet with open source tools*. The Pragmatic Bookshelf Raleigh, North Carolina, 2008.

Sobradelo, R. and Martí, J.: Bayesian event tree for long-term volcanic hazard assessment: application to Teide-Pico Viejo stratovolcanoes, Tenerife, Canary islands. *J Geophys Res* 115. doi:10.1029/2009JB006566, 2010.

Sobradelo, R., Martí, J., Mendoza-Rosas, A.T., and Gómez, G.: Volcanic hazard assessment for the canary islands (spain) using extreme value theory. *Nat Hazards Earth Syst Sci* 11(10):2741– 2753, 2011.

Woo, G.: *The mathematics of natural catastrophes*. Imperial College Press, London, 1999.

Appendix: Computation of the variance estimation for a particular eruptive scenario

Let us use a general notation for simplicity. Let Y be a random variable formed by the product of m random variables, $Y = X_1.X_2.....X_m$. In our case, Y will be a particular eruptive scenario whose variance we want to compute.

Then, the expected value E and variance V (also denoted $\hat{\sigma}^2$) of Y , are:

$$E(Y) = E(X_1.X_2.....X_m) = E \prod_{i=1}^m X_i = \prod_{i=1}^m E(X_i)$$

and

$$V(Y) = V(X_1.X_2.....X_m)$$

and so the expected value of a particular scenario is just the product of the expected value (posterior Dirichlet) of each of the m nodes. The same condition does not apply to the variance. That is, the variance of the product is not the product of the variances, so we use the Delta method, also called propagation error, to approximate this variance by applying a first order Taylor series expansion. We do a logarithmic transformation of the variable, and we get:

$$\log(Y) = \sum_{i=1}^m \log X_i$$

and, now by the independence condition of X_i

$$V(\log(Y)) = \sum_{i=1}^m V(\log X_i) \tag{3.5}$$

We apply the Delta method to approximate $\log(Y)$ and $\log(X_i)$, with $g(\delta) = \log(\delta)$, where δ is the estimator, and we get:

$$V(\log(Y)) \approx V(Y) \frac{1}{\delta^2}$$

Hence,

$$V(Y) = \delta^2 V(\log(Y)) \tag{3.6}$$

and similarly for $\log(X_i)$,

$$V(\log(X_i)) \approx V(X_i) \frac{1}{\delta_i^2}$$

Hence,

$$V(X_i) = \delta_i^2 V(\log(X_i))$$

and so, by equations 3.5 and 3.6

$$V(Y) = \delta^2 \sum_{i=1}^m V(\log X_i) = \delta^2 \sum_{i=1}^m \frac{1}{\delta_i^2} V(X_i)$$

For our particular case, we know that the estimator δ_k is modeled with the expected value of the random variable for node k that follows a Dirichlet distribution of parameters $\alpha_k + y_k$ (the posterior distribution of a particular branch for node k). The estimator δ is the expected value for that particular eruptive scenario, and $V(X_k)$ is the variance for the random variable in node k that follows a Dirichlet distribution of parameters $\alpha_k + y_k$. We thus derive Eq. 3.2:

$$\hat{\sigma}_j^2 = E(H)^2 \sum_{k=1}^m \frac{1}{[E(\theta_{kn}^*)]^2} V(\theta_{kn}^*)$$

And so we have written the variance for an eruptive scenario H as a function of the expected value and variances of the individual random variables used to model each particular node.

Long-term volcanic hazard assessment on El Hierro (Canary Islands)

Published in:

Natural Hazards and Earth System Sciences

Authors:

Laura Becerril^a

Stefania Bartolini^a

Rosa Sobradelo^a

Joan Martí^a

Jose Maria Morales^b

Inés Galindo^b

a) Institute of Earth Sciences Jaume Almera, ICTJA-CSIC, Group of Volcanology, SIMGEO (UB-CSIC) Lluís Sole i Sabaris s/n, 08028 Barcelona, Spain

b) Instituto Geológico y Minero de España (IGME) c/ Alonso Alvarado, 43-2A, 35003 Las Palmas de Gran Canaria, Spain

4.1 Abstract

Long-term hazard assessment, one of the bastions of risk-mitigation programs, is required for land-use planning and for developing emergency plans. To ensure quality and representative results, long-term volcanic hazard assessment requires several sequential steps to be completed, which include the compilation of geological and volcanological information, the characterisation of past eruptions, spatial and temporal probabilistic studies, and the simulation of different eruptive scenarios. Despite being a densely populated active volcanic region that receives millions of visitors per year, no systematic hazard assessment has ever been conducted on the Canary Islands. In this paper we focus our attention on El Hierro, the youngest of the Canary Islands and the most recently affected by an eruption. We analyse the past eruptive activity to determine the spatial and temporal probability, and likely style of a future eruption on the island, i.e. the where, when and how. By studying the past eruptive behaviour of the island and assuming that future eruptive patterns will be similar, we aim to identify the most likely volcanic scenarios and corresponding hazards, which include lava flows, pyroclastic fallout and pyroclastic density currents (PDCs). Finally, we estimate their probability of occurrence. The end result, through the combination of the most probable scenarios (lava flows, pyroclastic density currents and ashfall), is the first qualitative integrated volcanic hazard map of the island.

4.2 Introduction

The possibility of future eruptive activity, coupled with population growth and economic and cultural development in the majority of active volcanic areas, means that mitigative measures against volcanic risk, such as the development of volcanic hazard analyses, must be undertaken. These types of analyses are a fundamental part of risk management tasks that include the developing of volcanic hazard maps, land-use planning and emergency plans.

The volcanic hazard of a given area is the probability that it will be affected by a process of a certain volcanic magnitude within a specific time interval (Fournier d'Albe, 1979). Therefore, volcanic hazard assessment must necessarily be based on good knowledge of the past eruptive history of the volcanic area, which will

tell us "how" eruptions have occurred. It also requires the spatial probability of occurrence of a hazard to be determined; i.e. "where" the next eruption can take place (volcanic susceptibility) and its extent, as well as its temporal probability, in other words "when" the next eruption may occur in the near future.

The complexity of any volcanic system and its associated eruptive processes, together with the lack of data that is typical of so many active volcanoes and volcanic areas (and in particular those with long periods between eruptions), make volcanic hazard quantification a challenge. Long-term hazard assessment is necessary to know how the next eruption could be. It is based on the past history of the volcano and the information needed comes from the geological record. Unlike short-term assessment that evaluates hazards from days to a few months, using data provided by monitoring networks, long-term assessment is estimated from years to decades, where the main source of information is mainly structural data from past eruptions (Marzocchi et al., 2006). Different steps need to be followed sequentially in any long-term volcanic hazard assessment. The first step consists of evaluating the likelihood of a future eruption, which will provide an indication of which areas are most likely to host future vents (Martí and Felpeto, 2010). The long-term spatial probability of vent opening can be estimated using structural data such as vents, dykes, faults, fractures and eruptive fissure-alignments obtained from geological and geophysical studies. These data can be converted into Probability Density Functions (PDFs) and then combined to obtain the final susceptibility map (Martin et al., 2004; Felpeto et al., 2007; Connor and Connor, 2009; Martí and Felpeto, 2010; Cappello et al., 2012; Bartolini et al., 2013; Becerril et al., 2013). Susceptibility maps show the spatial probability of hosting new future eruptions. This term has been commonly used during the last years by other authors in the volcanic field (Felpeto et al., 2007; Cappello et al., 2010, 2011, 2012; Martí and Felpeto, 2010; Vicari et al., 2011; Alcorn et al., 2013; Bartolini et al., 2013; Becerril et al., 2013).

The next step corresponds to the temporal probability estimation of any possible volcanic event. Long-term forecasting is based on historical and geological data, as well as on theoretical models, and refers to the time window available before an unrest episode occurs in the volcanic system. In this regard, some authors use probabilistic statistical methods based on the Bayesian event tree for long-term volcanic hazard assessment (Newhall and Hoblitt, 2002; Marzocchi et al., 2008; Sobradelo and Martí, 2010), while some others use a deterministic approach (Voight

and Cornelius, 1991; Kilburn, 2003; see also Hill et al., 2001).

Once spatial and temporal probabilities have been estimated, the next step forward consists of computing several scenarios as a means of evaluating the potential extent of the main expected volcanic and associated hazards. Most of these studies are based on the use of simulation models and Geographical Information Systems (GIS) that allow volcanic hazards such as lava flows, PDCs and ash fallout to be modelled and visualised (Pareschi et al., 2000; Felpeto et al., 2007; Toyos et al., 2007; Crisci et al., 2008; Cappello et al., 2012; Martí et al., 2012; Alcorn et al., 2013).

All of these steps should be undertaken to evaluate the potential volcanic hazards of any active volcanic area. Similar approaches have been applied in volcanic areas such as Auckland, New Zealand (Bebbington and Cronin, 2011); Etna, Sicily (Cappello et al., 2013); and Tenerife, Spain (Martí et al., 2012); Perú (Sandri et al., 2014). Nevertheless, other procedures have also been applied in order to assess volcanic hazards in Campi Flegrei, Italy (Lirer et al., 2001); Furnas (São Miguel, Azores) Vesuvius in Italy (Chester et al., 2002); and Auckland, New Zealand (Sandri et al., 2012). Compared with these previous approaches, our study offers a procedure that facilitates undertaking volcanic hazard assessment in a systematic way, which can be easily applied to other volcanic areas around the world.

The Canary Islands are the only area of Spain in which volcanic activity has occurred in the last 600 years, representing one of the world's largest oceanic volcanic zones. The geodynamic environment in which the archipelago lies and the characteristics of its recent and historical volcanism suggest that the volcanic activity that has characterised this archipelago for more than 60 Ma will continue in the future. Previous volcanic hazard studies conducted on the Canary Islands have not followed a systematic method. Most work to date has focused on Tenerife and Lanzarote (Gómez-Fernández, 1996; Araña et al., 2000; Felpeto et al., 2001, 2007; Felpeto, 2002; Carracedo et al., 2004a, b, 2005; Martí and Felpeto, 2010; Sobradelo and Martí, 2010; Martí et al., 2012; Bartolini et al., 2013), although other studies have been carried out on Gran Canaria (Rodríguez-González, 2009), El Hierro (Becerril et al., 2013) and one for the Canary Islands as a whole (Sobradelo et al., 2011).

In this study we focus on El Hierro and conduct a long-term volcanic hazard assessment by taking into account spatial and temporal probabilities. Despite being

small and submarine in nature (Martí et al., 2013), the most recent eruption on El Hierro (October 2011–February 2012) highlighted the need for volcanic hazard studies, given the negative impact on tourism and the local economy of any volcanic event. Although this eruption was not different in terms of magma volume and volcanic products from most eruptions that historically occurred in the Canarian Archipelago, this eruption marked the end of a 40-year period of quiescence in this volcanic region. El Hierro has a population of 10 960 inhabitants (www.ine.es), or 0.51% of the total population of the Canary Islands. Its main economic resources are tourism and fishery, two aspects that may be – and in fact were – seriously affected by the impact of volcanic activity.

In this work we present a systematic analysis of the volcanic hazards present on this island that includes the following steps: (1) characterisation of past volcanism in the study area; (2) estimation of spatio-temporal probabilities; (3) simulation of the most probable eruptive scenarios such as lava flows, pyroclastic fallout and pyroclastic density currents (PDCs); and (4) assessment of the volcanic hazard.

4.3 Geological setting

The Canary Islands extend for roughly 500 km in a chain that has developed on the passive margin of the African plate in the eastern central Atlantic Ocean (Fig. 4.1, inset). The Canarian Archipelago is the result of long-term volcanic and tectonic activity that started around 60 Ma (Robertson and Stillman, 1979; Le Bas et al., 1986; Araña and Ortiz, 1991; Marinoni and Pasquaré, 1994). A number of contrasting models – including the presence of a hotspot, the propagation of a fracture from the Atlas Mountains and mantle decompression melting associated with uplift of tectonic blocks – have been mooted to explain the origin of the Canary Islands (Le-Pichon and Fox, 1971; Anguita and Hernán, 1975; Schmincke, 1982; Araña and Ortiz, 1991; Hoernle and Schmincke, 1993; Hoernle et al., 1995; Carracedo et al., 1998; Anguita and Hernán, 2000).

Although all of the islands (except La Gomera) have been witness to Holocene volcanic activity, volcanism has historically been restricted to La Palma, Lanzarote, El Hierro and Tenerife (Fig. 4.1, inset). In all cases, historical eruptive activity has produced mafic eruptions ranging in intensity from Hawaiian to violent Strombolian (Valentine and Gregg, 2008 and references therein) and have given rise to lavas and

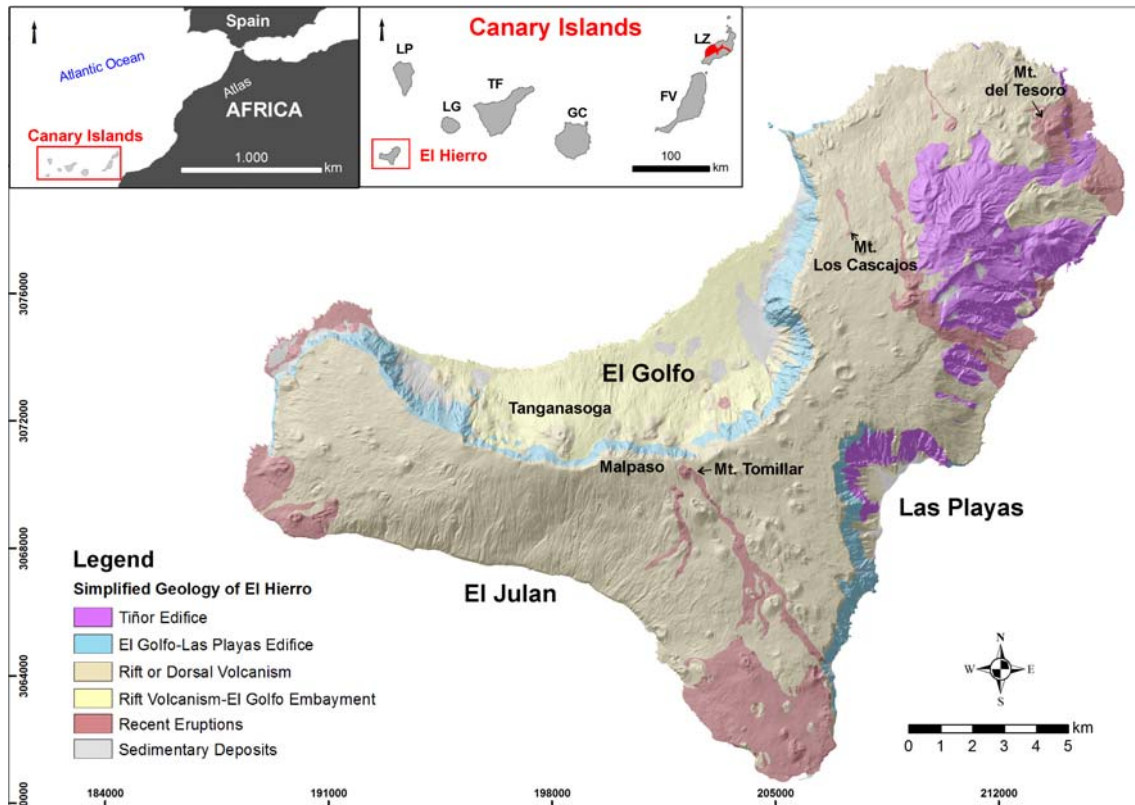


Figure 4.1: Geological map of El Hierro Island. At the left top part of the figure, location of the Canary Islands is presented where LZ represents Lanzarote; FV represents Fuerteventura; GC represents Gran Canaria; TF represents Tenerife; LG represents La Gomera; LP represents La Palma; EH represents El Hierro. Timanfaya eruption in Lanzarote has been coloured in red

scoria cones. Typically, the islands' historical eruptions have occurred in active rift zones along eruptive fissures and have occasionally generated alignments of cones. Other than the case of the Timanfaya eruption in 1730 in Lanzarote (Fig. 4.1, inset), which lasted for 6 years, the duration of eruptions has ranged from a few weeks to a few months. The total volume of erupted magma ranges from 0.01 to $> 1.5 \text{ km}^3$ (DRE, dense rock equivalent), the upper extreme occurring in the case of the Timanfaya eruption. In all cases the resulting volcanic cones were constructed during single eruptive episodes (i.e. they should be referred to as monogenetic) that usually involved several distinctive phases with no significant temporal separations between them. Monogenetic volcanic fields consist of individual, commonly mafic volcanoes, built in single, relatively short-lived eruptions. These volcanoes usually take the form of scoria cones, tuff rings, maars or tuff cones; scoria cones are the most common landform and show a great diversity in size, morphology and eruptive

products (Valentine and Gregg, 2008; Kereszturi and Németh, 2012). Individual volcanic edifices are characteristically small in volume, typically $< 0.1 \text{ km}^3$ of DRE, but the eruption can be complex with many different phases and styles of activity (Németh, 2010). Situated in the southwestern corner of the archipelago, El Hierro is the youngest of the Canary Islands; its oldest subaerial rocks have been dated at 1.12 Ma (Guillou et al., 1996). It rises from a depth of 4000 m to around 1500 m a.s.l. and has an estimated total edifice volume of about 5500 km^3 (Schminke and Sumita, 2010). It corresponds to a shield structure formed by different volcanic edifices and includes three rift zones on which recent volcanism has been concentrated (Guillou et al., 1996; Carracedo et al., 2001) (Fig. 4.1). Other relevant morphological features include the collapse scars of El Golfo, Las Playas and El Julan (Fig. 4.1). The emergent parts of these rifts are characterised by steep narrow ridges, corresponding to aligned dyke complexes with clusters of cinder cones. Pre-historical eruptions have been recognised on all three rifts on El Hierro (Guillou et al., 1996; Carracedo et al., 2001).

Recent subaerial volcanism on El Hierro is monogenetic and is mostly characterised by the eruption of mafic magmas as well as the intrusion of subvolcanic bodies ranging in composition from picrobasalts to basanites (Pellicer, 1977; Stroncik et al., 2009), which have generally erupted along the rift zones. Some felsic dykes and lava flows associated with the older parts of the island have also been reported (Guillou et al., 1996; Carracedo et al., 2001) but are volumetrically subordinate to the mafic material. In addition, an explosive felsic eruption has been documented in association with the final episodes of the construction of the edifice of El Golfo–Las Playas (later than 158 ka), before it was destroyed by a massive landslide (Pedrazzi et al., 2014). Mafic eruptions typically occur from fissures, and produce proximal fallout, ballistic ejecta and lava flows. PDC deposits have also been reported in cases in which eruptions are related to hydromagmatic episodes (Balcells and Gómez, 1997; Pedrazzi et al., 2014).

The erupted volume of magma in eruptions on El Hierro typically ranges from less than 0.0001 to 0.1 km^3 (DRE), values that are of the same order as most of the other historical eruptions on the Canaries (Sobradelo et al., 2011). One of the most important eruptive episodes in the last few thousand years on El Hierro was the Tanganasoga eruption (Fig. 4.1), which occurred inside the depression of El Golfo along a N–S-oriented fissure, at most 20 ka (Carracedo et al., 2001). Several cones

and emission centres formed, giving rise to one of the largest volcanic edifices on the island via the accumulation of ankaramitic lavas and pyroclastic deposits (Carracedo et al., 2001) (Fig. 4.1). In addition to the subaerial volcanism, bathymetric studies (Gee et al., 2001) have revealed that a significant number of well-preserved volcanic cones exist on the submarine flanks of the island, in particular on the continuation of the southern rift, which suggests that significant submarine volcanic activity has also occurred recently. As a confirmation of this observation, a submarine eruption occurred from 10 October 2011 to the end of February 2012 on the southern rift zone, 2 km off the coast of El Hierro (Martí et al., 2013).

4.4 Methods

The spatial probabilities of hosting new vents were estimated using the study by Becerril et al. (2013) of volcanic susceptibility on El Hierro, which takes into account most of the structural data (vents, eruptive fissures, dykes and faults) available from the island. The temporal part of the long-term volcanic hazard assessment was carried out with the Bayesian-event tree-based software HASSET (Sobradelo et al., 2014a) using geochronological data for El Hierro and historical data from the whole archipelago. Hazard scenarios of lava flows, fallout and PDCs were obtained with the VORIS tool (Felpeto et al., 2007) since they are the most likely volcanic scenarios on the island. The data collection required for each hazard assessment was divided into three parts (spatial, temporal, and scenarios), according to the use made of each data set.

4.5 How: characterisation of the eruptions

The characterisation of past volcanic eruptions – typically based on the determination of eruptive parameters derived from the study of erupted products found in the geological records – is crucial for understanding past eruptive behaviour and for forecasting future volcanic activity.

Recent volcanic activity on El Hierro is largely characterised by monogenetic mafic volcanism and the building of more than 220 cones, most of which are scoria cones that correspond to the most recent eruptive cycle (rift volcanism).

Hawaiian and Strombolian activity are the most common eruptive styles observed on the island (Becerril, 2009), which have formed extensive lava flow fields, spatter and cinder cones made of scoria agglutinates and well-bedded lapilli scoria and ash, respectively. Violent Strombolian activity – refereeing to explosive activity that produces sustained eruption columns up to ~ 10 km high (without reaching the tropopause) and with the dominant clast sizes being ash to lapilli (Valentine, 1998; Arrighi et al., 2001; Valentine and Gregg, 2008) – has been also recognised through the presence of several distal ash deposits on the geological record of the island. Phreatomagmatic episodes generating rhythmic laminated sequences of coarse juvenile ash and lapilli-rich beds with accidental lithic fragments also occurred at the interior of the island but in less frequency than those mentioned above. In addition, some hydromagmatic eruptions occurred along the coast, producing tuff ring deposits on the western part of the island (Becerril, 2009). Eruptions related to felsic magmas and producing either trachytic lava flows (Guillou et al., 1996) or trachytic pyroclastic deposits (Pellicer, 1977; Balcells and Gómez, 1997) have also been described. In this sense, it is remarkable that the occurrence of a base-surge-type explosive eruption that generated dilute pyroclastic surge deposits covering an area of more than 15 km^2 around the Malpaso area (Fig. 4.1) (Pedrazzi et al., 2014).

We also took into account the final constructive cycle (158 ka–present) of the island to characterise of the size of the eruptions. The volume of the cones was calculated using ARCGIS 10.0 (ESRI[©]) through the analysis of a digital elevation model (DEM), subtracting the current DEM topography to the restored paleotopography. The volume of lava flows and distal pyroclastic deposits was calculated taking into account their areal extent and thickness variations. This provided a first-order estimate of the erupted volume, despite the lack of a precise paleotopography. In terms of the total volume of erupted material, the largest eruptions that occurred during the final growing cycle on El Hierro correspond to volumes of the order of $0.15\text{--}0.042 \text{ km}^3$ (Tanganasoga, Mt. del Tesoro, the latter was calculated by Rodríguez-González et al., 2012). A minimum value is for Mt. Los Cascajos, with just 0.0016 km^3 . The volcanic explosivity index (VEI) (Newhall and Self, 1982) and dense rock equivalent (DRE) derived from the volumetric data of the eruptions were also calculated. Most of VEI values are in the range of 0–2, whilst the erupted volume of magma (using mean magma density of 2.8 g cm^{-3} , an average rock density of 2.44 g cm^{-3} obtained from laboratory analysis of El Hierro samples, and applying

the equation: $DRE (km^3) = \text{volume of volcanic deposit } (km^3) \times \text{density of volcanic deposit } (kg m^{-3}) / \text{magma density } (kg m^{-3})$ for most of the recent eruptions on El Hierro lies within the range of 0.0001–0.1 km³ (DRE). The DRE calculation was based on the volume of exposed materials (lavas and pyroclastic deposits) so our total volumes are minimum estimates, but similar to those assigned to other monogenetic fields, which normally have volumes between 0.0001 and a few cubic kilometres for individual eruptions (e.g. Kereszturi et al., 2013). For example, the erupted volume of magma on the Canary Islands typically ranges from 0.001 to 0.2 km³ (DRE) (Sobradelo et al., 2011). In the Garrotxa volcanic field (Spain) the total volume of extruded magma in each eruption ranges from 0.01 to 0.2 km³ (DRE) (Bolós et al., 2014). The volumes of basaltic eruptions on Terceira (Açores, Portugal) range in size from 0.1 km³ to less than 0.001 km³ (DRE) (Self, 1976). In the case of Auckland (New Zealand), monogenetic field volumes are in the range of 0.00007 to 0.698 km³ (Kereszturi et al., 2013).

By comparing pre- and post-eruption high-resolution bathymetries, the total bulk volume erupted during the submarine eruption of 2011–2013 was estimated at 0.33 km³ (Rivera et al., 2013).

Most of the lava flows on El Hierro that were emplaced from cones located on and off the rift zones reached the sea. Therefore, it was not possible to measure precisely the maximum lengths of past lava flows. Nevertheless, the Mt. del Tomillar (Fig. 4.1) lava flow, which did not reach the sea, has a total length of 8 km. However, for further simulations (Sect. 4.10) we considered this value as a minimum length for the lava flows and used 15 km as a more reliable length. The mean thickness of lava flows was obtained from the average value (3 m) of individual flows measured in the field.

4.6 Where: spatial analysis

An essential step in obtaining a volcanic hazard map is to determine the most likely areas to host new eruption vents, a task based on the drawing of susceptibility maps based on geological, structural and geophysical data (Martí and Felpeto, 2010). Structural elements such as vents, eruptive fissures, dykes and faults are used to pinpoint areas where next eruptions may most likely occur. A volcanic susceptibility map shows the spatial distribution of vent opening for future eruption and represents

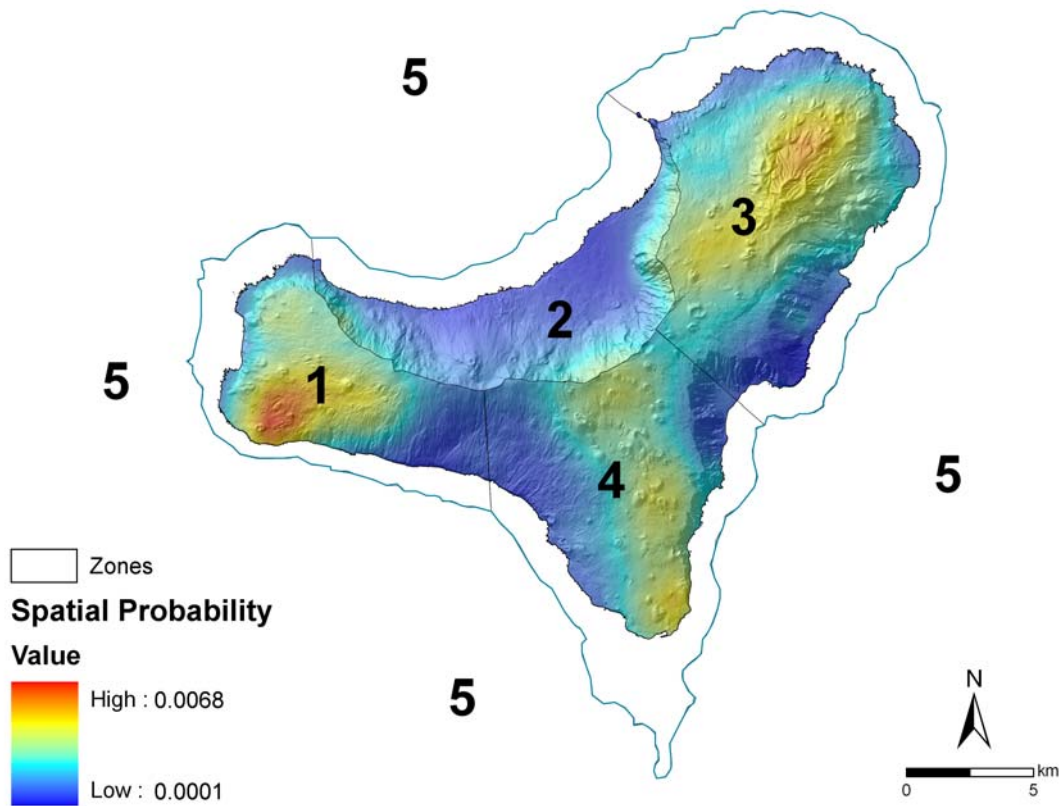


Figure 4.2: Onshore spatial probability distribution of future volcanic eruptions map of El Hierro Island, showing the divisions of the sectors. Modified from Becerril et al. (2013)

the basis for further temporal and spatial probability analysis and the definition of eruptive scenarios. We used the susceptibility map developed by Becerril et al. (2013) following the methodology employed by Cappello et al. (2012) (Fig. 4.2). This map is based on the five data sets representing the volcano-structural elements on El Hierro: (1) subaerial vents and eruptive fissures pertaining to the island's rift volcanism, which include sub-recent and recent eruptions; (2) submarine vents and eruptive fissures inferred from bathymetric data; (3) eruptive fissures and emission centres identified on the Tiñor and El Golfo–Las Playas edifices; (4) presence of dykes; (5) and presence of faults.

To carry out this spatial assessment, we subdivided the spatial probability map into 5 sectors (Fig. 4.2) based on susceptibility values, topographic constraints and expected hazards. First, we differentiated the subaerial and the submarine area, taking into account differences in the expected hazards. After that, the emergent

part of the island was subdivided according to areas with different structural controls (different strike of the volcano-structures as dykes and fissures), different topographical constrains (zones 1, 3 and 4 represent rift areas, while zone 2 is an embayment), and different susceptibility values according to the map developed by Becerril et al. (2013). This map enables us to select the areas with the greatest likelihood of hosting future scenarios.

4.7 When: temporal analysis

Temporal analyses were performed using HASSET (Sobradelo et al., 2014a) a Bayesian event tree structure with eight nodes representing different steps to evaluate the temporal probability and evolving from a more general node of unrest to the more specific node of the extent of the hazard (Sobradelo and Martí, 2010).

We based the study of temporal probability on the catalogue of eruptions documented in Table 4.1. In all, 25 eruptions are documented from the last 158 ka, data confirmed by the relative stratigraphy established during our field work. Six of these eruptions took place during the previous 11 700 years (Holocene), but only 2 unrest episodes have been documented in the last 600 years (historical period). The information from these eruptions was used to characterise the past eruptive activity on El Hierro and to estimate some of the input parameters required for our hazard assessment.

However, due to the scarcity of dated eruptions and to the certainty that not all the eruptions that occurred in this period have been identified and/or dated, we also used in our temporal analysis as data for the last 600 years (15th century to 2013) the historical data set for the whole of the Canary Islands (see Sobradelo et al., 2011). Therefore, using HASSET we were able to estimate the probability that a volcanic episode will occur in the forecasting time interval (the next 20 years). Given that the data set time window is 600 years, we thus obtained 30 time intervals of data for the study period. Here we restrict our data set to the historical period, which includes the recent submarine eruption (2011) and the seismic unrest of 1793. The remaining 23 eruptions in this catalogue – referred to as pre-historical – will be used to assign prior weights to nodes 2 to 8.

Table 4.1: The principal characteristics of the eruptions identified during the last constructive episode of El Hierro. The eruptions included in this table are those for which geochronological data exist and that are consistent with the field-relative stratigraphy established in this study. In addition to the geochronological data and the corresponding references, the rest of the information included in the table corresponds to information related to the first nodes in the HASSET (Sobradelo et al., 2014a) event tree used in this study. (See text for more details)

ID	Unrest	Origin	Outcome	Location	Composition	Hazard	Extent	Reference
1	2011	magmatic	magmatic eruption	5	Mafic	lava flow	medium	Martí et al. (2013)
2	1793	seismic	no eruption	?				Hernández Pacheco (1982)
3	2500 ± 70 (BP)	magmatic	magmatic eruption	3a	Mafic	ballistic + lava flow	medium	Carracedo et al. (2001)
4	4230 (BP)	magmatic	magmatic eruption	3a	Mafic	ballistic + lava flow	short	Fúster et al. (1993)
5	8000 ± 2000 (BP)	magmatic	magmatic eruption	1a	Mafic	ballistic + lava flow	short	Pérez Torrado et al. (2011)
6	9000 (BP)	magmatic	magmatic eruption	3a	Mafic	ballistic + lava flow	medium	Rodríguez-González et al. (2012)
7	12 000 ± 7000 (BP)	magmatic	magmatic eruption	2a	Mafic	lava flow	short	Guillou et al. (1996)
8	15 000 ± 3000 (BP)	magmatic	magmatic eruption	2a	Mafic	lava flow	short	Guillou et al. (1996)
9	15 000 ± 2000 (BP)	magmatic	magmatic eruption	4b	Mafic	lava flow	short	Carracedo et al. (2001)
10	21 000 ± 3000 (BP)	magmatic	magmatic eruption	2a	Mafic	lava flow	short	Guillou et al. (1996)
11	31 000 ± 2000 (BP)	magmatic	magmatic eruption	4b	Mafic	lava flow	short	Carracedo et al. (2001)
12	38 700 ± 12 600 (BP)	magmatic	magmatic eruption	2b	Mafic	lava flow	short	Longpré et al. (2011)
13	41 000 ± 2000 (BP)	magmatic	magmatic eruption	4b	Mafic	lava flow	short	Carracedo et al. (2001)
14	44 000 ± 3000 (BP)	magmatic	magmatic eruption	4b	Mafic	lava flow	short	Guillou et al. (1996)
15	76 000 ± 6000 (BP)	magmatic	magmatic eruption	3b	Mafic	lava flow	short	Guillou et al. (1996)
16	80 000 ± 40 000 (BP)	magmatic	magmatic eruption	3a	Felsic	lava flow	medium-large	Fúster et al. (1993)
17	86 600 ± 8300 (BP)	magmatic	magmatic eruption	1a	Mafic	lava flow	short	Longpré et al. (2011)
18	94 500 ± 12 600 (BP)	magmatic	magmatic eruption	4a	Mafic	lava flow	short	Longpré et al. (2011)
19	115 300 ± 6900 (BP)	magmatic	magmatic eruption	4a	Mafic	lava flow	short	Longpré et al. (2011)
20	126 000	magmatic	magmatic eruption	5	Mafic	lava flow	short	Klügel et al. (2011)
21	133 000 ± 200	magmatic	magmatic eruption	5	Felsic	lava flow	short	Van der Bogard (2013)
22	134 000 (BP)	magmatic	magmatic eruption	3a	Mafic	lava flow	short	Szérémeta et al. (1999)
23	142 000 ± 2000 (BP)	magmatic	magmatic eruption	5	Felsic	lava flow	short	Van der Bogard (2013)
24	145 000 ± 4000 (BP)	magmatic	magmatic eruption	3b	Mafic	lava flow	short	Guillou et al. (1996)
25	158 000 ± 4000 (BP)	magmatic	magmatic eruption	3a	Mafic	lava flow	short	Guillou et al. (1996)

4.8 Input data for HASSET

4.8.1 Node 1: unrest

This node estimates the temporal probability of a reawakening of the system in the next time window by examining the number of past, non-overlapping, equal-length time windows that encompass an episode of unrest. Implicitly, this node estimates the recurrence time with a Bayesian approach that does not use the time series. It did not take into account the repose period between eruptions or the possible non-stationary nature of the data. However, Sobradelo et al. (2011) used extreme value theory to study the historical recurrence of monogenetic volcanism on the Canary Islands since the first written records appeared at the beginning of the 15th century. By modelling the inter-period times with a non-homogeneous generalised Pareto–Poisson distribution, this study estimated as of 2010 that the probability of an eruption of a magnitude > 2 anywhere on the Canary Islands in the next 20 years was 0.97 ± 0.00024 .

In order to compute the probability of having (at least) an unrest episode in the next 20 years, we need two pieces of information: (1) our starting beliefs or weights for each possibility (yes, no) and (2) the number of past events during the period of study. As per the number of past events, it shows that in the last 600 years (historical period), there have been two episodes of unrest identified at El Hierro (a seismic unrest and the latest magmatic unrest in 2011 which resulted in eruption). As per the starting weights for each option, if we did not have any information at all we would start with the state of total ignorance or total epistemic uncertainty, and give 50/50 chance to each option. However, this is not the case, as in the study of the volcanic recurrence for the Canary Islands as of 2010 (based on volcanic records from the islands of Tenerife, La Palma and Lanzarote) (Sobradelo et al., 2011), there is an estimated 97% probability of at least one eruption in the next 20 years, anywhere on the Canary Islands (including El Hierro). Therefore, rather than starting with a 50/50 chance, this study allowed us to assign our a priori beliefs for the “unrest” node in the island of El Hierro (yes = 97, no = 3), and then we used the 2 historical episodes of unrest documented in El Hierro to update those initial beliefs.

The reason why we used the 2 historical events in the catalogue of El Hierro, and not the remaining 23 pre-historical events, was to avoid misleading results in the probability of unrest. If we had used the entire catalogue we would have said to the

model that there was on average 1 eruption every 7900 years (158 000/20), which is not realistic, as the catalogue is incomplete. For that reason we updated our prior beliefs with the historical part of the catalogue that we were most confident with. Given our confidence in these results, we were able to assign an epistemic uncertainty of 50 to our data weights, which means that new evidence regarding intervals with non-eruptive behaviour will not significantly modify our prior assumptions. As shown by the posterior probabilities in column 6 of Table 4.2, despite 28 intervals out of 30 (600 years/20 estimated time intervals) with no unrest, the posterior probability of unrest in the next 20 years is still significantly large.

4.8.2 Node 2: origin

We considered four types of unrest that could occur on El Hierro: magmatic, geothermal, seismic and others. In spite of the predominant magmatic and seismic behaviour in past activity, we cannot exclude either geothermal activity or false unrest. In fact, hydromagmatic deposits exist in the interior of the island that were most probably associated with the presence of shallow aquifers. Some of these deposits also contain hydrothermally altered lithic clasts, which also suggest the existence of localised hydrothermal systems. Thus, it was impossible to rule out the possibility of geothermal unrest. False unrest can occur when non-volcanic signals are recorded together with volcanic signals. For example, changes in the gravity field, ground deformation or even seismicity unrelated to any volcanic activity could be associated with variations in the recharge and/or extraction of meteoric water into/from aquifers in El Hierro. Even so, we still believe that in monogenetic volcanism magmatic changes are the main source of unrest and so we gave the greatest weight to magmatic unrest (0.96) and split the rest evenly among the other options. The prior weights were assigned on the basis of a priori beliefs and so we allocated a value of 10 to the epistemic uncertainty since we still expect the majority of unrest to be of magmatic origin. However, it is still important to give more weight to new evidence.

4.8.3 Node 3: outcome

A study of global volcanic unrest in the 21st century (Phillipson et al., 2013) shows that 64 % of unrest episodes lead to eruptions. On the other hand, in light of previous

studies on El Hierro (Carracedo et al., 2001; Pedrazzi et al., 2014), we were unable to rule out the possibility that, aside from a magmatic eruption, a sector failure or a phreatic explosion might also follow on from an episode of unrest.

Therefore, we assigned a weight of 0.64 to the magmatic eruption and split the remaining 0.36 evenly between the alternative nodes. As these weights were assigned based on general studies and a priori beliefs that did not necessarily include data from El Hierro, we gave a value of 10 to the epistemic uncertainty. As with the previous node, we did not give a total epistemic uncertainty, as we still believe that the largest weight should be for the magmatic eruption branch; however, we still want new evidence to be able to contribute significantly to updating our prior weights. The two data points in our historical catalogue already include an episode of unrest that did not evolve into an eruption and so we should expect the prior weight of 0.12 assigned to the “No eruption” node to be substantially increased after the new evidence is entered in the model and the posterior probabilities are computed (Table 4.2, column 6).

4.8.4 Node 4: location

We divided the island into 5 zones and 11 subzones to be able to perform a volcanic hazard assessment of El Hierro based on the past geological information described above (Fig. 4.3). These five main zones were established according to the structural (susceptibility) and topographic characteristics of the island, whilst the subdivisions were made by taking into account the potential occurrence of hydrovolcanic episodes. Thus, subzones 1b–4b represent areas that could include the focus of and/or be affected by hydrovolcanic episodes caused by the interaction of seawater with the erupting magma. Given the data, regarding such episodes in the past geological record, we considered that the offshore zone between the bathymetric line of 200 m and the onshore area near the coast, which already includes several hydrovolcanic edifices, was suitable for the occurrence of such processes (Fig. 4.3). Moreover, subzones 3c and 4c in the interior of the island provide evidence of phreatomagmatic eruptions in the past.

The susceptibility analysis of the island, based on the study by Becerril et al. (2013) (Fig. 4.2), allowed us to assign the prior weights to each node with a high degree of confidence, as shown in Table 4.2. The reliability of the susceptibility map enables us to assign a data weight of 50 (since the prior weights were estimated

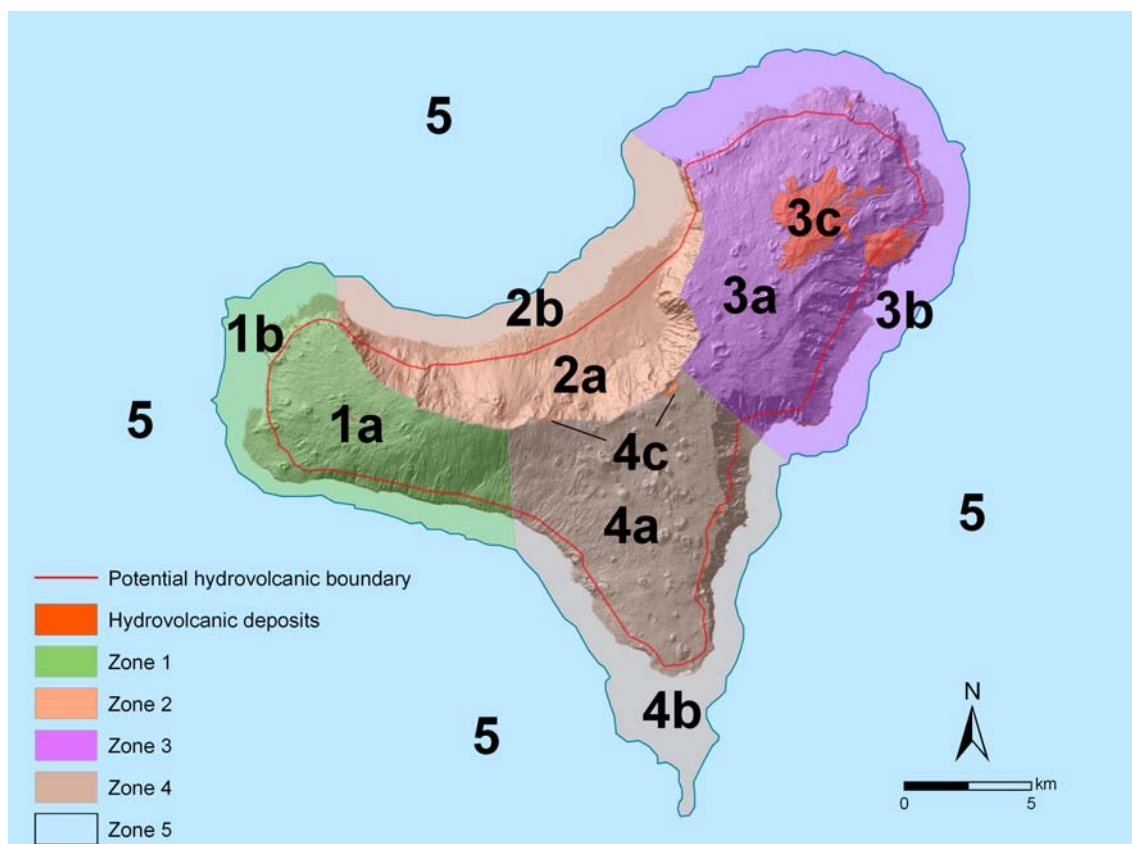


Figure 4.3: Sectors and subsectors defined on El Hierro. Sectors 1–4 show onshore division while sector 5 represents the offshore area. The division is based on differences in structural patterns, spatial probability of hosting new vents and expected hazards. Subsectors a–c take into account the potential occurrence of hydrovolcanic episodes

using past data from El Hierro) accounting for the uncertainties in the data catalogue. For this reason, we felt very confident in the initial distribution of the prior weights and any new evidence is likely to confirm them. Of the two historical events, one was in zone 5 (2011–2012 eruption). This unrest lasted 4 months before leading to an eruption which was fully monitored by the Instituto Geográfico Nacional (López et al., 2012). The other one refers to the 1793 seismic unrest whose location is uncertain, although historical documents describe it as being in the northwest submarine area, i.e. zone 5.

4.8.5 Node 5: composition

From the pre-historical set of 23 eruptions shown in Table 4.1, 87% correspond to mafic events and 13% to felsic events. As we were aware of the incompleteness

of the data catalogue, especially in the oldest part, we were not confident if this was indeed the proportion for the composition of prior weights. Some – or many – felsic eruptions may not be documented for example, the Malpaso member, a felsic explosive eruption, has been identified on the upper part of El Golfo–Las Playas volcano (Pedrazzi et al., 2014) but was not included in our catalogue because we lack a precise date. The prior weights are not random, as they are based on well-documented data. For this reason, we assigned an epistemic uncertainty of 10 to our data weights so that if new evidence arrives, these prior values are still accounted for (but more so if there is new evidence), thereby ensuring that any new data will contribute significantly to updating our prior beliefs.

4.8.6 Node 6: size

The erupted volume of magma on the Canary Islands typically ranges from 0.001–0.2 km³ (DRE) (Sobradelo et al., 2011). Due to a lack of accurate volume data, we assumed that volume values on El Hierro were of the same order as in most of the historical eruptions in the Canaries. The last eruption (2011–2012) was characterised by lava flows of medium extent with VEI 2 and so, by using this information, we were able to assign the weights for VEI 1, VEI 2 and VEI 3, as 0.31, 0.62 and 0.07, respectively.

In the particular case of El Hierro, we observed cases of hydrovolcanic episodes associated with PDC. This would imply VEI sizes that are greater than those on which these prior weights are estimated. Furthermore, the data documented in Sobradelo et al. (2011) is based on Magnitude size, as there was not enough information to estimate the corresponding VEI. For this reason and owing to the lack of magnitude information for the catalogue of eruptions on El Hierro, we were not confident of the prior weights assigned and so an epistemic uncertainty value of 1 was the most appropriate, and would also ensure that if new evidence arrives for different sectors, it will contribute significantly to updating our prior knowledge. In this way, we gave more weight to the new evidence than to our prior beliefs.

4.8.7 Node 7: hazard

Based on past activity, possible eruption products include ballistic ejecta, fallout, PDCs and lava flows with the prior weights shown in Table 4.2, computed using

the 23 pre-historic eruptions in Table 4.1. Most mafic eruptions generated lava flows and proximal fallout. However, a revision of the deposits generated from past volcanic events also reveals that some eruptions located close to the coastline correspond to hydrovolcanic episodes generating PDC deposits. In a similar way, some of the hydrovolcanic deposits found on land near the coast in fact originated from very shallow submarine eruptions. Thus, there is reason to include in subzone b (Fig. 4.3) both coastal and offshore zones to a maximum depth of 200 m, based on the assumption that vents located in these subzones could generate hydrovolcanic phases and produce PDCs.

Of all the possible hazard products, we were confident that ballistic ejecta, fallout, PDCs and lava flows could occur and so we gave zero weight to the remaining options (lahar, debris avalanche and others). However, for the same reasons given for the composition weights (felsic vs. mafic), we assigned a value of 10 to the epistemic uncertainties, as these data weights could change if we had a more complete data catalogue; however, they are still not completely uninformative, as they are based on past records. In this way, we ensure that new evidence will be well accounted for in new updates and that prior weights are not fully dropped when this new evidence arrives.

4.8.8 Node 8: extent

Extent refers to the distance reached by eruption products (lava flows, ballistic ejecta, fallout and PDCs) from eruption points that can be deduced from the geological record. The extent of products from the eruptions documented on El Hierro is comparable to those on the rest of the Canary Islands. We considered small distances for those short lava flows that reach up to 5 km, medium distances (5–15 km) for PDC deposits, ballistics and lava flows that reach the sea, and large extent mainly for fall out deposits that can expand more than 15 km. As with the previous node, on the basis of data from the oldest eruptions (Table 4.1), 87% of extents are small, while 9% are medium and 4% large. We assigned a positive weight to a scenario that gives rise to a large extent of products that will account for the potentially more explosive eruptions seen in the geological record that relate to felsic eruptions or even hydromagmatic eruptions. For the same reasons given for the previous node, we assigned an epistemic value of 10 to all branches.

Table 4.2: Input data for HASSET (columns 1 to 5) and output probability vectors and standard deviations (columns 6 and 7). Prior weights and data weights are estimated using pre-historical data, a priori beliefs and published studies on global volcanic unrest during the last century. Past data are based on the eruptions recorded in the last 600 years, considered as the historical period for the Canary Islands

Node name	Event	Past data	Prior weight	Data weight	Probability estimate	Standard deviation
Unrest	Yes	2	0.97	50	0.64	0.07
Unrest	No	28	0.03	50	0.36	0.07
Origin	Magmatic	1	0.94	10	0.88	0.09
Origin	Geothermal	0	0.02	10	0.02	0.03
Origin	Seismic	1	0.02	10	0.08	0.07
Origin	Other	0	0.02	10	0.02	0.03
Outcome	Magmatic erupt	1	0.64	10	0.62	0.13
Outcome	Sector failure	0	0.12	10	0.10	0.08
Outcome	Phreatic explos	0	0.12	10	0.10	0.08
Outcome	No eruption	1	0.12	10	0.17	0.10
Location	Zone 1	1	0.16	50	0.17	0.05
Location	Zone 2	0	0.07	50	0.07	0.03
Location	Zone 3	0	0.29	50	0.28	0.06
Location	Zone 4	0	0.16	50	0.15	0.05
Location	Zone 5	1	0.32	50	0.33	0.06
Composition	Mafic	1	0.87	10	0.88	0.09
Composition	Felsic	0	0.13	10	0.12	0.09
Size	VEI 1–	0	0.31	1	0.25	0.19
Size	VEI 2	1	0.62	1	0.70	0.21
Size	VEI 3+	0	0.07	1	0.06	0.10
Size	n.a.	0	0	0	0.00	0.00
Hazard	Ballistic	1	0.12	10	0.15	0.09
Hazard	Fallout	1	0.05	10	0.09	0.07
Hazard	PDC	0	0.03	10	0.03	0.04
Hazard	Lava flow	1	0.8	10	0.73	0.11
Hazard	Lahars	0	0	0	0.00	0.00
Hazard	Debris avalan	0	0	0	0.00	0.00
Hazard	Other	0	0	0	0.00	0.00
Extent	Short	0	0.87	10	0.80	0.11
Extent	Medium	1	0.09	10	0.16	0.10
Extent	Large	0	0.04	10	0.04	0.05

4.9 Results

Columns 6 and 7 in Table 4.2 show the output from HASSET. Although we started with 28 time windows with no unrest, the posterior probability of unrest in the next 20 years is significantly large (64 %; 36 % for no unrest), due to the high value of the data weight. The same effect occurs with the node location, in which the posterior probabilities remain in the same proportion as the prior weights. The episode of seismic unrest in 1793 has updated our prior beliefs from 2 to 8 %, given that we assigned low confidence levels to the initial values. In general, comparing columns 4 and 6 in Table 4.2, we can see how past data can significantly change the prior probabilities for which we assumed low confidence (10 or less – large epistemic uncertainty), while prior weights assigned with high confidence remain consistent after new evidence is entered in the model.

Looking at the different scenarios (as a combination of the first nodes and branches up to node location) (Table 4.3a), we see that the 5 most likely scenarios are a basaltic eruption with magmatic unrest in zones 5, 3, 1, 4 and 2 (in that order) with probabilities of occurrence over the next 20 years of 0.11 ± 0.04 , 0.10 ± 0.03 , 0.06 ± 0.02 , 0.05 ± 0.02 and 0.02 ± 0.01 , respectively, for any VEI and any type of hazard or extent. However, although some of these estimates have a large standard deviation due to sizeable uncertainties in the input data, they are consistent with observations from the past. Thus, using the information in the data catalogue, we estimated the long-term probability of a basaltic eruption with magmatic unrest in zone 5 (submarine area) occurring in the next 20 years to be 0.11 ± 0.04 .

If we now look at the most likely scenarios that also include size, hazard and the extent of the eruption, the five next most likely scenarios are basaltic eruptions of VEI 2 with magmatic unrest that generate short lava flows. However, in this case zone 2 is no longer among the 5 most likely scenarios and an eruption in zone 5 with a VEI of 1 or less becomes the fifth most likely to occur in the next 20 years (probability of 0.01 ± 0.01). Once again, the standard deviation for these estimates is large, implying that the variability due to uncertainties in the input data is also large. In this case, we estimated that the most probable scenario (0.04 ± 0.02) is a submarine (zone 5) mafic magmatic eruption of VEI 2 generating short lava flows.

Table 4.3: (a) Most likely scenarios for node location. (b) Most likely scenarios for node extent

Scenario	Probability estimate	Standard deviation
(a)		
1. Yes-magmatic-magmatic eruption-Zone 5	0.11	0.04
2. Yes-magmatic-magmatic eruption-Zone 3	0.10	0.03
3. Yes-magmatic-magmatic eruption-Zone 1	0.06	0.02
4. Yes-magmatic-magmatic eruption-Zone 4	0.05	0.02
5. Yes-magmatic-magmatic eruption-Zone 2	0.02	0.01
(b)		
1. Basaltic eruption with magmatic unrest in zone 5, VEI 2, that generates lava flows of short extent	0.04	0.02
2. Basaltic eruption with magmatic unrest in zone 3, VEI 2, that generates lava flows of short extent	0.04	0.02
3. Basaltic eruption with magmatic unrest in zone 1, VEI 2, that generates lava flows of short extent	0.02	0.01
4. Basaltic eruption with magmatic unrest in zone 4, VEI 2, that generates lava flows of short extent	0.02	0.01
5. Basaltic eruption with magmatic unrest in zone 5, VEI ≤ 1 , that generates lava flows of short extent	0.01	0.01

4.10 Eruptive scenarios

Hazard assessment must be based on the simulation of different volcanic processes across the susceptibility map (e.g. Martí et al., 2012). In order to illustrate potential future eruptions on El Hierro, we simulated scenarios assuming the results obtained with HASSET and considering the most probable hazards (i.e. lava flows, fallout and PDCs) that could occur in the event of such eruptions. We mainly considered eruptions that occur on land or in shallow submarine environments (at a depth of less than 200 m) (Fig. 4.3). We did not consider deeper submarine eruptions even though their socio-economic impact may in fact not be negligible, as seen in the 2011–2012 eruption. However, we assumed that the direct impact of hazards caused by these deeper submarine eruptions on the island was not relevant for the purpose of this study.

For the simulations we used light detection and ranging (LIDAR) technology based on the digital elevation model (DEM) of the island with a cell size of 10 m generated by the National Geographic Institute (IGN).

4.11 Lava flow scenarios

Bearing in mind the previously obtained susceptibility values (Fig. 4.2) (Becerril et al., 2013), we simulated lava flow scenarios taking into account only those pixels located on land (lava flows generated in submarine eruptions, even in shallow waters, were assumed not to cause any direct impact on the island). Lava flow simulations based on VORIS 2.0.1 rely on a probabilistic model that assumes that topography is the most important factor in determining the path of a lava flow (Felpeto et al., 2007 and references therein). As explained before, simulations of lava flows were conducted on land and are based on the pixels that lie on the different spatial probability values ranging from 0.00037 to 0.0068.

In the model, the input parameters for the lava flows were constrained by maximum flow lengths and thicknesses taken from field measurements. Considering that most lava flows in the past reached the sea, we assumed flow lengths of about 15 km. The thickness used as input for the models was 3 m, which was obtained from the average value of individual flows measured in the field. The results provide a map that gives the probability that any particular cell is invaded by a lava flow (Fig. 4.4).

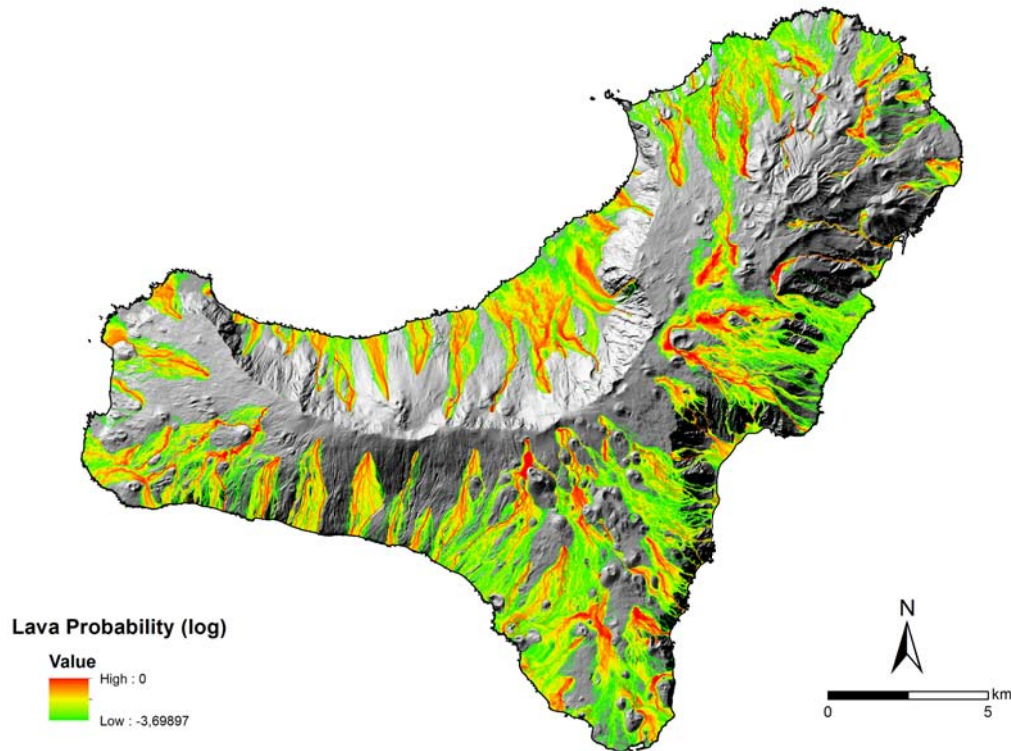


Figure 4.4: Lava flow scenarios for El Hierro performed with VORIS 2.0.1. Vents from lava flows that have been simulated represent those with the highest spatial probabilities (see susceptibility map in Fig. 2). Red colours are those areas with the highest probability to be invaded by lava flows

4.12 Scenarios for pyroclastic density currents (PDCs)

The pyroclastic density currents (PDCs) identified on El Hierro are all associated with hydrovolcanic episodes and mostly relate to mafic vents located in the coastal zone, or episodes occurring at shallow submarine depths that generated deposits that are now exposed along the coast. However, we also considered the possibility that this type of explosive episode could occur on land with more evolved compositions and larger run-out distances, as is the case of the Malpaso member identified in the centre of the island (Pedrazzi et al., 2014). PDCs were simulated with an energy cone model (Sheridan and Malin, 1983) using as input parameters topography, the collapse equivalent height (H) and the collapse equivalent angle (θ), which is obtained through the arctangent of the ratio between H_c and L , where L represents

the run-out length (Felpeto et al., 2007; Toyos et al., 2007). Run-out distances were considered to be equivalent to the most distal exposure of PDC deposits found on the island, which were calculated to have lengths of 5, 1 and 0.5 km. These distances are relative to the most distal deposits of the studied PDCs.

Collapse equivalent heights were chosen in the range of 250–300 m above the possible vent site in order to constrain the best Hc that matches real deposits. Based on the calibration, a collapse equivalent of 250 and an angle of 11° were determined for a pyroclastic flow deposit, resembling the known Malpaso member felsic flow deposit. For those vents located in the coastal zone or associated with mafic eruptions, we simulated PDCs with a collapse equivalent of 250 m and angles in the range of around 4–27° (low values for base surge explosions and high values for column collapse phases) (Sheridan and Malin, 1983). Although the topography of the area has been modified since the eruption of the Malpaso member, the area and extent of the simulated deposits were still similar to the real PDC deposit. With these constraints, PDC simulations were carried out in the areas with the highest spatial probabilities (Fig. 4.5a). The areas close to the PDC deposits of El Hierro were also selected to simulate scenarios (Fig. 4.5b). Figure 4.5a and b show coverage areas with different Heim coefficients and VEI values.

4.13 Fallout

Fallout from the eruptions on El Hierro was simulated by assuming a violent Strombolian eruption (e.g. Tanganasoga eruption, Fig. 4.1), characterised by the formation of an eruptive column up to 10 km high (Arrighi et al., 2001), having significant impacts over distances of several tens of kilometres from the vent (Valentine and Gregg, 2008), which would represent one of the most probable high intensity eruptions that could occur on the island. Nevertheless, we do not rule out the possibility of a subplinian eruption, characterised by columns ranging between 10 and 20 km altitude, having potential impacts over much larger regions and even globally (Valentine and Gregg, 2008 and references therein) in the event that more felsic magmas are involved in the process. Simulations were conducted using an advection-diffusion model based on the assumption that particle motion is controlled by advection from wind, particle diffusion and their terminal settling velocity (Pfeiffer et al., 2005; Felpeto et al., 2007). All the simulations were conducted with one vent located in

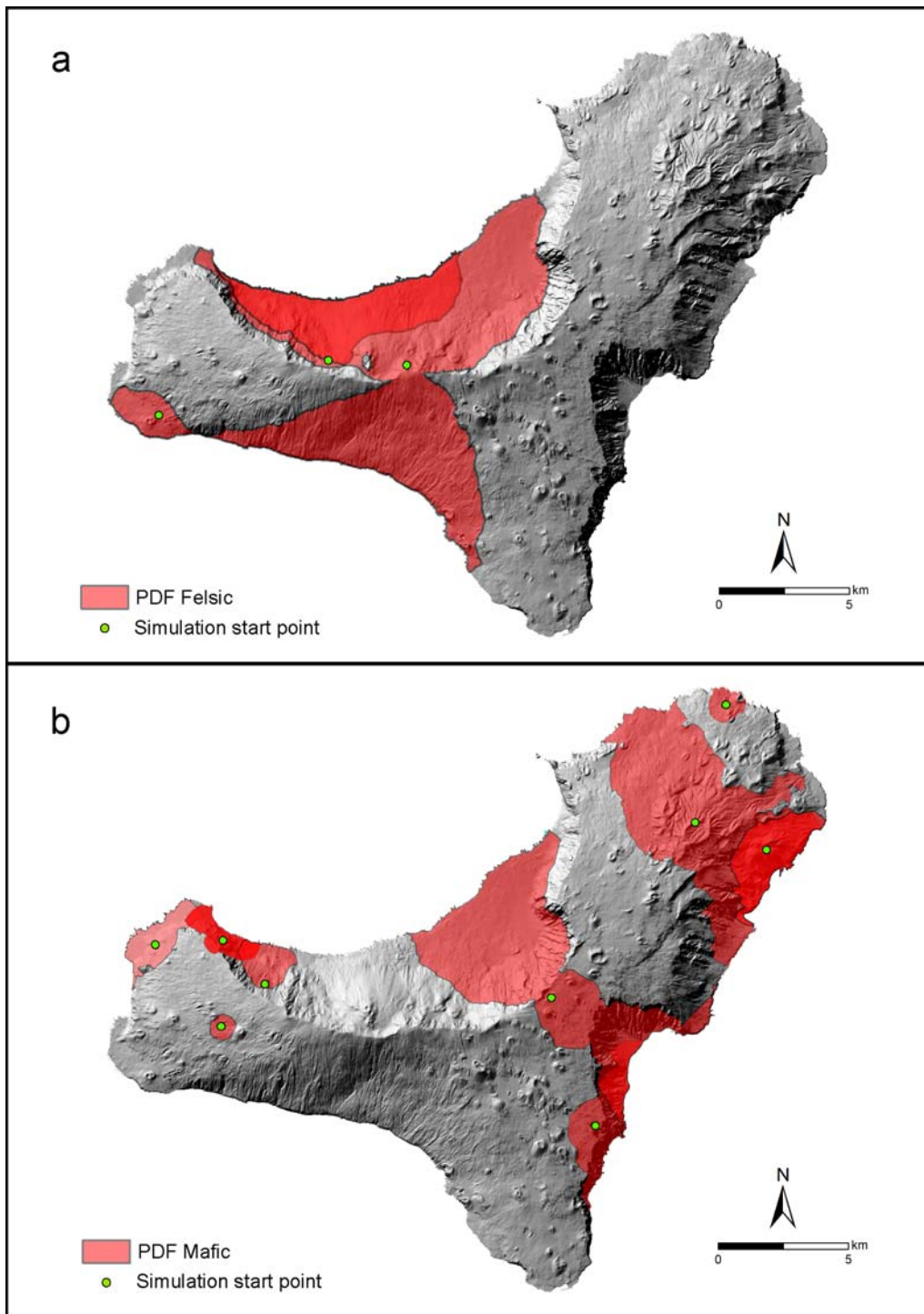


Figure 4.5: PDC scenarios performed with VORIS 2.0.1. Covered areas with different collapse equivalent heights (H_c), collapse equivalent angles (θ) and VEI values (see the text for more detail). (a) VEI 2 corresponding to felsic eruptions; (b) VEI 1 corresponding to mafic eruptions

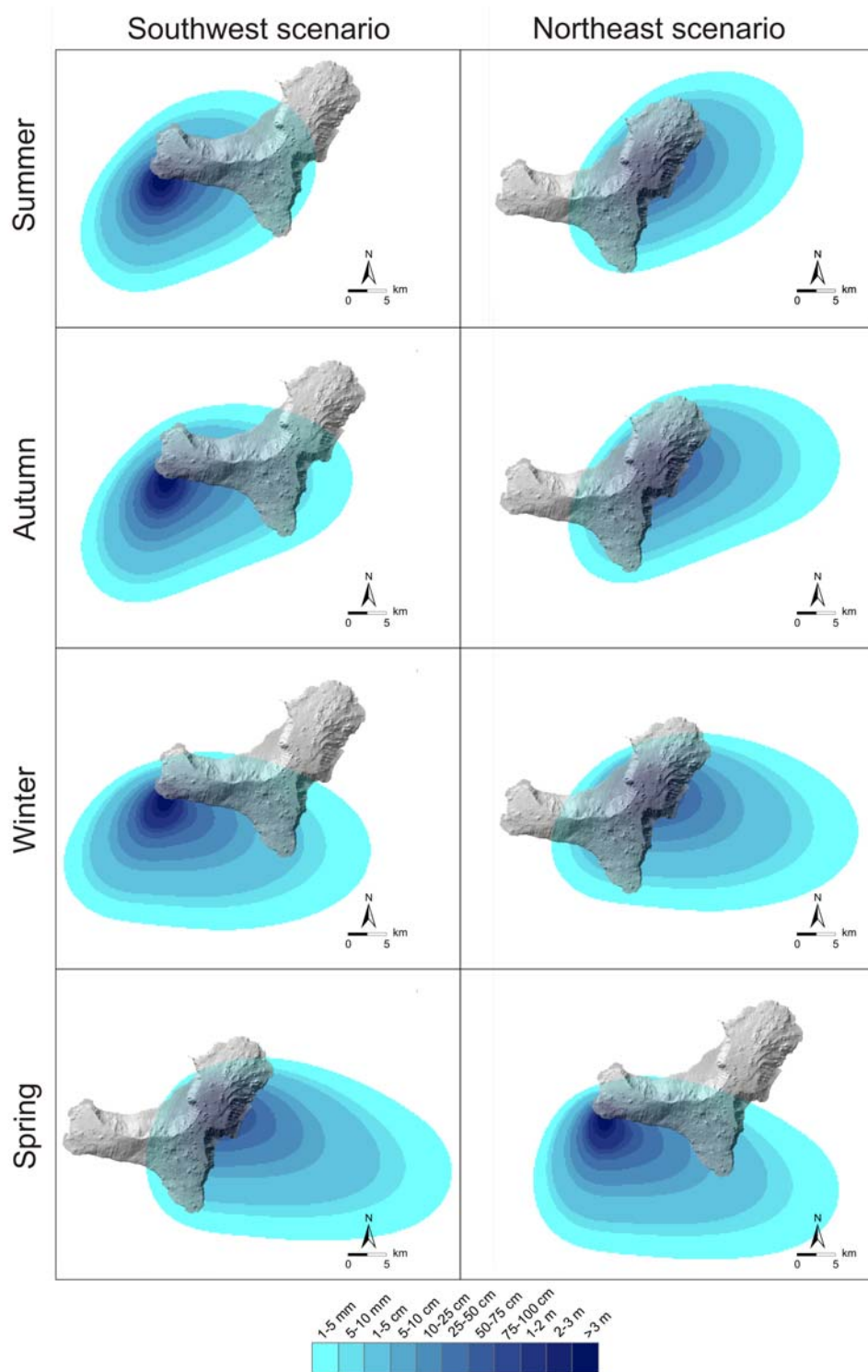


Figure 4.6: Ashfall scenarios from a violent Strombolian eruption performed with VORIS 2.0.1. (1) Simulation at the highest probability vent; (2) simulation at an area close the main areas of population. Both simulations were performed for summer, autumn, winter and spring

the highest spatial probability area and another on the eastern side of the island, the most vulnerable area for a volcanic event and where the main villages, airport and port are situated.

Data inputs of wind profiles were compiled from the University of Wyoming Department of Atmospheric Science sounding database (<http://weather.uwyo.edu/upperair/sounding.html>). We focused the attention of our study on the fallout scenarios for the average wind value of each season during the last decade. Wind direction and intensity were chosen at different vertical heights (500, 1000, 2000, 4000 and 6000 m).

Input parameters for the simulation were obtained from fieldwork and bibliographic data. Results are shown in Fig. 4.6, with particle distribution in a 5 km high eruptive column related to a violent Strombolian eruption, generating 0.03 km³ of deposits. Particle sizes were considered in a range from -6 to 2Φ , thereby covering the entire range of particle sizes observed in the field.

4.14 Total hazard map

Combination of the most probable scenarios related to basaltic eruptions of VEI 2 that generate lava flows, fallout and PDCs in case of hydrovolcanic events, provided the first total qualitative volcanic hazard map of El Hierro (Fig. 4.7b). The most probable areas to be affected by the three most likely scenarios were used to define the areas with the greatest and lowest overall volcanic hazard (Fig. 4.7b). This is an approach similar to that taken by Lindsay et al. (2005) in the Lesser Antilles. We distinguished four levels of hazard depending on the number of individual hazards (Fig. 4.7a) that overlap on each point (pixel) of the map. The superposition was done taking into account the spatial probability and the extension of each scenario, given more weight to the most probable scenario, i.e. lava flows originating from areas with high spatial vent opening probability. The resulting map shows that, although El Hierro is not a highly populated island, some medium- and high-volcanic-hazard zones coincide with some of the main inhabited areas. However, it must be noted that this hazard level delineation is reliant on the current information, which may be subject to further revision thus implying possible changes in the hazard assessment.

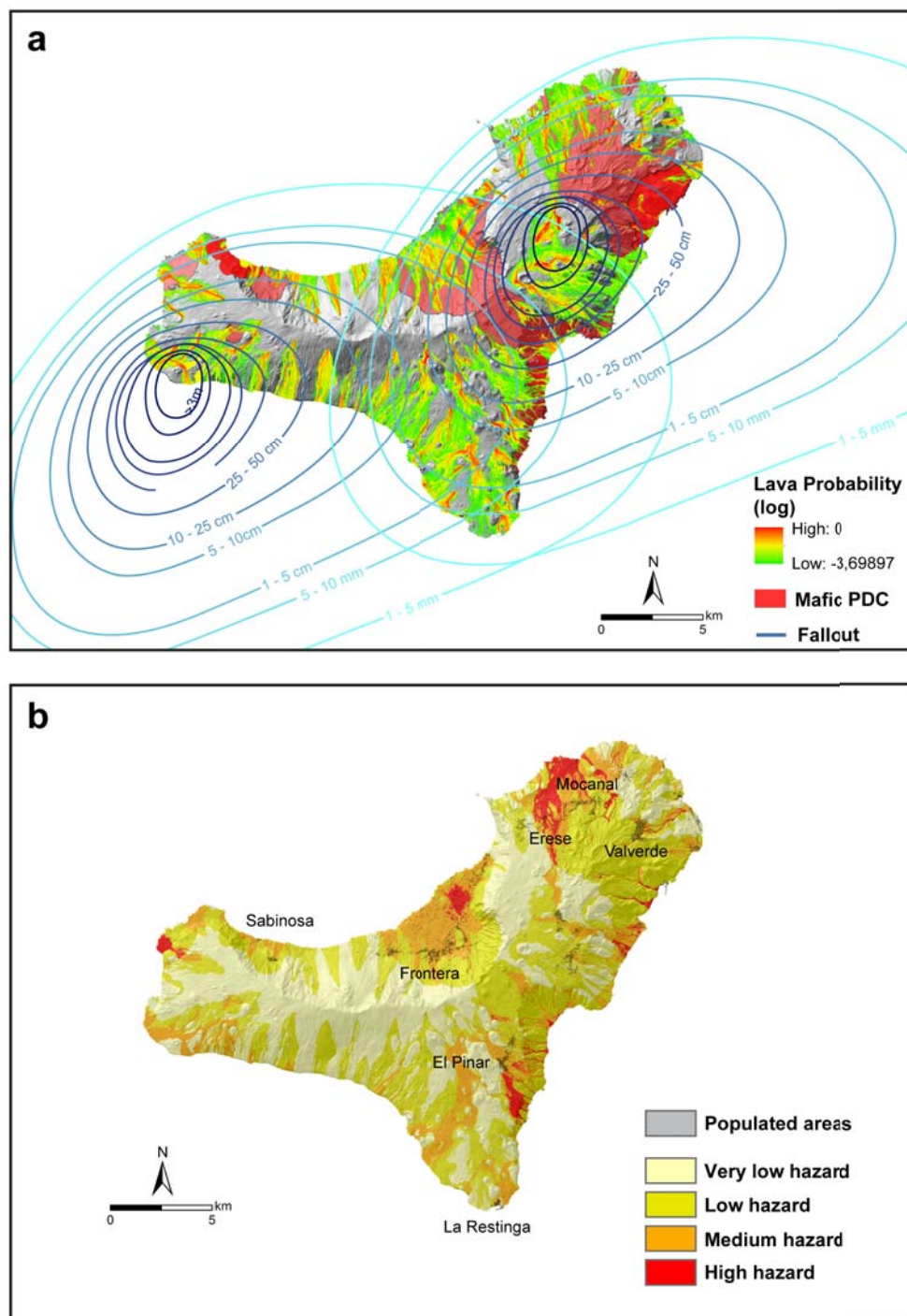


Figure 4.7: (a) Superposition of the most probable scenarios; (b) qualitative hazard map of El Hierro (zones 1–4) constructed from the combination of the most likely scenarios. This map shows the overall integrated volcanic hazard zones for El Hierro based on lava flows, PDCs and ashfall scenarios. We distinguish four levels of hazard, from very low to high hazard, depending on the number of individual hazards that overlap on each point (pixel) of the map (see text for more explanation)

4.15 Discussion and conclusions

Mafic monogenetic eruptions (Table 4.1) are the most common eruption type to have occurred in El Hierro's recent geological past, especially over the last 158 ka (Pellicer, 1977, 1979). Consequently, we assume that they also represent the most likely eruption types in the near future. These eruptions generated small-size cones, lava flows, proximal scoria, fallout and, occasionally, PDCs. The size of most of these eruptions ranged from typical Strombolian to violent Strombolian (some of them associated with hydrovolcanic phases). In Fig. 4.7a the most likely expected scenarios on the island are represented together. The presence of a relatively recent eruption of phonolitic composition of medium size called Malpaso member and described as a PDC (Pedrazzi et al., 2014) is also remarkable, as it opens up the possibility that eruptions other than monogenetic magmatic and/or hydrovolcanic mafic ones may also occur on El Hierro. Although associated with much greater hazard intensities, this type of eruption has a much lower probability of occurrence.

The catalogue of eruptions that have occurred on El Hierro in the last 158 ka is far from complete. This is evident when trying to establish the relative stratigraphy of volcanic deposits, as there are a large number of units of known origin intercalated between the reported units. Although the establishment of a complete volcano-stratigraphy of El Hierro (and, in particular, of its last constructive episode) is still required, the available number of reported eruptions (for which the corresponding geochronology based on radiometric dating exists) is large enough to provide a preliminary volcanic hazard assessment with a sufficient degree of confidence.

The application of available tools such as HASSET (Sobradelo et al., 2014a) and VORIS 2.0.1 (Felpeto et al., 2007), specifically designed to undertake volcanic hazard assessment based on current knowledge of past eruptive activity and using probabilistic methods and simulation models, allows us to obtain an initial long-term hazard assessment, which can be easily updated and improved with the incorporation of new information such as a more complete volcano-stratigraphy and geochronology. This is an essential tool that should enable local authorities to apply more rational territorial planning and to design more adequate emergency plans to face future volcanic crises. The experience gained from the last eruption on El Hierro in 2011–2012 showed that the lack of tools such as the one described in the present study can lead scientific advisors and decision-makers to consider possible eruptive scenarios

that have a very low probability of occurrence, whilst ignoring others with a high probability of occurrence – for example, the submarine eruption that in the end turned out to be the true scenario. This lack of any systematic study of past eruptive activity hampered the forecasting of the most probable scenarios and led to a certain confusion regarding the potential outcome of the impending eruption. This in turn affected the way in which information was transmitted to the population and to the scale of the decisions made, some of which were unnecessarily over-protective (Sobradelo et al., 2014b).

The advantage of conducting a probabilistic hazard assessment is that the results obtained can be updated whenever new information becomes available. Such an approach permits work to start even when only a little information exists and then enables results to improve over time. Thus, appropriate mitigation policies can be based on less, but more precise and realistic information. In the case of El Hierro, despite sufficient knowledge of past eruptive activity, the available information was not structured in a comprehensive way that was easy to manage and be used by decision-makers or even by the scientists who were providing advice. The results obtained in the present study, that is, the development of a probabilistic long-term volcanic hazard assessment that includes dynamic scenarios and a qualitative hazard map (Fig. 4.7a and b), offer basis on which to build the strategies that are required to successfully face up to and minimise the impact of future volcanic eruptions on the island.

Our approach offers a method that facilitates accomplishing volcanic hazard assessment in a homogeneous and systematic way. The approach is based on the history of the volcano being deduced from the geological record, which allows determining how, where, and when the next eruption could be. Similar approaches have been applied in other volcanic areas where the application of available tools similar to ours have also allowed us to obtain an initial long-term hazard assessment. This is the case of Auckland Volcanic Field in New Zealand (Sandri et al., 2012) or Misti volcano in Peru (Sandri et al., 2014), where a Bayesian approach using BET_VH tool (Marzocchi et al., 2010) and other simulation tools are applied to compute the temporal and spatial probabilities. Our methodology uses different free tools that have been developed to contribute to the long-term hazard assessment, both in spatial (VORIS 2.0.1, Felpeto et al., 2007) and temporal analyses (HASSET, Sobradelo et al., 2014a). The main advantage of using VORIS 2.0.1 is that it

creates scenarios of different kind of hazards such as lava flows, PDCs and ashfall. Other works have focused on the simulation of only one scenario using non-free tools (e.g. lava flows for Etna volcano: Cappello et al., 2010, 2011; Tarquini and Favalli, 2010). On the other hand, although some parts of the HASSET tool (that evaluate temporal probabilities) coincide with BET_EF and BET_VH tools presented by Marzocchi et al. (2008, 2010), HASSET is built on a Quantum Gis (QGIS) platform and considers different kinds of unrest episodes (seismic, geothermal, others), and moreover takes into account the kind of outcome (e.g. phreatic explosion and sector failure) and the magma composition, overcoming the limitations of previous event tree models (Sobradelo et al., 2014a). Another important advantage of using these tools is that new data or new model results can be easily included in the procedure to update the hazard assessment. Other works focused on the evaluation of the potential hazards related to a specific kind of hazard of a particular area (e.g. phreatomagmatic volcanic hazards; Németh and Cronin, 2011) could take the advantages of our methodology and implement it in an easy and successful way for future and completeness of volcanic hazard evaluation.

Acknowledgments

This research was partially funded by IGME, CSIC and the European Commission (FT7 Theme: ENV.2011.1.3.3-1; Grant 282759: “VUELCO”), and MINECO grant CGL2011-16144-E. We would like to thank X. Bolós and J. P. Galve for their help in the development of figures. We also want to thank J. Lindlay and K. Németh for their very useful suggestions that have enabled us to significantly improve our manuscript. The English text was corrected by Michael Lockwood.

References

Alcorn, R., Panter, K. S., and Gorsevski, P. V.: A GIS-based volcanic hazard and risk assessment of eruptions sourced within Valles Caldera, New Mexico, *J. Volcanol. Geoth. Res.*, 267, 1–14, 2013.

Anguita, F. and Hernán, F.: A propagating fracture model versus a hot spot origin for the Canary Islands, *Earth Planet. Sc. Lett.*, 27, 11–19, 1975.

Anguita, F. and Hernán, F.: The Canary Islands origin: a unifying model, *J. Volcanol. Geoth. Res.*, 103, 1–26, 2000.

Araña, V. and Ortiz, R.: The Canary Islands: Tectonics, magmatism, and geodynamic framework, in: *Magmatism in Extensional Structural Settings and the Phanerozoic African Plate*, edited by: Kampunzu, A. and Lubala, R., Springer, New York, 209–249, 1991.

Araña, V., Felpeto, A., Astiz, M., García, A., Ortiz, R., and Abella, R.: Zonation of the main volcanic hazards (lava flows and ash fall) in Tenerife, Canary Islands. A proposal for a surveillance network, *J. Volcanol. Geoth. Res.*, 103, 377–391, 2000.

Arrighi, S., Principe, C., and Rosi, M.: Violent Strombolian and subplinian eruptions at Vesuvius during post-1631 activity, *Bull. Volcanol.*, 63, 126–150, 2001.

Balcells, R. and Gómez, J. A.: *Memorias y mapas geológicos del Plan MAGNA a escala 1 : 25.000 de las Hojas correspondientes a la isla de El Hierro*, Geol. Surv. of Spain, Madrid, 1997.

Bartolini, S., Cappello, A., Martí, J., and Del Negro, C.: QVAST: a new Quantum GIS plugin for estimating volcanic susceptibility, *Nat. Hazards Earth Syst. Sci.*, 13, 3031–3042, doi: 10.5194/nhess-13-3031-2013, 2013.

Bebbington, M. and Cronin, S. J.: Spatio-temporal hazard estimation in the Auckland Volcanic Field, New Zealand, with a new event-order model, *Bull. Volcanol.*, 73, 55–72, 2011.

Becerril, L.: Approach to volcanic hazard and its effects in coastal areas of the Canary Islands, Master's thesis, Universidad de Las Palmas de Gran Canaria, Las Palmas, Spain, available on line at: <http://hdl.handle.net/10553/4595>, 2009.

Becerril, L., Cappello, A., Galindo, I., Neri, M., and Del Negro, C.: Spatial probability distribution of future volcanic eruptions at El Hierro Island (Canary Islands, Spain), *J. Volcanol. Geoth. Res.*, 257, 21–30, doi:10.1016/j.jvolgeores.2013.03.005, 2013.

Bolós, X., Planagumà, L., and Martí, J.: Volcanic stratigraphy of the Quaternary La Garrotxa Volcanic Field (NE Iberian Peninsula), *J. Quaternary. Sci.*, in press, 2014.

Cappello A., Del Negro C. and Vicari A.: Lava flow susceptibility map of Mt Etna based on numerical simulations, in: *From Physics to Control through an Emergent View*, World Sci. Ser. Nonlin. Sci. B, 5, 201–206, 2010.

Cappello, A., Vicari, A. M., and Del Negro, C.: Assessment and modeling of

lava flow hazard on Mt. Etna volcano, *B. Geofis. Teor. Appl.*, 52, 299–308, 2011.

Cappello, A., Neri, M., Acocella, V., Gallo, G., Vicari, A., and Del Negro, C.: Spatial vent opening probability map of Mt Etna volcano (Sicily, Italy), *Bull. Volcanol.*, 74, 2083–2094, 2012.

Cappello, A., Bilotta, G., Neri, M., and Del Negro, C.: Probabilistic modeling of future volcanic eruptions at Mount Etna, *J. Geophys. Res.*, 118, 1925–1935, doi:10.1002/jgrb.50190, 2013.

Carracedo, J. C., Day, S., Guillou, H., Rodríguez Badiola, E., Canas, J. A., and Pérez-Torrado, F. J.: Hotspot volcanism close to a passive continental margin: the Canary Islands, *Geol. Mag.*, 135, 591–604, 1998.

Carracedo, J. C., Rodríguez Badiola, E., Guillou, H., de La Nuez, H. J., and Pérez Torrado, F. J.: Geology and Volcanology of the Western Canaries: La Palma and El Hierro, *Estud. Geol.* 57, 171–295, 2001.

Carracedo, J. C., Guillou, H., Paterne, M., Scaillet, S., Rodríguez Badiola, E., Paris, R., Pérez Torrado, F. J., and Hansen Machín, A.: Análisis del riesgo volcánico asociado al flujo de lavas en Tenerife (Islas Canarias): escenarios previsibles para una futura erupción en la isla, *Estud. Geol.*, 60, 63–93, 2004a.

Carracedo, J. C., Guillou, H., Paterne, M., Scaillet, S., Rodríguez Badiola, E., Paris, R., Pérez Torrado, F. J., and Hansen, A.: Avance de un mapa de peligrosidad volcánica de Tenerife (escenarios previsibles para una futura erupción en la isla), Servicio de Publicaciones de la Caja General de Ahorros de Canarias (CajaCanarias), Tenerife, 46 pp., 2004b.

Carracedo, J. C., Pérez Torrado, F. J., Rodríguez Badiola, E., Hansen, A., Paris, R., Guillou, H., and Scaillet, S.: Análisis de los riesgos geológicos en el Archipiélago Canario: Origen, características, probabilidades y tratamiento, *Anuario de Estudios Atlánticos*, 51, 513–574, 2005.

Chester, D. K., Dikken, C. J. L., and Duncanc, A. M.: Volcanic hazard assessment in western Europe, *J. Volcanol. Geoth. Res.*, 115, 411–435, 2002.

Connor, C. B. and Connor, L. J.: Estimating spatial density with kernel methods, in: *Volcanic and Tectonic Hazard Assessment for Nuclear Facilities*, edited by: Connor, C. B., Chapman, N. A., Connor, L. J., Cambridge University Press, 346–368, 2009.

Crisci, G. M., Iovine, G., Di Gregorio, S., and Lupiano, V.: Lava-flow hazard on the SE flank of Mt. Etna (Southern Italy), *J. Volcanol. Geoth. Res.*, 177, 778–796,

2008.

Felpeto, A.: Modelización física y simulación numérica de procesos eruptivos para la generación de mapas de peligrosidad volcánica, Ph.D. thesis, University of Madrid, Madrid, Spain, 250 pp., 2002.

Felpeto, A., Araña, V., Ortiz, R., Astiz, M., and García, A.: Assessment and modelling of lava flow hazard on Lanzarote (Canary Islands), *Nat. Hazards*, 23, 247–257, 2001.

Felpeto, A., Martí, J., and Ortiz, R.: Automatic GIS-based system for volcanic hazard assessment, *J. Volcanol. Geoth. Res.*, 166, 106–116, 2007.

Fournier d'Albe, E. M.: Objectives of volcanic monitoring and prediction, *J. Geol. Soc. Lond.*, 136, 321–326, 1979.

Fúster, J. M., Hernán, F., Cendrero, A., Coello, J., Cantangrel, J. M., Ancochea, E., and Ibarrola, E.: Geocronología de la isla de El Hierro (Islas Canarias), *Boletín de la Real Sociedad Española de Historia Natural, (Geología)*, 88, 86–97, 1993.

Gee, M. J. R., Masson, D. G., Watts, A. B., and Mitchell, N. C.: Offshore continuation of volcanic rift zones, El Hierro, Canary Islands, *J. Volcanol. Geoth. Res.*, 105, 107–119, doi:10.1016/S0377-0273(00)00241-9, 2001.

Gómez-Fernández, F.: Desarrollo de una Metodología para el Análisis del Riesgo Volcánico en el marco de un Sistema de Información Geográfica, Ph.D. thesis, University of Madrid, Madrid, Spain, 255 pp., 1996.

Guillou, H., Carracedo, J. C., Pérez-Torrado, F. J., and Rodríguez Badiola, E.: K-Ar ages and magnetic stratigraphy of a hotspot-induced, fast grown oceanic island: El Hierro, Canary Islands, *J. Volcanol. Geoth. Res.* 73, 141–155, 1996.

Hernández Pacheco, A.: Sobre una posible erupción en 1793 en la Isla del Hierro (Canarias), *Estud. Geol.*, 38, 15–25, 1982.

Hill, D. P., Dzurisin, D., Ellsworth, W. L., Endo, E. T., Galloway, D. L., Gerlach, T. M., Johnston, M. S. J., Langbein, J., McGee, K. A., Miller, C. D., Oppenheimer, D., and Sorey, M. L.: Response plan for volcano hazards in the Long Valley Caldera and Mono craters region California, *Bull. Geol. Surv.*, 65, 2185, 2001.

Hoernle, K. and Schmincke, H. U.: The role of partial melting in the 15 Ma geochemical evolution of Gran Canaria: a blob model for the Canary hotspot, *J. Petrol.*, 34, 599–626, 1993.

Hoernle, K., Zhang, Y. S., and Graham, D.: Seismic and geochemical evidence for large-scale mantle upwelling beneath the eastern Atlantic and western and central

Europe, *Nature*, 374, 34–39, 1995.

Kereszturi, G. and Németh, K.: Monogenetic Basaltic Volcanoes: Genetic Classification, Growth, Geomorphology and Degradation, in: *Updates in Volcanology – New Advances in Understanding Volcanic Systems*, edited by: Németh, K., InTech, 3–88, doi:10.5772/51387, 2012.

Kereszturi, G., Németh, K., Cronin, S. J., Agustín-Flores, J., Smith I. E. M., and Lindsay, J.: A model for calculating eruptive volumes for monogenetic volcanoes – Implication for the Quaternary Auckland Volcanic Field, New Zealand, *J. Volcanol. Geoth. Res.*, 266, 16–33, 2013.

Kilburn, C. R. J.: Multiscale fracturing as a key to forecasting volcanic eruptions, *J. Volcanol. Geoth. Res.*, 125, 271–289, 2003.

Klügel, A., Hansteen, T. H., van den Bogaard, P., Strauss, H., and Hauff, F.: Holocene fluid venting at an extinct Cretaceous seamount, Canary archipelago, *Geology*, 39, 855–858, 2011.

Le Bas, M. J., Rex, D. C., and Stillmann, C. J.: The early magmatic chronology of Fuerteventura, Canary Islands, *Geol. Mag.*, 123, 287–298, 1986.

Le-Pichon, X. and Fox, P. J.: Marginal offsets, fracture zones, and the early opening of the North Atlantic, *J. Geophys. Res.*, 76, 2156–2202, 1971.

Lindsay, J. M., Robertson, R., Shepherd, J., and Ali, S.: *Volcanic Hazard Atlas of the Lesser Antilles, Trinidad and Tobago*, The Seismic Research Unit, University of the West Indies, Trinidad and Tobago, 1–47, 2005.

Lirer, L., Petrosino, P., and Alberico, I.: Volcanic hazard assessment at volcanic fields: the Campi Flegrei case history, *J. Volcanol. Geoth. Res.*, 101, 55–75, 2001.

Longpré, M. A., Chadwick, J. P., Wijbrans, J., and Iping, R.: Age of the El Golfo debris avalanche, El Hierro (Canary Islands): New constraints from laser and furnace $^{40}\text{Ar}/^{39}\text{Ar}$ dating, *J. Volcanol. Geoth. Res.*, 203, 76–80, 2011.

López, C., Blanco, M. J., Abella, R., Brenes, B., Cabrera-Rodríguez, V. M., Casas, B., Domínguez-Cerdeña, I., Felpeto, A., Fernández de Villalta, M., Del Fresno, C., García, O., García-Arias, M. J., García-Canada, L., Gomis-Moreno, A., González-Alonso, E., Guzmán-Pérez, J., Iribarren, I., López-Díaz, R., Luengo-Oroz, N., Meletlidis, S., Moreno, M., Moure, D., Pereda de Pablo, J., Rodero, C., Romero, E., Sainz-Maza, S., Sentre-Domingo, M. A., Torres, P. A., Trigo, P., and Villasante-Marcos, M.: Monitoring the unrest of El Hierro (Canary Islands) before the onset of the 2011 Submarine Eruption, *Geophys. Res. Lett.*, 39, L13303,

doi:10.1029/2012GL051846, 2012.

Marinoni, L. B. and Pasquaré, G.: Tectonic evolution of the emergent part of a volcanic ocean island: Lanzarote, Canary Islands, *Tectonophysics*, 239, 111–137, doi:10.1016/0040-1951(94)90110-4, 1994.

Martí, J. and Felpeto, A.: Methodology for the computation of volcanic susceptibility. An example for mafic and felsic eruptions on Tenerife (Canary Islands), *J. Volcanol. Geoth. Res.* 195, 69–77, doi:10.1016/j.jvolgeores.2010.06.008, 2010.

Martí, J., Sobradelo, R., Felpeto, A., and García, O.: Eruptive scenarios of phonolitic volcanism at Teide-Pico Viejo volcanic complex (Tenerife, Canary Islands), *Bull. Volcanol.*, 74, 767–782, doi:10.1007/s00445-011-0569-6, 2012.

Martí, J., Pinel, V., López, C., Geyer, A., Abella, R., Tárraga, M., Blanco, M. J., Castro, A., and Rodríguez, C.: Causes and mechanisms of El Hierro submarine eruption (2011–2012) (Canary Islands), *J. Geophys. Res.*, 118, 1–17, 2013.

Martin, A. J., Umeda, K., Connor, C. B., Weller, J. N., Zhao, D., and Takahashi, M.: Modeling long-term volcanic hazards through Bayesian inference: an example from the Tohoku volcanic arc Japan, *J. Geophys. Res.*, 109, B10208, doi:10.1029/2004JB003201, 2004.

Marzocchi, W., Sandri, L., and Furlan, C.: A quantitative model for volcanic hazard assessment, in: *Statistics in Volcanology*, edited by: Mader, H. M., Coles, S. G., Connor, C. B., and Connor, L. J., Special Publication of IAVCEI, Geological Society of London, London, 2006.

Marzocchi, W., Sandri, L., and Selva, J.: BET_EF: A probabilistic tool for long- and short-term eruption forecasting, *Bull. Volcanol.*, 70, 623–632, 2008.

Marzocchi, W., Sandri, L., and Selva, J.: BET_VH: a probabilistic tool for long-term volcanic hazard assessment, *Bull. Volcanol.*, 72, 705–716, 2010.

Németh, K.: Monogenetic Volcanic Fields: Origin, Sedimentary Record, and Relationship with Polygenetic Volcanism, in: *What Is a Volcano? Gsa Special Papers Volume 470*, edited by: Cañón-Tapia, E. and Szakács, A., Geological Society of America, Boulder, Colorado, 43–67, 2010.

Németh, K. and Cronin, S. J.: Drivers of explosivity and elevated hazard in basaltic fissure eruptions: The 1913 eruption of Ambrym Volcano, Vanuatu (SW-Pacific), *J. Volcanol. Geoth. Res.*, 201, 194–209, 2011.

Newhall, C. G. and Hoblitt, R. P.: Constructing event trees for volcanic crisis, *Bull. Volcanol.*, 64, 3–20, doi:10.1007/s004450100173, 2002.

Newhall, G. G. and Self, S.: The Volcanic Explosivity Index (VEI): An estimate of explosive magnitude of historic eruptions, *J. Volcanol. Geoth. Res.*, 87, 1231–1238, 1982.

Pareschi, M. T., Cavarra, L., Favalli, M., Giannini, F., and Meriggi, A.: GIS and Volcanic Risk Management, *Nat. Hazards*, 21, 361–379, 2000.

Pedrazzi, D., Becerril, L., Martí, J., Meletlidis, S., and Galindo, I.: Explosive felsic volcanism on El Hierro (Canary Islands), *Bull. Volcanol.*, in press, 2014.

Pellicer, M. J.: Estudio volcanológico de la isla de El Hierro (Islas Canarias), *Estud. Geol.*, 33, 181–197, 1977.

Pellicer, M. J.: Estudio geoquímico del vulcanismo de la isla de Hierro, Archipiélago Canario, *Estud. Geol.*, 35, 15–29, 1979.

Pérez-Torrado, F. J., Rodríguez-González, A., Carracedo, J. C., Fernández-Turiel, J. L., Guillou, H., Hansen, A., and Rodríguez Badiola, E.: Edades C-14 Del Rift ONO de El Hierro (Islas Canarias), in: *El Cuaternario en España y Áreas Afines*, Avances en 2011, edited by: Turu, V. and Constante, A., Asociación Española para el Estudio del Cuaternario (AEQUA), Andorra, 101–104, 2011.

Pérez-Torrado, F. J., Carracedo, J. C., Rodríguez-González, A., Soler, V., Troll, V. R., and Wiesmaier, S.: La erupción submarina de La Restinga en la isla de El Hierro, Canarias: Octubre 2011–Marzo 2012, *Estud. Geol.*, 68, 5–27, 2012.

Pfeiffer, T., Costa, A., and Macedonio, G.: A model for the numerical simulation of tephra fall deposits, *J. Volcanol. Geoth. Res.*, 140, 273–294, 2005.

Phillipson, G., Sobradelo, R., and Gottsmann, J.: Global volcanic unrest in the 21st century: An analysis of the first decade, *J. Volcanol. Geoth. Res.*, 264, 183–196, 2013.

Rivera, J., Lastras, G., Canals, M., Acosta, J., Arrese, B., Hermida, N., Micallef, A., Tello, O., and Amblas, D.: Construction of an oceanic island: Insights from the El Hierro (Canary Islands) 2011–2012 submarine volcanic eruption, *Geology*, 41, 355–358, doi:10.1130/G33863.1, 2013.

Robertson, A. H. F. and Stillman, C. J.: Submarine volcanic and associate sedimentary rocks of the Fuerteventura Basal Complex, Canary Islands, *Geol. Mag.*, 116, 203–214, 1979.

Rodríguez-González, A.: El Vulcanismo Holoceno de Gran Canaria: Aplicación de un sistema de Información Geográfica, Ph.D. thesis, University of Las Palmas de Gran Canaria, Las Palmas de Gran Canaria, Spain, 424 pp., 2009.

Rodríguez-González, A., Pérez-Torrado, F. J., Fernandez-Turiel, J. L., Carracedo, J. C., and Guillou, H.: GIS-based geomorphological modeling of coastal platform-forming eruptions: Montaña del Tesoro volcano (El Hierro, Canary Islands), *Geotemas*, Sociedad Geológica de Madrid, Madrid, 13 pp., 2012.

Sandri, L., Jolly, G., Lindsay, J., Howe, T., and Marzocchi, W.: Combining long- and short-term probabilistic volcanic hazard assessment with cost-benefit analysis to support decision making in a volcanic crisis from the Auckland Volcanic Field, New Zealand, *Bull. Volcanol.*, 74, 705–723, 2012.

Sandri, L., Thouret, J. C., Constantinescu, R., Biass, S., and Tonini, R.: Long-term multi-hazard assessment for El Misti volcano (Peru), *Bull. Volcanol.*, 76, 771–797, doi:10.1007/s00445-013-0771-9, 2014.

Schmincke, H. U.: Volcanic and chemical evolution of the Canary Islands, in: *Geology of the Northwest African continental margin*, edited by: von Rad, U., Hinz, K., Sarnthein, M., and Seibold, E., Springer, Berlin, Heidelberg, New York, 273–306, 1982.

Schmincke, H. U. and Sumita, M.: *Geological Evolution of the Canary Islands*. Görres-Verlag, Koblenz, Germany, p. 200, 2010.

Self, S.: The Recent volcanology of Terceira, Azores, *J. Geol. Soc. Lond.*, 132, 645–666, 1976.

Sheridan, M. F. and Malin, M. C.: Application of computer-assisted mapping to volcanic hazard evaluation of surge eruption: Vulcano, Lipari, Vesuvius. *Explosive Volcanism*, *J. Volcanol. Geoth. Res.*, 17, 187–202, 1983.

Sobradelo, R. and Martí, J.: Bayesian event tree for long-term volcanic hazard assessment: Application to Teide-Pico Viejo stratovolcanoes, Tenerife, Canary Islands, *J. Geophys. Res.*, 115, B05206, doi:10.1029/2009JB006566, 2010.

Sobradelo, R., Martí, J., Mendoza-Rosas, A. T., and Gómez, G.: Volcanic hazard assessment for the Canary Islands (Spain) using extreme value theory, *Nat. Hazards Earth Syst. Sci.*, 11, 2741–2753, doi:10.5194/nhess-11-2741-2011, 2011.

Sobradelo, R., Bartolini, S., and Martí, J.: HASSET: a probability event tree tool to valuate future volcanic scenarios using Bayesian inference Presented as a plugin for QGIS, *Bull. Volcanol.*, 76, 770–785, doi:10.1007/s00445-013-0770-x, 2014a.

Sobradelo, R., Martí, J., Kilburn, C., and López, C.: Probabilistic approach to decision making under uncertainty during volcanic crises, *Nat. Hazards*, submitted, 2014b.

Stroncik, N. A., Klügel, A., and Hansteen, T. H.: The magmatic plumbing system beneath El Hierro (Canary Islands): constraints from phenocrysts and naturally quenched basaltic glasses in submarine rocks, *Contrib. Mineral. Petrol.*, 157, 593–607, 2009.

Székely, N., Laj, C., Guillout, H., Kissel, C., Mazaud, A., and Carracedo, J. C.: Geomagnetic paleosecular variation in the Brunhes period, from the island of El Hierro (Canary Islands), *Earth Planet. Sc. Lett.*, 165, 241–253, 1999.

Tarquini, S. and Favalli, M.: Changes of the susceptibility to lava flow invasion induced by morphological modifications of an active volcano: the case of Mount Etna, Italy, *Nat. Hazards*, 54, 537–546, 2010.

Toyos, G. P., Cole, P. D., Felpeto, A., and Martí, J.: A GIS-based methodology for hazard mapping of small pyroclastic density currents, *Nat. Hazards*, 41, 99–112, 2007.

Valentine, G. A.: Eruption column physics, in: *From Magma to Tephra – Modelling Physical Processes of Explosive Volcanic Eruptions*, edited by: Freundt, A., Rosi, M., Elsevier, Amsterdam, 91–138, 1998.

Valentine, G. A. and Gregg, T. K. P.: Continental basaltic volcanoes – processes and problems, *J. Volcanol. Geotherm. Res.*, 177, 857–873, 2008.

Van der Bogard, P.: The origin of the Canary Island Seamount Province-New ages of old seamounts, *Scientific Rep.*, 3, 1–7, 2013.

Vicari, A., Bilotta, G., Bonfiglio, S., Cappello, A., Ganci, G., Hérault, A., Rustico, E., Gallo, G., and Del Negro, C.: LAV@HAZARD: a web-GIS interface for volcanic hazard assessment, *Ann. Geophys.-Italy*, 54, 662–670, 2011.

Voight, B. and Cornelius, R. R.: Prospects for eruption prediction in near-real-time, *Nature*, 350, 695–698, 1991.

Volcanic hazard on Deception Island (South Shetland Islands, Antarctica)

Published in:

Journal of Volcanology and Geothermal Research

Authors:

Stefania Bartolini^a

Adelina Geyer^a

Joan Martí^a

Dario Pedrazzi^a

Gerardo Aguirre-Díaz^b

a) Institute of Earth Sciences Jaume Almera, ICTJA-CSIC, Group of Volcanology, SIMGEO (UB-CSIC) Lluís Sole i Sabaris s/n, 08028 Barcelona, Spain

b) Centro de Geociencias, Universidad Nacional Autónoma de México, Campus Juriquilla, Querétaro, Qro. 76230, Mexico

5.1 Abstract

Deception Island is the most active volcano in the South Shetland Islands and has been the scene of more than twenty identified eruptions over the past two centuries. In this contribution we present the first comprehensive long-term volcanic hazard assessment for this volcanic island. The research is based on the use of probabilistic methods and statistical techniques to estimate volcanic susceptibility, eruption recurrence and the most likely future eruptive scenarios. We perform a statistical analysis of the time series of past eruptions and the spatial extent of their products, including lava flows, fallout, pyroclastic density currents and lahars. The Bayesian event tree statistical method HASSET is applied to calculate eruption recurrence, while the QVAST tool is used in an analysis of past activity to calculate the possibility that new vents will open (volcanic susceptibility). On the basis of these calculations, we identify a number of significant scenarios using the GIS-based VORIS 2.0.1 and LAHARZ software and evaluate the potential extent of the main volcanic hazards to be expected on the island. This study represents a step forward in the evaluation of volcanic hazard on Deception Island and the results obtained are potentially useful for long-term emergency planning.

Keywords

Deception Island · Volcanic hazard · Volcanic susceptibility · Bayesian event tree · Eruptive scenarios

5.2 Introduction

Deception Island is the most active volcano in the South Shetland Islands group (Antarctica) and more than 20 eruptions have taken place there over the past two centuries (Orheim, 1972; Pallàs et al., 2001; Smellie, 2002a). Located at the spreading centre of the Bransfield Strait marginal basin (Fig. 5.1), this island consists of a horse-shoe-shaped composite volcanic system truncated by the formation of the collapse caldera that occupies the central part of the island (Valencio et al. 1979; Smellie 1988; Martí et al., 2013) (Fig. 5.2a). The most recent eruptions took place in the late 1960s and 1970s and destroyed or severely damaged the scientific bases

operating on the island (Baker et al., 1975; Roobol, 1982) (Figs. 5.3a,b). Interestingly, during the final eruption strong winds and the unusually low tropopause in the area (Smellie, 1999) led to an important spread of volcanic ejecta that reached distances of over 150 km (Pallàs et al., 2001; Fretzdorff and Smellie, 2002; Pedrazzi et al., 2014).

Since its discovery in 1820, the island's natural harbours in Port Foster Bay (e.g. Pendulum Cove and Whalers Bay) (Fig. 5.2b) have been actively used during different peaks in the commercial exploitation of the Southern Ocean (Roobol, 1982; Smellie and López-Martínez, 2002). Between 1905 and 1930, the island served as the shore base for the Antarctic's most important whaling industry (Fig. 5.3c) and also played a military role during World War I due to its strategic location between the Atlantic and Pacific Oceans. This resulted in the construction of a British scientific station, which was occupied from 1944 until it was destroyed in 1969 (Roobol, 1982; Smellie and López-Martínez, 2002) (Fig. 5.3a). Following the British initiative, Argentina and Chile also established scientific bases on the island that, likewise, were either destroyed or abandoned after the eruptions occurring between 1967 and 1970 (Fig. 5.3b). After occasional expeditions to Deception Island, Britain, Spain and Argentina recommenced scientific activity in 1986. Argentina re-occupied and reconstructed its station (Fig. 3f), while Spain constructed a new station in 1989 (Fig. 5.3e); these two scientific bases operate every year during the Antarctic summer.

The number of tourists that visit Antarctica has increased since the first commercial cruise in 1966 and today over 30,000 visitors arrive during the austral summer (2012-2013) (IAATO, *International Association of Antarctica Tour Operators*) (Fig. 5.4a). Deception Island and Half Moon Island (Fig. 5.4) are two of the most popular destinations; specifically, the Antarctic Specially Protected Area (ASPA) sub-site of Whalers Bay (Fig. 5.2) receives over 15,000 visitors every year (Fig. 5.4b), while other sectors such as Telefon Bay or Pendulum Cove (Fig. 5.2) are visited by up to 5,000 tourists annually (Fig. 5.4b).

The recent eruptions (1967, 1969 and 1970) have demonstrated that volcanic activity on Deception Island may become a cause for concern for tourists, scientists and the military personnel working on or near the island. Livingston and Deception Islands host a total of five research stations and three field camps, while Greenwich and King George Islands are home to 10 all-year and two temporary research stations

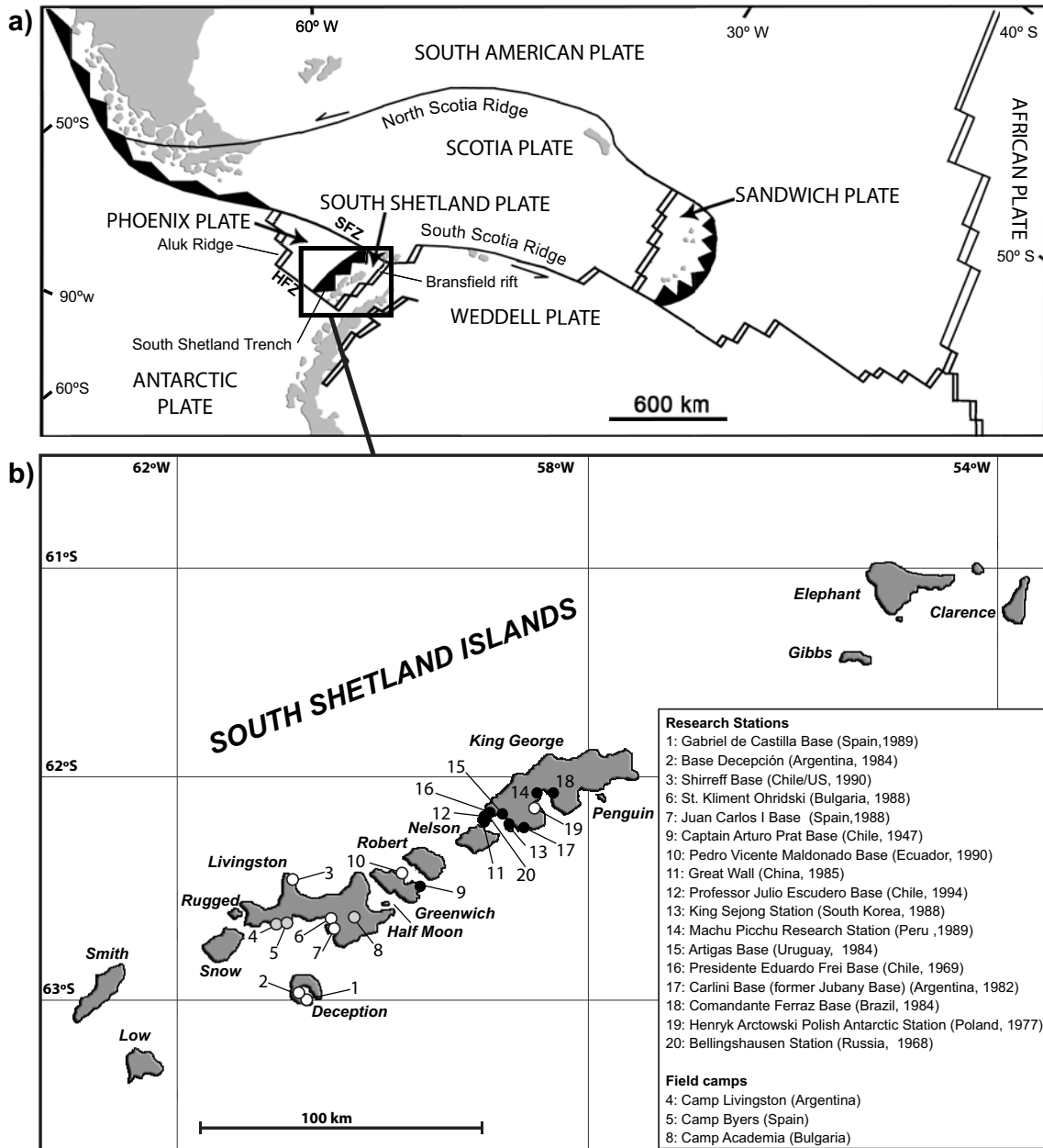


Figure 5.1: a) Simplified regional tectonic map and location of the South Shetland Islands (modified from Ibañez et al., 2003). HFZ: Hero Fracture Zone, SFZ: Shetland Fracture Zone. b) Location of Deception Island (modified from Grad et al., 1992). Black and white dots indicate nearby year-round and temporary (only austral summer) research stations, respectively. Grey dots correspond to temporary field camps

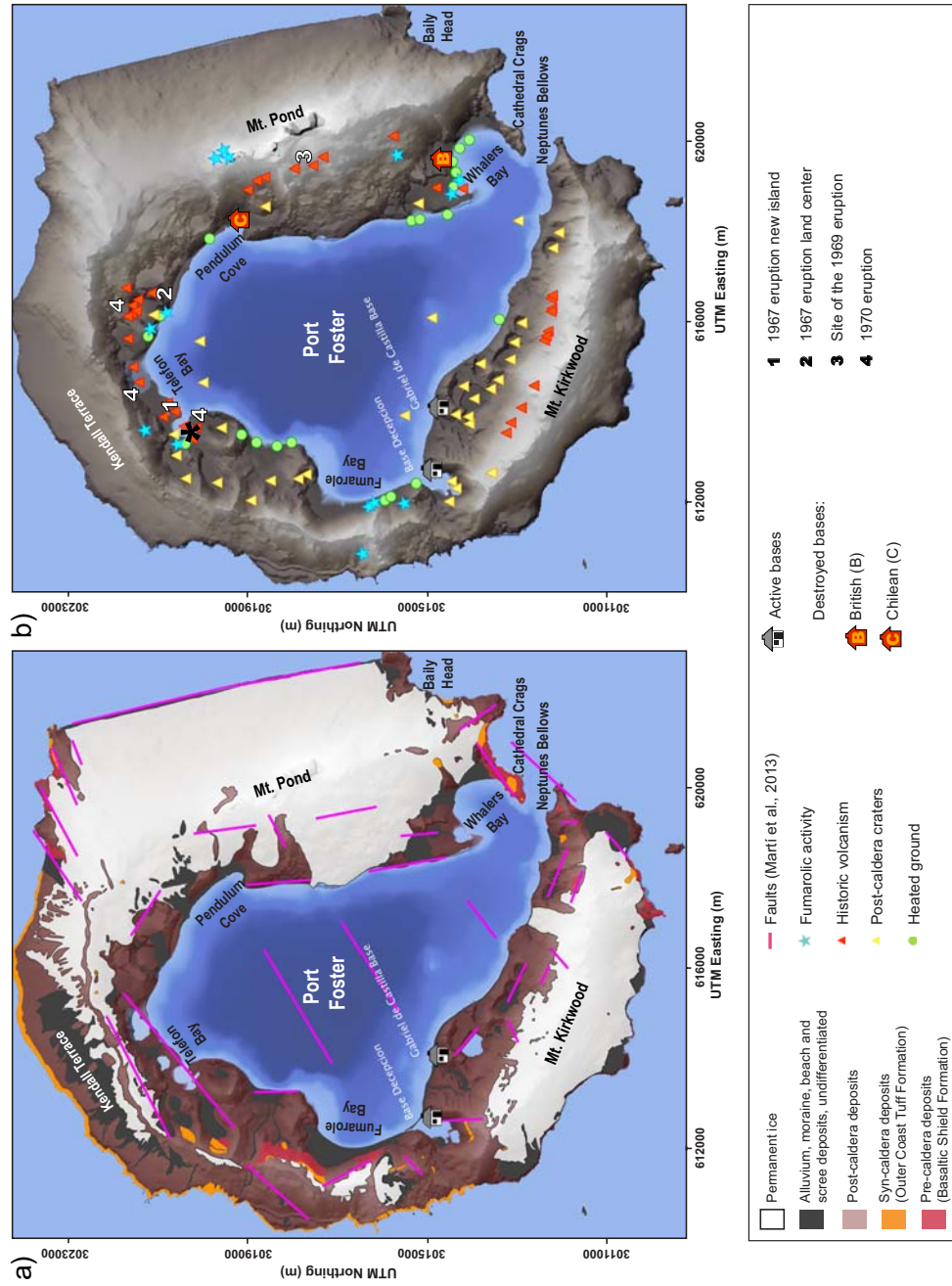


Figure 5.2: a) Simplified geological and tectonic map of Deception Island modified from Martí et al. (2013) and Smellie et al. (2002). b) The sites of the historical volcanic vents, observable fumarolic activity and heated ground are also indicated (data obtained from Spatial Data Infrastructure for Deception Island SIMAC, <http://www.simac.uca.es>, Torrecillas et al., 2006). As well as the historical vents, we have identified the post-caldera craters that, while not directly related to historical volcanic eruptions, clearly correspond to post-caldera volcanism

(Fig. 5.2). For example, during the 1970 eruption, a considerable amount of ash – including a fine ash fall deposit of 4 mm on Arturo Prat station on Greenwich Island and about 1 mm on Bellingshausen station on King George Island (Baker et al., 1975, Pedrazzi et al., 2014) – fell far from the island.

Aside from a paper by Roobol (1982) and the relatively recent work of Smellie (2002a), to the authors' knowledge no accurate volcanic hazard assessment has ever been conducted for Deception Island. Furthermore, previously hazard maps were either restricted to a single hazard (Roobol, 1982) (Fig. 5.5a) or were non-systematic (Smellie, 2002a) (Fig. 5.5b). As pointed out by Smellie (2002a), as a popular destination for tourists and an area of constant scientific research, properly elaborated hazard maps and related assessments are now more necessary than ever. The latter are indispensable for the elaboration of emergency plans aimed at mitigating the potential human and economic losses of any future volcanic eruptions on Deception Island.

In order to improve the hazard assessment on Deception Island, it is important to estimate the temporal and spatial probabilities of future eruptions. In this paper, we carry out a threat analysis for Deception Island using the National Volcano Early Warning System (NVEWS) template (Ewert et al., 2005) and compare it with other volcanoes of similar characteristics. Then, we present a systematic analysis of the temporal and spatial long-term hazard assessment of the island using available geological data, including the past eruption record, stratigraphic information and volcano-structural data. We used HASSET (Sobradelo et al., 2014) to estimate the probability that a volcanic episode will occur within the forecast interval and to evaluate the long-term probability of different types of hazards on the island. For the spatial analysis we applied QVAST (Bartolini et al., 2013) to obtain the susceptibility map, and LAHARZ and VORIS 2.0.1 (Hoblitt et al., 1995; Schilling, 1998; Felpeto et al., 2007) to generate different eruptive scenarios such as lahars, lava flows, pyroclastic density currents (PDCs) and fallout. The ultimate aim of this work was to generate a qualitative hazard map for Deception Island depicting the most probable scenarios and, consequently, to understand the potential impact that future eruptions could have on research stations, tourists, and ships in and around the island.

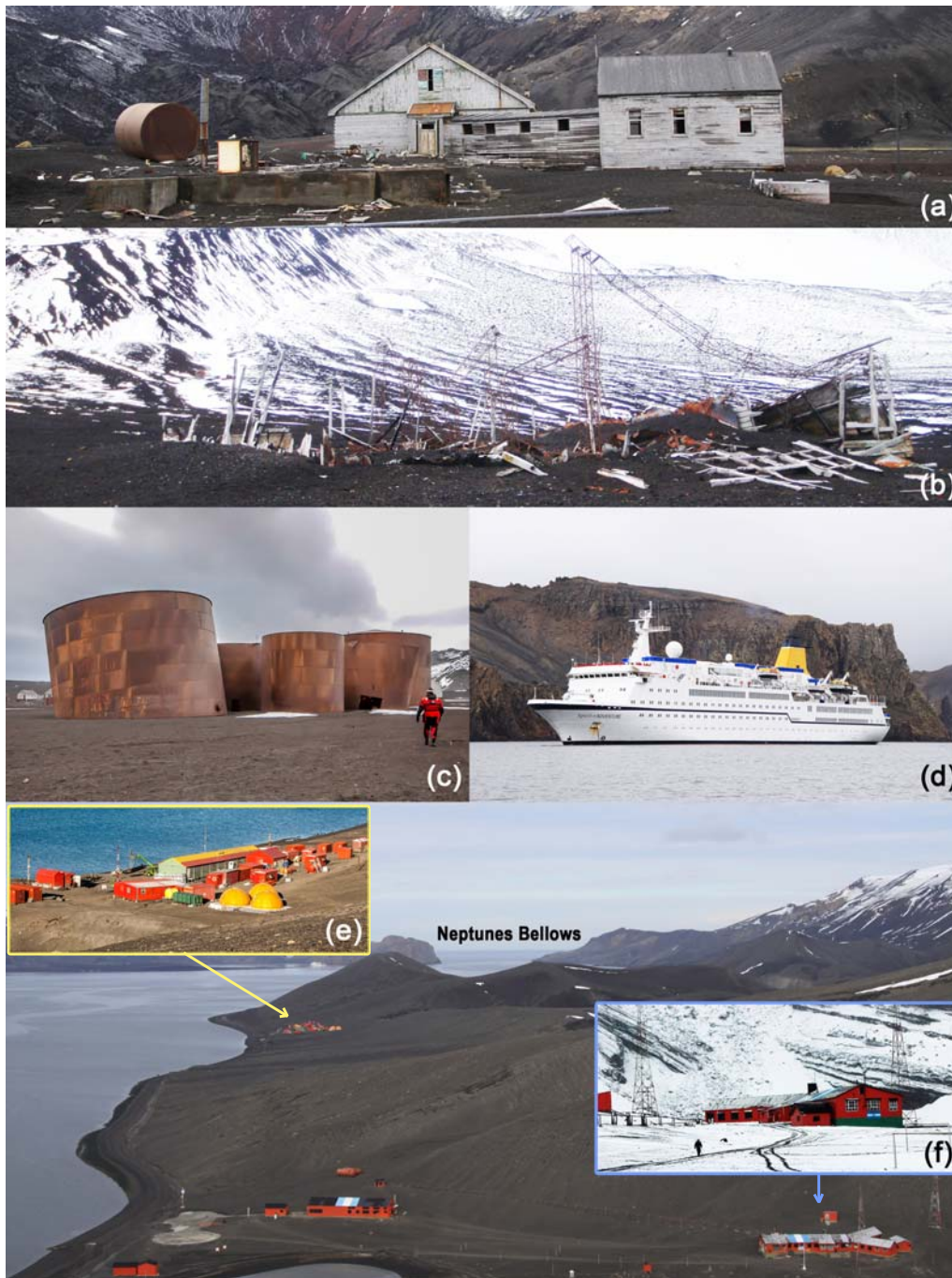


Figure 5.3: Remains of the British (a) and Chilean (b) bases in Whalers Bay and Pendulum Cove, respectively (see Fig. 5.2b for exact locations). Remains of the Norwegian whaling station in Whalers Bay (c). Current Spanish Gabriel de Castilla (e) and Argentinian Base Decepcion (f) scientific bases (see Fig. 5.2 for exact locations). (d) Photograph of a tourist cruise ship entering Port Foster through Neptunes Bellows. (Authors: A. Villaseñor (a), (b) and (d); J. Galeano (c), (e) and (f))

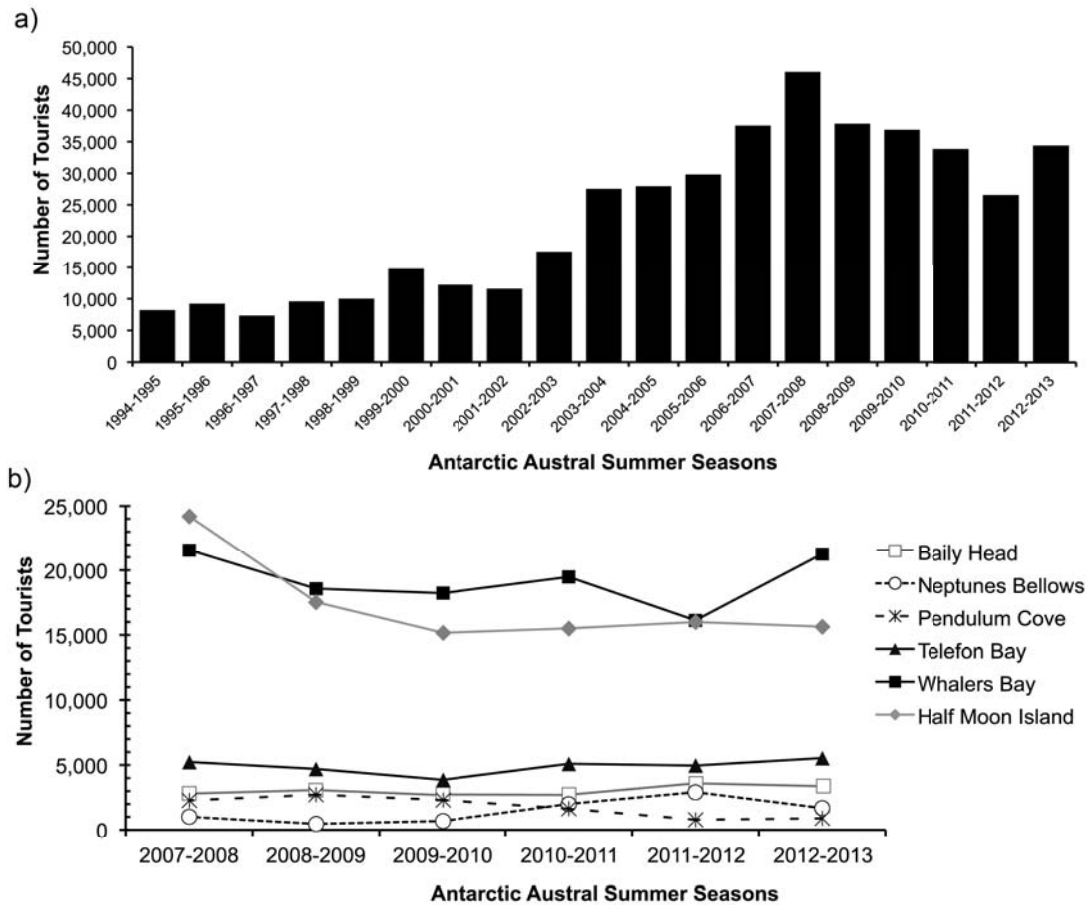


Figure 5.4: a) Visitors to Antarctica during the austral summers over the past two decades. b) Amount of visitors to specific Deception Island sites over the last five years (source: International Association of Antarctica Tour Operators (IAATO, <http://www.iaato.org>))

5.3 Geological setting

Deception Island is a sizeable active Quaternary volcano with a large central collapse caldera that is located at the south-western end of the Bransfield Strait, a marginal basin lying between the Antarctic Peninsula and the South Shetland Islands (Fig. 5.1). The related volcanic ridge has traditionally been interpreted as a Late Cenozoic extensional structure produced as a consequence of back-arc spreading (Roach, 1978; Peccerillo et al., 1991) linked to subduction of the Phoenix Plate beneath the Antarctic Plate (González-Ferrán, 1985). Deception, Penguin and Bridgeman islands and a number of other submerged volcanic vents are associated with the spreading centre. In particular, Deception Island is located near the intersection

between the axis of the Bransfield basin and the extension of the Hero Fracture Zone (Fig. 5.1).

The construction of the island can be separated into three main phases: pre-, syn- and post-caldera (Smellie, 2001; Martí et al., 2013). The first phase was characterised by the construction of the volcanic shield and is represented by the Basaltic Shield Formation, outcropping mainly at Baily Head and along the nearly vertical caldera wall at Fumarole Bay (Fig. 5.2a). The Outer Coast Tuff Formation (i.e. syn-caldera phase deposits) (Hawkes, 1961; Smellie, 2001; Martí et al., 2013) was deposited unconformably over the shield-related units and forms an almost continuous outcrop along the outer part of the island (Fig. 5.2a). The post-caldera phase, which includes the recent historical eruptions, consists of eruptive vents scattered across the whole island: all but one are found along the structural borders of the caldera and most correspond to previous regional tectonic faults (Fig. 5.2a) (Smellie, 2002a; Martí et al., 2013).

The magnetic polarity of the exposed rocks and K-Ar data indicate that Deception Island is younger than 0.75 Ma (Valencio et al., 1979) and that its subaerial part has mostly been constructed over the last 0.2 Ma (Keller et al., 1992). Indeed, the correlation between the exposed rocks and the tephras found elsewhere in the region suggests that these rocks are probably even younger than 0.1 Ma (Martí et al., 2013). The age of the collapse event remains unclear due to a lack of geochronological data and the fact that none of the tephra layers found in the various ice and marine/lacustrine sediment cores extracted around the Antarctic region appear to correlate with this event (Smellie, 1999; Pallàs et al., 2001). Since all the tephra related to the post-caldera volcanism recorded in the region are from the Middle Holocene or younger (Smellie, 1999; Moreton, 1999), Martí et al (2013) speculate that the caldera may have formed in the late Pleistocene-early Holocene.

5.4 Recent Volcanic Activity & Volcanic Hazards

The 1967, 1969 and 1970 eruptions on Deception Island have been well documented (González-Ferrán et al., 1971; Orheim, 1972; Baker et al., 1975; Roobol, 1982; Smellie, 1999, 2002a, 2002b; Moreton, 1999; Pedrazzi et al., 2014). First-hand observations exist for the first two as they occurred during austral summer. The December 1967 event created a new island around four aligned vents in Telefon Bay

Table 5.1: Principal characteristics of the volcanic eruptions and unrest periods recorded over the last 372 years (1641–2013). Only eruptions of known age and consistent with the relative field stratigraphy established in this study are included (error according to the time interval provided by the bibliography). Information about the nodes in the HASSET tool (Sobradelo et al., 2014) is also included. See text for more details.)

Year	Node 1 Unrest	Node 2 Origin	Node 3 Outcome	Node 4 Location	Node 5 Composition	Node 6 Size	Node 7 Hazard	Node 8 Extent	Source
1999	Yes	Geoth	No erup	-	-	-	-	-	Ibañez et al. (2003)
1992	Yes	Geoth	No erup	-	-	-	-	-	Ibañez et al. (2003)
1970	Yes	Magm	Magm	Telefon Ridge	Mafic	3	Ballistic Fall out PDC	L	González-Ferran et al. (1971) Baker et al. (1975)
1969	Yes	Magm	Magm	Mt. Pond	Mafic	3	Lava flow Lahars PDC	M	Baker et al. (1975)
1967	Yes	Magm Seis	Magm	Telefon Ridge Port Foster	Mafic	3	Ballistic Fall out PDC	M	Baker et al. (1975) Valenzuela et al. (1968)
1943 ± 12	Yes	Magm	Magm	Mt. Pond	Mafic	≥3	-	-	Roobol (1973) Pàllas et al. (2001)
1918 ± 12	Yes	Geoth	No Erup	-	-	-	-	-	Roobol (1980) Roobol (1982)
1915 ± 3	Yes	Magm	Magm	-	Mafic	3	Ballistic Fall out	L	Pàllas et al. (2001) Hodgson et al. (1998)
1892 ± 64	Yes	Magm	Magm	Telefon Ridge	-	<3	-	-	Roobol (1973)
1879 ± 49	Yes	Magm	Magm	Mt. Pond	-	≤3	Ballistic Fall out Lava flow	-	Smellie (2002a)
1869 ± 40	Yes	Magm	Magm	Mt. Pond	Mafic	≤3	-	-	Roobol (1973)
1842	Yes	Magm	Magm	Mt. Kirkwood	Felsic	2	Lava flow	S	Roobol (1980) Smiley in Wilkes (1845) Hawkes (1961)
1838 - 1839	Yes	Magm	Magm	Mt. Kirkwood	-	>3	Lava flow	-	Pallàs et al. (2001) Roobol (1980) Whittle in Wilkes (1845) Birkenmajer (1991)
1827 ± 2	Yes	Magm	Magm	Mt. Pond	Mafic	4	-	-	Roobol (1973) Roobol (1980) Kendall (1831) Pàllas et al. (2001)
1820 ± 1	Yes	Magm	Magm	-	Mafic	<3	Ballistic Fall out	L	Palais et al. (1989)
1795 ± 5	Yes	Magm	Magm	Telefon	-	-	-	-	Roobol (1973) Roobol (1980) Kendall (1831) Pàllas et al. (2001)
1750 ± 50	Yes	Magm	Magm	Mt. Kirkwood	Mafic	≥3	-	-	Pallàs et al. (2001)
1700	Yes	Magm	Magm	-	-	≥3	-	-	Moreton (1999) Smellie (1999)
1641	Yes	Magm	Magm	-	Mafic	>3	Ballistic Fall out	L	Aristarain and Delmas (1998) Delmas (1992)

Table 5.2: Additional geochronological data about the recorded volcanic eruptions on Deception Island between 35,400 B.P. and 450 B.P. (error according to the time interval provided by the bibliography). This information provides the main characteristics of the eruptive style of the island for the application of the Bayesian Event Tree method.)

Year	Node 1 Unrest	Node 2 Origin	Node 3 Outcome	Node 4 Location	Node 5 Composition	Node 6 Size	Node 7 Hazard	Node 8 Extent	Source
450	Yes	Magm	Magm	-	Mafic	≥ 3	-	L	Björck et al. (1991) Moreton (1999) Smellie (1999)
750	Yes	Magm	Magm	-	Mafic	≥ 3	-	L	Björck et al. (1991) Moreton (1999) Smellie (1999)
1050	Yes	Magm	Magm	-	Mafic	≥ 3	-	L	Moreton (1999) Smellie (1999)
1350	Yes	Magm	Magm	-	Mafic	≥ 3	-	L	Björck et al. (1991) Moreton (1999) Smellie (1999)
1850	Yes	Magm	Magm	-	Mafic	≥ 3	-	L	Moreton (1999) Smellie (1999)
2100	Yes	Magm	Magm	-	Mafic	≥ 3	-	L	Moreton (1999) Smellie (1999)
2250	Yes	Magm	Magm	-	-	≥ 3	-	L	Moreton (1999) Smellie (1999)
2500	Yes	Magm	Magm	-	Mafic	≥ 3	-	L	Moreton (1999) Smellie (1999)
2700 \pm 50	Yes	Magm	Magm	-	Mafic	≥ 3	-	L	Björck et al. (1991) Moreton (1999) Smellie (1999)
3500	Yes	Magm	Magm	-	-	≥ 3	-	L	Moreton (1999) Smellie (1999)
4700	Yes	Magm	Magm	-	Mafic	≥ 3	-	L	Björck et al. (1991) Moreton (1999) Smellie (1999)
5200	Yes	Magm	Magm	-	Mafic	≥ 3	-	L	Smellie (1999) Mathies et al. (1990)
8700(?)	Yes	Magm	Magm	-	Mafic	≥ 3	-	L	Smellie (1999) Mathies et al. (1990)
10,670	Yes	Magm	Magm	-	-	> 3	-	L	Moreton (1999) Smellie (1999)
21,660	Yes	Magm	Magm	-	-	> 3	-	L	Moreton (1999) Smellie (1999)
26,400	Yes	Magm	Magm	-	-	> 3	-	L	Moreton (1999) Smellie (1999)
35,400	Yes	Magm	Magm	-	-	> 3	-	L	Moreton (1999) Smellie (1999)

and a land vent located 2.5 km to the east (Fig. 5.2b). The February 1969 eruption occurred when a 4-km-long fissure opened beneath glacial ice along the eastern interior side of the caldera (Smellie, 2002a). This activity resulted in catastrophic floods and lahars, and the construction of several small cinder cones (Baker et al., 1975; Smellie, 2002b). Unlike the two previous events, there were no eyewitnesses to the 1970 eruption. Ash fell on the Chilean station *Arturo Prat* on Greenwich Island on August 13, 1970 and during the early morning on the same day near the Soviet station Bellingshausen on the King George Islands.

The tephra record from Deception Island (Orheim, 1972) and neighbouring islands (Pallàs et al., 2001) and ice and sediment (marine and lacustrine) cores reveal a series of over 30 post-caldera eruptions during the Holocene (Tables 5.1 and 5.2). However, even the most detailed record such as that provided by Mt. Pond glacier (Fig. 5.2a) probably only records some of the post-caldera eruptions on the island (Orheim, 1972; Smellie, 2002b) and a considerably higher number of eruptions may well have occurred. The record of the eruptions from the eighteenth to the twentieth centuries includes periods of great activity (e.g. 1906–1912, 1818–1828) with several temporally closely spaced eruptions, followed by decades of dormancy (e.g. 1912–1967) (Orheim, 1972; Roobol, 1982; Smellie, 2002b). Despite the inherent difficulties involved in predicting the date of the next eruption on Deception Island, it is still reasonable to expect further episodes to occur as part of these most recent activity cycles (Shultz, 1972). The unrest episodes in 1992 and 1999 demonstrate that the volcanic system is still active (Ibañez et al., 2003) and, as has been remarked in published research work, the occurrence of a future eruption on the island cannot be ruled out.

All post-caldera volcanism corresponds to eruptions of small volume (e.g. < 0.05 km³ for each of the 1967, 1969, and 1970 eruptions) and their explosivity will have varied in terms of their consistent phreatomagmatic nature. The interacting water may be simply seawater from Port Foster Bay, water from the underground aquifer or even melt water from the glaciers. The presence of Deception Island tephra in marine sediments in the Scotia Sea (e.g. Moreton and Smellie, 1998) or in ice cores from the South Pole (e.g. Aristarain and Delmas, 1998) suggests that some post-caldera eruptions may have been much more violent than those experienced in recent centuries.

The main direct volcanic hazards identified on Deception Island include (Smellie,

2002a) ash fall, pyroclastic density currents (mainly surges), lava flows and lahars, while indirect volcanic hazards could involve (Smellie, 2002a) steam fields, fumaroles, heated ground, structural collapses and rock falls, hydrothermal eruptions, volcanic gases, earthquakes and tsunamis.

Due to the strong winds and the unusually low tropopause (8-10 km) in the area (Smellie, 1999), ash fall deposits – even in historical eruptions – are rapidly displaced over neighbouring islands and the Antarctic continent. Indeed, ashes from the latest eruption on Deception Island were observed on King George Island (>150 km distance) (Baker et al., 1975). Additionally, numerous layers of Deception Island ash are preserved in marine sediments in the Scotia Sea (>800 km distance) (Moreton and Smellie, 1998). Close to the vent, ash fallout can lead to severe building damage, as in the case of the abandoned Chilean station at Pendulum Cove (Fig. 5.3b). This base was covered (and burned down) by ash from the 1969 fissure eruption, the closest vents of which were 400–500 m away (Smellie, 2002b). Smellie (2002a) has pointed out that since the prevailing winds on Deception Island are mainly from the west, the eastern side of the island is highly exposed to ash fall. Nevertheless, during the most recent eruptions, almost the entire island received some ash fall (Baker et al., 1975; Smellie, 2002a).

In the first volcanic hazard assessment on Deception Island, Roobol (1982) indicated that there were no relevant pyroclastic flows on the island. Nevertheless, Smellie (2002a) specifies that pyroclastic flows have occurred in the past but were only abundant during the caldera-forming eruption (Outer Coast Tuff Formation). Even so, dilute pyroclastic density currents (i.e. pyroclastic surges) are a characteristic feature of many Deception Island post-caldera eruptions. In most cases, mapped surge deposits extend for about 2 km from the vents (Pedrazzi et al., 2014) and may travel across water (Smellie, 2002a).

Lava fountaining and flows have also been a common feature throughout the eruptive history of the island (Roobol, 1982; Smellie, 2002a). The main hazard related to lava flows is the damage or destruction they cause by burying, crushing or burning as they progress. Even though they tend to be confined to valleys and can be easily outrun, the most important problem is that they can generate *jökulhlaups*, i.e. floods of molten water released from the glacier due to the opening of subglacial vents and the partial melting of the ice cover (Roobol, 1982; Smellie, 2002a, 2002b). In fact, Baker et al. (1975) state that the most recent eruptions demonstrate that

these floods are the main hazards to human life and property on the island. The same authors indicate that the most suitable sites for scientific stations on the shores around Port Foster are also the most vulnerable to the effects of this particular hazard.

These lahars or volcanic mudflows consist of substantial volumes of melt water, often highly charged with debris. Their great bulk density and velocity make them highly destructive. In fact, the *jökulhlaups* produced by the 1969 eruption were responsible for the destruction of the British scientific station at Whalers Bay (Baker et al., 1975). Lahars are characterised by having well-defined topographical limits since they are confined to valleys (Smellie, 2002a). Thus, the location of the eruptive vent, i.e. in ice-free areas or below the permanent ice caps on Mt. Kirkwood and Mt. Pond (Fig. 5.2b), is crucial for determining the potential hazards to be expected during a future eruption on Deception Island.

Other secondary hazards such as steam fields, fumaroles and ground heating are also common on the island, and are mostly confined to the inside of the caldera along the shores of Port Foster (Baker et al., 1975; Roobol, 1980; Smellie, 2002a) (Fig. 5.2b). Ground temperatures of <40-60°C are common but at Pendulum Cove and Fumarole Bay, they may reach up to 70°C and 100°C, respectively (Smellie, 2002a). These temperatures fluctuate daily, mainly with the tides. In 1920–21, for example, sudden subsidence of the sea floor beneath Whalers Bay caused the sea to boil and affected the ships in the area (Smellie, 2002a).

Seismicity may also be an issue in the area. During 1992 and 1999, two seismic crises related to episodes of deep magma injection led to the evacuation of the island (Ibañez et al., 2003). In general terms, current activity is characterised by strong hydrothermal circulation and intense seismicity with frequent volcano-tectonic and long-period events (Smellie, 2002a; Zandomenighi et al., 2009).

In addition, tsunamis triggered by eruptions and slope failures have occurred on Deception Island in the past (Smellie, 2002a). This is an important problem since they may block Neptunes Bellows, the only exit from (and entry into) Port Foster and make it difficult or even impossible to sail through this narrow, shallow channel. On a smaller scale, rock falls in strategically important places could cause major problems and, for example, the collapse of Cathedral Crags could block Neptunes Bellows and prevent ships from entering/leaving the island's interior bay (Smellie, 2002a).

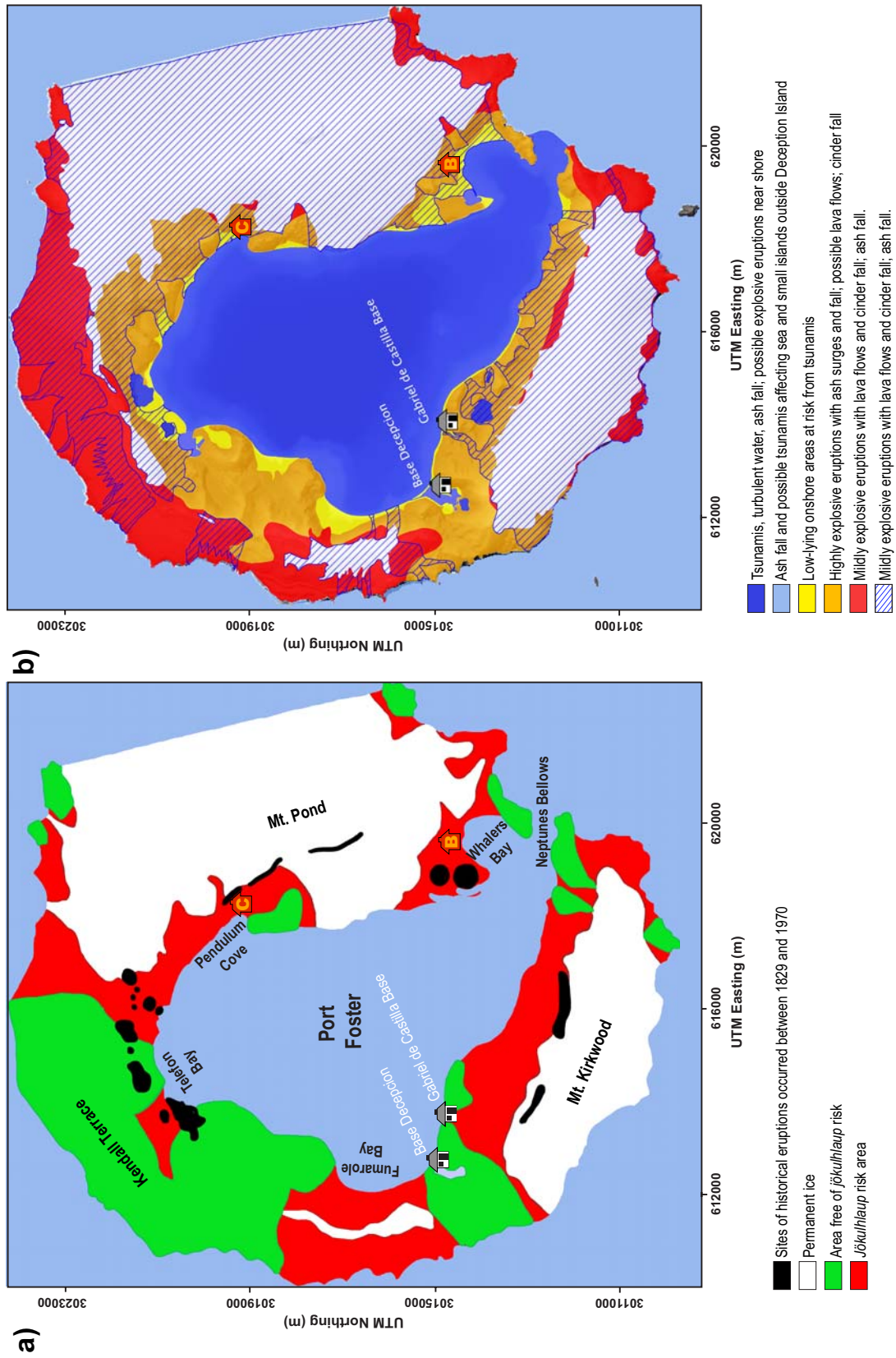


Figure 5.5: Hazard maps presented by Roobol (1982) (a) and Smellie (2002a) (b)

5.5 Threat Analysis

The quantification of the threat posed by volcanoes to their surroundings is vital when trying to define the required monitoring level for each volcano. In order to perform this quantification, Ewert et al. (2005) developed the National Volcano Early Warning System (NVEWS). The rationale behind NVEWS was to assess the threat posed by volcanoes in the United States via an analysis scheme divided into two main factor groups. First, those directly associated with the volcanic hazard and second, those related to exposure of human, social and economical elements potentially affected by the hazard. The individual factors are summed into a hazard score and an exposure score, which are then multiplied to generate the volcano's overall threat score. The total threat score obtained classifies the volcanic threat into one of five threat categories (Ewert et al., 2005): very low (6-0), low (6-30), moderate high (30-63), high (63 -113) and very high (> 113).

In recent years several authors have applied the NVEWS analysis to other volcanoes (e.g. Kinvig et al., 2010; Martí et al., 2012). Scores given to each factor (labelled from (a) to (y)) and the final results are given in Table 5.3. A brief explanation of the different scores is included in the next section; full details and references for the NVEWS analysis performed for Deception Island is included as a Microsoft Excel spread sheet in Supplementary Material 1. For each factor we have tried to determine the maximum and minimum score in an attempt to quantify the uncertainty caused by the lack of data in some cases. The obtained threat score for Deception Island is between 113.9 and 180, which corresponds to a high-to-very-high level of threat (Ewert et al., 2005).

5.5.1 Hazard factors

Deception Island corresponds to a composite volcanic system that includes a central collapse caldera that was responsible for the creation of Port Foster (a). Nevertheless, post-caldera volcanism is apparently restricted to small-size eruptions up to VEI 4, as indicated by the deposits on the island and the tephra records elsewhere in the region (b). Some indices of bimodal volcanism and deposits found at distances of over 500 km away suggest that more powerful eruptions may have taken place (e.g. Aristarain and Delmas, 1998; Caselli and Agosto, 2004; Smellie, 2002a) (c) and (d).

Table 5.3: Deception Island NVEWS (National Volcano Early Warning System) scoring factors.)

		Score (max)	Score (min)	References
<i>Hazard factors</i>				
(a)	Volcano type	1	1	[1][2][3]
(b)	Maximum Volcano Explosivity Index (VEI)	1	1	[1][2][3]
(c)	Explosive activity	1	1	[1][2][3]
(d)	Major explosive activity	1	0	[1][2][3]
(e)	Eruption recurrence	4	4	[3][4][5]
(f)	Holocene pyroclastic flows?	1	1	[3]
(g)	Holocene lava flows?	1	1	[3][4]
(h)	Holocene lahars?	1	1	[3]
(i)	Holocene tsunami (s)?	1	1	[3]
(j)	Hydrothermal explosion potential	1	1	[3]
(k)	Sector collapse potential	1	1	[3]
(l)	Primary lahar source	1	1	[3][4][6]
(m)	Observed seismic unrest	1	1	[7]
(n)	Observed ground deformation	1	1	[8]
(o)	Observed fumarolic or magmatic degassing	1	1	[7]
<i>Total hazard factors</i>		18	17	
<i>Exposure factors</i>				
(p)	Volcano Population Index (VPI) at 30 km	3	1.7	
(q)	Population downstream or downslope	0	0	
(r)	Historical fatalities	0	0	
(s)	Historical evacuations	0	0	[7][9]
(t)	Local aviation exposure	1	1	
(u)	Regional aviation exposure	2	0	
(v)	Power infrastructure	1	1	
(w)	Transportation infrastructure	1	1	
(x)	Major development of sensitive areas	1	1	
(y)	Volcano is significant part of a populated island	1	1	
<i>Total exposure factors</i>		10	6.7	
<i>Relative threat ranking (THF x TEF)</i>		180	113.9	

- [1] Aristarain and Delmas (1998)
- [2] Caselli and Agosto (2004)
- [3] Smellie (2002a)
- [4] Roobol (1982)
- [5] Orheim (1972)
- [6] Baker et al. (1975)
- [7] Ibañez et al. (2003)
- [8] Prates et al. (2013)
- [9] Smith et al. (2003)

The historical period in Deception Island is relatively short as it starts in 1820. Since then, over 15 eruptions have occurred on the island at Mt. Kirkwood (e.g. 1842, 1838–1839), Mt. Pond (e.g. 1969), Whalers Bay (e.g. 1829–1908), Pendulum Cove (e.g. 1800–1828, 1830–1927, 1931–1955) and Telefon Bay (e.g. 1967, 1970). During the Holocene, at least 30 eruptions occurred on Deception Island (Tables 5.1 and 5.2) including all the volcanic hazards described in the previous section (e). As mentioned above, there is evidence of pyroclastic surges and flows (f), lava flows (g) and ash fall. The constant fumarolic activity on the island and the evidence of phreatomagmatic eruptions fully justify the hydrothermal potential of the island (Smellie, 2002a) (h). There is also evidence of sector collapses (k) that may have led to tsunamis (j) inside Port Foster or beyond the island (Smellie, 2002a). As well, the permanent ice on Mt. Pond and Mt. Kirkwood also provide a primary source for a lahar in the event of an eruption occurring underneath these ice caps (l).

In 1992 and 1999, an episode of volcanic unrest took place on Deception Island that was characterised by a great increase in seismic activity (m) and changes in the hydrothermal system and fumarolic activity (o) (Ibañez et al., 2003). Ground deformation has been also observed on the island during recent scientific surveys (e.g. Prates et al., 2013) (n).

5.5.2 Exposure factor

When evaluating the threat on Deception Island it is important to take into account the fact that it is only populated during the austral summer. However, in neighbouring areas a few stations are inhabited during the winter and there is a permanent population on King George Island (Fig. 5.1). Thus, the threat analysis presented here refers mainly to the summer, especially for the maximum scores.

The first exposure factor is the volcano population index (VPI) within a 30-km radius of the volcano summit or the most recent active event. On Deception Island, this distance consists of the entire island and includes the Spanish and Bulgarian bases on Livingston Island (Fig. 5.1). These two bases, together with the ones on Deception Island itself, may be home to 50–100 people (i.e. a VPI of 1.7–2) (p). However, as one of the main Antarctic touristic destinations, we should also consider the possibility that a fully laden tourist vessel is present on the island, with which the VPI increases to 3 or more. There is no population downstream of the volcano within the 30 km VPI circle (q) and no fatalities have ever been recorded during

the eruptions on Deception Island (r). The Chilean and British stations and the Argentinian and Spanish bases were evacuated during the 1967 and 1969 eruptions and the seismic crisis of 1992, respectively (Ibañez et al., 2003, Smith et al., 2003), and no permanent populations remain (s).

In terms of local aviation exposure, the only airport on the South Shetland Islands is on King George Island, about 150 km away (t): a maximum of two flights per day would represent around 100 passengers (u). The power infrastructures for both the Spanish and the Argentinian bases and all accessible ports within Port Foster (e.g. Whalers Bay or Pendulum Cove) are located within the flowage hazard zones (v), (w). Finally, several parts of the island are considered Antarctic Specially Protected Areas and the Holocene volcanic deposits cover over 25

5.6 Volcanic hazard assessment: spatial and temporal analysis

The main steps in the volcanic hazard assessment on Deception Island (Fig. 5.6) can be divided into long- and short-term analyses. Long-term hazard assessment is based on the past history of the volcano and requires information from the geological record. This analysis enables us to determine the eruption recurrence and the possible nature of a forthcoming eruption. Short-term hazard assessment, on the other hand, provides complementary information resulting from the combination of a long-term analysis with real-time monitoring data gathered during a crisis or an unrest episode, and helps forecast where and when the eruption might take place and the most likely eruptive scenarios. To evaluate the long-term volcanic hazard, for this study we carried out both temporal and spatial analyses: the former evaluates in a probabilistic way possible outcomes of volcanic unrest within a specific time frame, while the latter uses simulation models to predict the most probable eruptive scenarios and which areas could be affected by a future eruptive event. The susceptibility analysis enables us to identify which areas have the greatest likelihood of hosting new vents.

Since the results from these temporal and spatial analyses are highly dependent on the data used, the selection of the data source is one of the most important steps to be undertaken during a hazard evaluation. Due to the logistic difficulties involved in performing repeated field studies or other surveying in the area, only previously

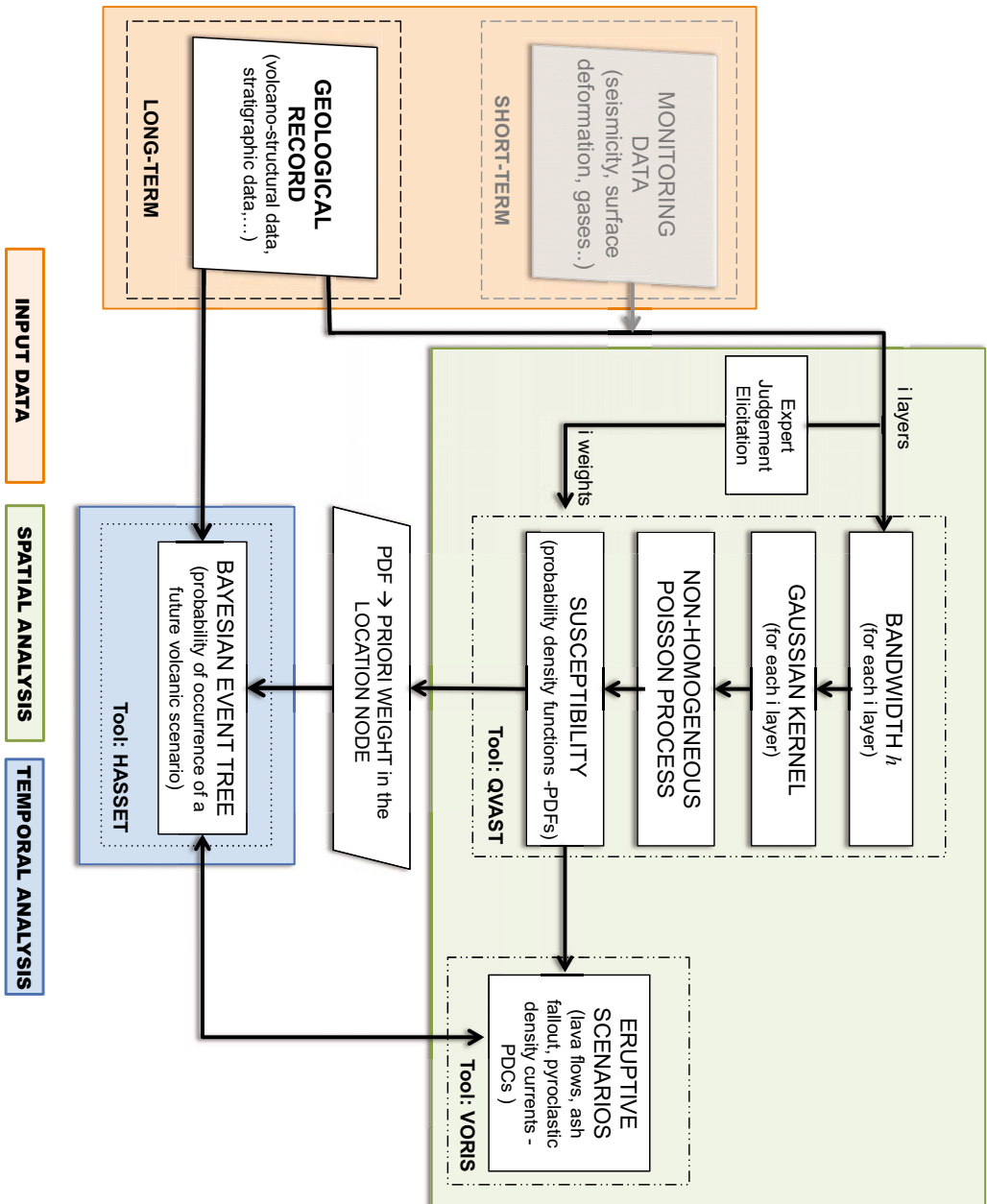


Figure 5.6: Flow chart for the volcanic hazard assessment. Tools used in this study are also indicated

published peer-reviewed information has been used in addition to our own data in this systematic volcanic hazard assessment. In the coming sections we provide a general overview of the different tools applied in this study, as well as a careful description of the required input data. For further detailed information regarding each specific tool, readers are referred to the original papers.

5.6.1 Susceptibility analysis

The first step in a long-term spatial analysis is to evaluate the susceptibility (probability of vent opening; Martí and Felpeto, 2010) of the volcanic area. For Deception Island we paid special attention to recent volcanic structural indicators such as vent locations and alignments, fumarolic activity and heated ground sites (Fig. 5.2). Vent locations were divided into post-caldera craters (no precise dating but recognisable in the field and from satellite images) and the historical volcanism described in the bibliography (Wilkes, 1845; Valenzuela et al., 1970; González-Ferrán et al., 1971; Baker et al., 1975; Roobol, 1980; Smellie, 2002b; Pedrazzi et al., 2014). The lineament structures shown in Figure 2a are taken from the simplified structural map of Deception Island in Martí et al. (2013). On the island, a NE–SW oriented regional tectonic trend, almost parallel to the expansion axis of the Bransfield Strait, is clearly predominant; NW–SE and N–S oriented faults are also present (Martí et al., 2013). Figure 5.2b also includes areas with clear signals of hydrothermal processes (e.g. fumaroles, heated ground) possibly related to the heating of shallow aquifers by magma intrusions at depth (Ortiz et al. 1987; Ramos et al. 1989; Rey et al., 1995; López-Martínez et al., 2000; Patrick and Smellie, 2013).

Susceptibility is generally calculated using probabilistic methods that estimate probability density functions (PDFs) by calculating a kernel function for each data location (Martin et al., 2004; Felpeto et al., 2007; Connor et al., 2012; Cappello et al., 2012, 2013; Becerril et al., 2013; Bartolini et al., 2013). The smoothness and the modelling ability of the kernel function is controlled by the smoothing parameter or bandwidth h , which determines how the probabilities spread out from the volcanic structures or vents (Diggle, 1985; Connor and Hill, 1995; Lutz and Gutmann, 1995; Cappello et al., 2012). Thus, for small h values, the kernel function gives high probability estimates in the vicinity of the existing volcanic structures. Conversely, when high bandwidth values are assigned, the probability estimates are distributed in a more homogeneous way throughout the entire area under study. The h values

LAYER	h (m)
Post-caldera craters (field work, analyzing orthophotos)	1170
Historic volcanism (Wilkes, 1845; Valenzuela et al., 1970; González-Ferrán et al., 1971; Baker et al., 1975; Roobol, 1980; Smellie, 2002b; Pedrazzi et al., 2014)	528
Lineaments (Martí et al., 2013)	3294
Fumarolic activity (López-Martinez et al., 2000; Smellie and López-Martinez, 2002)	4071
Heated ground (López-Martinez et al., 2000; Smellie and López-Martinez, 2002)	1001

Table 5.4: Bandwidth parameters for all the available datasets on Deception Island obtained using the modified LSCV (Least Square Cross Validation) method (Cappello et al., 2013) in the QVAST tool (Bartolini et al., 2013)

obtained for our dataset from Deception Island are given in Table 5.4.

For the present work, the bandwidth and the corresponding Gaussian Kernels and PDFs for all available datasets (vent locations, vent alignments, dykes, etc.) were evaluated with QVAST (Bartolini et al., 2013). We chose the modified version of the Least Square Cross Validation (LSCV) method to evaluate h (Cappello et al., 2012, 2013) and computed the final susceptibility map (Fig. 5.7) assuming a non-homogeneous Poisson process. To obtain the final susceptibility map, we had to combine all the PDFs evaluated for each volcano-structural data in a weighted sum. These weights were assigned using expert elicitation judgment (see Aspinall, 2006; Neri et al., 2008) by experts from the Group of Volcanology of Barcelona on the basis of structural criteria (see Martí and Felpeto, 2010), which provide initial indicative probability distributions associated with each PDF. We obtained the following values: 0.4 for the historical volcanism, 0.4 for the post-caldera craters, 0.1 for lineament structures, 0.05 for fumarolic activity and 0.05 for heated ground.

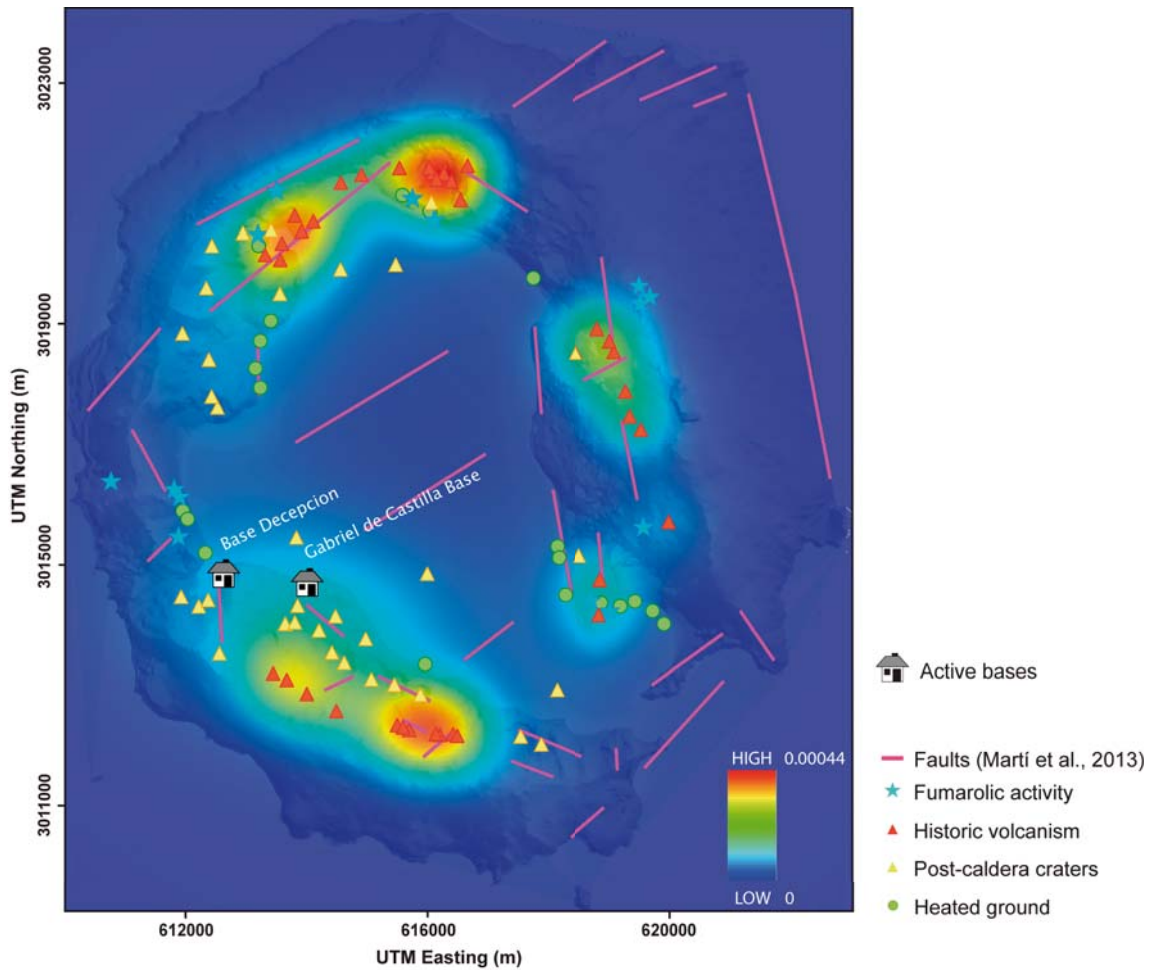


Figure 5.7: Susceptibility map of future eruptions on Deception Island calculated with QVAST (Bartolini et al., 2013)

5.6.2 Temporal analysis

The temporal analysis was computed using HASSET (Sobradelo et al., 2014), an event tree structure that uses Bayesian inference to estimate the probability of occurrence of a future volcanic scenario (Sobradelo and Martí, 2010) and to predict the five most likely scenarios. An event tree is a probabilistic model that can be used to calculate the probability of occurrence for any possible volcano-related event (Newhall and Hoblitt, 2002; Aspinall and Woo, 1994; Marzocchi et al., 2008, 2010; Aspinall, 2006; Neri et al., 2008; Martí et al., 2008; Sobradelo and Martí, 2010; Becerril et al., 2014). This graphic representation of events in the form of nodes and branches depicts all relevant possible outcomes of volcanic unrest in progressively

greater levels of detail.

Input data for the HASSET event tree model consists of geological and/or physical models, past data, present and past monitoring observations, and expert opinion. Three parameters must be entered at each branch to run the model: past data, prior weight and data weight (Sobradelo and Martí, 2010; Sobradelo et al., 2014). Past data consists of information about the volcanic area corresponding to observational data or data collected from the bibliography. We assume that the future behaviour of the volcano will be similar to its recent past history. In probabilistic terms, prior weight represents uncertainty before data are gathered and it is assigned on the basis of the priori beliefs regarding the volcanic area under study. Data weight represents how well we know the system. This value represents the epistemic uncertainty related to our knowledge of the system and the quality and quantity of data we have about the system. The more data we have, the better we know the system and the lower the epistemic uncertainty (Woo, 1999; Sobradelo and Martí, 2010).

The study of temporal probability on Deception Island was based on the catalogue of eruptions documented in Tables 5.1 and 5.2. Information from these eruptions was used to characterise past eruptive activity and to estimate some of the input parameters required for our hazard assessment. Due to the certainty that not all post-caldera eruptions occurred on Deception Island have been identified and/or dated, we computed only those volcanic eruptions and unrest periods recorded for the last 372 years (1641–2013), the period for which the available stratigraphic record and geochronological data are most precise. Therefore, using HASSET we were able to estimate the probability of a volcanic episode occurring within the forecasting time interval (the following 2 years). This forecasting time interval was chosen on the basis of the model and represents the minimum time window range needed to evaluate the probability of having at least one eruption in the range considered (see Sobradelo and Martí, 2010). The time window of the dataset is 372 years and so we obtained 186 time intervals of data for the study period. As we restricted our dataset to the last 372 years, the eruptions in this catalogue were used to assign prior weights to nodes 2 to 8. Table 5.5 shows the Bayesian event tree structure for Deception Island, as well as the input parameters for each branch. Figure 5.8 shows the probability for each event tree branch.

Furthermore, using HASSET it is possible to compute the total probability for any particular scenario and then compare results. Once all probability density func-

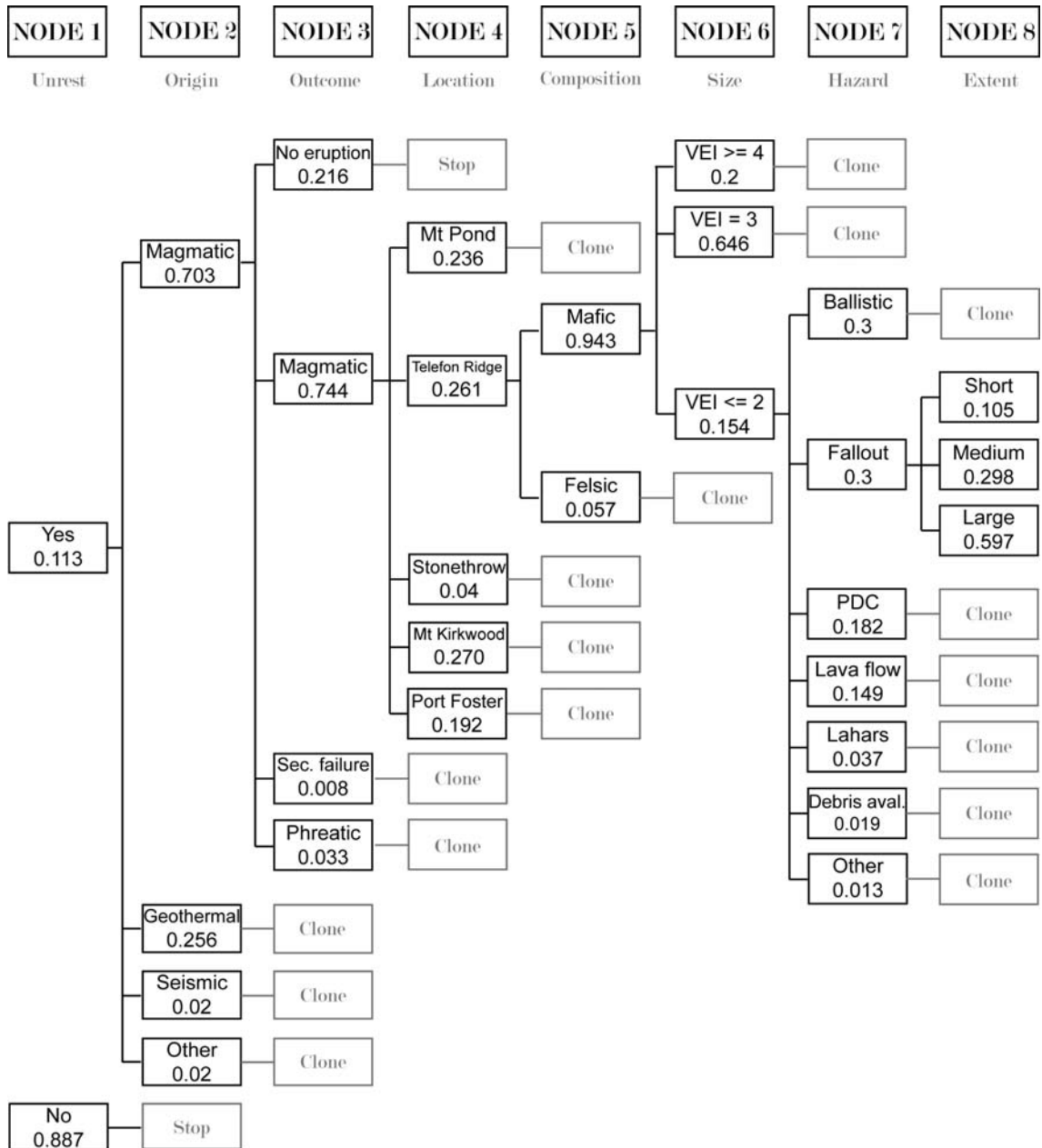


Figure 5.8: Bayesian event tree structure for Deception Island including results for the probability estimate using the HASSET tool (Sobradelo et al., 2014)

Table 5.5: Input data for HASSET (Sobradelo et al., 2014). Prior weights and data weights are estimated using data on Deception Island volcanic activity. Past data are based on the eruptions recorded over the last 372 years

#	NODE NAME	EVENT EVENT	PAST DATA	PRIOR WEIGHT	DATA WEIGHT
1	UNREST	Yes	19	0.30	10
1	UNREST	No	167	0.70	10
2	ORIGIN	Magmatic	16	0.50	10
2	ORIGIN	Geothermal	3	0.40	10
2	ORIGIN	Seismic	0	0.05	10
2	ORIGIN	Other	0	0.05	10
3	OUTCOME	Magmatic eruption	16	0.60	10
3	OUTCOME	Sector failure	0	0.02	10
3	OUTCOME	Phreatic explosion	0	0.08	10
3	OUTCOME	No eruption	3	0.30	10
4	LOCATION	Mt. Pond	5	0.20	50
4	LOCATION	Telefon Ridge	4	0.25	50
4	LOCATION	Stonethrow Ridge	0	0.05	50
4	LOCATION	Mt. Kirkwood	3	0.28	50
4	LOCATION	Port Foster	1	0.22	50
5	COMPOSITION	Mafic	10	0.95	50
5	COMPOSITION	Felsic	1	0.05	50
6	SIZE	$VEI \geq 4$	3	0.20	10
6	SIZE	$VEI = 3$	9	0.70	10
6	SIZE	$VEI \leq 2$	3	0.10	10
6	SIZE	-	-	-	-
7	HAZARD	Ballistic	6	0.30	30
7	HAZARD	Fallout	6	0.30	30
7	HAZARD	PDC	3	0.20	30
7	HAZARD	Lava flow	4	0.12	30
7	HAZARD	Lahars	1	0.03	30
7	HAZARD	Debris avalanche	0	0.03	30
7	HAZARD	Other	0	0.02	30
8	EXTENT	Short	1	0.10	50
8	EXTENT	Medium	2	0.30	50
8	EXTENT	Large	4	0.60	50

tions for each branch of each node and the conditional probability assessment are calculated, all these probabilities can be combined to estimate the total long-term probability of a particular event. Thus, we evaluated the total probability for different eruptive scenarios for the five different sectors that we established for Deception Island according to susceptibility and topographic criteria, as is permitted by HASSET and explained below (Fig. 5.9).

Node 1: Unrest

This first node estimates the temporal probability that the system will reactivate during the next time window. The probability that an unrest phase will occur (or not) during the next time window can be obtained by analysing the number of past time windows that encompass an episode of unrest. It does not take into account the periods of repose between eruptions or the possible non-stationary nature of the data (Sobradelo and Martí, 2010; Sobradelo et al., 2014).

As mentioned above, the existing eruptive record of Deception Island may be incomplete. First, the island is uninhabited for most of the year and so direct observations of unrest periods, whether a prelude or not to a volcanic eruption, are clearly biased towards the period when observers are present. Second, most of the information comes from ice-core studies and reports from Antarctic expeditions. Thus, the number of unrest periods occurring during the temporal window used in this analysis may be underestimated. For this reason, we assigned an epistemic uncertainty of 10 to our data weights, which means that new evidence on intervals with eruptive or non-eruptive behaviour will modify our prior assumptions. We assigned a 0.30 prior weight to unrest and 0.70 of prior weight to ‘no’ unrest.

Node 2: Origin

The origin node takes into account four types of unrest that could occur in a volcanic area: magmatic involving the movement of fresh magma, geothermal, seismic and others. Two intense seismic crises in 1992 and 1999 have been registered in 15 years of monitoring (Ibañez et al., 2003). This high seismicity was probably associated with the activity of the main geothermal system installed inside the

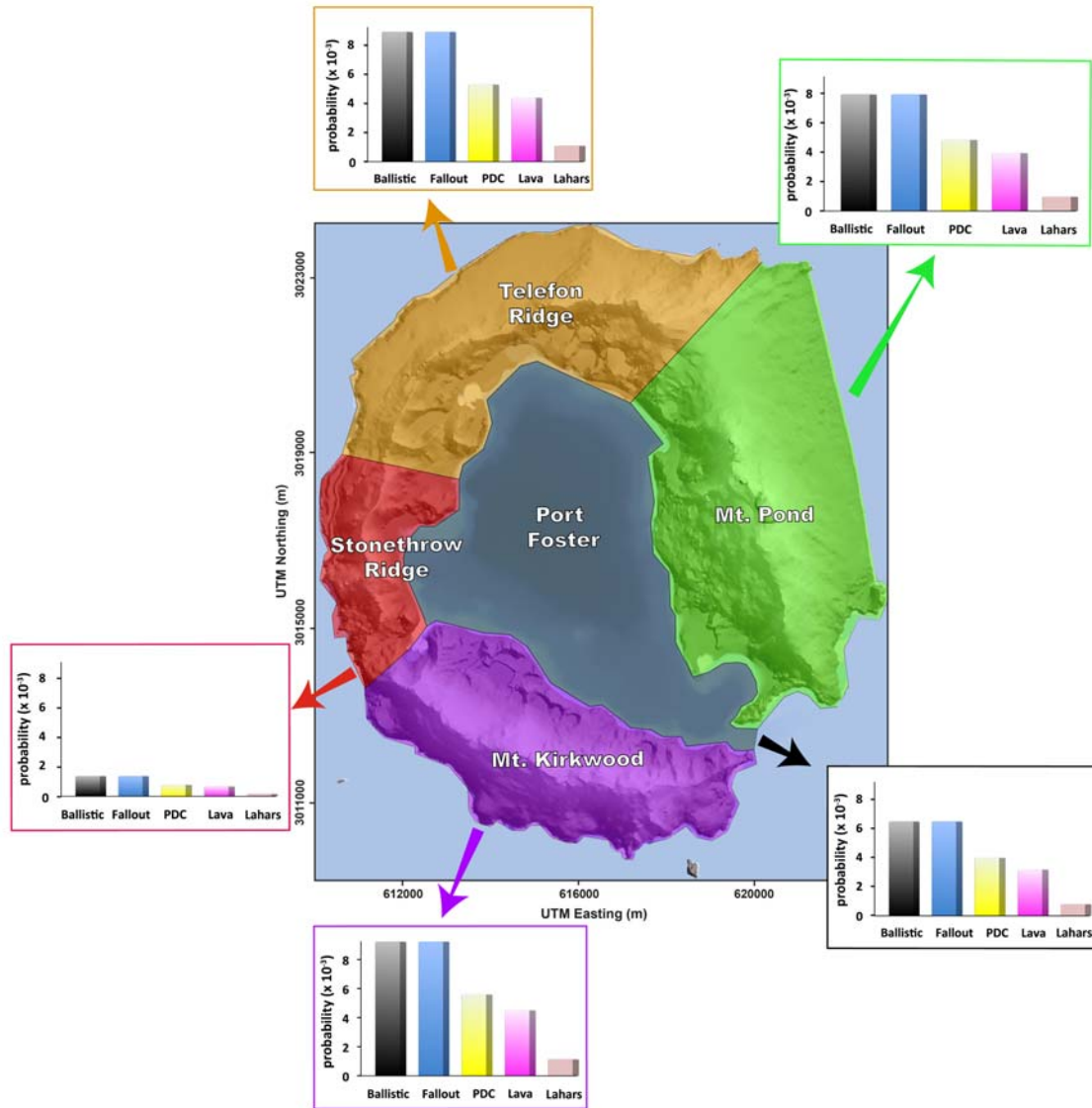


Figure 5.9: Sectors on Deception Island based on volcanic susceptibility and topographic criteria. The probabilities of the different hazards in each zone of Deception Island obtained with the application HASSET (Sobradelo et al., 2014) are also shown (see text for more explanation)

caldera depression (Martí et al., 2013). Despite the predominantly magmatic character of past activity on the island, we cannot exclude the possibility of geothermal behaviour without any associated fresh magma movements as occurs in other caldera systems with high geothermal activity (e.g. Campi Flegrei, Gottsmann et al., 2006; Nysiros, Gottsmann et al., 2007). In this sense, we have to assume that seismo-volcanic signals can also be associated with a shallow geothermal aquifer and deep hot materials (but not necessarily fresh magma), which gives rise to the resonance of fluid-filled fractures (Ibañez et al., 2003). In fact, these seismic measurements are not continuous and have only been registered over the past 15 years; there is thus a lack of seismic information and other similar but unrecorded periods of intense seismic activity may have gone unnoticed (Ibañez et al., 2003). For this reason, we assigned 0.5 for magmatic origin, 0.4 for geothermal origin, and split the rest evenly among the other options.

The prior weights are assigned on the basis of *a priori* beliefs and so we assigned a value of 10 to the epistemic uncertainty since we still expect the majority of unrest to be of magmatic origin. However, it is important to give a certain weight to new evidence.

Node 3: Outcome

A study of volcanic unrest in the historical period of Deception Island shows that 84

Given that these weights were assigned on the basis of incomplete data, we assigned a value of 10 to the epistemic uncertainty. We did not assign total epistemic uncertainty as we still believe that the largest weight should be for the magmatic eruption with no eruption branches; however, we still want new evidence to be able to contribute significantly to the updating of our prior weights.

Node 4: Location

The location node divides Deception Island into five main zones according to its topographic characteristics and the nature of past activity (volcanic susceptibility and past hazards). The five zones are shown in Figure 5.9.

Mount Pond (zone 1) and Mount Kirkwood (zone 4) represent zones with the

presence of extensive glaciers on their summits. The 1969 subglacial eruption took place on Mount Pond (Smellie, 2002b) and gave rise to the Costa Recta, a retreated scarp produced by a normal NNW–SSE-orientated fault (Fernández-Ibañez et al., 2005). Mount Kirkwood is characterised by the lava flows from the 1842 eruption. In the vicinity of Mount Kirkwood there are two scientific-military bases, the *Base Decepcion* (Argentina) and the *Gabriel de Castilla* station (Spain), both of which only operate during the Antarctic summer. The eruptive episodes from 1967 and 1970 were located on Telefon Ridge (zone 2) and Telefon Bay was largely filled by products from these eruptions, although three new smaller bays were created in flooded craters that formed during the final eruption in 1970 (Smellie, 2001). Stonethrow Ridge (zone 3) was formed after the caldera collapse and is characterised by lava flows and deposits of red and black scorias (Agusto et al., 2007). Port Foster (zone 5), the sea-flooded depression formed by the caldera collapse, occupies the central part of the island and is characterised by major normal faults bounding the caldera depression (Maestro et al., 2007; Martí et al., 2013).

The susceptibility analysis of the island based on the methodology described above allows us to assign prior weights to each node with a high degree of confidence, as shown in Table 5.5. The reliability of the susceptibility map allows us to assign a data weight of 50 since the prior weights were estimated using past data from Deception Island based on the volcano-structural data and on the location of past and current hydrothermal activity. For this reason, we are confident of the initial distribution of these prior weights.

Node 5: Composition

Most of the post-caldera volcanic activity on Deception Island corresponds to the eruption of basaltic and andesitic magmas (González-Ferrán et al., 1971; Smellie, 2001), of which only one is of dacitic composition (Table 5.1). Therefore, we assigned a weight of 0.95 for mafic composition and 0.05 for felsic composition. We assigned an epistemic uncertainty of 50, which means that new evidence regarding the composition of the historical eruptions will not modify substantially our prior assumptions.

Node 6: Size

The erupted volume on Deception Island ranges from 0.01 to 0.1 km³ of magma, with post-caldera activity varying from magmatic Strombolian to phreatomagmatic sub-Plinian in nature (Baker et al., 1975; Keller et al., 1992; Smellie, 1988, 1999). The values that characterize this activity on the island can be linked to small batches of deep-sourced magmas (Martí et al., 2013). Taking into account the recorded data, we attributed to VEI ≤ 2, VEI = 3 and VEI ≥ 4, the values of 0.10, 0.70 and 0.20, respectively. We assigned as a prior weight for the epistemic uncertainty a value of 10 as new evidence on the volumes or sizes of the historical eruptions will help significantly update our prior knowledge.

Node 7: Hazard

Post-caldera eruptions are characterised by the generation of ballistic ejecta, scoria fallout, PDCs, lava flows and lahars. Based on information on past activity, we assigned 0.3 for both ballistic ejecta and fallout, 0.2 for PDC, 0.12 for lava flows, 0.03 for both lahars and debris avalanches, and 0.02 for others. However, for the same reasons given for the size weights, we assigned a value of 30 to the epistemic uncertainties, as these prior weights may vary somewhat if an improved data catalogue – especially based on studies of the ice record – of past volcanic deposits can be obtained.

Node 8: Extent

Node extent refers to the distance reached by eruption products such as lava flows, ballistic, fallout, lahars and PDCs. The extent of the recent volcanic products on Deception Island varies considerably and, while lava flows may emplace only very close to the vents, ash fallout can be carried over 100 km due to the strong winds and the characteristic tropopause height of the area. In this analysis, we considered products located near the vents to be of small extent, products emplaced on the island to be of medium extent, and products emplaced beyond Deception Island to be of large extent. According to this and the geological record, 0.1 of extents were small, while 0.3 were medium and 0.6 large. We assigned an epistemic value of 50 to all branches, as new data will not affect significantly this information.

5.6.3 Eruptive scenarios

The second step is to simulate different eruptive scenarios using information on the spatial probability of a new vent opening indicated on the calculated susceptibility map. The result is a final qualitative hazard map created by the superposition of the different analysed scenarios. Simulations were conducted using VORIS 2.0.1 (Felpeto et al., 2007; available at <http://www.gvb-csic.es/GVB/VORIS/VORIS.htm>) and LAHARZ (Schilling, 1998; available at <http://vulcan.wr.usgs.gov/Projects/LAHARZ/framework.html>), two automatic systems developed in a GIS framework (ArcGis®) that enable volcanic hazard maps and eruptive scenarios based on geological record information to be elaborated. The VORIS 2.0.1 tool generates quantitative hazard maps for lava flows and PDCs and simulates fallout deposits for a single vent. LAHARZ is able to map lahar inundation zones.

Eruptive scenarios were calculated using information from recent historical eruptions and on the basis of the premise that future eruptions (if any) will be similar to those documented on the island from 1842, 1967, 1969 and 1970. Taking into account the main types of primary volcanic hazards identified during the historical eruptions (Smellie, 2002a), the eruptive scenarios predict the existence of ash fall, lava flows, dilute pyroclastic density currents and lahars. Furthermore, as obtained in the Bayesian Event Tree analysis, we have also a not null probability for ballistic ejecta and debris avalanches hazards. In this first analysis, we have decided not to include these two hazards due to the scarcity of input parameters to run the models.

Ash fall

Ash fall can be expected to occur on Deception Island in the event of more than one type of eruptive style. The style considered in this study was a violent Strombolian eruption, which coincides with recent eruption styles and corresponds to the most significant hazard in terms of probability of occurrence according to the long-term event tree constructed in section 5.2 (Temporal analysis). The input data regarding the eruptive column and ash particle size were inferred from the 1967, 1969 and 1970 eruptions (Valenzuela et al., 1970; González-Ferrán et al., 1971; Baker et al., 1975; Roobol, 1980; Smellie, 2002b; Pedrazzi et al., 2014), which were relatively small in volume ($<0.05 \text{ km}^3$) with eruptive columns that were probably less than 10-km high (Smellie, 2002b; Pedrazzi et al., 2014). Ash fallout simulations were based

on the advection-diffusion model (Folch and Felpeto, 2005), whereby the vertical mass distribution is computed using Suzuki's approximation (Suzuki, 1983; Felpeto et al., 2007). Wind data for the advection model correspond to records from the Bellingshausen station and were provided by the British Antarctic Survey (http://www.antarctica.ac.uk/met/READER/upper_air/uawind.html). Monthly records were used to calculate average annual wind velocities and directions at intervals of about 1,500 m up to an altitude of 20,000 m for a 30-year period (from 1969 to 1999). The wind roses for the time period considered are included as Supplementary Material 2.

We focused our attention on the fallout scenarios corresponding to the average wind velocity and direction values for each season. Up to five different wind direction inputs and intensities at different vertical heights can be used with the VORIS 2.0.1 tool. We chose data from altitudes between 1,500 and 12,000 m. Westerly winds prevail in general throughout the year, but with a more north-westerly direction in summer and winter. This is due to the fact that the data used come from a station that is strongly affected by the climatological low pressure that forms over the Bellingshausen Sea that generates predominantly north to north-westerly winds (Turner and Pendlebury, 2004). Wind speed averages range between 20 and 50 m/s. All the simulations were conducted assuming a single eruptive vent located in the area with the highest spatial probability during each season.

Results are shown in Figure 5.10, with particles distributed in a 5-km-high eruptive column produced by a violent Strombolian eruption generating 0.03 km³ of deposits. The column height and volume values are the same as for the 1969 eruption (Ortiz et al., 1987; Smellie, 2002b). We considered particle sizes ranging from -6 to 2ϕ (i.e. 64 mm to 0.25 mm), which cover the entire range of particle sizes observed in the volcanic deposits of the 1970 eruption (González-Ferrán et al., 1971; Shultz, 1972; Pedrazzi et al., 2014). It is clear that, as in the 1967 and 1969 eruptions (Smellie, 2002a), ash fall may also affect the southern part of the island, thereby hindering the exit of ships sailing from inside Port Foster (Fig. 5.3d). Moreover, as shown in Figure 10, ash fall may even cause problems for vessels operating several kilometres away from Deception Island.

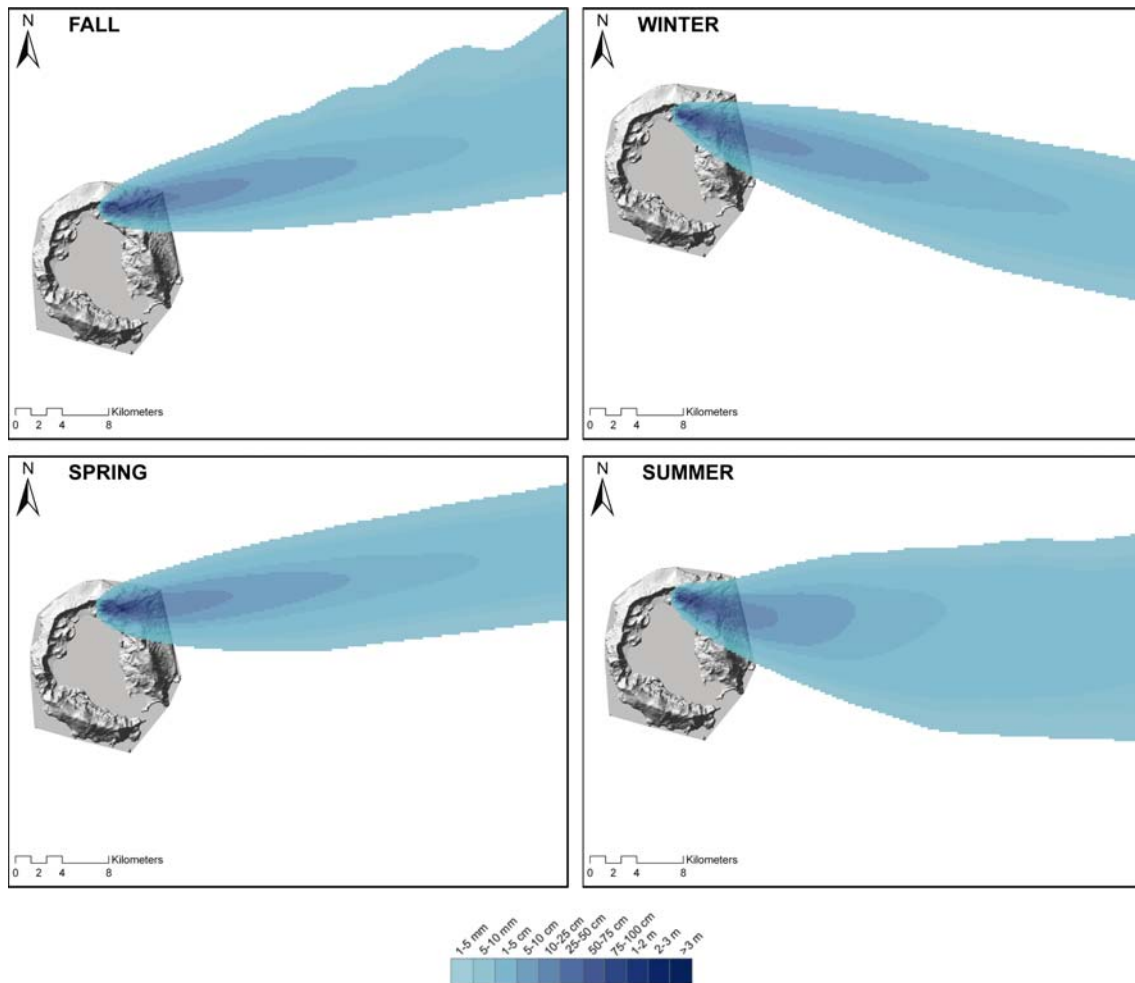


Figure 5.10: Ash fallout simulations (thickness) with a 5-km column height and volume of 0.3 km^3 . All four seasons are simulated using wind data from the *Bellinghousen* station

Lava flows

The lava flow (probabilistic) model applied is based on the assumption that topography and flow thickness play major roles in determining lava paths (Felpeto et al., 2007 and references therein). Input parameters required by the model include a Digital Elevation Model (DEM), maximum flow lengths and height correction (i.e. average thickness of the flow). In the case of Deception Island, simulations were run over a DEM with a cell size of 30 meters. Small lava flows that accumulated near the eruptive vent and did not flow over long distances were generated in the historical eruptions (Smellie, 2002a). The eruption with the largest lava flow was that of 1842, from Mt. Kirkwood, which reaches a maximum length of 5 km. Thus,

we assumed flow lengths in the range 1–5 km. The thickness used as input data for the models was 3 m, corresponding to the average value of individual flows measured in the field. The simulations were run for all cells in the DEM and the sum of the 5,000 iterations provided a map with the probability for any particular cell of being covered by a lava flow. Figure 5.11a consists of a lava-flow simulation probability map, which shows that there is a high probability that the caldera interior around the shores of Port Foster will be affected by lava flows. From this map it is clear that both scientific stations on the island and the evacuation routes proposed by the Spanish military staff (based on logistical criteria) are all located in areas with a moderate-to-high probability of being affected by lava flows.

PDCs

Pyroclastic density currents (PDCs) were simulated using the energy cone model (Sheridan and Malin, 1983) with input parameters of topography, the collapse equivalent height (H_c) and angle (θ). The latter is obtained by the arctangent of the ratio between H_c and L , where L represents the run-out length (Felpeto et al., 2007; Toyos et al., 2007). The output of the model is the maximum potential extent that can be affected by the flow (Malin and Sheridan, 1982; Toyos et al., 2007; Felpeto et al., 2007). The collapse equivalent height values range from 100 m up to about 1000 m (for very large eruptions), while the angle values range from about 4° for base surge explosions to 27° for column collapse phases (Sheridan and Malin, 1983). The result of each simulation is the area potentially attainable by a PDC.

On Deception Island, mapped surge deposits extend about 2 km from known vents and are small in volume (Smellie, 2002a). Collapse equivalent heights were chosen in the range of 200–500 m above the possible vent site in order to constrain the best H_c matching real deposits. We simulated PDCs with a collapse angle of 12° calculated from the ratio between the H_c and the run-out length. Results are shown in Figure 5.11b. The map obtained represents the sum of the simulation for all cells in the DEM for a collapse column of 400 meters and an inclination of the energy cone of 12° . The map shows how the interior area of Mt. Kirkwood has a high probability of being affected by dilute pyroclastic density currents that would affect the scientific stations and the evacuation routes. In addition, Telefon Ridge has a moderate-high probability of being invaded by PDCs, which would also affect evacuation routes.

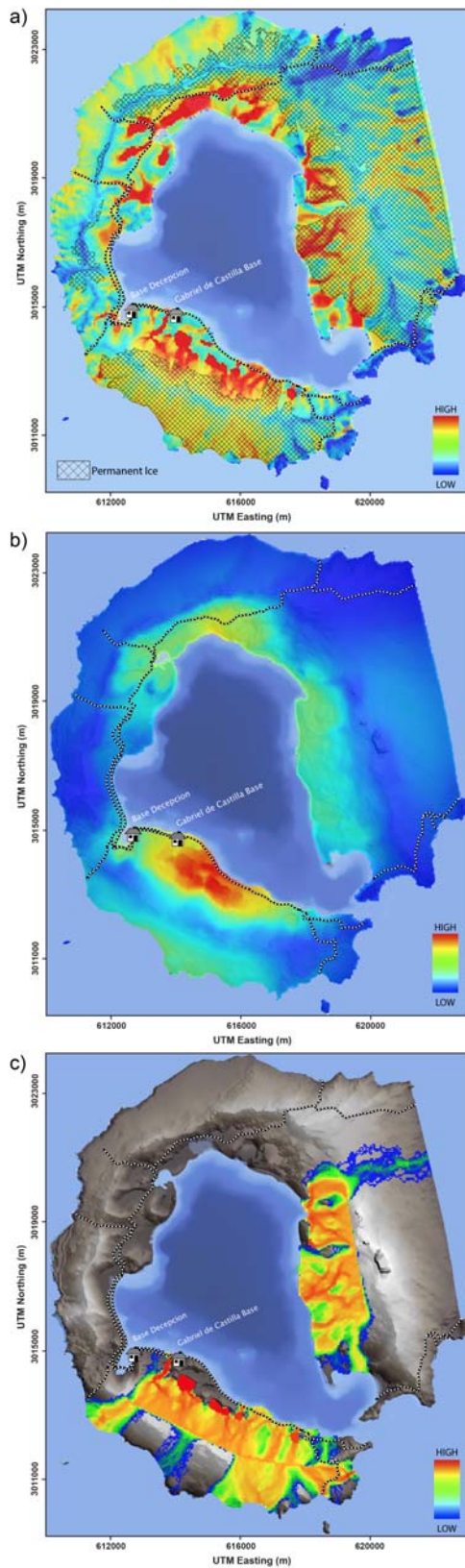


Figure 5.11: Lava flow (a), PDC (b) and lahar (c) simulation probability maps. Evacuation routes provided by the Spanish military staff are indicated by dotted lines

Lahars

The LAHARZ semi-empirical code creates hazard-zonation maps that depict estimates of the location and extent of areas inundated by lahars (Hoblitt et al., 1995, Schilling, 1998). The input parameters of this model are the Digital Elevation Model (DEM) and lahar volume, which provide an automated method for mapping areas of potential lahar inundation.

The lahar eruptive scenario was computed bearing in mind the fact that, in association with subglacial eruptions, lahars affected Deception Island during past activity (Smellie, 2002a, 2002b). Based on the estimated volumes from the 1969 eruption located under the Mt. Pond glacier (Smellie, 2002b), simulations were run with a volume of few millions of m³ originating along fissures in the two principal glacier zones, Mt. Pond and Mt. Kirkwood (Fig. 5.2a). These summits have extensive thin glaciers that could represent a significant hazard, creating a large and sudden discharge of melt water that would overflow the glacier.

Figure 5.11c shows a lahar simulation with hazard gradations ranging from low to high probabilities. The map shows how lahars could flood and reach the sea, and seriously damage the Gabriel de Castilla station on the way. From the map it is clear, as in the case of lava flows, that evacuation routes are located in moderate-to-high probability areas.

5.6.4 Hazard map

Finally, we obtained a qualitative hazard map with four levels of hazard (Fig. 5.12): very low, low, moderate and high. We established these levels on the basis of a combination of simulations for an area invaded by lava flows, lahars, and PDCs. The map shows that in the interior of the caldera there is mostly a moderate-to-high risk of being affected by one of the hazard scenarios considered. The highest hazard level is confined to the north-eastern flanks of Mt. Kirkwood, Pendulum Cove and the south-eastern slopes of Telefon Ridge (Fig. 5.12). The few areas with only a very low hazard level are mainly limited to Baily Head and Entrance Point (Fig. 5.12). From the hazard map it is clear that the two scientific stations on the island are both located in moderate-to-high hazard zones. Moreover, some of the evacuation routes run through areas possessing very high hazard level.

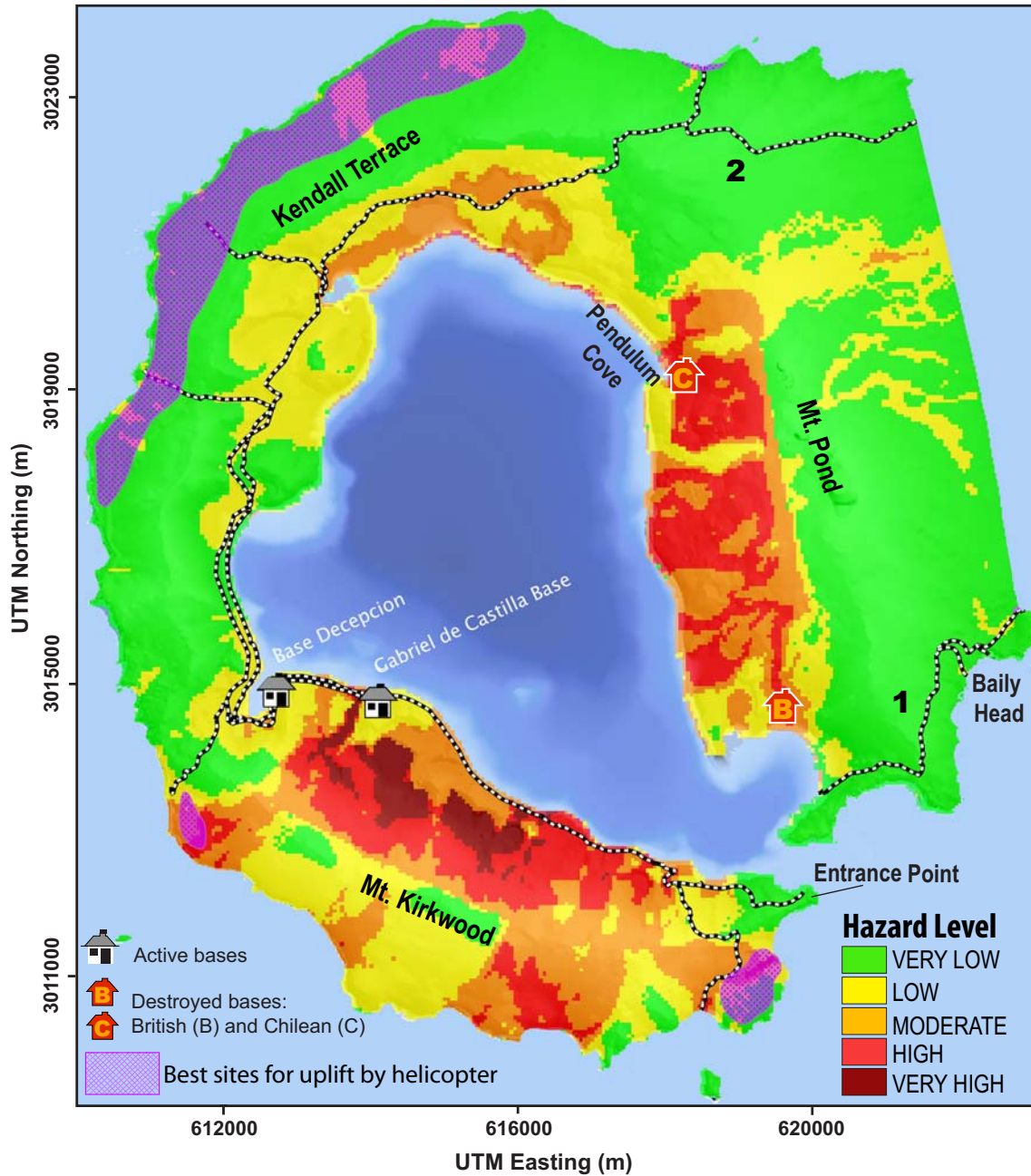


Figure 5.12: Qualitative hazard map for Deception Island. The evacuation routes provided by the Spanish military staff and the best sites for helicopter uplift according to Smellie (2002a) are also indicated

5.7 Discussion

Deception Island is the most active volcanic complex in the South Shetland Islands. Despite the important continuous research activity and the increasing number of tourists per year, no detailed hazard assessment has ever been conducted for the island. Two previous attempts have been made: Roobol (1982) mainly focused on assessing the zones threatened by lahars and constructed a model using topographic data and the extent of the ice cap, while Smellie (2002a) basically used observations of the extent of the products from the most recent historical eruptions in 1842, 1967, 1969 and 1970.

It is clear that hazard assessment on Deception Island may be limited by the lack of a complete geological record (e.g. chronological and stratigraphic data). Nonetheless, the threat evaluation and the spatio-temporal analysis presented here do provide a comprehensive hazard assessment for the island. Despite the intrinsic limitations of the methodology (partially due to the scarcity of data), we believe that this first analysis – albeit subject to improvement by new data – represents an important tool in management planning and in preparation for possible evacuations.

Even by assuming conservative values for some of the evaluated factors, the threat score obtained using the NVEWS test (Ewert et al., 2005) gives a range of 113.9–180, which places Deception island in the category of a volcano with a high-to-very-high threat, comparable to Crater Lake, St. Helens, Novarupta and Katmai in the USA (Ewert et al., 2005). According to Ewert et al. (2005), these high-threat volcanoes should be closely monitored in real-time. In more detail, the monitoring network must be able to track changes occurring in the system as they happen and to apply models to the on-going and expected activity. On Deception Island, Spanish seismologists monitor the island with five seismometers and one array during the austral summer (Carmona et al., 2012). During some campaigns other scientific groups also measure ground deformation and temperature (e.g. Prates et al., 2013; Peci et al., 2014). In light of the NVEWS recommendations, the volcano-monitoring network on Deception Island should be improved, especially considering the important tourist and scientific activity occurring during the Antarctic summer.

The present hazard assessment is relevant as an analysis of the adequacy of the current evacuation routes and locations of the active scientific stations. From Figure 5.12, it is clear that both *Base Decepcion* and *Gabriel de Castilla* station

are located in areas of moderate to high hazard. Previous work dealing with hazard assessment on Deception Island have already advised against the construction of permanent buildings on the shores of Port Foster (Roobol, 1982; Smellie, 2002a). Baker and co-authors (1975) highlighted that it would be “evidently unwise” to construct any new stations or any other kind of installation on the island. Roobol (1982) proposed that the safest place would be along Kendall Terrace outside the ring-fault zone (Fig. 5.5a) and argued that, if two different constructions were installed there, it seemed extremely unlikely that one would not survive the other in case of an eruption. Figure 5.12 demonstrates that the destroyed Chilean and British stations were, indeed, located in areas with high hazard level.

As is clearly suggested by the range of volcanic hazards identified on Deception Island, and given the increasing number of tourists and scientific expeditions visiting the island and its surroundings, it is important to identify escape routes in case of a sudden volcanic eruption. The escape strategy provided by the Spanish military staff is illustrated in Figure 5.12. However, the evacuation routes from both scientific stations run through zones with high hazard level. Indeed, as Smellie (2002a) remarks, all possible escape routes from the inner bay to the outer coast are demanding since they include climbing up on to the steep caldera walls. So, because the routes are physically arduous, even fit persons may end exhausted. It should be added that it is almost impossible to use ground vehicles to transport people and, if possible, considerable skill and local knowledge of the routes are required (cf. Smellie, 2002a).

All routes to the outer coast would take hours to complete – a minimum of two hours for the easiest route (Fig. 5.12, label 1) and over three or four hours (or more) for the most difficult ones (Fig. 5.12, label 2). According to Smellie (2002a), there are no recommended safe routes over snow and ice because the inherent difficulties of travelling over glaciers (e.g. crevasses, whiteout, slippery surfaces). So, glacier travel should be avoided unless with trained guides using suitable equipment, although this is unlikely to be readily available in an emergency (cf. Smellie, 2002a). It should be added that the existing evacuation routes shown in Figure 5.12 were defined without any accurate hazard assessment and taking into account only logistical considerations. Thus, the results presented here should encourage a revision of the distribution and course of the evacuation routes.

The evacuation of the island would be difficult for a number of other reasons.

First, it is possible that the entrance to Port Foster would be blocked or difficult to sail through due to the eruption, a tsunamis or any other of the hazards outlined here. Thus, all ships present within the bay when an eruption begins should set sail immediately, preferably after uplifting all people on the ground (Smellie, 2002a). Vessels should also avoid sailing too close to Cathedral Crags given the possibility of rock falls from these unstable cliffs.

Another aspect to be taken into account is that all rescue ships and helicopters should avoid passing through or under the eruption ash cloud due to the possibility of damage to machinery caused by ash particles. This is an important difficulty during rescue operations given that the hazard assessment developed in this study and, above all, the eruptive simulations reveal the possibility that Neptune's Bellows will be affected by ash fall. This would hamper any rescue operation and navigation routes, as well as activity on other islands. On the other hand, PDCs and lava flows are more constrained to the area around the vents, but these could still affect the research stations and create a problem for the existing evacuation routes.

5.8 Conclusions

Here we present a long-term volcanic hazard assessment of Deception Island that takes into account both temporal and spatial probabilities. The computation of the latter probabilities for the different eruptive scenarios is important in the evaluation of the hazard level on different parts of the island. These values can be easily updated and improved with the incorporation of new information such as a more complete volcanic stratigraphy and geochronological data.

The hazard probability map shows that the research stations could be affected by PDCs and that a large area of the island could be covered by ash fallout. Furthermore, the opening of new fissures in the glacier zones could generate lahars that would reach the research stations and affect evacuation routes. These results are useful for planning and choosing suitable routes for evacuating the island during a volcanic crisis in the Antarctic summer when the island is populated.

Finally, it is worth mentioning that this long-term assessment may help decision makers when faced with difficult situations such as the allocation of resources for hazard prevention and evacuation whose objective is to reduce the loss of life due to the potential impact of volcanic hazards.

Acknowledgements

This work was supported by the European Commission (FP7 Theme: ENV.2011.1.3.3-1; Grant 282759: VUELCO) and the MICINN grant CTM2011-13578-E. AG is grateful for her Juan de la Cierva Grant (JCI-2010-06092) and Ramón y Cajal contract (RYC-2012-11024). We would like to thank all the military staff from the Spanish Antarctic Base Gabriel de Castilla for their constant help and for the logistic support, without which this research would have been impossible. We would also like to thank Manuel Bañón for his help with the meteorological information. The authors are grateful to two anonymous reviewers for their insightful comments and review of the manuscript, which have helped us improve this work. We also thank the Editor Lionel Wilson for handling this paper. The English text was corrected by Michael Lockwood.

References

Aristarain, A.J. and Delmas, R.J.: Ice record of a large eruption of Deception Island Volcano (Antarctica) in the XVIIIth century. *J. Volcanol. Geotherm. Res.* 80, 17-25, 1998.

Aspinall, W. P. and Woo, G.: An impartial decision-making procedure using expert judgment to assess volcanic hazards, in *Large Explosive Eruptions*. *Accad. Naz. dei Lincei, Rome. Atti Conv. Lincei* 112, 211-220, 1994.

Aspinall, W.P.: Structured elicitation of expert judgment for probabilistic hazard and risk assessment in volcanic eruptions. In: Mader, H.M., Coles, S.G., Connor, C.B., Connor, L.J. (Eds.), *Statistics in Volcanology*. : Special Publication of IAV-CEI, 1. *Geol. Soc. London*, pp. 15–30, 2006.

Baker. P.E., McReath, I., Harvey. M.R., Roobol, M.J., and Davies. T.G.: The geology of the South Shetland Islands: V. Volcanic evolution of Deception Island. *Br. Antarct. Surv. Sci. Rep.*, 78-81, 1975.

Bartolini, S., Cappello, A., Martí, J., and Del Negro, C.: QVAST: a new Quantum GIS plugin for estimating volcanic susceptibility. *Nat. Hazards Earth Syst. Sci.* 13, 3031–3042, 2013.

Becerril, L., Cappello, A., Galindo, I., Neri, M., and Del Negro, C.: Spatial probability distribution of future volcanic eruptions at El Hierro Island (Canary

Islands, Spain). *J. Volcanol. Geotherm. Res.* 257, 21-30, 2013.

Becerril, L., Bartolini, S., Sobradelo, R., Martí, J., Morales, J. M., and Galindo, I.: Long-term volcanic hazard assessment on El Hierro (Canary Islands). *Nat. Hazards Earth Syst. Sci.* 14, 1853-1870, 2014.

Birkenmajer, K.: Lichenometric dating of a mid_19th century lava eruption at Deception Island (West Antarctica). *Bulletin of the Polish Academy of Science, Earth Sciences* 39, 1-9, 1991.

Björck, S., Sandgren, P., and Zale, R.: Late Holocene tephrochronology of the Northern Antarctic Peninsula. *Quaternary Research* 36, 322-328, 1991.

Cappello, A., Neri, M., Acocella, V., Gallo, G., Vicari, A., and Del Negro, C.: Spatial vent opening probability map of Etna volcano (Sicily, Italy). *Bull. Volcanol.* 74, 2083-2094, 2012.

Cappello, A., Bilotta, G., Neri, M., and Del Negro, C.: Probabilistic modeling of future volcanic eruptions at Mount Etna. *J. Geophys. Res. Solid Earth* 118, 1-11, 2013.

Carmona, E., Almendros, J., Martín, R., Cortés, G., Alguacil, G., Moreno, J., Martín, B., Martos, A., Serrano, I., Stich, D., and Ibáñez, J.M.: Avances y mejoras en el monitoreo sísmico de Isla Decepción (Antártida). *Proceedings de la 7^a Asamblea Hispano-Portuguesa de Geodesia y Geofísica*, pp. 267- 271, 2012.

Caselli, A.T. and Augusto, M.R.: Recent hydrovolcanic deposits with evidence of magmatic immiscibility on Deception Island, Antarctica. *Depósitos hidrovolcánicos recientes con indicios de inmiscibilidad magmática en la isla Decepción (Antártida)*. *Rev. Asoc. Geol. Argent.* 59(3), 495-500, 2004.

Connor, C.B. and Hill, B.E.: Three nonhomogenous Poisson models for the probability of basaltic volcanism: application to the Yucca Mountain region, Nevada. *J. Geophys. Res.* 100(B6), 107-110, 1995.

Connor, L.J., Connor, C.B., Meliksetian, K., and Savov, I.: Probabilistic approach to modeling lava flow inundation: a lava flow hazard assessment for a nuclear facility in Armenia. *J. Appl. Volcanol.* 1(3), 1-19, 2012.

Delmas, R.J.: Environmental information from ice cores. *Rev. Geophys.* 30, 1-21, 1992.

Diggle, P. J.: A kernel method for smoothing point process data. *Applied Statistics, J. R. Stat. Soc. Ser. C.* 34, 138-147, 1985.

Ewert, J., Guffanti, M., and Murray, T.: An assessment of volcanic threat and

monitoring capabilities in the United States: Framework for a National Volcanic Early Warning System, NVEWS. US Geoll. Sur. Open-File Rep. 1164, 1–62, 2005.

Felpeto, A., Martí, J., and Ortiz, R.: Automatic GIS-based system for volcanic hazard assessment. *J. Volcanol. Geotherm. Res.* 166, 106–116, 2007.

Fernández-Ibañez, F., Perez-Lopez, R., Martinez-Diaz, J.J., Paredes, C., Giner-Robles, J.L., Caselli, A.T., and Ibañez, J.M.: Costa Recta beach, Deception Island, West Antarctica: a retreated scarp of a submarine fault. *Antarctic Sci.* 17, 418–426, 2005.

Folch, A. and Felpeto, A.: A coupled model for dispersal of tephra during sustained explosive eruptions. *J. Volcanol. Geotherm. Res.* 145, 337–349, 2005.

Fretzdorff, S. and Smellie, J.L.: Electron microprobe characterization of ash layers in sediments from the central Bransfield basin (Antarctic Peninsula): evidence for at least two volcanic sources. *Antarctic Sci.* 14(4), 412–421, 2002.

González-Ferrán, O., Munizaga, F., and Moreno, H.: Síntesis de la evolución volcánica de la isla Decepción y la erupción de 1970. *Instituto Antártico Chileno, Serie Científica* 2(1), 1–14, 1971.

González-Ferrán, O.: Volcanic and tectonic evolution of the northern Antarctic Peninsula - Late Cenozoic to Recent. In: Husebye, E.S., Johnson, G.L. Kristoffersen, Y. (Eds.), *Geophysics of the Polar Regions, Tectonophysics*, 114, pp. 389–409, 1985.

Gottsmann, J., Folch, A., and Rymer, H.: Unrest at Campi Flegrei: a contribution to the magmatic versus hydrothermal debate from inverse and finite element modelling. *J. Geophys. Res.* 111, B07203, 2006.

Gottsmann, J., Carniel, R., Coppo, N., Wooller, L., Hautman, S., and Rymer, H.: Oscillations in hydrothermal systems as a source of periodic unrest at caldera volcanoes: multiparameter insights from Nisyros, Greece. *Geophys. Res. Lett.* 34, L07307, 2007.

Grad, M., Guterch, A., and Sroda, P.: Upper crustal structure of Deception Island area, Bransfield Strait, West Antarctica. *Antarctic Sci.* 4, 469–476, 1992.

Hawkes, D.D.: The geology of the South Shetland Islands: II. The geology and petrology of Deception Island. *Falkland Islands Dependencies Survey Scientific Reports* 27, 43, 1961.

Hoblitt, R.P., Walder, J.S., Driedger, C.L., Scott, K.M., Pringle, J.T., and Vallance, J.W.: Volcano hazards from Mount Rainier, Washington. *U.S. Geological Survey Open-File Report* 95- 273, pp. 10, 1995.

Hodgson, A.D., Dyson, C.L., Jones, V.J., and Smellie, J.L.: Tephra analysis of sediments from Midge Lake (South Shetland Islands) and Sombre Lake (South Orkney Islands), Antarctica. *Antarctic Sci.* 10, 13-20, 1998.

Ibañez, J., Almendros, J., Carmona, E., Martínez-Arévalo, C., and Abril, M.: The recent seismo-volcanic activity at Deception Island volcano. *Deep-Sea Res. II* 50, 1611–1629, 2003.

Keller, R.A., Fisk, M.R., White, W.M., and Birkenmajer, K.: Isotopic and trace element constraints on mixing and melting models of marginal basin volcanism, Bransfield Strait, Antarctica. *Earth Planet Sci. Lett.* 111, 287–303, 1992.

Kendall, E.N.: An account of the Island of Deception, one of the New Shetland Isles. Extracted from the private journal of Lieutenant Kendal, R.N., embarked on board his Majesty's sloop *CJumticieer*, Captain Foster, on a scientific voyage; and communicated by John Barrow, Esq., F.R.S. *Journal of the Royal Geographical Society*, London 1, 62-66, 1831.

Kinvig, H.S., Winson, A., and Gottsmann, J.: Analysis of volcanic threat from Nisyros Island, Greece, with implications for aviation and population exposure. *Nat. Hazards Earth Syst. Sci.* 10, 1101–1113, 2010.

López-Martínez, J., Serrano, E., Rey, J., and Smellie, J.L.: Geomorphological map of Deception Island. BAS GEOMAP Series, Sheet 6-B, 1:25,000. *Br. Antarct. Surv.*, Cambridge, 2000.

Lutz, T. M. and Gutmann, J. T.: An improved method for determining and characterizing alignments of point-like features and its implications for the Pinacate volcanic field, Sonoran, Mexico. *J. Geophys. Res.* 100, 17659–17670, 1995.

Maestro, A., Somoza, L., Rey, J., Martínez-Frías, J., and López-Martínez, J.: Active tectonics, fault patterns, and stress field of Deception Island: a response to oblique convergence between the Pacific and Antarctic plates. *Jour. South Am. Earth Sci.* 23, 256–268, 2007.

Malin, M.C. and Sheridan, M.F.: Computer-assisted mapping of pyroclastic surges. *Science* 217, 637–640, 1982.

Martí, J., Aspinall, W., Sobradelo, R., Felpeto, A., Geyer, A., Ortiz, R., Baxter, P., Cole, P., Pacheco, J., Blanco, M., and Lopez, C.: A long-term volcanic hazard event tree for Teide-Pico Viejo stratovolcanoes (Tenerife, Canary Islands). *J. Volcanol. Geotherm. Res.* 178(3), 543-552, 2008.

Martí, J. and Felpeto, A.: Methodology for the computation of volcanic suscep-

tibility: Application to Tenerife Island (Canary Islands). *J. Volcanol. Geotherm. Res.* 195, 69-77, 2010.

Martí, J., Sobradelo, R., Felpeto, A., and García, O.: Eruptive scenarios of phonolitic volcanism at Teide-Pico Viejo volcanic complex (Tenerife, Canary Islands). *Bull. Volcanol.* 74, 767–782, 2012.

Martí, J., Geyer, A., and Aguirre-Diaz, G.: Origin and evolution of the Deception Island caldera (South Shetland Islands, Antarctica). *Bull. Volcanol.* 75, 732, 2013.

Martin, A.J., Umeda, K., Connor, C.B., Weller, J.N., Zhao, D., and Takahashi, M.: Modeling long-term volcanic hazards through Bayesian inference: an example from the Tohoku volcanic arc Japan, *J. Geophys. Res.* 109, B10208, 2004.

Marzocchi, W., Sandri, L., and Selva, J.: BET EF: a probabilistic tool for long- and short-term eruption forecasting. *Bull. Volcanol.* 70(5), 623–632, 2008.

Marzocchi, W., Sandri, L., and Selva, J.: BET VH: a probabilistic tool for long-term volcanic hazard assessment. *Bull. Volcanol.* 72, 705–716, 2010.

Mathies, D., Mäusbacher, R., and Storzer, D.: Deception Island tephra: a stratigraphical marker for limnic and marine sediments in Bransfield Strait area, Antarctica. *Zentralbl. Geol. Paläontol. Teil (1-2)*, 153-165, 1990.

Moreton, S.G. and Smellie, J.L.: Identification and correlation of distal tephra layer; in deep-sea sediment cores, Scotia Sea, Antarctica. *Annals of Glaciology* 27, 285-289, 1998.

Moreton, S.C.: Quaternary tephrochronology of the Scotia Sea and Bellingshausen Sea, Antarctica. Ph.D. thesis, Cheltenham and Gloucester College of Higher Education, pp. 164, unpublished, 1999.

Neri, A., Aspinall, W.P., Cioni, R., Bertagnini, A., Baxter, P.J., Zuccaro, G., Andronico, D., Barsotti, S., Cole, P.D., Esposti Ongaro, T., Hincks, T.K., Macedonio, G., Papale, P., Rosi, M., Santacroce, R., and Woo, G.: Developing an event tree for probabilistic hazard and risk assessment at Vesuvius. *J. Volcanol. Geotherm. Res.* 178(3), 397-415, 2008.

Newhall, C. G. and Hoblitt, R. P.: Constructing event trees for volcanic crisis. *Bull. Volcanol.* 64, 3–20, 2002.

Orheim, O.: A 200-year record of glacier mass balance at Deception Island, southwest Atlantic Ocean, and its bearing on models of global climate change, Institute of Polar Studies, Ohio State University, 118, 1972.

Ortiz, R., Araña, V., Vila, J., Viramonte, J.G., and Mazzuoli, R.: Mecanismos de

erupción de la reciente actividad volcánica en Decepción, *Actas II Simposio Español de Estudios Antárticos, CSIC*, 217–227, 1987.

Palais, J.M., Kirchner, S., and Delmas, R.: Identification and correlation of volcanic eruption horizons in a 1000 year ice-core record from the South Pole. *Antarctic Journal US Review* 24, 101-104, 1989.

Pallàs, R., Smellie, J.L., Casas, J.M., and Calvet, J.: Using tephrochronology to date temperate ice: correlation between ice tephros on Livingston Island and eruptive units on Deception Island volcano (South Shetland Islands, Antarctica). *The Holocene* 11(2), 149-160, 2001.

Patrick, M. and Smellie, J.L.: Synthesis. A spaceborne inventory of volcanic activity in Antarctica and southern oceans, 2000–10. *Antarctic Sci.* 25(4), 475–500, 2013.

Peccerillo, A., Tripodo, A., Villari, L., Currieri, S., and Zimbalaiti, E.: Genesis and evolution of volcanism in back-arc areas. A case history, the Island of Deception (Western Antarctica). *Periodico di Mineralogia* 60, 29-44, 1991.

Pedrazzi, D., Aguirre Díaz, G., Bartolini, S., Martí, J., and Geyer, A.: The 1970 eruption on Deception Island (Antarctica): eruptive dynamics and implications for volcanic hazards. *J. Geol. Soc. London*, in press, 2014.

Peci, L.M., Berrocoso, M., Fernández-Ros, A., García, A., Marrero, J.M., and Ortiz, R.: Embedded ARM System for Volcano Monitoring in Remote Areas: Application to the Active Volcano on Deception Island (Antarctica). *Sensors* 14, 672-690, 2014.

Prates, G., Berrocoso, M., Fernández-Ros, A., and García, A.: Enhancement of sub-daily positioning solutions for surface deformation monitoring at Deception volcano (South Shetland Islands, Antarctica). *Bull. Volcanol.* 75(2), 1-10, 2013.

Ramos, M., Ortiz, R., Diez-Gil, J.L., and Viramonte, J.: Anomalías térmicas y balance de flujo energético sobre el suelo del volcán Decepción, Isla Decepción (Shetland del Sur). *Actas del III Simposium Español de Estudios Antárticos, CSIC*, 203-219, 1989.

Rey, J., Somoza, L., and Martínez-Frías, J.: Tectonic, volcanic, and hydrothermal event sequence on Deception Island (Antarctica). *Geo Mar. Lett.* 15, 1–8, 1995.

Roach, P.J.: The nature of back-arc extension in Bransfield Basin. *Geophys. J. Royal Astron. Soc.* 53, 165, 1978.

- Roobol, M.J.: Historic volcanic activity at Deception Island. *Br. Antarct. Surv. Bull.* 32, 23-30, 1973.
- Roobol, M.J.: A model for the eruptive mechanism of Deception Island from 1820 to 1970. *Br. Antarct. Surv. Bull.* 49, 137-156, 1980.
- Roobol, M.J.: The volcanic hazard at Deception Island, South Shetland Islands. *Br. Antarct. Surv. Bull.* 51, 237-245, 1982.
- Schilling, S.P.: LAHARZ: GIS program for automated mapping of lahar-inundation hazard zones. U.S. Geological Survey Open-File Report, pp. 98-638, 1998.
- Sheridan, M. F. and Malin, M. C.: Application of computer-assisted mapping to volcanic hazard evaluation of surge eruption: Vulcano, Lipari, Vesuvius, explosive volcanism. *J. Volcanol. Geotherm. Res.* 17, 187-202, 1983.
- Shultz, C.H.: Eruption at Deception Island, Antarctica, August 1970. *Geol. Soc. Am. Bull.* 83(9), 2837-2842, 1972.
- Smellie, J.L.: Recent observations on the volcanic history of Deception Island, South Shetland Islands. *Br. Antarct. Surv. Bull.* 81, 83-85, 1988.
- Smellie, J.L.: The upper Cenozoic tephra record in the south polar region: a review. *Glob. Planet Chang.* 21, 51-70, 1999.
- Smellie, J.L.: Lithostratigraphy and volcanic evolution of Deception Island, South Shetland Islands. *Antarctic Sci.* 13, 188-209, 2001.
- Smellie, J.L.: Volcanic hazard. In: López-Martínez, J., Smellie, J.L., Thomson, J.W., Thomson, M.R.A. (Eds.), *Geology and geomorphology of Deception Island*. Cambridge, Br. Antarct. Surv., Natural Environmental Research Council 2002, pp. 47-53, 2002a.
- Smellie, J.L.: The 1969 subglacial eruption on Deception Island (Antarctica): events and processes during an eruption beneath a thin glacier and implications for volcanic hazards. *Volcano-Ice Interactions on Earth and Mars*. Geol. Soc. London, Special Publications 202, 59-79, 2002b.
- Smellie, J.L. and López-Martínez, J.: Introduction. In: López-Martínez, J., Smellie, J.L., Thomson, J.W., Thomson, M.R.A. (Eds.), *Geology and geomorphology of Deception Island*. Cambridge, British Antarctic Survey, Natural Environmental Research Council 2002, pp. 1-6, 2002.
- Smellie, J.L., López-Martínez, J., and others: *Geology and geomorphology of Deception Island*. BAS GEOMAP series, Sheets 6-A and 6-B, 1:25 000. Cambridge, Br. Antarct. Surv., Cambridge, pp. 78, 2002.

Smith, R.L., Baldwin, R.J., Glatts, R.C., Chereskin, T.K., Ruhl, H., and Lagun, V.: Weather, ice, and snow conditions at Deception Island, Antarctica: long time-series photographic monitoring. *Deep-Sea Research II* 50, 1649–1664, 2003.

Sobradelo, R. and Martí, J.: Bayesian event tree for long-term volcanic hazard assessment: Application to Teide-Pico Viejo stratovolcanoes, Tenerife, Canary Islands. *J. Geophys. Res.* 115, B05206, 2010.

Sobradelo, R., Bartolini, S., and Martí, J.: HASSET: a probability event tree tool to valuate future volcanic scenarios using Bayesian inference presented as a plugin for QGIS. *Bull. Volcanol.* 76, 770, 2013.

Suzuki, T.: A Theoretical Model for Dispersion of Tephra. In: Shimozuru, D., Yokoyama, I. (Eds.), *Arc Volcanism, Physics and Tectonics*. Terra Scientific Publishing Company, Tokyo, 1983.

Torrecillas, C., Berrocoso, M., and García-García, A.: The Multidisciplinary Scientific Information Support System (SIMAC) for Deception Island. In: D. Fütterer, D. Damaske, G. Kleinschmidt, H. Miller and F. Tessensohn (Editors), *Antarctica*. Springer Berlin Heidelberg, pp. 397-402, 2006.

Toyos, G. P., Cole, P. D., Felpeto, A., and Martí, J.: A GIS-based methodology for hazard mapping of small pyroclastic density currents. *Nat. Hazards* 41, 99–112, 2007.

Turner, J. and Pendlebury, S.: *The International Antarctic Weather Forecasting Handbook*. Br. Antarct. Surv., Cambridge, 2004.

Valencio, A., Mendía, E., and Vilas, J.: Palaeomagnetism and K-Ar age of Mesozoic and Cenozoic igneous rocks from Antarctica. *Earth Planet. Sci. Lett.* 45, 61-68, 1979.

Valenzuela, E., Chávez, L., and Munizaga, F.: Informe preliminar sobre la erupción de la isla Decepción ocurrida en diciembre de 1967. Instituto Antártico Chileno Serie 1, 5-16, 1968.

Valenzuela, E., Chávez, L., and Munizaga, F.: Actividad volcánica en isla Decepción, Antártica, 1967. Instituto Antártico Chileno Serie 1, 25-40, 1970.

Wilkes, C.: *American Exploring Expedition: Narrative of the United States Exploring Expedition during the years 1838-1842 I-V*, Lea and Blanchard, Philadelphia, 1845.

Woo, G.: *The mathematics of natural catastrophes*. Imperial College Press, London, 1999.

Zandomenghi, D., Barclay, A., Almendros, J., Ibáñez, J.M., Wilcock, W.S.D., and Ben-Zvi, T.: The crustal structure of Deception Island Volcano from P wave seismic tomography: tectonic and volcanic implications. *J. Geophys. Res.* 11, B06310, 2009.

Supplementary material 1

HAZARDS FACTORS	SCORE (max)	SCORE (min)
Volcano type If volcano type is cinder cone, basaltic field, small shield, or fissure vents: Score=0 If volcano type is stratocone, lava domes, complex volcano, maar or caldera: Score=1	1	1
Maximum Volcano Explosivity Index (VEI) If maximum known VEI < or = 2: Score=0 If maximum known VEI=3 or 4: Score=1 If maximum known VEI=5 or 6: Score=2 If maximum known VEI < or = 7: Score=3 If no maximum VEI is listed by GVP and if volcano type=0: Score=0 If no maximum VEI is listed by GVP but volcano type=1: Score=1 If no known Holocene eruptions and the volcano is not a silicic caldera system: Score=0	1	1
Explosive activity If explosive activity (VEI > or = 3) within the past 500 years: Score=1	1	1
Major explosive activity If major explosive activity (VEI > or = 4) within past 5,000 years: Score=1	1	0
Eruption recurrence If eruption interval is 1-99 years: Score=4 If eruption interval is 100-1,000 years: Score=3 If eruption interval is 1,000 to 5,000 years: Score=2 If eruption interval is 5,000-10,000 years, or if no Holocene eruptions but it is a large-volume restless silicic system that has erupted in the last 100,000 years: Score=1 If no known Holocene eruption: Score=0	4	4
Holocene pyroclastic flows? If yes: Score=1	1	1
Holocene lava flows? If Holocene lava flows have traveled beyond the immediate eruption site or flanks and reached populated areas: Score=1	1	1
Holocene-lahars? If Holocene lahars have traveled beyond the flanks and reached populated areas: Score=1	1	1
Holocene tsunami (s)? Has it produced a tsunami within the Holocene? If yes: Score=1	1	1
Hydrothermal explosion potential If the volcano has had Holocene phreatic explosive activity, and/or the volcano has thermal features that are extensive enough to pose a potential for explosive activity: Score=1	1	1
Sector collapse potential If the volcano has produced a sector collapse in Quaternary time and has rebuilt its edifice, or, has high relief, steep flanks and demonstrated or inferred alteration: Score=1	1	1
Primary lahar source If volcano has a source of permanent water/ice on edifice, water volume >10e6 m3: Score=1	1	1
<i>Subtotal HAZARDS FACTORS</i>	15	14
HISTORICAL UNREST FACTORS	SCORE (max)	SCORE (min)
Observed seismic unrest Since the last eruption, in the absence of eruptive activity, within 20 km of the volcanic edifice? If yes: Score=1	1	1
Observed ground deformation Since the last eruption, in the absence of eruptive activity, inflation or other evidence of magma injection? If yes: Score=1	1	1
Observed fumarolic or magmatic degassing Since the last eruption, in the absence of eruptive activity, either heat source or magmatic gases? If yes: Score=1	1	1
<i>Subtotal HISTORICAL UNREST FACTORS</i>	3	3
TOTAL HAZARD FACTORS	18	17
EXPOSURE FACTORS	SCORE (max)	SCORE (min)
Volcano Population Index (VPI) at 30 km		

Calculated with LandScan population database. Visitor statistics for volcanoes in National Parks and other destination recreation areas are added to the VPI factor where available.

Population downstream or downslope

Population outside the 30 km VPI circle included within the extent of Holocene flow deposits or reasonable inundation modeling. This factor to be used only with volcanoes that have a primary lahar hazard e.g. Cascade stratovolcanoes or significant lava flow hazard e.g. Mauna Loa.

Historical fatalities

If yes, and a permanent population is still present: Score=1

Historical evacuations

If yes, and a permanent population is still present: Score=1

Local aviation exposure

If any type volcano is within 50 km of a jet-service airport, Score=1;
 If a Type 1 volcano is within 300 km of a jet-service airport, Score=1;
 If a Type 1 volcano is within 300 km of a major international airport, Score=2;
 If none of these criteria are met, Score=0.

Regional aviation exposure

This score is based on the log10 of approximate daily passenger traffic in each region. At present, in the U.S., this score ranges from 4 to 5.15. The regional risk code is applied only to type 1 volcanoes and those type 0 volcanoes that have produced explosive eruptions.

Power infrastructure

Is there power infrastructure e.g., power generation/transmission/distribution for electricity, oil, or gas within flowage hazard zones, or in an area frequently downwind of the volcano and close enough to be considered at some risk? If yes, Score=1

Transportation infrastructure

Is there transportation infrastructure e.g. port facilities, rail lines, major roads within flowage hazard zones, or in an area frequently downwind of the volcano and close enough to be considered at some risk? If yes, Score=1

Major development or sensitive areas

Are there major developments or sensitive areas threatened e.g., National Park facilities, flood control projects, government facilities, developed tourist/recreation facilities, manufacturing or other significant economic activity? If yes, Score=1

Volcano is a significant part of a populated island

Holocene volcanic deposits cover 25% of land mass. If yes, score=1

	3	1.7
Population downstream or downslope	0	0
Historical fatalities	0	0
Historical evacuations	0	0
Local aviation exposure	1	1
Regional aviation exposure	2	0
Power infrastructure	1	1
Transportation infrastructure	1	1
Major development or sensitive areas	1	1
Volcano is a significant part of a populated island	1	1
TOTAL EXPOSURE FACTORS	10	6.7

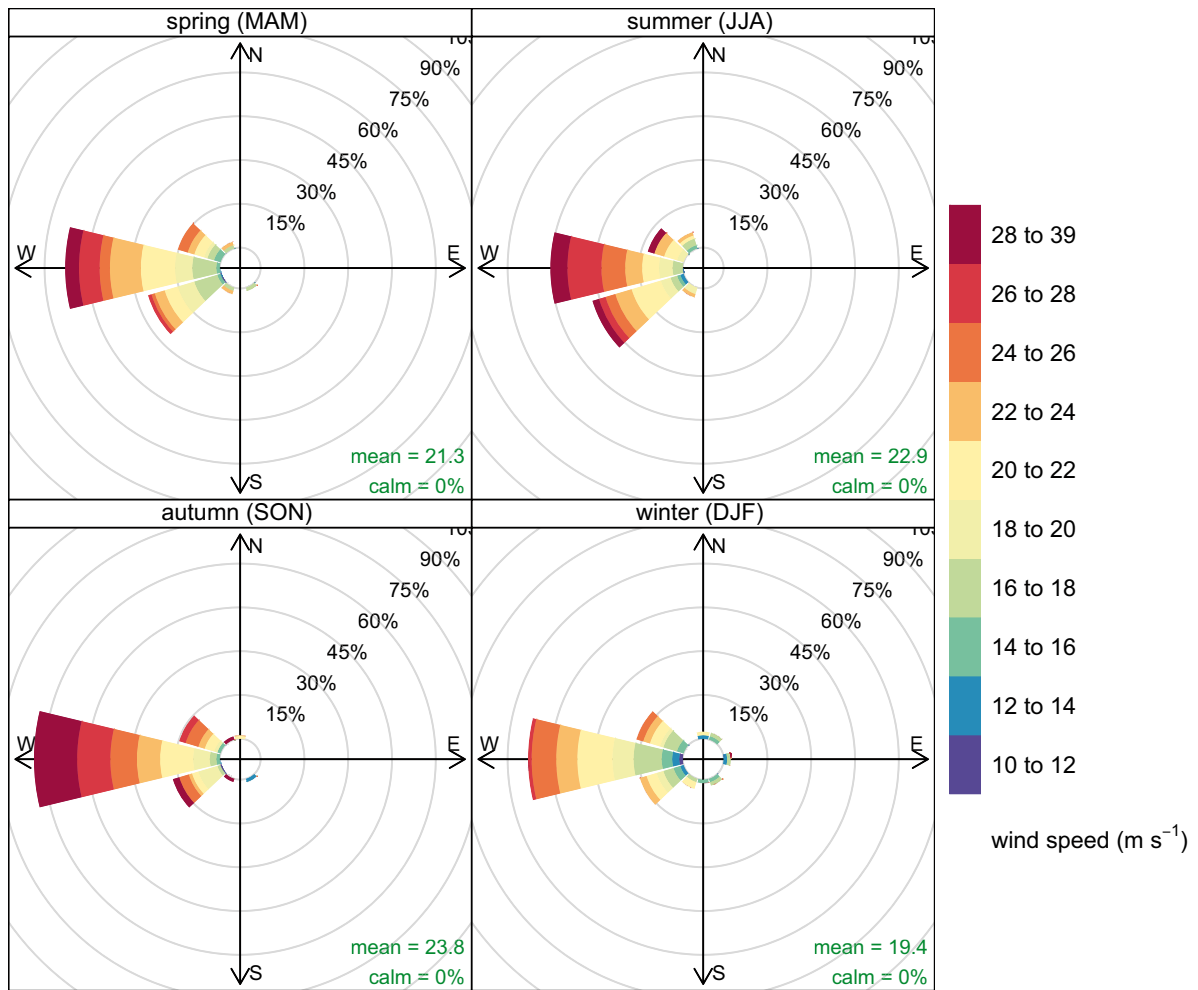
RELATIVE THREAT RANKING

	TOTAL HAZARD FACTORS	X	TOTAL EXPOSURE FACTORS	=	
max. VALUE	18	x	10	=	180
min. VALUE	17	x	6.7	=	113.9

VERY HIGH Threat	>113
HIGH Threat	113-63
MODERATE HIGH Threat	63-30
LOW Threat	30-6
VERY LOW Threat	6-0

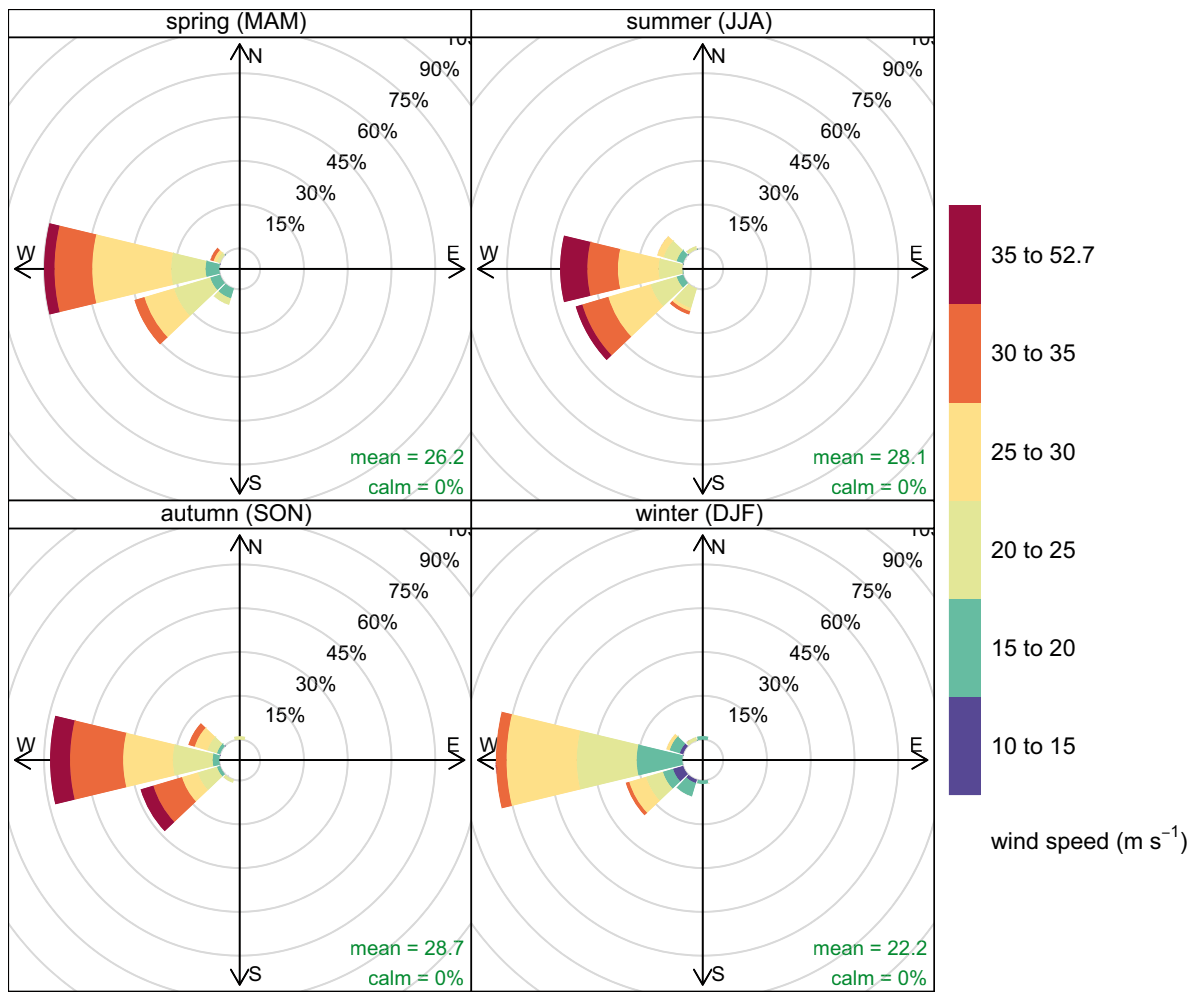
Supplementary material 2

WIND ANNUAL AVERAGE (speed and direction) AT 1500 m



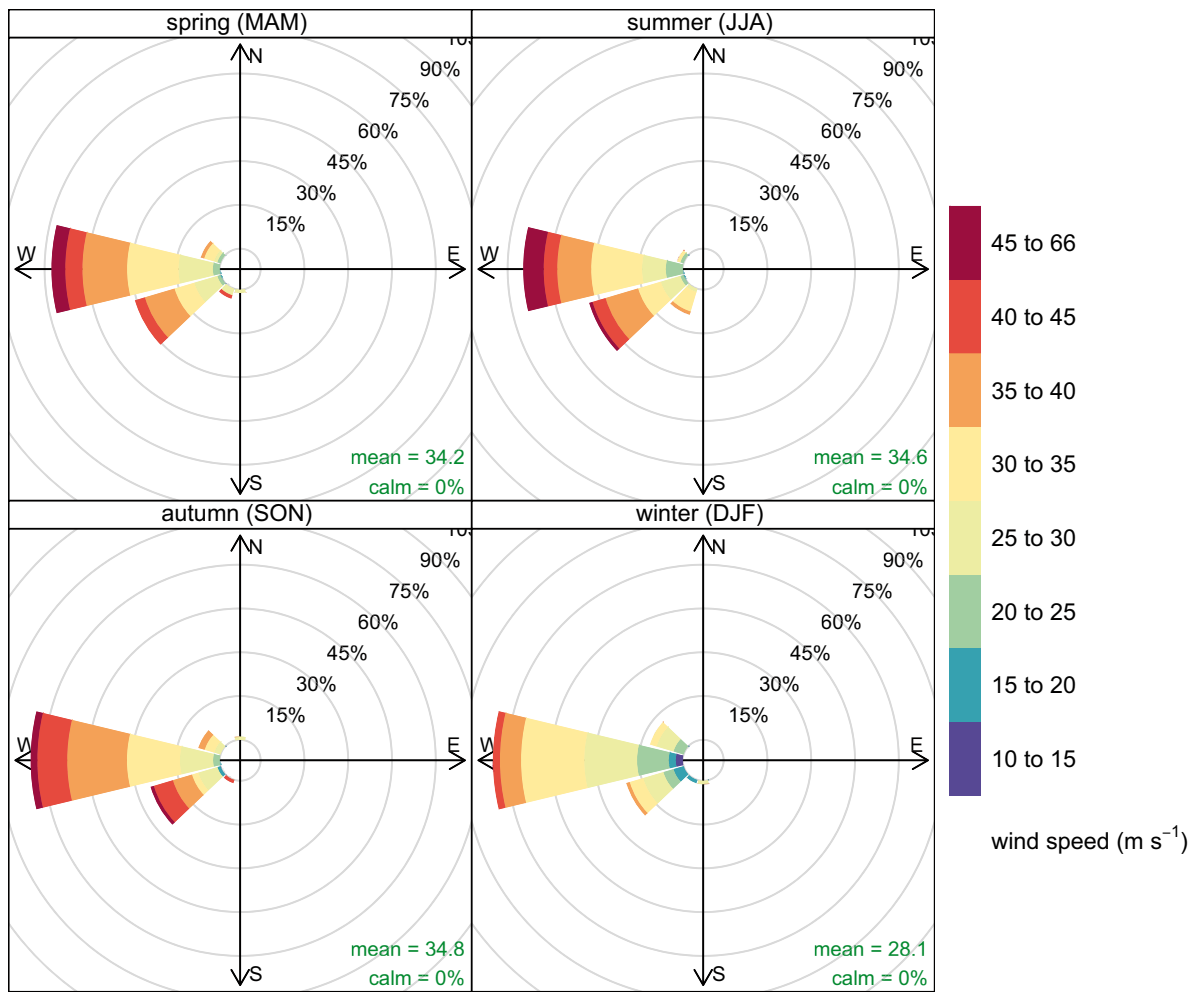
Frequency of counts by wind direction (%)

WIND ANNUAL AVERAGE (speed and direction) AT 3000 m



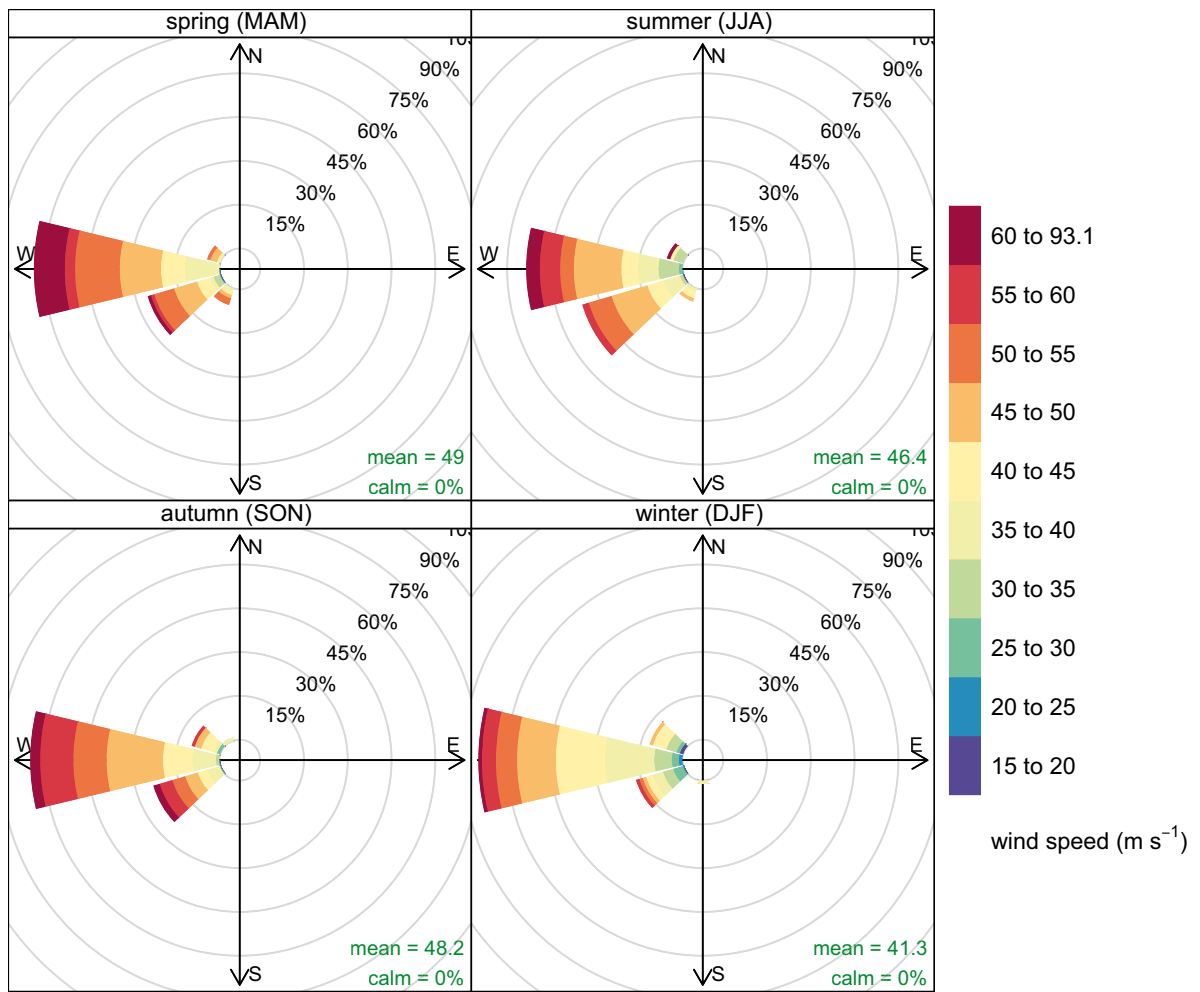
Frequency of counts by wind direction (%)

WIND ANNUAL AVERAGE (speed and direction) AT 5500 m



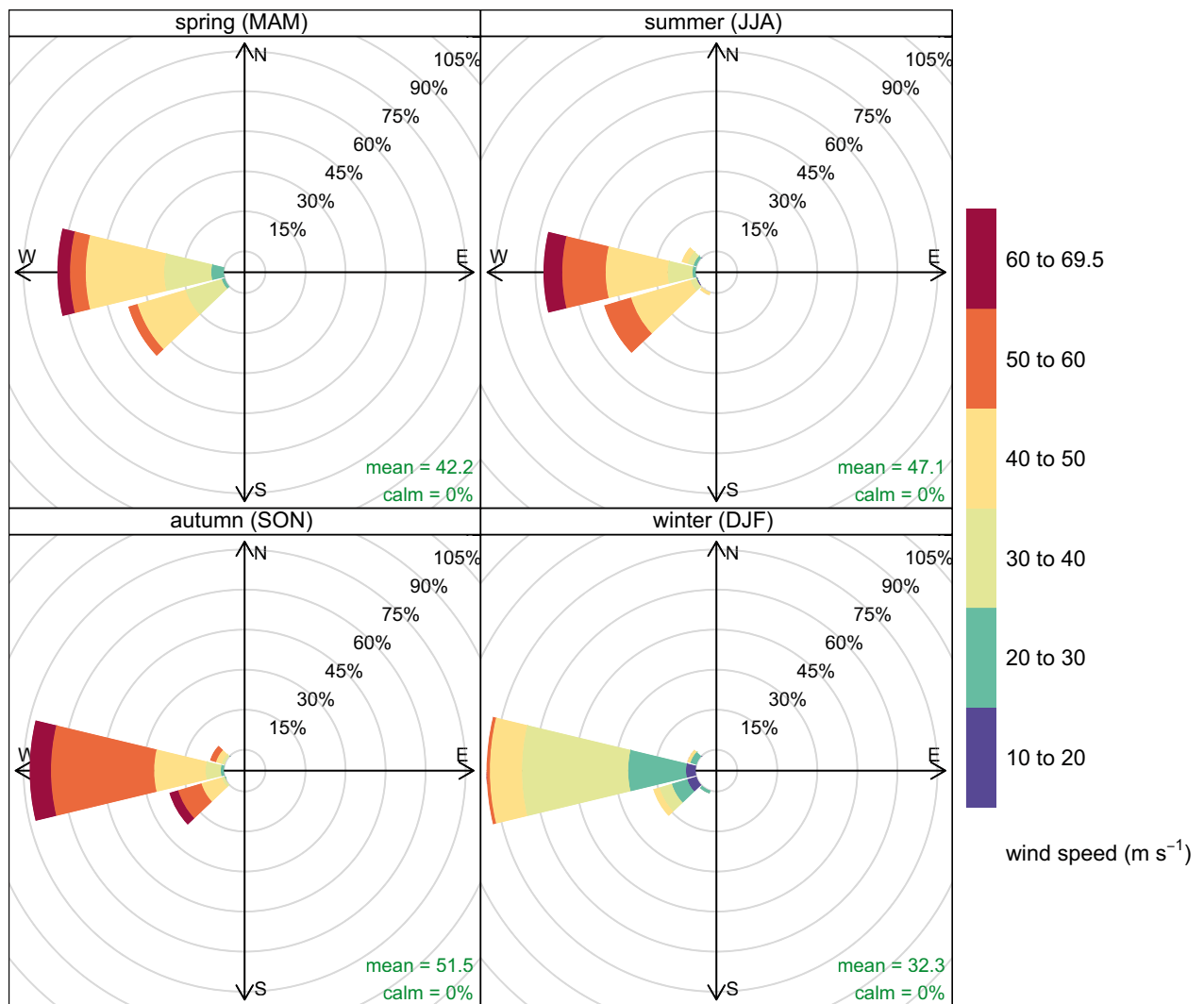
Frequency of counts by wind direction (%)

WIND ANNUAL AVERAGE (speed and direction) AT 9000 m



Frequency of counts by wind direction (%)

WIND ANNUAL AVERAGE (speed and direction) AT 12000 m



Frequency of counts by wind direction (%)

Hazard assessment at the Quaternary La Garrotxa Volcanic Field (NE Iberia)

Submitted to:

Journal of Quaternary Science

Authors:

Stefania Bartolini^a

Xavier Bolós^a

Joan Martí^a

Elisabeth Riera Pedra^a

Llorenç Planagumà^b

a) Group of volcanology, (SIMGEO-UB), Institute of Earth Sciences Jaume Almera, ICTJA-CSIC, Barcelona, Spain

b) Tosca, Environment Services of Education. Casal dels Volcans, Av. Santa Coloma, 17800 Olot, Spain

6.1 Abstract

La Garrotxa Volcanic Field (GVF), located in NE Iberian Peninsula, is one of the Quaternary alkaline volcanic provinces of the European Cenozoic Rifts System. This volcanic zone has been active during the last 12 Ma, being the last dated eruption of early Holocene age. The volcanic activity varies from Hawaiian to Violent Strombolian, showing numerous episodes of phreatomagmatic activity, and has been controlled by the main regional normal faults generated during the Neogene extension that affected the area. Despite the potentiality for future eruptions and the fact that this is a densely populated and industrialised area, volcanic hazard assessment has not been conducted yet. In this work, we present the first comprehensive evaluation of volcanic hazard at La Garrotxa Volcanic Field, through (1) an evaluation of the volcanic susceptibility, (2) a temporal recurrence rate analysis, (3) a simulation of different eruptive scenarios, such as lava flow, pyroclastic density current (PDC), and ash fall, and (4) the elaboration of a qualitative hazard map. The final hazard map shows La Garrotxa volcanic field subdivided into five different levels of hazards and aims to become useful for land use management planning and elaboration of emergency plans.

Keywords

Garrotxa Volcanic Field · Volcanic hazard · Volcanic susceptibility · Recurrence rate · European Cenozoic Rifts System

6.2 Introduction

The impact of a natural event, as a volcanic eruption, can significantly affect human life. Long periods of quiescence are quite common in many volcanic areas and this often leads to a reduction of the alert level. The consequence is not being prepared to deal with a volcanic crisis. For this reason it is necessary to evaluate the possible hazards that could affect the studied area and develop volcanic hazard and risk maps. Volcanic hazard assessment is part of the scientific task to be achieved in an active volcanic area where population could be affected by an eruptive episode. Possible future volcanic activity can be understood and predicted by analysing the

past eruptive behaviour, through the study of the geological record.

Most of the hazard assessment studies conducted during last years refer to composite or stratovolcanoes located close to populated areas, for which volcanic threat is always present (e.g.: Somma-Vesuvio, Italy (Lirer et al., 2001); Campi Flegrei and Somma-Vesuvio (Alberico et al., 2011); Teide-Pico Viejo, Canary Islands (Martí et al., 2008); Popocatepetl, Mexico (Siebe and Macías, 2006); Mt. Cameroon, Africa (Favalli et al., 2012); Etna, Italy (Cappello et al., 2011)). However, monogenetic volcanic fields are commonly not regarded as potentially dangerous and only a few studies concerning hazard assessment have been conducted in such environments (e.g.: Auckland volcanic field, New Zealand (Bebbington and Cronin, 2011), El Hierro, Canary Islands (Becerril et al., 2014); Tohoku volcanic arc, Japan (Martin et al., 2004)). This is probably due to the relative small size of their eruptions and their episodic recurrence, sometimes separated by inter-eruptive periods of thousands to ten thousands years. Nevertheless, numerous Quaternary monogenetic volcanic fields exist around the World, covering periods of activity from several millions of years to present, sometimes with high potentiality to erupt in the near future (Wood, 1980; Cas and Wright, 1987; Kereszturi and Németh, 2012). Examples of monogenetic eruptions occurred in recent times after long periods of quiescence are not uncommon (e.g.: Jorullo, Mexico (Guilbaud et al., 2011), Parícutin, Mexico (Scandone, 1979), El Hierro, Canary Islands (Becerril et al., 2014)). All this tells us that undertaking hazard assessment in Quaternary monogenetic fields is also necessary as a precautionary measure to reduce volcanic risk, even if no signals of volcanic activity are now present.

La Garrotxa Volcanic Field (GVF) has been active from 0.7 Ma to early Holocene (Araña et al., 1983; Bolós et al., 2014a). Since 2013, this volcanic field is considered as an active volcanic area jointly to other Spanish volcanic zones, such as the Canary Islands (see Spanish for Official Bulletin of the State (B.O.E) of February 11th of 2013). In addition, this area is highly populated with urban, agricultural, industrial and communication infrastructure including an international airport. However, no studies have addressed the assessment of volcanic hazard and risk, essential task that should enable local authorities to apply more rational territorial planning and to design more adequate emergency plans in order to face future volcanic crises.

The aim of this study is to obtain a qualitative long-term volcanic hazard map of the GVF, taking into account that an important part of this zone lies underneath

the city of Olot (almost 40,000 inhabitants). This is a highly industrialised and urbanised area covering about 30 km². Recent studies (Bolós et al 2014a, b, and c) have permitted to obtain a detailed picture of the stratigraphic evolution and structural controls of this volcanic zone, filling the gap of an incomplete knowledge due to urban and industrial construction, and due to a dense carpet of vegetation covering most of volcanic deposits.

Taking advantage of this new geological and volcanological knowledge of the area, we conduct its hazard assessment assuming that the future eruptive behaviour will be similar to the last eruptive activity, thus taking as the main reference for a potential future eruption the eruption of Croscat, the last dated (11-13 ka) of the GVF (Fig. 6.1a and Fig. 6.2). We first describe the main geological, stratigraphic, structural, and volcanological features of the area. Then we compute the volcanic susceptibility by identifying those zones with a higher probability of hosting a new vent. This information is then used to compute different simulations of eruptive scenarios. Finally, we obtain a qualitative hazard map that allows us to identify different levels of hazard in the study area.

6.3 General features of the GVF

GVF is the youngest part of the Catalan Volcanic Zone (CVZ), situated in the NE part of Iberian Peninsula (Fig. 6.1b). This basaltic monogenetic field is one of the Quaternary alkaline volcanic provinces belonging to the European Cenozoic Rift System (Martí et al., 1992; Dèzes et al., 2004). The CVZ ranges in age from >12 Ma to early Holocene and it is mainly represented by alkaline basalts and basanites (Martí et al., 1992; Cebriá et al., 2000). GVF is characterised by small-sized cinder cones formed along widely dispersed fissure zones during monogenetic, short-lived eruptions. Hydromagmatic events were also common. Each eruption was caused by an individual batch of magma that was transported rapidly from the source region, each batch representing the products of an individual partial melting event (Martí et al., 1992; Bolós et al., 2014b). The magma ascent rates indicate that only a relatively short time was required for magma to reach the surface (Bolós et al., 2014b). The intermittent character of this volcanism (Martí et al., 1992) indicates that each eruptive episode corresponds to an intermittent reactivation of the main fault system every 5,000 – 20,000 years. These tectonic reactivations would

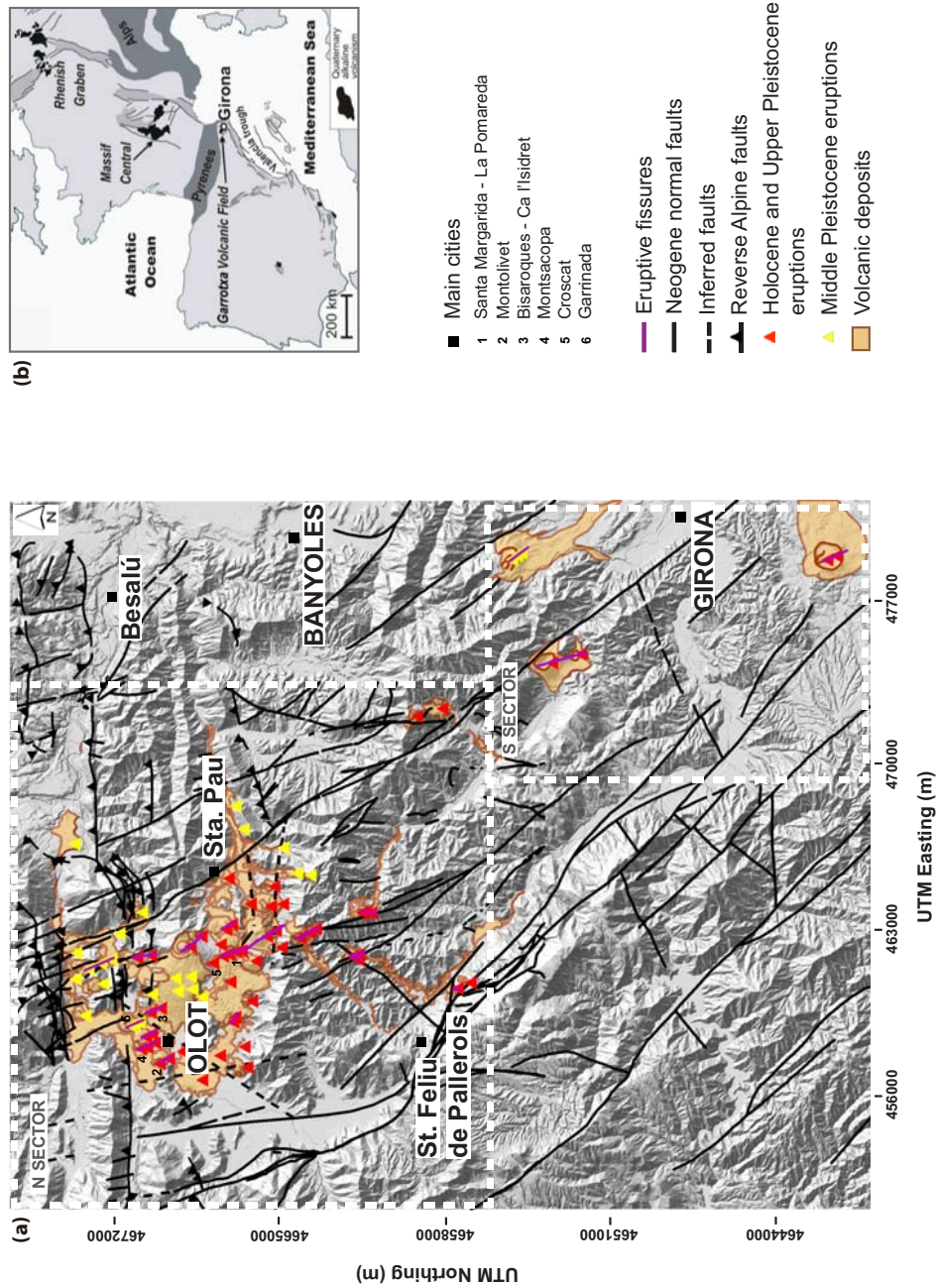


Figure 6.1: a) Simplified geological map of the GVF modified from Bolós et al. (2014b). The sites of the historical volcanic vents, divided into Holocene-Upper Pleistocene and Middle Pleistocene, fissures, normal and transtensional Neogene faults, inferred faults, and reverse Alpine faults. b) Location of the study area

permit the ascent of deep magma and the opening of subordinate fractures in the uppermost crust, which would erupt on the surface each time in a different location in the volcanic field (Bolós et al., 2014b).

The GVF embraces two geographically distinct zones, the larger one located in the north in the area of La Garrotxa and a southerly area that contains fewer but larger and more complex volcanic edifices (Martí et al., 2011; Bolos et al 2014a) (Fig. 6.1a). Although both corresponding to tectonically controlled depressions, the northern sector has a substrate of thick layers of Tertiary affected by Alpine reverse faults and Quaternary sediments. Geophysical data and volcano-structural analysis show that the previous Alpine tectonic structures played no apparent role in controlling the loci of this volcanism (Bolós et al., 2014b). In the southern sector is floored by unconsolidated Quaternary sediments in combination with the Palaeozoic basement.

GVF is formed by more than 50 well preserved monogenetic volcanic cones, distributed along the fracture system of NNW-SSE direction (Barde-Cabusson et al., 2014), corresponding to the Neogene extensional faults system, associated to the main transtensional faults that constrain this volcanic field (Bolós et al., 2014b).

The total volume of extruded magma in each eruption is typical of the monogenetic volcanism (0.01–0.2 km³ Dense-Rock Equivalent (DRE)) (Cimarelli et al., 2013; Bolós et al., 2014a), suggesting that the magma available to feed each eruption was also very limited. Strombolian and phreatomagmatic episodes alternated in most of these eruptions giving rise to complex stratigraphic successions composed of a wide range of pyroclastic deposits (Martí and Mallarach, 1987; Martí et al., 2011).

Most volcanoes show different phases during the same eruptive event. The activity varies from Hawaiian to Violent Strombolian, whereby we found alternate deposits of phreatic phases produced by vapour explosions that only erupted lithic clasts from the substrate, with typical phreatomagmatic phases that generated a wide diversity of pyroclastic density currents and fallout deposits, with typically Strombolian phases including explosive and effusive episodes (Martí et al., 2011).

6.4 Methods

Long-term volcanic hazard assessment is defined as the evaluation of the eruption recurrence and the possible nature of a forthcoming eruption, based on the past

history of the volcano and information from the geological record (Marzocchi et al., 2006; Becerril et al., 2014; Bartolini et al., 2014). To evaluate the long-term volcanic hazard, different steps need to be followed sequentially (see Alcorn et al., 2013; Becerril et al., 2014; Bartolini et al., 2014). In this study, we carried out both temporal and spatial analyses: the former evaluates the recurrence rate of the volcanic activity in the studied area, while the latter uses simulation models to predict the most probable eruptive scenarios and which areas could be affected by a future eruptive event. Since the results from these temporal and spatial analyses are highly dependent on the data used, the selection of the data source is one of the most important steps to be undertaken during the hazard evaluation.

The susceptibility analysis is the first step and enables us to identify which areas have the greatest likelihood of hosting new vents (Martí and Felpeto, 2010). Once the susceptibility analysis has been estimated, the next step consists of computing several eruptive scenarios as a means of evaluating the potential extent of the main expected volcanic and associated hazards. The evaluation of volcanic susceptibility and eruptive scenarios are based on the use of simulation models and Geographical Information Systems (GIS) that allow volcanic hazards to be modelled. Volcanic susceptibility was calculated using QVAST tool (Bartolini et al., 2013), and modelling of eruptive scenarios, which include lava flows, pyroclastic density currents (PDCs), and fallout, used the VORIS 2.0.1 tool (Felpeto et al., 2007). For detailed information regarding each specific tool, readers are referred to the original papers.

6.5 Characterisation of past eruptive activity

To forecast the future behaviour of the volcanic area under study we need to know its past eruptive history. So, we need to characterise the past volcanic activity through the determination of eruptive parameters derived from the study of the erupted products. The last dated and well-studied eruptive episode of La Garrotxa corresponds to the Croscat volcano, one of the most representative edifices of the N sector of the studied area (Fig. 6.1a and Fig. 6.2), so that we take it as the past eruption example to be used to define future eruptive scenarios. This volcano is approximately 160 meters high and has a base diameter of 950 meters and it has been dated in $11,500 \pm 1,500$ years (Martí et al., 2011; Puiguriguer, 2012; Bolós et al., 2014a).

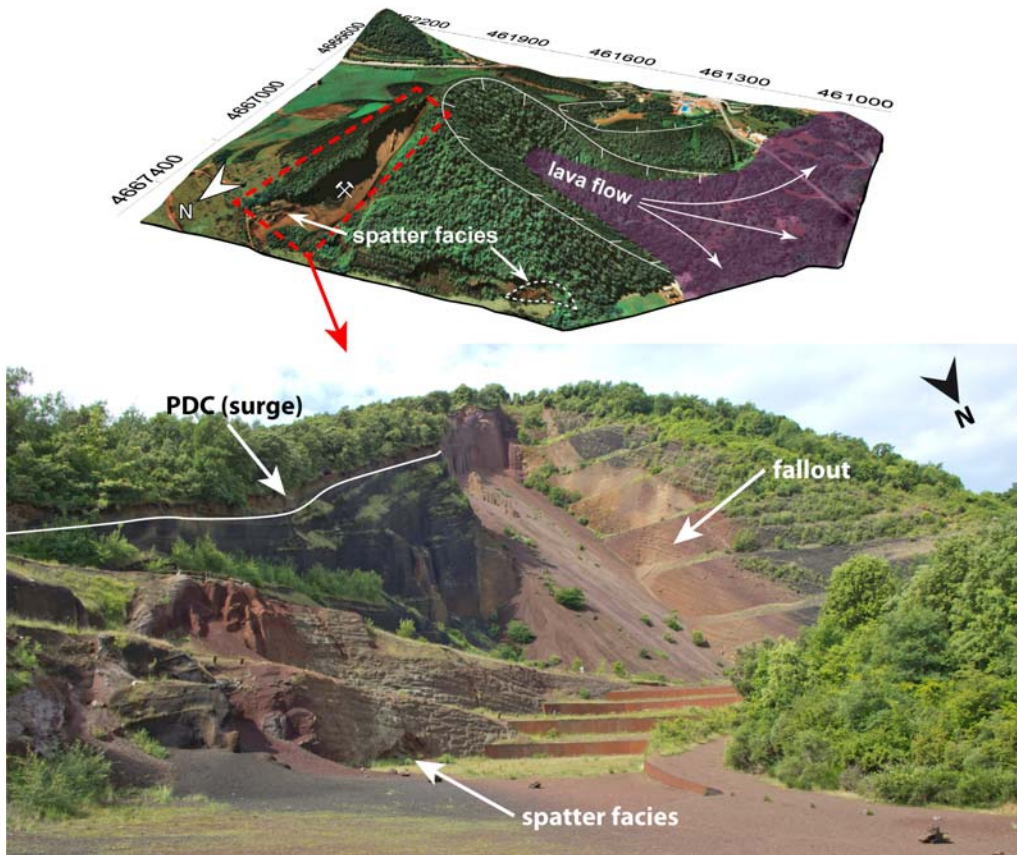


Figure 6.2: Croscat volcano: 3D view with the main volcanic deposits (modified from Bolós et al. (2014a)) and a panoramic view of an outcrop showing the main deposits

Recent studies show as Croscat has a complicated eruptive sequence (Martí et al 2011; Bolos et al., 2014a). The Croscat volcano corresponds to the cone building phase of a more complex eruption that occurred along the longest eruptive fissure identified in this volcanic field (Fig. 6.2). This eruption also created the Santa Margarida and La Pomareda vent sites at both end of the fissure with the Croscat volcano in the middle of it. For the purpose of this study we only consider the Croscat cone building phase. The Croscat activity generated three main scoria fallout units (Di Traglia et al., 2009; Martí et al., 2011) (Fig. 6.2). The lower one corresponds to a spatter deposit formed during a Hawaiian phase that generated also the spatter deposit of La Pomareda at the northern end of the eruptive fissure (Martí et al., 2011; Bolós et al., 2014a). The middle unit conformably overlies the basal spatter and is formed by a several metres thick, poorly stratified Strombolian coarse

lapilli size scoria deposit with several scoria bomb beds. The upper unit constitutes the main volume of the Croscat cone and is formed by a well stratified to thinly laminated, medium to fine lapilli size scoria deposit, more than ten metres thick that contains sparse scoria bombs and blocks and that forms most of the intermediate to distal outcrops towards the east of the volcano, that can be recognised at distances farther than 5 km. It also covers the Pomareda spatter and the phreatomagmatic deposits and the explosion crater of Santa Margarida. The topmost unit of the Croscat pyroclastic succession corresponds to a few metres thick, lithic-rich, thinly laminated pyroclastic surge deposit, thus indicating the return to phreatomagmatic activity towards the end of the eruption. This deposit extends for several kilometres to the east, covering area of 8.4 km².

The last eruptive phase of Croscat corresponds to a lava flow that covered an area of 5 km² and flowed more than 10 km west, with an average thickness of 10 m of the emplacement, which emplacement caused the breaching of the western flank of the cone. The total volume of magma (DRE) emitted during the Croscat eruption is of the order of 0.2 km³.

6.6 Volcanic susceptibility

The first step to undertake hazard assessment is to determine the location of possible new eruptive vents, i.e. the susceptibility analysis (Felpeto et al., 2007; Martí and Felpeto, 2010). In monogenetic volcanism volcanic susceptibility contains a high degree of randomness caused by the changes in regional and/or local stress fields originated by tectonic or lithological contrasts (Martí et al., 2013). So, to reduce the uncertainty in the spatial forecasting, the calculation of the probability of the opening of new emission centres should take into account all available volcano-structural parameters (fractures, faults, location of vents, eruptive fissures, etc. . .). In the case of the GVF, the input parameters we used were the location of past recognisable eruptive vents and fissures, but also structural elements related to this volcanism such as fractures and faults identified in previous geological and geophysical studies (Barde-Cabusson et al., 2014; Bolós et al., 2014b, 2014c).

Once all the input parameters are obtained, the next step is to apply different statistical methods in order to obtain the corresponding probability density functions (PDFs) required to obtain the final susceptibility map (Martin et al., 2004; Felpeto

et al., 2007; Connor and Connor, 2009; Martí and Felpeto, 2010; Cappello et al., 2012; Becerril et al., 2013; Bartolini et al., 2013). The PDFs for the GVF were obtained through the application of the QVAST tool (Bartolini et al., 2013). The most important factor is the smoothing coefficient h that determines the shape and, consequently, the resulting PDF. It depends on a combination of different factors such as the size of the volcanic field and the degree of clustering or density of the volcano-structural data (Cappello et al., 2012; Becerril et al., 2013; Bartolini et al., 2013). The smoothing factor values we used were: (a) 1568 m for Holocene and Upper Pleistocene volcanism vents and fissures, (b) 1900 m for Middle Pleistocene volcanism vents and fissures, (c) 363 m for normal and transtensional Neogen faults, and (d) 5856 m for inferred faults. The PDFs obtained are shown in Figure 6.3.

Once the PDF is obtained for each type of structural data, we need to combine them in a Non-Homogeneous Poisson Process (NHPP) to obtain the final susceptibility map. These weights were assigned using expert elicitation judgment (see Aspinall, 2006; Neri et al., 2008) by members from the Group of Volcanology of Barcelona on the basis of structural criteria (see Martí and Felpeto, 2010), which provide initial indicative probability distributions associated with each PDF. We obtained the following values: 0.5 for the Holocene and Upper Pleistocene volcanism (vents and alignments), 0.25 for the Middle Pleistocene craters and lineaments, 0.15 for normal and transtensional Neogen faults, and 0.07 for inferred faults.

The final susceptibility map obtained is shown in Figure 6.4. The map represents those areas with more or less probability to host a new vent and is important as input parameter in the eruptive scenarios simulation to localise the starting point for simulating lava flows, PDCs, and ash fall.

6.7 Temporal recurrence rate

Temporal analysis to determine the recurrence rate of the volcanic activity is an important issue in hazard assessment, as it allows to calculate the temporal probability of occurrence of a new event.

The approach that we used to calculate the temporal recurrence rate λ_t is based on the repose-time method (Ho et al., 1991; Connor and Conway, 2000). In this method, the average recurrence rates of volcanic events depend only on the measure of the relative activity of the Garrotxa volcanic field (for details of volcanic events

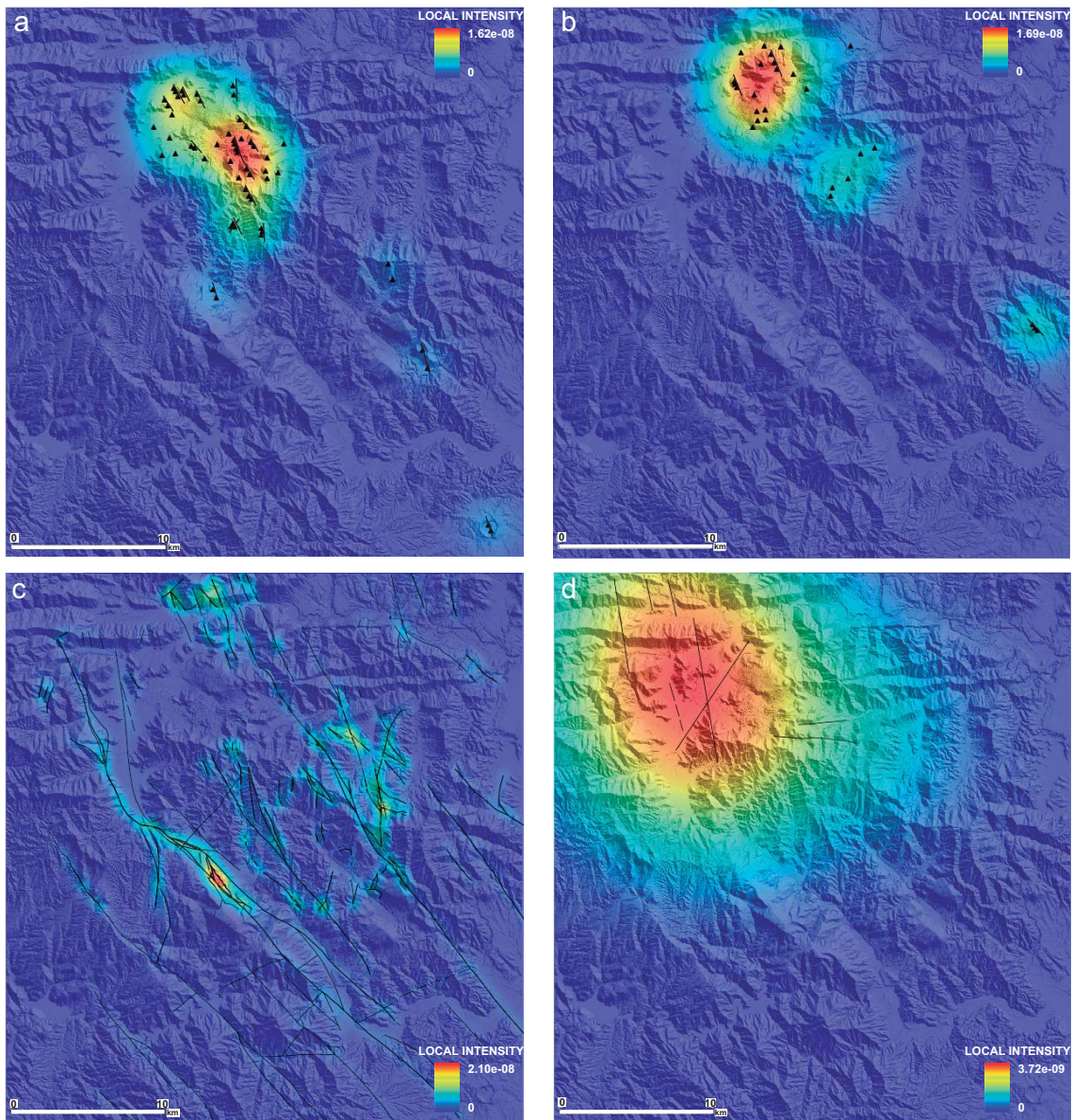


Figure 6.3: PDFs of the five different layers (a–e) considered for the susceptibility analysis: (a) Holocene and Upper Pleistocene volcanism vents (dots) and fissures (lines); (b) Middle Pleistocene volcanism vents (dots) and fissures (lines); (c) Normal and transtentional Neogen faults; and (d) Inferred faults

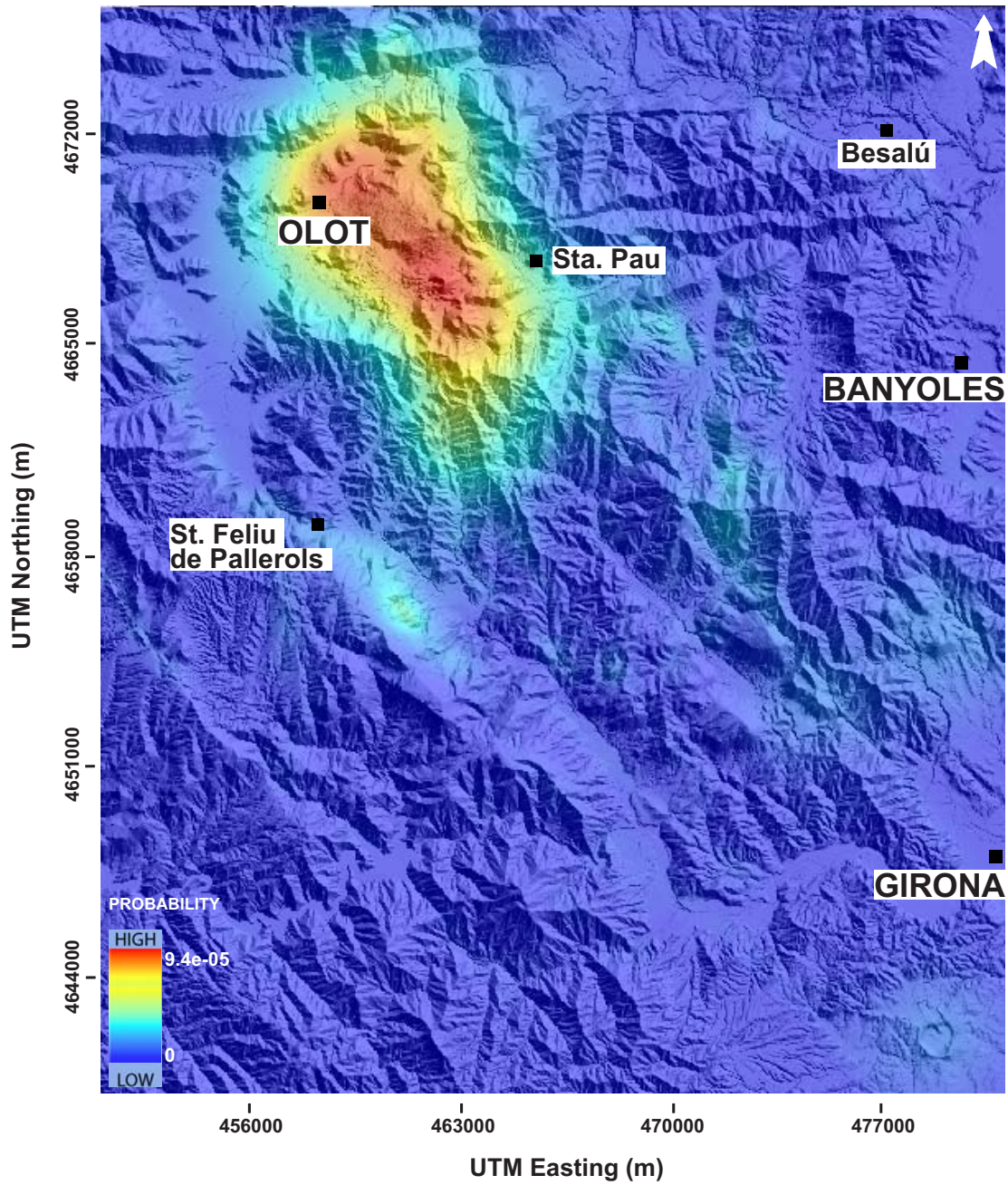


Figure 6.4: Susceptibility map of future eruptions on GVF calculated with QVAST (Bartolini et al., 2013)

in the GVF see Table 2 in Bolós et al., 2014a). Average recurrence rates of volcanic events are a simple measure of the relative activity in volcanic fields, defined using a maximum likelihood estimator that averages events over a specific period of volcanic activity (Connor and Conway, 2000):

$$\lambda_t = \frac{N - 1}{t_0 - t_y} \quad (6.1)$$

where N is the total number of eruptions or vents, t_0 is the age of the oldest event and t_y is the age of the youngest event. For the GVF we obtain a long-term average recurrence rate of $7.7 * 10^{-5}$ volcanic events per year (v/yr).

6.8 Eruptive scenarios

Eruptive scenarios were computed using a VORIS 2.0.1 tool (Felpeto et al., 2007; available at <http://www.gvb-csic.es/GVB/VORIS/VORIS.htm>), developed in a GIS framework (ArcGis®), which enables to elaborate volcanic hazard maps and eruptive scenarios based on geological record information. The VORIS 2.0.1 tool generates quantitative hazard maps for lava flows and PDCs and simulates fallout deposits for a single vent. A 50 m resolution digital elevation model (DEM) was used for topography during the lava flow and PDC simulations. The DEM was generated by the Institut Cartogràfic i Geològic de Catalunya (ICGC, <http://www.icc.cat>).

In the following subsections we present the input parameters for the models based on the eruptive behaviour of the Croscat volcano described before.

6.8.1 Lava flow

Lava flow model is a probabilistic model based on the assumption that the topography and flow thickness play major roles in determining the path followed by the lava flow (Felpeto et al., 2007 and references therein). Input data for the simulation are a Digital Elevation Model (DEM), the maximum flow lengths and height correction (i.e. average thickness of the flow). The Croscat lava flow flowed for more than 10 km, which is a distance in accordance to other lava flows of the same area (Martí et al., 2011). Thus, we assumed maximum flow lengths in our simulation of the order of 12 km. The thickness used as input data for the models was 10 m, corresponding to the average value of individual flows (Croscat and others) measured in the field.

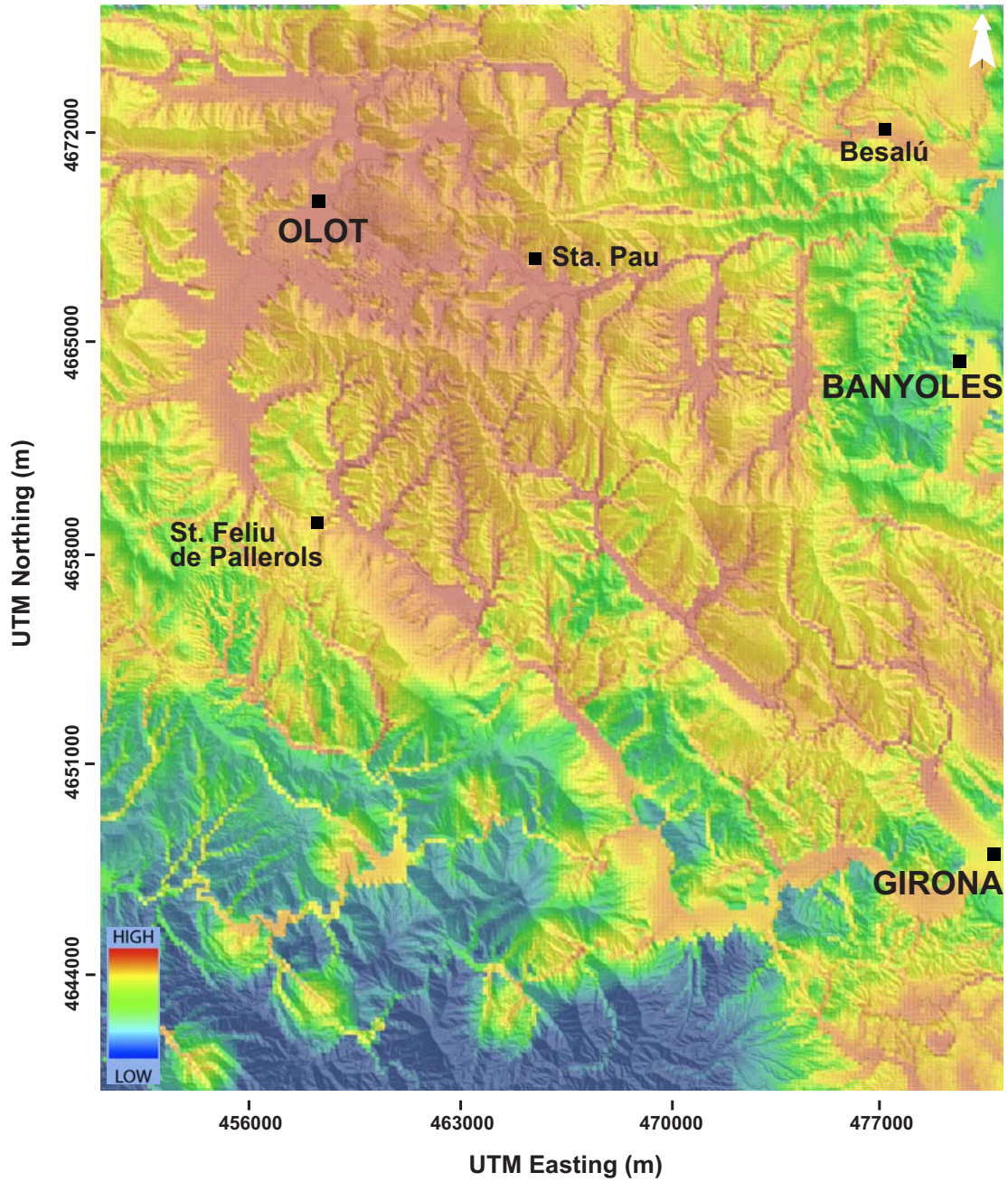


Figure 6.5: Lava flow simulation probability map

We ran simulations for all cells in the DEM and the sum of the 5,000 iterations provided a map with the probability for any particular cell of being covered by a lava flow.

The result of the simulation in the GVF is shown in Figure 6.5. It consists of a lava flow simulation probability map, which shows that there is a moderate-to-high probability that the municipalities of Olot and Girona, two populated areas, will be affected by lava flows.

6.8.2 Pyroclastic density current

Numerical simulation for PDCs is based on the concept of the energy cone model (Malin and Sheridan, 1982; Felpeto et al., 2007; Toyos et al., 2007), constrained by the topography, collapse equivalent height of the column, and friction parameter, known as the collapse equivalent angle. The output of the model is the maximum potential extent that can be affected by the PDC.

The eruptive constraints of the PDC simulation were estimated from the extent of Croscat eruption, one of the best examples of a PDC from the GVF. The runout length was considered equivalent to the most distal exposure of Croscat uppermost phreatomagmatic pyroclastic density current deposit, which lies about 5 km from the crater towards the southeast. To reproduce a PDC deposit similar to that from Croscat, collapse equivalent heights of 400 m above the vent were chosen together with an angle of 6° . The result shows that a PDC could reach with high probability a large area (about 8 km diameter) around the municipality of Olot (Fig. 6.6).

6.8.3 Ash fall

The numerical model for the simulation of ash fall is an advection-diffusion model where the vertical distribution of mass is calculated using the Suzuki approach (Suzuki, 1983; Felpeto et al., 2007). The main input parameters are the volume emitted during the eruption, the height of the column, the particles grain-size characteristics, and the wind data. The result of the ash fall simulation is the thickness of the ash deposit in the analysed area.

The eruptive style considered in this study was a violent Strombolian eruption, which coincides with the main magmatic phase of the Croscat eruption. The corresponding input data were obtained from distribution of the fallout deposits, consid-

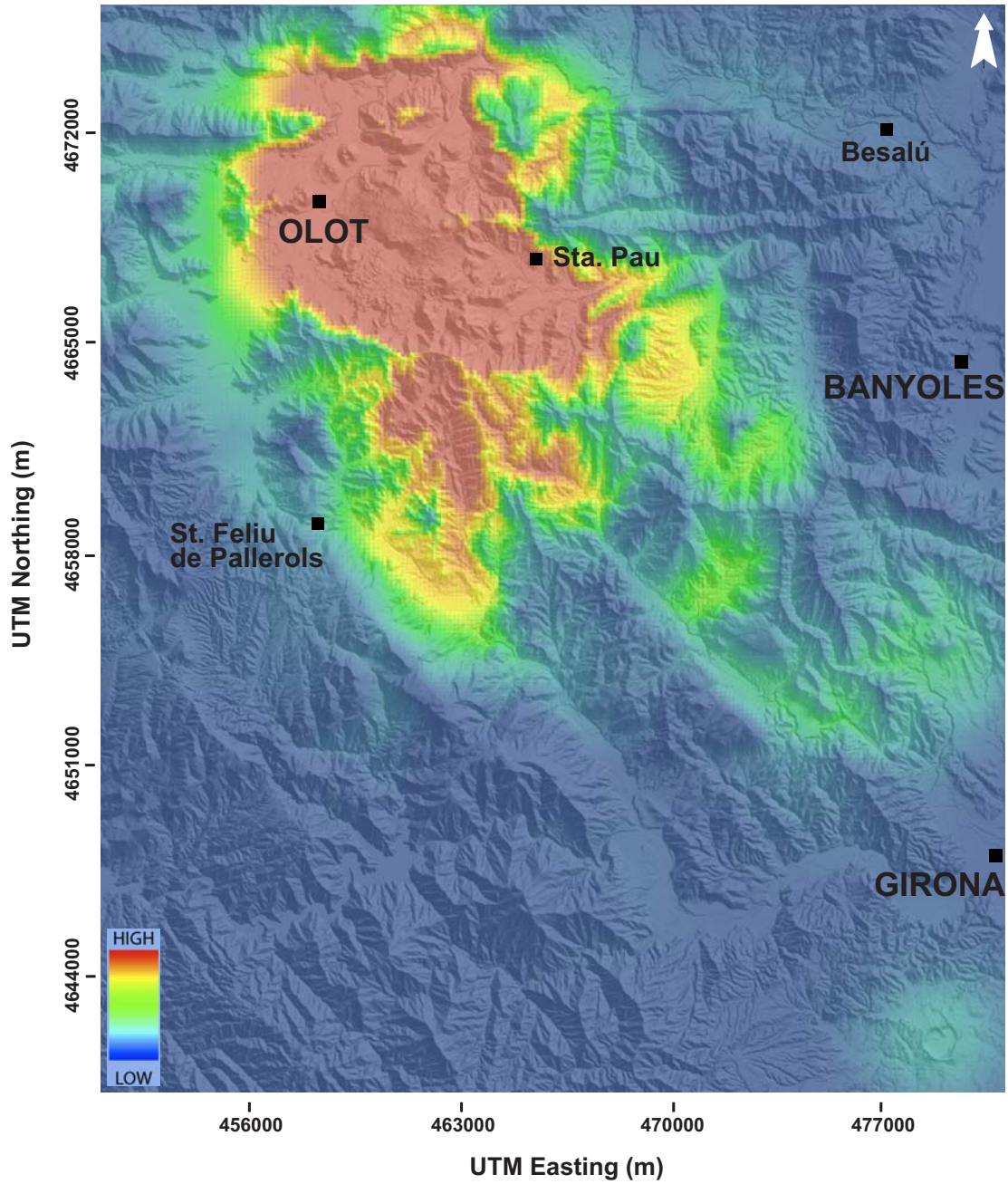


Figure 6.6: PDC simulation probability map

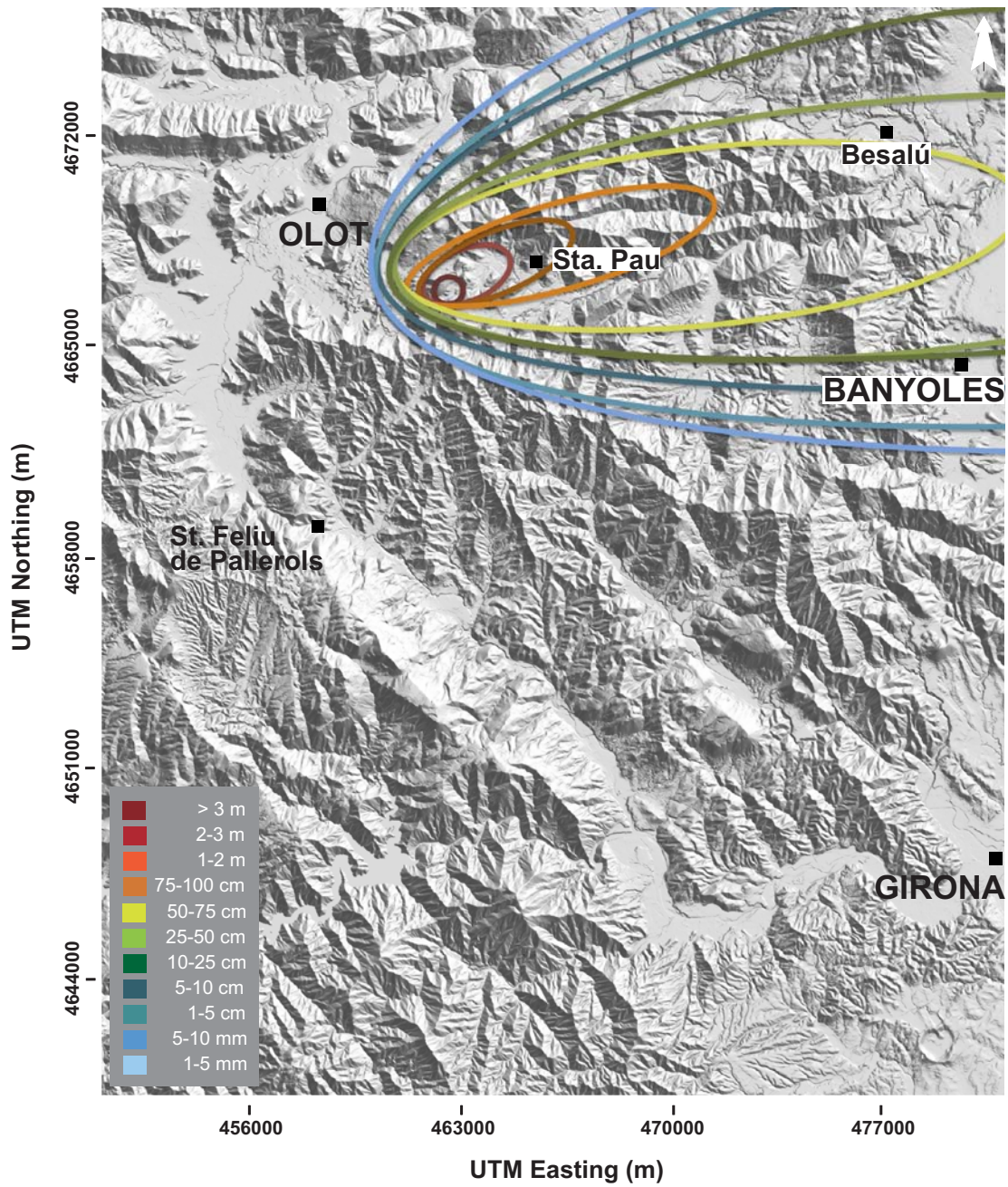


Figure 6.7: Ash fallout simulations with a 8-km column height and volume of 0.05 km^3

ering that the total volume of magma (DRE) emitted was of the order of 0.2 km^3 (Martí et al., 2011). We assumed a volume of about 0.05 km^3 for the fallout phase and an eruptive column about 8 km high, considering that the tephra deposits from this volcanic episode had reached Banyoles Lake 25 km towards the East (Höbig et al., 2012). Westerly and southwesterly winds prevail in general throughout the year at intervals of about 1500 m up to an altitude of 9,000 m (Farnell and Llasat, 2013). Up to five different wind direction inputs and intensities at different vertical heights can be set with the VORIS 2.0.1 tool. Data on particle size were obtained from field studies and grain-size analysis of selected samples sieved in the laboratory.

The result shows that a fallout with the characteristics described above and with W-SW predominant winds could affect a large area of the northwesterly sector of the GVF around the municipality of Olot (Fig. 6.7), according to the ash deposits found in Banyoles lake (Höbig et al., 2012).

6.9 Discussion and conclusions

The long-term hazard assessment is a necessary task to be undertaken at Quaternary monogenetic volcanic fields, even if eruptive activity has not been recorded in recent (historical or pre-historical) times. Most of these volcanic regions show very long recurrence periods, so that they are frequently regarded as non-active. However, the fact that volcanic activity has been present a long time ago, normally for several millions of years, and the fact that the same geodynamic conditions that gave rise to these volcanisms in most cases still prevail, constitute sufficient evidence to consider these areas with the necessary caution to assume that future eruptions may have a low probability but are not impossible. The demographic expansion of most of these areas recommends undertaking hazard assessment as a precaution measure in order to reduce the potential risk that could affect them.

The GVF is a typical monogenetic field in which the lack of data and the absence of recent eruptions could lead us to assume that volcanic hazard and, consequently, risk is inexistent. On the contrary, all geological indicators suggest that the area is subjected to the same geodynamic conditions that favoured the initiation and continuation of this volcanism, so that we must consider this volcanic area as potentially active. In fact the important socio-economic development of the area and the high number of infrastructures, including an international airport, requires to

evaluate the potential hazard of the zone and to identify those areas that could be affected by an eruption of the same type than the ones occurred more recently.

Based on a susceptibility analysis and the identification of the most common eruptive types and products from the geological record, we have applied the available tools, such as QVAST (Bartolini et al., 2013) and VORIS 2.0.1 (Felpeto et al., 2007), designed to undertake volcanic hazard assessment and to update the results whenever new information becomes available. These tools allowed us to simulate different eruptive scenarios and to develop a long-term qualitative hazard map of the area.

The volcanic hazard map of the GVF (Fig. 6.8) has been obtained using a combination of the lava flow, PDC, and fallout eruptive scenario simulations, and represents how the area could be affected by future eruptive events. This first hazard map also takes into account the results of ash fall simulations strictly dependent on the average of the wind directions and velocities, which means that it will be updated if new data were available based on the meteorological predictions. We have considered five different levels of hazard, from very low to very high, thus indicating the relative probability for the area of being affected by any of the hazards considered in this work. The final qualitative hazard map (Fig. 6.8) will be useful to minimise the impact of future volcanic eruptions in the area, allowing local authorities to use it as a reference for land-use planning and for the elaboration of an emergency plan for the GVF.

Acknowledgements

This research has been partially funded by the European Commission (FP7 Theme: ENV.2011.1.3.3-1; Grant 282759: VUELCO). We would like to thank Jordi Zapata of the Museu dels Volcans d'Olot for his help with the meteorological information. The English text was corrected by Michael Lockwood.

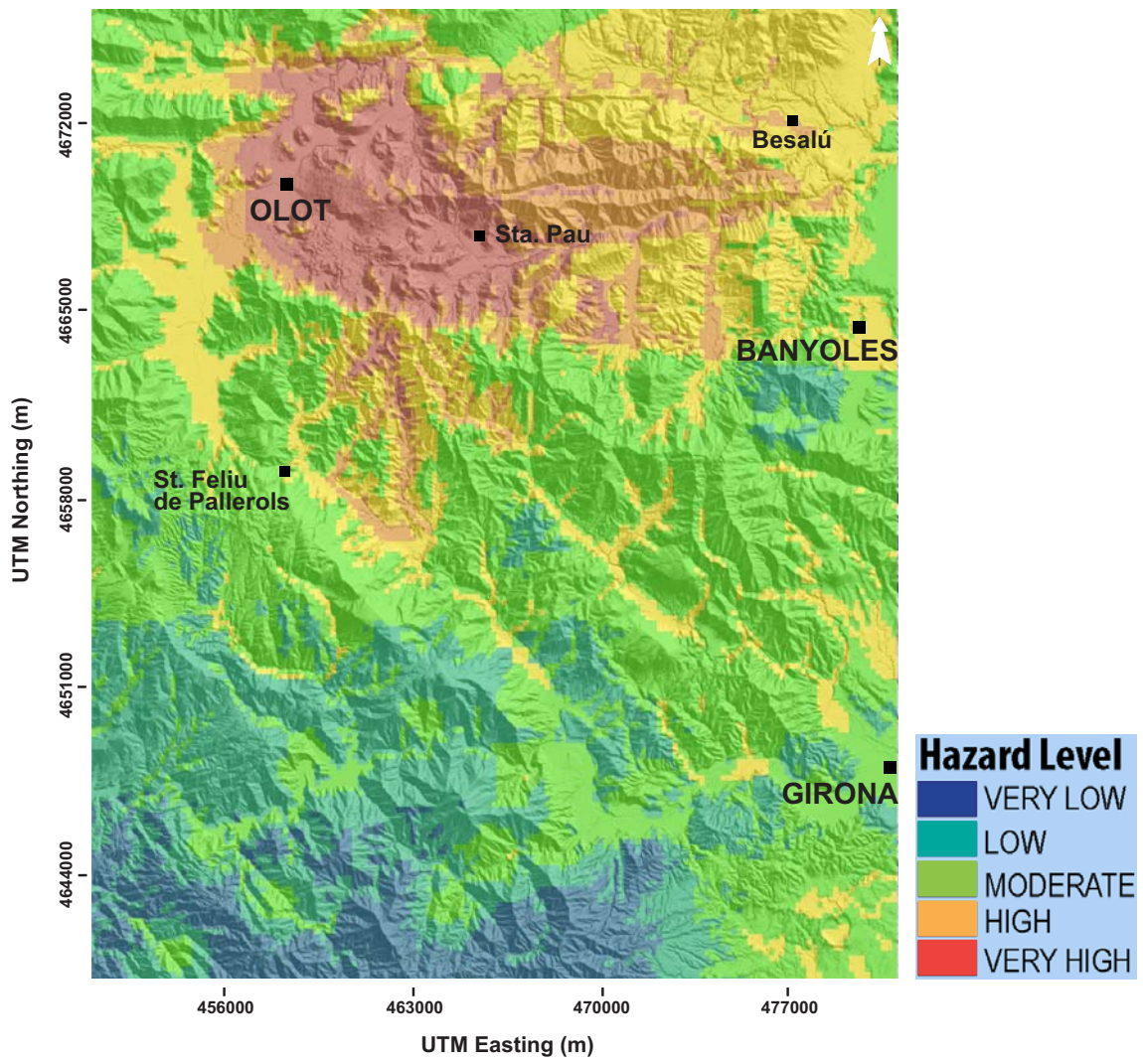


Figure 6.8: Qualitative hazard map for GVF

References

Alberico, I., Petrosino, P., and Lirer, L.: Volcanic hazard and risk assessment in a multi-source volcanic area: the example of Napoli city (Southern Italy). *Natural Hazards and Earth System Science* 11, 1-14, 2001.

Alcorn, R., Panter, K.S., and Gorsevski, P.V.: A GIS-based volcanic hazard and risk assessment of eruptions sourced within Valles Caldera, New Mexico. *Journal of Volcanology and Geothermal Research* 267, 1-14, 2013.

Araña, V., Aparicio, A., Martín Escorza, C., García Cacho, L., Ortiz, R., Vaquer, R., Barberi, F., Ferrara, G., Albert, J., and Gassiot, X.: Neogene-Quaternary volcanism of Catalunya: structural, petrological, and geodynamic characteristics. *Acta Geologica Hispanica* 18, 1-17, 1983.

Aspinall, W.P.: Structured elicitation of expert judgment for probabilistic hazard and risk assessment in volcanic eruptions. In: Mader, H.M., Coles, S.G., Connor, C.B., Connor, L.J. (Eds.), *Statistics in Volcanology*. Special Publication of IAVCEI, 1. Geological Society of London, pp. 15–30, 2006.

Barde-Cabusson, S., Gottsman, J., Martí, J., Bolós, X., Camacho, A.G., Geyer, A., Planagumà, L., Ronchin, E., and Sanchez, A.: Structural control of monogenetic volcanism in the Garrotxa volcanic field (Northeastern Spain) from gravity and self-potential measurements. *Bulletin of Volcanology* 76, 788, 2014.

Bartolini, S., Cappello, A., Martí, J., and Del Negro, C.: QVAST: a new Quantum GIS plugin for estimating volcanic susceptibility. *Natural Hazards Earth System Science* 13, 3031–3042, 2013.

Bartolini, S., Geyer, A., Martí, J., Pedrazzi, D., and Aguirre-Díaz, G.: Volcanic hazard on Deception Island (South Shetland Islands, Antarctica). *Journal of Volcanology and Geothermal Research*, in press, 2014.

Bebbington, M.S. and Cronin, S.J.: Spatio-temporal hazard estimation in the Auckland Volcanic Field, New Zealand, with a new event-order model. *Bulletin of Volcanology* 73, 55–72, 2011.

Becerril, L., Bartolini, S., Sobradelo, R., Martí, J., Morales, J. M., and Galindo, I.: Long-term volcanic hazard assessment on El Hierro (Canary Islands). *Natural Hazards and Earth System Science* 14, 1853-1870, 2014.

Bolós, X., Planagumà, L., and Martí, J.: Volcanic stratigraphy and evolution of the Quaternary monogenetic volcanism in the Catalan Volcanic Zone (NE Spain).

Journal of Quaternary Science 29(6), 547–560, 2014a.

Bolós, X., Martí, J., Becerril, L., Planagumà, L., Grosse, P., and Barde-Cabusson, S.: Volcano-structural analysis of La Garrotxa Volcanic Field (NE Iberia): implications on the plumbing system. *Tectonophysics*, under-review, 2014b.

Bolós, X., Barde-Cabusson, S., Pedrazzi, D., Martí, J., Casas, A., Lovera, R., and Nadal-Sala, D.: Geophysical exploration on the subsurface geology in the monogenetic La Garrotxa Volcanic Field (NE Iberian Peninsula). *International Journal of Earth Science*, <http://dx.doi.org/10.1007/s00531-014-1044-3>, 2014c.

Cappello, A., Vicari, A., and Del Negro, C.: Assessment and modeling of lava flow hazard on Etna volcano. *Bollettino di Geofisica Teorica ed Applicata* 52 (2), 299-308, 2011.

Cappello, A., Neri, M., Acocella, V., Gallo, G., Vicari, A., and Del Negro, C.: Spatial vent opening probability map of Mt Etna volcano (Sicily, Italy). *Bulletin of Volcanology* 74(9), 2083-2094, 2012.

Cas, R.A.F. and Wright, J.V.: Volcanic successions (modern and ancient). A geological approach to processes products and successions. Allen and Unwin, London, 1987.

Cebrià, J.M., López-Ruiz, J., Doblas, M., Oyarzun, R., Hertogen, J., and Benito, R.: Geochemistry of the Quaternary alkali basalts of Garrotxa (NE Volcanic Province, Spain): a case of double enrichment of the mantle lithosphere. *Journal of Volcanology and Geothermal Research* 102, 217-235, 2000.

Cimarelli, C., Di Traglia, F., de Rita, D., Gimeno Torrente, D., and Fernandez Turiel, J.L.: Space–time evolution of monogenetic volcanism in the mafic Garrotxa Volcanic Field (NE Iberian Peninsula). *Bulletin of Volcanology* 75, 758, 2013.

Connor, C.B. and Conway, F.M.: Basaltic Volcanic Fields. In: *Encyclopedia of Volcanology*. Academic Press, pp. 331-343, 2000.

Connor, C.B. and Connor, L.J.: Estimating spatial density with kernel methods. In: Connor, C.B., Chapman, N.A., Connor, L.J. (Eds.), *Volcanic and Tectonic Hazard Assessment for Nuclear Facilities*. Cambridge University Press, pp. 346–368, 2009.

Dèzes, P., Schmid, S.M., and Ziegler, P.A.: Evolution of the European Cenozoic Rift System: interaction of the Alpine and Pyrenean orogens with their foreland lithosphere. *Tectonophysics* 389, 1–33, 2004.

Di Traglia, F., Cimarelli, C., de Rita, D., and Gimeno Torrente, D.: Changing

eruptive styles in basaltic explosive volcanism: examples from Croscat complex scoria cone, Garrotxa Volcanic Field (NE Iberian Peninsula). *Journal of Volcanology and Geothermal Research* 180, 89–109, 2009.

Farnell, C. and Llasat, M.C.: Proposal of three thermodynamic variables to discriminate between storms associated with hail and storms with intense rainfall in Catalonia. *Tethys* 10, 25–34, 2013.

Favalli, M., Tarquini, S., Papale, P., Fornaciai, A., and Boschi, E.: Lava flow hazard and risk maps at Mount Cameroon volcano. *Bulletin of Volcanology* 74, 423–439, 2012.

Felpeto, A., Martí, J., and Ortiz, R.: Automatic GIS-based system for volcanic hazard assessment. *Journal of Volcanology and Geothermal Research* 166, 106–116, 2007.

Guilbaud, M.N., Siebe, C., Layer, P., Salinas, S., Castro-Govea, R., Garduño Monroy, V.H., and Le Corvec, N.: Geology, geochronology, and tectonic setting of the Jorullo volcano region, Michoacán, México. *Journal of Volcanology and Geothermal Research* 201, 97–112, 2011.

Ho, C-H., Smith, E.I., Feuerbach, D.L., and Naumann, T.R.: Eruptive calculation for the Yucca Mountain site, USA: statistical estimation of recurrence rates. *Bulletin of Volcanology* 54, 50–56, 1991.

Höbig, N., Weber, M.E., Kehl, M., Weniger, G.C., Julià, R., Melles, M., Fülöp, R.H., Vogel, H., and Reicherter, K.: Lake Banyoles (northeastern Spain): A Last Glacial to Holocene multi-proxy study with regard to environmental variability and human occupation. *Quaternary International* 274, 205–218, 2012.

Lirer, L., Petrosino, P., and Alberico, I.: Volcanic hazard assessment at volcanic fields: the Campi Flegrei case history. *Journal of Volcanology and Geothermal Research* 101(1–4), 55–75, 2001.

Malin, M.C. and Sheridan, M.F.: Computer-assisted mapping of pyroclastic surges. *Science* 217, 637–640, 1982.

Martí, J. and Mallarach, J.M.: Erupciones hidromagmáticas en el volcanismo cuaternario de Olot. *Estudios Geológicos* 43, 31–40, 1987.

Martí, J., Mitjavila, J., Roca, E., and Aparicio, A.: Cenozoic magmatism of the Valencia trough (western Mediterranean): relationship between structural evolution and volcanism. *Tectonophysics* 203, 145–165, 1992.

Martí, J., Aspinall, W., Sobradelo, R., Felpeto, A., Geyer, A., Folch, A., Teixidó,

F., Ortiz, R., Baxter, P., Cole, P., Pacheco, J., Blanco, M.J., and Lopez, C.: A long-term volcanic hazard event tree for Teide-Pico Viejo stratovolcanoes (Tenerife, Canary Islands). *Journal of Volcanology and Geothermal Research* 178, 543–552, 2008.

Martí, J. and Felpeto, A.: Methodology for the computation of volcanic susceptibility. An example for mafic and felsic eruptions on Tenerife (Canary Islands). *Journal of Volcanology and Geothermal Research* 195, 69–77, 2010.

Martí, J., Planagumà, L., Geyer, A., Canal, E., and Pedrazzi, D.: Complex interaction between Strombolian and phreatomagmatic eruptions in the Quaternary monogenetic volcanism of the Catalan Volcanic Zone (NE of Spain). *Journal of Volcanology and Geothermal Research* 201, 178–193, 2011.

Martí, J., Pinel, V., López, C., Geyer, A., Abella, R., Tárraga, M., Blanco, M.J., Castro, A., and Rodríguez, C.: Causes and mechanisms of the 2011–2012 El Hierro (Canary Islands) submarine eruption, *Journal of Geophysical Research: Solid Earth* 118, 823–839, 2013.

Martin, A.J., Umeda, K., Connor, C.B., Weller, J.N., Zhao, D., and Takahashi, M.: Modeling long-term volcanic hazards through Bayesian inference: an example from the Tohoku volcanic arc Japan, *Journal of Geophysical Research* 109, B10208, 2004.

Marzocchi, W., Sandri, L., and Furlan, C.: A quantitative model for volcanic hazard assessment. In: Mader, H.M., Coles, S.G., Connor, C.B., Connor, L.J. (Eds.), *Statistics in Volcanology*. Special Publication of IAVCEI, 1. Geological Society of London, pp. 15–30, 2006.

Neri, A., Aspinall, W.P., Cioni, R., Bertagnini, A., Baxter, P.J., Zuccaro, G., Andronico, D., Barsotti, S., Cole, P.D., Esposti Ongaro, T., Hincks, T.K., Macedonio, G., Papale, P., Rosi, M., Santacroce, R., and Woo, G.: Developing an event tree for probabilistic hazard and risk assessment at Vesuvius. *Journal of Volcanology and Geothermal Research* 178(3), 397–415, 2008.

Puiguirguer, M., Alcalde, G., Bassols, E., Burjachs, F., Expósito, I., Planagumà, Ll., Saña, M., and Yll, E.: ¹⁴C dating of the last Croscat volcano eruption (Garrotxa Region, NE Iberian Peninsula). *Geologica Acta* 10(1), 43–47, 2012.

Scandone R.: Effusion rate and energy balance of Paricutin eruption (1943–1952), Michoacan, Mexico. *Journal of Volcanology and Geothermal Research* 6, 49–59, 1979.

Siebe, C. and Macías, J.L.: Volcanic hazards in the Mexico City metropolitan area from eruptions at Popocatepetl, Nevado de Toluca, and Jocotitlán stratovolcanoes and monogenetic scoria cones in the Sierra Chichinautzin Volcanic Field. *Special Papers, Geological Society of America* 402, 253, 2006.

Suzuki, T.: A theoretical model for dispersion of tephra. In: Shimozuru, D., Yokoyama, I., (Eds.). *Arc Volcanism: Physics and Tectonics*, Terra Scientific Publishing Company (TERRAPUB), Tokyo, pp. 93–113, 1983.

Toyos, G. P., Cole, P. D., Felpeto, A., and Martí, J.: A GIS-based methodology for hazard mapping of small pyroclastic density currents. *Natural Hazards* 41, 99–112, 2007.

Kereszturi, G. and Németh, K.: Monogenetic Basaltic Volcanoes: Genetic Classification, Growth, Geomorphology and Degradation. In: Németh, K. (Editor). *Updates in Volcanology - New Advances in Understanding Volcanic Systems*, Jeddah, Kingdom of Saudi Arabia, 2012.

Wood, C.A.: Morphometric evolution of cinder cones. *Journal of Volcanology and Geothermal Research* 7, 387–413, 1980.

VERDI: a new Volcanic managEmEnt Risk Database desIgn

Submitted to:

Journal of Volcanology and Geothermal Research

Authors:

Stefania Bartolini^a

Laura Becerril^a

Joan Martí^a

a) Group of volcanology, (SIMGEO-UB), Institute of Earth Sciences Jaume Almera, ICTJA-CSIC, Barcelona, Spain

7.1 Abstract

One of the most important issues in modern volcanology is the assessment of volcanic risk, which will depend – amongst other factors – on both the quantity and quality of the available volcanic data and an optimum storage mechanism. This will require the design of purpose-built databases that take into account data format and availability and afford easy data storage and sharing, and will provide for a more complete risk assessment that combines different analyses but avoids any duplication of information. Data contained in any such database should facilitate spatial and temporal analysis that will (1) produce probabilistic hazard models for future vent opening, (2) simulate volcanic hazards and (3) assess their socio-economic impact. We describe the design of a new spatial database structure, VERDI (**V**olcanic **m**anag**E**ment **R**isk **D**atabase **d**es**I**gn), which allows different types of data, including geological, volcanological, meteorological, monitoring and socio-economic information, to be manipulated, organized and managed. The root of the question is to ensure that VERDI will serve as a tool for connecting different kinds of data sources, GIS platforms and modelling applications. We present an overview of the database design, its components and the attributes that play an important role in the database model. The potential of the VERDI structure is here shown through its application on El Hierro (Canary Islands) and the possibilities it offers in regard to data organization. The VERDI database will in coming years provide scientists and decision makers with a useful tool that will assist in volcanic risk assessment and hazard prioritization.

Keywords

Database design · Volcanic risk · Decision making · El Hierro

7.2 Introduction

Volcanic risk assessment and management are complex issues due largely to the nature, variety and availability of the data they handle (De la Cruz-Reyna, 1996). The quality of the data will determine the evaluation of the volcanic risk, which is an essential part of risk-based decision making in land-use planning and emer-

gency management. The first step in the evaluation of volcanic risk consists of obtaining and organizing all pertinent data derived from disciplines such as geology, volcanology, geochemistry, petrology and seismology, as well as vulnerability and socio-economic information relating to the elements that are potentially at risk. Some of the most relevant issues include how and where to store the data, in which format should it be made available, and how to facilitate its use and exchange. Thus, it is essential to design an appropriate database that is specifically adapted to the task of evaluating and managing volcanic risk.

The design of an appropriate database for risk assessment and management should aim to organize all the available and necessary information on volcanic risk assessment in a standardized way that is easy to consult and exchange.

As in any other field, the first step in designing a database for volcanic risk assessment and management is the definition of its architecture. This must allow for effective interaction between the different information fields and offer users a clear vision of its internal organization and rapid access to its contents. Nevertheless, it will be the quantity and quality of the information contained in the database that will determine the reliability and validity of the final risk analysis. Subsequent steps will consist of the creation, maintenance and updating of all data related to volcanic risk. It is important to ensure that the database will be able to evolve freely from a simple to a more complex structure and be updated when new data are available.

To facilitate its operability and the visualisation of the data the database must be integrated into a GIS (Geographical Information System). A GIS is an organized integration of software, hardware and geographic data designed to capture, store, manipulate, analyze and represent georeferenced information (Longley et al., 2005). In recent years, the use of GIS and the improvement of the modelling of volcanic processes have become useful tools in volcanic hazard and risk assessment. In fact, susceptibility, hazard, vulnerability and risk maps have been generated using GIS tools (Pareschi et al., 2000; Felpeto et al., 2007; Barreca et al., 2013) and can be represented in a GIS environment as a support for spatial decision making (Cova, 1999).

Furthermore, thematic volcanic risk maps can facilitate land-use planning and appropriate actions required during emergencies. In fact, hazard and risk maps are key tools in emergency management: the former depicts the hazard at any particular location, while the latter shows the spatial variation of both hazard and vulnerability

(Lirer et al., 2001).

To date, the databases used in volcanology have been created to store and analyze different types of information and have been employed to analyze, for example, (1) the impacts of volcanic phenomena on people (Witham, 2005); (2) potentially active volcanoes situated in regions of high geodynamic unrest (Gogu et al., 2006); (3) collapse calderas (Geyer and Martí, 2008); (4) volcano monitoring data that include instrumentally and visually recorded changes in seismicity, ground deformation, gas emission and other parameters (WOVOdat (Venezky and Newhall, 2007)); (5) global volcanic unrest (Phillipson et al., 2013); and (6) active faults on Mt. Etna (Barreca et al., 2013). In particular, efforts have been made to construct a Global Volcanic Risk database of large magnitude explosive volcanic eruptions (LaMEVE (Croweller et al., 2012)). However, none of the existing databases is based on a simple architecture that contains all the necessary information for volcanic risk analysis and management.

Here we present **Volcanic management Risk Database design** (VERDI), the architecture for a geodatabase for volcanic risk assessment and management. The rationale behind constructing this database is the need to create a comprehensive structure including all known or identified fields that might contribute to the assessment of volcanic risk. The database also aims to make the task of volcanic risk management easier for decision makers. Currently, relevant data are stored in a variety of different formats and are not always easily accessible. Thus, this new way of compiling extensive data aims to provide an accessible and useful structure that will facilitate information sharing and risk assessment. This new database has been designed to work in a GIS environment.

The ultimate aim of VERDI is to create a platform for expanding, updating and sharing information that is open to the incorporation of new data. In the future, a web site could be set up to make it a truly user-friendly application.

In this paper, we also present an example of the applicability of VERDI, taking as example the island of El Hierro (Canary Islands, Spain). We show how all the available data necessary for conducting a preliminary risk assessment can be integrated and discuss the limitations of existing data and the inherent advantages in storing data in the proposed form.

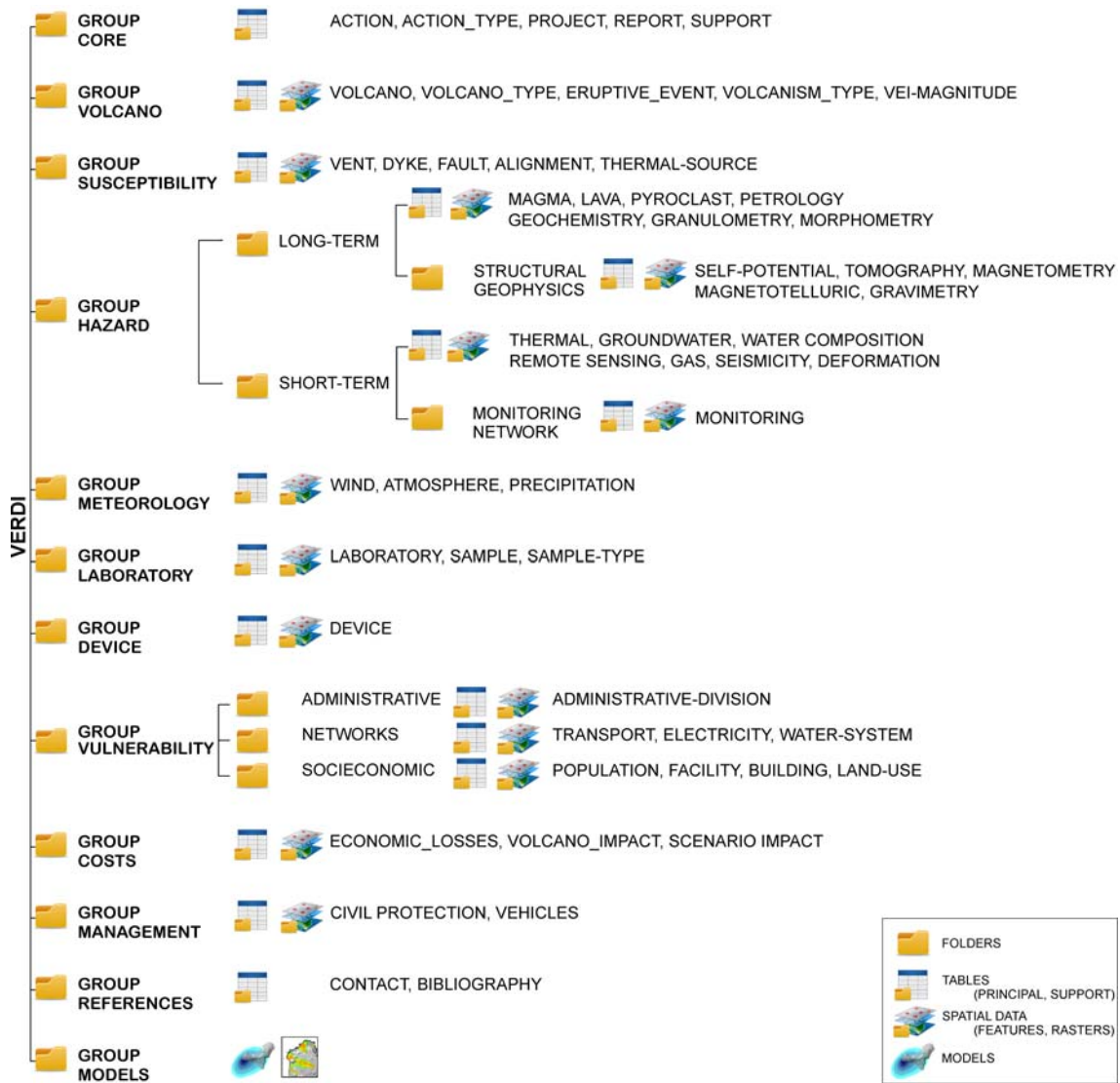


Figure 7.1: VERDI database design structure

7.3 VERDI architecture

A simplified version of the VERDI database design structure is shown in Figure 7.1. The full version of the VERDI structure and the user manual will be published online on the website of the CSIC Barcelona Volcanology Group (<http://www.GVB-csic.es/>).

The design of the database has taken into account the type of data required and possible inter-relationships in order to avoid duplication.

The first steps in the creation of the database model were the collection of metadata, the analysis of the required features and the calculation of the expected output responses. This phase included the creation of information groups and the definition of the table fields and the relationships between tables.

In order to optimize the accurate evaluation of volcanic risk, VERDI contains 12 information groups regarding past and current volcanic activity and the associated hazards and the potential vulnerability of the elements that may be affected by such hazards. The information included in each group is recorded in individual tables. Additionally, VERDI includes spatial features that can be visualized with a GIS application. The rationale behind the VERDI architecture is based on the principle that all the information concerning the evaluation of volcanic risk should be comparable, consistent and available for future comparisons and data analyses.

In the following subsections we offer a brief description of each information group and the type of data included therein.

7.3.1 GroupCore

GroupCore is the central group of VERDI and represents the metadata information of all the actions that could be incorporated into the database as new data. This group governs the recorded information added to each group of the database, thereby controlling the insertion of new data.

The tables contained in this group are ACTION, ACTION_TYPE, PROJECT, REPORT and SUPPORT (Fig. 7.2): ACTION and ACTION_TYPE correspond to actions and the type of actions, respectively, that generate new data (volcanic event, fieldwork, bibliography, etc.); PROJECT is a reference to a project undertaken by an institution such as a ministry or an institute; the REPORT table describes the action and includes information about the project related to the action; and SUPPORT

adds information about the entity that is managing or funding the project. Table 7.1 shows the structure and field details of each table contained in this group.

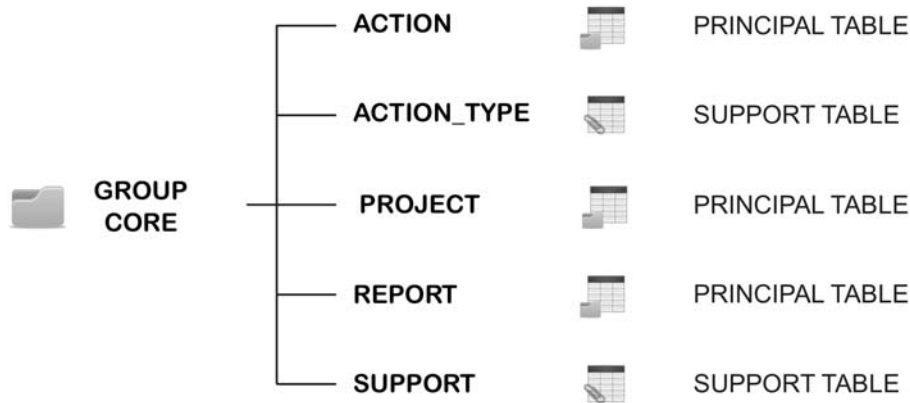


Figure 7.2: *GroupCore* structure

7.3.2 GroupVolcano

This group contains information about the volcano or the studied volcanic area and includes data on the volcanic event itself, the characteristics of the type of volcanism and the magnitude of the event (Fig. 7.3).

The table VOLCANO provides general information about the location of the volcano and volcanic area, which will normally be associated with spatial information included in a shapefile of polygons or in raster images. Spatial features contain a folder with additional information such as Digital Elevation Models (DEM), hillshades and orthophotos.

VOLCANO_TYPE completes the information about the volcano and identifies different types and features of volcanoes (stratovolcano, shield volcano, etc...). ERUPTIVE_EVENT provides information about eruptive events including date and location and enables the volcano-stratigraphy of the volcano and the study area to be obtained. ACTIVITY_TYPE characterizes the eruptive behaviour of the volcano thus: Hawaiian, Strombolian, Vulcanian, Peléan/Plinian, Plinian, Ultraplinian and/or Caldera. The size and magnitude of the eruption is contained in the VEI_MAGNITUDE table, which includes parameters such as volume, column height, fragmentation index, dispersion index, Dense-Rock Equivalent (DRE), mag-

Table 7.1: *GroupCore* tables

Table	Field	Info	Type
ACTION			
	action_id	primary key	AutoNumber
	action_date	date of the data entry	dd/mm/yyyy
	actionT_cd	type of the new data entry (foreign key ACTION_TYPE table)	Integer
	report_cd	report reference (foreign key REPORT table)	Integer
	project_cd	project reference (foreign key PROJECT table)	Integer
	support_cd	who funds the action (foreign key SUPPORT table)	Integer
	contact_cd	contact reference (foreign key CONTACT table)	Integer
ACTION_TYPE			
	actionT_id	primary key	AutoNumber
	actionT_info	different types of data entry (Volcanic Event, Fieldwork,...)	Text
PROJECT			
	project_id	primary key	AutoNumber
	project_ref	code of the project reference	Text
	project_name	name of the project	Text
	project_start	date when project starts	dd/mm/yyyy
	project_end	date when project finishes	dd/mm/yyyy
REPORT			
	report_id	primary key	AutoNumber
	report_name	name of the report	Text
	report_start	date when report starts	dd/mm/yyyy
	report_end	date when report finishes	dd/mm/yyyy
	report_info	info report	Text
SUPPORT			
	support_id	primary key	AutoNumber
	support_info	info about the entity that manages or funds the project	Text

nitide (Pyle, 2000) and the Volcanic Explosivity Index (VEI) according to Newhall and Self's (1982) classification (Newhall and Self, 1982).

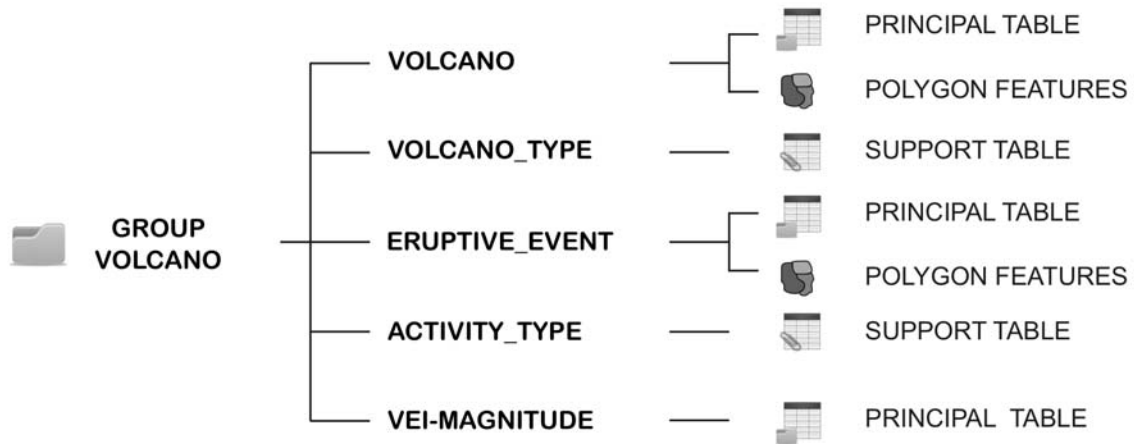


Figure 7.3: *GroupVolcano* structure

7.3.3 GroupSusceptibility

Volcanic susceptibility (i.e. the probability of vent opening) represents an important step in simulating eruptive scenarios and developing hazard maps (Martí and Felpeto, 2010). Thus, *GroupSusceptibility* contains information on all structural elements such as vents, dykes, faults, fractures and eruptive fissure-alignments obtained from both geological and geophysical studies. The location of gas emissions or water springs, as well as thermal anomalies related to the volcanic activity, are also included in this group. All of these elements enable susceptibility maps in long-term analyses to be generated. During volcanic unrest episodes, real-time monitoring information – in particular regarding the location of the volcano-tectonic seismicity and surface deformation – can be added to permit the susceptibility to be re-evaluated. This group also contains a GEOPHYSICS subgroup with information on structural geophysics that includes data derived from structural studies using different geophysical techniques such as self-potential, tomography, magnetometry, magnetotelluric and gravimetry. This type of geophysical data is useful in susceptibility analyses and in both short- and long-term hazard evaluation. In addition, it is useful for studying dispersed volcanic fields and their relation to local tectonics (Barde-Cabusson et al., 2014) and can thus facilitate a complete analysis of the

probability of future activity in monogenetic fields and improve understanding of the internal structure of composite volcanoes (Rout et al., 1993; Blakely et al., 1997; Connor et al., 2000; Kiyosugi et al., 2010).

Moreover, in both short- and long-term hazard assessment the monitoring and interpretation of geophysical parameters such as temporal gravity changes, seismicity and ground deformation can benefit from integration with structural geophysical data. Figure 7.4 shows the organization of this group.

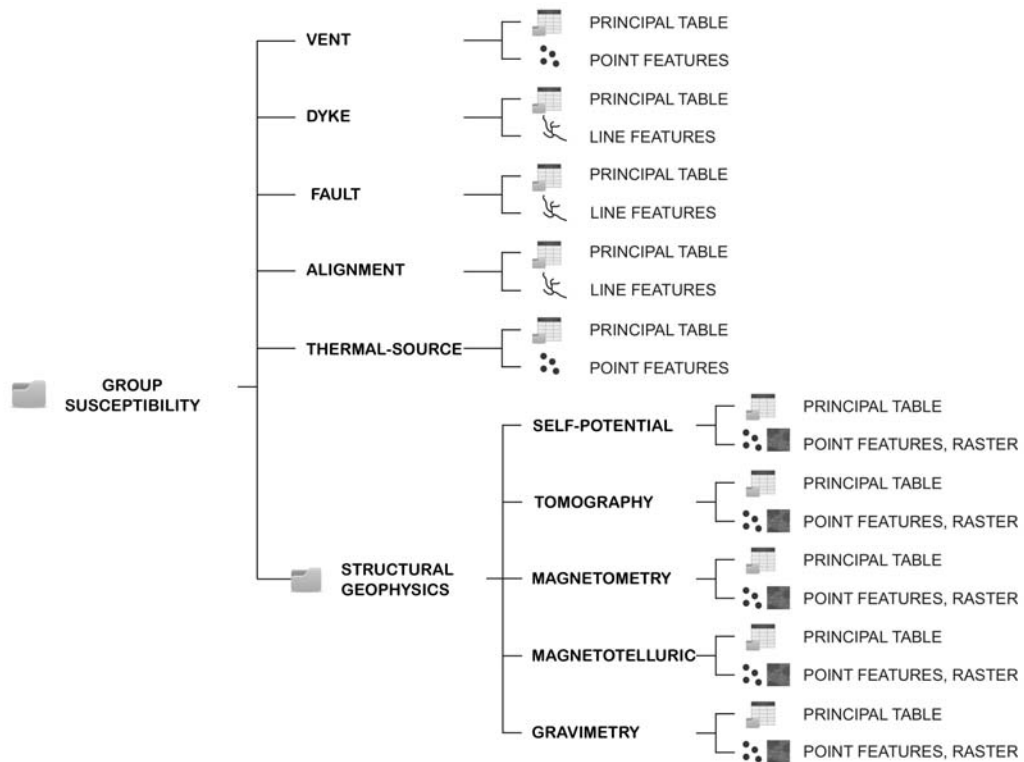


Figure 7.4: *GroupSusceptibility* structure

7.3.4 GroupHazard

GroupHazard contains basic data for computing volcanic hazards to be employed in simulation models that take susceptibility information into account. This group constitutes the information on which territorial and emergency plans should be based and has been divided into LONG TERM and SHORT TERM subgroups (see Fig. 7.5).

The tables of the LONG TERM hazard subgroup contain mainly data regarding the products generated during the past activity of the volcano. The information required comes mainly from geological and historical records and laboratory analyses. This subgroup includes the following information split into different tables: magma and volcanic products (lava flows, pyroclastic deposits, etc.); petrological and geochemical data from volcanic rock samples; granulometry classification of pyroclasts based on sieved samples; and morphometry.

The SHORT TERM hazard subgroup tables contain monitoring data collected during an unrest episode. These data are useful for short-term hazard assessments. The information is usually organized in terms of volcanic monitoring networks (seismicity, deformation, gas, thermal, groundwater, remote sensing images, etc.).

7.3.5 GroupMeteorology

GroupMeteorology includes the information required for the analysis of wind profiles, atmospheric parameters and precipitation data (see Fig. 7.6). These parameters are very important as inputs for ash-fall simulations. Other important parameters included in this group are related to the atmospheric diffusion coefficient, the eruption style and the grain-size classification. Ash-fall simulations are very useful in volcanic risk assessment and consider the impact of volcanic ash not only on the population and infrastructures but also on aircraft safety (Johnson et al., 2012).

7.3.6 GroupLaboratory

GroupLaboratory contains information supplementing the *GroupSusceptibility* and *GroupHazard* groups that relates to the laboratories in which sample analyses are conducted. This group specifies the kind of samples used, the analytical tests applied and the results obtained (see Fig. 7.7). This group is important for controlling the quality of data used to characterise the expected type of eruption (e.g. lava composition) by means of the analysis of past products.

7.3.7 GroupDevice

GroupDevice provides information about the measurement devices in tables such as PETROLOGY, SELF_POTENTIAL, MONITORING, and WIND. A large amount



Figure 7.5: *GroupHazard* structure

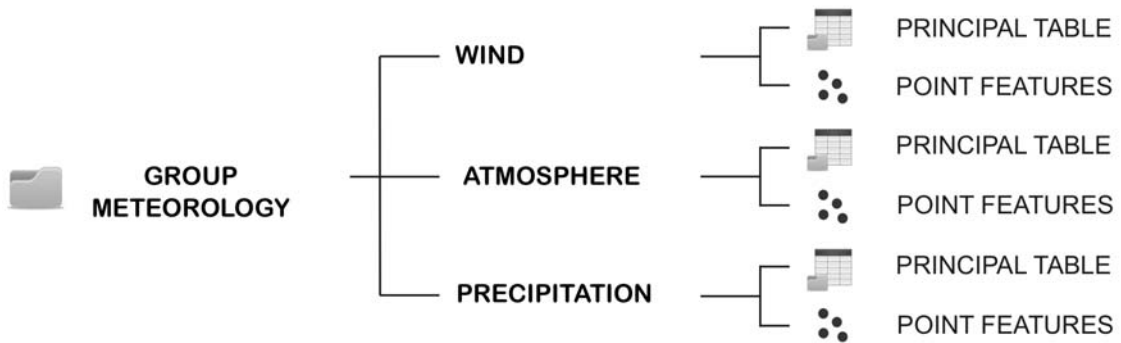


Figure 7.6: *GroupMeteorology* structure



Figure 7.7: *GroupLaboratory* structure

of information in the database is obtained through the use of instruments such as seismographs and microscopes and the *DEVICE* table (Fig. 7.8) contains the names, models, types and functions of these devices.

7.3.8 GroupVulnerability

This group includes all the elements that could be affected by a destructive volcanic event.

Vulnerability is the potential of exposed elements to be directly or indirectly damaged by a given hazard (Scaini et al., 2014). There are many types of vulnerability – physical, infrastructural, social and economic – and in combination they

Figure 7.8: *GroupDevice* structure

constitute the vulnerability of the system (Menoni et al., 2011). Physical vulnerability due to volcanic activity has been widely observed and studied, in particular in recent decades (Blong and McKee, 1995; Annen and Wagner, 2003; Spence, 2004; Baxter et al., 2005; Spence et al., 2005; Gomes et al., 2006; Martí et al., 2008; Zuccaro et al., 2008; Scaini et al., 2014).

Thus, the VERDI database includes administrative divisions, infrastructure networks (TRANSPORT, ELECTRICITY, and WATER_SYSTEM tables), as well as a socio-economic table that includes POPULATION information, FACILITY, BUILDING and LANDUSE (Fig. 9). A LAND_USE classification is included because correct land-use planning is fundamental in minimising both loss of life and damage to property (Pareschi et al., 2000). The information contained in this part of the database is very important in the organization of evacuation plans, the reduction of potential losses caused by the impact of volcanic and associated hazards, the design of land-planning measures, and the evaluation of potential economic losses.

7.3.9 GroupCosts

GroupCosts (Figure 7.10) represents the huge economic losses (human life, infrastructure, property, productivity, etc.) that volcanic activity can cause. Estimating the economic costs associated with volcanic eruptions is very difficult due to their duration and the variety of the types of impacts (Annen and Wagner, 2003). However, the quantitative estimation of economic losses is of primary importance when

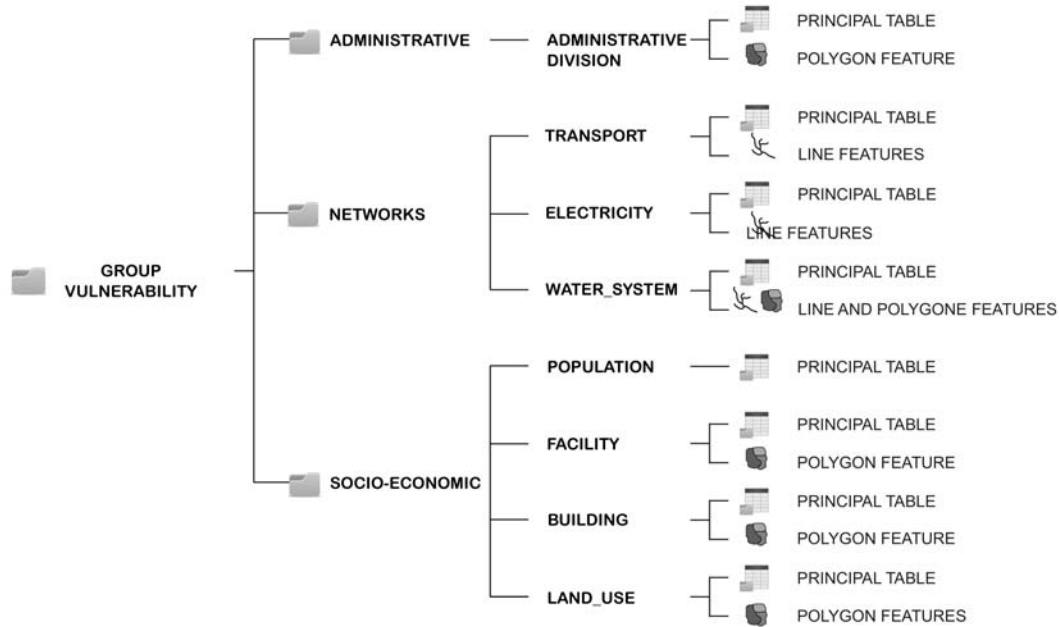


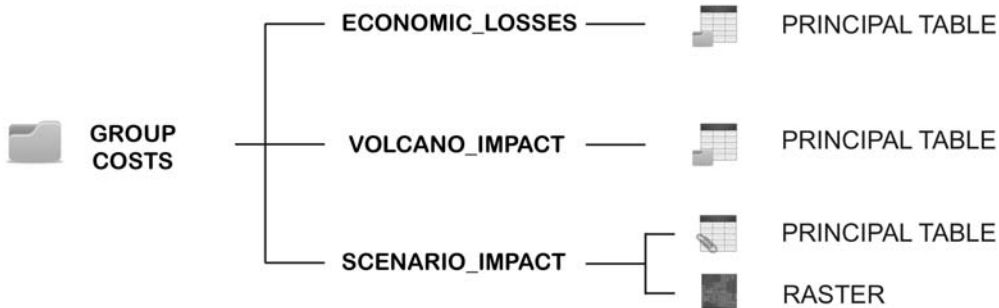
Figure 7.9: *GroupVulnerability* structure

providing mitigation recommendations aimed at reducing damage (Spence et al., 2005).

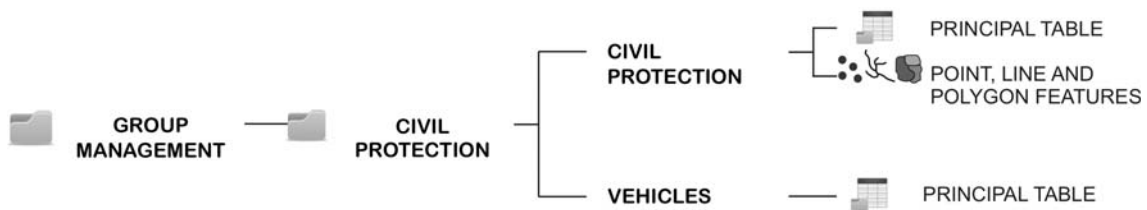
The `ECONOMIC_LOSSES` and `VOLCANO_IMPACT` tables refer to the economic and human losses evaluated after a volcanic crisis and the economic impact for a specific volcanic event. The third table, `SCENARIO_IMPACT`, represents a support table that allows a cost evaluation to be added when a volcanic hazard scenario is computed and enables the human losses expected during a volcanic crisis to be calculated.

7.3.10 GroupManagement

GroupManagement (Figure 7.11) is a useful group for decision makers and risk managers that should include ideally all types of emergency services (e.g. police, fire department, Red Cross, NGOs, etc.), although in most cases Civil Protection bodies will take responsibility during a volcanic crisis. Volcanic crises require continuous

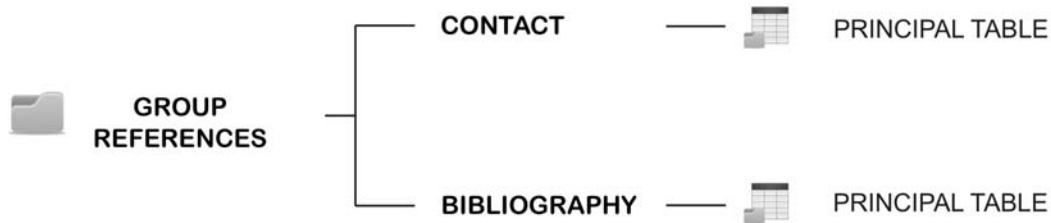
Figure 7.10: *GroupCosts* structure

close collaboration between civil protection bodies and scientists in order to best analyse observational and monitoring data, to evaluate short-term hazards, to draw up plans for optimizing existing monitoring networks, to install new instruments and to provide advice in decision making (Bertolaso et al., 2009).

Figure 7.11: *GroupManagement* structure

7.3.11 GroupReferences

GroupReferences contains contact information for key people and institutions, as well as bibliographic references (see Figure 7.12) related to the data contained in the database. This group is important for obtaining the reference for any input into the VERDI database and thus enables the origin of the data to be known; in this way, if necessary, the person or team in question can be contacted if there is any explanation needed for the data introduced.

Figure 7.12: *GroupReferences* structure

7.3.12 GroupModels

GroupModels contains examples of hazard-modelling tools. It includes the most relevant available software and a summary of both the required main input parameters and the output formats.

In recent years, new tools have been developed for generating hazard and risk maps, evaluating long- and short-term hazards, simulating different eruptive scenarios and designing evacuation plans. Examples of these tools include QVAST (Bartolini et al., 2013), VORIS (Felpeto et al., 2007), a model for lava flow simulation (Connor et al., 2012), HASSET (Sobradelo et al., 2014), BET_EF (Marzocchi et al., 2008), BET_VH (Marzocchi et al., 2010), HAZMAP (Bonadonna et al., 2002; Macedonio et al., 2005), FALL3D (Costa et al., 2006; Folch et al., 2009), TEPHRA2 (Connor et al., 2001), PUFFIN (Patra et al., 2013), VOLCFLOW (Kelfoun and Druitt, 2005), TITAN2D (Sheridan et al., 2005) and EJECT (Mastin, 2001).

Simplified schematic tables are given in the Supplementary Material with the main input parameters required for the above-listed tools.

7.4 VERDI usefulness: case study of El Hierro

One of the main obstacles when attempting to develop a robust database is the lack of quality, well-gathered data. This issue can be made simpler and easier in part by selecting small areas in which to test the operability database. With this aim in

mind, a pilot project to check the feasibility of VERDI was set up with information available from the island of El Hierro (Canary Island, Spain).

The last eruption on El Hierro occurred in 2011–2012 (López et al., 2012; Martí et al., 2013) and demonstrated the importance of reliable data and tools that can enable scientific advisors and decision-makers to consider possible future eruptive scenarios. Furthermore, this was the first ever eruption in the Canary Islands to be tracked in real-time (López et al., 2012).

Most of eruptions occurring on El Hierro are similar in type and in size, and consist of the emission of mafic lava flows, the ballistic projection of pyroclasts and proximal fallout from low fire-fountains. Its simple volcanic history, relative homogeneous petrology and the new data collected during the last eruption, among other factors, prompted us to select El Hierro as a case study for testing the methodology proposed here.

In order to show the functionality of the VERDI database, we describe here two hypothetical phases in the volcanic risk assessment on El Hierro. We analyze the most representative and necessary information in each of the two periods: (1) the pre-eruption or emergency planning phase of the volcanic process and (2) the unrest episode itself. In these examples we try to summarize the information required to complete a qualitative volcanic risk analysis for the island, show how to find and to store data, and outline the advantages of organizing the available data.

Indeed, we believe that the availability of a well-organized database at the beginning of an unrest phase could become a very useful tool for decision-makers and for the scientists that have to provide assessment.

7.4.1 Emergency planning phase

The emergency planning phase is a moment of relative calm during the volcanic activity in which long-term volcanic hazard and risk assessment become feasible.

During this phase, the research, compilation and interpretation of different types of data should be carried out. Furthermore, available information should be organized and stored in the database and completed by further fieldwork, library searches and monitoring wherever data is lacking.

Once uploaded, the data must be filtered before being used as inputs for spatial and temporal analysis and for defining eruptive scenarios. The results obtained from the aforementioned analysis will become a useful tool for institutions such as Civil

Protection when developing their emergency plans.

We assume that the Canary Islands Civil Protection Organization needs to know what impact the most likely eruption scenarios on El Hierro will have on the population and the other exposed elements (property, infrastructures, communication networks, etc.). For this analysis different data layers will have to be superimposed in order to reach a final risk assessment. Figure 7.13 shows the different data and steps to be performed in a GIS environment.

The first step is to obtain the Digital Elevation Model (DEM) of El Hierro and general information about the volcanic area and the eruptive event (see *GroupVolcano*). The DEM of this area can be freely obtained from the website of Spanish Instituto Geográfico Nacional (IGN, <http://centrodedescargas.cnig.es/CentroDescargas/index.jsp>).

The second step involves the collection of volcano-structural data via new field-work measurements and bathymetric information, as well as the analysis of geological maps, orthophotos and aerial photographs (Becerril et al., 2013). Once the whole volcano-structural elements have been assembled, they can be geo-referenced on the DEM.

The susceptibility map, i.e. the spatial distribution of new vent openings, is based on the analysis of the aforementioned volcano-structural data. One of the tools that facilitates this type of analysis is QVAST (Bartolini et al., 2013) (the main input parameters required are specified in the Supplementary Material).

All necessary data for conducting the susceptibility analysis is contained in *GroupSusceptibility*. In our example, we need to collect as much data as possible to improve the accuracy of the spatial probability of a new vent opening. In the case of El Hierro, data referring to past vent locations, dykes, eruptive fissures and faults are used. To compile information related to vents, we refer to the table VENT in VERDI that contains information about all known emission centres on the island. This table is linked to a point shapefile that permits us to visualize the vents and use them in QVAST to obtain probability density functions. This procedure can also be carried out with the other volcano-structural elements.

The result will be a raster file (map) in which each pixel has a value that represents the probability that it will host a new emission centre. In the specific case of El Hierro, this map has already been published by Becerril et al. (2013).

Once the susceptibility map has been drawn up, eruptive scenarios for hazard

assessment can be computed. In Becerril et al. (2014), different eruptive scenarios such as lava flow, ash fall and pyroclastic density currents (PDC) were considered and enabled a qualitative volcanic hazard map to be generated.

VORIS (Felpeto et al., 2007), which requires different types of input data parameters that are presented and organized in VERDI, was used to produce this map (see Supplementary Material). All the information obtained during fieldwork, be it from the bibliography or from devices (i.e. meteorological data), is vital in determining these parameters.

Once the distribution of the eruptive scenarios has been developed, Civil Protection is then able to evaluate the most likely eruption scenarios for the island and their impact on the population and other exposed features. For this, relevant data on elements such as population and transport networks must be obtained for analysis. For example, Population data for El Hierro can be downloaded from the website of the Spanish Instituto Nacional de Estadística (INE, <http://www.ine.es/>). Data on transport networks can be obtained from the IGN website and OpenStreetMap (<http://downloads.cloudmade.com/>), the latter a tool used by public administrations, NGOs and even Civil Protection bodies to manage in the aftermath of disasters such as the Haiti earthquake.

The acquisition of this information allows evacuation routes and even a preliminary evaluation of general losses due to volcanic hazards such as lava flows to be calculated.

7.4.2 Unrest phase

Entry into the unrest phase means that the volcanic system has reawakened. During this phase, monitoring data plays an important role and is essential as a support for decision making. For this reason, the VERDI database contains monitoring information distributed in different groups and tables. *GroupHazard* contains precursor data such as deformation, seismic activity and groundwater monitoring for short-term hazard assessment; the MONITORING table summarizes all the monitoring networks within a volcanic area.

The 2011–2012 eruption on El Hierro was preceded by three months of unrest. From July 2011 onwards a dense multi-parametric monitoring network including seismic and magnetic stations and GPS recorders were deployed throughout the island by the Instituto Geográfico Nacional (IGN). Data recorded during this unrest

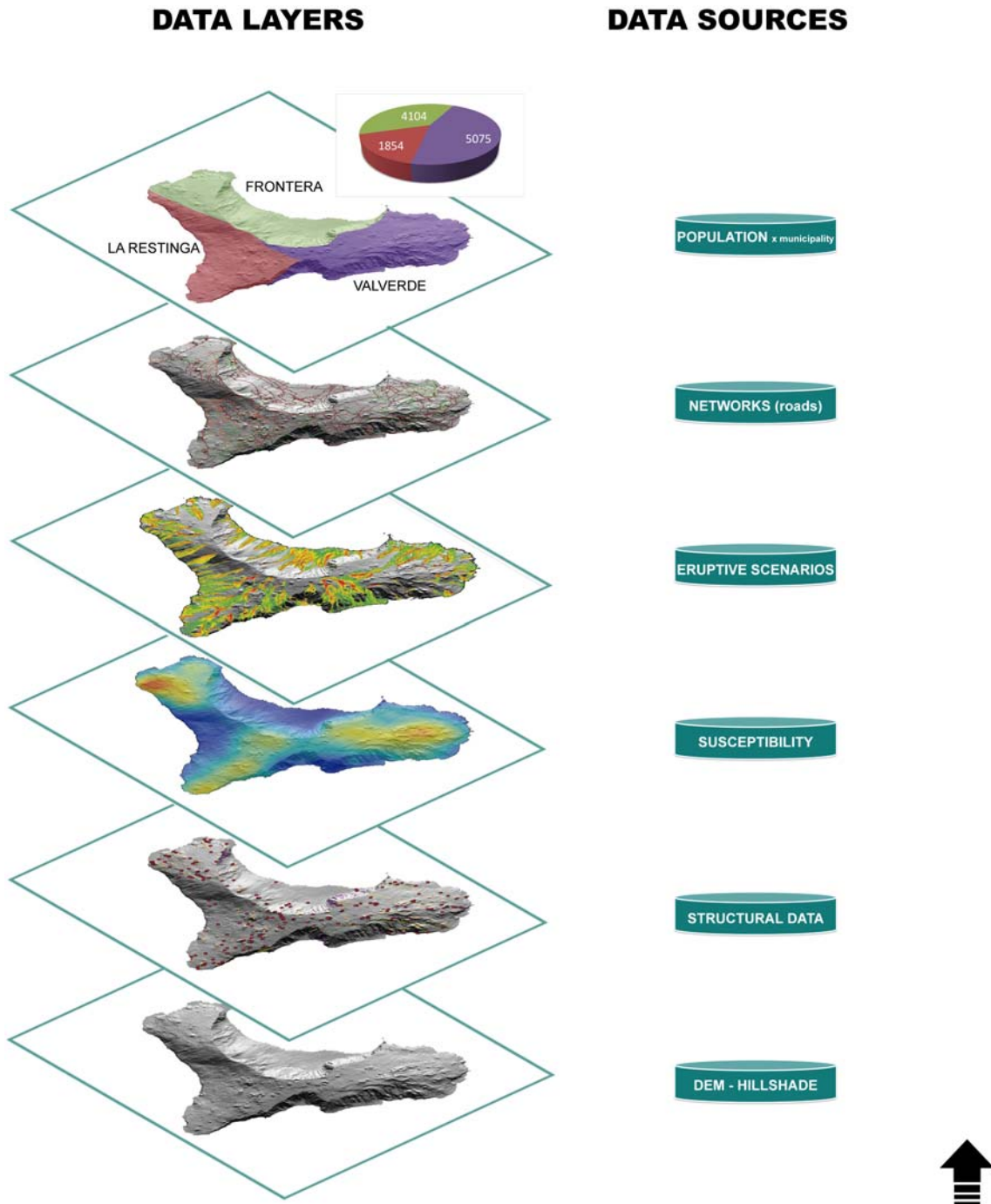


Figure 7.13: Data layers in a GIS environment

Table 7.2: GroupCosts: SCENARIO_IMPACT table

Table	Field	Info	Type
SCENARIO_IMPACT			
	scenarioImpact_id	primary key	Auto Number
	scenarioImpact_type	type of scenario simulation (lava, pdc, ashfall, ...)	Text
	scenarioImpact_pop	population affected by eruptive scenario	Integer
	scenarioImpact_facility	facility affected by eruptive scenario	Integer
	scenarioImpact_building	building affected by eruptive scenario	Integer
	scenarioImpact_landUse	land use affected by eruptive scenario	Integer
	scenarioImpact_transport	transport affected by eruptive scenario	Integer
	scenarioImpact_electricity	electricity affected by eruptive scenario	Integer
	scenarioImpact_waterSystem	water system affected by eruptive scenario	Integer
	population_cd	foreign key POPULATION table	Integer
	volcano_cd	foreign key VOLCANO table	Integer

episode contributed to the understanding of the reawakening of the volcanic activity on the island. In general, this monitoring network assisted authorities in emergency management (López et al., 2012) and prepared them for the eruption that finally started on 10 October 2011, 2 km off the southern coast.

During an unrest phase, the updating of the possible eruptive scenarios computed during the emergency planning is necessary, mainly because the arrival of new data such as seismic information can change previous susceptibility analysis and, consequently, eruption forecasts. This may involve a change in the direction taken by the crisis management.

During an unrest phase economic losses may be estimated by using information derived from spatial and temporal analysis.

It is imperative that data regarding possible costs, along with an a priori analysis of losses, are stored right from the beginning of the process (Baxter et al., 2005). In VERDI, we have added a support table (Table 7.2) for cost evaluation when a hazard volcanic scenario is computed.

At the end of this phase, all the data obtained are uploaded to the database to facilitate future risk evaluations.

7.5 Conclusions and final remarks

VERDI is a new design for a database for risk assessment. Its logical structure has been conceived in order to facilitate the interaction between data sets and to guarantee the maintenance and evolution of the system. It is essential that the database structure permits the exchange of standardized information and the updating of data in order to prevent redundancy and repetitiveness. The VERDI database design aims to make scientific research easier and to promote information-sharing for volcanic surveillance, susceptibility, hazard and vulnerability. Its structure is linked to a spatial database in a GIS environment, which is used to create susceptibility, hazard, vulnerability, and risk maps.

VERDI is a new design for a database for risk assessment. Its logical structure has been conceived in order to facilitate the interaction between data sets and to guarantee the maintenance and evolution of the system. It is essential that the database structure permits the exchange of standardized information and the updating of data in order to prevent redundancy and repetitiveness. The VERDI database

design aims to make scientific research easier and to promote information-sharing for volcanic surveillance, susceptibility, hazard and vulnerability. Its structure is linked to a spatial database in a GIS environment, which is used to create susceptibility, hazard, vulnerability, and risk maps.

A future role for VERDI will be the publication of an interactive web site that will enable registered users to access and share the information in the database, thereby allowing VERDI to become more dynamic and to continue to develop. However, we cannot ignore the inherent limitations of available data and the effect that this may have on the interpretation of the compiled information. It is therefore vital to acknowledge that both data and interpretations are dynamic, that is, they have to be subject to continuous revision and updating. For this reason, VERDI needs to be freely available to all scientists interested in volcanic risk assessment since only contributions from all will allow VERDI to grow and evolve into the useful tool we envisage.

Acknowledgements

This research has been partially funded by the European Commission (FP7 Theme: ENV.2011.1.3.3-1; Grant 282759: VUELCO) and the MINECO grant CGL2011-16144-E. We thank Xavier Castelltort for their suggestions and Jorge Pedro Galve for thorough and helpful views.

References

Annen, C. and Wagner, J.J.: The Impact of Volcanic Eruptions During the 1990s. *Nat. Hazards Rev.* 4(4), 169-175, 2003.

Barde-Cabusson, S., Gottsmann, J., Martí, J., Bolós, X., Camacho, A.G., Geyer, A., Planagumà, Ll., Ronchin, E., and Sánchez, A.: Structural control of monogenetic volcanism in the Garrotxa volcanic field (Northeastern Spain) from gravity and self-potential measurements. *Bull. Volcanol.* 76, 788, 2014.

Barreca, G., Bonforte, A., and Neri, M.: A pilot GIS database of active faults of Mt. Etna (Sicily): A tool for integrated hazard evaluation. *J. Volcanol. Geotherm. Res.* 251, 170-186, 2013.

Bartolini, S., Cappello, A., Martí, J., and Del Negro, C.: QVAST: A new Quantum GIS plugin for estimating volcanic susceptibility. *Nat. Hazards Earth Syst. Sci.* 13(11), 3031-3042, 2013.

Baxter, P., Cole, P., Spence, R., Neri, A., Zuccaro, G., and Boyle, R.: The Impacts of Pyroclastic Surges on Buildings at the Eruption of the Soufriere Hills Volcano, Montserrat. *Bull. Volcanol.* 67, 292-313, 2005.

Becerril, L., Cappello, A., Galindo, I., Neri, M., and Del Negro, C.: Spatial probability distribution of future volcanic eruptions at El Hierro Island (Canary Islands, Spain). *J. Volcanol. Geoth. Res.* 257, 21-30, 2013.

Becerril, L., Bartolini, S., Sobradelo, R., Martí, J., Morales, J.M., and Galindo, I.: Long-term volcanic hazard assessment on El Hierro (Canary Islands). *Nat. Hazards Earth Syst. Sci. Discuss.* 2, 1799-1835, 2014.

Bertolaso, G., De Bernardinis, B., Bosi, V., Cardaci, C., Ciolli, S., Colozza, R., Cristiani, C., Mangione, D., Ricciardi, A., Rosi, M., Scalzo, A., and Soddu, P.: Civil protection preparedness and response to the 2007 eruptive crisis of Stromboli volcano, Italy. *J. Volcanol. Geotherm. Res.* 182, 269277, 2009.

Blakely, R.J., Christiansen, R.L., Guffanti, M., Wells, R.E., Donnelly-Nolan, J.M., Muffler, L.J.P., Clynne, M.A., and Smith, J.G.: Gravity anomalies, Quaternary vents, and Quaternary faults in the southern Cascade Range, Oregon and California: implications for arc and backarc evolution. *J. Geophys. Res.* 102(B10), 22513–22527, 1997.

Blong, R. and McKee, C.: *The Rabaul eruption 1994: Destruction of a town*, National Hazards Research Centre, Mcquarie University, Sydney, 1995.

Bonadonna, C., Macedonio, G., and Sparks, R.S.J.: Numerical modelling of tephra fallout associated with dome collapses and Vulcanian explosions: application to hazard assessment in Montserrat. In: Druitt, T.H., Kokelaar, B.P. (Eds.). *The eruption of Soufrière Hills Volcano, Montserrat, from 1995 to 1999*. Geological Society of London, Memoir, London, pp. 517-537, 2002.

Connor, C.B., Stamatakos, J.A., Ferrill, D.A., Hill, B.E., Ofoegbu, G.I., Conway, F.M., Sagar, B., and Trapp, J.: Geologic factors controlling patterns of small-volume basaltic volcanism: application to a volcanic hazards assessment at Yucca Mountain, Nevada. *J. Geophys. Res.* 105, 417–432, 2000.

Connor, C.B., Hill, B.E., Winfrey, B., Franklin, N.M., and LaFemina, P.C.: Estimation of volcanic hazards from tephra fallout. *Nat. Hazards Rev.* 2, 33-42,

2001.

Connor, L.J., Connor, C.B., Meliksetian, K., and Savov, I.: Probabilistic approach to modeling lava flow inundation: a lava flow hazard assessment for a nuclear facility in Armenia. *J. Appl. Volcanol.* 1(3), 1-19, 2012.

Costa, A., Macedonio, G., and Folch, A.: A three-dimensional Eulerian model for transport and deposition of volcanic ashes. *Earth Planet Sci. Lett.* 241, 634-647, 2006.

Cova, T.J.: GIS in emergency management. In: Longley, P.A., Goodchild, M.F., Maguire, D.J., Rhind, D.W. (Eds.), *Geographical Information Systems: Principles, Techniques, Applications, and Management*. John Wiley and Sons Ltd, New York, pp. 845-858, 1999.

Crosweller, H.S., Arora, B., Brown, S.K., Cottrell, E., Deligne, N.I., Ortiz, N., Hobbs, L.K., Kiyosugi, K., Loughlin, S.C., Lowndes, J., Nayembil, M., Siebert, L., Sparks, R.S.J., Takarada, S., and Venzke, E.: Global database on large magnitude explosive volcanic eruptions (LaMEVE). *J. Appl. Volcanol.* 1, 2012.

De la Cruz-Reyna, S.: Long-term probabilistic analysis of future explosive eruptions. In: Scarpa, R., Tilling, R.I. (Eds.), *Monitoring and mitigation of volcanic hazards*. Springer-Verlag, Berlin, pp. 599-629, 1996.

Felpeto, A., Martí, J., and Ortiz, R.: Automatic GIS-based system for volcanic hazard assessment. *J. Volcanol. Geotherm. Res.* 166, 106116, 2007.

Folch, A., Costa, A., and Macedonio, G.: FALL3D: A computational model for transport and deposition of volcanic ash. *Comput. Geosci.* 35, 1334-1342, 2009.

Geyer, A. and Martí, J.: The new worldwide collapse caldera database (CCDB): A tool for studying and understanding caldera processes. *J. Volcanol. Geotherm. Res.* 175, 334-354, 2008.

Gogu, R.C., Dietrich, V.J., Bernhard, J., Schwandner, F.M., and Hurni, L.: A geo-spatial data management system for potentially active volcanoes-GEOWARN project. *Comput. Geosci.* 32, 29-41, 2006.

Gomes, A., Gaspar, J.L., and Queiroz, G.: Seismic vulnerability of dwellings at Sete Cidades Volcano (S. Miguel Island, Azores). *Nat. Hazards Earth Syst. Sci.* 6, 4148, 2006.

Johnson, B., Turnbull, K., Brown, P., Burgess, R., Dorsey, J., Baran, A.J., Webster, H., Haywood, J., Cotton, R., Ulanowski, Z., Hesse, E., Woolley, A., and Rosenberg, P.: In-situ observations of volcanic ash clouds from the FAAM aircraft

during the eruption of Eyjafjallajökull in 2010. *J. Geophys. Res.* 117, D00U24, 2012.

Kelfoun, K. and Druitt, T.H.: Numerical modeling of the emplacement of Soconpa rock avalanche, Chile. *J. Geophys. Res.: Solid Earth* (19782012), 110(B12), 2005.

Kiyosugi, K., Connor, C.B., Zhao, D., Connor, L.J., and Tanaka, K.: Relationships between volcano distribution, crustal structure, and P-wave tomography: an example from the Abu Monogenetic Volcano Group, SW Japan. *Bull. Volcanol.* 72, 331–340, 2010.

Lirer, L., Petrosino, P., Alberico, I., and Postiglione, I.: Long-term volcanic hazard forecasts based on Somma-Vesuvio past eruptive activity. *Bull. Volcanol.* 63, 45-60, 2001.

López, C., Blanco, M.J., Abella, R., Brenes, B., Cabrera-Rodríguez, V.M., Casas, B., Domínguez-Cerdeña, I., Felpeto, A., Fernández de Villalta, M., Del Fresno, C., García, O., García-Arias, M.J., García-Canada, L., Gomis-Moreno, A., González-Alonso, E., Guzmán-Pérez, J., Iribarren, I., López-Díaz, R., Luengo-Oroz, N., Meletlidis, S., Moreno, M., Moure, D., Pereda de Pablo, J., Rodero, C., Romero, E., Sainz-Maza, S., Sentre-Domingo, M.A., Torres, P.A., Trigo, P., and Villasante-Marcos, M.: Monitoring the unrest of El Hierro (Canary Islands) before the onset of the 2011 Submarine Eruption. *Geophys. Res. Lett.* 39, 2012.

Macedonio, G., Costa, A., and Longo, A.: A computer model for volcanic ash fallout and assessment of subsequent hazard. *Comput. Geosci.* 31(7), 837-845, 2005.

Martí, J., Spence, R.J.S., Calogero, E., Ordonez, A., Felpeto, A., and Baxter, P.: Estimating building exposure and impact to volcanic hazards in Icod de los Vinos, Tenerife (Canary Islands). *J. Volcanol. Geotherm. Res.* 178(3), 553-561, 2008.

Martí, J. and Felpeto, A.: Methodology for the computation of volcanic susceptibility: Application to Tenerife Island (Canary Islands). *J. Volcanol. Geotherm. Res.* 195, 69-77, 2010.

Martí, J., Pinel, V., López, C., Geyer, A., Abella, R., Tárraga, M., Blanco, M.J., Castro, A., and Rodríguez, C.: Causes and mechanisms of the 2011-2012 El Hierro (Canary Islands) submarine eruption. *J. Geophys. Res: Solid Earth* 118(3), 823-839, 2013.

Marzocchi, W., Sandri, L., and Selva, J.: BET EF: a probabilistic tool for long-

and short-term eruption forecasting. *Bull. Volcanol.* 70, 623-632, 2008.

Marzocchi, W., Sandri, L., and Selva, J.: BET VH: a probabilistic tool for long-term volcanic hazard assessment. *Bull. Volcanol.* 72, 705-716, 2010.

Mastin, L.G.: A simple calculator of ballistic trajectories for blocks ejected during volcanic eruptions. U.S. Geological Survey Open-File Report 01-45, pp. 16, 2001.

Menoni, S., Costa, L., Galderisi, A., and Margottini, C.: Methodological framework for an Integrated multi-scale vulnerability and resilience assessment. ENSURE, Del 4.1.1. ENSURE project, WP4, deliverable 4.1.1, pp. 96, 2011.

Newhall, C.G. and Self, S.: The volcanic explosivity index (VEI): an estimate of the explosive magnitude for historical eruptions. *J. Geophys. Res.* 87, 12311238, 1982.

Longley, P.A., Goodchild, M.F., Maguire, D.J., and Rhind, D.W.: *Geographic Information Systems and Science*. 2nd ed. John Wiley and Sons Ltd, England, pp. 517, 2005.

Pareschi, M.T., Cavarra, L., Favalli, F., Gianni, F., and Meriggi, A.: GIS and volcanic risk management. *Nat. Hazards* 21, 361379, 2000.

Patra, A.K., Bursikb, M., Dehne, J., Jonesc, M., Madankana, R., Mortone, D., Pavolonisf, M., Pitmand, E.B., Pougetb, S., Singha, T., Singlaa, P., Stefanescua, E.R., and Webleye, P.: Challenges in Developing DDDAS Based Methodology for Volcanic Ash Hazard Analysis Effect of Numerical Weather Prediction Variability and Parameter Estimation. *Procedia Computer Science* 18, 1871-1880, 2013.

Phillipson, G., Sobradelo, R., and Gottsmann, J.: Global volcanic unrest in the 21st century: An analysis of the first decade. *J. Volcanol. Geotherm. Res.* 264, 183-196, 2013.

Pyle, D.M.: Sizes of volcanic eruptions. In: Sigurdsson, H. (Ed.), *Encyclopedia of Volcanoes*. Academic, San Diego (California), 263269, 2000.

Rout, D.J., Cassidy, J., Locke, C.A., and Smith, I.E.: Geophysical evidence for temporal and structural relationships within the monogenetic basalt volcanoes of the Auckland volcanic field, northern New Zealand. *J. Volcanol. Geotherm. Res.* 57(1), 71-83, 1993.

Scaini, C., Felpeto, A., Martí, J., and Carniel, R.: A GIS-based methodology for the estimation of potential volcanic damage and its application to Tenerife Island, Spain. *J. Volcanol. Geotherm Res.* 278-279, 40-58, 2014.

Sheridan, M.F., Stinton, A.J., Patra, A., Pitman, E.B., Bauer, A., and Nichita, C.C.: Evaluating Titan2D mass-flow model using the 1963 Little Tahoma Peak avalanches, Mount Rainier, Washington. *J. Volcanol. Geophys. Res.* 139, 89-102, 2005.

Sobradelo, R., Bartolini, S., and Martí, J.: HASSET: a probability event tree tool to valuate future volcanic scenarios using Bayesian inference presented as a plugin for QGIS. *Bull. Volcanol.* 76, 770, 2013.

Spence, R.J.S.: Risk and regulation: can improved government action reduce the impacts of natural disasters?. *Building Research and Information* 32(5), 391-402, 2004.

Spence, R.J.S., Kelman, I., Calogero, E., Toyos, G., Baxter, P., and Komorowski, J.C.: Modelling expected physical impacts and human casualties from explosive volcanic eruptions. *Nat. Hazards Earth Syst. Sci.* 5, 1003-1015, 2005.

Venezky, D.Y. and Newhall, C.G.: WOVOdat design document: The schema, table descriptions, and create table statements for the database of worldwide volcanic unrest (WOVOdat version 1.0). US Geological Survey Open-File Report 2007-1117, pp.184, 2007.

Witham, C.: Volcanic disasters and incidents: a new database. *J. Volcanol. Geotherm. Res.* 148, 191-233, 2005.

Zuccaro, G., Cacace, F., Spence, R., and Baxter, P.: Impact of explosive eruption scenarios at Vesuvius. *J. Volcanol. Geotherm. Res.* 178(3), 416-453, 2008.

Supplementary material

SUPPLEMENTARY MATERIAL

GroupModels: hazard model tools

Table I . Susceptibility input parameters

parameter	QVAST	VORIS 2.0.1	Connor et al., 2012
GIS data (DEM, volcano-structural data)	X	X	X
bandwidtht evaluation	X		
Gauss kernel	X	X	X
Cauchy kernel		X	
grid size	X		X
output format	geoTIFF	Arc/Info Binary Grid	ASCII
reference	Bartolini et al., 2013	Felpeto et al., 2007	Connor et al., 2012

Table II . Temporal analysis input parameters

parameter	HASSET	BET_EF	BET_VH
unrest	X	X	X
origin	X	X	
outcome	X	X	
location	X	X	X
size	X	X	X
composition	X		
hazard	X		X
distance	X		X
overcoming threshold			X
output format	.csv, .png, .pdf	.bmp, .kml	maps in GoogleEarth, GIS, .gif
reference	Sobradelo et al., 2013	Marzocchi et al., 2008	Marzocchi et al., 2010

Table III . Susceptibility input parameters

parameter	VORIS 2.0.1	Connor et al., 2012
GIS data (DEM, volcano-structural data)	X	X
flow lenght	X	
lava thickness	X	X
lava flow volume		X
iteration volume		X
number of simulations	X	X
output format	Arc/Info Binary Grid	ASCII
reference	Felpeto et al., 2007	Connor et al., 2012

Table IV . Fallout input parameters

parameter	VORIS 2.0.1	HAZMAP	FALL 3D	TEPHRA 2	PUFFIN
GIS data (DEM, source point)	X	X	X	X	X
eruption duration		X	X	X	X
exit velocity		X	X	X	X
vent magma temperature		X	X	X	X
mass eruption rate		X	X	X	X
column height	X	X	X	X	X
erupted mass	X	X	X	X	X
metereological input data	X	X	X	X	X
horizontal diffusion coefficient	X	X	X	X	X
vertical diffusion coefficient	X	X	X	X	X
granulometry	X	X	X	X	X
output format	Arc/Info Binary Grid	.out, ASCII, ASCII Grid, ASCII Binary Grid	ASCII, netCDF	.txt	.cdf, .jpg, .txt, .gif, .kmz
reference	Felpeto et al., 2007	Macedonio et al., 2014	Folch et al., 2014	Connor et al., 2011	Bursik et al., 2013

Table V . PDC input parameters

parameter	VORIS 2.0.1	VOLCFLOW
GIS data (DEM)	X	X
collapse equivalent height	X	
collapse equivalent angle	X	X
time		X
internal friction angle		X
bed friction angle		X
viscosity		X
turbulence		X
density		X
output format	Arc/Info Binary Grid	.avi, .dat
reference	Felpeto et al., 2007	Kelfoun et al., 2005

Table VI . Ballistic input parameters

parameter	EJECT
drag properties	X
block properties	X
atmospheric properties	X
tailwind speed	X
initial velocity	X
extent zone	X
ejection angle	X
distance of landing point below takeoff point	X
output format	.txt
reference	Mastin et al., 2011

Table VII . Lahars input parameters

parameter	TITAN 2D	VOLCFLOW
GIS data (DEM)	X	X
time	X	X
collapse equivalent angle	X	X
time		X
internal friction angle	X	X
bed friction angle	X	X
viscosity		X
turbulence		X
discharge plane	X	
output format	tecplot.plt, mshplot.plt, GMFG Viz, XDMF/Paraview, Web Viz, grass sites	.avi, .dat
reference		Kelfoun et al., 2005

Summary of results & Discussion

This Ph.D. Thesis consists of six research papers that represent the logical time evolution of the research project, from the development of spatial and temporal tools for assessing long-term volcanic hazard to their application in different monogenetic volcanic fields, until the design of a new spatial database for the evaluation of volcanic risk.

The first tool was designed to evaluate volcanic susceptibility, that is the spatial probability of the appearance of a future vent opening, based on the past activity of the volcanic area and their structural controls. Through QVAST (**Q**GIS for **VolcAnic SuscepTibility**) tool it is possible (a) to calculate the bandwidth (e.g.: degree of randomness in the distribution of past vents) using different methods, (b) to evaluate the probability density function (PDF) using a Gaussian kernel, (c) to assign the weights to each PDF, and (d) to elaborate the susceptibility map. This tool is very appropriate for monogenetic volcanism where volcanoes are commonly clustered within fields and may occur in any geotectonic and environmental setting (Connor and Conway, 2000; Valentine and Gregg, 2008; Kereszturi and Németh, 2012). The results show the importance of choosing the optimal bandwidth parameter and for this reason the strength of QVAST lies in the possibility to choose between different methods. This manuscript “QVAST: a new Quantum GIS plugin for estimating volcanic susceptibility” has been published on November 27th, 2013 in *Natural Hazards and Earth System Sciences* 13 (2013), 3031-3042, with Impact Factor 1.826. Authors: S. Bartolini, A. Cappello, J. Martí, and C. Del Negro.

The second tool we have developed uses Bayesian Inference and event tree model for long-term volcanic hazard assessment. In comparison with previous event trees based on Bayesian methodology (e.g., BET_EF and BET_VH (Marzocchi et al., 2008, 2010)), the new model presented here overcomes their limitations by allowing a larger set of future volcanic scenarios in their probability estimation, and thus extending their use to a wide range of volcanic systems. HASSET (Hazard Assess-

ment Event Tree) also permits to automatically update the probabilities when new evidence arrives or the system becomes active and monitoring data on precursors exist. Further, it determines the five most likely scenarios based on the information given by the user. This new tool was created in a realistic, simple, and practical way, focusing discussion and drawing attention to possible scenarios that otherwise would go unnoticed or underestimated. Although this method was initially applied to the Teide-Pico Viejo stratovolcanoes in Tenerife, it can also be used with other similar volcanoes and in monogenetic volcanic fields as it offers a wide structure and applicability. HASSET can be used to identify the relative importance of several scenarios by comparing their probabilities and is useful for land use planning and preparedness actions. This manuscript “HASSET: a probability event tree tool to evaluate future volcanic scenarios using Bayesian inference” has been published online on December 6th, 2013 in the *Bulletin of Volcanology* 76 (2013), 770, doi:10.1007/s00445-013-0770-x, with Impact Factor 2.667. Authors: R. Sobradelo, S. Bartolini, and J. Martí.

The third work is case study of these applications to El Hierro (Canary Islands). The methodology presented is based on the characterization of past eruptions and the compilation of the volcano-structural data to study the spatio-temporal probabilities and to simulate different eruptive scenarios. Additionally, combining the most probable scenarios, we provided the first total qualitative hazard map of El Hierro. The result obtained from our approach shows that, although El Hierro is not a highly populated island, some medium- and high-volcanic-hazard zones coincide with some of the main inhabited areas. Furthermore, the results obtained offer the basis on which to build the strategies that are required to successfully face up and to minimise the impact of future volcanic eruptions on the island. This manuscript “Long-term volcanic hazard assessment on El Hierro (Canary Islands)” has been published on July 28th, 2014 in *Natural Hazards and Earth System Sciences* 14 (2014), 1853-1870, with Impact Factor 1.826. Authors: L. Becerril, S. Bartolini, R. Sobradelo, J. Martí, J.M. Morales, and I. Galindo.

The fourth work was conducted at Deception Island, representing a step forward in the evaluation of volcanic hazard on the island and the results obtained are potentially useful for long-term emergency planning. The present hazard assessment is relevant for the analysis of the adequacy of the current evacuation routes and locations of the active scientific stations. The hazard probability map shows that

the research stations could be affected by pyroclastic density currents and that a large area of the island could be covered by ash fallout. Furthermore, the opening of new fissures in the glacier zones could generate lahars that would reach the research stations and affect evacuation routes. It should be added that the existing evacuation routes were defined without any accurate hazard assessment and taking into account only logistical considerations. Thus, the results presented here should encourage a revision of the distribution and course of the evacuation routes. Moreover, it is worth mentioning that this long-term assessment may help decision makers when faced with difficult situations such as the allocation of resources for hazard prevention and evacuation whose objective is to reduce the loss of life due to the potential impact of volcanic hazards. This manuscript “Volcanic hazard on Deception Island (South Shetland Islands, Antarctica)” has been accepted for publication in the *Journal of Volcanology and Geothermal Research* on 11th August 2014, with Impact Factor 2.515. Authors: S. Bartolini, A. Geyer, J. Martí, D. Pedrazzi, and G. Aguirre-Díaz.

The fifth work evaluates the long-term hazard assessment of La Garrotxa Volcanic Field (NE Spain). In this work, an evaluation of different volcanic hazards is computed, through an evaluation of the susceptibility, temporal recurrence rate analysis, simulation of different eruptive scenarios, and obtention of a final hazard map. As in most of the Quaternary monogenetic volcanic fields, the lack of data and of recent eruptions could let us to assume that volcanic hazard and, consequently, risk is inexistent or non-significant. Well the contrary, all geological indicators suggest that the area is subjected to the same geodynamic conditions that favoured the initiation and continuation of this volcanism, so that we must consider this volcanic area as potentially active. The final hazard map shows La Garrotxa volcanic field subdivided into four different levels of hazards and will be useful for a land use planning and for the elaboration of an emergency plan for this volcanic area that should help to minimise the impact of future volcanic eruptions. This manuscript “Hazard assessment at the Quaternary La Garrotxa Volcanic Field (NE Iberia)” has been submitted for publication to the *Journal of Quaternary Science*, with Impact Factor 2.661. Authors: S. Bartolini, X. Bolós, J. Martí, E. Riera Pedra, and Ll. Planagumà.

The last research paper aims at designing a new spatial database, VERDI (**V**olcanic **managE**ment **R**isk **D**atabase des**I**gn). In fact, the first step in the evaluation of volcanic risk consists of obtaining and organizing all pertinent data derived from differ-

ent disciplines such as geology, volcanology, geochemistry, petrology and seismology, as well as vulnerability and socio-economic information relating to the elements that are potentially at risk. In order to optimize the accurate evaluation of volcanic risk, VERDI contains 12 information groups regarding past and current volcanic activity and the associated hazards and the potential vulnerability of the elements that may be affected by such hazards. Some of the most relevant issues include how and where to store the data, in which format should it be made available, and how to facilitate its use and exchange. The objective of the VERDI database is to make scientific research easier and to promote information-sharing for volcanic surveillance, susceptibility, hazard and vulnerability. This manuscript “VERDI: a new Volcanic managEment Risk Database desIgn” has been submitted on May 16th, 2014 in the Journal of Volcanology and Geotherma Research, with impact factor 2.515. Authors: S. Bartolini, L. Becerril, J. Martí.

The results presented in this Ph.D. Thesis evidence the importance of the evaluation of the volcanic hazard but especially the development of free and easy-use e-tools designed to obtain it. The potentiality of using QVAST and HASSET lies on the fact that they are free tools and developed on accessible and dynamic graphical user interfaces. The main advantage of using these tools is that new data or new model results can be easily included in the procedure to update the hazard assessment. Furthermore, the use of non-free tools makes difficult the exchange of information and the opportunity to be tested in different volcanic fields by different users. In addition, QVAST provides different methods for estimating the optimal bandwidth parameter, such as the Least Square Cross Validation (Cappello et al., 2012), the h_{opt} score (Silverman, 1986), and the Sum of Asymptotic Mean Squared Error selector (Connor et al., 2012), and new methods can be easily added. Whereas, although some parts of the HASSET tool coincide with BET_EF and BET_VH tools presented by Marzocchi et al. (2008, 2010), HASSET overcomes the limitations of previous event tree models by allowing a larger set of future volcanic scenarios in their probability estimation, considering different kinds of unrest episodes, taking into account the kind of outcome, and the magma composition.

Statistical methodologies are useful when the information about the past eruptive history and present state of activity of the volcanic area is incomplete, and much more effort is required before being confident to forecast its future behavior precisely. Another important aspects are the input parameters that play a major

role to determine the result of the models applied (Felpeto et al., 2007; Bartolini et al., 2013). Nowadays, none of the existing databases is based on a simple architecture that contains all the necessary information for volcanic risk analysis and management (e.g. WOVOdat (Venezky and Newhall, 2007); LaMEVE (Crosweller et al., 2012)). So, The rationale behind the VERDI architecture is based on the principle that all the information concerning the evaluation of volcanic risk should be comparable, consistent and available for future comparisons and data analyses.

This thesis has analyzed and computed a homogeneous and systematic methodology to evaluate volcanic hazard in monogenetic volcanic fields where no previous studies or no accurate volcanic hazard assessment has ever been conducted. In fact, in monogenetic volcanic fields are often regarded as non-active, so there is an alert reduction. On the contrary, to consider these volcanic areas as potentially active and to undertake volcanic hazard assessment for risk-based decision-making in land-use planning and emergency management and, consequently, to improve the security of the inhabitants and infrastructures. The suitability of the tools and methodology designed in this Ph.D. Thesis, tested at different case studies, allows them to be applied to other volcanic areas of similar characteristics and, consequently, will contribute to reduce effectively volcanic risk.

Conclusions

Modern volcanology is an interdisciplinary science that aims at studying the process behind volcanic eruptions and assessing volcanic hazard in order to reduce volcanic risk. The application of available tools such as QVAST (Bartolini et al., 2013), HASSET (Sobradelo et al., 2013), based on current knowledge of past eruptive activity and using probabilistic methods, such as the kernel density estimation and the Bayesian inference, and the possibility to simulate different eruptive scenarios, allows us to obtain a long-term hazard assessment, which can be easily updated and improved with the incorporation of new information such as a more complete volcano-stratigraphy and geochronology. This is an essential purpose and these free tools which should enable local authorities to apply more rational territorial planning and to design more adequate emergency plans to face future volcanic crises.

In this work we have presented different statistical methodologies and used different tools to interpret volcanic data and providing good examples to assess long-term volcanic hazard in monogenetic volcanic fields, using El Hierro (Canary Islands, Spain), Deception Island (South Shetland Islands, Antarctica), La Garrotxa (NE of Spain) as case studies. We performed a statistical analysis to extract information about the future behavior of the volcano by looking at the geological and historical activity of the volcanic system in each case. The Bayesian event tree statistical method HASSET was applied to calculate eruption recurrence, while the QVAST tool was used in an analysis of past activity to calculate the possibility that new vents will open (volcanic susceptibility). On the basis of these calculations, we identified a number of significant scenarios using the GIS-based tools (i.e. VORIS 2.0.1 (Felpeto et al., 2007), LAHARZ (Schilling, 1998)) and evaluated the potential extent of the main volcanic hazards to be expected on the volcanic areas. The results obtained allowed to evaluate and generate volcanic hazard maps with different levels of hazards.

These tools are part of a larger project consisting of several modules that will

interact with each other to elaborate an analysis report on the current situation of the volcano. Future research work includes to complete the spatial QVAST and temporal HASSET tools with a short term probability, including monitoring data, to be used during a volcanic crisis and to create other modules that allow also to evaluate eruptive scenarios, the vulnerability, and the risk. This architecture could be useful not only for the scientific community but also for decision making during volcanic crises. Furthermore, model results should be updated when new volcanic data and new geological records become available. We also suggest that all the basic information required to conduct hazard and risk assessment should be available and stored in a same database. A future role for a new database design, such as VERDI, will be the publication of an interactive web site that will enable registered users to access and share the information in the database, thereby allowing VERDI to become more dynamic and to continue to develop. As the most important aim of the modern volcanology is based on reducing the risk, our future research work will be also addressed to create a complete multihazard tool that takes into account the volcanic hazard not as an isolated process but as a set of natural hazards.

References

Alberico, I., Petrosino, P., Lirer, L.: Volcanic hazard and risk assessment in a multi-source volcanic area: the example of Napoli city (Southern Italy). *Natural Hazards Earth System Science* 11, 1-14, 2011.

Alcorn, R., Panter, K. S., and Gorsevski, P. V.: A GIS-based volcanic hazard and risk assessment of eruptions sourced within Valles Caldera, New Mexico, *J. Volcanol. Geoth. Res.*, 267, 1–14, 2013.

Barreca, G., Bonforte, A., Neri, M.: A pilot GIS database of active faults of Mt. Etna (Sicily): A tool for integrated hazard evaluation. *J. Volcanol. Geotherm. Res.* 251, 170-186, 2013.

Bartolini, S., Cappello, A., Martí, J., Del Negro, C.: QVAST: a new Quantum GIS plugin for estimating volcanic susceptibility, *Nat. Hazards Earth Syst. Sci.*, 13, 3031–3042, doi: 10.5194/nhess-13-3031-2013, 2013.

Bebbington, M., Cronin, S. J.: Spatio-temporal hazard estimation in the Auckland Volcanic Field, New Zealand, with a new event-order model, *Bull. Volcanol.*, 73, 55–72, 2011.

Becerril, L., Bartolini, S., Sobradelo, R., Martí, J., Morales, J. M., Galindo, I., 2014. Long-term volcanic hazard assessment on El Hierro (Canary Islands). *Nat. Hazards Earth Syst. Sci.* 14, 1853-1870.

Blong, R.: Volcanic hazards and risk management. In: Sigurdsson H et al. (eds) *Encyclopedia of volcanoes*. Academic, San Diego, pp 1215–1227, 2000.

Cappello, A., Vicari, A. M., Del Negro, C.: Assessment and modeling of lava flow hazard on Mt. Etna volcano, *B. Geofis. Teor. Appl.*, 52, 299–308, 2011.

Cappello, A., Neri, M., Acocella, V., Gallo, G., Vicari, A., Del Negro, C.: Spatial vent opening probability map of Mt Etna volcano (Sicily, Italy), *Bull. Volcanol.*, 74, 2083–2094, 2012.

Cappello, A., Bilotta, G., Neri, M., and Del Negro, C.: Probabilistic modeling of future volcanic eruptions at Mount Etna, *J. Geophys. Res.*, 118, 1925–1935, doi:10.1002/jgrb.50190, 2013.

Cas, R.A.F., Wright, J.V.: Volcanic successions (modern and ancient). A geo-

REFERENCES

logical approach to processes products and successions. Allen and Unwin, London, 1987.

Chester, D. K., Dikken, C. J. L., and Duncan, A. M.: Volcanic hazard assessment in western Europe, *J. Volcanol. Geoth. Res.*, 115, 411–435, 2002.

Connor, C.B., Hill, B.E.: Three nonhomogenous Poisson models for the probability of basaltic volcanism: application to the Yucca Mountain region, Nevada. *J. Geophys. Res.* 100(B6), 107–110, 1995.

Connor, C.B., Conway, F.M.: Basaltic Volcanic Fields. In: *Encyclopedia of Volcanology*. Academic Press, pp. 331-343, 2000.

Connor, L.J., Connor, C.B., Meliksetian, K., Savov, I., 2012. Probabilistic approach to modeling lava flow inundation: a lava flow hazard assessment for a nuclear facility in Armenia. *J. Appl. Volcanol.* 1(3), 1-19.

Crisci, G. M., Iovine, G., Di Gregorio, S., and Lupiano, V.: Lava-flow hazard on the SE flank of Mt. Etna (Southern Italy), *J. Volcanol. Geoth. Res.*, 177, 778–796, 2008.

Crosweller, H.S., Arora, B., Brown, S.K., Cottrell, E., Deligne, N.I., Ortiz, N., Hobbs, L.K., Kiyosugi, K., Loughlin, S.C., Lowndes, J., Nayembil, M., Siebert, L., Sparks, R.S.J., Takarada, S., Venzke, E.: Global database on large magnitude explosive volcanic eruptions (LaMEVE). *J. Appl. Volcanol.* 1, 2012.

De la Cruz-Reyna, S.: Long-term probabilistic analysis of future explosive eruptions. In: Scarpa, R., Tilling, R.I. (Eds.), *Monitoring and mitigation of volcanic hazards*. Springer-Verlag, Berlin, pp. 599-629, 1996.

Diggle, P. J.: A kernel method for smoothing point process data. *Applied Statistics*, *J. R. Stat. Soc. Ser. C.* 34, 138–147, 1985.

Favalli, M., Tarquini, S., Papale, P., Fornaciai, A., and Boschi, E.: Lava flow hazard and risk at Mt. Cameroon volcano, *Bull. Volcanol.*, 74, 423–439, doi:10.1007/s00445-011-0540-6, 2011.

Favalli, M., Tarquini, S., Papale, P., Fornaciai, A., Boschi, E.: Lava flow hazard and risk maps at Mount Cameroon volcano. *Bulletin of Volcanology* 74, 423-439, 2012.

Felpeto, A., Martí, J., Ortiz, R.: Automatic GIS-based system for volcanic hazard assessment, *J. Volcanol. Geoth. Res.*, 166, 106–116, doi:10.1016/j.jvolgeores.2007.07.008, 2007.

Fiske, R.S., Jackson, E.D.: Orientation and growth of Hawaiian volcanic rifts:

REFERENCES

the effect of regional structure and gravitational stresses. *Proc. R. Soc. Lond.*, 329, 299-326, 1972.

Fournier d'Albe, E. M.: Objectives of volcanic monitoring and prediction, *J. Geol. Soc. Lond.*, 136, 321–326, 1979.

Geyer, A., Martí, J.: The new worldwide collapse caldera database (CCDB): A tool for studying and understanding caldera processes. *J. Volcanol. Geotherm. Res.* 175, 334-354, 2008.

Gogu, R.C., Dietrich, V.J., Bernhard, J., Schwandner, F.M., Hurni, L.: A geo-spatial data management system for potentially active volcanoes-GEOWARN project. *Comput. Geosci.* 32, 29-41, 2006.

Guilbaud, M.N., Siebe, C., Layer, P., Salinas, S., Castro-Govea, R., Garduño Monroy, V.H., Le Corvec, N.: Geology, geochronology, and tectonic setting of the Jorullo volcano region, Michoacán, México. *Journal of Volcanology and Geothermal Research* 201, 97–112, 2011.

Hill, D. P., Dzurisin, D., Ellsworth, W. L., Endo, E. T., Galloway, D. L., Gerlach, T. M., Johnston, M. S. J., Langbein, J., McGee, K. A., Miller, C. D., Oppenheimer, D., and Sorey, M. L.: Response plan for volcano hazards in the Long Valley Caldera and Mono craters region California, *Bull. Geol. Surv.*, 65, 2185, 2001.

Jaquet, O., Connor, C. B., and Connor, L.: Probabilistic Methodology for Long Term Assessment of Volcanic Hazards, IHLRMW, Las Vegas, USA, 2008.

Kereszturi, G., Németh, K.: Monogenetic Basaltic Volcanoes: Genetic Classification, Growth, Geomorphology and Degradation, in: Updates in Volcanology- New Advances in Understanding Volcanic Systems, edited by: Németh, K., InTech, 3–88, doi:10.5772/51387, 2012.

Kilburn, C. R. J.: Multiscale fracturing as a key to forecasting volcanic eruptions, *J. Volcanol. Geoth. Res.*, 125, 271–289, 2003.

Lirer, L., Petrosino, P., and Alberico, I.: Volcanic hazard assessment at volcanic fields: the Campi Flegrei case history, *J. Volcanol. Geoth. Res.*, 101, 55–75, 2001.

Lutz, T. M., Gutmann, J. T., 1995. An improved method for determining and characterizing alignments of point-like features and its implications for the Pinacate volcanic field, Sonoran, Mexico. *J. Geophys. Res.* 100, 17659–17670.

Martí, J., Aspinall, W., Sobradelo, R., Felpeto, A., Geyer, A., Ortiz, R., Baxter, P., Cole, P., Pacheco, J., Blanco, M., Lopez, C., 2008. A long-term volcanic hazard event tree for Teide-Pico Viejo stratovolcanoes (Tenerife, Canary Islands). *J.*

Volcanol. Geotherm. Res. 178(3), 543-552.

Martí, J. and Felpeto, A.: Methodology for the computation of volcanic susceptibility. An example for mafic and felsic eruptions on Tenerife (Canary Islands), *J. Volcanol. Geoth. Res.* 195, 69–77, doi:10.1016/j.jvolgeores.2010.06.008, 2010.

Martí, J., Sobradelo, R., Felpeto, A., García, O.: Eruptive scenarios of phonolitic volcanism at Teide-Pico Viejo volcanic complex (Tenerife, Canary Islands), *Bull. Volcanol.*, 74, 767–782, doi:10.1007/s00445-011-0569-6, 2012.

Martin, A. J., Umeda, K., Connor, C. B., Weller, J. N., Zhao, D., and Takahashi, M.: Modeling long-term volcanic hazards through Bayesian inference: an example from the Tohoku volcanic arc Japan, *J. Geophys. Res.*, 109, B10208, doi:10.1029/2004JB003201, 2004.

Marzocchi, W., Sandri, L., Selva, J.: BET_EF: A probabilistic tool for long- and short-term eruption forecasting, *Bull. Volcanol.*, 70, 623–632, doi:10.1007/s00445-007-0157-y, 2008.

Marzocchi, W., Sandri, L., Selva, J.: BET_VH: a probabilistic tool for long-term volcanic hazard assessment, *Bull. Volcanol.*, 72, 705–716, 2010.

Newhall, C. G., Hoblitt, R. P.: Constructing event trees for volcanic crisis, *Bull. Volcanol.*, 64, 3–20, doi:10.1007/s004450100173, 2002.

Pareschi, M. T., Cavarra, L., Favalli, M., Giannini, F., and Meriggi, A.: GIS and Volcanic Risk Management, *Nat. Hazards*, 21, 361–379, 2000.

Phillipson, G., Sobradelo, R., Gottsmann, J.: Global volcanic unrest in the 21st century: An analysis of the first decade, *J. Volcanol. Geoth. Res.*, 264, 183–196, 2013.

Sandri, L., Jolly, G., Lindsay, J., Howe, T., Marzocchi, W.: Combining long- and short-term probabilistic volcanic hazard assessment with cost-benefit analysis to support decision making in a volcanic crisis from the Auckland Volcanic Field, New Zealand, *Bull. Volcanol.*, 74, 705–723, 2012.

Sandri, L., Thouret, J. C., Constantinescu, R., Biass, S., Tonini, R.: Long-term multi-hazard assessment for El Misti volcano (Peru), *Bull. Volcanol.*, 76, 771–797, doi:10.1007/s00445-013-0771-9, 2014.

Scandone R.: Effusion rate and energy balance of Paricutin eruption (1943-1952), Michoacan, Mexico. *Journal of Volcanology and Geothermal Research* 6, 49-59, 1979.

Schilling, S.P.: LAHARZ: GIS program for automated mapping of lahar-inundation

REFERENCES

- hazard zones. U.S. Geological Survey Open-File Report, pp. 98-638, 1998.
- Siebe, C., Macías, J. L.: Volcanic hazards in the Mexico City metropolitan area from eruptions at Popocatepetl, Nevado de Toluca, and Jocotitlán stratovolcanoes and monogenetic scoria cones in the Sierra Chichinautzin Volcanic Field. *Special Papers, Geological Society of America* 402, 253, 2006.
- Silverman, B. W.: *Density Estimation for Statistics and Data Analysis*, Chapman & Hall, London, 1986.
- Sobradelo, R., Martí, J.: Bayesian event tree for long-term volcanic hazard assessment: Application to Teide-Pico Viejo stratovolcanoes, Tenerife, Canary Islands, *J. Geophys. Res.*, 115, B05206, doi:10.1029/2009JB006566, 2010.
- Sobradelo, R., Geyer, A., Martí, J.: Statistical data analysis of the CCDB (Collapse Caldera Database): Insights on the formation of caldera systems. *Journal of Volcanology and Geothermal Research*, 198:241–252, 2010.
- Sobradelo, R., Bartolini, S., Martí, J.: HASSET: a probability event tree tool to evaluate future volcanic scenarios using Bayesian inference Presented as a plugin for QGIS, *Bull. Volcanol.*, 76, 770–785, doi:10.1007/s00445-013-0770-x, 2013.
- Toyos, G. P., Cole, P. D., Felpeto, A., Martí, J.: A GIS-based methodology for hazard mapping of small pyroclastic density currents, *Nat. Hazards*, 41, 99–112, 2007.
- Valentine, G. A., Gregg, T. K. P.: Continental basaltic volcanoes – processes and problems, *J. Volcanol. Geotherm. Res.*, 177, 857–873, 2008.
- Venezky, D.Y., Newhall, C.G.: WOVODat design document: The schema, table descriptions, and create table statements for the database of worldwide volcanic unrest (WOVODat version 1.0). US Geological Survey Open-File Report 2007-1117, pp.184, 2007.
- Voight, B., Cornelius, R. R.: Prospects for eruption prediction in near-real-time, *Nature*, 350, 695–698, 1991.
- Walker, G.P.L.: Volcanic rift zones and their intrusion swarms. *J. Volcanol. Geotherm. Res.*, 94, 21–34, 1999.
- Witham, C.: Volcanic disasters and incidents: a new database. *J. Volcanol. Geotherm. Res.*, 148, 191-233, 2005.
- Wood, C.A.: Morphometric evolution of cinder cones. *J. Volcanol. Geotherm. Res.*, 7, 387–413, 1980.

REFERENCES

PART II

Appendix 1

Contribution to the papers

Inform from the supervisors of the thesis on the impact factor or the categorization of journal publications to be found in the doctoral thesis and the report of the thesis supervisor explaining the participation in the paper of the coauthors.



JOAN MARTÍ I MOLIST, Professor d'Investigació del CSIC adscrit a l'Institut de Ciències de la Terra "Jaume Almera" de Barcelona i Director de la Tesi Doctoral realitzada per Stefania Bartolini titulada "VOLCANIC HAZARD ASSESSMENT IN MONOGENETIC VOLCANIC FIELDS"

CERTIFICA:

1. que, d'acord amb la normativa vigent de la Universitat de Barcelona referent a la presentació de Tesis Doctorals, aquesta Tesi Doctoral es presenta com a compendi de les següents publicacions científiques de les que s'indica el seu factor d'impacte a l'any de la publicació:

- **Stefania Bartolini**, Annalisa Cappello, Joan Martí, and Ciro Del Negro, 2013. QVAST: a new Quantum GIS plugin for estimating volcanic susceptibility. Natural Hazards and Earth System Sciences.
Factor d'impacte: 1.826
<http://www.nat-hazards-earth-syst-sci.net/13/3031/2013/nhess-13-3031-2013.html>
- Rosa Sobradelo, **Stefania Bartolini**, and Joan Martí, 2013. HASSET: a probability event tree tool to evaluate future volcanic scenarios using Bayesian inference. Bulletin of Volcanology.
Factor d'impacte: 2.667
<http://link.springer.com/article/10.1007%2Fs00445-013-0770-x>
- Laura Becerril, **Stefania Bartolini**, Rosa Sobradelo, Joan Martí, José María Morales, and Inés Galindo, 2014. Long-term volcanic hazard assessment on El Hierro (Canary Islands). Natural Hazards and Earth System Sciences.
Factor d'impacte: 1.826
<http://www.nat-hazards-earth-syst-sci.net/14/1853/2014/nhess-14-1853-2014.html>



- **Stefania Bartolini**, Adelina Geyer, Joan Martí, Dario Pedrazzi, and Gerardo Aguirre-Díaz, 2014. Volcanic hazard on Deception Island (South Shetland Islands, Antarctica). Journal of Volcanology and Geothermal Research.
Factor d'impacte: 2.515
- **Stefania Bartolini**, Xavier Bolós, Joan Martí, Elisabeth Riera Pedra, and Llorenç Planagumà, 2014. Hazard assessment at the Quaternary La Garrotxa Volcanic Field (NE Iberia). Journal of Quaternary Science.
Factor d'impacte: 2.661
- **Stefania Bartolini**, Laura Becerril, and Joan Martí, 2014. VERDI: a new Volcanic management Risk Database design. Journal of Volcanology and Geothermal Research.
Factor d'impacte: 2.515

2. que tots els treballs han estat realitzats en col·laboració amb altres investigadors, havent estat la doctorant la persona encarregada de realitzar la major part del treball, la seva planificació, redacció i revisió, en aquelles publicacions en que és el primer autor, en els que el paper dels altres firmants ha estat l'assessorament científic, aportació de dades complementaries i/o participació en els treballs. Igualment, en els altres treballs inclosos, el paper de la doctorant ha estat destacat i del tot necessari per la consecució dels resultats obtinguts.

I perquè així consti i a tots el efectes oportuns signo el present certificat a Barcelona a 20 de agost de dos mil catorze.

Appendix 2

QVAST: a new Quantum GIS plugin for estimating volcanic susceptibility



QVAST: a new Quantum GIS plugin for estimating volcanic susceptibility

S. Bartolini¹, A. Cappello², J. Marti¹, and C. Del Negro²

¹Group of volcanology, (SIMGEO-UB), Institute of Earth Sciences Jaume Almera, ICTJA-CSIC, Barcelona, Spain

²Istituto Nazionale di Geofisica e Vulcanologia, Sezione di Catania, Osservatorio Etneo, Catania, Italy

Correspondence to: S. Bartolini (sbartolini@ictja.csic.es)

Received: 16 July 2013 – Published in Nat. Hazards Earth Syst. Sci. Discuss.: 22 August 2013

Revised: 18 October 2013 – Accepted: 23 October 2013 – Published: 27 November 2013

Abstract. One of the most important tasks of modern volcanology is the construction of hazard maps simulating different eruptive scenarios that can be used in risk-based decision making in land-use planning and emergency management. The first step in the quantitative assessment of volcanic hazards is the development of susceptibility maps (i.e., the spatial probability of a future vent opening given the past eruptive activity of a volcano). This challenging issue is generally tackled using probabilistic methods that use the calculation of a kernel function at each data location to estimate probability density functions (PDFs). The smoothness and the modeling ability of the kernel function are controlled by the smoothing parameter, also known as the bandwidth. Here we present a new tool, QVAST, part of the open-source geographic information system Quantum GIS, which is designed to create user-friendly quantitative assessments of volcanic susceptibility. QVAST allows the selection of an appropriate method for evaluating the bandwidth for the kernel function on the basis of the input parameters and the shapefile geometry, and can also evaluate the PDF with the Gaussian kernel. When different input data sets are available for the area, the total susceptibility map is obtained by assigning different weights to each of the PDFs, which are then combined via a weighted summation and modeled in a non-homogeneous Poisson process. The potential of QVAST, developed in a free and user-friendly environment, is here shown through its application in the volcanic fields of Lanzarote (Canary Islands) and La Garrotxa (NE Spain).

1 Introduction

Volcano susceptibility is defined as the spatial probability of vent opening (Marti and Felpeto, 2010) and constitutes one of the first steps in the assessment of volcanic hazards and the construction of hazard maps of eruptive products (e.g., lava flows, ash, and pyroclastic density currents). The exact site of a new eruption – a central vent or a vent located on the flanks of a stratovolcano, or at any other apparently randomly distributed point in a larger monogenetic volcanic field – is of critical importance in determining the potential outcome of an eruption. For the same eruption, different eruption scenarios and, consequently, different potential impacts are to be expected depending on the exact location of the vent and on the geographic and demographic characteristics of the area. Hence, evaluating where future eruptive vents are most likely to open greatly influences volcanic hazard assessment (Cappello et al., 2011a, b).

The exact path that the over-pressurized magma will take from its accumulation site to the earth's surface – and hence the site of any new vent – will be determined by geological structure and stress distribution inside the crust. We know that the energetic investment by the magma on this path will be the minimum and that it will be parallel to the trajectory of the main principal stress and normal to the minimum principal stress (Gudmundsson, 2008, 2012). However, we do not have any direct criteria that enable us to determine this route a priori since we lack detailed 3-D knowledge of the stress field of the area. In the long term it is possible to base some approaches on the location of previous eruptions and on the structural characteristics of the volcano or the volcanic area. On the other hand, in the short term it is also possible to take

into account monitoring data from the volcanic field. Therefore, the estimation of the most probable vent site is not an impossible task and can be undertaken as part of volcanic hazard assessment. This is a less difficult task in stratovolcanoes for which good knowledge of past eruptive history exists and where real-time volcano monitoring is currently being performed. However, volcano susceptibility assessment is more complex in monogenetic volcanic fields, as has been shown by the recent eruption at El Hierro (Martí et al., 2013), where stress conditions may change from one eruption to another.

Published works in this field (Connor and Hill, 1995; Felpeto et al., 2007; Jaquet et al., 2008; Martí and Felpeto, 2010; Favalli et al., 2011; Connor et al., 2012; Cappello et al., 2012, 2013) report the use of kernel density functions to evaluate susceptibility. However, this technique is based mainly on the assumption that new vents will not form far from existing ones (Martin et al., 2004; Jaquet et al., 2008). This is an a priori hypothesis for long-term hazard assessment, in which the use of volcano structural alignments (eruptive fissures, fractures, dykes) and the location of past centers of emission assumes implicitly that the general stress field has not changed significantly since the formation of these structures. Conversely, when dealing with short-term hazard assessment, monitoring data (Martí and Felpeto, 2010) – which provide important information regarding the evolution of magma migration and its ascent to the surface – play a major role in determining volcanic susceptibility.

A kernel function is a density function used to obtain the intensity of volcanic events. It is based on the distance from nearby volcanoes and a smoothing constant h (Martin et al., 2004), which indicates the spatial probability that a new eruptive vent will form. A Gaussian kernel is a kernel function describing a normal distribution that is used in volcanology to estimate local volcanic event densities in volcanic fields (Martin et al., 2004; Connor et al., 2012; Cappello et al., 2012).

The aim of this work is to (i) analyze different approaches to evaluate the smoothing parameter h (also known as the bandwidth), (ii) estimate for each approach the corresponding probability density function (PDF) and (iii) assess long-term spatial susceptibility in monogenetic volcanic fields. We describe here a new user-friendly plugin known as QVAST (QGIS for VolcAnic SuscepTibility) for the free geographic information system Quantum GIS (QGIS), which can make these calculations and help users to choose the best option in each particular case (Fig. 1). We describe the QVAST interface step by step via two different applications: the first in Lanzarote (Canary Islands, Spain) and the second in La Garrotxa (NE Spain). These two case studies show QVAST's great flexibility and its ability to identify the most likely zones to host new eruptions in monogenetic volcanic fields.

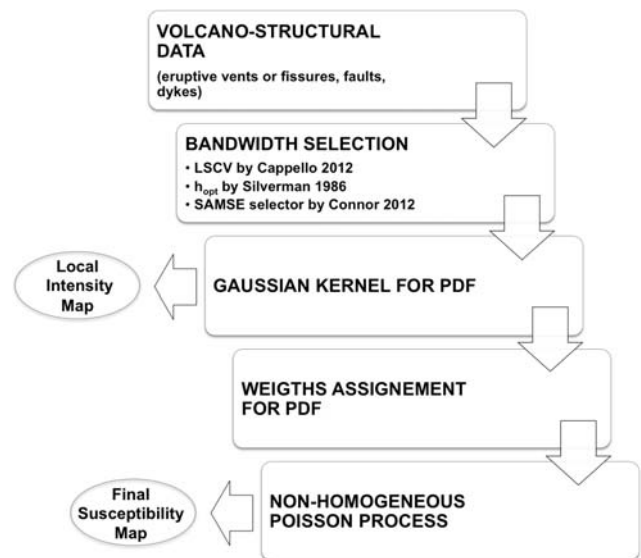


Fig. 1. Flowchart showing the main steps available in QVAST.

2 Optimal bandwidth in kernel density estimation

The probability distribution in a kernel technique is strongly influenced by a smoothing parameter or bandwidth, which determines how probabilities are distributed in terms of the distance from the volcanic structures or vents. The smoothness of the kernel density estimate is evident compared to the discreteness of the histogram, as bin width of a histogram, for continuous random variables (Scott, 1979). An optimal smoothing bandwidth is based on the clustering behavior of the volcanic structures and varies proportionally with the volcanic field size and vent density. Indeed, narrow bandwidths accentuate densities near the locations of past events. Conversely, broad bandwidths may oversmooth the density estimate, resulting in unreasonably low density estimates near clusters of past events, or overestimate densities at greater distances from past events. In a Gaussian kernel function, the bandwidth is equivalent to the variance of the kernel (Connor et al., 2012).

In volcanic hazard applications, the choice of the optimal bandwidth is difficult and depends on the field size and degree of cluster determining the probability distribution at distance from volcanic structures or eruptive vents.

QVAST provides a number of different methods for estimating the optimal bandwidths. The least square cross-validation (LSCV – Cappello et al., 2012) is made available for the volcanic structures with linear geometries (e.g., dykes, eruptive fissures, faults), and three methods are provided for the eruptive vents: the LSCV, the \hat{h} score (Silverman, 1986) and the sum of asymptotic mean squared error (SAMSE) selector H (Connor et al., 2012).

An exhaustive description of each of these methods is hereinafter provided.

2.1 Least square cross-validation (Cappello et al., 2012)

Least square cross-validation (LSCV) is a procedure that uses an iterative approach to determine the optimal bandwidth for fixed kernel functions. Initially proposed by Rudemo (1982) and Bowman (1984), the LSCV uses the minimization of the integrated square error between the estimated distribution and the true distribution.

In our QGIS plugin, we used the version proposed by Wornton (1995), defined as

$$\text{LSCV}_h = \frac{1}{\pi h^2 n} + \frac{1}{4\pi h^2 n^2} \times \sum_{i=1}^n \sum_{j=1}^n \left(\exp \left[\frac{-d_{ij}^2}{4h^2} \right] - 4 \exp \left[\frac{-d_{ij}^2}{2h^2} \right] \right), \quad (1)$$

where h is the smoothing factor, n the total number of historical data and d_{ij} the Euclidean distance between the i th and the j th points, when dealing with eruptive vents.

Conversely, if historical data consist of broken lines containing a number of linear segments, QVAST uses a modified version of LSCV (Cappello et al., 2012; Becerril et al., 2013; Cappello et al., 2013), where d_{ij} is the “minimax distance” (i.e., the minimum value of the maximum distances between each end point of the i th volcanic structure and all the end points of the j th volcanic structure).

2.2 The h_{opt} score (Silverman, 1986)

The Silverman method determines the optimal bandwidth h based on the assumption that the location of the vent opening is a random variable. The generalization of the Silverman’s rule of thumb (Silverman, 1986) in the multivariate case is as follows (Scott, 1992; Härdle et al., 2004):

$$\hat{h} = n^{1/(d+4)} \hat{\sigma}. \quad (2)$$

In the bivariate case $d = 2$, n is the length of the samples (x and y are the Cartesian coordinates), and $\hat{\sigma}$ is the standard deviation. Thus, we obtain

$$\hat{h} = n^{1/6} \sqrt{\frac{\sigma_x^2 + \sigma_y^2}{2}}, \quad (3)$$

where σ_x and σ_y are the standard deviations of the x and y coordinates, respectively.

2.3 The sum of asymptotic mean squared error selector (Connor et al., 2012)

The pilot bandwidth selector is a modified asymptotic mean integrated squared error (AMISE) method developed by Duong and Hazelton (2003) to evaluate the optimal bandwidth in kernel density estimation.

Despite their mathematical complexity, SAMSE bivariate bandwidth selectors can help find optimal bandwidths using

actual data locations, and so remove subjectivity from the process (Connor et al., 2012). In Duong and Hazelton (2003), the bivariate kernel density is defined by

$$\hat{f}(x; \mathbf{H}) = n^{-1} \sum_{i=1}^n K_{\mathbf{H}}(\mathbf{x} - \mathbf{X}_i), \quad (4)$$

where n is the sample size, $\mathbf{x} = (x_1, x_2)^T$, $\mathbf{X}_i = (X_{i1}, X_{i2})^T$, for $i = 1, 2, \dots, n$, and K is the bivariate kernel that depends on \mathbf{H} , the bandwidth matrix that is symmetric and positive definite. To measure the performance of \hat{f} , a SAMSE pilot selector is used, which is simpler and more parsimonious than the AMISE selectors.

The SAMSE selector is freely available within the “ks” package of the R Project for Statistical Computing (Duong, 2007; Hornik, 2009) and can be expressed as follows:

$$H = Hpi(x, nstage, pilot = 'samse', pre = 'sphere'), \quad (5)$$

where \mathbf{x} is a vector or matrix of data (vents), $nstage$ is the number of stages in the plugin bandwidth selector, $pilot$ is the pilot estimation, and “pre” concerns the pre-transformations.

The spatial density estimates are based on the distribution of past events within a volcanic field and the time period under consideration, and can be used as the basis for estimating the probability of the opening of new vents within a region. Connor et al. (2012) define an event as the opening of a new vent at a new location during a new episode of volcanic activity.

The optimal bandwidth matrix obtained using Eq. (5) represents smoothing in E–W and N–S directions, the upper left and lower right diagonal elements, respectively.

3 Kernel density estimation

Kernel density estimation is a well-known, non-parametric approach to the estimation of probability density functions using a finite number of samples. The shape of kernel function – be it Cauchy kernel (Martin et al., 2004), Epanechnikov kernel (Lutz and Gutmann, 1995) or Gaussian kernel (Connor and Hill, 1995) – is important in probability calculations, even if it is less relevant than other parameters (Connor and Hill, 1995; Lutz and Gutmann, 1995).

In the general case, if X_i denotes samples of size n , then the kernel density estimate of λ in the point x is given by

$$\lambda(x) = \frac{1}{n} \sum_{i=1}^n K_h(x, X_i), \quad (6)$$

where K_h is a kernel function with bandwidth h , satisfying the condition that $\int K_h(x, \cdot) dx = 1$ to ensure that $\lambda(x)$ is a density. In the Gaussian formulation,

$$\lambda(x) = \frac{1}{2\pi n h^2} \sum_{i=1}^n \exp \left(-\frac{d_i^2}{2h^2} \right). \quad (7)$$

4 Interface and tools of QVAST

Available open-source desktop GISs have notable differences in quality and performance (Sherman, 2008; Chen et al., 2010). Quantum GIS (QGIS) is a free, open-source and cross-platform software, distributed at www.QGIS.org. It includes all of the common GIS functions and features and possesses an intuitive and user-friendly interface. One of the great advantages of QGIS is the availability of plugins from official and third-party repositories that provide a large number of additional functions. These features make QGIS the most suitable software for our plugin.

QVAST is developed in Python script, an interpreted, general-purpose, high-level programming language, whose codes can be packaged into stand-alone executable programs (using sub-process calls to R) and C++ codes. A graphical user interface (GUI) is available to provide users with a dynamic graphical window in QGIS.

QVAST includes different methods for choosing the optimal value for the bandwidth, which depends on the size of the volcanic field and the degree of clustering in the available data. The PDF is constructed using a kernel density estimator, which is a function centered at each data sample location that exerts an influence on the surrounding region (Diggle, 1985). It is employed to estimate how the density of new vent openings varies across a study area in accordance with the distribution of past eruptions and the bandwidth. Different types of kernels can be used to describe the spatial density, e.g., the Cauchy (Martin et al., 2004), Epanechnikov (Lutz and Gutmann, 1995), Gaussian (Connor and Hill, 1995), or elliptical (Kiyosugi et al., 2010) kernels. Here we use the Gaussian kernel, which responds well to the clustering phenomena commonly observed in volcanic distributions (Weller et al., 2006).

Long-term spatial susceptibility is obtained through a non-homogeneous Poisson process (NHPP), where the PDFs and their relative weights are combined through a weighted sum. QVAST allows users to assign different weights to each of the PDFs depending on the relevance and reliability of data sets. Once the user has installed the plugin in the QGIS plugins folder, a new option called “Volcano” appears in the QGIS menu bar where the QVAST model is installed.

The QVAST structure consists of three main modules (Fig. 2):

1. Estimation of the optimal bandwidth starting from different geometric layers (points and polylines);
2. Evaluation of the Gaussian kernel and generation of the PDF in the volcanic area under study;
3. Calculation of the susceptibility map from one or more PDFs. In this latter case, QVAST allows users to assign different weights to each layer.

The first window that appears after launching the plugin is the evaluation of the bandwidth. A drop-down menu contains the shapefile layers added in the “Layers” menu in the QGIS project. To estimate the optimal bandwidth in case of a group of sample points (e.g., eruptive vents), QVAST offers three different methods: LSCV, the \hat{h} score and the SAMSE selector H . If the GIS layer consists of linear volcanic structures (e.g., dykes, eruptive fissures, or faults), only the LSCV score can be used. Otherwise, the plugin allows the user to introduce the optimal value for the bandwidth by hand (if known) and continue directly to the construction of the PDF.

Once the layer and the method for evaluating the bandwidth have been selected, the value of the smoothing parameter is calculated using the “CALCULATE BANDWIDTH” button.

The second window enables the PDF with the Gaussian kernel to be evaluated using the calculated optimal bandwidth. To evaluate the Gaussian kernel on the selected layer, QVAST needs the following input parameters: the surface area on which the calculation is to be performed (raster layer), the grid resolution (which should be clearly smaller than the size of the volcanic area under study), the bandwidth value, the output name, and the output path where the results are to be saved. The surface area can be less than the entire digital elevation model (DEM) if the user is only interested in a particular area. The result of the Gaussian kernel is a PDF in GeoTIFF raster format, which is automatically added as a new layer to the active QGIS project. The results show the distribution of the PDF in the volcanic area related to the input layer selected.

The third window enables simultaneously considering different layers to which different weights can be assigned and thus calculate the final susceptibility map. Once the grid size and the weight for each PDF have been defined, QVAST calculates the weighted sum and evaluates the final raster map that represents the spatial susceptibility. The map is presented in a GeoTIFF raster format and is added to the layer.

Hence, the steps needed to obtain the final susceptibility can be summarized as follows (Fig. 1):

1. Gathering of all volcano structural data available;
2. Optimal bandwidth selection using different methods;
3. Application of the Gaussian kernel to obtain the PDF;
4. Assignment of a relative weight to each PDF;
5. Creation of the susceptibility map with an NHPP.

The functionality and flexibility provided by QVAST have been demonstrated in Lanzarote and La Garrotxa volcanic fields. Different methods were used to identify the optimal bandwidth, and different results were obtained when different weights to the PDFs were assigned.

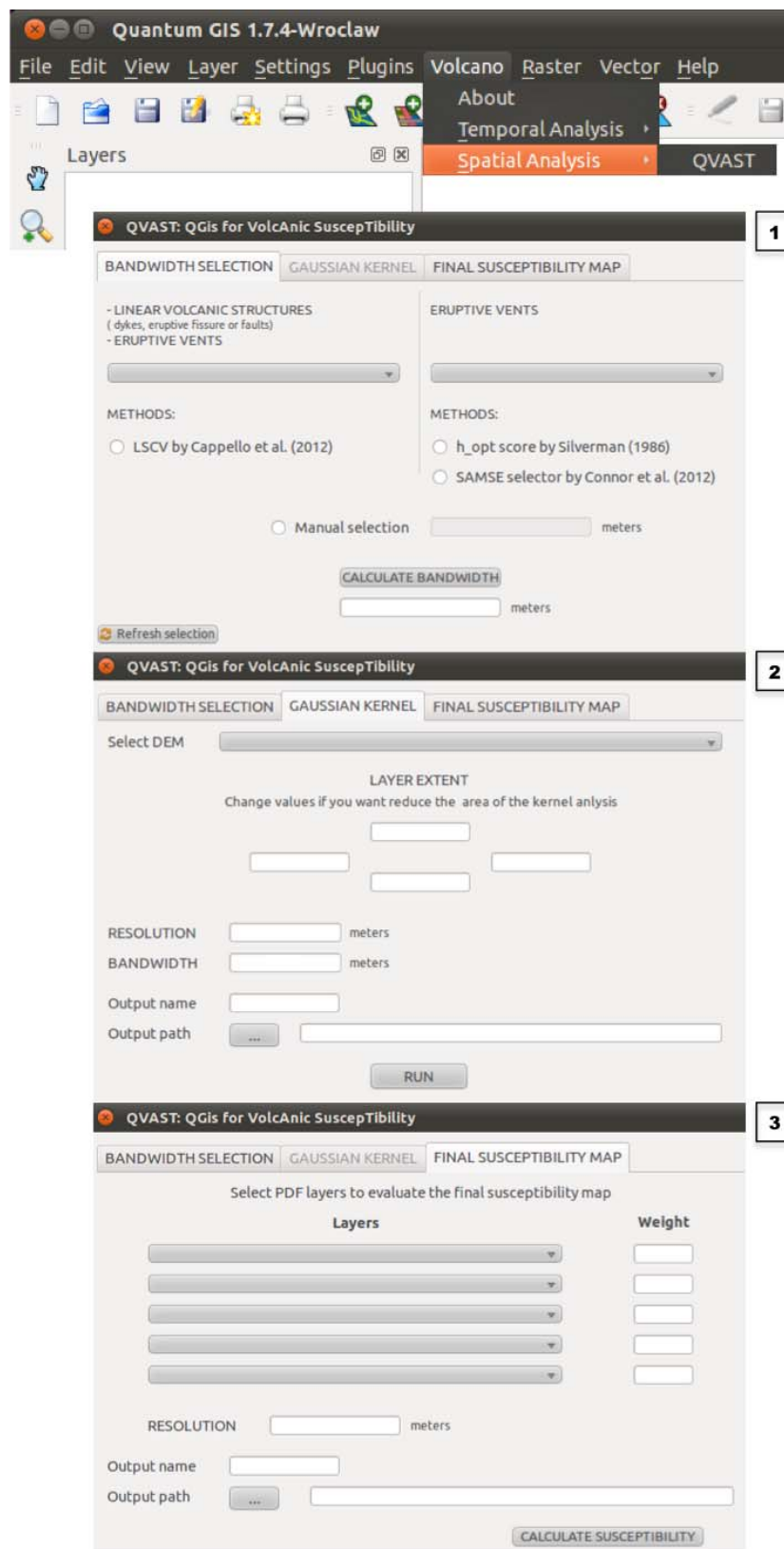


Fig. 2. QVAST main interface: screenshots of the optimal bandwidth selection (1), for the parameter needed by the Gaussian kernel (2) and for the assignment of weights to the different PDFs (3).



Fig. 3. Geographical setting of the Canary Islands.

5 Applying QVAST: Lanzarote (Canary Islands, Spain) and La Garrotxa (NE Spain)

5.1 Lanzarote: geological context

Lanzarote lies in the northeast of the Canary Islands archipelago (Fig. 3). It forms the emergent part of the so-called East Canary Ridge (ECR), a NNE–SSW linear volcanic structure located on atypical oceanic crust, at least 11 km thick (Banda et al., 1981), lying between the continental rise and the Canary Basin.

The geological evolution of Lanzarote involves two main stages: the first pre-erosional during the Miocene–Pliocene and the second – divided into two periods of volcanic activity – post-erosional during the Quaternary (Marinoni and Pasquaré, 1994).

Sub-aerial volcanic activity has been almost continuous during the past 20 Myr and reveals that these islands are part of a sector of the lithosphere in which the thermal and dynamic anomalies that lead to the production and ascent of alkaline basaltic magmas have persisted for an exceptionally long period (Coello et al., 1992; Blanco-Montenegro et al., 2005).

In historical times eruptions on Lanzarote took place during the 18th and 19th centuries. The eruption between 1730 and 1736 was one of the earth's biggest ever historical eruptions. A large number of volcanic cones were formed along an around 15 km long fissure. During the eruption 3–5 km³ of lava were emitted, covering an area of approximately 200 km² (Carracedo et al., 1992; Felpeto et al., 2001).

The structural evolution results from a complex interaction between the magmatism and both the regional stress field and the local stress field generated during the growth of the island itself. Hence, the present structural architecture is the result of a complex magmatic and tectonic evolution characterized by variations in the stress field that have been at work from the Miocene to the present day (Camacho et al., 1991).

5.2 La Garrotxa: geological context

The Catalan Volcanic Zone (CVZ, NE Iberian Peninsula) is one of the alkaline Quaternary volcanic provinces that form

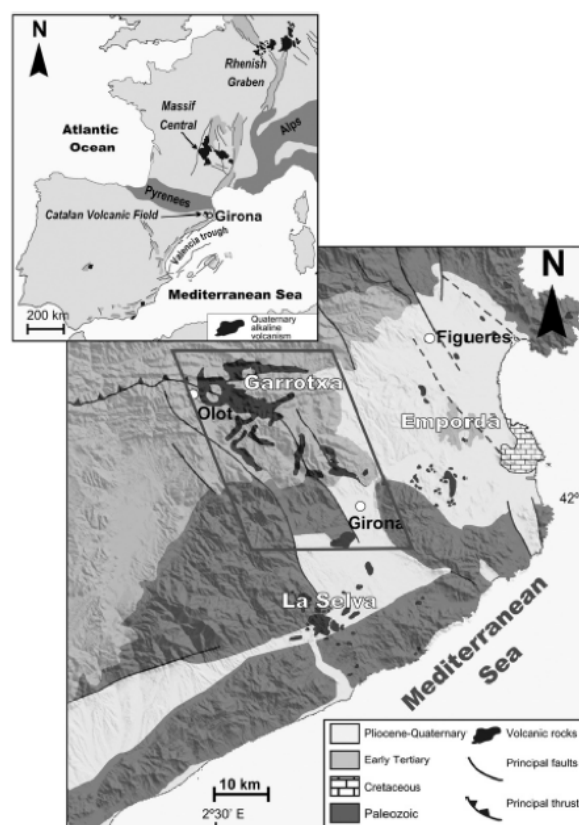


Fig. 4. Geographical and geological settings of the La Garrotxa volcanic field (Martí et al., 2011).

part of the European rift system (Fig. 4). The age of its volcanism has not yet been fully defined. Available data indicate that volcanic activity started over 12 Ma ago and continued up to the beginning of the Holocene. Despite being significant in both extension and volume, this volcanism – whose eruptions continued up to the Holocene – is poorly known in comparison to the contemporaneous alkaline volcanism in other parts of western and central Europe. Volcanism in the CVZ lies predominantly in a NW–SE direction corresponding to the graben system present in the area. Various vents in the area can be aligned in the same NW–SE direction in parallel to the local fault systems. The volcanism younger than 0.5 Ma is mostly concentrated in an area of about 100 km² located between the cities of Olot and Girona. This basaltic volcanic field exhibits scoria cones, lava flows, tuff rings, and maars. Magmatic eruptions range from Hawaiian to violent Strombolian. Phreatomagmatism is also common and has contributed to the construction of more than half of the region's volcanic edifices. It is frequently associated with Strombolian activity but has also acted independently, thereby giving rise to a large variety of different types of eruptive sequences (Martí et al., 2011).

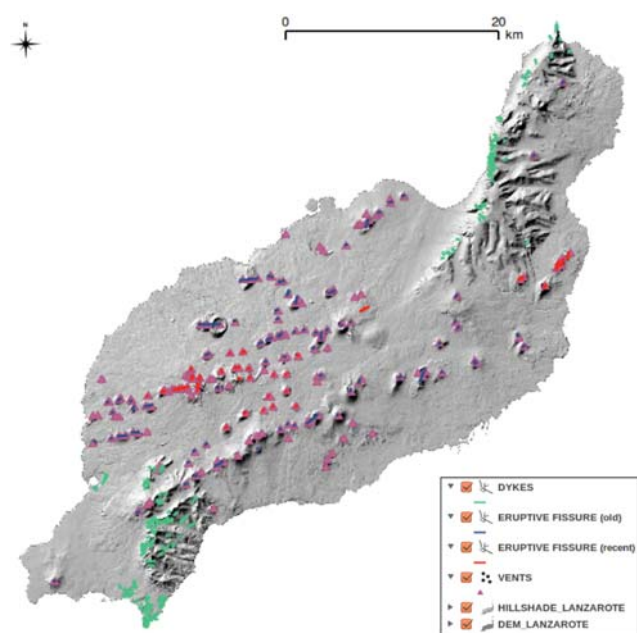


Fig. 5. Main volcano structural data (dykes, vent alignments and emission centers) used to build the susceptibility map of Lanzarote. The topographic base is 25 m resolution DEM.

5.3 Data sets and bandwidth estimation

DEMs created by the Instituto Geográfico Nacional (IGN) for Lanzarote and by the Institut Cartogràfic de Catalunya (ICC) for La Garrotxa with a cell size of 25×25 m were used in these analyses. Volcano structural data were retrieved by the Instituto Geológico y Minero de España (IGME, 1988) for Lanzarote and by the Institut Geològic de Catalunya (IGC, 2007) for la Garrotxa.

Volcanic susceptibility was estimated by studying separately all structural data in order to identify different data sets that could be used for the probabilistic analysis. Using the available literature and geological maps, we were able to identify vent locations, vent alignments, and dykes.

5.3.1 Application to Lanzarote

Volcanic structures on Lanzarote are shown in Fig. 5. Specifically, we considered 256 dykes and two layers of vent alignments containing 75 older vent alignments and 30 more recent vent alignments, formed during the Holocene. Since both dykes and vent alignments can be represented as poly-line shapefiles, QVAST used the LSCV method to calculate the optimal values for the bandwidth, which were found to be the following:

- 351 m for dykes,
- 3000 m for the oldest vent alignments,
- 2304 m for the most recent vent alignments.

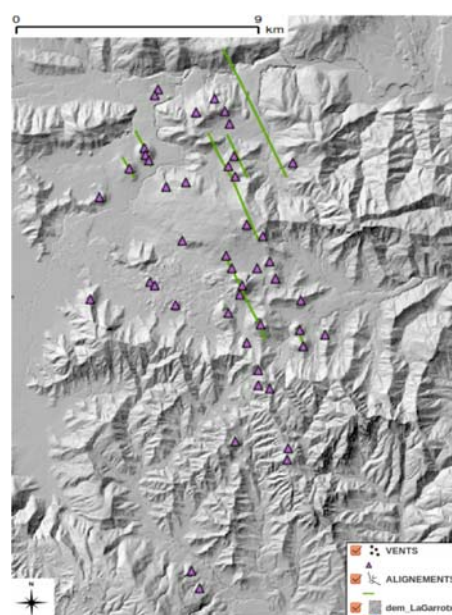


Fig. 6. Main volcano structural data (dykes, vent alignments and emission centers) used to build the susceptibility map of La Garrotxa. The topographic base is 25 m resolution DEM.

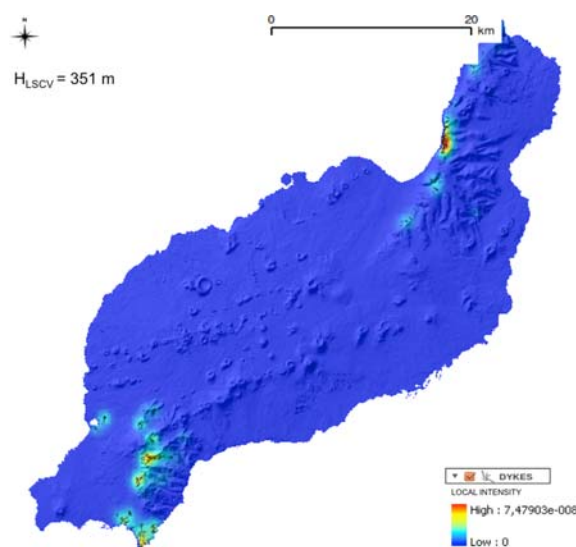


Fig. 7. PDF of Lanzarote dykes calculated with the Gaussian kernel using a bandwidth of 351 m.

As well, we identified a total of 187 emission centers (Quaternary pyroclastic cones and eruptive vents), most of which are distributed in the central part of the island in a NE–SW direction (Marinoni and Pasquaré, 1994).

The evaluation of the bandwidth for the vent locations was performed using the three methods available in QVAST and the following results were obtained: (i) 333 m with the LSCV method, (ii) 3844 m with Silverman's method, and (iii) 3934 m with the SAMSE selector.

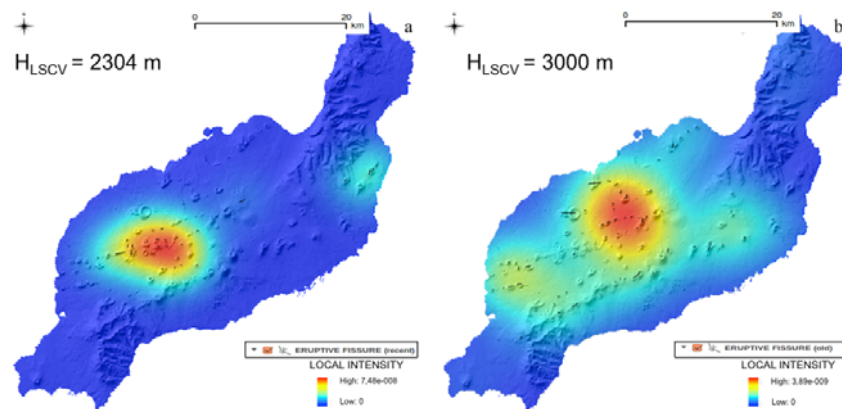


Fig. 8. PDFs calculated with the Gaussian kernel for the most recent (a) and the oldest (b) vent alignments of Lanzarote.

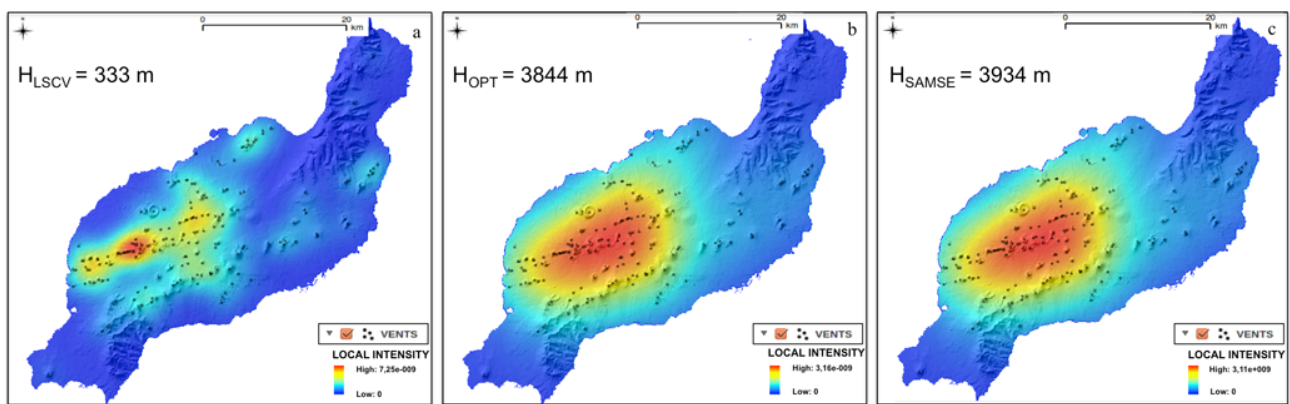


Fig. 9. PDFs of Lanzarote emission centers calculated with the Gaussian kernel using different bandwidths: 333 m as computed by the LSCV method (a), 3844 m as by the h_{opt} score (b), and 3934 m as by the SAMSE selector (c).

The PDFs for each layer evaluated using the Gaussian kernel and a 500 m spaced grid are shown for dykes in Fig. 7, for vent alignments in Fig. 8, and for emission centers in Fig. 9.

Given that the PDF generated using the bandwidth obtained with the LSCV seems to provide the best reflection of the current clustering of the emission centers observed, we decided to use this method for the final susceptibility map.

5.3.2 Application to La Garrotxa

Volcanic structures in La Garrotxa are shown in Fig. 6. Specifically, we considered vent alignments and emission centers.

Given that the vent alignments can be represented as polyline shapefiles, QVAST used the LSCV method to calculate the optimal value for the bandwidth, which was found to be 4012 m.

In addition, we identified a total of 45 emission centers aligned in a NW–SE direction, parallel to the fault systems (Martí et al., 2011).

As on Lanzarote, the evaluation of the bandwidth for the vent locations was performed using the three methods available in QVAST, which gave the following results: (i) 2002 m with the LSCV method, (ii) 1774 m with Silverman's method, and (iii) 1567 m with the SAMSE selector.

The PDFs for each layer evaluated using the Gaussian kernel and a 500 m spaced grid are shown for vent alignments in Fig. 10 and for emission centers in Fig. 11.

The PDFs obtained for the vent locations using different bandwidth values generate similar local intensity results. Taking into account isolated vents, we decided to use Silverman's method for the final susceptibility map since it seems to provide the best reflection of the degree of clustering currently observed.

5.4 Susceptibility map

The spatial probability of future vent openings is obtained by applying an NHPP to each potential vent (x, y) as follows:

$$\text{susc}(x, y) = 1 - \exp(-\Lambda(x, y)\Delta x \Delta y), \quad (8)$$

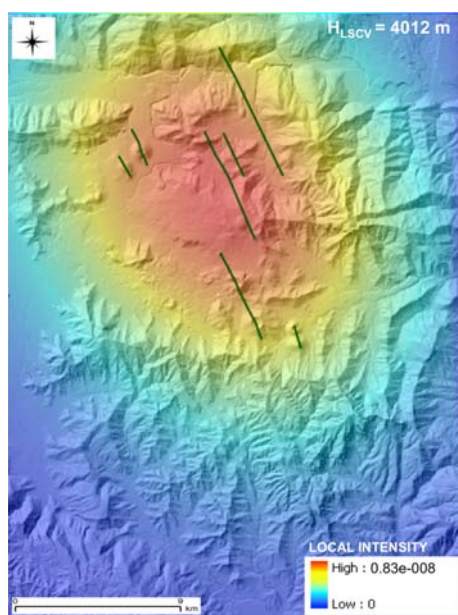


Fig. 10. PDFs calculated with the Gaussian kernel for the vent alignments of La Garrotxa.

where $\Delta x \Delta y$ is the size of the grid cell ($500 \text{ m} \times 500 \text{ m}$) and $\Lambda(x, y)$ is the weighted sum of the four PDFs and their relative weights.

QVAST provides two opportunities for assigning the weights that reflect the importance and reliability of each input data set. In the first, the user does not assign any specific individual weight and so QVAST defines the same constant value for all PDFs in the computation of the final probability map. In the second case, weights are assigned using expert judgment on the basis of structural criteria (Aspinall, 2006; Neri et al., 2008; Martí and Felpeto, 2010), which provides initial indicative probability distributions to be associated with each PDF.

In this case study, we demonstrated the flexibility of QVAST by generating two different susceptibility maps.

In the first map, the same weight (i.e., 0.25) was assigned to each PDF under the assumption that the probability of all future vent openings is influenced equally by all volcano structural data.

In the second case, we assigned to each of the PDFs the following weights for Lanzarote:

- 0.05 for dykes,
- 0.15 for the oldest vent alignments,
- 0.3 for the most recent vent alignments,
- 0.5 for the emission centers;

and for La Garrotxa, the following weights:

- 0.3 for the vent alignments,
- 0.7 for the emission centers.

On Lanzarote, the highest weight (50%) was assigned to the emission centers in the center of the island, where eruptions occurred in historical times. This means that new eruptions are given the greatest likelihood of occurring close to the most recent eruptions. Decreasing importance was awarded to the most recent vent alignments, the oldest vent alignments and dykes. Obviously, the total sum of weights is equal to 1. In La Garrotxa, the highest weight (70%) was assigned to the emission centers.

The two final susceptibility maps for Lanzarote are shown in Fig. 12 and for La Garrotxa in Fig. 13.

As it is obvious, on Lanzarote the susceptibility obtained using the same weight for all PDFs (Fig. 12a) provides a very homogeneous probability distribution, with the highest values corresponding to exposed dykes. This is disputable, since these dykes are volcanic structures that are clustered as a wide swarm chiefly at the headwalls of the main landslide and have probably been buried by recent volcanic products in other areas. Hence it is not clear whether they have acted as feeders or not (Becerril et al., 2013).

Conversely, the susceptibility map obtained using different weights (Fig. 12b) would appear to be more accurate and reliable, and reflects coherently the recent distribution of alignments located in the central part of the island in a NE–SW direction.

If we change the assigned weights, results differ for Lanzarote but not for La Garrotxa. In fact, in this latter volcanic field, the susceptibility maps obtained using the same (Fig. 13a) and different weights (Fig. 13b) for the PDFs are both coherent. The choice of the final technique for constructing hazard maps depends on the reliability of the method used to assign the weights.

6 Conclusions

The elaboration of a susceptibility map based on the quantification of objective geological and geophysical data is the first and most important step in the quantitative assessment of volcanic hazard and risk. Here we have presented QVAST, the new tool for calculating volcanic susceptibility that works under QGIS, a free and user-friendly GIS environment.

QVAST is built to evaluate volcanic susceptibility, that is, the spatial probability of the appearance of a future vent opening, based on the activity of the volcanic area under study. The main steps involved are as follows: (i) calculation of the bandwidth using different methods, (ii) evaluation of the PDF using a Gaussian kernel, (iii) assignment of the weights to each PDF, and (iv) evaluation of the susceptibility map using an NHPP.

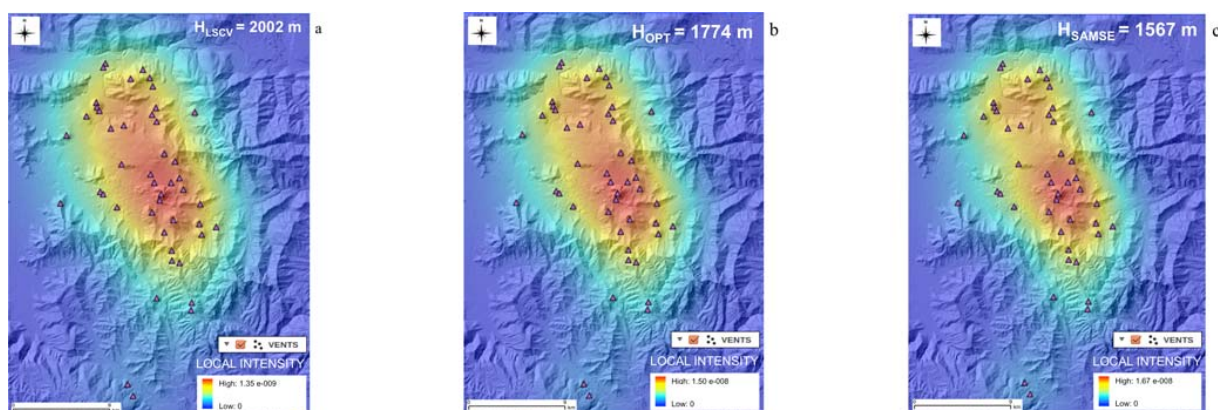


Fig. 11. PDFs of La Garrotxa emission centers calculated with the Gaussian kernel using different bandwidths: 2002 m as computed by the LSCV method (a), 1774 m as by the h_{opt} score (b), and 1567 m as by the SAMSE selector (c).

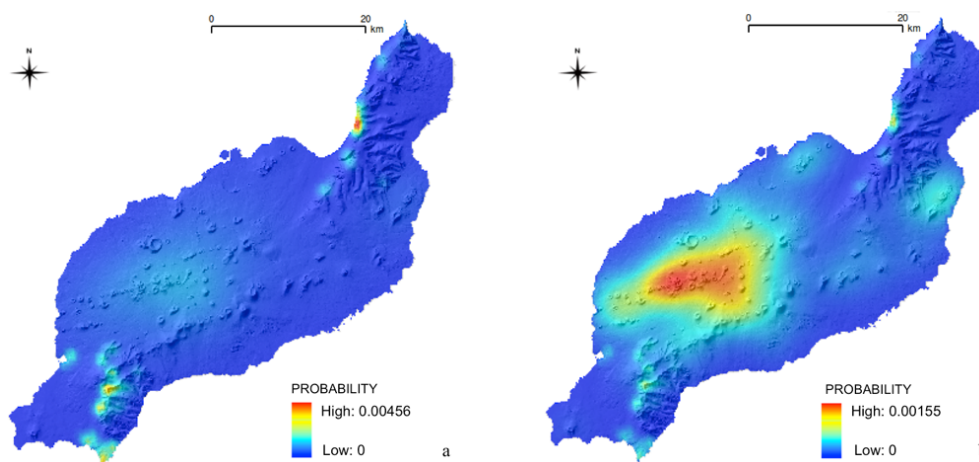


Fig. 12. Lanzarote susceptibility maps calculated assigning the same weights to all PDFs (a) and variable weights, i.e., 0.05 for dykes, 0.15 for the oldest vent alignments, 0.3 for the most recent vent alignments and 0.5 for the emission centers (b).

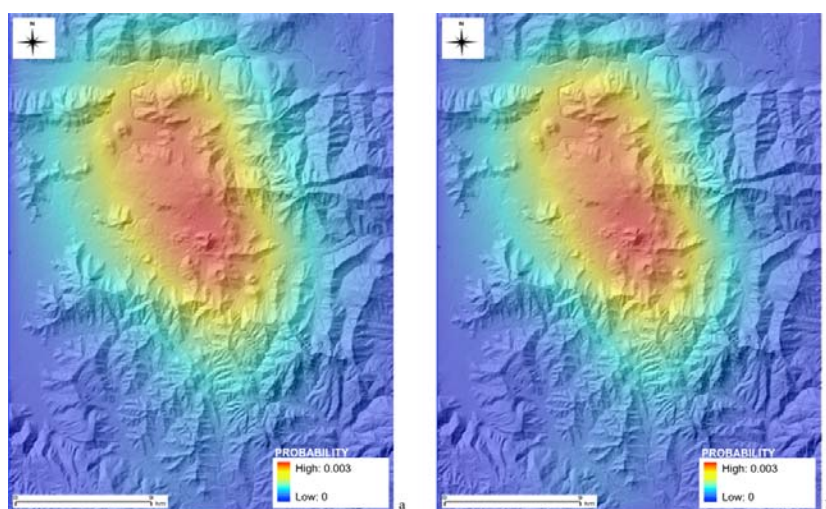


Fig. 13. La Garrotxa susceptibility maps calculated assigning the same weights to all PDFs (a) and variable weights, i.e., 0.03 for alignments and 0.7 for the emission centers (b).

The comparison of different volcanic fields shows the importance of choosing the optimal bandwidth parameters. The strength of QVAST lies in the possibility of selecting various methods for evaluating the bandwidth parameter and for obtaining the final susceptibility map. The volcanic fields of Lanzarote and La Garrotxa are excellent case studies for learning how to use this interface and for comparing the different results generated using different bandwidths for the kernel; this thus allows an optimal bandwidth for the volcanic field to be chosen.

QVAST is part of a larger project consisting of several modules (implemented in QGIS) that will interact and will analyze the current situation of volcano fields as part of the task of generating hazard maps.

In the cases of Lanzarote and La Garrotxa, although data availability is somewhat restricted, the preliminary results obtained are good enough to be used as a starting point for generating eruptive scenarios that can aid local territorial planning and risk-mitigation programs. Thus, we propose that this tool should be used as a common way for determining the susceptibility of future volcanic eruptions in active regions and as a necessary tool in the reduction of volcanic risks.

Future work will include the spatiotemporal analysis of future vent openings and the construction of volcanic hazard maps, all of which will be of great help to the governmental bodies in charge of territorial planning and the development of mitigation plans.

Acknowledgements. This work was supported by the European Commission (FP7 Theme: ENV.2011.1.3.3-1; grant 282759: VUELCO) and developed in the frame of TecnoLab, the Laboratory for the Technological Advance in Volcano Geophysics organized by INGV-CT and UNICT. The authors thank Rosa Sobradelo, Erika Ronchin, and Elisabeth Riera Pedra for improving the paper. The English text was corrected by Michael Lockwood. We thank Olivier Jaquet and an anonymous reviewer for the supportive comments that helped to improve the manuscript, and the Editor Antonio Costa for his efficient handling.

Edited by: A. Costa

Reviewed by: O. Jaquet and one anonymous referee

References

- Aspinall, W. P.: Structured elicitation of expert judgment for probabilistic hazard and risk assessment in volcanic eruptions, in: *Statistics in Volcanology*, edited by: Mader, H. M., Coles, S. G., Connor, C. B., and Connor, L. J., Geological Society of London, Special Publication of IAVCEI, 1, 15–30, 2006.
- Banda, E., Dafiobeitia, J. J., Surifiach, E., and Ansoorge, J.: Features of crustal structure under the Canary Islands, *Earth Planet. Sci. Lett.*, 55, 11–24, 1981.
- Becerril, L., Cappello, A., Galindo, I., Neri, M., and Del Negro, C.: Spatial probability distribution of future volcanic eruptions at El Hierro Island (Canary Islands, Spain), *J. Volcanol. Geoth. Res.*, 257, 21–30, doi:10.1016/j.jvolgeores.2013.03.005, 2013.
- Blanco-Montenegro, I., Montesinos, F. G., García, A., Vieira, R., and Villalaín, J. J.: Paleomagnetic determinations on Lanzarote from magnetic and gravity anomalies: Implications for the early history of the Canary Islands, *J. Geophys. Res. Solid Earth*, 110, 1–12, doi:10.1029/2005JB003668, 2005.
- Bowman, A. W.: An alternative Method of Cross Validation for the Smoothing of Density Estimates, *Biometrika*, 71, 353–360, 1984.
- Camacho, A. G., Vieira, R., and Toro, C.: Microgravimetric model of the Las Cañadas caldera (Tenerife), *J. Volcanol. Geother. Res.*, 47, 75–80, 1991.
- Cappello, A., Vicari, A., and Del Negro, C.: Assessment and modeling of lava flow hazard on Etna volcano, *Boll. Geofis. Teor. Appl.*, 52, 299–308, doi:10.4430/bgta0003, 2011a.
- Cappello, A., Vicari, A., and Del Negro, C.: Retrospective validation of a lava flow hazard map for Mount Etna volcano, *Ann. Geophys.*, 54, 634–640, doi:10.4401/ag-5345, 2011b.
- Cappello, A., Neri, M., Acocella, V., Gallo, G., Vicari, A., and Del Negro, C.: Spatial vent opening probability map of Etna volcano (Sicily, Italy), *Bull. Volcanol.*, 74, 2083–2094, doi:10.1007/s00445-012-0647-4, 2012.
- Cappello, A., Bilotta, G., Neri, M., and Del Negro, C.: Probabilistic modeling of future volcanic eruptions at Mount Etna, *J. Geophys. Res. Solid Earth*, 118, 1–11, doi:10.1002/jgrb.50190, 2013.
- Carracedo, J. C., Rodríguez Badiola, E., and Soler, V.: The 1730–1736 eruption of Lanzarote, Canary Islands: a long, high-magnitude basaltic fissure eruption, *J. Volcanol. Geotherm. Res.*, 53, 239–250, 1992.
- Chen, D., Shams, S., Carmona-Moreno, C., and Leone, A.: Assessment of open source gis software for water resources management in developing countries, *J. Hydro-environ. Res.*, 4, 253–264, 2010.
- Coello, J., Cantagrel, J. M., Hernán, F., Fúster, J. M., Ibarrola, E., Ancochea, E., Casquet, C., Jamond, C., Díaz de Terán, J. R., and Cendrero, A.: Evolution of the eastern volcanic ridge of the Canary Islands based on new K-Ar data, *J. Volcanol. Geotherm. Res.*, 53, 251–274, 1992.
- Connor, C. B. and Hill, B. E.: Three nonhomogenous Poisson models for the probability of basaltic volcanism: application to the Yucca Mountain region, Nevada, *J. Geophys. Res.*, 100, 10107–10125, 1995.
- Connor, L. J., Connor, C. B., Meliksetian, K., and Savov, I.: Probabilistic approach to modeling lava flow inundation: a lava flow hazard assessment for a nuclear facility in Armenia, *J. Appl. Volcanol.*, 1, 1–19, doi:10.1186/2191-5040-1-3, 2012.
- Diggle, P. J.: A kernel method for smoothing point process data, *Applied Statistics*, *J. R. Stat. Soc. Ser. C*, 34, 138–147, 1985.
- Duong, T.: ks: Kernel Density Estimation and Kernel Discriminant Analysis for Multivariate Data in R, *J. Stat. Soft.*, 21, 1–16, 2007.
- Duong, T. and Hazelton, M.: Plug-in bandwidth matrices for bivariate kernel density estimation, *J. Nonparametr. Stat.*, 15, 17–30, 2003.
- Favalli, M., Tarquini, S., Papale, P., Fornaciai, A., and Boschi, E.: Lava flow hazard and risk at Mt. Cameroon volcano, *Bull. Volcanol.*, 74, 423–439, doi:10.1007/s00445-011-0540-6, 2011.

- Felpeto, A., Araña, V., Ortiz, R., Astiz, M., and García, A.: Assessment and modelling of lava flow hazard on Lanzarote (Canary Islands), *Nat. Hazards*, 23, 247–257, 2001.
- Felpeto, A., Martí, J., and Ortiz, R.: Automatic GIS-based system for volcanic hazard assessment, *J. Volcanol. Geotherm. Res.*, 166, 106–116, 2007.
- Gudmundsson, A.: Magma-chamber geometry, fluid transport, local stresses and rock behavior during collapse caldera formation, in: *Caldera Volcanism*, edited by: Gottsmann, J. and Martí, J., *Developments in Volcanology*, 10, Elsevier, Amsterdam, 313–349, 2008.
- Gudmundsson, A.: Strengths and strain energies of volcanic edifices: implications for eruptions, collapse calderas, and landslides, *Nat. Hazards Earth Syst. Sci.*, 12, 2241–2258, doi:10.5194/nhess-12-2241-2012, 2012.
- Härdle, W., Müller, M., Sperlich, S., and Werwatz, A.: *Nonparametric and Semiparametric Models, An Introduction*, Springer Series in Statistics, Springer, Berlin, 2004.
- Hornik, K.: The R FAQ, available at: <http://CRAN.R-project.org/doc/FAQ/R-FAQ.html>, ISBN 3-900051-08-9, 2009.
- Jaquet, O., Connor, C. B., and Connor, L.: *Probabilistic Methodology for Long Term Assessment of Volcanic Hazards*, IHLRMW, Las Vegas, USA, 2008.
- Kiyosugi, K., Connor, C. B., Zhao, D., Connor, L. J., and Tanaka, K.: Relationships between temporal-spatial distribution of monogenetic volcanoes, crustal structure, and mantle velocity anomalies: An example from the Abu monogenetic volcano group, southwest Japan, *Bull. Volcanol.*, 72, 331–340, doi:10.1007/s00445-009-0316-4, 2010.
- Lutz, T. M. and Gutmann, J. T.: An improved method for determining and characterizing alignments of point-like features and its implications for the Pinacate volcanic field, Sonoran, Mexico, *J. Geophys. Res.*, 100, 17659–17670, 1995.
- Marinoni, L. B., and Pasquaré, G.: Tectonic evolution of the emergent part of a volcanic ocean island: Lanzarote, Canary Islands, *Tectonophysics*, 239, 111–135, 1994.
- Martí, J. and Felpeto, A.: Methodology for the computation of volcanic susceptibility: Application to Tenerife Island (Canary Islands), *J. Volcanol. Geother. Res.*, 195, 69–77, 2010.
- Martí, J., Planagumà, L., Geyer, A., Canal, E., and Pedrazzi, D.: Complex interaction between Strombolian and phreatomagmatic eruptions in the Quaternary monogenetic volcanism of the Catalan Volcanic Zone (NE of Spain), *J. Volcanol. Geotherm. Res.*, 201, 178–193, doi:10.1016/j.jvolgeores.2010.12.009, 2011.
- Martí, J., Castro, A., Rodríguez, C., Costa, F., Carrasquilla, S., Pedreira, R., and Bolos, X.: Correlation of Magma Evolution and Geophysical Monitoring during the 2011–2012 El Hierro (Canary Islands) Submarine Eruption, *J. Petrology*, 54, 1349–1373, doi:10.1093/petrology/egt014, 2013.
- Martin, A. J., Umeda, K., Connor, C. B., Weller, J. N., Zhao, D., and Takahashi, M.: Modeling long-term volcanic hazards through Bayesian inference: an example from the Tohoku volcanic arc Japan, *J. Geophys. Res.*, 109, B10208, doi:10.1029/2004JB003201, 2004.
- Neri, A., Aspinall, W. P., Cioni, R., Bertagnini, A., Baxter, P. J., Zuccaro, G., Andronico, D., Barsotti, S., Cole, P. D., Esposti Ongaro, T., Hincks, T. K., Macedonio, G., Papale, P., Rosi, M., Santacroce, R., and Woo, G.: Developing an Event Tree for probabilistic hazard and risk assessment at Vesuvius, *J. Volcanol. Geotherm. Res.*, 178, 397–415, doi:10.1016/j.jvolgeores.2008.05.014, 2008.
- Rudemo, M.: Empirical choice of histograms and kernel density estimators, *Scandinavian J. Stat.*, 9, 65–78, 1982.
- Scott, D. W.: On optimal and data-based histograms, *Biometrika*, 66, 605–610, 1979.
- Scott, D. W.: *Multivariate Density Estimation: Theory, Practice, and Visualization* (Wiley Series in Probability and Statistics), Wiley Interscience Publications, ISBN-13: 978-0471547709, 1992.
- Sherman, G. E.: *Desktop GIS. Mapping our Planet with Open Source Tools*, The Pragmatic Bookshelf, Raleigh, North Carolina, USA, 2008.
- Silverman, B. W.: *Density Estimation for Statistics and Data Analysis*, Chapman & Hall, London, 1986.
- Weller, J. N., Martin, A. J., Connor, C. B., Connor, L. J., and Karakhanian, A.: Modelling the spatial distribution of volcanoes: an example from Armenia, in: *Statistics in volcanology*, edited by: Mader, H. M., Coles, S. G., Connor, C. B., and Connor, L. J., *Spec. Pub. IAVCEI, Geol. Soc. London*, 77–88, 2006.
- Worton, B. J.: Using Monte Carlo simulation to evaluate kernel-based home range estimators, *J. Wild. Manag.*, 59, 794–800, 1995.

Appendix 3

HASSET:

A probability event tree tool to evaluate future volcanic scenarios using Bayesian Inference.

Presented as a plug-in for QGIS

HASSET: a probability event tree tool to evaluate future volcanic scenarios using Bayesian inference

Presented as a plug-in for QGIS

Rosa Sobradelo · Stefania Bartolini · Joan Martí

Received: 29 March 2013 / Accepted: 11 October 2013 / Published online: 6 December 2013
© The Author(s) 2013. This article is published with open access at Springerlink.com

Abstract Event tree structures constitute one of the most useful and necessary tools in modern volcanology for assessment of hazards from future volcanic scenarios (those that culminate in an eruptive event as well as those that do not). They are particularly relevant for evaluation of long- and short-term probabilities of occurrence of possible volcanic scenarios and their potential impacts on urbanized areas. In this paper, we introduce Hazard Assessment Event Tree (HASSET), a probability tool, built on an event tree structure that uses Bayesian inference to estimate the probability of occurrence of a future volcanic scenario and to evaluate the most relevant sources of uncertainty from the corresponding volcanic system. HASSET includes hazard assessment of noneruptive and nonmagmatic volcanic scenarios, that is, episodes of unrest that do not evolve into volcanic eruption but have an associated volcanic hazard (e.g., sector collapse and phreatic explosion), as well as unrest episodes triggered by external triggers rather than the magmatic system alone. Additionally, HASSET introduces the Delta method to assess precision of the probability

estimates, by reporting a 1 standard deviation variability interval around the expected value for each scenario. HASSET is presented as a free software package in the form of a plug-in for the open source geographic information system Quantum Gis (QGIS), providing a graphically supported computation of the event tree structure in an interactive and user-friendly way. We also include further in-depth explanations for each node together with an application of HASSET to Teide-Pico Viejo volcanic complex (Spain).

Keywords Volcanic hazard · Event tree · Probability estimation · Bayesian inference · QGIS

Introduction

Volcanic systems near urbanized areas require sound risk evaluation to support decision makers during the critical times of emergency management, as well as before the onset of volcanic unrest, to build preparedness plans and define land use management. Assessment of volcanic hazard from future eruptive scenarios in probabilistic ways has become a widely used technique for risk evaluation in recent years (Newhall and Hoblitt 2002; Marzocchi et al. 2004, 2006, 2008, 2010; Aspinall 2006; Neri et al. 2008; Martí et al. 2008a, 2011; Sobradelo and Martí 2010; Sobradelo et al. 2011). Volcanic hazard is the probability of any particular area being affected by a destructive volcanic event within a given period of time (Blong 2000). So, to quantify volcanic hazard, we need to estimate probabilities of occurrence of a particular eruptive scenario in time and space. Despite the limitations in the construction of an event tree usually imposed by the lack of knowledge about the past and present behavior of active volcanoes, it is clear from the

Editorial responsibility: E. S. Calder

Electronic supplementary material The online version of this article (doi:10.1007/s00445-013-0770-x) contains supplementary material, which is available to authorized users.

R. Sobradelo (✉) · S. Bartolini · J. Martí
Group of Volcanology, (SIMGEO-UB) CSIC Institute of Earth Sciences “Jaume Almera”, Lluís Sole i Sabaris s/n,
08028 Barcelona, Spain
e-mail: rsobradelo@ictja.csic.es

R. Sobradelo
Aon Benfield UCL Hazard Centre, Department of Earth Sciences, University College London,
Gower Street, London WC1E 6BT, UK

works previously cited and experiences from volcanic crises (Aspinall and Cook 1998) that construction of an event tree is extremely useful for hazard assessment.

Future probabilities of occurrence of an eruptive scenario can be analyzed for both the short term and long term. Short- and long-term forecasts of eruption are defined based on the expected time interval over which the volcanic system enters unrest and/or shows significant variations. For the purpose of our analysis, long-term volcanic hazard refers to the time window before the volcanic system goes into unrest, and short-term volcanic hazard refers to the unrest phase. Consequently, long-term forecasting is mainly based on geological, historical and geochronological data, and theoretical models, while short-term forecasting is complemented with information from continuous monitoring.

The complexity of any volcanic system and its associated eruptive processes, together with the lack of data that characterize many active volcanoes, particularly those with long intervals between events, make volcanic hazard quantification very challenging, as there is often not enough observational data to build a robust statistical model. However, it is important to find a way to summarize the uncertainty of a volcanic scenario in a structured and systematic way, so that when new evidence arrives, we can update these uncertainties in a consistent and rigorous way. This will allow paths to decisions to be documented and later tracked, rather than being based on intuition or gut feelings.

Bayesian inference is based on the principle that every state of uncertainty can be modeled with a probability distribution. It provides a numerical instrument, based on rigorous mathematical modeling, to define and interpret uncertainties. As more data arrives, the method incorporates the new evidences in order to progressively reduce uncertainty. The precision of the probability estimates for each possible eruptive scenario will depend heavily on the available data. We begin with the state of total ignorance and use noninformative priors to quantify our uncertainty before observing the data, and later update these with the arrival of new evidence from geochronological and geophysical data, to get the posterior probabilities, which provide an estimate of the uncertainty after observing the data. Due to the poor and incomplete data catalogue often used when doing eruption estimates, aleatoric (stochastic) and epistemic (data or knowledge limited) uncertainties are significant, and we need to find a way to correctly evaluate them.

The aleatoric (stochastic) uncertainty is a consequence of the intrinsic complexity of a system, hence a limitation to our ability to predict the evolution of the system in a deterministic way. The aleatoric uncertainty introduces a component of randomness in the outcomes, regardless of our physical knowledge of the system. The epistemic uncertainty is directly related to our knowledge of the system and

the quality and quantity of data we have about the system. The more data we have, the better we know the system and the lower the epistemic uncertainty (Woo 1999).

In this paper, we present Hazard Assessment Event Tree (HASSET), a probability tool that uses Bayesian inference in an event tree structure to assess volcanic hazard of future volcanic scenarios. It evaluates the most relevant sources of uncertainty in estimating the probability of occurrence of a future volcanic event. HASSET is presented as a free software package in the form of a plug-in for the open source geographic information system Quantum Gis (QGIS), providing a graphically supported computation of the event tree structure in an interactive and user-friendly way. It is built on the Bayesian event tree model proposed by Sobradelo and Martí (2010) and expanded further to include two additional and important nodes to account for the type and extension of the hazard phenomena. Additionally, HASSET introduces the Delta method to approximate the precision in the probability estimates, by constructing a 1 standard deviation variability interval around the expected probability value for each scenario.

It is important to mention that some parts of our tool overlap with the BET_EF and BET_VH tools presented by Marzocchi et al. (2008, 2010). These tools use Bayesian theory in an event tree structure. HASSET is built on QGIS platform, taking advantage of additional features of this geographic information system, and BET_EF and BET_VH are presented in the form of an independent software. The main differences are that HASSET evaluates the hazard associated with magmatic and nonmagmatic unrest episodes, by accounting for unrest induced by external triggers (geothermal, seismic), as opposed to internal triggers alone (magmatic) (this will be further described in the next section). HASSET evaluates the hazard associated with eruptive and noneruptive volcanic scenarios (e.g., phreatic explosion and sector failure) and looks at the hazard for different types of magma composition and different vent locations, together with the geological hazard and its extent. This allows for identification of important eruptive scenarios which otherwise would go unnoticed. In this respect, HASSET overcomes the limitations of previous event tree models by allowing a larger set of future volcanic scenarios in their probability estimation, and thus extending their use to a wider range of volcanic systems, accounting for aleatoric and epistemic uncertainties, and reducing the additional bias that the human decision component adds to the use of alternative techniques for estimating event tree probabilities (Aspinall 2006; Loughlin et al. 2002). In this paper, we will focus on the long-term volcanic hazard assessment of the system, so we will base our analysis on the past behavior of the volcano.

HASSET: Hazard Assessment Event Tree

An event tree is a tree graph representation of events in the form of nodes and branches and it was first introduced to volcanology by Newhall and Hoblitt (2002) as a tool for volcanic hazard assessment. Each node represents a step and contains a set of possible branches (outcomes for that particular category). The nodes are alternative steps from a general prior event, state, or condition through increasingly specific subsequent events to final outcomes. The objective is to outline all relevant possible outcomes of volcanic unrest, at progressively higher degrees of detail, and assess the probability of each hazard scenario occurring within a specified future time interval. HASSET uses this event tree structure (Fig. 1a) to make these estimations based on a statistical methodology, further described below, called Bayesian inference (Rice 2007) (Fig. 1b, c). All nodes are independent and the corresponding branches are mutually

exclusive and exhaustive. That is, they cannot happen simultaneously and they sum up to 1. These are initial conditions set for simplicity and practical application of the Bayesian inference methodology. In general, an event tree can have any form or shape and the nodes need not be independent or mutually exclusive, in which case a different mathematical approach is needed. Future work is needed to address this issue and eliminate the dependency and mutually exclusive restrictions to make a free form event tree structure. However, it remains to be proven whether the presumed accuracy increase in the probability estimates would justify the additional complexity that dependency and nonmutually exclusive assumptions would introduce in the model settings and calculations.

HASSET accounts for the possibility of flank vent eruptions (as opposed to only central), making it also useful for monogenetic volcanism. A novelty of HASSET is that it accounts for nonmagmatic unrest (geothermal or seismic), as opposed to only magmatic, and for noneruptive scenarios

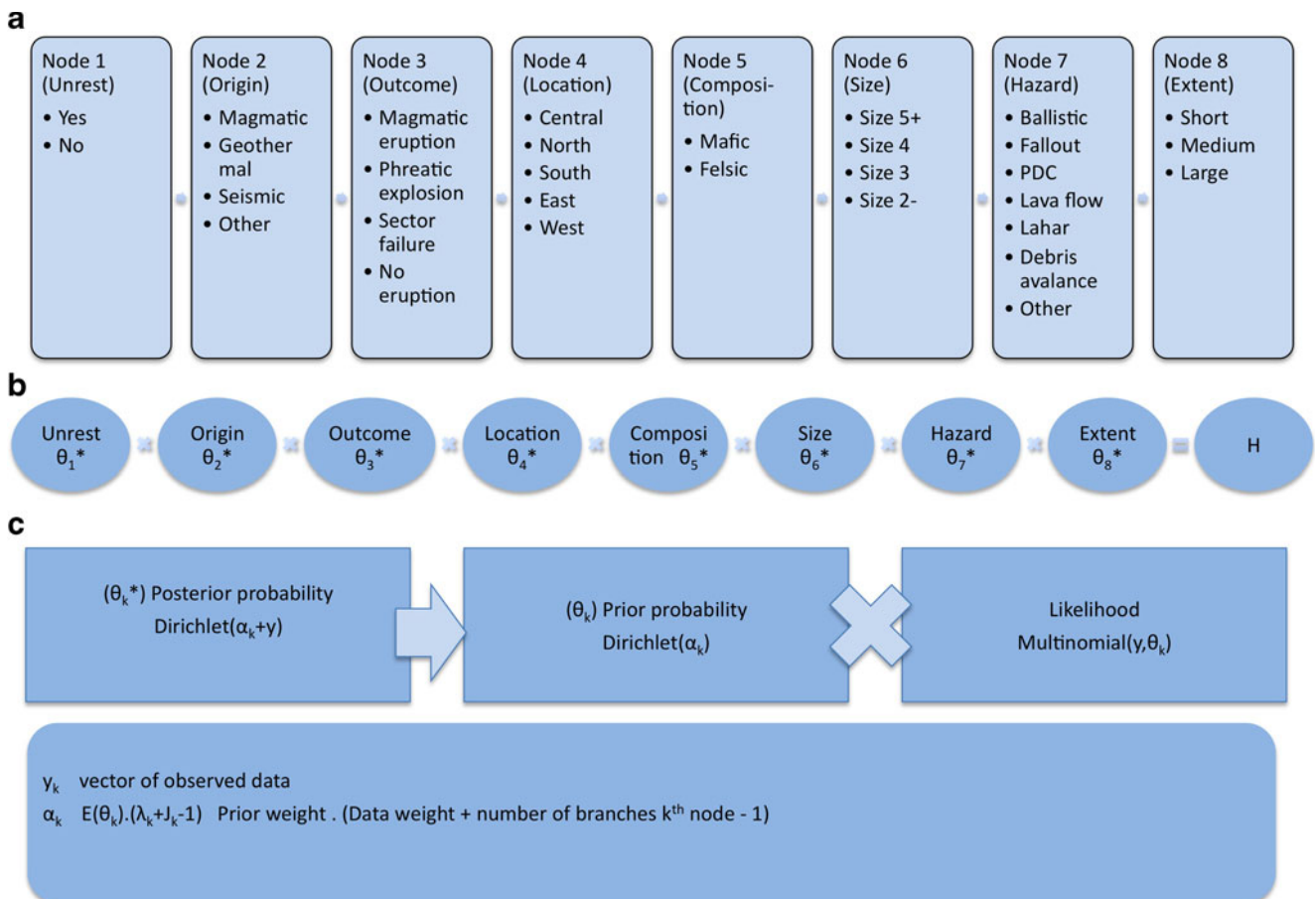


Fig. 1 HASSET event tree structure (a) formed by eight nodes and corresponding mutually exclusive and exhaustive branches to account for all possible scenarios likely to occur in a volcanic system. By the condition of independence of the nodes, the probability of a

particular eruptive scenario, as a combination of branches across nodes, is the product of the individual probabilities of occurrence of each branch in that scenario (b). These probabilities are calculated using a Bayesian inference approach (c). (See text for further details)

(phreatic explosions or sector failure), as opposed to volcanic eruptions only. Also, it accounts for felsic or mafic composition, and their associated volcanic hazards as possible outputs of an eruption, together with the extent reached by each hazard.

Event tree structure

Each possible volcanic scenario is a combination of one branch per node evolving from a more general node of unrest (yes or no) to the more specific node of the extent of the hazard. Below is a detailed explanation of each node and corresponding branches (see Sobradelo and Martí (2010) for further details on the event tree methodology). It is possible to stop at a particular node if we want to evaluate the hazard at a more general level. Each possible volcanic scenario is made up from the following nodes:

Node 1, Unrest: Yes or No. Given that we have the capacity to differentiate the origin of the precursory signals, we define unrest in a particular time window τ as any modification of the background activity of the volcano or volcanic area recorded by the monitoring network, and which may or may not be followed by an eruption of any kind.

Node 2, Origin: We define four possible sources of unrest, which comprises events (above background) recorded by the network, that are likely to happen, magmatic, geothermal, seismic, and other. Assuming we can define the precursors that identify the source of the unrest, it is crucial in a complex volcanic system to differentiate between unrest caused by internal triggers or caused by external triggers, which ultimately may condition the outcome and further development of the system. Every eruption type, including a phreatic episode, requires the presence of fresh magma at shallow depths in the volcanoes. However, we do not discard the possibility of starting an eruption process from an unrest directly associated with the hydrothermal system or even due to external triggers, such as regional tectonics, if eruptible magma is already present in the system. It is also important to mention that the interior of a volcanic system may react to changes in the regional stress field or regional tectonics, so a seismic trigger for unrest cannot be ruled out.

Node 3, Outcome: We consider here the outcome of the unrest being of four different types, magmatic eruption, sector failure, phreatic explosion (triggered by unrest of any type, where no magma is expelled in the eruption), no eruption (there is unrest but no further outcome develops). It is important to address the hazard associated with noneruptive scenarios in the event of unrest. That

is, the hazard could arise in response to internal or external triggers that do not evolve into a magmatic eruption but rather originate a sector failure or a phreatic episode. These volcanic scenarios should not be left out when assessing volcanic hazard, especially for a volcano with a hydrothermal system or a shallow aquifer.

Magmatic eruptions can be preceded directly by magmatic unrest, which may or may not itself be preceded by sector failure. A magmatic eruption can also be triggered indirectly by geothermal or seismic unrest, in which case, externally driven decompression of the shallow volcanic system would be required. This could be achieved by sector failure or tectonic fracture opening. When the unrest is geothermal or seismic, for a magmatic eruption to occur, an initial sector collapse or fracture opening is needed to decompress the whole system. In discussing a magmatic eruption which was originated by geothermal or seismic unrest, we assume that a sector failure or a tectonically induced fracture opening has previously occurred.

Sector failure alone, triggered by magmatic, geothermal, or seismic unrest, corresponds with the sector collapse itself, not being followed by an eruption. A sector failure followed by a magmatic eruption is considered in the previous branch (magmatic eruption), caused indirectly by a magmatic unrest triggering a sector collapse (see Sobradelo and Martí (2010)).

Node 4, Location: We segment possible locations for an imminent eruption into five different areas, which can be customized and named accordingly. By default, we have named them as *central*, *north*, *south*, *east*, and *west*, and the coverage area for each location would vary for each volcanic system according to topography, surroundings, and/or important topographic barriers which may impose a different level of hazard and risk depending on what side of the volcano the eruption occurs.

Node 5, Composition: Mafic or felsic. The magma composition will determine two main types of eruptions associated with different hazard implications, as felsic magmas are generally associated with more violent eruptions than mafic magmas. The importance in distinguishing these two outcomes for node 5 is the different level of hazard associated with each one (Martí et al. 2008b). For simplicity in the model, we will assume the two branches are exclusive, and thus a branch for mixed composition is left out. We are aware some compositions can be a mix of both mafic and felsic magmas, but for the purpose of the hazard estimation, we will assume that a magma with felsic composition will fall in the category of *felsic*, regardless of the proportion.

Node 6, Size: This node represents the size of the eruption, assigned to one of four categories, $size \geq 5$, $size 4$, $size 3$, $size \leq 2$. The size can be expressed in terms of

either the volcanic explosive index (VEI), or simply the magnitude of the eruption, as a function of the erupted volume. Also, the four category groups can be modified to better fit a particular volcanic system. For instance, one may be interested in merging $size \leq 2$ and $size 3$ into one group $size \leq 3$ and segmenting group $size \geq 5$ into two additional categories, say $size 5$ and $size \geq 6$. Similarly, as VEI is not necessarily an integer, the branches could be defined as bins, e.g., VEI 5 could correspond to $3.5 < VEI \leq 4.5$. The only condition is that the groups are mutually exclusive and exhaustive.

Node 7, Hazard: This node and the following are a new contribution of this paper to the event tree structure from (Sobradelo and Martí 2010). Here, we list the most relevant hazardous phenomena originating from a volcanic eruption, *ballistic*, *fallout*, *PDC*, *lava flows*, *lahars*, *debris avalanche*, and include a seventh branch called *other* to account for the remaining hazards, like *direct blast*, to make the branches exhaustive (this is another difference with BET_VH (Marzocchi et al. 2010) where Node 6 phenomena is left open without an upper bound). We assume, without loss of generality, that any two hazards do not happen at exactly the same time (this is, $P(A_1 \cap A_2) = 0$, where hazard A_1 could be ballistic and hazard A_2 could be Fallout), but with a time interval in between, so that the condition of mutual exclusivity still holds, and so does the condition of exhaustivity of the branches, where $P(A_1 \cup A_2 \cup \dots \cup A_7) = P(A_1) + P(A_2) + \dots + P(A_7) = 1$, A_1, A_2, \dots, A_7 are the different branches in the node. This is a conservative assumption, as we may be overestimating the total probability of two hazard events by not subtracting the probability of the intersection (by definition $P(A_1 \cup A_2) = P(A_1) + P(A_2) - P(A_1 \cap A_2)$). With this in mind, we compute the probability of more than one hazard associated with the same eruption by adding the individual probabilities of each scenario alone. The issue of possible dependency of the branches does not affect us here as we are analyzing scenarios with primary hazards alone, as opposed to scenarios with secondary hazards. This should be assessed in future work, as during a volcanic eruption with multiple phases, the probability of a second hazard being triggered after a primary one has happened is strongly determined by the dependency of the hazards. In this case, the issues of correlation and multicollinearity of the different hazards should be addressed (Rice 2007).

Ballistic: We consider here blocks and bombs that are sent ballistically and can happen in any eruption with explosive phases, including phreatic phases (without fresh magma), dome explosions, strombolian, plinian, etc.

Fallout: Here, we include ashfall originating from pyroclasts in strombolian eruptions as fire fountains, to ash fall from an eruption column.

Pyroclastic density current (PDC): This includes the spectrum of currents from dense to dilute. Dense flows will only have a runout since they are mostly small volume confined to the valleys, but the diluted ones and large pyroclastic flows can have an important lateral extension. In some cases, as frequently occurs with dome collapse PDCs, the only measurable parameter is runout, as they are mostly confined to the valleys, but sometimes there are PDCs that have an important extension so we must consider both.

Lava flows: All types of lava flows of any composition or rheology.

Lahar: Debris flows and mudflows, related to ice melting, rain, etc.

Debris avalanche: We include here collapse of nonexplosive lava domes or sector collapses of the volcanic edifice, regardless of their origin.

Other: So far, we have included what we consider to be the six most likely hazards. There are additional phenomena that could also occur (direct blast, gas emissions, etc.), but they are not so likely to happen as to justify their own branch, so we grouped them all together. However, the branches in this node could be easily renamed if there is evidence that alternative hazards should be included instead.

Node 8, Extent: This node refers exclusively to the maximum distance and areal extent reached by a volcanic hazard regardless of the nature and potential impact it may cause. It is a measure of the expected zone that will be affected by a particular hazard but it does not estimate any degree of vulnerability. The extent has to be estimated separately for each volcano or volcanic zone by comparing the maximum and minimum extent of each volcano or volcanic area, and should not be compared among different volcanoes even when these might show similar characteristics. This is an important node for completion of a thorough hazard assessment because the area affected by a particular eruptive scenario refers to the spatial part of the definition of hazard. We consider three types of mutually exclusive and exhaustive extents, *short*, *medium*, and *large*, with respect to the eruptive vent.

Each option will fall inside an area previously defined by the user for that particular volcanic system, based on different levels of exposure. For each analysis, the area covered (and maximum distance reached) by each type of hazard will be previously defined, so that a *short*, *medium*, or *large* extent will refer, respectively, to the distance and area from the source regardless of what type of hazard reaches there.

In the case of single vents, the application is straightforward, but in volcanic systems with an option for multiple vents, we will consider the largest volcanic susceptibility values (i.e., maximum probability of vent opening) and proceed in the same way as with a single vent, assuming a larger area. Obviously, the interpretation of the results will be different if there is a large lava flow versus a large PDC, for example, and this should be reflected on the conditional probabilities computed later.

Probability estimates

We will use Bayesian inference to compute the probability of occurrence for each scenario. The fundamental principle of Bayesian statistics is that what is known about anything that is incompletely or imperfectly known can be described as a probability distribution. See Sobradelo and Martí (2010) and references within for further details

on how the Bayesian methodology is applied to the event tree. Our knowledge about a random variable θ given the observed data is expressed through its posterior distribution $p(\theta|y) \propto p(\theta) \times p(y|\theta)$. That is, the posterior distribution is proportional to the prior distribution times the likelihood. The prior distribution, $p(\theta)$, expresses our uncertainty about θ before seeing the data. The posterior distribution, $p(\theta|y)$, expresses our uncertainty about θ after seeing the data. The likelihood function allows us to use the past data (y_k) at node k to modify the a priori beliefs or prior distribution.

By the condition of independence of the nodes, the probability of a particular eruptive scenario, as a combination of branches across nodes, is the product of the individual probabilities of occurrence of each branch in that scenario (Fig. 1b). For example scenario j , the probability of having magmatic unrest that evolves into a central vent basaltic

Table 1 Volcanic data used for the Teide-Pico Viejo case study (see Sobradelo and Martí (2010) and references within for in-depth explanation of the catalogue and corresponding source)

Eruption name	Year	Node 1 Unrest	Node 2 Origin	Node 3 Outcome	Node 4 Location	Node 5 Composition	Node 6 Size	Node 7 Hazard	Node 8 Extent
Chahorra	1798	Yes	Magmatic	Eruption M	West	Mafic	VEI \leq 2	Lava flows Fallout	Short Medium
Mta Reventada	895 bp	Yes	Magmatic	Eruption M	North	Mafic	VEI \leq 2	Lava flows Fallout	Short Short
Lavas Negras	1150 bp	Yes	Magmatic	Eruption M	Central	Felsic	VEI \leq 2	Lava flows	Large
Roques Blancos	1714 bp	Yes	Magmatic	Eruption M	North	Felsic	VEI 4	Lava flows	Large
Mta Blanca	2000 bp	Yes	Magmatic	Eruption M	East	Felsic	VEI 3	Lava flows Fallout	Short Medium
PV surges	(2528-2000) bp	Yes	Magmatic	Eruption M	Central	Mafic	VEI \leq 2	PDCs Ballistic	Short Short
Hoya del Cedro	(2528-2000) bp	Yes	Magmatic	Eruption M	North	Felsic	VEI 4	Fallout	Medium
Mta Majua	(2528-2000) bp	Yes	Magmatic	Eruption M	South	Felsic	VEI \leq 2	Fallout	Short
Mta de la Cruz	(2528-2000) bp	Yes	Magmatic	Eruption M	East	Mafic	VEI \leq 2	Lava flows Fallout	Short Short
Arenas Blancas	(2528-2000) bp	Yes	Magmatic	Eruption M	East	Felsic	VEI \leq 2	Lava flows	Medium
Mta Los Conejos	(2528-2000) bp	Yes	Magmatic	Eruption M	East	Mafic	VEI \leq 2	Lava flows Fallout	Short Short
Bocas de Maria	(2528-2000) bp	Yes	Magmatic	Eruption M	East	Mafic	VEI \leq 2	Lava flows Fallout	Short Short
Mta Las Lajas	(2528-2000) bp	Yes	Magmatic	Eruption M	East	Felsic	VEI \leq 2	Lava flows Fallout	Short Short
El Boqueron	2528 bp	Yes	Magmatic	Eruption M	North	Felsic	VEI 4	Fallout	Large
Cañada Blanca	(5911-2528) bp	Yes	Magmatic	Eruption M	Central	Felsic	VEI 3	Lava flows	Medium
Abejera Baja	5911 bp	Yes	Magmatic	Eruption M	North	Felsic	VEI 4	Lava flows	Medium
Abejera Alta	5486 bp	Yes	Magmatic	Eruption M	North	Felsic	VEI 4	Lava flows	Medium
Pico Cabras	(7900-5486) bp	Yes	Magmatic	Eruption M	North	Felsic	VEI 4	Lava flows	Large

eruption of VEI 4, generating a lava flow of short runout, in the time interval $(t_0, t_0 + \tau)$ is:

$$H_j = \theta_1^*(\text{unrest}) \times \theta_2^*(\text{magmatic}) \times \theta_3^*(\text{eruption}) \times \theta_4^*(\text{central}) \times \theta_5^*(\text{basaltic}) \times \theta_6^*(\text{VEI 4}) \times \theta_7^*(\text{lavas}) \times \theta_8^*(\text{short}) \quad (1)$$

Where the posterior probability for a specific branch in node k , denoted θ_k^* for simplicity, is the expected value of a random variable that follows a Dirichlet distribution of parameters $(\alpha_k + y_k)$ (Fig. 1c). The parameter α_k is equal to $E[\theta_k](\lambda_k + J_k - 1)$, where $E[\theta_k]$ is an input to the model and corresponds to the prior weight. $E[\theta_k]$ is computed from alternative physical models and a priori beliefs, and accounts for the aleatoric uncertainty. J_k is the number of branches in node k and λ_k is the data weight, also input to the model, and controls the confidence at which $E[\theta_k]$ is

considered a reliable estimate. λ_k accounts for the epistemic uncertainty. The choice of the Dirichlet (Beta) distribution is itself rather subjective. In general, theoretical models, a priori beliefs, and/or expert elicitation provide estimations of the expected average of the prior distribution that represents the “best guess.” Further details on this choice can be found in Marzocchi et al. (2004).

How precise are the probability estimates?

The probability estimate we assign to each scenario is, as explained in the previous section, the product of the individual probabilities for each branch. This property is attributed to the condition of independence of the nodes, which allows us to write the expected value of the product as the product of the individual expected values. The expected value

Table 2 *.csv file with volcanic data formatted and ready to upload into HASSET

Node #	Node	Branch	Past events	Prior weight	Data weight
1	Unrest	Yes	18	0.5	1
1	Unrest	No	62	0.5	1
2	Origin	Magmatic	18	0.25	1
2	Origin	Geothermal	0	0.25	1
2	Origin	Seismic	0	0.25	1
2	Origin	Other	0	0.25	1
3	Outcome	Magmatic Eruption	18	0.25	1
3	Outcome	Sector Failure	0	0.25	1
3	Outcome	Phreatic Explosion	0	0.25	1
3	Outcome	No Eruption	0	0.25	1
4	Location	Central	3	0.2	1
4	Location	North	7	0.2	1
4	Location	South	1	0.2	1
4	Location	East	6	0.2	1
4	Location	West	1	0.2	1
5	Composition	Mafic	3	0.5	1
5	Composition	Felsic	15	0.5	1
6	Size	VEI ≥ 5	0	0.25	1
6	Size	VEI4	6	0.24	1
6	Size	VEI3	3	0.25	1
6	Size	VEI ≤ 2	9	0.25	1
7	Hazard	Ballistic	1	0.14	1
7	Hazard	Fallout	10	0.15	1
7	Hazard	PDC	1	0.14	1
7	Hazard	Lava flow	14	0.15	1
7	Hazard	Lahard	0	0.14	1
7	Hazard	Debris avalanche	0	0.14	1
7	Hazard	Other	0	0.14	1
8	Extent	Short	15	.4	1
8	Extent	Medium	7	.3	1
8	Extent	Large	4	.3	1

(mean) is a measure of central tendency used to describe a probability distribution (Dirichlet in this case), together with the variance (or standard deviation). Unfortunately, the same property does not apply to the variance, the measure of dispersion around the mean, used to estimate the precision. Since the variance of the product cannot be written as the product of the variance of each individual variable, we have to use alternative methods to estimate or approximate this. One way is using the Delta method (Rice 2007). Hence, to assess the precision in the probability estimate for eruptive scenario \hat{H}_j , we use the Delta method to estimate the variance $\hat{\sigma}_j^2$ and corresponding standard deviation $\hat{\sigma}_j = \sqrt{\hat{\sigma}_j^2}$.

Using the Delta method to determine the asymptotic distribution of $\hat{\sigma}_j^2$, we get:

$$\hat{\sigma}_j^2 = E(H)^2 \sum_{k=1}^m \frac{Var(\theta_{kn}^*)}{[E(\theta_{kn}^*)]^2} \quad (2)$$

Where,

$$E(\theta_{kn}^*) = \frac{\alpha_{kn} + y_{kn}}{\sum_{i=1}^{J_k} (\alpha_{ki} + y_{ki})} \quad (3)$$

and

$$Var(\theta_{kn}^*) = \frac{E[\theta_{kn}^*](1 - E[\theta_{kn}^*])}{\lambda_k + J_k} \quad (4)$$

are the expected value and variance from the posterior distribution for θ_{kn}^* in branch n and node k . See Appendix for details on how to derive Eq. 2. Hence, we have written the variance for an eruptive scenario H_j as a function of the expected value and variances of the individual random variables, θ_{kn}^* , involved in that scenario. See Sobradelo and Martí (2010) Eq. (4)–(10) for further details on how to derive Eqs. 3 and 4.

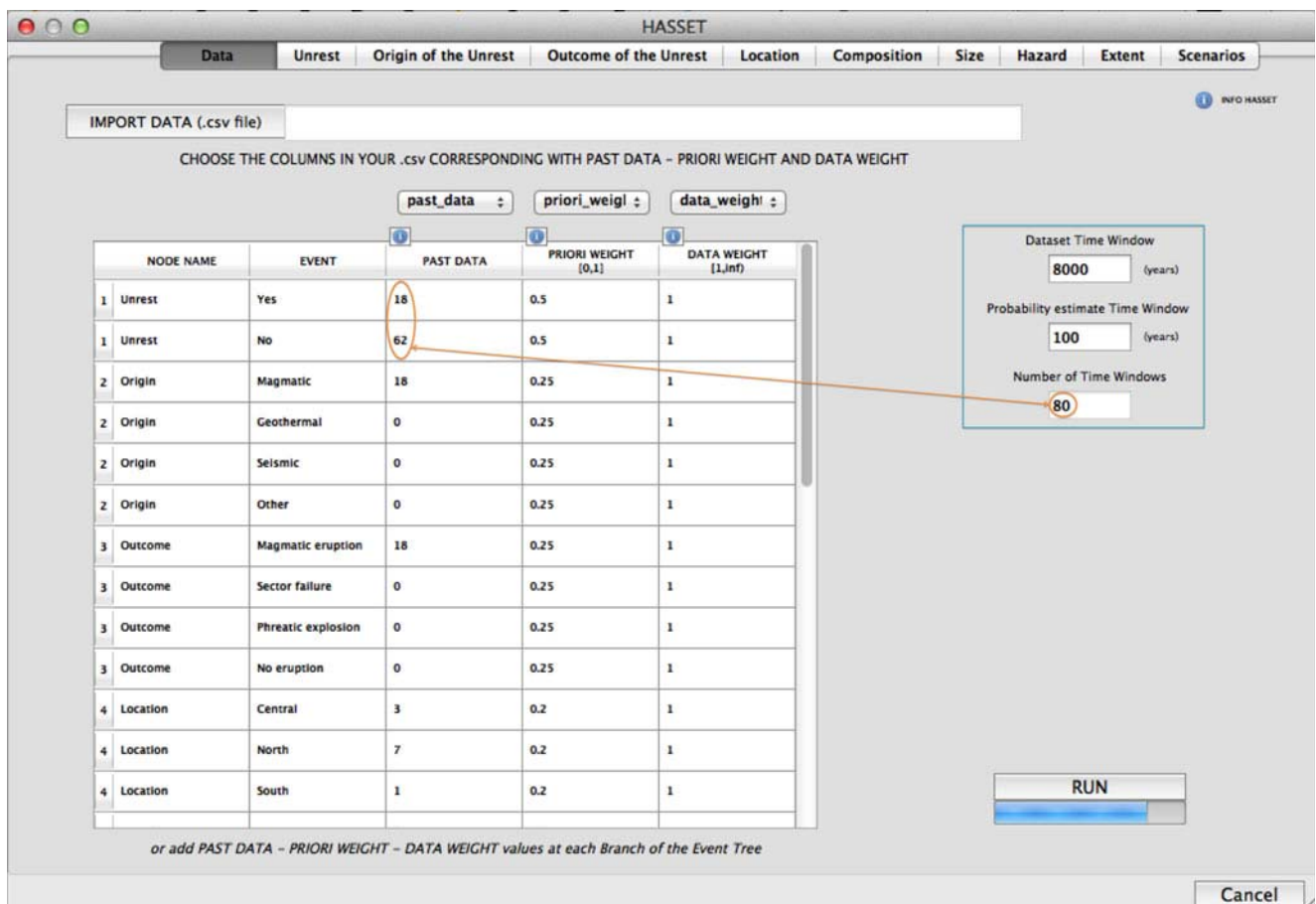


Fig. 2 This is the main window of HASSET, where the user has to define the input parameters of the model. A “Browse .csv file” button allows the user to visualize only the *.csv files in the user computer in order to import the data. The three drop-down menus allow the user to import the information for past events, prior and data weights

directly from the *.csv. The information can also be entered manually. The location names and the size bins need to be defined. The “Dataset” total time and “Probability estimate Time Windows” need to be defined. The “Number of Time Windows” has to be the same as the sum of “unrest” and “no unrest” episodes entered

HASSET software: a QGIS plug-in to perform hazard assessment using Bayesian event tree methodology

Geographic information systems (GIS) are increasingly being used in environmental management as a powerful tool to store, visualize, and model environmental processes in support of management decisions (Longley et al. 2001; Renschler 2005; Chen et al. 2010). Open source desktop GIS have been developed in different countries, with some differences in performance (Sherman 2008; Chen et al. 2010). We have decided to use the QGIS (www.qgis.org) for its functionalities and the ability to run it on Linux, Mac OSX, and Windows, as well as the open possibility of connecting HASSET with a mapping format structure. Currently, the software has been developed for Mac OS (tested on version 10.7.4 and above) and Linux (tested

on Ubuntu 10.10 and above). The version for Windows OS is under development. HASSET is available upon request to the authors or it can be downloaded online at the website of the CSIC Group of Volcanology of Barcelona (<http://www.gvb-csic.es>) on the “Software & Databases” tab.

The original R code for the Bayesian model was adapted to a Python script, and the HASSET program was developed and implemented in QGIS as an accessible and dynamic graphical user interface (GUI) plug-in, which, once properly installed following a few easy steps, creates a new option in the QGIS menu bar called “volcano,” where the HASSET model is installed. Along with HASSET, an html manual (HASSET_MANUAL) with step-by-step explanations on how to use it is also provided.

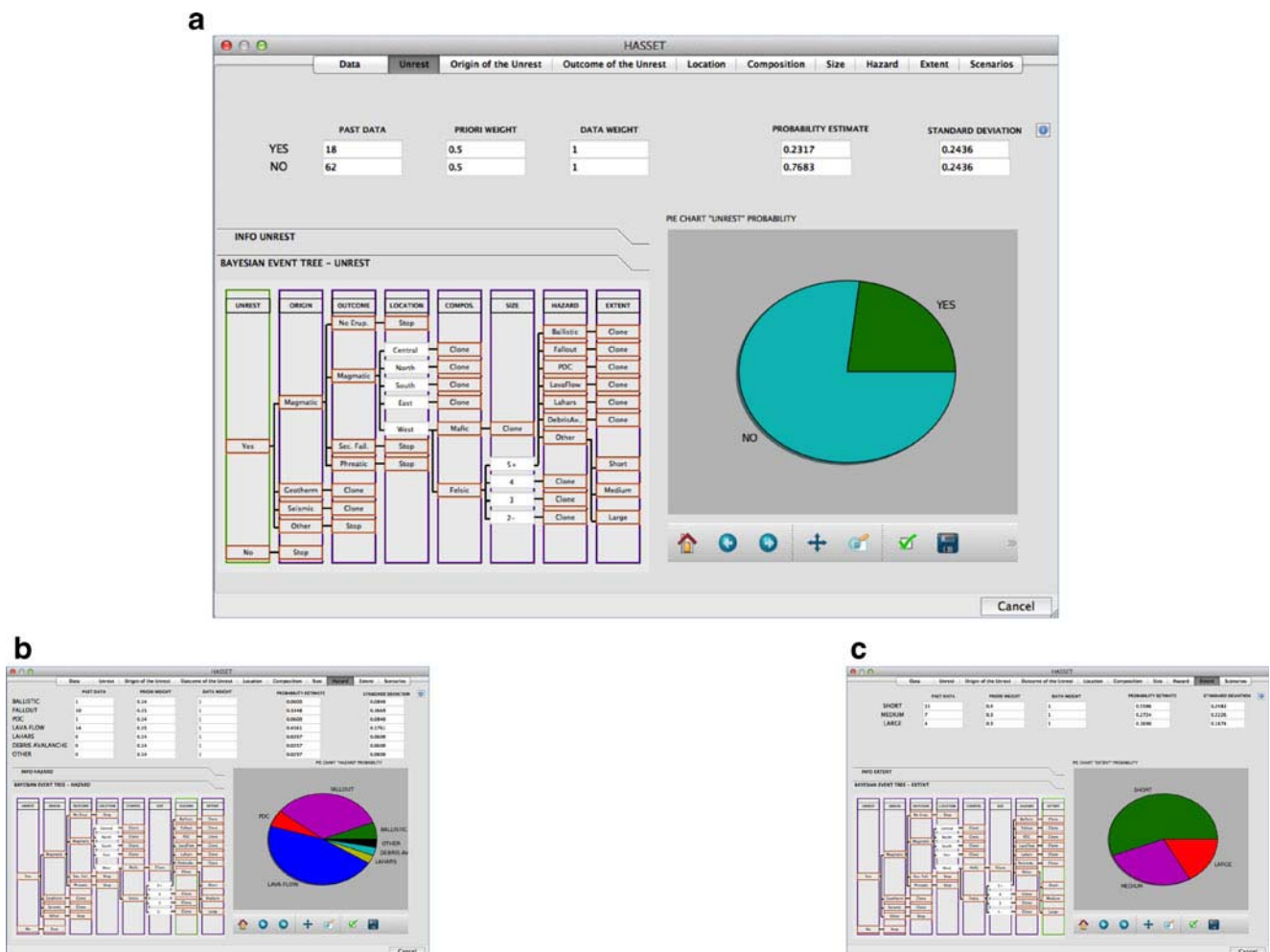


Fig. 3 The first result is represented by the probability estimated at each node and by the corresponding precision. All nodes are visualized with the individual results for each branch. In this example, we show the results for nodes **a** unrest, **b** hazard, and **c** extent. The results are

displayed as a numeric value, but also in a pie chart that can be zoomed in, saved to a file or used to show a graphical view of the probability. The node tabs contain an information button with further details and the current node is highlighted on the event tree scheme

HASSET implements the Bayesian event tree method described earlier, where the user previously defines a forecasting time interval. The user provides all volcanological data for the analysis, which HASSET then merges using the Bayesian event tree approach described above and in the Appendix. To do that, a user-friendly interface will guide the user through all the steps. The first step, and most important, is to enter all the data for the analysis. The second step is to compute the probability estimates for each branch in the event tree and corresponding variability. The third step computes the total probability estimate for different scenarios. It is important to highlight the advantages of having a simple GUI that makes it easy for the user to input the data parameters and generate results with the correct interpretations. HASSET also allows the user to edit and save the output in various formats (more details in the manual).

In the next section, we describe the tool using an example. In summary, HASSET allows the user to easily:

- Browse the csv file and select input data or enter data manually.
- Enter the dataset time window and decide the forecasting time interval.
- Identify five different locations and size values relevant to a particular volcanic system.
- Evaluate probability at each branch (RUN button).
- Calculate total probability for any particular scenario and compare up to five different scenarios.
- Sum the total probability of the scenarios selected.
- Visualize the five most likely scenarios out of all the possibilities for the selected nodes.
- Access the information in each step and locate where we are in the event tree for each node.

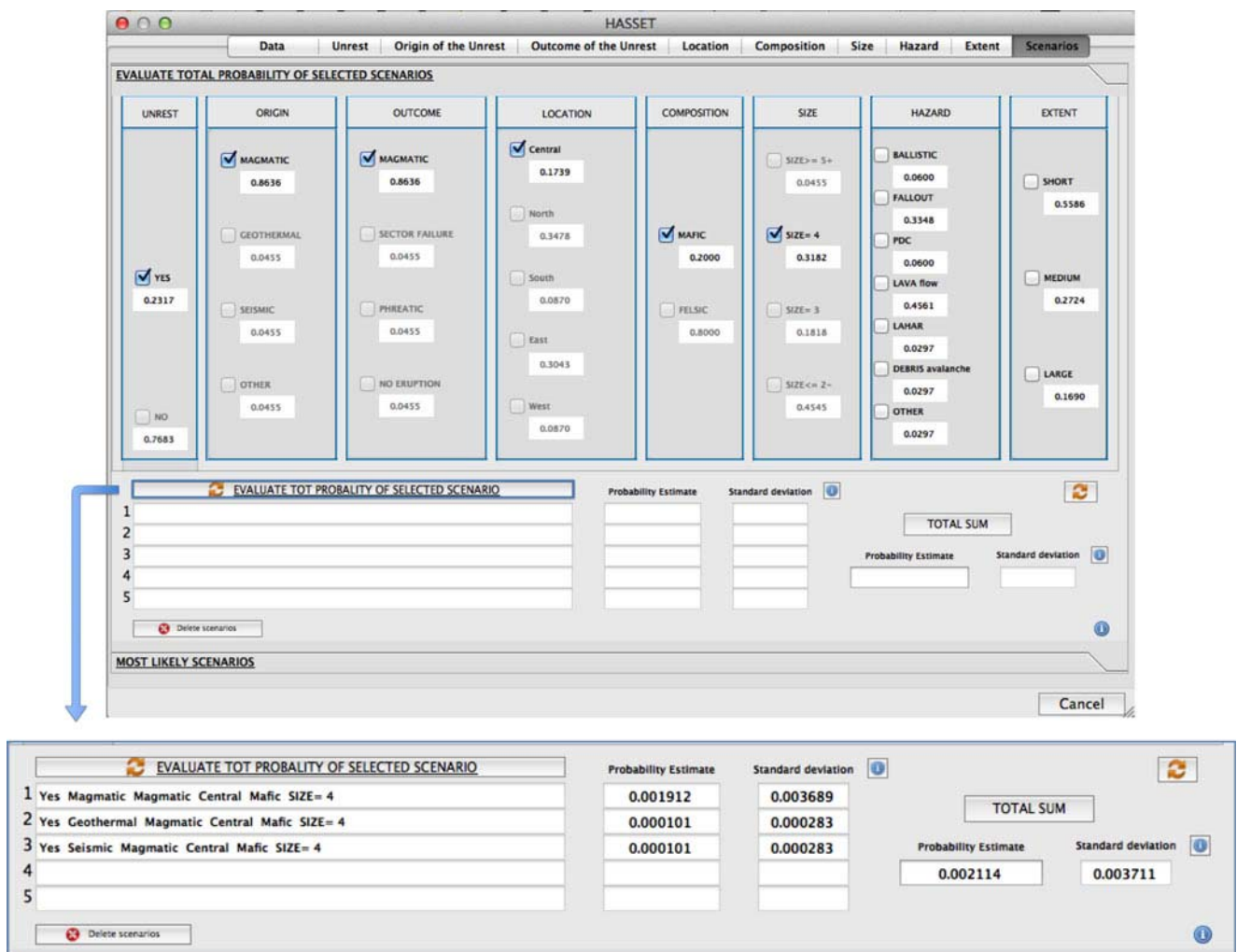


Fig. 4 The “Scenarios” window represents the Event Tree structure with all the nodes and branches. The results obtained in the first analysis of HASSET, i.e., the probability values at each node, are also

shown. Here, the user has the possibility to evaluate the probability of different volcanic scenarios by choosing different combinations of branches

HASSET applied to Teide-Pico Viejo volcanic complex

Here, we use the existing data catalogue for Teide-Pico Viejo (TPV) as shown in Table 1. More in-depth explanation of the data can be found in Sobradelo and Martí (2010) and references within.

In this example, we want to assess the long-term volcanic hazard of TPV for the next 100 years, so we set $\tau = 100$. For node 4, we consider five different locations: central, north, south, east, and west, and for Node 6, we use VEI to define four different sizes: $VEI \leq 2$, $VEI 3$, $VEI 4$, $VEI \geq 5$ (see Sobradelo and Martí (2010)). All of the volcanic data input for HASSET, as well as the prior distribution and model beliefs, input as data and prior weights, are reported in Table 2. Note that even if there are no records of unrest with geothermal or seismic origin, we do not rule out this as a possible future scenario, because in our example, there is a

hydrothermal system underneath the volcanic complex. We account for these additional sources of volcanic hazard by assigning positive weights to the corresponding branches, and assume the lack of records in the dataset could be due to incompleteness in the data catalogue. Not accounting for these scenarios could underestimate the volcanic hazard. The same applies to the noneruptive volcanic scenarios (sector failure and phreatic explosion) despite no records in the data catalogue. In this example, we assumed that every unrest episode results in an eruption, as we do not have records otherwise. Alternative models and expert elicitation are used to adjust the input data and assign weights to the priors and the data. Here, we assume maximum epistemic uncertainty (i.e., the minimum data weight value of 1) and proportional prior weights (refer to Sobradelo and Martí (2010) for further details).

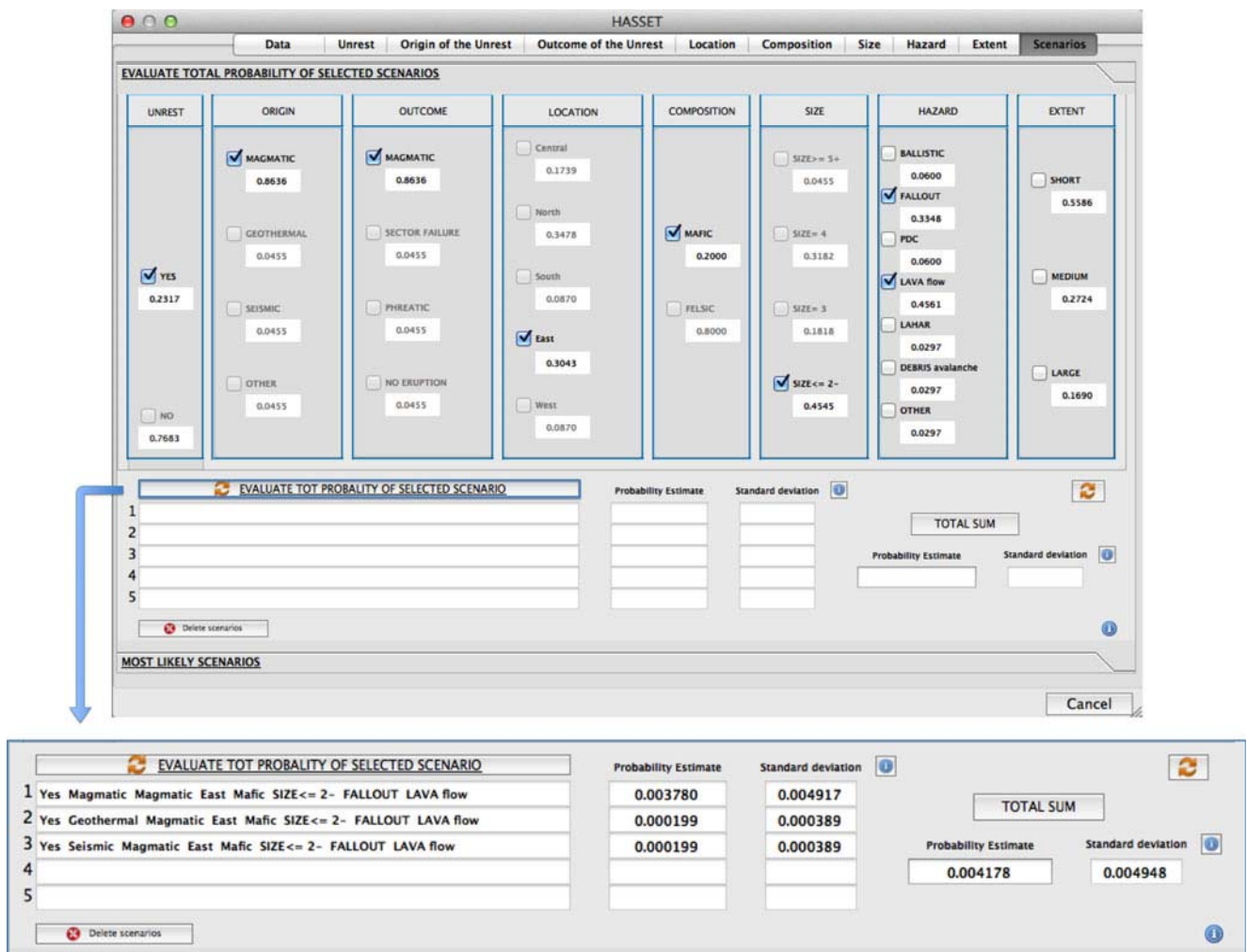


Fig. 5 The probability estimate for various volcanic scenarios can be compared and visualized with the “EVALUATE TOTAL PROBABILITY OF SELECTED SCENARIOS” button. Only five scenarios can be

visualized at the same time and the “Delete scenarios” button is used to erase the selected scenarios and perform a new scenario analysis

A crucial determinant of the reliability of the results is the data used in the study, and so it is the first step of introduction of the input parameters. The user has the possibility of manually entering the data shown in Table 1 or uploading it from a comma-separated (csv) file (Table 2), where the input data for past events, priori weight, and data weight are selected from a drop-down menu. Figure 2 shows a screenshot of the first window where the data are uploaded into the HASSET GUI.

As mentioned earlier, the extent of a volcanic hazard is a relative measure of the maximum distance reached, or the area covered by a particular event. It has to be estimated separately for each volcano or volcanic zone by comparing the maximum and minimum extent of each hazard in particular.

In the case of Teide-Pico Viejo, regardless of the type of hazard reaching the area, we consider short extent any area within 3 km of the volcanic region of study, medium extent would be the area between 3 and 15 km, and large extent any area further than 15 km. Impact may be assessed by comparing a combination of hazard and extent, for instance the hazard from a lava flow of medium extent compared to a PDC of large extent.

As the time over which eruptions in our dataset took place is 8,000 years and we want to estimate the probability of at least one eruption in the next 100 years, we have 80 time intervals of data for the study. For each branch, we count the number of intervals where at least one event of that type has occurred. For example, out of 80 time intervals, 18 observed an episode of unrest and 62 did not.

Once the data is entered, HASSET computes a probability estimate and corresponding standard deviation for each branch of all the eight nodes, and displays them in table and graphical format for simplicity. Figure 3a shows an example of how the *unrest* tab displays the output on HASSET. The initial beliefs are entered for this node in columns for prior and data weight. We can see the 80 time windows of which 18 had an episode of unrest and 62 did not. With these data, the probability estimate of having at least one unrest episode in the next time window of 100 years is 23.17 %, versus the complement 76.83 % of no unrest. The pie chart in Fig. 3 displays graphically these probabilities. On the event tree graph (Fig. 3), we see the node of unrest highlighted in green to show the user at what point of the event tree are we. The same applies for all of the remaining seven nodes. Figure 3b

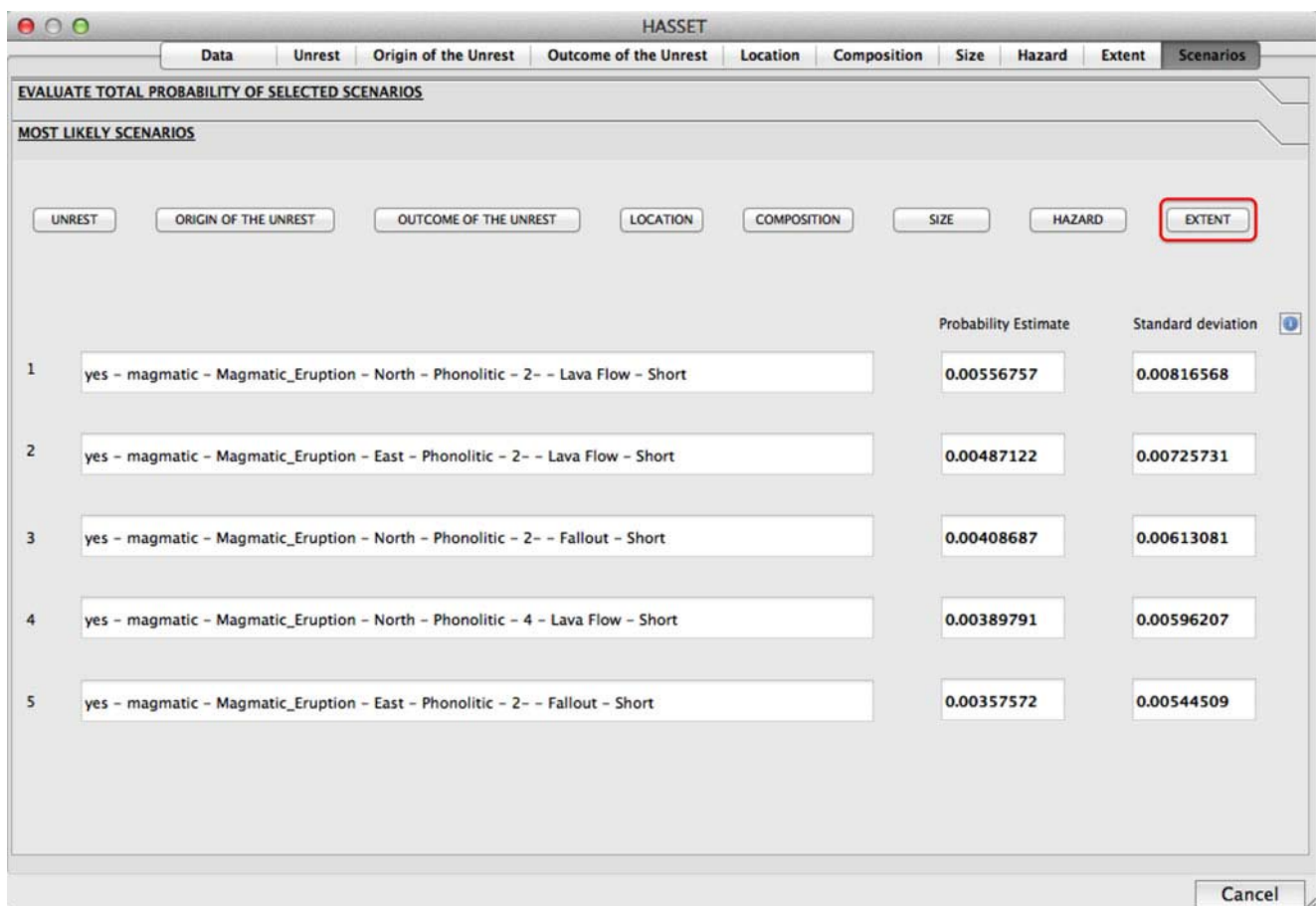


Fig. 6 This window shows at each node (e.g., Extent) the five most likely scenarios, i.e., the ones with the highest probability estimates. See text for explanations

and c show the results for the *hazards* and *extent* node, where after observing the data, we compute that fallout and lava flows account for nearly 80 % of the total probability estimate of the occurrence of these particular hazards in the next 100 years, while the possibility of any of this hazard affecting a medium/large area is not far from 50 % (22.26 and 18.74 %, respectively). Note that the variability interval for each estimate is very wide, as we are assuming maximum epistemic uncertainty and noninformative priors. Figures 4 and 5 show the scenario selection tab, where the entire event tree is displayed with all the nodes and corresponding probability estimates for each branch. From this window, we can now evaluate all scenarios of interest by clicking on the desired branch. Note that some eruptive scenarios are formed of different combinations, as shown in the bottom part of the figures, where a magmatic eruption can be triggered by different types of unrest, and so HASSET allows for computation and summing of all cases. Also note that the *hazards* node allows the user to select more than one option (Fig. 5), since the same eruption could produce different hazards.

When studying a particular volcanic system, it could be the case that we are not interested in a particular eruptive scenario but more so knowing what the most likely eruptive scenarios are. One of the prime features of HASSET is that it includes an option to identify the five most likely scenarios to occur up to a particular node. In Fig. 6, we see that the most likely scenarios to occur are magmatic eruptions, mainly of VEI 2 or less, on the north or east sides of the volcano producing lava flows and fallout of short extent.

Discussion and conclusions

HASSET is a probability tool built on an event tree structure of possibilities that outlines possible future volcanic scenarios, eruptive and noneruptive, originated by internal or external triggers, and then uses Bayesian theory to estimate a probability of occurrence for each scenario. Further, it determines the five most likely scenarios based on the information given. The main goal of this tool is to focus discussion and draw attention to possible scenarios that otherwise would go unnoticed or underestimated. The reliability of the results will strongly depend on the reliability of the volcanological information provided. With HASSET, we wanted to create a realistic, simple, and practical tool that brings a particular hazard assessment technique closer to the decision maker or the monitoring expert, to help structure and focus discussion on the main aspects of the volcanic hazard. This tool could be useful for land use planning and preparedness actions.

The interpretation of the individual probability estimates for each scenario is subjective. The absolute value of the

estimate will strongly depend on the accuracy and completeness of the data, as mentioned earlier, but also on the starting assumptions of independence of the nodes and the choice of mathematical technique to model the uncertainty surrounding the corresponding volcanic system. We turn to probability models when we want to make inferences and decisions about the future in view of uncertainty. We observe the past history of a volcanic system and assume that the future behavior will be similar, and then, based on the data provided, extract a probability model that may guide decisions and make inferences about future scenarios. The model selection is an additional source of uncertainty. HASSET provides a systematic and structured way of using all of the available information such as models, state of the volcano, geochronological and historical data, expert opinion and theoretical beliefs, to analyze the uncertainty surrounding a volcano, based on robust and well-established mathematical theory, that will enable us to rapidly update our estimates when new evidence arrives.

HASSET is a probabilistic approach that accounts for the epistemic (data or knowledge limited) and aleatory (stochastic) uncertainties (given reliable input information), providing a more realistic assessment of the probability estimates.

HASSET can be used to identify the relative importance of several scenarios by comparing their probabilities of occurrence, providing an important tool for the decision maker to redirect resources and prioritize emergency plans, based on what is most likely to occur. Note that the five most likely scenarios, identified through HASSET, may very well not be the five most threatening, in terms of the risk they pose, because the model does not consider what is exposed to the hazards. The relative interpretation of the probability estimates will depend on the decision maker, his or her perception of risk, and the level of loss considered acceptable.

HASSET is part of a larger project to build an architecture for decision making during volcanic crises, incorporating information from other relevant sources like cost, loss, vulnerability, spatial hazards, etc. It represents the first of several modules, temporal and spatial, that will also be implemented in QGIS and will interact with each other to elaborate an analysis report on the current situation of the volcano. The next step of HASSET is to add monitoring data to perform short-term volcanic hazard assessment.

Acknowledgments This work was supported by the European Commission (FP7 Theme: ENV.2011.1.3.3-1; grant 282759: VUELCO). The authors are grateful to Henry Odbert and an anonymous reviewer for their insightful comments and thorough review of the manuscript, which has helped us improve considerably this work. We also thank the Associate Editor Eliza Calder for handling this paper and for her editing and scientific corrections.

Open Access This article is distributed under the terms of the Creative Commons Attribution License which permits any use, distribution, and reproduction in any medium, provided the original author(s) and the source are credited.

Appendix: Computation of the variance estimation for a particular eruptive scenario

Let us use a general notation for simplicity. Let Y be a random variable formed by the product of m random variables, $Y = X_1 \cdot X_2 \cdot \dots \cdot X_m$. In our case, Y will be a particular eruptive scenario whose variance we want to compute.

Then, the expected value E and variance V (also denoted $\hat{\sigma}^2$) of Y , are:

$$E(Y) = E(X_1 \cdot X_2 \cdot \dots \cdot X_m) = E \prod_{i=1}^m X_i = \prod_{i=1}^m E(X_i)$$

and

$$V(Y) = V(X_1 \cdot X_2 \cdot \dots \cdot X_m)$$

and so the expected value of a particular scenario is just the product of the expected value (posterior Dirichlet) of each of the m nodes. The same condition does not apply to the variance. That is, the variance of the product is not the product of the variances, so we use the Delta method, also called propagation error, to approximate this variance by applying a first order Taylor series expansion. We do a logarithmic transformation of the variable, and we get:

$$\log(Y) = \sum_{i=1}^m \log X_i$$

and, now by the independence condition of X_i

$$V(\log(Y)) = \sum_{i=1}^m V(\log X_i) \quad (5)$$

We apply the Delta method to approximate $\log(Y)$ and $\log(X_i)$, with $g(\delta) = \log(\delta)$, where δ is the estimator, and we get:

$$V(\log(Y)) \approx V(Y) \frac{1}{\delta^2}$$

Hence,

$$V(Y) = \delta^2 V(\log(Y)) \quad (6)$$

and similarly for $\log(X_i)$,

$$V(\log(X_i)) \approx V(X_i) \frac{1}{\delta_i^2}$$

Hence,

$$V(X_i) = \delta_i^2 V(\log(X_i))$$

and so, by Eqs. 5 and 6

$$V(Y) = \delta^2 \sum_{i=1}^m V(\log X_i) = \delta^2 \sum_{i=1}^m \frac{1}{\delta_i^2} V(X_i)$$

For our particular case, we know that the estimator δ_k is modeled with the expected value of the random variable for node k that follows a Dirichlet distribution of parameters $\alpha_k + y_k$ (the posterior distribution of a particular branch for node k). The estimator δ is the expected value for that particular eruptive scenario, and $V(X_k)$ is the variance for the random variable in node k that follows a Dirichlet distribution of parameters $\alpha_k + y_k$. We thus derive Eq. 2:

$$\hat{\sigma}_j^2 = E(H)^2 \sum_{k=1}^m \frac{1}{[E(\theta_{kn}^*)]^2} V(\theta_{kn}^*)$$

And so we have written the variance for an eruptive scenario H as a function of the expected value and variances of the individual random variables used to model each particular node.

References

- Aspinall W, Cook R (1998) Expert judgement and the Montserrat volcano eruption. In: Mosleh A et al. (eds) Proceedings of the 4th international conference on Probabilistic Safety Assessment and Management PSAM4, 13–14 September. Springer, New York, pp 2113–2118
- Aspinall WP (2006) Structured elicitation of expert judgment for probabilistic hazard and risk assessment in volcanic eruptions. In: Mader HM et al. (eds) Statistics in volcanology. Special Publication of IAVCEI, Geological Society of London
- Blong R (2000) Volcanic hazards and risk management. In: Sigurdsson H et al. (eds) Encyclopedia of volcanoes. Academic, San Diego, pp 1215–1227
- Chen D, Shams S, Carmona-Moreno C, Leone A (2010) Assessment of open source gis software for water resources management in developing countries. J Hydro Environ Res 4(3):253–264
- Longley PA, Goodchild MF, Maguire DJ, Rhin DW (2001) Geographic information, systems and science. Wiley, Chichester
- Loughlin S, Baxter P, Aspinall W, Darroux B, Harford C, Miller AD (2002) Eyewitness accounts of the 25 June 1997 pyroclastic flows and surges at Soufriere Hills Volcano, Montserrat, and implications for disaster mitigation. Geol Soc Lond Mem 2002(21):211–230
- Martí J, Aspinall W, Sobrado R, Felpeto A, Geyer A, Ortiz R, Baxter P, Cole P, Pacheco J, Blanco M, Lopez C (2008a) A long-term volcanic hazard event tree for Teide-Pico Viejo stratovolcanoes (Tenerife, Canary Islands). J Volcanol Geotherm Res 178(3):543–552
- Martí J, Geyer A, Andújar J, Teixidó F, Costa F (2008b) Assessing the potential for future explosive activity from Teide-Pico Viejo stratovolcanoes (Tenerife, Canary Islands). J Volcanol Geotherm Res 178(3):529–542. Evaluating Explosive Eruption Risk at European Volcanoes - Contribution from the EXPLORIS Project
- Martí J, Sobrado R, Felpeto A, García O (2011) Eruptive scenarios of phonolitic volcanism at Teide-Pico Viejo volcanic complex (Tenerife, Canary Islands). Bull Volcanol 74:767–782

- Marzocchi W, Sandri L, Gasparini P, Newhall C, Boschi E (2004) Quantifying probabilities of volcanic events: the example of volcanic hazard at Mount Vesuvius. *J Geophys Res* 109. doi:[10.1029/2004JB003155](https://doi.org/10.1029/2004JB003155)
- Marzocchi W, Sandri L, Furlan C (2006) A quantitative model for volcanic hazard assessment. In: Mader HM, et al. (eds) *Statistics in volcanology*. Special Publication of IAVCEI, Geological Society of London
- Marzocchi W, Sandri L, Selva J (2008) BET_EF: a probabilistic tool for long- and short-term eruption forecasting. *Bull Volcanol* 70(5):623–632
- Marzocchi W, Sandri L, Selva J (2010) BET_VH: a probabilistic tool for long-term volcanic hazard assessment. *Bull Volcanol* 72:705–716
- Neri A, Aspinall W, Cioni R, Bertagnini A, Baxter P, Zuccaro G, Andronico D, Barsotti S, Cole P, Ongaro TE, Hincks T, Macedonio G, Papale P, Rosi M, Santacroce R, Woo G (2008) Developing an event tree for probabilistic hazard and risk assessment at vesuvius. *J Volcanol Geotherm Res* 178(3):397–415
- Newhall CG, Hoblitt RP (2002) Constructing event trees for volcanic crisis. *Bull Volcanol* 64:3–20
- Renschler CS (2005) Scales and uncertainties in using models and gis for volcano hazard prediction. *J Volcanol Geotherm Res* 139(1–2):73–87
- Rice JA (2007) *Mathematical statistics and data analysis*. Duxbury, Belmont
- Sherman GE (2008) *Desktop GIS. Mapping our planet with open source tools*. The Pragmatic Bookshelf Raleigh, North Carolina
- Sobradelo R, Martí J (2010) Bayesian event tree for long-term volcanic hazard assessment: application to Teide-Pico Viejo stratovolcanoes, Tenerife, Canary islands. *J Geophys Res* 115. doi:[10.1029/2009JB006566](https://doi.org/10.1029/2009JB006566)
- Sobradelo R, Martí J, Mendoza-Rosas AT, Gómez G (2011) Volcanic hazard assessment for the canary islands (spain) using extreme value theory. *Nat Hazards Earth Syst Sci* 11(10):2741–2753
- Woo G (1999) *The mathematics of natural catastrophes*. Imperial College Press, London

Appendix 4

Long-term volcanic hazard assessment on El Hierro (Canary Islands)



Long-term volcanic hazard assessment on El Hierro (Canary Islands)

L. Becerril¹, S. Bartolini¹, R. Sobradelo¹, J. Martí¹, J. M. Morales², and I. Galindo²

¹Institute of Earth Sciences Jaume Almera, ICTJA-CSIC, Group of Volcanology, SIMGEO (UB-CSIC) Lluís Solé i Sabarís s/n, 08028 Barcelona, Spain

²Instituto Geológico y Minero de España (IGME) c/Alonso Alvarado, 43-2A, 35003 Las Palmas de Gran Canaria, Spain

Correspondence to: L. Becerril (laurabcar@gmail.com)

Received: 22 January 2014 – Published in Nat. Hazards Earth Syst. Sci. Discuss.: 24 February 2014

Revised: 10 June 2014 – Accepted: 13 June 2014 – Published: 28 July 2014

Abstract. Long-term hazard assessment, one of the bastions of risk-mitigation programs, is required for land-use planning and for developing emergency plans. To ensure quality and representative results, long-term volcanic hazard assessment requires several sequential steps to be completed, which include the compilation of geological and volcanological information, the characterisation of past eruptions, spatial and temporal probabilistic studies, and the simulation of different eruptive scenarios. Despite being a densely populated active volcanic region that receives millions of visitors per year, no systematic hazard assessment has ever been conducted on the Canary Islands. In this paper we focus our attention on El Hierro, the youngest of the Canary Islands and the most recently affected by an eruption. We analyse the past eruptive activity to determine the spatial and temporal probability, and likely style of a future eruption on the island, i.e. the where, when and how. By studying the past eruptive behaviour of the island and assuming that future eruptive patterns will be similar, we aim to identify the most likely volcanic scenarios and corresponding hazards, which include lava flows, pyroclastic fallout and pyroclastic density currents (PDCs). Finally, we estimate their probability of occurrence. The end result, through the combination of the most probable scenarios (lava flows, pyroclastic density currents and ashfall), is the first qualitative integrated volcanic hazard map of the island.

1 Introduction

The possibility of future eruptive activity, coupled with population growth and economic and cultural development in the majority of active volcanic areas, means that mitigative measures against volcanic risk, such as the development of volcanic hazard analyses, must be undertaken. These types of analyses are a fundamental part of risk management tasks that include the developing of volcanic hazard maps, land-use planning and emergency plans.

The volcanic hazard of a given area is the probability that it will be affected by a process of a certain volcanic magnitude within a specific time interval (Fournier d'Albe, 1979). Therefore, volcanic hazard assessment must necessarily be based on good knowledge of the past eruptive history of the volcanic area, which will tell us “how” eruptions have occurred. It also requires the spatial probability of occurrence of a hazard to be determined; i.e. “where” the next eruption can take place (volcanic susceptibility) and its extent, as well as its temporal probability, in other words “when” the next eruption may occur in the near future.

The complexity of any volcanic system and its associated eruptive processes, together with the lack of data that is typical of so many active volcanoes and volcanic areas (and in particular those with long periods between eruptions), make volcanic hazard quantification a challenge. Long-term hazard assessment is necessary to know how the next eruption could be. It is based on the past history of the volcano and the information needed comes from the geological record. Unlike short-term assessment that evaluates hazards from days to a few months, using data provided by monitoring networks,

long-term assessment is estimated from years to decades, where the main source of information is mainly structural data from past eruptions (Marzocchi et al., 2006). Different steps need to be followed sequentially in any long-term volcanic hazard assessment. The first step consists of evaluating the likelihood of a future eruption, which will provide an indication of which areas are most likely to host future vents (Martí and Felpeto, 2010). The long-term spatial probability of vent opening can be estimated using structural data such as vents, dykes, faults, fractures and eruptive fissure-alignments obtained from geological and geophysical studies. These data can be converted into Probability Density Functions (PDFs) and then combined to obtain the final susceptibility map (Martin et al., 2004; Felpeto et al., 2007; Connor and Connor, 2009; Martí and Felpeto, 2010; Cappello et al., 2012; Bartolini et al., 2013; Becerril et al., 2013). Susceptibility maps show the spatial probability of hosting new future eruptions. This term has been commonly used during the last years by other authors in the volcanic field (Felpeto et al., 2007; Cappello et al., 2010, 2011, 2012; Martí and Felpeto, 2010; Vicari et al., 2011; Alcorn et al., 2013; Bartolini et al., 2013; Becerril et al., 2013).

The next step corresponds to the temporal probability estimation of any possible volcanic event. Long-term forecasting is based on historical and geological data, as well as on theoretical models, and refers to the time window available before an unrest episode occurs in the volcanic system. In this regard, some authors use probabilistic statistical methods based on the Bayesian event tree for long-term volcanic hazard assessment (Newhall and Hoblitt, 2002; Marzocchi et al., 2008; Sobradelo and Martí, 2010), while some others use a deterministic approach (Voight and Cornelius, 1991; Kilburn, 2003; see also Hill et al., 2001).

Once spatial and temporal probabilities have been estimated, the next step forward consists of computing several scenarios as a means of evaluating the potential extent of the main expected volcanic and associated hazards. Most of these studies are based on the use of simulation models and Geographical Information Systems (GIS) that allow volcanic hazards such as lava flows, PDCs and ash fallout to be modelled and visualised (Pareschi et al., 2000; Felpeto et al., 2007; Toyos et al., 2007; Crisci et al., 2008; Cappello et al., 2012; Martí et al., 2012; Alcorn et al., 2013).

All of these steps should be undertaken to evaluate the potential volcanic hazards of any active volcanic area. Similar approaches have been applied in volcanic areas such as Auckland, New Zealand (Bebbington and Cronin, 2011); Etna, Sicily (Cappello et al., 2013); and Tenerife, Spain (Martí et al., 2012); Perú (Sandri et al., 2014). Nevertheless, other procedures have also been applied in order to assess volcanic hazards in Campi Flegrei, Italy (Lirer et al., 2001); Furnas (São Miguel, Azores) Vesuvius in Italy (Chester et al., 2002); and Auckland, New Zealand (Sandri et al., 2012). Compared with these previous approaches, our study offers a procedure that facilitates undertaking volcanic hazard

assessment in a systematic way, which can be easily applied to other volcanic areas around the world.

The Canary Islands are the only area of Spain in which volcanic activity has occurred in the last 600 years, representing one of the world's largest oceanic volcanic zones. The geodynamic environment in which the archipelago lies and the characteristics of its recent and historical volcanism suggest that the volcanic activity that has characterised this archipelago for more than 60 Ma will continue in the future. Previous volcanic hazard studies conducted on the Canary Islands have not followed a systematic method. Most work to date has focused on Tenerife and Lanzarote (Gómez-Fernández, 1996; Araña et al., 2000; Felpeto et al., 2001, 2007; Felpeto, 2002; Carracedo et al., 2004a, b, 2005; Martí and Felpeto, 2010; Sobradelo and Martí, 2010; Martí et al., 2012; Bartolini et al., 2013), although other studies have been carried out on Gran Canaria (Rodríguez-González, 2009), El Hierro (Becerril et al., 2013) and one for the Canary Islands as a whole (Sobradelo et al., 2011).

In this study we focus on El Hierro and conduct a long-term volcanic hazard assessment by taking into account spatial and temporal probabilities. Despite being small and submarine in nature (Martí et al., 2013), the most recent eruption on El Hierro (October 2011–February 2012) highlighted the need for volcanic hazard studies, given the negative impact on tourism and the local economy of any volcanic event. Although this eruption was not different in terms of magma volume and volcanic products from most eruptions that historically occurred in the Canarian Archipelago, this eruption marked the end of a 40-year period of quiescence in this volcanic region. El Hierro has a population of 10 960 inhabitants (www.ine.es), or 0.51 % of the total population of the Canary Islands. Its main economic resources are tourism and fishery, two aspects that may be – and in fact were – seriously affected by the impact of volcanic activity.

In this work we present a systematic analysis of the volcanic hazards present on this island that includes the following steps: (1) characterisation of past volcanism in the study area; (2) estimation of spatio-temporal probabilities; (3) simulation of the most probable eruptive scenarios such as lava flows, pyroclastic fallout and pyroclastic density currents (PDCs); and (4) assessment of the volcanic hazard.

2 Geological setting

The Canary Islands extend for roughly 500 km in a chain that has developed on the passive margin of the African plate in the eastern central Atlantic Ocean (Fig. 1, inset). The Canarian Archipelago is the result of long-term volcanic and tectonic activity that started around 60 Ma (Robertson and Stillman, 1979; Le Bas et al., 1986; Araña and Ortiz, 1991; Marinoni and Pasquaré, 1994). A number of contrasting models – including the presence of a hotspot, the propagation of a fracture from the Atlas Mountains and mantle

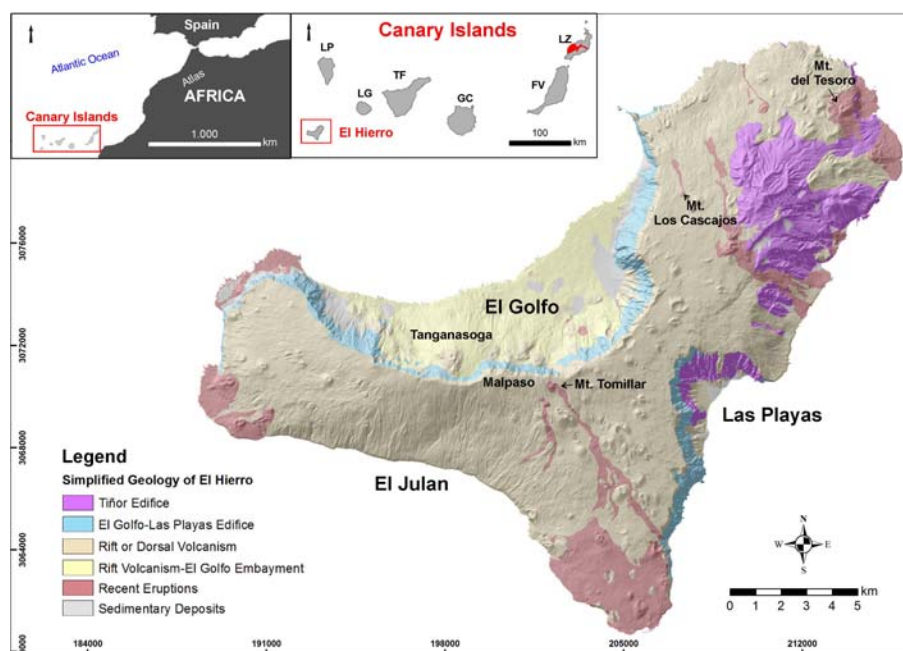


Figure 1. Geological map of El Hierro Island. At the left top part of the figure, location of the Canary Islands is presented where LZ represents Lanzarote; FV represents Fuerteventura; GC represents Gran Canaria; TF represents Tenerife; LG represents La Gomera; LP represents La Palma; EH represents El Hierro. Timanfaya eruption in Lanzarote has been coloured in red.

decompression melting associated with uplift of tectonic blocks – have been mooted to explain the origin of the Canary Islands (Le-Pichon and Fox, 1971; Anguita and Hernán, 1975; Schmincke, 1982; Araña and Ortiz, 1991; Hoernle and Schmincke, 1993; Hoernle et al., 1995; Carracedo et al., 1998; Anguita and Hernán, 2000).

Although all of the islands (except La Gomera) have been witness to Holocene volcanic activity, volcanism has historically been restricted to La Palma, Lanzarote, El Hierro and Tenerife (Fig. 1, inset). In all cases, historical eruptive activity has produced mafic eruptions ranging in intensity from Hawaiian to violent Strombolian (Valentine and Gregg, 2008 and references therein) and have given rise to lavas and scoria cones. Typically, the islands' historical eruptions have occurred in active rift zones along eruptive fissures and have occasionally generated alignments of cones. Other than the case of the Timanfaya eruption in 1730 in Lanzarote (Fig. 1, inset), which lasted for 6 years, the duration of eruptions has ranged from a few weeks to a few months. The total volume of erupted magma ranges from 0.01 to $> 1.5 \text{ km}^3$ (DRE, dense rock equivalent), the upper extreme occurring in the case of the Timanfaya eruption. In all cases the resulting volcanic cones were constructed during single eruptive episodes (i.e. they should be referred to as monogenetic) that usually involved several distinctive phases with no significant temporal separations between them. Monogenetic volcanic fields consist of individual, commonly mafic volcanoes, built in single, relatively short-lived eruptions. These volcanoes usually take the form of scoria cones, tuff rings, maars or tuff

cones; scoria cones are the most common landform and show a great diversity in size, morphology and eruptive products (Valentine and Gregg, 2008; Kereszturi and Németh, 2012). Individual volcanic edifices are characteristically small in volume, typically $< 0.1 \text{ km}^3$ of DRE, but the eruption can be complex with many different phases and styles of activity (Németh, 2010). Situated in the southwestern corner of the archipelago, El Hierro is the youngest of the Canary Islands; its oldest subaerial rocks have been dated at 1.12 Ma (Guillou et al., 1996). It rises from a depth of 4000 m to around 1500 m a.s.l. and has an estimated total edifice volume of about 5500 km^3 (Schmincke and Sumita, 2010). It corresponds to a shield structure formed by different volcanic edifices and includes three rift zones on which recent volcanism has been concentrated (Guillou et al., 1996; Carracedo et al., 2001) (Fig. 1). Other relevant morphological features include the collapse scars of El Golfo, Las Playas and El Julian (Fig. 1). The emergent parts of these rifts are characterised by steep narrow ridges, corresponding to aligned dyke complexes with clusters of cinder cones. Pre-historical eruptions have been recognised on all three rifts on El Hierro (Guillou et al., 1996; Carracedo et al., 2001).

Recent subaerial volcanism on El Hierro is monogenetic and is mostly characterised by the eruption of mafic magmas as well as the intrusion of subvolcanic bodies ranging in composition from picobasalts to basanites (Pellicer, 1977; Stroncik et al., 2009), which have generally erupted along the rift zones. Some felsic dykes and lava flows associated with the older parts of the island have also been reported (Guillou

et al., 1996; Carracedo et al., 2001) but are volumetrically subordinate to the mafic material. In addition, an explosive felsic eruption has been documented in association with the final episodes of the construction of the edifice of El Golfo–Las Playas (later than 158 ka), before it was destroyed by a massive landslide (Pedrazzi et al., 2014). Mafic eruptions typically occur from fissures, and produce proximal fallout, ballistic ejecta and lava flows. PDC deposits have also been reported in cases in which eruptions are related to hydromagmatic episodes (Balcells and Gómez, 1997; Pedrazzi et al., 2014).

The erupted volume of magma in eruptions on El Hierro typically ranges from less than 0.0001 to 0.1 km³ (DRE), values that are of the same order as most of the other historical eruptions on the Canaries (Sobradelo et al., 2011). One of the most important eruptive episodes in the last few thousand years on El Hierro was the Tanganasoga eruption (Fig. 1), which occurred inside the depression of El Golfo along a N–S-oriented fissure, at most 20 ka (Carracedo et al., 2001). Several cones and emission centres formed, giving rise to one of the largest volcanic edifices on the island via the accumulation of ankaramitic lavas and pyroclastic deposits (Carracedo et al., 2001) (Fig. 1). In addition to the sub-aerial volcanism, bathymetric studies (Gee et al., 2001) have revealed that a significant number of well-preserved volcanic cones exist on the submarine flanks of the island, in particular on the continuation of the southern rift, which suggests that significant submarine volcanic activity has also occurred recently. As a confirmation of this observation, a submarine eruption occurred from 10 October 2011 to the end of February 2012 on the southern rift zone, 2 km off the coast of El Hierro (Martí et al., 2013).

3 Methods

The spatial probabilities of hosting new vents were estimated using the study by Becerril et al. (2013) of volcanic susceptibility on El Hierro, which takes into account most of the structural data (vents, eruptive fissures, dykes and faults) available from the island. The temporal part of the long-term volcanic hazard assessment was carried out with the Bayesian-event tree-based software HASSET (Sobradelo et al., 2014a) using geochronological data for El Hierro and historical data from the whole archipelago. Hazard scenarios of lava flows, fallout and PDCs were obtained with the VORIS tool (Felpeto et al., 2007) since they are the most likely volcanic scenarios on the island. The data collection required for each hazard assessment was divided into three parts (spatial, temporal, and scenarios), according to the use made of each data set.

4 How: characterisation of the eruptions

The characterisation of past volcanic eruptions – typically based on the determination of eruptive parameters derived from the study of erupted products found in the geological records – is crucial for understanding past eruptive behaviour and for forecasting future volcanic activity.

Recent volcanic activity on El Hierro is largely characterised by monogenetic mafic volcanism and the building of more than 220 cones, most of which are scoria cones that correspond to the most recent eruptive cycle (rift volcanism).

Hawaiian and Strombolian activity are the most common eruptive styles observed on the island (Becerril, 2009), which have formed extensive lava flow fields, spatter and cinder cones made of scoria agglutinates and well-bedded lapilli scoria and ash, respectively. Violent Strombolian activity – refereeing to explosive activity that produces sustained eruption columns up to ~10 km high (without reaching the tropopause) and with the dominant clast sizes being ash to lapilli (Valentine, 1998; Arrighi et al., 2001; Valentine and Gregg, 2008) – has been also recognised through the presence of several distal ash deposits on the geological record of the island. Phreatomagmatic episodes generating rhythmic laminated sequences of coarse juvenile ash and lapilli-rich beds with accidental lithic fragments also occurred at the interior of the island but in less frequency than those mentioned above. In addition, some hydromagmatic eruptions occurred along the coast, producing tuff ring deposits on the western part of the island (Becerril, 2009). Eruptions related to felsic magmas and producing either trachytic lava flows (Guillou et al., 1996) or trachytic pyroclastic deposits (Pellicer, 1977; Balcells and Gómez, 1997) have also been described. In this sense, it is remarkable that the occurrence of a base-surge-type explosive eruption that generated dilute pyroclastic surge deposits covering an area of more than 15 km² around the Malpaso area (Fig. 1) (Pedrazzi et al., 2014).

We also took into account the final constructive cycle (158 ka–present) of the island to characterise of the size of the eruptions. The volume of the cones was calculated using ARCGIS 10.0 (ESRI[©]) through the analysis of a digital elevation model (DEM), subtracting the current DEM topography to the restored paleo-topography. The volume of lava flows and distal pyroclastic deposits was calculated taking into account their areal extent and thickness variations. This provided a first-order estimate of the erupted volume, despite the lack of a precise paleo-topography. In terms of the total volume of erupted material, the largest eruptions that occurred during the final growing cycle on El Hierro correspond to volumes of the order of 0.15–0.042 km³ (Tanganasoga, Mt. del Tesoro, the latter was calculated by Rodríguez-González et al., 2012). A minimum value is for Mt. Los Cascajos, with just 0.0016 km³. The volcanic explosivity index (VEI) (Newhall and Self, 1982) and dense rock equivalent (DRE) derived from the volumetric

data of the eruptions were also calculated. Most of VEI values are in the range of 0–2, whilst the erupted volume of magma (using mean magma density of 2.8 g cm^{-3} , an average rock density of 2.44 g cm^{-3} obtained from laboratory analysis of El Hierro samples, and applying the equation: $\text{DRE (km}^3) = \text{volume of volcanic deposit (km}^3) \times \text{density of volcanic deposit (kg m}^{-3}) / \text{magma density (kg m}^{-3})$) for most of the recent eruptions on El Hierro lies within the range of $0.0001\text{--}0.1 \text{ km}^3$ (DRE). The DRE calculation was based on the volume of exposed materials (lavas and pyroclastic deposits) so our total volumes are minimum estimates, but similar to those assigned to other monogenetic fields, which normally have volumes between 0.0001 and a few cubic kilometres for individual eruptions (e.g. Kereszturi et al., 2013). For example, the erupted volume of magma on the Canary Islands typically ranges from 0.001 to 0.2 km^3 (DRE) (Sobradelo et al., 2011). In the Garrotxa volcanic field (Spain) the total volume of extruded magma in each eruption ranges from 0.01 to 0.2 km^3 (DRE) (Bolós et al., 2014). The volumes of basaltic eruptions on Terceira (Açores, Portugal) range in size from 0.1 km^3 to less than 0.001 km^3 (DRE) (Self, 1976). In the case of Auckland (New Zealand), monogenetic field volumes are in the range of 0.00007 to 0.698 km^3 (Kereszturi et al., 2013).

By comparing pre- and post-eruption high-resolution bathymetries, the total bulk volume erupted during the submarine eruption of 2011–2013 was estimated at 0.33 km^3 (Rivera et al., 2013).

Most of the lava flows on El Hierro that were emplaced from cones located on and off the rift zones reached the sea. Therefore, it was not possible to measure precisely the maximum lengths of past lava flows. Nevertheless, the Mt. del Tomillar (Fig. 1) lava flow, which did not reach the sea, has a total length of 8 km. However, for further simulations (Sect. 6.1) we considered this value as a minimum length for the lava flows and used 15 km as a more reliable length. The mean thickness of lava flows was obtained from the average value (3 m) of individual flows measured in the field.

5 Where: spatial analysis

An essential step in obtaining a volcanic hazard map is to determine the most likely areas to host new eruption vents, a task based on the drawing of susceptibility maps based on geological, structural and geophysical data (Martí and Felpeto, 2010). Structural elements such as vents, eruptive fissures, dykes and faults are used to pinpoint areas where next eruptions may most likely occur. A volcanic susceptibility map shows the spatial distribution of vent opening for future eruption and represents the basis for further temporal and spatial probability analysis and the definition of eruptive scenarios. We used the susceptibility map developed by Becerril et al. (2013) following the methodology employed by Cappello et al. (2012) (Fig. 2). This map is based on the

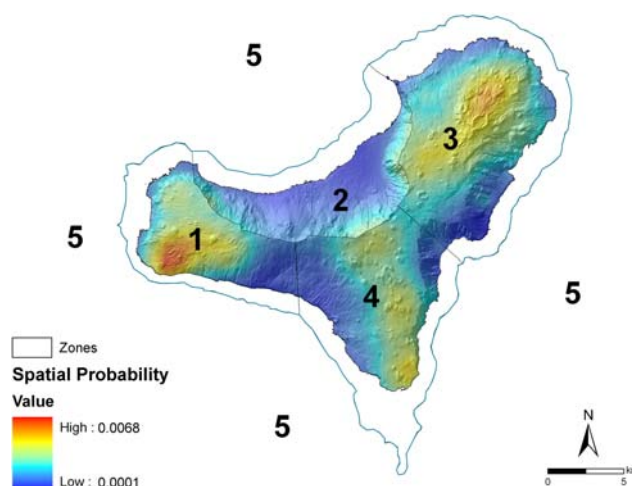


Figure 2. Onshore spatial probability distribution of future volcanic eruptions map of El Hierro Island, showing the divisions of the sectors. Modified from Becerril et al. (2013).

five data sets representing the volcano-structural elements on El Hierro: (1) subaerial vents and eruptive fissures pertaining to the island's rift volcanism, which include sub-recent and recent eruptions; (2) submarine vents and eruptive fissures inferred from bathymetric data; (3) eruptive fissures and emission centres identified on the Tiñor and El Golfo–Las Playas edifices; (4) presence of dykes; (5) and presence of faults.

To carry out this spatial assessment, we subdivided the spatial probability map into 5 sectors (Fig. 2) based on susceptibility values, topographic constraints and expected hazards. First, we differentiated the subaerial and the submarine area, taking into account differences in the expected hazards. After that, the emergent part of the island was subdivided according to areas with different structural controls (different strike of the volcano-structures as dykes and fissures), different topographical constraints (zones 1, 3 and 4 represent rift areas, while zone 2 is an embayment), and different susceptibility values according to the map developed by Becerril et al. (2013). This map enables us to select the areas with the greatest likelihood of hosting future scenarios.

6 When: temporal analysis

Temporal analyses were performed using HASSET (Sobradelo et al., 2014a) a Bayesian event tree structure with eight nodes representing different steps to evaluate the temporal probability and evolving from a more general node of unrest to the more specific node of the extent of the hazard (Sobradelo and Martí, 2010).

We based the study of temporal probability on the catalogue of eruptions documented in Table 1. In all, 25 eruptions are documented from the last 158 ka, data confirmed by the relative stratigraphy established during our field work. Six of

Table 1. The principal characteristics of the eruptions identified during the last constructive episode of El Hierro. The eruptions included in this table are those for which geochronological data exist and that are consistent with the field-relative stratigraphy established in this study. In addition to the geochronological data and the corresponding references, the rest of the information included in the table corresponds to information related to the first nodes in the HASSET (Sobradelo et al., 2014a) event tree used in this study. See text for more details.

ID	Unrest	Origin	Outcome	Location	Composition	Hazard	Extent	Reference
1	2011	magmatic	magmatic eruption	5	Mafic	lava flow	medium	Martí et al. (2013)
2	1793	seismic	no eruption	?				Hernández Pacheco (1982)
3	2500 ± 70 (BP)	magmatic	magmatic eruption	3a	Mafic	ballistic + lava flow	medium	Carracedo et al. (2001)
4	4230 (BP)	magmatic	magmatic eruption	3a	Mafic	ballistic + lava flow	short	Fúster et al. (1993)
5	8000 ± 2000 (BP)	magmatic	magmatic eruption	1a	Mafic	ballistic + lava flow	short	Pérez Torrado et al. (2011)
6	9000 (BP)	magmatic	magmatic eruption	3a	Mafic	ballistic + lava flow	medium	Rodríguez-González et al. (2012)
7	12 000 ± 7000 (BP)	magmatic	magmatic eruption	2a	Mafic	lava flow	short	Guillou et al. (1996)
8	15 000 ± 3000 (BP)	magmatic	magmatic eruption	2a	Mafic	lava flow	short	Guillou et al. (1996)
9	15 000 ± 2000 (BP)	magmatic	magmatic eruption	4b	Mafic	lava flow	short	Carracedo et al. (2001)
10	21 000 ± 3000 (BP)	magmatic	magmatic eruption	2a	Mafic	lava flow	short	Guillou et al. (1996)
11	31 000 ± 2000 (BP)	magmatic	magmatic eruption	4b	Mafic	lava flow	short	Carracedo et al. (2001)
12	38 700 ± 12 600 (BP)	magmatic	magmatic eruption	2b	Mafic	lava flow	short	Longpré et al. (2011)
13	41 000 ± 2000 (BP)	magmatic	magmatic eruption	4b	Mafic	lava flow	short	Carracedo et al. (2001)
14	44 000 ± 3000 (BP)	magmatic	magmatic eruption	4b	Mafic	lava flow	short	Guillou et al. (1996)
15	76 000 ± 6000 (BP)	magmatic	magmatic eruption	3b	Mafic	lava flow	short	Guillou et al. (1996)
16	80 000 ± 40 000 (BP)	magmatic	magmatic eruption	3a	Felsic	lava flow	medium–large	Fúster et al. (1993)
17	86 600 ± 8300 (BP)	magmatic	magmatic eruption	1a	Mafic	lava flow	short	Longpré et al. (2011)
18	94 500 ± 12 600 (BP)	magmatic	magmatic eruption	4a	Mafic	lava flow	short	Longpré et al. (2011)
19	115 300 ± 6900 (BP)	magmatic	magmatic eruption	4a	Mafic	lava flow	short	Longpré et al. (2011)
20	126 000	magmatic	magmatic eruption	5	Mafic	lava flow	short	Klügel et al. (2011)
21	133 000 ± 200	magmatic	magmatic eruption	5	Felsic	lava flow	short	Van der Bogard (2013)
22	134 000 (BP)	magmatic	magmatic eruption	3a	Mafic	lava flow	short	Szérémeta et al. (1999)
23	142 000 ± 2000 (BP)	magmatic	magmatic eruption	5	Felsic	lava flow	short	Van der Bogard (2013)
24	145 000 ± 4000 (BP)	magmatic	magmatic eruption	3b	Mafic	lava flow	short	Guillou et al. (1996)
25	158 000 ± 4000 (BP)	magmatic	magmatic eruption	3a	Mafic	lava flow	short	Guillou et al. (1996)

these eruptions took place during the previous 11 700 years (Holocene), but only 2 unrest episodes have been documented in the last 600 years (historical period). The information from these eruptions was used to characterise the past eruptive activity on El Hierro and to estimate some of the input parameters required for our hazard assessment.

However, due to the scarcity of dated eruptions and to the certainty that not all the eruptions that occurred in this period have been identified and/or dated, we also used in our temporal analysis as data for the last 600 years (15th century to 2013) the historical data set for the whole of the Canary Islands (see Sobrado et al., 2011). Therefore, using HASSET we were able to estimate the probability that a volcanic episode will occur in the forecasting time interval (the next 20 years). Given that the data set time window is 600 years, we thus obtained 30 time intervals of data for the study period. Here we restrict our data set to the historical period, which includes the recent submarine eruption (2011) and the seismic unrest of 1793. The remaining 23 eruptions in this catalogue – referred to as pre-historical – will be used to assign prior weights to nodes 2 to 8.

7 Input data for HASSET

7.1 Node 1: unrest

This node estimates the temporal probability of a reawakening of the system in the next time window by examining the number of past, non-overlapping, equal-length time windows that encompass an episode of unrest. Implicitly, this node estimates the recurrence time with a Bayesian approach that does not use the time series. It did not take into account the repose period between eruptions or the possible non-stationary nature of the data. However, Sobrado et al. (2011) used extreme value theory to study the historical recurrence of monogenetic volcanism on the Canary Islands since the first written records appeared at the beginning of the 15th century. By modelling the inter-period times with a non-homogeneous generalised Pareto–Poisson distribution, this study estimated as of 2010 that the probability of an eruption of a magnitude > 2 anywhere on the Canary Islands in the next 20 years was 0.97 ± 0.00024 .

In order to compute the probability of having (at least) an unrest episode in the next 20 years, we need two pieces of information: (1) our starting beliefs or weights for each possibility (yes, no) and (2) the number of past events during the period of study. As per the number of past events, it shows that in the last 600 years (historical period), there have been two episodes of unrest identified at El Hierro (a seismic unrest and the latest magmatic unrest in 2011 which resulted in eruption). As per the starting weights for each option, if we did not have any information at all we would start with the state of total ignorance or total epistemic uncertainty, and give 50/50 chance to each option. However, this is not the

case, as in the study of the volcanic recurrence for the Canary Islands as of 2010 (based on volcanic records from the islands of Tenerife, La Palma and Lanzarote) (Sobrado et al., 2011), there is an estimated 97 % probability of at least one eruption in the next 20 years, anywhere on the Canary Islands (including El Hierro). Therefore, rather than starting with a 50/50 chance, this study allowed us to assign our a priori beliefs for the “unrest” node in the island of El Hierro (yes = 97, no = 3), and then we used the 2 historical episodes of unrest documented in El Hierro to update those initial beliefs.

The reason why we used the 2 historical events in the catalogue of El Hierro, and not the remaining 23 pre-historical events, was to avoid misleading results in the probability of unrest. If we had used the entire catalogue we would have said to the model that there was on average 1 eruption every 7900 years ($158\,000/20$), which is not realistic, as the catalogue is incomplete. For that reason we updated our prior beliefs with the historical part of the catalogue that we were most confident with. Given our confidence in these results, we were able to assign an epistemic uncertainty of 50 to our data weights, which means that new evidence regarding intervals with non-eruptive behaviour will not significantly modify our prior assumptions. As shown by the posterior probabilities in column 6 of Table 2, despite 28 intervals out of 30 (600 years/20 estimated time intervals) with no unrest, the posterior probability of unrest in the next 20 years is still significantly large.

7.2 Node 2: origin

We considered four types of unrest that could occur on El Hierro: magmatic, geothermal, seismic and others. In spite of the predominant magmatic and seismic behaviour in past activity, we cannot exclude either geothermal activity or false unrest. In fact, hydromagmatic deposits exist in the interior of the island that were most probably associated with the presence of shallow aquifers. Some of these deposits also contain hydrothermally altered lithic clasts, which also suggest the existence of localised hydrothermal systems. Thus, it was impossible to rule out the possibility of geothermal unrest. False unrest can occur when non-volcanic signals are recorded together with volcanic signals. For example, changes in the gravity field, ground deformation or even seismicity unrelated to any volcanic activity could be associated with variations in the recharge and/or extraction of meteoric water into/from aquifers in El Hierro. Even so, we still believe that in monogenetic volcanism magmatic changes are the main source of unrest and so we gave the greatest weight to magmatic unrest (0.96) and split the rest evenly among the other options. The prior weights were assigned on the basis of a priori beliefs and so we allocated a value of 10 to the epistemic uncertainty since we still expect the majority of unrest to be of magmatic origin. However, it is still important to give more weight to new evidence.

Table 2. Input data for HASSET (columns 1 to 5) and output probability vectors and standard deviations (columns 6 and 7). Prior weights and data weights are estimated using pre-historical data, a priori beliefs and published studies on global volcanic unrest during the last century. Past data are based on the eruptions recorded in the last 600 years, considered as the historical period for the Canary Islands.

Node name	Event	Past data	Prior weight	Data weight	Probability estimate	Standard deviation
Unrest	Yes	2	0.97	50	0.64	0.07
Unrest	No	28	0.03	50	0.36	0.07
Origin	Magmatic	1	0.94	10	0.88	0.09
Origin	Geothermal	0	0.02	10	0.02	0.03
Origin	Seismic	1	0.02	10	0.08	0.07
Origin	Other	0	0.02	10	0.02	0.03
Outcome	Magmatic eruption	1	0.64	10	0.62	0.13
Outcome	Sector failure	0	0.12	10	0.10	0.08
Outcome	Phreatic explosion	0	0.12	10	0.10	0.08
Outcome	No eruption	1	0.12	10	0.17	0.10
Location	Zone 1	1	0.16	50	0.17	0.05
Location	Zone 2	0	0.07	50	0.07	0.03
Location	Zone 3	0	0.29	50	0.28	0.06
Location	Zone 4	0	0.16	50	0.15	0.05
Location	Zone 5	1	0.32	50	0.33	0.06
Composition	Mafic	1	0.87	10	0.88	0.09
Composition	Felsic	0	0.13	10	0.12	0.09
Size	VEI 1–	0	0.31	1	0.25	0.19
Size	VEI 2	1	0.62	1	0.70	0.21
Size	VEI 3+	0	0.07	1	0.06	0.10
Size	n.a.	0	0	0	0.00	0.00
Hazard	Ballistic	1	0.12	10	0.15	0.09
Hazard	Fallout	1	0.05	10	0.09	0.07
Hazard	PDC	0	0.03	10	0.03	0.04
Hazard	Lava flow	1	0.8	10	0.73	0.11
Hazard	Lahars	0	0	0	0.00	0.00
Hazard	Debris avalanche	0	0	0	0.00	0.00
Hazard	Other	0	0	0	0.00	0.00
Extent	Short	0	0.87	10	0.80	0.11
Extent	Medium	1	0.09	10	0.16	0.10
Extent	Large	0	0.04	10	0.04	0.05

7.3 Node 3: outcome

A study of global volcanic unrest in the 21st century (Phillipson et al., 2013) shows that 64 % of unrest episodes lead to eruptions. On the other hand, in light of previous studies on El Hierro (Carracedo et al., 2001; Pedrazzi et al., 2014), we were unable to rule out the possibility that, aside from a magmatic eruption, a sector failure or a phreatic explosion might also follow on from an episode of unrest.

Therefore, we assigned a weight of 0.64 to the magmatic eruption and split the remaining 0.36 evenly between the alternative nodes. As these weights were assigned based on general studies and a priori beliefs that did not necessarily include data from El Hierro, we gave a value of 10 to the epistemic uncertainty. As with the previous node, we did not give a total epistemic uncertainty, as we still believe that the largest weight should be for the magmatic eruption branch; however, we still want new evidence to be able to

contribute significantly to updating our prior weights. The two data points in our historical catalogue already include an episode of unrest that did not evolve into an eruption and so we should expect the prior weight of 0.12 assigned to the “No eruption” node to be substantially increased after the new evidence is entered in the model and the posterior probabilities are computed (Table 2, column 6).

7.4 Node 4: location

We divided the island into 5 zones and 11 subzones to be able to perform a volcanic hazard assessment of El Hierro based on the past geological information described above (Fig. 3). These five main zones were established according to the structural (susceptibility) and topographic characteristics of the island, whilst the subdivisions were made by taking into account the potential occurrence of hydrovolcanic episodes. Thus, subzones 1b–4b represent areas that

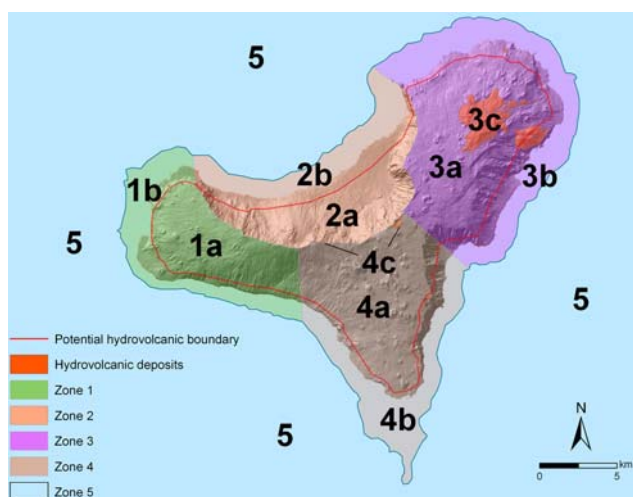


Figure 3. Sectors and subsectors defined on El Hierro. Sectors 1–4 show onshore division while sector 5 represents the offshore area. The division is based on differences in structural patterns, spatial probability of hosting new vents and expected hazards. Subsectors a–c take into account the potential occurrence of hydrovolcanic episodes.

could include the focus of and/or be affected by hydrovolcanic episodes caused by the interaction of seawater with the erupting magma. Given the data, regarding such episodes in the past geological record, we considered that the offshore zone between the bathymetric line of 200 m and the onshore area near the coast, which already includes several hydrovolcanic edifices, was suitable for the occurrence of such processes (Fig. 3). Moreover, subzones 3c and 4c in the interior of the island provide evidence of phreatomagmatic eruptions in the past.

The susceptibility analysis of the island, based on the study by Becerril et al. (2013) (Fig. 2), allowed us to assign the prior weights to each node with a high degree of confidence, as shown in Table 2. The reliability of the susceptibility map enables us to assign a data weight of 50 (since the prior weights were estimated using past data from El Hierro) accounting for the uncertainties in the data catalogue. For this reason, we felt very confident in the initial distribution of the prior weights and any new evidence is likely to confirm them. Of the two historical events, one was in zone 5 (2011–2012 eruption). This unrest lasted 4 months before leading to an eruption which was fully monitored by the Instituto Geográfico Nacional (López et al., 2012). The other one refers to the 1793 seismic unrest whose location is uncertain, although historical documents describe it as being in the north-west submarine area, i.e. zone 5.

7.5 Node 5: composition

From the pre-historical set of 23 eruptions shown in Table 1, 87 % correspond to mafic events and 13 % to felsic events.

As we were aware of the incompleteness of the data catalogue, especially in the oldest part, we were not confident if this was indeed the proportion for the composition of prior weights. Some – or many – felsic eruptions may not be documented for example, the Malpaso member, a felsic explosive eruption, has been identified on the upper part of El Golfo–Las Playas volcano (Pedrazzi et al., 2014) but was not included in our catalogue because we lack a precise date. The prior weights are not random, as they are based on well-documented data. For this reason, we assigned an epistemic uncertainty of 10 to our data weights so that if new evidence arrives, these prior values are still accounted for (but more so if there is new evidence), thereby ensuring that any new data will contribute significantly to updating our prior beliefs.

7.6 Node 6: size

The erupted volume of magma on the Canary Islands typically ranges from 0.001–0.2 km³ (DRE) (Sobradelo et al., 2011). Due to a lack of accurate volume data, we assumed that volume values on El Hierro were of the same order as in most of the historical eruptions in the Canaries. The last eruption (2011–2012) was characterised by lava flows of medium extent with VEI 2 and so, by using this information, we were able to assign the weights for VEI 1, VEI 2 and VEI 3, as 0.31, 0.62 and 0.07, respectively.

In the particular case of El Hierro, we observed cases of hydrovolcanic episodes associated with PDC. This would imply VEI sizes that are greater than those on which these prior weights are estimated. Furthermore, the data documented in Sobradelo et al. (2011) is based on Magnitude size, as there was not enough information to estimate the corresponding VEI. For this reason and owing to the lack of magnitude information for the catalogue of eruptions on El Hierro, we were not confident of the prior weights assigned and so an epistemic uncertainty value of 1 was the most appropriate, and would also ensure that if new evidence arrives for different sectors, it will contribute significantly to updating our prior knowledge. In this way, we gave more weight to the new evidence than to our prior beliefs.

7.7 Node 7: hazard

Based on past activity, possible eruption products include ballistic ejecta, fallout, PDCs and lava flows with the prior weights shown in Table 2, computed using the 23 pre-historic eruptions in Table 1. Most mafic eruptions generated lava flows and proximal fallout. However, a revision of the deposits generated from past volcanic events also reveals that some eruptions located close to the coastline correspond to hydrovolcanic episodes generating PDC deposits. In a similar way, some of the hydrovolcanic deposits found on land near the coast in fact originated from very shallow submarine eruptions. Thus, there is reason to include in subzone b (Fig. 3) both coastal and offshore zones to a maximum depth

of 200 m, based on the assumption that vents located in these subzones could generate hydrovolcanic phases and produce PDCs.

Of all the possible hazard products, we were confident that ballistic ejecta, fallout, PDCs and lava flows could occur and so we gave zero weight to the remaining options (lahar, debris avalanche and others). However, for the same reasons given for the composition weights (felsic vs. mafic), we assigned a value of 10 to the epistemic uncertainties, as these data weights could change if we had a more complete data catalogue; however, they are still not completely uninformative, as they are based on past records. In this way, we ensure that new evidence will be well accounted for in new updates and that prior weights are not fully dropped when this new evidence arrives.

7.8 Node 8: extent

Extent refers to the distance reached by eruption products (lava flows, ballistic ejecta, fallout and PDCs) from eruption points that can be deduced from the geological record. The extent of products from the eruptions documented on El Hierro is comparable to those on the rest of the Canary Islands. We considered small distances for those short lava flows that reach up to 5 km, medium distances (5–15 km) for PDC deposits, ballistics and lava flows that reach the sea, and large extent mainly for fall out deposits that can expand more than 15 km. As with the previous node, on the basis of data from the oldest eruptions (Table 1), 87% of extents are small, while 9% are medium and 4% large. We assigned a positive weight to a scenario that gives rise to a large extent of products that will account for the potentially more explosive eruptions seen in the geological record that relate to felsic eruptions or even hydromagmatic eruptions. For the same reasons given for the previous node, we assigned an epistemic value of 10 to all branches.

8 Results

Columns 6 and 7 in Table 2 show the output from HASSET. Although we started with 28 time windows with no unrest, the posterior probability of unrest in the next 20 years is significantly large (64%; 36% for no unrest), due to the high value of the data weight. The same effect occurs with the node location, in which the posterior probabilities remain in the same proportion as the prior weights. The episode of seismic unrest in 1793 has updated our prior beliefs from 2 to 8%, given that we assigned low confidence levels to the initial values. In general, comparing columns 4 and 6 in Table 2, we can see how past data can significantly change the prior probabilities for which we assumed low confidence (10 or less – large epistemic uncertainty), while prior weights assigned with high confidence remain consistent after new evidence is entered in the model.

Looking at the different scenarios (as a combination of the first nodes and branches up to node location) (Table 3a), we see that the 5 most likely scenarios are a basaltic eruption with magmatic unrest in zones 5, 3, 1, 4 and 2 (in that order) with probabilities of occurrence over the next 20 years of 0.11 ± 0.04 , 0.10 ± 0.03 , 0.06 ± 0.02 , 0.05 ± 0.02 and 0.02 ± 0.01 , respectively, for any VEI and any type of hazard or extent. However, although some of these estimates have a large standard deviation due to sizeable uncertainties in the input data, they are consistent with observations from the past. Thus, using the information in the data catalogue, we estimated the long-term probability of a basaltic eruption with magmatic unrest in zone 5 (submarine area) occurring in the next 20 years to be 0.11 ± 0.04 .

If we now look at the most likely scenarios that also include size, hazard and the extent of the eruption, the five next most likely scenarios are basaltic eruptions of VEI 2 with magmatic unrest that generate short lava flows. However, in this case zone 2 is no longer among the 5 most likely scenarios and an eruption in zone 5 with a VEI of 1 or less becomes the fifth most likely to occur in the next 20 years (probability of 0.01 ± 0.01). Once again, the standard deviation for these estimates is large, implying that the variability due to uncertainties in the input data is also large. In this case, we estimated that the most probable scenario (0.04 ± 0.02) is a submarine (zone 5) mafic magmatic eruption of VEI 2 generating short lava flows.

9 Eruptive scenarios

Hazard assessment must be based on the simulation of different volcanic processes across the susceptibility map (e.g. Martí et al., 2012). In order to illustrate potential future eruptions on El Hierro, we simulated scenarios assuming the results obtained with HASSET and considering the most probable hazards (i.e. lava flows, fallout and PDCs) that could occur in the event of such eruptions. We mainly considered eruptions that occur on land or in shallow submarine environments (at a depth of less than 200 m) (Fig. 3). We did not consider deeper submarine eruptions even though their socio-economic impact may in fact not be negligible, as seen in the 2011–2012 eruption. However, we assumed that the direct impact of hazards caused by these deeper submarine eruptions on the island was not relevant for the purpose of this study.

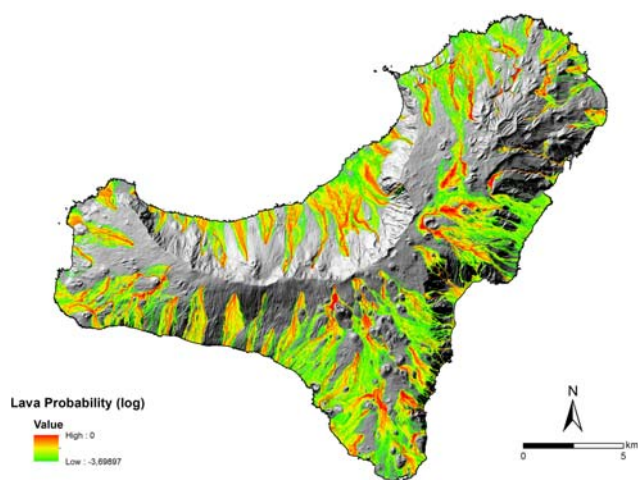
For the simulations we used light detection and ranging (LIDAR) technology based on the digital elevation model (DEM) of the island with a cell size of 10 m generated by the National Geographic Institute (IGN).

10 Lava flow scenarios

Bearing in mind the previously obtained susceptibility values (Fig. 2) (Becerril et al., 2013), we simulated lava flow

Table 3. (a) Most likely scenarios for node location. (b) Most likely scenarios for node extent.

Scenario	Probability estimate	Standard deviation
(a)		
1. Yes-magmatic-magmatic eruption-Zone 5	0.11	0.04
2. Yes-magmatic-magmatic eruption-Zone 3	0.10	0.03
3. Yes-magmatic-magmatic eruption-Zone 1	0.06	0.02
4. Yes-magmatic-magmatic eruption-Zone 4	0.05	0.02
5. Yes-magmatic-magmatic eruption-Zone 2	0.02	0.01
(b)		
1. Basaltic eruption with magmatic unrest in zone 5, VEI 2, that generates lava flows of short extent	0.04	0.02
2. Basaltic eruption with magmatic unrest in zone 3, VEI 2, that generates lava flows of short extent	0.04	0.02
3. Basaltic eruption with magmatic unrest in zone 1, VEI 2, that generates lava flows of short extent	0.02	0.01
4. Basaltic eruption with magmatic unrest in zone 4, VEI 2, that generates lava flows of short extent	0.02	0.01
5. Basaltic eruption with magmatic unrest in zone 5, VEI ≤ 1 , that generates lava flows of short extent	0.01	0.01

**Figure 4.** Lava flow scenarios for El Hierro performed with VORIS 2.0.1. Vents from lava flows that have been simulated represent those with the highest spatial probabilities (see susceptibility map in Fig. 2). Red colours are those areas with the highest probability to be invaded by lava flows.

scenarios taking into account only those pixels located on land (lava flows generated in submarine eruptions, even in shallow waters, were assumed not to cause any direct impact on the island). Lava flow simulations based on VORIS 2.0.1 rely on a probabilistic model that assumes that topography is the most important factor in determining the path of a lava flow (Felpeto et al., 2007 and references therein). As

explained before, simulations of lava flows were conducted on land and are based on the pixels that lie on the different spatial probability values ranging from 0.00037 to 0.0068.

In the model, the input parameters for the lava flows were constrained by maximum flow lengths and thicknesses taken from field measurements. Considering that most lava flows in the past reached the sea, we assumed flow lengths of about 15 km. The thickness used as input for the models was 3 m, which was obtained from the average value of individual flows measured in the field. The results provide a map that gives the probability that any particular cell is invaded by a lava flow (Fig. 4).

11 Scenarios for pyroclastic density currents (PDCs)

The pyroclastic density currents (PDCs) identified on El Hierro are all associated with hydrovolcanic episodes and mostly relate to mafic vents located in the coastal zone, or episodes occurring at shallow submarine depths that generated deposits that are now exposed along the coast. However, we also considered the possibility that this type of explosive episode could occur on land with more evolved compositions and larger run-out distances, as is the case of the Malpaso member identified in the centre of the island (Pedrazzi et al., 2014). PDCs were simulated with an energy cone model (Sheridan and Malin, 1983) using as input parameters topography, the collapse equivalent height (H) and the collapse equivalent angle (θ), which is obtained through the

arctangent of the ratio between H_c and L , where L represents the run-out length (Felpeto et al., 2007; Toyos et al., 2007). Run-out distances were considered to be equivalent to the most distal exposure of PDC deposits found on the island, which were calculated to have lengths of 5, 1 and 0.5 km. These distances are relative to the most distal deposits of the studied PDCs.

Collapse equivalent heights were chosen in the range of 250–300 m above the possible vent site in order to constrain the best H_c that matches real deposits. Based on the calibration, a collapse equivalent of 250 and an angle of 11° were determined for a pyroclastic flow deposit, resembling the known Malpaso member felsic flow deposit. For those vents located in the coastal zone or associated with mafic eruptions, we simulated PDCs with a collapse equivalent of 250 m and angles in the range of around 4 – 27° (low values for base surge explosions and high values for column collapse phases) (Sheridan and Malin, 1983). Although the topography of the area has been modified since the eruption of the Malpaso member, the area and extent of the simulated deposits were still similar to the real PDC deposit. With these constraints, PDC simulations were carried out in the areas with the highest spatial probabilities (Fig. 5a). The areas close to the PDC deposits of El Hierro were also selected to simulate scenarios (Fig. 5b). Figure 5a and b show coverage areas with different Heim coefficients and VEI values.

12 Fallout

Fallout from the eruptions on El Hierro was simulated by assuming a violent Strombolian eruption (e.g. Tanganasoga eruption, Fig. 1), characterised by the formation of an eruptive column up to 10 km high (Arrighi et al., 2001), having significant impacts over distances of several tens of kilometres from the vent (Valentine and Gregg, 2008), which would represent one of the most probable high intensity eruptions that could occur on the island. Nevertheless, we do not rule out the possibility of a subplinian eruption, characterised by columns ranging between 10 and 20 km altitude, having potential impacts over much larger regions and even globally (Valentine and Gregg, 2008 and references therein) in the event that more felsic magmas are involved in the process. Simulations were conducted using an advection-diffusion model based on the assumption that particle motion is controlled by advection from wind, particle diffusion and their terminal settling velocity (Pfeiffer et al., 2005; Felpeto et al., 2007). All the simulations were conducted with one vent located in the highest spatial probability area and another on the eastern side of the island, the most vulnerable area for a volcanic event and where the main villages, airport and port are situated.

Data inputs of wind profiles were compiled from the University of Wyoming Department of Atmospheric Science sounding database (<http://weather.uwyo.edu/upperair/>

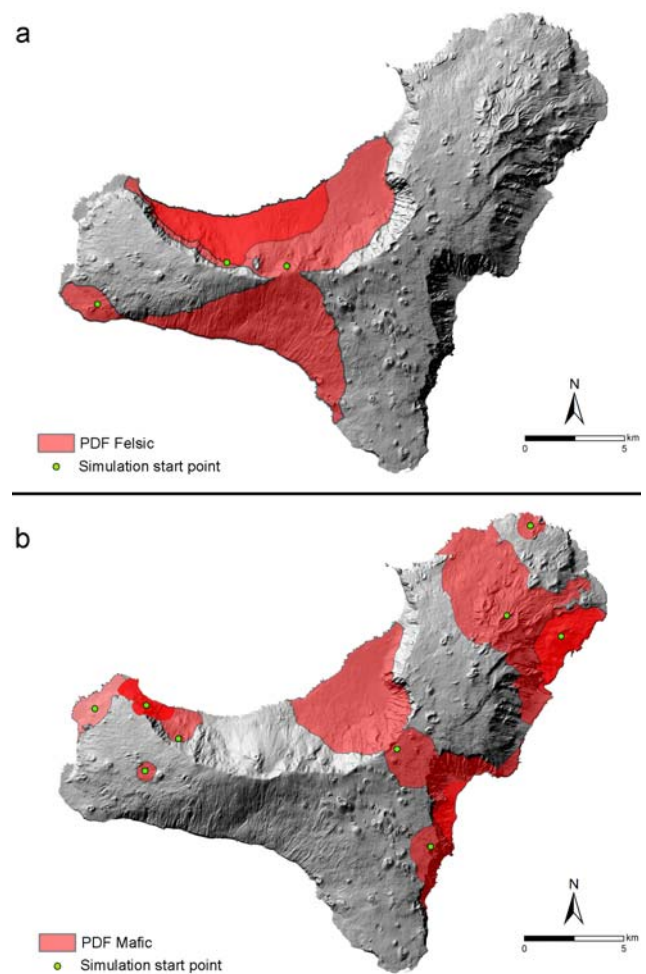


Figure 5. PDC scenarios performed with VORIS 2.0.1. Covered areas with different collapse equivalent heights (H_c), collapse equivalent angles (θ) and VEI values (see the text for more detail). **(a)** VEI 2 corresponding to felsic eruptions; **(b)** VEI 1 corresponding to mafic eruptions.

sounding.html). We focused the attention of our study on the fallout scenarios for the average wind value of each season during the last decade. Wind direction and intensity were chosen at different vertical heights (500, 1000, 2000, 4000 and 6000 m).

Input parameters for the simulation were obtained from fieldwork and bibliographic data. Results are shown in Fig. 6, with particle distribution in a 5 km high eruptive column related to a violent Strombolian eruption, generating 0.03 km^3 of deposits. Particle sizes were considered in a range from -6 to 2Φ , thereby covering the entire range of particle sizes observed in the field.

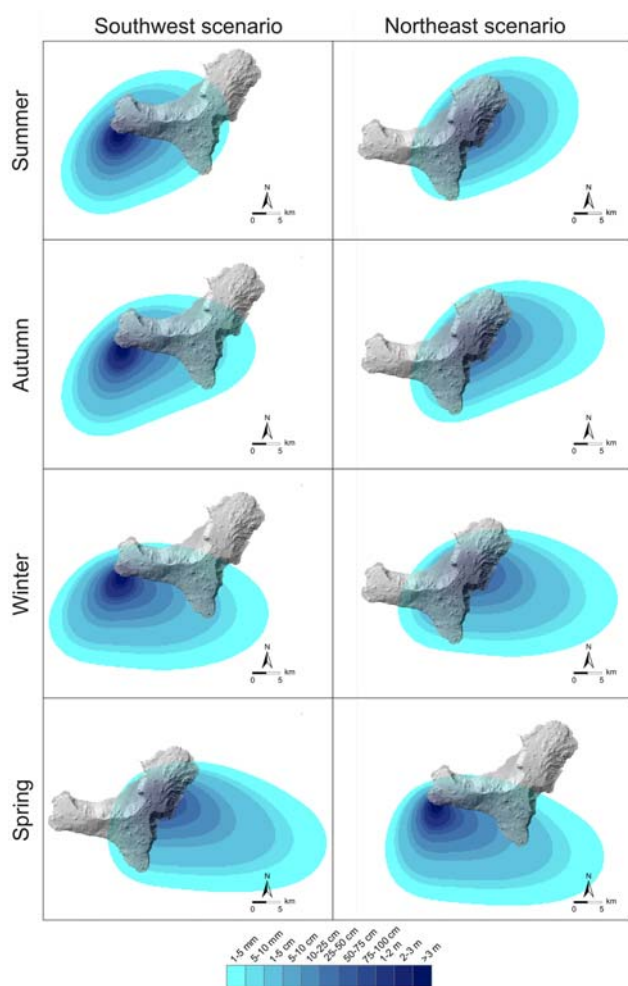


Figure 6. Ashfall scenarios from a violent Strombolian eruption performed with VORIS 2.0.1. (1) Simulation at the highest probability vent; (2) simulation at an area close the main areas of population. Both simulations were performed for summer, autumn, winter and spring.

13 Total hazard map

Combination of the most probable scenarios related to basaltic eruptions of VEI 2 that generate lava flows and PDCs in case of hydrovolcanic events, provided the first total qualitative volcanic hazard map of El Hierro (Fig. 7b). The most probable areas to be affected by the three most likely scenarios were used to define the areas with the greatest and lowest overall volcanic hazard (Fig. 7b). This is an approach similar to that taken by Lindsay et al. (2005) in the Lesser Antilles. We distinguished four levels of hazard depending on the number of individual hazards (Fig. 7a) that overlap on each point (pixel) of the map. The superposition was done taking into account the spatial probability and the extension of each scenario, given more weight to the most probable scenario, i.e. lava flows originating from areas with high spatial vent opening probability. The resulting

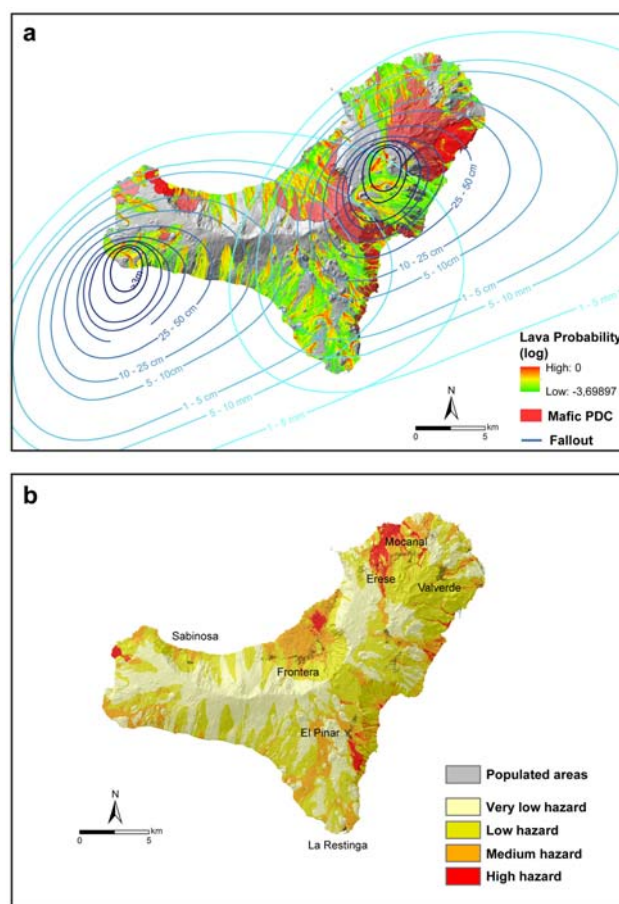


Figure 7. (a) Superposition of the most probable scenarios; (b) qualitative hazard map of El Hierro (zones 1–4) constructed from the combination of the most likely scenarios. This map shows the overall integrated volcanic hazard zones for El Hierro based on lava flows, PDCs and ashfall scenarios. We distinguish four levels of hazard, from very low to high hazard, depending on the number of individual hazards that overlap on each point (pixel) of the map (see text for more explanation).

map shows that, although El Hierro is not a highly populated island, some medium- and high-volcanic-hazard zones coincide with some of the main inhabited areas. However, it must be noted that this hazard level delineation is reliant on the current information, which may be subject to further revision thus implying possible changes in the hazard assessment.

14 Discussion and conclusions

Mafic monogenetic eruptions (Table 1) are the most common eruption type to have occurred in El Hierro's recent geological past, especially over the last 158 ka (Pellicer, 1977, 1979). Consequently, we assume that they also represent the most likely eruption types in the near future. These eruptions generated small-size cones, lava flows, proximal scoria, fallout

and, occasionally, PDCs. The size of most of these eruptions ranged from typical Strombolian to violent Strombolian (some of them associated with hydrovolcanic phases). In Fig. 7a the most likely expected scenarios on the island are represented together. The presence of a relatively recent eruption of phonolitic composition of medium size called Malpaso member and described as a PDC (Pedrazzi et al., 2014) is also remarkable, as it opens up the possibility that eruptions other than monogenetic magmatic and/or hydrovolcanic mafic ones may also occur on El Hierro. Although associated with much greater hazard intensities, this type of eruption has a much lower probability of occurrence.

The catalogue of eruptions that have occurred on El Hierro in the last 158 ka is far from complete. This is evident when trying to establish the relative stratigraphy of volcanic deposits, as there are a large number of units of known origin intercalated between the reported units. Although the establishment of a complete volcano-stratigraphy of El Hierro (and, in particular, of its last constructive episode) is still required, the available number of reported eruptions (for which the corresponding geochronology based on radiometric dating exists) is large enough to provide a preliminary volcanic hazard assessment with a sufficient degree of confidence.

The application of available tools such as HASSET (Sobradelo et al., 2014a) and VORIS 2.0.1 (Felpeto et al., 2007), specifically designed to undertake volcanic hazard assessment based on current knowledge of past eruptive activity and using probabilistic methods and simulation models, allows us to obtain an initial long-term hazard assessment, which can be easily updated and improved with the incorporation of new information such as a more complete volcano-stratigraphy and geochronology. This is an essential tool that should enable local authorities to apply more rational territorial planning and to design more adequate emergency plans to face future volcanic crises. The experience gained from the last eruption on El Hierro in 2011–2012 showed that the lack of tools such as the one described in the present study can lead scientific advisors and decision-makers to consider possible eruptive scenarios that have a very low probability of occurrence, whilst ignoring others with a high probability of occurrence – for example, the submarine eruption that in the end turned out to be the true scenario. This lack of any systematic study of past eruptive activity hampered the forecasting of the most probable scenarios and led to a certain confusion regarding the potential outcome of the impending eruption. This in turn affected the way in which information was transmitted to the population and to the scale of the decisions made, some of which were unnecessarily over-protective (Sobradelo et al., 2014b).

The advantage of conducting a probabilistic hazard assessment is that the results obtained can be updated whenever new information becomes available. Such an approach permits work to start even when only a little information exists and then enables results to improve over time. Thus, appropriate mitigation policies can be based on less, but more

precise and realistic information. In the case of El Hierro, despite sufficient knowledge of past eruptive activity, the available information was not structured in a comprehensive way that was easy to manage and be used by decision-makers or even by the scientists who were providing advice. The results obtained in the present study, that is, the development of a probabilistic long-term volcanic hazard assessment that includes dynamic scenarios and a qualitative hazard map (Fig. 7a and b), offer basis on which to build the strategies that are required to successfully face up to and minimise the impact of future volcanic eruptions on the island.

Our approach offers a method that facilitates accomplishing volcanic hazard assessment in a homogeneous and systematic way. The approach is based on the history of the volcano being deduced from the geological record, which allows determining how, where, and when the next eruption could be. Similar approaches have been applied in other volcanic areas where the application of available tools similar to ours have also allowed us to obtain an initial long-term hazard assessment. This is the case of Auckland Volcanic Field in New Zealand (Sandri et al., 2012) or Misti volcano in Peru (Sandri et al., 2014), where a Bayesian approach using BET_VH tool (Marzocchi et al., 2010) and other simulation tools are applied to compute the temporal and spatial probabilities. Our methodology uses different free tools that have been developed to contribute to the long-term hazard assessment, both in spatial (VORIS 2.0.1, Felpeto et al., 2007) and temporal analyses (HASSET, Sobradelo et al., 2014a). The main advantage of using VORIS 2.0.1 is that it creates scenarios of different kind of hazards such as lava flows, PDCs and ashfall. Other works have focused on the simulation of only one scenario using non-free tools (e.g. lava flows for Etna volcano: Cappello et al., 2010, 2011; Tarquini and Favalli, 2010). On the other hand, although some parts of the HASSET tool (that evaluate temporal probabilities) coincide with BET_EF and BET_VH tools presented by Marzocchi et al. (2008, 2010), HASSET is built on a Quantum Gis (QGIS) platform and considers different kinds of unrest episodes (seismic, geothermal, others), and moreover takes into account the kind of outcome (e.g. phreatic explosion and sector failure) and the magma composition, overcoming the limitations of previous event tree models (Sobradelo et al., 2014a). Another important advantage of using these tools is that new data or new model results can be easily included in the procedure to update the hazard assessment. Other works focused on the evaluation of the potential hazards related to a specific kind of hazard of a particular area (e.g. phreatomagmatic volcanic hazards; Németh and Cronin, 2011) could take the advantages of our methodology and implement it in an easy and successful way for future and completeness of volcanic hazard evaluation.

Acknowledgements. This research was partially funded by IGME, CSIC and the European Commission (FT7 Theme: ENV.2011.1.3.3-1; Grant 282759: “VUELCO”), and MINECO grant CGL2011-16144-E. We would like to thank X. Bolós and J. P. Galve for their help in the development of figures. We also want to thank J. Lindlay and K. Németh for their very useful suggestions that have enabled us to significantly improve our manuscript. The English text was corrected by Michael Lockwood.

Edited by: A. Costa

Reviewed by: J. Lindsay and K. Németh

References

- Alcorn, R., Panter, K. S., and Gorsevski, P. V.: A GIS-based volcanic hazard and risk assessment of eruptions sourced within Valles Caldera, New Mexico, *J. Volcanol. Geoth. Res.*, 267, 1–14, 2013.
- Anguita, F. and Hernán, F.: A propagating fracture model versus a hot spot origin for the Canary Islands, *Earth Planet. Sc. Lett.*, 27, 11–19, 1975.
- Anguita, F. and Hernán, F.: The Canary Islands origin: a unifying model, *J. Volcanol. Geoth. Res.*, 103, 1–26, 2000.
- Araña, V. and Ortiz, R.: The Canary Islands: Tectonics, magmatism, and geodynamic framework, in: *Magmatism in Extensional Structural Settings and the Phanerozoic African Plate*, edited by: Kampunzu, A. and Lubala, R., Springer, New York, 209–249, 1991.
- Araña, V., Felpeto, A., Astiz, M., García, A., Ortiz, R., and Abella, R.: Zonation of the main volcanic hazards (lava flows and ash fall) in Tenerife, Canary Islands. A proposal for a surveillance network, *J. Volcanol. Geoth. Res.*, 103, 377–391, 2000.
- Arrighi, S., Principe, C., and Rosi, M.: Violent Strombolian and subplinian eruptions at Vesuvius during post-1631 activity, *Bull. Volcanol.*, 63, 126–150, 2001.
- Balcells, R. and Gómez, J. A.: *Memorias y mapas geológicos del Plan MAGNA a escala 1 : 25.000 de las Hojas correspondientes a la isla de El Hierro*, Geol. Surv. of Spain, Madrid, 1997.
- Bartolini, S., Cappello, A., Martí, J., and Del Negro, C.: QVAST: a new Quantum GIS plugin for estimating volcanic susceptibility, *Nat. Hazards Earth Syst. Sci.*, 13, 3031–3042, doi:10.5194/nhess-13-3031-2013, 2013.
- Bebbington, M. and Cronin, S. J.: Spatio-temporal hazard estimation in the Auckland Volcanic Field, New Zealand, with a new event-order model, *Bull. Volcanol.*, 73, 55–72, 2011.
- Becerril, L.: Approach to volcanic hazard and its effects in coastal areas of the Canary Islands, Master’s thesis, Universidad de Las Palmas de Gran Canaria, Las Palmas, Spain, available on line at: <http://hdl.handle.net/10553/4595>, 2009.
- Becerril, L., Cappello, A., Galindo, I., Neri, M., and Del Negro, C.: Spatial probability distribution of future volcanic eruptions at El Hierro Island (Canary Islands, Spain), *J. Volcanol. Geoth. Res.*, 257, 21–30, doi:10.1016/j.jvolgeores.2013.03.005, 2013.
- Bolós, X., Planagumà, L., and Martí, J.: Volcanic stratigraphy of the Quaternary La Garrotxa Volcanic Field (NE Iberian Peninsula), *J. Quaternary. Sci.*, in press, 2014.
- Cappello, A., Del Negro, C. and Vicari, A.: Lava flow susceptibility map of Mt Etna based on numerical simulations, in: *From Physics to Control through an Emergent View*, World Sci. Ser. Nonlin. Sci. B, 5, 201–206, 2010.
- Cappello, A., Vicari, A. M., and Del Negro, C.: Assessment and modeling of lava flow hazard on Mt. Etna volcano, *B. Geofis. Teor. Appl.*, 52, 299–308, 2011.
- Cappello, A., Neri, M., Acocella, V., Gallo, G., Vicari, A., and Del Negro, C.: Spatial vent opening probability map of Mt Etna volcano (Sicily, Italy), *Bull. Volcanol.*, 74, 2083–2094, 2012.
- Cappello, A., Bilotta, G., Neri, M., and Del Negro, C.: Probabilistic modeling of future volcanic eruptions at Mount Etna, *J. Geophys. Res.*, 118, 1925–1935, doi:10.1002/jgrb.50190, 2013.
- Carracedo, J. C., Day, S., Guillou, H., Rodríguez Badiola, E., Canas, J. A., and Pérez-Torrado, F. J.: Hotspot volcanism close to a passive continental margin: the Canary Islands, *Geol. Mag.*, 135, 591–604, 1998.
- Carracedo, J. C., Rodríguez Badiola, E., Guillou, H., de La Nuez, H. J., and Pérez Torrado, F. J.: Geology and Volcanology of the Western Canaries: La Palma and El Hierro, *Estud. Geol.* 57, 171–295, 2001.
- Carracedo, J. C., Guillou, H., Paterne, M., Scaillet, S., Rodríguez Badiola, E., Paris, R., Pérez Torrado, F. J., and Hansen Machín, A.: Análisis del riesgo volcánico asociado al flujo de lavas en Tenerife (Islas Canarias): escenarios previsibles para una futura erupción en la isla, *Estud. Geol.*, 60, 63–93, 2004a.
- Carracedo, J. C., Guillou, H., Paterne, M., Scaillet, S., Rodríguez Badiola, E., Paris, R., Pérez Torrado, F. J., and Hansen, A.: Avance de un mapa de peligrosidad volcánica de Tenerife (escenarios previsibles para una futura erupción en la isla), Servicio de Publicaciones de la Caja General de Ahorros de Canarias (CajaCanarias), Tenerife, 46 pp., 2004b.
- Carracedo, J. C., Pérez Torrado, F. J., Rodríguez Badiola, E., Hansen, A., Paris, R., Guillou, H., and Scaillet, S.: Análisis de los riesgos geológicos en el Archipiélago Canario: Origen, características, probabilidades y tratamiento, *Anuario de Estudios Atlánticos*, 51, 513–574, 2005.
- Chester, D. K., Dibbenb, C. J. L., and Duncanc, A. M.: Volcanic hazard assessment in western Europe, *J. Volcanol. Geoth. Res.*, 115, 411–435, 2002.
- Connor, C. B. and Connor, L. J.: Estimating spatial density with kernel methods, in: *Volcanic and Tectonic Hazard Assessment for Nuclear Facilities*, edited by: Connor, C. B., Chapman, N. A., Connor, L. J., Cambridge University Press, 346–368, 2009.
- Crisi, G. M., Iovine, G., Di Gregorio, S., and Lupiano, V.: Lava-flow hazard on the SE flank of Mt. Etna (Southern Italy), *J. Volcanol. Geoth. Res.*, 177, 778–796, 2008.
- Felpeto, A.: Modelización física y simulación numérica de procesos eruptivos para la generación de mapas de peligrosidad volcánica, Ph.D. thesis, University of Madrid, Madrid, Spain, 250 pp., 2002.
- Felpeto, A., Araña, V., Ortiz, R., Astiz, M., and García, A.: Assessment and modelling of lava flow hazard on Lanzarote (Canary Islands), *Nat. Hazards*, 23, 247–257, 2001.
- Felpeto, A., Martí, J., and Ortiz, R.: Automatic GIS-based system for volcanic hazard assessment, *J. Volcanol. Geoth. Res.*, 166, 106–116, doi:10.1016/j.jvolgeores.2007.07.008, 2007.
- Fournier d’Albe, E. M.: Objectives of volcanic monitoring and prediction, *J. Geol. Soc. Lond.*, 136, 321–326, 1979.

- Fúster, J. M., Hernán, F., Cendrero, A., Coello, J., Cantangrel, J. M., Ancochea, E., and Ibarrola, E.: Geocronología de la isla de El Hierro (Islas Canarias), *Boletín de la Real Sociedad Española de Historia Natural*, (Geología), 88, 86–97, 1993.
- Gee, M. J. R., Masson, D. G., Watts, A. B., and Mitchell, N. C.: Offshore continuation of volcanic rift zones, El Hierro, Canary Islands, *J. Volcanol. Geoth. Res.*, 105, 107–119, doi:10.1016/S0377-0273(00)00241-9, 2001.
- Gómez-Fernández, F.: Desarrollo de una Metodología para el Análisis del Riesgo Volcánico en el marco de un Sistema de Información Geográfica, Ph.D. thesis, University of Madrid, Madrid, Spain, 255 pp., 1996.
- Guillou, H., Carracedo, J. C., Pérez-Torrado, F. J., and Rodríguez Badiola, E.: K-Ar ages and magnetic stratigraphy of a hotspot-induced, fast grown oceanic island: El Hierro, Canary Islands, *J. Volcanol. Geoth. Res.* 73, 141–155, 1996.
- Hernández Pacheco, A.: Sobre una posible erupción en 1793 en la Isla del Hierro (Canarias), *Estud. Geol.*, 38, 15–25, 1982.
- Hill, D. P., Dzurisin, D., Ellsworth, W. L., Endo, E. T., Galloway, D. L., Gerlach, T. M., Johnston, M. S. J., Langbein, J., McGee, K. A., Miller, C. D., Oppenheimer, D., and Sorey, M. L.: Response plan for volcano hazards in the Long Valley Caldera and Mono craters region California, *Bull. Geol. Surv.*, 65, 2185, 2001.
- Hoernle, K. and Schmincke, H. U.: The role of partial melting in the 15 Ma geochemical evolution of Gran Canaria: a blob model for the Canary hotspot, *J. Petrol.*, 34, 599–626, 1993.
- Hoernle, K., Zhang, Y. S., and Graham, D.: Seismic and geochemical evidence for large-scale mantle upwelling beneath the eastern Atlantic and western and central Europe, *Nature*, 374, 34–39, 1995.
- Kereszturi, G. and Németh, K.: Monogenetic Basaltic Volcanoes: Genetic Classification, Growth, Geomorphology and Degradation, in: *Updates in Volcanology-New Advances in Understanding Volcanic Systems*, edited by: Németh, K., InTech, 3–88, doi:10.5772/51387, 2012.
- Kereszturi, G., Németh, K., Cronin, S. J., Agustín-Flores, J., Smith I. E. M., and Lindsay, J.: A model for calculating eruptive volumes for monogenetic volcanoes – Implication for the Quaternary Auckland Volcanic Field, New Zealand, *J. Volcanol. Geoth. Res.*, 266, 16–33, 2013.
- Kilburn, C. R. J.: Multiscale fracturing as a key to forecasting volcanic eruptions, *J. Volcanol. Geoth. Res.*, 125, 271–289, 2003.
- Klügel, A., Hansteen, T. H., van den Bogaard, P., Strauss, H., and Hauff, F.: Holocene fluid venting at an extinct Cretaceous seamount, Canary archipelago, *Geology*, 39, 855–858, 2011.
- Le Bas, M. J., Rex, D. C., and Stillmann, C. J.: The early magmatic chronology of Fuerteventura, Canary Islands, *Geol. Mag.*, 123, 287–298, 1986.
- Le-Pichon, X. and Fox, P. J.: Marginal offsets, fracture zones, and the early opening of the North Atlantic, *J. Geophys. Res.*, 76, 2156–2202, doi:10.1029/JB076i026p06294, 1971.
- Lindsay, J. M., Robertson, R., Shepherd, J., and Ali, S.: Volcanic Hazard Atlas of the Lesser Antilles, Trinidad and Tobago, The Seismic Research Unit, University of the West Indies, Trinidad and Tobago, 1–47, 2005.
- Lirer, L., Petrosino, P., and Alberico, I.: Volcanic hazard assessment at volcanic fields: the Campi Flegrei case history, *J. Volcanol. Geoth. Res.*, 101, 55–75, 2001.
- Longpré, M. A., Chadwick, J. P., Wijbrans, J., and Iping, R.: Age of the El Golfo debris avalanche, El Hierro (Canary Islands): New constraints from laser and furnace $^{40}\text{Ar}/^{39}\text{Ar}$ dating, *J. Volcanol. Geoth. Res.*, 203, 76–80, 2011.
- López, C., Blanco, M. J., Abella, R., Brenes, B., Cabrera-Rodríguez, V. M., Casas, B., Domínguez-Cerdeña, I., Felpeto, A., Fernández de Villalta, M., Del Fresno, C., García, O., García-Arias, M. J., García-Canada, L., Gomis-Moreno, A., González-Alonso, E., Guzmán-Pérez, J., Iribarren, I., López-Díaz, R., Luengo-Oroz, N., Meletlidis, S., Moreno, M., Moure, D., Pereda de Pablo, J., Rodero, C., Romero, E., Sainz-Maza, S., Sentre-Domingo, M. A., Torres, P. A., Trigo, P., and Villasante-Marcos, M.: Monitoring the unrest of El Hierro (Canary Islands) before the onset of the 2011 Submarine Eruption, *Geophys. Res. Lett.*, 39, L13303, doi:10.1029/2012GL051846, 2012.
- Marinoni, L. B. and Pasquaré, G.: Tectonic evolution of the emergent part of a volcanic ocean island: Lanzarote, Canary Islands, *Tectonophysics*, 239, 111–137, doi:10.1016/0040-1951(94)90110-4, 1994.
- Martí, J. and Felpeto, A.: Methodology for the computation of volcanic susceptibility. An example for mafic and felsic eruptions on Tenerife (Canary Islands), *J. Volcanol. Geoth. Res.* 195, 69–77, doi:10.1016/j.jvolgeores.2010.06.008, 2010.
- Martí, J., Sobradelo, R., Felpeto, A., and García, O.: Eruptive scenarios of phonolitic volcanism at Teide-Pico Viejo volcanic complex (Tenerife, Canary Islands), *Bull. Volcanol.*, 74, 767–782, doi:10.1007/s00445-011-0569-6, 2012.
- Martí, J., Pinel, V., López, C., Geyer, A., Abella, R., Tárraga, M., Blanco, M. J., Castro, A., and Rodríguez, C.: Causes and mechanisms of El Hierro submarine eruption (2011–2012) (Canary Islands), *J. Geophys. Res.*, 118, 1–17, doi:10.1002/jgrb.50087, 2013.
- Martin, A. J., Umeda, K., Connor, C. B., Weller, J. N., Zhao, D., and Takahashi, M.: Modeling long-term volcanic hazards through Bayesian inference: an example from the Tohoku volcanic arc Japan, *J. Geophys. Res.*, 109, B10208, doi:10.1029/2004JB003201, 2004.
- Marzocchi, W., Sandri, L., and Furlan, C.: A quantitative model for volcanic hazard assessment, in: *Statistics in Volcanology*, edited by: Mader, H. M., Coles, S. G., Connor, C. B., and Connor, L. J., Special Publication of IAVCEI, Geological Society of London, London, 2006.
- Marzocchi, W., Sandri, L., and Selva, J.: BET_EF: A probabilistic tool for long- and short-term eruption forecasting, *Bull. Volcanol.*, 70, 623–632, doi:10.1007/s00445-007-0157-y, 2008.
- Marzocchi, W., Sandri, L., and Selva, J.: BET_VH: a probabilistic tool for long-term volcanic hazard assessment, *Bull. Volcanol.*, 72, 705–716, 2010.
- Németh, K.: Monogenetic Volcanic Fields: Origin, Sedimentary Record, and Relationship with Polygenetic Volcanism, in: *What Is a Volcano? Gsa Special Papers Volume 470*, edited by: Cañón-Tapia, E. and Szakács, A., Geological Society of America, Boulder, Colorado, 43–67, 2010.
- Németh, K. and Cronin, S. J.: Drivers of explosivity and elevated hazard in basaltic fissure eruptions: The 1913 eruption of Ambrym Volcano, Vanuatu (SW-Pacific), *J. Volcanol. Geoth. Res.*, 201, 194–209, 2011.

- Newhall, C. G. and Hoblitt, R. P.: Constructing event trees for volcanic crisis, *Bull. Volcanol.*, 64, 3–20, doi:10.1007/s004450100173, 2002.
- Newhall, G. G. and Self, S.: The Volcanic Explosivity Index (VEI): An estimate of explosive magnitude of historic eruptions, *J. Volcanol. Geoth. Res.*, 87, 1231–1238, 1982.
- Pareschi, M. T., Cavarra, L., Favalli, M., Giannini, F., and Meriggi, A.: GIS and Volcanic Risk Management, *Nat. Hazards*, 21, 361–379, 2000.
- Pedrazzi, D., Becerril, L., Martí, J., Meletlidis, S., and Galindo, I.: Explosive felsic volcanism on El Hierro (Canary Islands), *Bull. Volcanol.*, in press, 2014.
- Pellicer, M. J.: Estudio volcanológico de la isla de El Hierro (Islas Canarias), *Estud. Geol.*, 33, 181–197, 1977.
- Pellicer, M. J.: Estudio geoquímico del vulcanismo de la isla de El Hierro, Archipiélago Canario, *Estud. Geol.*, 35, 15–29, 1979.
- Pérez-Torrado, F. J., Rodríguez-González, A., Carracedo, J. C., Fernández-Turiel, J. L., Guillou, H., Hansen, A., and Rodríguez Badiola, E.: Edades C-14 Del Rift ONO de El Hierro (Islas Canarias), in: *El Cuaternario en España y Áreas Afines, Avances en 2011*, edited by: Turu, V. and Constante, A., Asociación Española para el Estudio del Cuaternario (AEQUA), Andorra, 101–104, 2011.
- Pérez-Torrado, F. J., Carracedo, J. C., Rodríguez-González, A., Soler, V., Troll, V. R., and Wiesmaier, S.: La erupción submarina de La Restinga en la isla de El Hierro, Canarias: Octubre 2011–Marzo 2012, *Estud. Geol.*, 68, 5–27, doi:10.3989/egol.40918.179, 2012.
- Pfeiffer, T., Costa, A., and Macedonio, G.: A model for the numerical simulation of tephra fall deposits, *J. Volcanol. Geoth. Res.*, 140, 273–294, 2005.
- Phillipson, G., Sobradelo, R., and Gottsmann, J.: Global volcanic unrest in the 21st century: An analysis of the first decade, *J. Volcanol. Geoth. Res.*, 264, 183–196, 2013.
- Rivera, J., Lastras, G., Canals, M., Acosta, J., Arrese, B., Hermida, N., Micallef, A., Tello, O., and Amblas, D.: Construction of an oceanic island: Insights from the El Hierro (Canary Islands) 2011–2012 submarine volcanic eruption, *Geology*, 41, 355–358, doi:10.1130/G33863.1, 2013.
- Robertson, A. H. F. and Stillman, C. J.: Submarine volcanic and associate sedimentary rocks of the Fuerteventura Basal Complex, Canary Islands, *Geol. Mag.*, 116, 203–214, 1979.
- Rodríguez-González, A.: El Vulcanismo Holoceno de Gran Canaria: Aplicación de un sistema de Información Geográfica, Ph.D. thesis, University of Las Palmas de Gran Canaria, Las Palmas de Gran Canaria, Spain, 424 pp., 2009.
- Rodríguez-González, A., Pérez-Torrado, F. J., Fernández-Turiel, J. L., Carracedo, J. C., and Guillou, H.: GIS-based geomorphological modeling of coastal platform-forming eruptions: Montaña del Tesoro volcano (El Hierro, Canary Islands), *Geotemas, Sociedad Geológica de Madrid, Madrid*, 13 pp., 2012.
- Sandri, L., Jolly, G., Lindsay, J., Howe, T., and Marzocchi, W.: Combining long- and short-term probabilistic volcanic hazard assessment with cost-benefit analysis to support decision making in a volcanic crisis from the Auckland Volcanic Field, New Zealand, *Bull. Volcanol.*, 74, 705–723, 2012.
- Sandri, L., Thouret, J. C., Constantinescu, R., Biass, S., and Tonini, R.: Long-term multi-hazard assessment for El Misti volcano (Peru), *Bull. Volcanol.*, 76, 771–797, doi:10.1007/s00445-013-0771-9, 2014.
- Schmincke, H. U.: Volcanic and chemical evolution of the Canary Islands, in: *Geology of the Northwest African continental margin*, edited by: von Rad, U., Hinz, K., Sarnthein, M., and Seibold, E., Springer, Berlin, Heidelberg, New York, 273–306, 1982.
- Schmincke, H. U. and Sumita, M.: *Geological Evolution of the Canary Islands*. Görres-Verlag, Koblenz, Germany, p. 200, 2010.
- Self, S.: The Recent volcanology of Terceira, Azores, *J. Geol. Soc. Lond.*, 132, 645–666, 1976.
- Sheridan, M. F. and Malin, M. C.: Application of computer-assisted mapping to volcanic hazard evaluation of surge eruption: Vulcano, Lipari, Vesuvius. *Explosive Volcanism, J. Volcanol. Geoth. Res.*, 17, 187–202, 1983.
- Sobradelo, R. and Martí, J.: Bayesian event tree for long-term volcanic hazard assessment: Application to Teide-Pico Viejo stratovolcanoes, Tenerife, Canary Islands, *J. Geophys. Res.*, 115, B05206, doi:10.1029/2009JB006566, 2010.
- Sobradelo, R., Martí, J., Mendoza-Rosas, A. T., and Gómez, G.: Volcanic hazard assessment for the Canary Islands (Spain) using extreme value theory, *Nat. Hazards Earth Syst. Sci.*, 11, 2741–2753, doi:10.5194/nhess-11-2741-2011, 2011.
- Sobradelo, R., Bartolini, S., and Martí, J.: HASSET: a probability event tree tool to evaluate future volcanic scenarios using Bayesian inference Presented as a plugin for QGIS, *Bull. Volcanol.*, 76, 770–785, doi:10.1007/s00445-013-0770-x, 2014a.
- Sobradelo, R., Martí, J., Kilburn, C., and López, C.: Probabilistic approach to decision making under uncertainty during volcanic crises, *Nat. Hazards*, submitted, 2014b.
- Stroncik, N. A., Klügel, A., and Hansteen, T. H.: The magmatic plumbing system beneath El Hierro (Canary Islands): constraints from phenocrysts and naturally quenched basaltic glasses in submarine rocks, *Contrib. Mineral. Petrol.*, 157, 593–607, 2009.
- Székely, N., Laj, C., Guillou, H., Kissel, C., Mazaud, A., and Carracedo, J. C.: Geomagnetic paleosecular variation in the Brunhes period, from the island of El Hierro (Canary Islands), *Earth Planet. Sc. Lett.*, 165, 241–253, 1999.
- Tarquini, S. and Favalli, M.: Changes of the susceptibility to lava flow invasion induced by morphological modifications of an active volcano: the case of Mount Etna, Italy, *Nat. Hazards*, 54, 537–546, 2010.
- Toyos, G. P., Cole, P. D., Felpeto, A., and Martí, J.: A GIS-based methodology for hazard mapping of small pyroclastic density currents, *Nat. Hazards*, 41, 99–112, 2007.
- Valentine, G. A.: Eruption column physics, in: *From Magma to Tephra – Modelling Physical Processes of Explosive Volcanic Eruptions*, edited by: Freundt, A., Rosi, M., Elsevier, Amsterdam, 91–138, 1998.
- Valentine, G. A. and Gregg, T. K. P.: Continental basaltic volcanoes – processes and problems, *J. Volcanol. Geotherm. Res.*, 177, 857–873, 2008.
- Van der Bogard, P.: The origin of the Canary Island Seamount Province–New ages of old seamounts, *Scientific Rep.*, 3, 1–7, 2013.

Appendix 5

Volcanic hazard on Deception Island (South Shetland Islands, Antarctica)

Accepted Manuscript

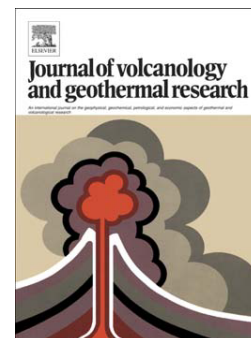
Volcanic hazard on Deception Island (South Shetland Islands, Antarctica)

S. Bartolini, A. Geyer, J. Martí, D. Pedrazzi, G. Aguirre-Díaz

PII: S0377-0273(14)00249-2
DOI: doi: [10.1016/j.jvolgeores.2014.08.009](https://doi.org/10.1016/j.jvolgeores.2014.08.009)
Reference: VOLGEO 5385

To appear in: *Journal of Volcanology and Geothermal Research*

Received date: 22 May 2014
Accepted date: 8 August 2014



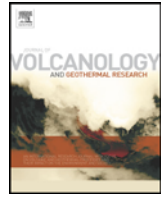
Please cite this article as: Bartolini, S., Geyer, A., Martí, J., Pedrazzi, D., Aguirre-Díaz, G., Volcanic hazard on Deception Island (South Shetland Islands, Antarctica), *Journal of Volcanology and Geothermal Research* (2014), doi: [10.1016/j.jvolgeores.2014.08.009](https://doi.org/10.1016/j.jvolgeores.2014.08.009)

This is a PDF file of an unedited manuscript that has been accepted for publication. As a service to our customers we are providing this early version of the manuscript. The manuscript will undergo copyediting, typesetting, and review of the resulting proof before it is published in its final form. Please note that during the production process errors may be discovered which could affect the content, and all legal disclaimers that apply to the journal pertain.



Contents lists available at ScienceDirect

Journal of Volcanology and Geothermal Research

journal homepage: www.elsevier.com/locate/jvolgeores

Volcanic hazard on Deception Island (South Shetland Islands, Antarctica)

Q14 S. Bartolini^{a,*}, A. Geyer^a, J. Martí^a, D. Pedrazzi^a, G. Aguirre-Díaz^b^a Institute of Earth Sciences Jaume Almera, ICTJA-CSIC, Group of Volcanology, SIMGEO (UB-CSIC), Lluís Solé i Sabarís s/n, 08028 Barcelona, Spain^b Centro de Geociencias, Universidad Nacional Autónoma de México, Campus Juriquilla, Querétaro, Qro. 76230, Mexico

ARTICLE INFO

Article history:
Received 22 May 2014
Accepted 8 August 2014
Available online xxx

Keywords:
Deception Island
Volcanic hazard
Volcanic susceptibility
Bayesian event tree
Eruptive scenarios

ABSTRACT

Deception Island is the most active volcano in the South Shetland Islands and has been the scene of more than twenty identified eruptions over the past two centuries. In this contribution we present the first comprehensive long-term volcanic hazard assessment for this volcanic island. The research is based on the use of probabilistic methods and statistical techniques to estimate volcanic susceptibility, eruption recurrence and the most likely future eruptive scenarios. We perform a statistical analysis of the time series of past eruptions and the spatial extent of their products, including lava flows, fallout, pyroclastic density currents and lahars. The Bayesian event tree statistical method HASSET is applied to calculate eruption recurrence, while the QVAST tool is used in an analysis of past activity to calculate the possibility that new vents will open (volcanic susceptibility). On the basis of these calculations, we identify a number of significant scenarios using the GIS-based VORIS 2.0.1 and LAHARZ software and evaluate the potential extent of the main volcanic hazards to be expected on the island. This study represents a step forward in the evaluation of volcanic hazard on Deception Island and the results obtained are potentially useful for long-term emergency planning.

© 2014 Published by Elsevier B.V.

1. Introduction

Deception Island is the most active volcano in the South Shetland Island group (Antarctica) and more than 20 eruptions have taken place there over the past two centuries (Orheim, 1972; Pallàs et al., 2001; Smellie, 2002a). Located at the spreading centre of the Bransfield Strait marginal basin (Fig. 1), this island consists of a horse-shoe-shaped composite volcanic system truncated by the formation of the collapse caldera that occupies the central part of the island (Valencio et al., 1979; Smellie, 1988; Martí et al., 2013) (Fig. 2a). The most recent eruptions took place in the late 1960s and 1970s and destroyed or severely damaged the scientific bases operating on the island (Baker et al., 1975; Roobol, 1982) (Fig. 3a, b). Interestingly, during the final eruption strong winds and the unusually low tropopause in the area (Smellie, 1999) led to an important spread of volcanic ejecta that reached distances of over 150 km (Pallàs et al., 2001; Fretzdorff and Smellie, 2002; Pedrazzi et al., 2014).

Since its discovery in 1820, the island's natural harbours in Port Foster Bay (e.g. Pendulum Cove and Whalers Bay) (Fig. 2b) have been actively used during different peaks in the commercial exploitation of the Southern Ocean (Roobol, 1982; Smellie and López-Martínez, 2002a,b). Between 1905 and 1930, the island served as the shore base for the Antarctic's most important whaling industry (Fig. 3c) and also played a military role during World War I due to its strategic location

between the Atlantic and Pacific Oceans. This resulted in the construction of a British scientific station, which was occupied from 1944 until it was destroyed in 1969 (Roobol, 1982; Smellie and López-Martínez, 2002a,b) (Fig. 3a). Following the British initiative, Argentina and Chile also established scientific bases on the island that, likewise, were either destroyed or abandoned after the eruptions occurring between 1967 and 1970 (Fig. 3b). After occasional expeditions to Deception Island, Britain, Spain and Argentina recommenced scientific activity in 1986. Argentina re-occupied and reconstructed its station (Fig. 3f), while Spain constructed a new station in 1989 (Fig. 3e); these two scientific bases operate every year during the Antarctic summer.

The number of tourists that visit Antarctica has increased since the first commercial cruise in 1966 and today over 30,000 visitors arrive during the austral summer (2012–2013) (IAATO, *International Association of Antarctica Tour Operators*) (Fig. 4a). Deception Island and Half Moon Island (Fig. 4) are two of the most popular destinations; specifically, the Antarctic Specially Protected Area (ASP) sub-site of Whalers Bay (Fig. 2) receives over 15,000 visitors every year (Fig. 4b), while other sectors such as Telefon Bay or Pendulum Cove (Fig. 2) are visited by up to 5000 tourists annually (Fig. 4b).

The recent eruptions (1967, 1969 and 1970) have demonstrated that volcanic activity on Deception Island may become a cause for concern for tourists, scientists and the military personnel working on or near the island. Livingston and Deception Islands host a total of five research stations and three field camps, while Greenwich and King George Islands are home to 10 all-year and two temporary research stations (Fig. 2). For example, during the 1970 eruption, a considerable amount of ash – including a fine ash fall deposit of 4 mm on Arturo Prat station

* Corresponding author. Tel.: +34 934095410.
E-mail address: sbartolini@ictja.csic.es (S. Bartolini).

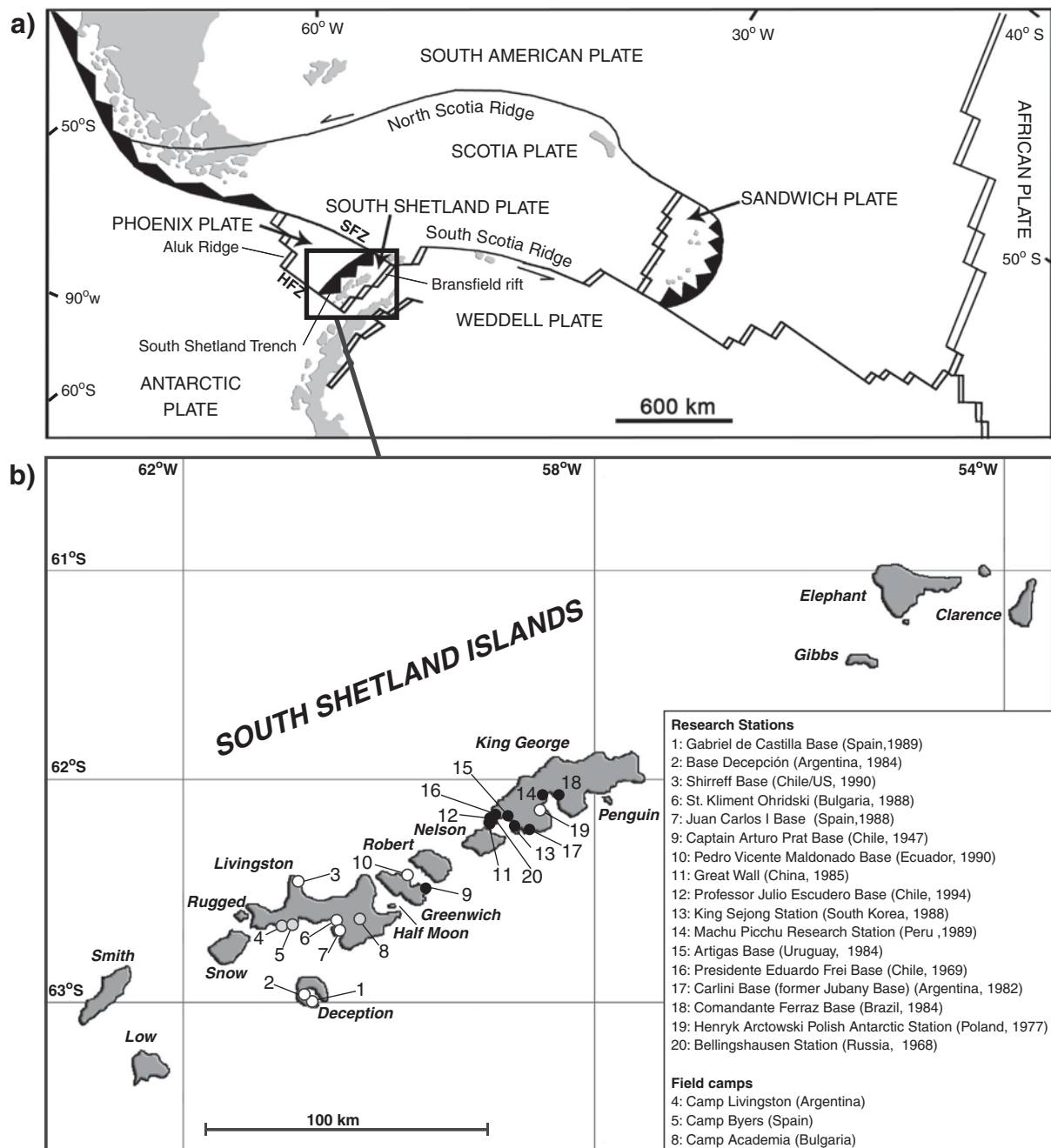


Fig. 1. a) Simplified regional tectonic map and location of the South Shetland Islands. HFZ: Hero Fracture Zone, SFZ: Shetland Fracture Zone. b) Location of Deception Island. Black and white dots indicate nearby year-round and temporary (only austral summer) research stations, respectively. Grey dots correspond to temporary field camps.

Panel a: modified from Ibañez et al. (2003); panel b: modified from Grad et al. (1992).

on Greenwich Island and about 1 mm on Bellingshausen station on King George Island (Baker et al., 1975; Pedrazzi et al., 2014) – fell far from the island.

Aside from a paper by Roobol (1982) and the relatively recent work of Smellie (2002a), to the authors' knowledge no accurate volcanic hazard assessment has ever been conducted for Deception Island. Furthermore, previously hazard maps were either restricted to a single hazard (Roobol, 1982) (Fig. 5a) or were non-systematic (Smellie, 2002a) (Fig. 5b). As pointed out by Smellie (2002a), as a popular destination for tourists and an area of constant scientific research, properly elaborated hazard maps and related assessments are now more necessary than ever. The latter are indispensable for the elaboration of emergency plans aimed at mitigating the potential human and economic losses of any future volcanic eruptions on Deception Island.

In order to improve the hazard assessment on Deception Island, it is important to estimate the temporal and spatial probabilities of future eruptions. In this paper, we carry out a threat analysis for Deception Island using the National Volcano Early Warning System (NVEWS) template (Ewert et al., 2005) and compare it with other volcanoes of similar characteristics. Then, we present a systematic analysis of the temporal and spatial long-term hazard assessment of the island using available geological data, including the past eruption record, stratigraphic information and volcano-structural data. We used HASSET (Sobradelo et al., 2014) to estimate the probability that a volcanic episode will occur within the forecast interval and to evaluate the long-term probability of different types of hazards on the island. For the spatial analysis we applied QVAST (Bartolini et al., 2013) to obtain the susceptibility map, and LAHARZ and VORIS (Hoblitt et al., 1995; Schilling, 1998; 111

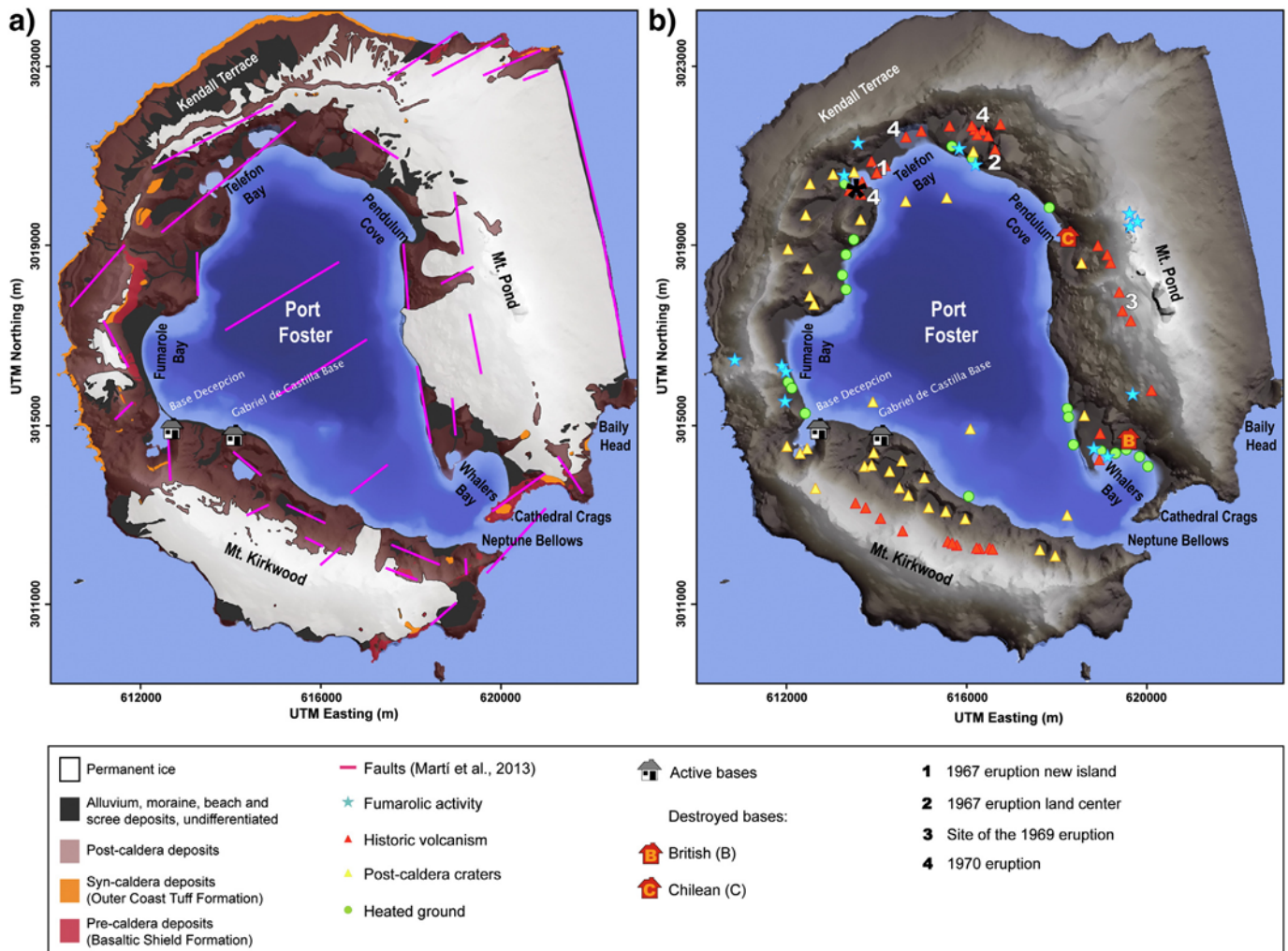


Fig. 2. a) Simplified geological and tectonic map of Deception Island. b) The sites of the historical volcanic vents, observable fumarolic activity and heated ground are also indicated (data obtained from Spatial Data Infrastructure for Deception Island SIMAC, <http://www.simac.uca.es>, Torrecillas et al., 2006). As well as the historical vents, we have identified the post-caldera craters that, while not directly related to historical volcanic eruptions, clearly correspond to post-caldera volcanism.

Q1 Panel a: modified from Martí et al. (2013) and Smellie (2002a,b).

112 Felpeto et al., 2007) to generate different eruptive scenarios such as
 113 lahars, lava flows, pyroclastic density currents (PDCs) and fallout. The
 114 ultimate aim of this work was to generate a qualitative hazard map
 115 for Deception Island depicting the most probable scenarios and, conse-
 116 quently, to understand the potential impact that future eruptions could
 117 have on research stations, tourists, and ships in and around the island.

118 2. Geological setting

119 Deception Island is a sizeable active Quaternary volcano with a large
 120 central collapse caldera that is located at the south-western end of the
 121 Bransfield Strait, a marginal basin lying between the Antarctic Peninsula
 122 and the South Shetland Islands (Fig. 1). The related volcanic ridge
 123 has traditionally been interpreted as a Late Cenozoic extensional struc-
 124 ture produced as a consequence of back-arc spreading (Roach, 1978;
 125 Peccerillo et al., 1991) linked to subduction of the Phoenix Plate beneath
 126 the Antarctic Plate (González-Ferrán, 1985). Deception, Penguin and
 127 Bridgeman islands and a number of other submerged volcanic vents
 128 are associated with the spreading centre. In particular, Deception Island
 129 is located near the intersection between the axis of the Bransfield basin
 130 and the extension of the Hero Fracture Zone (Fig. 1).

131 The construction of the island can be separated into three main
 132 phases: pre-, syn- and post-caldera (Smellie, 2001; Martí et al., 2013).
 133 The first phase was characterised by the construction of the volcanic

shield and is represented by the Basaltic Shield Formation, outcropping
 134 mainly at Baily Head and along the nearly vertical caldera wall at Fuma-
 135 role Bay (Fig. 2a). The Outer Coast Tuff Formation (i.e. syn-caldera phase
 136 deposits) (Hawkes, 1961; Smellie, 2001; Martí et al., 2013) was depos-
 137 ited unconformably over the shield-related units and forms an almost
 138 continuous outcrop along the outer part of the island (Fig. 2a). The
 139 post-caldera phase, which includes the recent historical eruptions,
 140 consists of eruptive vents scattered across the whole island: all but
 141 one are found along the structural borders of the caldera and most cor-
 142 respond to previous regional tectonic faults (Fig. 2a) (Smellie, 2002a;
 143 Martí et al., 2013).
 144

145 The magnetic polarity of the exposed rocks and K–Ar data indicate
 146 that Deception Island is younger than 0.75 Ma (Valencio et al., 1979)
 147 and that its subaerial part has mostly been constructed over the last
 148 0.2 Ma (Keller et al., 1992). Indeed, the correlation between the exposed
 149 rocks and the tephra found elsewhere in the region suggests that these
 150 rocks are probably even younger than 0.1 Ma (Martí et al., 2013).
 151 The age of the collapse event remains unclear due to a lack of geo-
 152 chronological data and the fact that none of the tephra layers
 153 found in the various ice and marine/lacustrine sediment cores ex-
 154 tracted around the Antarctic region appear to correlate with this
 155 event (Smellie, 1999; Pallàs et al., 2001). Since all the tephra related
 156 to the post-caldera volcanism recorded in the region are from the
 157 Middle Holocene or younger (Moreton, 1999; Smellie, 1999), Martí

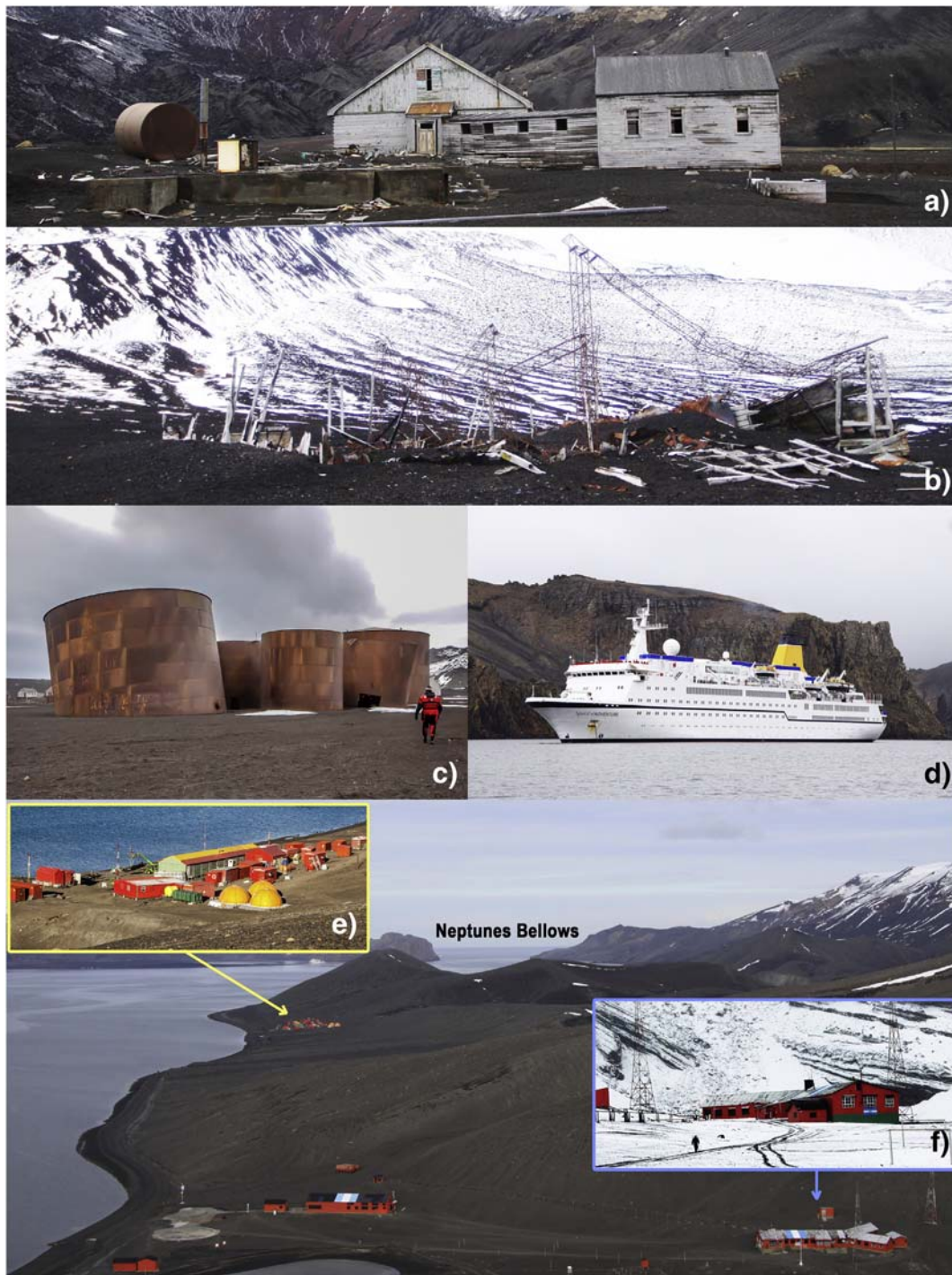


Fig. 3. Remains of the British (a) and Chilean (b) bases in Whalers Bay and Pendulum Cove, respectively (see Fig. 2b for exact locations). Remains of the Norwegian whaling station in Whalers Bay (c). Current Spanish *Gabriel de Castilla* (e) and Argentinian *Base Decepcion* (f) scientific bases (see Fig. 2 for exact locations). (d) Photograph of a tourist cruise ship entering Port Foster through Neptune's Bellows (authors: A. Villaseñor (a), (b) and (d); J. Galeano (c), (e) and (f)).

158 et al. (2013) speculate that the caldera may have formed in the late
159 Pleistocene–early Holocene.

160 3. Recent volcanic activity & volcanic hazards

161 The 1967, 1969 and 1970 eruptions on Deception Island have been
162 well documented (González-Ferrán et al., 1971; Orheim, 1972; Baker
163 et al., 1975; Roobol, 1982; Moreton, 1999; Smellie, 1999, 2002a,
164 2002b; Pedrazzi et al., 2014). First-hand observations exist for the first

two as they occurred during austral summer. The December 1967 165
event created a new island around four aligned vents in Telefon Bay 166
and a land vent located 2.5 km to the east (Fig. 2b). The February 167
1969 eruption occurred when a 4-km-long fissure opened beneath 168
glacial ice along the eastern interior side of the caldera (Smellie, 169
2002a). This activity resulted in catastrophic floods and lahars, and the
170 construction of several small cinder cones (Baker et al., 1975; Smellie,
171 2002b). Unlike the two previous events, there were no eyewitnesses
172 to the 1970 eruption. Ash fell on the Chilean station *Arturo Prat* on 173

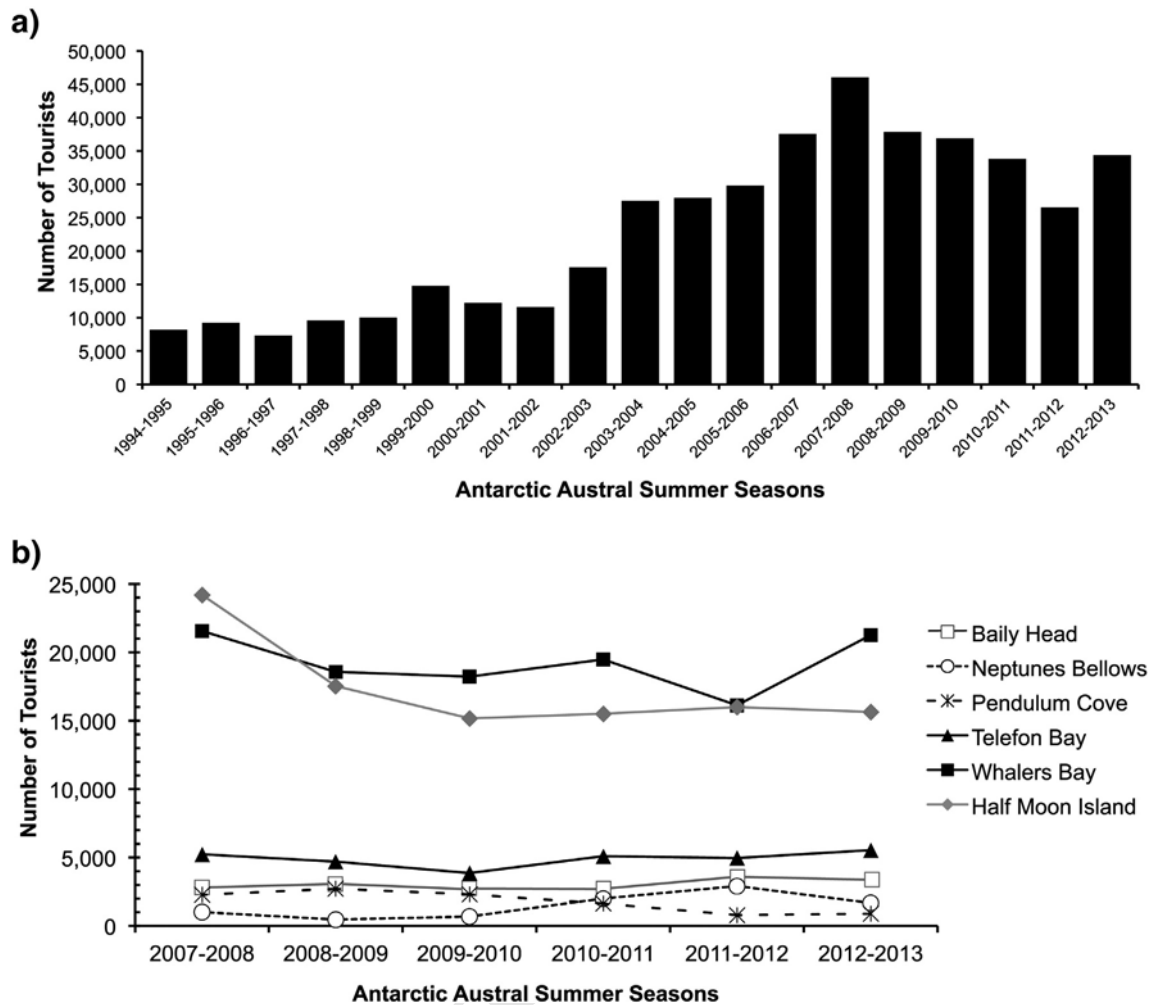


Fig. 4. a) Visitors to Antarctica during the austral summers over the past two decades. b) Amount of visitors to specific Deception Island sites over the last five years. Source: International Association of Antarctica Tour Operators (IAATO, <http://www.iaato.org>).

174 Greenwich Island on August 13, 1970 and during the early morning on
 175 the same day near the Soviet station *Bellingshausen* on the King George
 176 Islands.

177 The tephra record from Deception Island (Orheim, 1972) and
 178 neighbouring islands (Pallàs et al., 2001) and ice and sediment (marine
 179 and lacustrine) cores reveal a series of over 30 post-caldera eruptions
 180 during the Holocene (Tables 1 and 2). However, even the most detailed
 181 record such as that provided by Mt. Pond glacier (Fig. 2a) probably only
 182 records some of the post-caldera eruptions on the island (Orheim, 1972;
 183 Smellie, 2002b) and a considerably higher number of eruptions may
 184 well have occurred. The record of the eruptions from the eight-
 185 teenth to the twentieth centuries includes periods of great activity
 186 (e.g. 1906–1912, 1818–1828) with several temporally closely spaced
 187 eruptions, followed by decades of dormancy (e.g. 1912–1967) (Orheim,
 188 1972; Roobol, 1982; Smellie, 2002b). Despite the inherent difficulties
 189 involved in predicting the date of the next eruption on Deception Island,
 190 it is still reasonable to expect further episodes to occur as part of these
 191 most recent activity cycles (Shultz, 1972). The unrest episodes in 1992
 192 and 1999 demonstrate that the volcanic system is still active (Ibañez
 193 et al., 2003) and, as has been remarked in published research work, the
 194 occurrence of a future eruption on the island cannot be ruled out.

195 All post-caldera volcanisms correspond to eruptions of small volume
 196 (e.g. <0.05 km³ for each of the 1967, 1969, and 1970 eruptions)
 197 and their explosivity will have varied in terms of their consistent
 198 phreatomagmatic nature. The interacting water may be simply seawater
 199 from Port Foster Bay, water from the underground aquifer or even

200 melt water from the glaciers. The presence of Deception Island tephra
 201 in marine sediments in the Scotia Sea (e.g. Moreton and Smellie,
 202 1998) or in ice cores from the South Pole (e.g. Aristarain and Delmas,
 203 1998) suggests that some post-caldera eruptions may have been
 204 much more violent than those experienced in recent centuries.

205 The main direct volcanic hazards identified on Deception Island
 206 include (Smellie, 2002a) ash fall, pyroclastic density currents (mainly
 207 surges), lava flows and lahars, while indirect volcanic hazards
 208 could involve (Smellie, 2002a) steam fields, fumaroles, heated
 209 ground, structural collapses and rock falls, hydrothermal eruptions,
 210 volcanic gases, earthquakes and tsunamis.

211 Due to the strong winds and the unusually low tropopause (8–
 212 10 km) in the area (Smellie, 1999), ash fall deposits – even in historical
 213 eruptions – are rapidly displaced over neighbouring islands and the
 214 Antarctic continent. Indeed, ashes from the latest eruption on Deception
 215 Island were observed on King George Island (>150 km distance) (Baker
 216 et al., 1975). Additionally, numerous layers of Deception Island ash are
 217 preserved in marine sediments in the Scotia Sea (>800 km distance)
 218 (Moreton and Smellie, 1998). Close to the vent, ash fallout can lead to
 219 severe building damage, as in the case of the abandoned Chilean station
 220 at Pendulum Cove (Fig. 3b). This base was covered (and burned down)
 221 by ash from the 1969 fissure eruption, the closest vents of which
 222 were 400–500 m away (Smellie, 2002b). Smellie (2002a) has pointed
 223 out that since the prevailing winds on Deception Island are main-
 224 ly from the west, the eastern side of the island is highly exposed to
 225 ash fall. Nevertheless, during the most recent eruptions, almost the

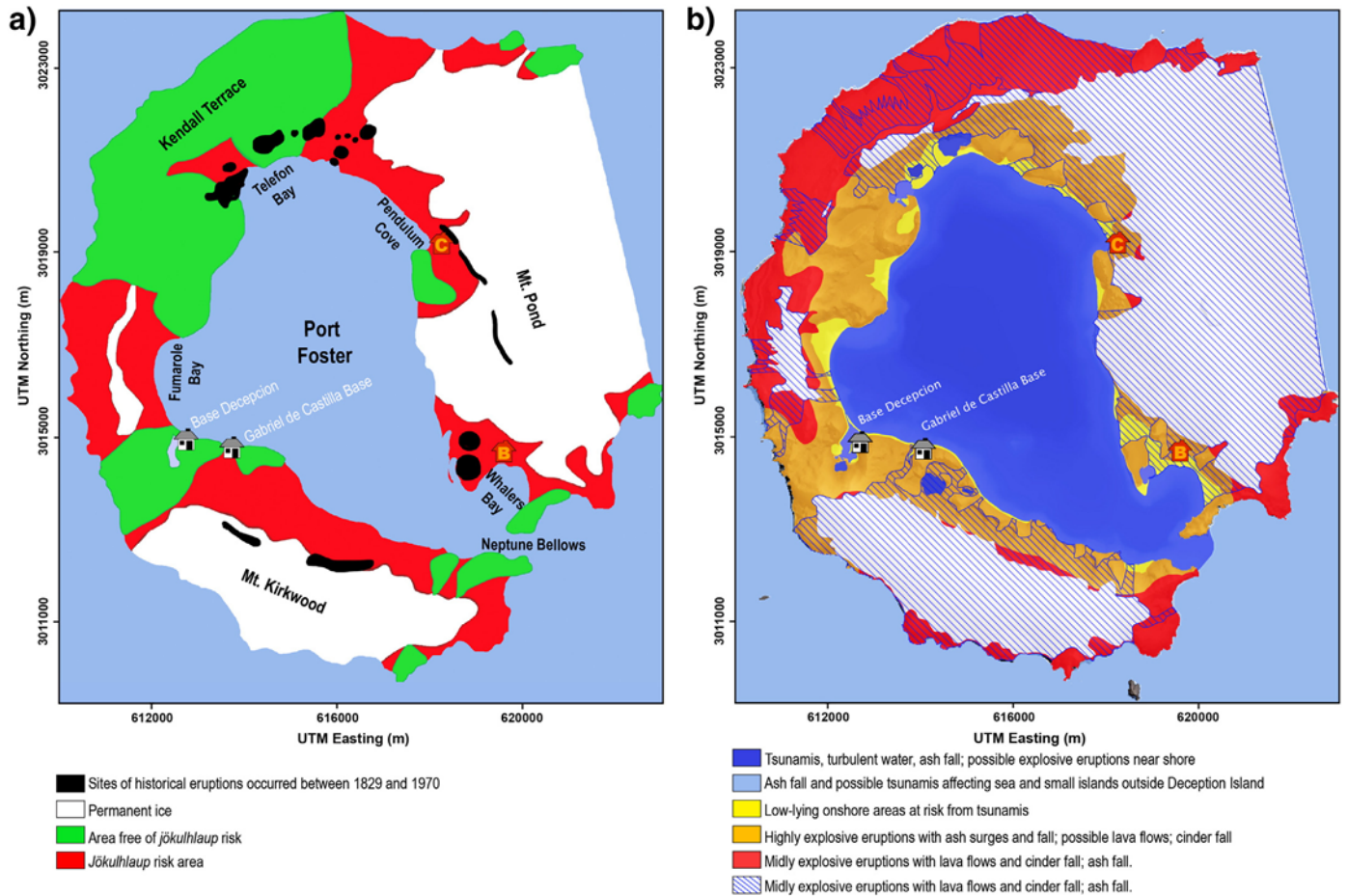


Fig. 5. Hazard maps presented by Roobol (1982)(a) and Smellie (2002a) (b).

entire island received some ash fall (Baker et al., 1975; Smellie, 2002a).

In the first volcanic hazard assessment on Deception Island, Roobol (1982) indicated that there were no relevant pyroclastic flows on the island. Nevertheless, Smellie (2002a) specifies that pyroclastic flows have occurred in the past but were only abundant during the caldera-forming eruption (Outer Coast Tuff Formation). Even so, dilute pyroclastic density currents (i.e. pyroclastic surges) are a characteristic feature of many Deception Island post-caldera eruptions. In most cases, mapped surge deposits extend for about 2 km from the vents (Pedrazzi et al., 2014) and may travel across water (Smellie, 2002a).

Lava fountaining and flows have also been a common feature throughout the eruptive history of the island (Roobol, 1982; Smellie, 2002a). The main hazard related to lava flows is the damage or destruction they cause by burying, crushing or burning as they progress. Even though they tend to be confined to valleys and can be easily outrun, the most important problem is that they can generate *jökulhlaups*, i.e. floods of molten water released from the glacier due to the opening of subglacial vents and the partial melting of the ice cover (Roobol, 1982; Smellie, 2002a,b). In fact, Baker et al. (1975) state that the most recent eruptions demonstrate that these floods are the main hazards to human life and property on the island. The same authors indicate that the most suitable sites for scientific stations on the shores around Port Foster are also the most vulnerable to the effects of this particular hazard.

These lahars or volcanic mudflows consist of substantial volumes of melt water, often highly charged with debris. Their great bulk density and velocity make them highly destructive. In fact, the *jökulhlaups* produced by the 1969 eruption were responsible for the destruction of the British scientific station at Whalers Bay (Baker et al., 1975). Lahars are

characterised by having well-defined topographical limits since they are confined to valleys (Smellie, 2002a). Thus, the location of the eruptive vent, i.e. in ice-free areas or below the permanent ice caps on Mt. Kirkwood and Mt. Pond (Fig. 2b), is crucial for determining the potential hazards to be expected during a future eruption on Deception Island.

Other secondary hazards such as steam fields, fumaroles and ground heating are also common on the island, and are mostly confined to the inside of the caldera along the shores of Port Foster (Baker et al., 1975; Roobol, 1980; Smellie, 2002a) (Fig. 2b). Ground temperatures of $40\text{--}60\text{ }^\circ\text{C}$ are common but at Pendulum Cove and Fumarole Bay, they may reach up to $70\text{ }^\circ\text{C}$ and $100\text{ }^\circ\text{C}$, respectively (Smellie, 2002a). These temperatures fluctuate daily, mainly with the tides. In 1920–21, for example, sudden subsidence of the sea floor beneath Whalers Bay caused the sea to boil and affected the ships in the area (Smellie, 2002a).

Seismicity may also be an issue in the area. During 1992 and 1999, two seismic crises related to episodes of deep magma injection led to the evacuation of the island (Ibañez et al., 2003). In general terms, current activity is characterised by strong hydrothermal circulation and intense seismicity with frequent volcano-tectonic and long-period events (Smellie, 2002a; Zandomenighi et al., 2009).

In addition, tsunamis triggered by eruptions and slope failures have occurred on Deception Island in the past (Smellie, 2002a). This is an important problem since they may block Neptune's Bellows, the only exit from (and entry into) Port Foster and make it difficult or even impossible to sail through this narrow, shallow channel. On a smaller scale, rock falls in strategically important places could cause major problems and, for example, the collapse of Cathedral Crags could block Neptune's Bellows and prevent ships from entering/leaving the island's interior bay (Smellie, 2002a).

t1.1 **Table 1**

t1.2 Principal characteristics of the volcanic eruptions and unrest periods recorded over the last 372 years (1641–2013). Only eruptions of known age and consistent with the relative field stratigraphy established in this study are included. Information about the nodes in the HASSET tool (Sobradelo et al., 2014) is also included. See text for more details.

t1.4	Year	Node 1 Unrest	Node 2 Origin	Node 3 Outcome	Node 4 Location	Node 5 Composition	Node 6 Size	Node 7 Hazard	Node 8 Extent	Source
t1.5	1999	Yes	Geothermal	No eruption	–	–	–	–	–	[1]
t1.6	1992	Yes	Geothermal	No eruption	–	–	–	–	–	[1]
t1.7	1970	Yes	Magmatic	Magmatic	Telefon Ridge	Mafic	3	Ballistic–fall out–PDC	Large	[2] [3]
t1.8	1969	Yes	Magmatic	Magmatic	Mt. Pond	Mafic	3	Lava flow–lahars–PDC	Medium	[3]
t1.9	1967	Yes	Magmatic (?) seismic	Magmatic	Telefon Ridge & Port Foster	Mafic	3	Ballistic–fall out–PDC	Medium	[3] [4]
t1.10	1943 ± 12 ^a	Yes	Magmatic	Magmatic	Mt. Pond	Mafic	≥3	–	–	[5] [6]
t1.11	1918 ± 12	Yes	Geothermal	No eruption	–	–	–	–	–	[7] [8]
t1.12	1915 ± 3	Yes	Magmatic	Magmatic	–	Mafic	3	Ballistic–fall out	Large	[6] [9]
t1.13	1892 ± 64	Yes	Magmatic	Magmatic	Telefon Ridge	–	<3	–	–	[5]
t1.14	1879 ± 49	Yes	Magmatic	Magmatic	Mt. Pond	–	≤3	Ballistic–fall out–lava flow	–	[10]
t1.15	1869 ± 40	Yes	Magmatic	Magmatic	Mt. Pond	Mafic	≤3	–	–	[5]
t1.16	1842	Yes	Magmatic	Magmatic	Mt. Kirkwood	Felsic	2	Lava flow	Small	[7] [11] [12]
t1.17	1838–1839	Yes	Magmatic	Magmatic	Mt. Kirkwood	–	>3	Lava flow	–	[6] [7] [13] [14]
t1.18	1827 ± 2	Yes	Magmatic	Magmatic	Mt. Pond	Mafic	4	–	–	[5] [7] [15] [16]
t1.19	1820 ± 1	Yes	Magmatic	Magmatic	–	Mafic	<3	Ballistic–fall out	Large	[17]
t1.20	1795 ± 5	Yes	Magmatic	Magmatic	Telefon Ridge	–	–	–	–	[5] [7] [15] [16]
t1.21	1750 ± 50	Yes	Magmatic	Magmatic	Mt. Kirkwood	Mafic	≥3	–	–	[6]
t1.22	1700	Yes	Magmatic	Magmatic	–	–	≥3	–	–	[18] [19]
t1.23	1641	Yes	Magmatic	Magmatic	–	Mafic	>3	Ballistic–fall out	Large	[20] [21]

t1.24 [1] Ibañez et al. (2003).

t1.25 [2] González-Ferrán et al. (1971).

t1.26 [3] Baker et al. (1975).

t1.27 **Q2** [4] Valenzuela et al. (1968).

t1.28 [5] Roobol (1973).

t1.29 [6] Pallàs et al. (2001).

t1.30 [7] Roobol (1980).

t1.31 [8] Roobol (1982).

t1.32 [9] Hodgson et al. (1998).

t1.33 [10] Smellie (2002a).

t1.34 [11] Smiley in Wilkes (1845).

t1.35 [12] Hawkes (1961).

t1.36 [13] Whittle in Wilkes (1845).

t1.37 [14] Birkenmajer (1991).

t1.38 [15] Kendall (1831).

t1.39 [16] Pallàs et al. (2001).

t1.40 [17] Palais et al. (1989).

t1.41 [18] Moreton (1999).

t1.42 [19] Smellie (1999).

t1.43 [20] Aristarain and Delmas (1998).

t1.44 **Q3** [21] Delmas (1992).

t1.45 ^a Error according to the time interval provided by the bibliography.

t2.1 **Table 2**

t2.2 Additional geochronological data about the recorded volcanic eruptions on Deception Island between 35,400 B.P. and 450 B.P. This information provides the main characteristics of the eruptive style of the island for the application of the Bayesian Event Tree method.

t2.4	Year (B.P.)	Node 1 Unrest	Node 2 Origin	Node 3 Outcome	Node 4 Location	Node 5 Composition	Node 6 Size	Node 7 Hazard	Node 8 Extent	Source
t2.5	450	Yes	Magmatic	Magmatic	–	Mafic	≥3	–	Large	[1] [2] [3]
t2.6	750	Yes	Magmatic	Magmatic	–	Mafic	≥3	–	Large	[1] [2] [3]
t2.7	1050	Yes	Magmatic	Magmatic	–	Mafic	≥3	–	Large	[2] [3]
t2.8	1350	Yes	Magmatic	Magmatic	–	Mafic	≥3	–	Large	[1] [2] [3]
t2.9	1850	Yes	Magmatic	Magmatic	–	Mafic	≥3	–	Large	[2] [3]
t2.10	2100	Yes	Magmatic	Magmatic	–	Mafic	≥3	–	Large	[2] [3]
t2.11	2250	Yes	Magmatic	Magmatic	–	–	≥3	–	Large	[2] [3]
t2.12	2500	Yes	Magmatic	Magmatic	–	Mafic	≥3	–	Large	[2] [3]
t2.13	2700 ± 50 ^a	Yes	Magmatic	Magmatic	–	Mafic	≥3	–	Large	[1] [2] [3]
t2.14	3500	Yes	Magmatic	Magmatic	–	–	≥3	–	Large	[2] [3]
t2.15	4700	Yes	Magmatic	Magmatic	–	Mafic	≥3	–	Large	[1] [2] [3]
t2.16	5200	Yes	Magmatic	Magmatic	–	Mafic	≥3	–	Large	[3] [4]
t2.17	8700 (?)	Yes	Magmatic	Magmatic	–	Mafic	≥3	–	Large	[3] [4]
t2.18	10,670	Yes	Magmatic	Magmatic	–	Mafic	>3	–	Large	[2] [3]
t2.19	21,660	Yes	Magmatic	Magmatic	–	Mafic	>3	–	Large	[2] [3]
t2.20	26,400	Yes	Magmatic	Magmatic	–	Mafic	>3	–	Large	[2] [3]
t2.21	35,400	Yes	Magmatic	Magmatic	–	Mafic	>3	–	Large	[2] [3]

t2.22 [1] Björck et al. (1991).

t2.23 [2] Moreton (1999).

t2.24 [3] Smellie (1999).

t2.25 [4] Mathies et al. (1990).

t2.26 ^a Error according to the time interval provided by the bibliography.

4. Threat analysis

The quantification of the threat posed by volcanoes to their surroundings is vital when trying to define the required monitoring level for each volcano. In order to perform this quantification, Ewert et al. (2005) developed the National Volcano Early Warning System (NVEWS). The rationale behind NVEWS was to assess the threat posed by volcanoes in the United States via an analysis scheme divided into two main factor groups. First, those directly associated with the volcanic hazard and second, those related to exposure of human, social and economical elements potentially affected by the hazard. The individual factors are summed into a hazard score and an exposure score, which are then multiplied to generate the volcano's overall threat score. The total threat score obtained classifies the volcanic threat into one of five threat categories (Ewert et al., 2005): very low (6–0), low (6–30), moderate high (30–63), high (63–113) and very high (>113).

In recent years several authors have applied the NVEWS analysis to other volcanoes (e.g. Kinvig et al., 2010; Martí et al., 2012). Scores given to each factor (labelled from (a) to (y)) and the final results are given in Table 3. A brief explanation of the different scores is included in the next section; full details and references for the NVEWS analysis performed for Deception Island are included as a Microsoft Excel spreadsheet in Supplementary Material 1. For each factor we have tried to determine the maximum and minimum scores in an attempt to quantify

Table 3
Deception Island NVEWS (National Volcano Early Warning System) scoring factors.

	Score (max)	Score (min)	References
Hazard factors			
(a) Volcano type	1	1	[1] [2] [3]
(b) Maximum Volcano Explosivity Index (VEI)	1	1	[1] [2] [3]
(c) Explosive activity	1	1	[1] [2] [3]
(d) Major explosive activity	1	0	[1] [2] [3]
(e) Eruption recurrence	4	4	[3] [4] [5]
(f) Holocene pyroclastic flows?	1	1	[3]
(g) Holocene lava flows?	1	1	[3] [4]
(h) Holocene-lahars?	1	1	[3]
(i) Holocene tsunami (s)?	1	1	[3]
(j) Hydrothermal explosion potential	1	1	[3]
(k) Sector collapse potential	1	1	[3]
(l) Primary lahar source	1	1	[3] [4] [6]
(m) Observed seismic unrest	1	1	[7]
(n) Observed ground deformation	1	1	[8]
(o) Observed fumarolic or magmatic degassing	1	1	[7]
Total hazard factors (THF)	18	16	
Exposure factors			
(p) Volcano Population Index (VPI) at 30 km	3	1.7	
(q) Population downstream or downslope	0	0	
(r) Historical fatalities	0	0	[3]
(s) Historical evacuations	0	0	[7] [9]
(t) Local aviation exposure	1	1	
(u) Regional aviation exposure	2	0	
(v) Power infrastructure	1	1	
(w) Transportation infrastructure	1	1	
(x) Major development or sensitive areas	1	1	
(y) Volcano is a significant part of a populated island	1	1	
Total exposure factors (TEF)	10	6.7	
Relative threat ranking (THF × TEF)	180	107.5	

[1] Aristarain and Delmas (1998).

[2] Caselli and Agosto (2004).

[3] Smellie (2002a).

[4] Roobol (1982).

[5] Orheim (1972).

[6] Baker et al. (1975).

[7] Ibañez et al. (2003).

[8] Prates et al. (2013).

[9] Smith et al. (2003).

the uncertainty caused by the lack of data in some cases. The obtained threat score for Deception Island is between 107.2 and 180, which corresponds to a high-to-very-high level of threat (Ewert et al., 2005).

4.1. Hazard factors

Deception Island corresponds to a composite volcanic system that includes a central collapse caldera that was responsible for the creation of Port Foster (a). Nevertheless, post-caldera volcanism is apparently restricted to small-size eruptions up to VEI 4, as indicated by the deposits on the island and the tephra records elsewhere in the region (b). Some indices of bimodal volcanism and deposits found at distances of over 500 km away suggest that more powerful eruptions may have taken place (e.g. Aristarain and Delmas, 1998; Smellie, 2002a; Caselli and Agosto, 2004) (c) and (d).

The historical period in Deception Island is relatively short as it starts in 1820. Since then, over 15 eruptions have occurred on the island at Mt. Kirkwood (e.g. 1842, 1838–1839), Mt. Pond (e.g. 1969), Whalers Bay (e.g. 1829–1908), Pendulum Cove (e.g. 1800–1828, 1830–1927, 1931–1955) and Telefon Bay (e.g. 1967, 1970). During the Holocene, at least 30 eruptions occurred on Deception Island (Tables 1 and 2) including all the volcanic hazards described in the previous section (e). As mentioned above, there is evidence of pyroclastic surges and flows (f), lava flows (g) and ash fall. The constant fumarolic activity on the island and the evidence of phreatomagmatic eruptions fully justify the hydrothermal potential of the island (Smellie, 2002a) (h). There is also evidence of sector collapses (k) that may have led to tsunamis (j) inside Port Foster or beyond the island (Smellie, 2002a). As well, the permanent ice on Mt. Pond and Mt. Kirkwood also provide a primary source for a lahar in the event of an eruption occurring underneath these ice caps (l).

In 1992 and 1999, an episode of volcanic unrest took place on Deception Island that was characterised by a great increase in seismic activity (m) and changes in the hydrothermal system and fumarolic activity (o) (Ibañez et al., 2003). Ground deformation has been also observed on the island during recent scientific surveys (e.g. Prates et al., 2013) (n).

4.2. Exposure factor

When evaluating the threat on Deception Island it is important to take into account the fact that it is only populated during the austral summer. However, in neighbouring areas a few stations are inhabited during the winter and there is a permanent population on King George Island (Fig. 1). Thus, the threat analysis presented here refers mainly to the summer, especially for the maximum scores.

The first exposure factor is the volcano population index (VPI) within a 30-km radius of the volcano summit or the most recent active event. On Deception Island, this distance consists of the entire island and includes the Spanish and Bulgarian bases on Livingston Island (Fig. 1). These two bases, together with the ones on Deception Island itself, may be home to 50–100 people (i.e. a VPI of 1.7–2) (p). However, as one of the main Antarctic touristic destinations, we should also consider the possibility that a fully laden tourist vessel is present on the island, with which the VPI increases to 3 or more. There is no population downstream of the volcano within the 30 km VPI circle (q) and no fatalities have ever been recorded during the eruptions on Deception Island (r). The Chilean and British stations and the Argentinian and Spanish bases were evacuated during the 1967 and 1969 eruptions and the seismic crisis of 1992, respectively (Ibañez et al., 2003; Smith et al., 2003), and no permanent populations remain (s).

In terms of local aviation exposure, the only airport on the South Shetland Islands is on King George Island, about 150 km away (t): a maximum of two flights per day would represent around 100 passengers (u). The power infrastructures for both the Spanish and the Argentinian bases and all accessible ports within Port Foster

371 (e.g. Whaler's Bay or Pendulum Cove) are located within the flowage
 372 hazard zones (v), (w). Finally, several parts of the island are consid-
 373 ered Antarctic Specially Protected Areas and the Holocene volcanic
 374 deposits cover over 25% of the island landmass (x), (y).

375 5. Volcanic hazard assessment: spatial and temporal analysis

376 The main steps in the volcanic hazard assessment on Deception
 377 Island (Fig. 6) can be divided into long- and short-term analyses.
 378 Long-term hazard assessment is based on the past history of the
 379 volcano and requires information from the geological record. This
 380 analysis enables us to determine the eruption recurrence and the
 381 possible nature of a forthcoming eruption. Short-term hazard assess-
 382 ment, on the other hand, provides complementary information result-
 383 ing from the combination of a long-term analysis with real-time monitoring
 384 data gathered during a crisis or an unrest episode, and helps forecast
 385 where and when the eruption might take place and the most likely erup-
 386 tive scenarios. To evaluate the long-term volcanic hazard, for this study
 387 we carried out both temporal and spatial analyses: the former evaluates
 388 in a probabilistic way possible outcomes of volcanic unrest within a
 389 specific time frame, while the latter uses simulation models to predict
 390 the most probable eruptive scenarios and which areas could be affected
 391 by a future eruptive event. The susceptibility analysis enables us to iden-
 392 tify which areas have the greatest likelihood of hosting new vents.

393 Since the results from these temporal and spatial analyses are highly
 394 dependent on the data used, the selection of the data source is one of the
 395 most important steps to be undertaken during a hazard evaluation.
 396 Due to the logistic difficulties involved in performing repeated field
 397 studies or other surveying in the area, only previously published peer-
 398 reviewed information has been used in addition to our own data in

399 this systematic volcanic hazard assessment. In the coming sections we
 400 provide a general overview of the different tools applied in this study,
 401 as well as a careful description of the required input data. For further
 402 detailed information regarding each specific tool, readers are referred
 403 to the original papers.

5.1. Susceptibility analysis

404 The first step in a long-term spatial analysis is to evaluate the suscep-
 405 tibility (probability of vent opening; Martí and Felpeto, 2010) of the
 406 volcanic area. For Deception Island we paid special attention to recent
 407 volcanic structural indicators such as vent locations and alignments,
 408 fumarolic activity and heated ground sites (Fig. 2). Vent locations
 409 were divided into post-caldera craters (no precise dating but recognisable
 410 in the field and from satellite images) and the historical volcanism
 411 described in the bibliography (Wilkes, 1845; Valenzuela et al., 1970;
 412 González-Ferrán et al., 1971; Baker et al., 1975; Roobol, 1980; Smellie,
 413 2002b; Pedrazzi et al., 2014). The lineament structures shown in Fig. 2a
 414 are taken from the simplified structural map of Deception Island in
 415 Martí et al. (2013). On the island, a NE-SW oriented regional tectonic
 416 trend, almost parallel to the expansion axis of the Bransfield Strait, is
 417 clearly predominant; NW-SE and N-S oriented faults are also present
 418 (Martí et al., 2013). Fig. 2b also includes those areas with clear signals of
 419 hydrothermal processes such as fumaroles or heated ground that can be
 420 related to the heating of shallow aquifers by convection gaseous inflowing
 421 from the underlying magma intrusions (Ortiz et al., 1987; Ramos et al.,
 422 1989; Rey et al., 1995; López-Martínez et al., 2000; Patrick and Smellie,
 423 2013).

424 Susceptibility is generally calculated using probabilistic methods
 425 that estimate probability density functions (PDFs) by calculating a

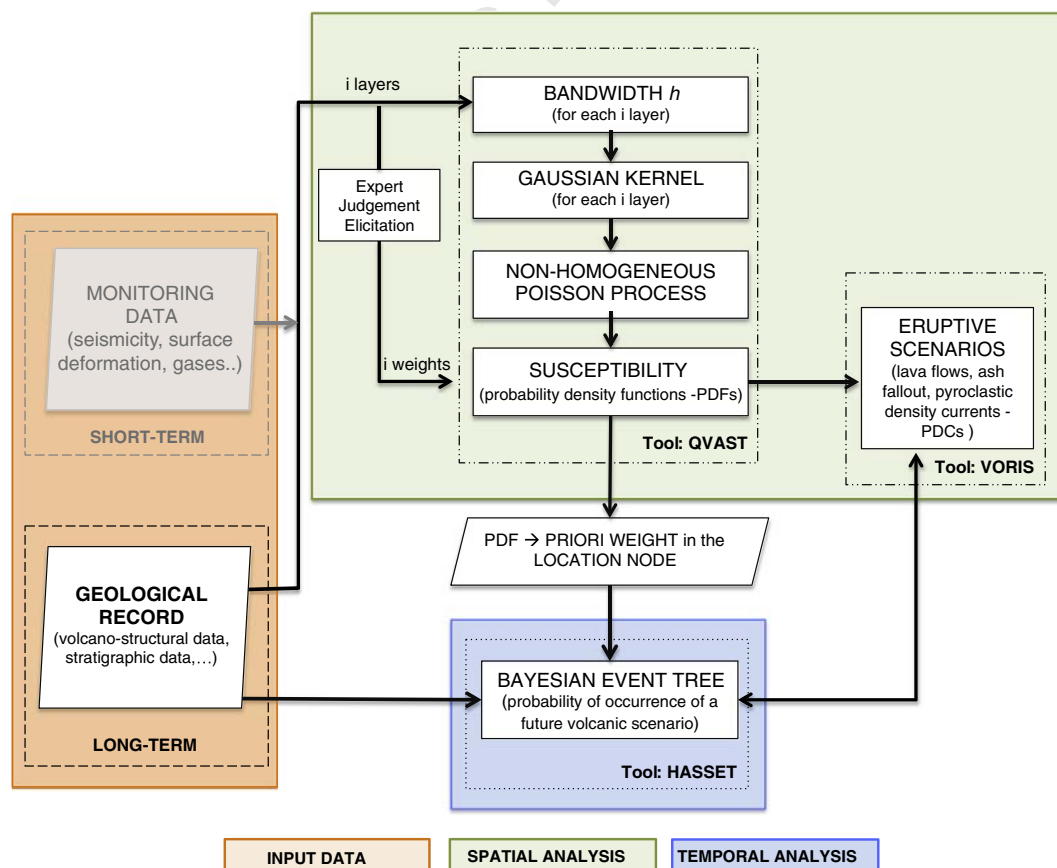


Fig. 6. Flow chart for the volcanic hazard assessment. Tools used in this study are also indicated.

Table 4

Bandwidth parameters for all the available datasets on Deception Island obtained using the modified LSCV (Least Square Cross Validation) method (Cappello et al., 2013) in the QVAST tool (Bartolini et al., 2013).

Layer	h (m)
Post-caldera craters (field work, analysing orthophotos)	1170
Historic volcanism (Wilkes, 1845; Valenzuela et al., 1970; González-Ferrán et al., 1971; Baker et al., 1975; Roobol, 1980; Smellie, 2002b; Pedrazzi et al., 2014)	528
Lineaments (Martí et al., 2013)	3294
Fumarolic activity (López-Martínez et al., 2000; Smellie and López-Martínez, 2002a,b)	4071
Heated ground (López-Martínez et al., 2000; Smellie and López-Martínez, 2002a,b)	1001

kernel function for each data location (Martin et al., 2004; Felpeto et al., 2007; Cappello et al., 2012; Connor et al., 2012; Bartolini et al., 2013; Becerril et al., 2013; Cappello et al., 2013). The smoothness and the modelling ability of the kernel function are controlled by the smoothing parameter or bandwidth h , which determines how the probabilities spread out from the volcanic structures or vents (Diggle, 1985; Connor and Hill, 1995; Lutz and Gutmann, 1995; Cappello et al., 2012). Thus, for small h values, the kernel function gives high probability estimates in the vicinity of the existing volcanic structures. Conversely, when

high bandwidth values are assigned, the probability estimates are distributed in a more homogeneous way throughout the entire area under study. The h values obtained for our dataset from Deception Island are given in Table 4.

For the present work, the bandwidth and the corresponding Gaussian Kernels and PDFs for all available datasets (vent locations, vent alignments, dykes, etc.) were evaluated with QVAST (Bartolini et al., 2013). We chose the modified version of the Least Square Cross Validation (LSCV) method to evaluate h (Cappello et al., 2012, 2013) and computed the final susceptibility map (Fig. 7) assuming a non-homogeneous Poisson process. To obtain the final susceptibility map, we had to combine all the PDFs evaluated for each volcano-structural data in a weighted sum. These weights were assigned using expert elicitation judgement (see Aspinall, 2006; Neri et al., 2008) by experts from the Group of Volcanology of Barcelona on the basis of structural criteria (see Martí and Felpeto, 2010), which provide initial indicative probability distributions associated with each PDF. We obtained the following values: 0.4 for the historical volcanism, 0.4 for the post-caldera craters, 0.1 for lineament structures, 0.05 for fumarolic activity and 0.05 for heated ground.

5.2. Temporal analysis

The temporal analysis was computed using HASSET (Sobradelo et al., 2014), an event tree structure that uses Bayesian inference to estimate the probability of occurrence of a future volcanic scenario (Sobradelo

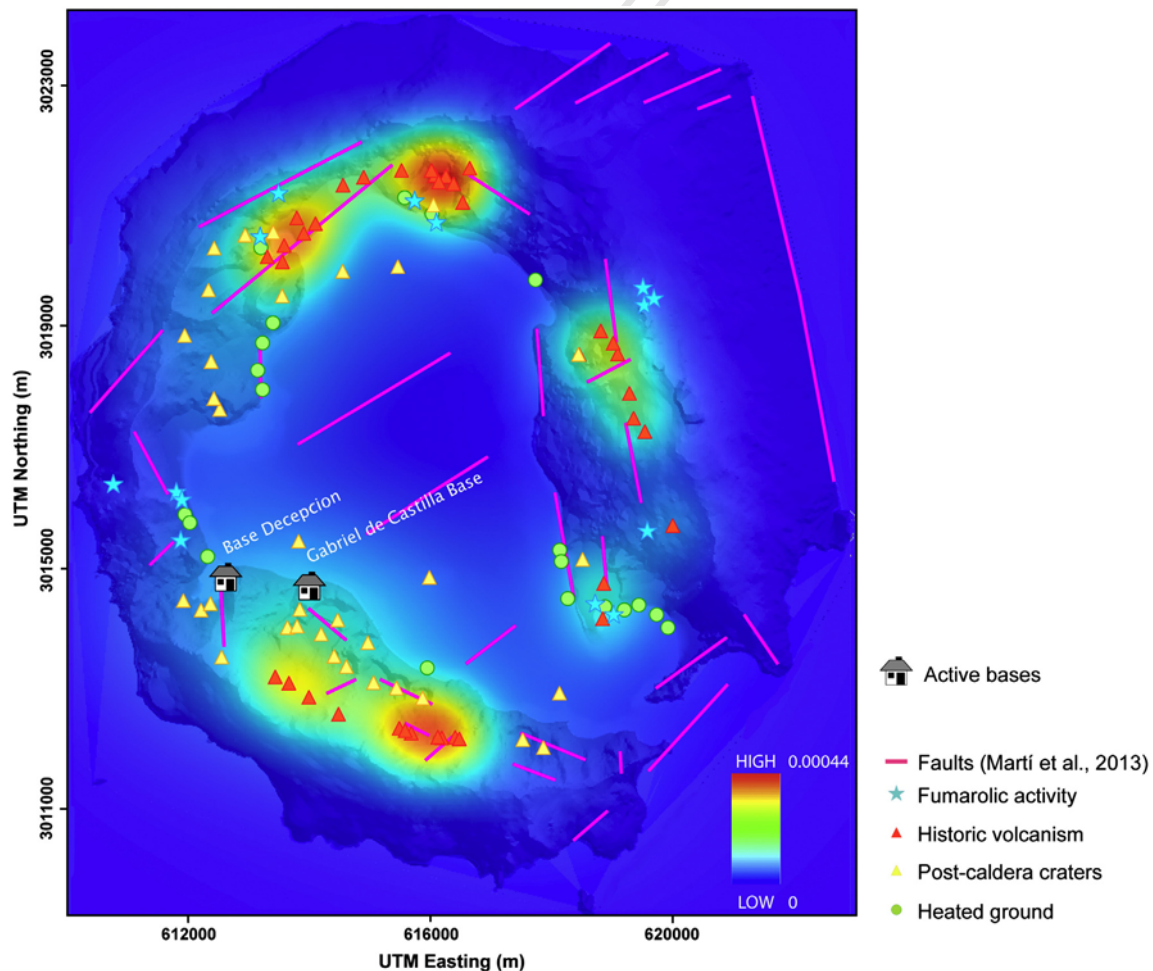


Fig. 7. Susceptibility map of future eruptions on Deception Island calculated with QVAST (Bartolini et al., 2013).

and Martí, 2010) and to predict the five most likely scenarios. An event tree is a probabilistic model that can be used to calculate the probability of occurrence for any possible volcano-related event (Aspinall and Woo, 1994; Newhall and Hoblitt, 2002; Aspinall, 2006; Martí et al., 2008; Marzocchi et al., 2008; Neri et al., 2008; Marzocchi et al., 2010; Sobradelo and Martí, 2010; Becerril et al., 2014). This graphic representation of events in the form of nodes and branches depicts all relevant possible outcomes of volcanic unrest in progressively greater levels of detail.

Input data for the HASSET event tree model consists of geological and/or physical models, past data, present and past monitoring observations, and expert opinion. Three parameters must be entered at each branch to run the model: past data, prior weight and data weight (Sobradelo and Martí, 2010; Sobradelo et al., 2014). Past data consists of information about the volcanic area corresponding to observational data or data collated from the bibliography. We assume that the future behaviour of the volcano will be similar to its recent past history. In probabilistic terms, prior weight represents uncertainty before data are gathered and it is assigned on the basis of the *a priori* beliefs regarding the volcanic area under study. Data weight represents how well we know the system. This value represents the epistemic uncertainty related to our knowledge of the system and the quality and quantity of data we have about the system. The more data we have, the better we know the system and the lower the epistemic uncertainty (Woo, 1999; Sobradelo and Martí, 2010).

The study of temporal probability on Deception Island was based on the catalogue of eruptions documented in Tables 1 and 2. Information from these eruptions was used to characterise past eruptive activity and to estimate some of the input parameters required for our hazard assessment. Due to the certainty that not all post-caldera eruptions occurred on Deception Island have been identified and/or dated, we computed only those volcanic eruptions and unrest periods recorded for the last 372 years (1641–2013), the period for which the available stratigraphic record and geochronological data are most precise. Therefore, using HASSET we were able to estimate the probability of a volcanic episode occurring within the forecasting time interval (the following 2 years). This forecasting time interval was chosen on the basis of the model and represents the minimum time window range needed to evaluate the probability of having at least one eruption in the range considered (see Sobradelo and Martí, 2010). The time window of the dataset is 372 years and so we obtained 186 time intervals of data for the study period. As we restricted our dataset to the last 372 years, the eruptions in this catalogue were used to assign prior weights to nodes 2 to 8. Table 5 shows the Bayesian event tree structure for Deception Island, as well as the input parameters for each branch. Fig. 8 shows the probability for each event tree branch.

Furthermore, using HASSET it is possible to compute the total probability for any particular scenario and then compare results. Once all probability density functions for each branch of each node and the conditional probability assessment are calculated, all these probabilities can be combined to estimate the total long-term probability of a particular event. Thus, we evaluated the total probability for different eruptive scenarios for the five different sectors that we established for Deception Island according to susceptibility and topographic criteria, as is permitted by HASSET and explained below (Fig. 9).

5.2.1. Node 1: unrest

This first node estimates the temporal probability that the system will reactivate during the next time window. The probability that an unrest phase will occur (or not) during the next time window can be obtained by analysing the number of past time windows that encompass an episode of unrest. It does not take into account the periods of repose between eruptions or the possible non-stationary nature of the data (Sobradelo and Martí, 2010; Sobradelo et al., 2014).

As mentioned above, the existing eruptive record of Deception Island may be incomplete. First, the island is uninhabited for most of

Table 5

Input data for HASSET (Sobradelo et al., 2014). Prior weights and data weights are estimated using data on Deception Island volcanic activity. Past data are based on the eruptions recorded over the last 372 years.

Node name	Event	Past data	Prior weight	Data weight	
1 Unrest	Yes	19	0.30	10	t5.1
1 Unrest	No	167	0.70	10	t5.2
2 Origin	Magmatic	16	0.50	10	t5.3
2 Origin	Geothermal	3	0.40	10	t5.4
2 Origin	Seismic	0	0.05	10	t5.5
2 Origin	Other	0	0.05	10	t5.6
3 Outcome	Magmatic eruption	16	0.6	10	t5.7
3 Outcome	Sector failure	0	0.02	10	t5.8
3 Outcome	Phreatic eruption	0	0.08	10	t5.9
3 Outcome	No eruption	3	0.30	10	t5.10
4 Location	Mt. Pond	5	0.20	50	t5.11
4 Location	Telefon Ridge	4	0.25	50	t5.12
4 Location	Stonethrow Ridge	0	0.05	50	t5.13
4 Location	Mt. Kirkwood	3	0.28	50	t5.14
4 Location	Port Foster	1	0.22	50	t5.15
5 Composition	Mafic	10	0.95	50	t5.16
5 Composition	Felsic	1	0.05	50	t5.17
6 Size	VEI ≥ 4	3	0.20	10	t5.18
6 Size	VEI = 3	9	0.70	10	t5.19
6 Size	VEI ≤ 2	3	0.10	10	t5.20
6 Size	–	–	–	–	t5.21
7 Hazard	Ballistic	6	0.30	30	t5.22
7 Hazard	Fallout	6	0.30	30	t5.23
7 Hazard	PDC	3	0.20	30	t5.24
7 Hazard	Lava flow	4	0.12	30	t5.25
7 Hazard	Lahars	1	0.03	30	t5.26
7 Hazard	Debris avalanche	0	0.03	30	t5.27
7 Hazard	Other	0	0.02	30	t5.28
8 Extent	Short	1	0.10	50	t5.29
8 Extent	Medium	2	0.30	50	t5.30
8 Extent	Large	4	0.60	50	t5.31

the year and so direct observations of unrest periods, whether a prelude or not to a volcanic eruption, are clearly biased towards the period when observers are present. Second, most of the information comes from ice-core studies and reports from Antarctic expeditions. Thus, the number of unrest periods occurring during the temporal window used in this analysis may be underestimated. For this reason, we assigned an epistemic uncertainty of 10 to our data weights, which means that new evidence on intervals with eruptive or non-eruptive behaviour will modify our prior assumptions. We assigned a 0.30 *prior* weight to unrest and 0.70 of prior weight to 'no' unrest.

5.2.2. Node 2: origin

The origin node takes into account four types of unrest that could occur in a volcanic area: magmatic involving the movement of fresh magma, geothermal, seismic and others. Two intense seismic crises in 1992 and 1999 have been registered in 15 years of monitoring (Ibañez et al., 2003). This high seismicity was probably associated with the activity of the main geothermal system installed inside the caldera depression (Martí et al., 2013). Despite the predominantly magmatic character of past activity on the island, we cannot exclude the possibility of geothermal behaviour without any associated fresh magma movements as occurs in other caldera systems with high geothermal activity (e.g. Campi Flegrei, Gottsmann et al., 2006; Nysiros, Gottsmann et al., 2007). In this sense, we have to assume that seismo-volcanic signals can also be associated with a shallow geothermal aquifer and deep hot materials (but not necessarily fresh magma), which gives rise to the resonance of fluid-filled fractures (Ibañez et al., 2003). In fact, these seismic measurements are not continuous and have only been registered over the past 15 years; there is thus a lack of seismic information and other similar but unrecorded periods of intense seismic activity may have gone unnoticed (Ibañez et al., 2003). For this reason, we assigned 0.5 for magmatic origin, 0.4 for geothermal origin, and split the rest evenly among the other options.

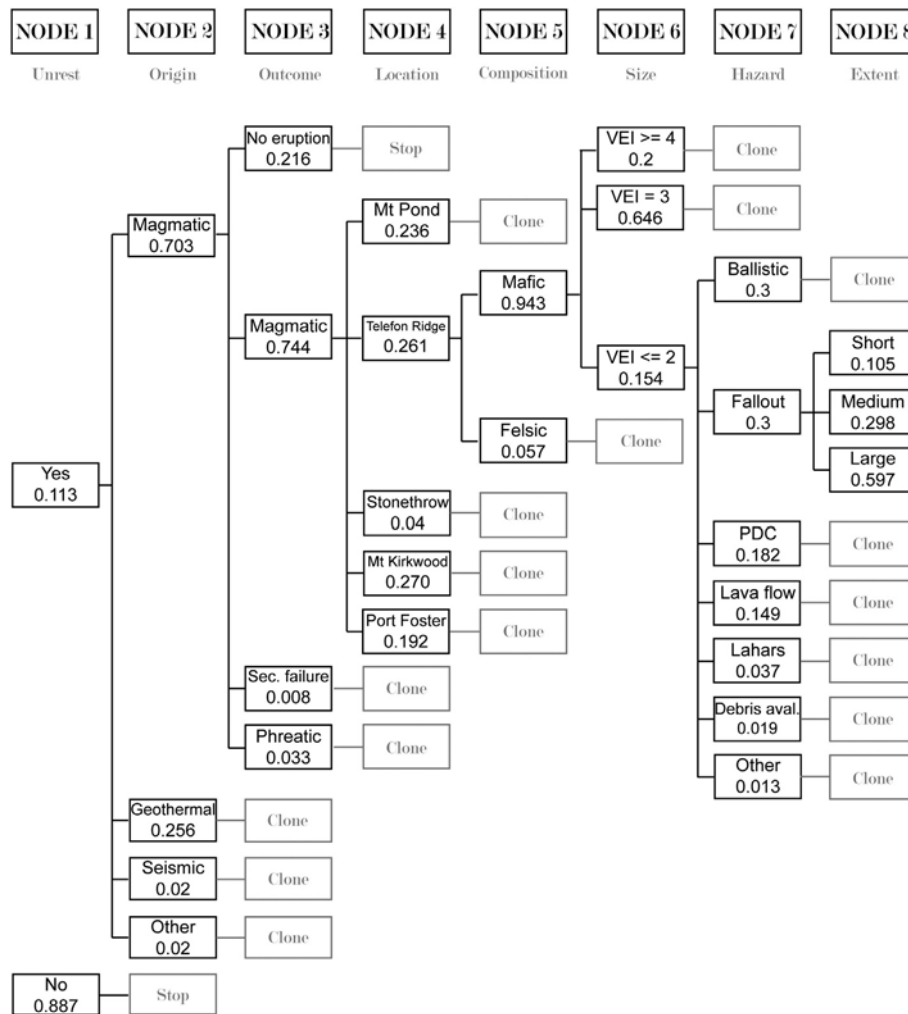


Fig. 8. Bayesian event tree structure for Deception Island including results for the probability estimate using the HASSET tool (Sobradelo et al., 2014).

557 The prior weights are assigned on the basis of a priori beliefs and so
 558 we assigned a value of 10 to the epistemic uncertainty since we still
 559 expect the majority of unrest to be of magmatic origin. However, it is
 560 important to give a certain weight to new evidence.

5.2.3. Node 3: outcome

561 A study of volcanic unrest in the historical period of Deception Island
 562 shows that 84% of unrest episodes have led to eruptions. Only three doc-
 563 umented unrest periods failed to generate volcanic activity. The lack of
 564 information about seismic activity caused by hydrothermal behaviour
 565 suggests that many other episodes of 'no eruption' could have occurred
 566 in addition to the documented ones. For this reason, we assigned 0.60 to
 567 magmatic eruption and 0.30 to 'no eruption'. The remaining 0.10 was
 568 split into the possibility of a phreatic explosion (prior weight of 0.8)
 569 and a sector failure (prior weight of 0.2) following an episode of unrest.

570 Given that these weights were assigned on the basis of incomplete
 571 data, we assigned a value of 10 to the epistemic uncertainty. We did
 572 not assign total epistemic uncertainty as we still believe that the largest
 573 weight should be for the magmatic eruption with no eruption branches;
 574 however, we still want new evidence to be able to contribute signifi-
 575 cantly to the updating of our prior weights.
 576

5.2.4. Node 4: location

577 The location node divides Deception Island into five main zones ac-
 578 cording to its topographic characteristics and the nature of past activity
 579

(volcanic susceptibility and past hazards). The five zones are shown in
 Fig. 9.

580 Mount Pond (zone 1) and Mount Kirkwood (zone 4) represent
 581 zones with the presence of extensive glaciers on their summits. The
 582 1969 subglacial eruption took place on Mount Pond (Smellie, 2002b)
 583 and gave rise to the Costa Recta, a retreated scarp produced by a normal
 584 NNW–SSE-orientated fault (Fernández-Ibañez et al., 2005). Mount
 585 Kirkwood is characterised by the lava flows from the 1842 eruption. In
 586 the vicinity of Mount Kirkwood there are two scientific-military bases,
 587 the *Deception* base (Argentina) and the *Gabriel de Castilla* station
 588 (Spain), both of which only operate during the Antarctic summer. The
 589 eruptive episodes from 1967 and 1970 were located on Telefon
 590 Ridge (zone 2) and Telefon Bay was largely filled by products from
 591 these eruptions, although three new smaller bays were created in
 592 flooded craters that formed during the final eruption in 1970 (Smellie,
 593 2001). Stonethrow Ridge (zone 3) was formed after the caldera collapse
 594 and is characterised by lava flows and deposits of red and black scorias
 595 (Augusto et al., 2007). Port Foster (zone 5), the sea-flooded depression
 596 formed by the caldera collapse, occupies the central part of the island
 597 and is characterised by major normal faults bounding the caldera
 598 depression (Maestro et al., 2007; Martí et al., 2013).
 599

600 The susceptibility analysis of the island based on the methodology
 601 described above allows us to assign prior weights to each node with a
 602 high degree of confidence, as shown in Table 5. The reliability of the sus-
 603 ceptibility map allows us to assign a data weight of 50 since the prior
 604 weights were estimated using past data from Deception Island based
 605

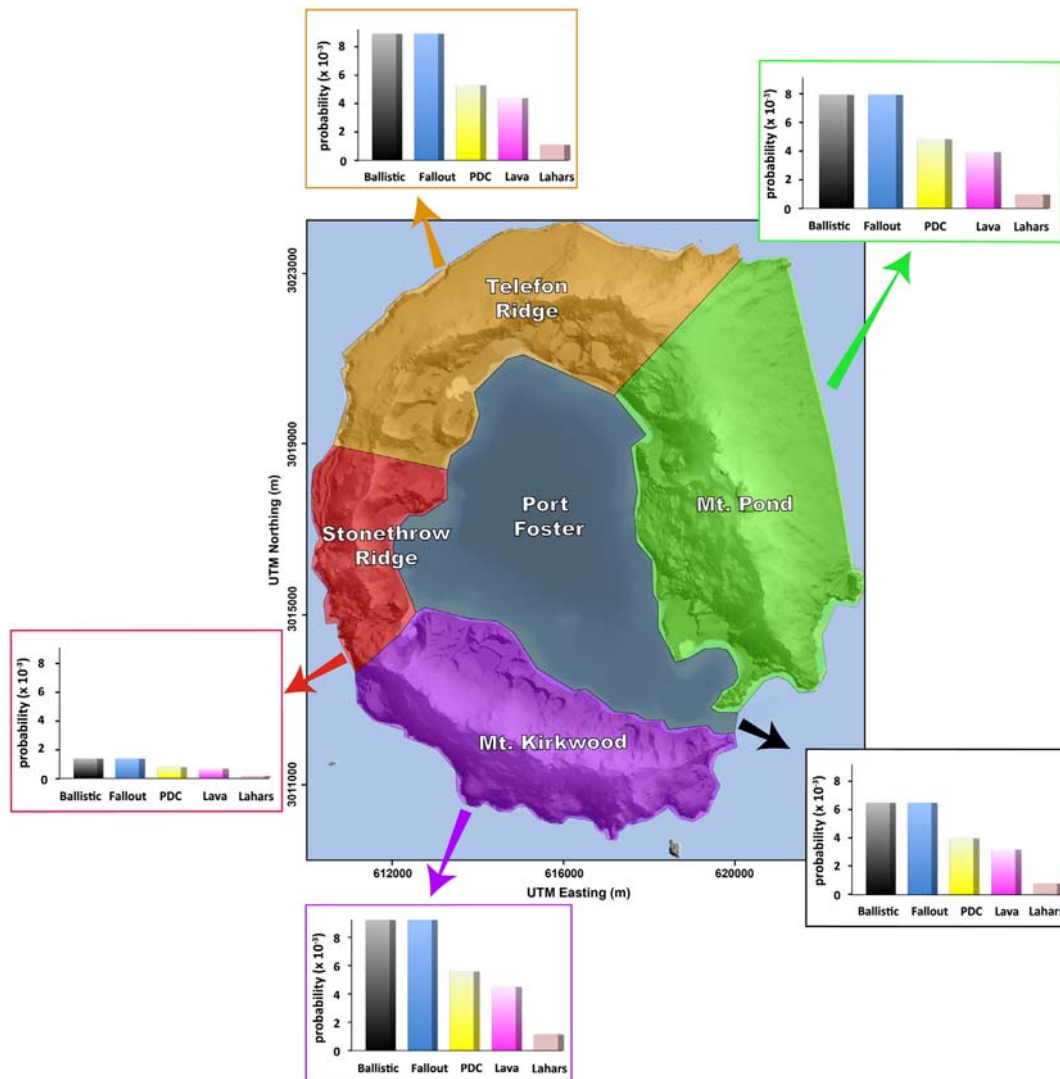


Fig. 9. Sectors on Deception Island based on volcanic susceptibility and topographic criteria. The probabilities of the different hazards in each zone of Deception Island obtained with the application HASSET (Sobradelo et al., 2014) are also shown (see text for more explanation).

606 on the volcano-structural data and on the location of past and current
607 hydrothermal activity. For this reason, we are confident of the initial
608 distribution of these prior weights.

609 5.2.5. Node 5: composition

610 Most of the post-caldera volcanic activity on Deception Island corre-
611 sponds to the eruption of basaltic and andesitic magmas (González-
612 Ferrán et al., 1971; Smellie, 2001), of which only one is of dacitic
613 composition (Table 1). Therefore, we assigned a weight of 0.95 for mafic
614 composition and 0.05 for felsic composition. We assigned an epistemic
615 uncertainty of 50, which means that new evidence regarding the com-
616 position of the historical eruptions will not modify substantially our
617 prior assumptions.

618 5.2.6. Node 6: size

619 The erupted volume on Deception Island ranges from 0.01 to
620 0.1 km³ of magma, with post-caldera activity varying from magmatic
621 Strombolian to phreatomagmatic sub-Plinian in nature (Baker et al.,
622 1975; Smellie, 1988; Keller et al., 1992; Smellie, 1999). The values that
623 characterise this activity on the island can be linked to small batches
624 of deep-sourced magmas (Martí et al., 2013). Taking into account the
625 recorded data, we attributed to $VEI \leq 2$, $VEI = 3$ and $VEI \geq 4$, the values
626 of 0.10, 0.70 and 0.20, respectively. We assigned as a prior weight for

the epistemic uncertainty a value of 10 as new evidence on the volumes
627 or sizes of the historical eruptions will help significantly update our
628 prior knowledge.
629

5.2.7. Node 7: hazard

630 Post-caldera eruptions are characterised by the generation of ballis-
631 tic ejecta, scoria fallout, PDCs, lava flows and lahars. Based on informa-
632 tion on past activity, we assigned 0.3 for both ballistic ejecta and
633 fallout, 0.2 for PDC, 0.12 for lava flows, 0.03 for both lahars and debris
634 avalanches, and 0.02 for others. However, for the same reasons given
635 for the size weights, we assigned a value of 30 to the epistemic uncer-
636 tainties, as these prior weights may vary somewhat if an improved
637 data catalogue – especially based on studies of the ice record – of past
638 volcanic deposits can be obtained.
639

5.2.8. Node 8: extent

640 Node extent refers to the distance reached by eruption products
641 such as lava flows, ballistic, fallout, lahars and PDCs. The extent of the
642 recent volcanic products on Deception Island varies considerably and,
643 while lava flows may emplace only very close to the vents, ash fallout
644 can be carried over 100 km due to the strong winds and the character-
645 istic tropopause height of the area. In this analysis, we considered prod-
646 ucts located near the vents to be of small extent, products emplaced on
647

the island to be of medium extent, and products emplaced beyond Deception Island to be of large extent. According to this and the geological record, 0.1 of extents were small, while 0.3 were medium and 0.6 large. We assigned an epistemic value of 50 to all branches, as new data will not affect significantly this information.

5.3. Eruptive scenarios

The second step is to simulate different eruptive scenarios using information on the spatial probability of a new vent opening indicated on the calculated susceptibility map. The result is a final qualitative hazard map created by the superposition of the different analysed scenarios. Simulations were conducted using VORIS 2.0.1 (Felpeto et al., 2007; available at <http://www.gvb-csic.es/GVB/VORIS/VORIS.htm>) and LAHARZ (Schilling, 1998; available at <http://vulcan.wr.usgs.gov/Projects/LAHARZ/framework.html>), two automatic systems developed in a GIS framework (ArcGis®) that enable volcanic hazard maps and eruptive scenarios based on geological record information to be elaborated. The VORIS 2.0.1 tool generates quantitative hazard maps for lava flows and PDCs and simulates fallout deposits for a single vent. LAHARZ is able to map lahar inundation zones.

Eruptive scenarios were calculated using information from recent historical eruptions and on the basis of the premise that future eruptions (if any) will be similar to those documented on the island from 1842, 1967, 1969 and 1970. Taking into account the main types of primary volcanic hazards identified during the historical eruptions (Smellie, 2002a), the eruptive scenarios predict the existence of ash fall, lava flows, dilute pyroclastic density currents and lahars. Furthermore, as obtained in the Bayesian Event Tree analysis, we have also a not null probability for ballistic ejecta and debris avalanche hazards. In this first analysis, we have decided not to include these two hazards due to the scarcity of input parameters to run the models.

5.3.1. Ash fall

Ash fall can be expected to occur on Deception Island in the event of more than one type of eruptive style. The style considered in this study was a violent Strombolian eruption, which coincides with recent eruption styles and corresponds to the most significant hazard in terms of probability of occurrence according to the long-term event tree constructed in Section 5.2 (Temporal probability). The input data regarding the eruptive column and ash particle size were inferred from the 1967, 1969 and 1970 eruptions (Valenzuela et al., 1970; González-Ferrán et al., 1971; Baker et al., 1975; Roobol, 1980; Smellie, 2002b; Pedrazzi et al., 2014), which were relatively small in volume ($<0.05 \text{ km}^3$) with eruptive columns that were probably less than 10 km high (Smellie, 2002b; Pedrazzi et al., 2014). Ash fallout simulations were based on the advection–diffusion model (Folch and Felpeto, 2005), whereby the vertical mass distribution is computed using Suzuki's approximation (Suzuki, 1983; Felpeto et al., 2007). Wind data for the advection model correspond to records from the Bellingshausen station and were provided by the British Antarctic Survey (http://www.antarctica.ac.uk/met/READER/upper_air/uawind.html). Monthly records were used to calculate average annual wind velocities and directions at intervals of about 1500 m up to an altitude of 20,000 m for a 30-year period (from 1969 to 1999). The wind roses for the time period considered are included as Supplementary Material 2.

We focused our attention on the fallout scenarios corresponding to the average wind velocity and direction values for each season. Up to five different wind direction inputs and intensities at different vertical heights can be used with the VORIS 2.0.1 tool. We chose data from altitudes between 1500 and 12,000 m. Westerly winds prevail in general throughout the year, but with a more north-westerly direction in summer and winter. This is due to the fact that the data used come from a station that is strongly affected by the climatological low pressure that forms over the Bellingshausen Sea that generates predominantly north to north-westerly winds (Turner and Pendlebury, 2004). Wind

speed averages range between 20 and 50 m/s. All the simulations were conducted assuming a single eruptive vent located in the area with the highest spatial probability during each season.

Results are shown in Fig. 10, with particles distributed in a 5-km-high eruptive column produced by a violent Strombolian eruption generating 0.03 km^3 of deposits. The column height and volume values are the same as for the 1969 eruption (Ortiz et al., 1987; Smellie, 2002b). We considered particle sizes ranging from -6 to 2Φ (i.e. 64 mm to 0.25 mm), which cover the entire range of particle sizes observed in the volcanic deposits of the 1970 eruption (González-Ferrán et al., 1971; Shultz, 1972; Pedrazzi et al., 2014). It is clear that, as in the 1967 and 1969 eruptions (Smellie, 2002a), ash fall may also affect the southern part of the island, thereby hindering the exit of ships sailing from inside Port Foster (Fig. 3d). Moreover, as shown in Fig. 10, ash fall may even cause problems for vessels operating several kilometres away from Deception Island.

5.3.2. Lava flows

The lava flow (probabilistic) model applied is based on the assumption that topography and flow thickness play major roles in determining lava paths (Felpeto et al., 2007 and the references therein). Input parameters required by the model include a Digital Elevation Model (DEM), maximum flow lengths and height correction (i.e. average thickness of the flow). In the case of Deception Island, simulations were run over a DEM with a cell size of 30 m. Small lava flows that accumulated near the eruptive vent and did not flow over long distances were generated in the historical eruptions (Smellie, 2002a). The eruption with the largest lava flow was that of 1842, from Mt. Kirkwood, which reaches a maximum length of 5 km. Thus, we assumed flow lengths in the range of 1–5 km. The thickness used as input data for the models was 3 m, corresponding to the average value of individual flows measured in the field. The simulations were run for all cells in the DEM and the sum of the 5000 iterations provided a map with the probability for any particular cell of being covered by a lava flow. Fig. 11a consists of a lava-flow simulation probability map, which shows that there is a high probability that the caldera interior around the shores of Port Foster will be affected by lava flows. From this map it is clear that both scientific stations on the island and the evacuation routes proposed by the Spanish military staff (based on logistical criteria) are all located in areas with a moderate-to-high probability of being affected by lava flows.

5.3.3. PDCs

Pyroclastic density currents (PDCs) were simulated using the energy cone model (Sheridan and Malin, 1983) with input parameters of topography, the collapse equivalent height (H_c) and angle (θ). The latter is obtained by the arctangent of the ratio between H_c and L , where L represents the run-out length (Felpeto et al., 2007; Toyos et al., 2007). The output of the model is the maximum potential extent that can be affected by the flow (Malin and Sheridan, 1982; Felpeto et al., 2007; Toyos et al., 2007). The collapse equivalent height values range from 100 m up to about 1000 m (for very large eruptions), while the angle values range from about 4° for base surge explosions to 27° for column collapse phases (Sheridan and Malin, 1983). The result of each simulation is the area potentially attainable by a PDC.

On Deception Island, mapped surge deposits extend about 2 km from known vents and are small in volume (Smellie, 2002a). Collapse equivalent heights were chosen in the range of 200–500 m above the possible vent site in order to constrain the best H_c matching real deposits. We simulated PDCs with a collapse angle of 12° calculated from the ratio between the H_c and the run-out length. Results are shown in Fig. 11b. The map obtained represents the sum of the simulation for all cells in the DEM for a collapse column of 400 m and an inclination of the energy cone of 12° . The map shows how the interior area of Mt. Kirkwood has a high probability of being affected by dilute pyroclastic density currents that would affect the scientific stations and the

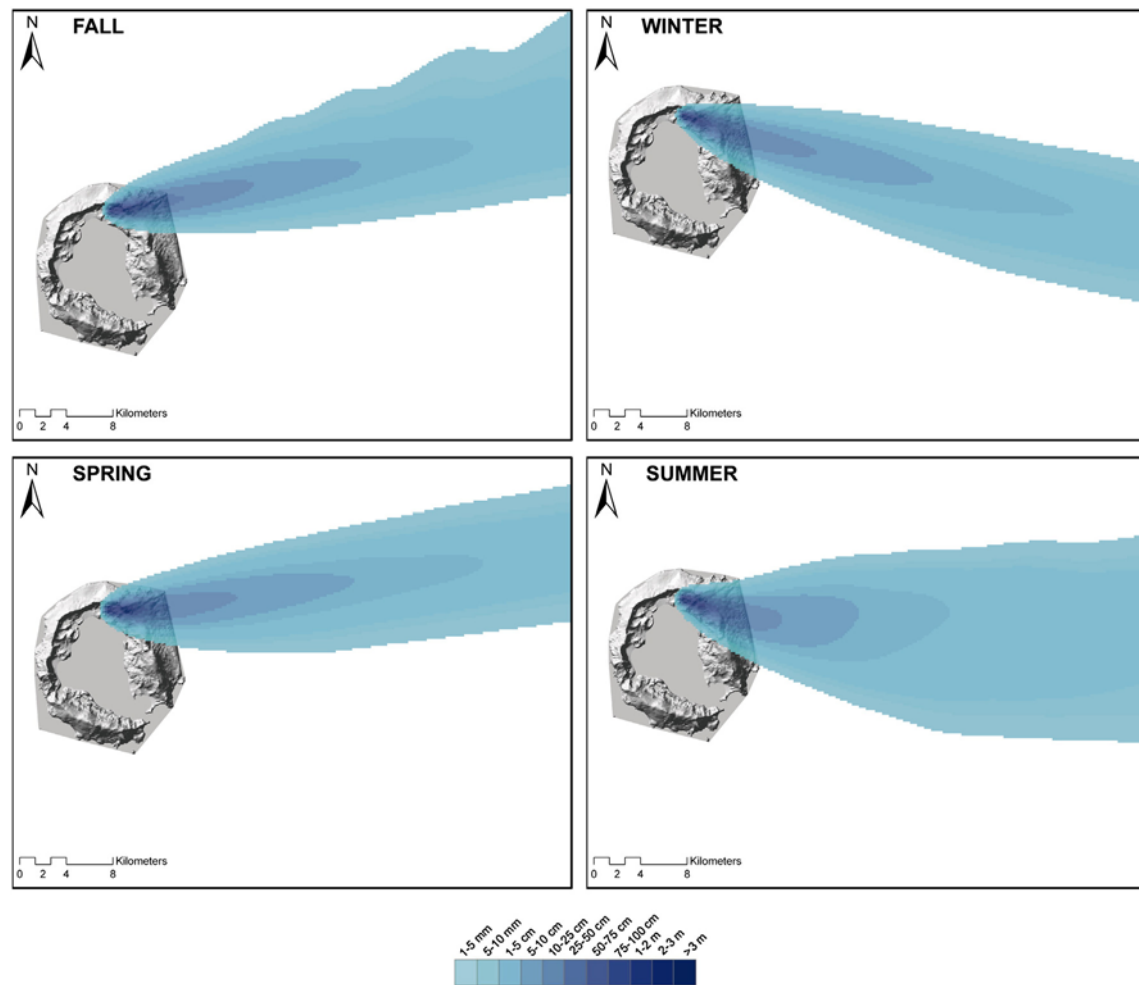


Fig. 10. Ash fallout simulations with a 5-km column height and volume of 0.3 km^3 . All four seasons are simulated using wind data from the *Bellinghousen* station.

775 evacuation routes. In addition, Telefon Ridge has a moderate–high prob-
 776 ability of being invaded by PDCs, which would also affect evacuation
 777 routes.

778 5.3.4. Lahars

779 The LAHARZ semi-empirical code creates hazard-zonation maps that
 780 depict estimates of the location and extent of areas inundated by lahars
 781 (Hoblitt et al., 1995; Schilling, 1998). The input parameters of this
 782 model are the Digital Elevation Model (DEM) and lahar volume, which
 783 provide an automated method for mapping areas of potential lahar
 784 inundation.

785 The lahar eruptive scenario was computed bearing in mind the fact
 786 that, in association with subglacial eruptions, lahars affected Deception
 787 Island during past activity (Smellie, 2002a,b). Based on the estimated
 788 volumes from the 1969 eruption located under the Mt. Pond glacier
 789 (Smellie, 2002b), simulations were run with a volume of few millions
 790 of m^3 originating along fissures in the two principal glacier zones,
 791 Mt. Pond and Mt. Kirkwood (Fig. 2a). These summits have extensive
 792 thin glaciers that could represent a significant hazard, creating a large
 793 and sudden discharge of melt water that would overflow the glacier.

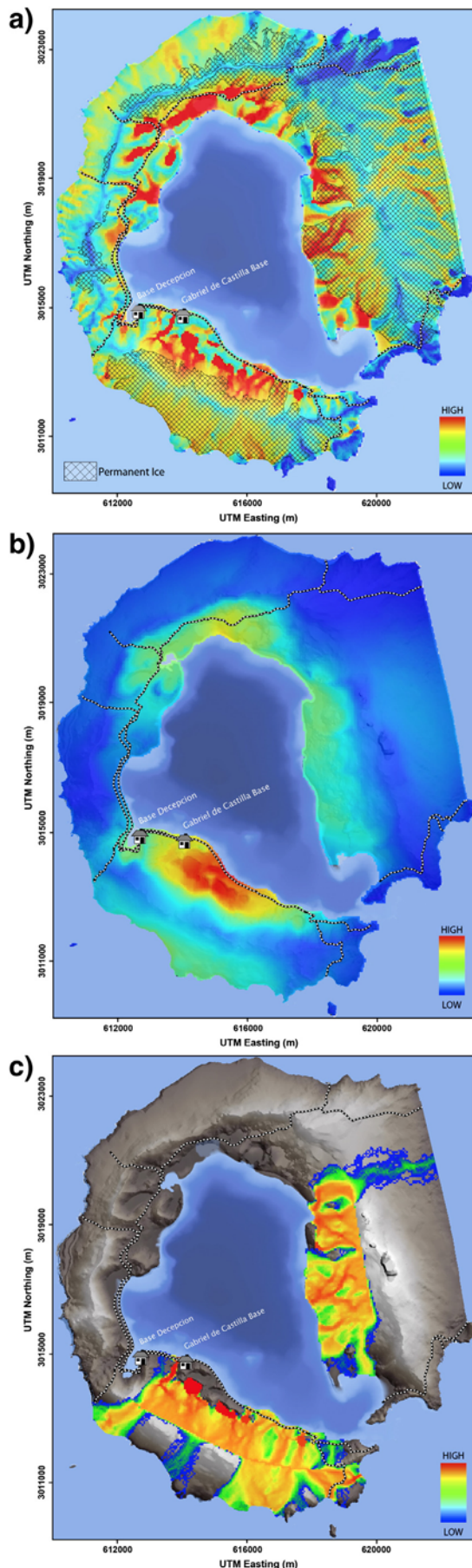
794 Fig. 11c shows a lahar simulation with hazard gradations ranging
 795 from low to high probabilities. The map shows how lahars could flood
 796 and reach the sea, and seriously damage the *Gabriel de Castilla* station
 797 on the way. From the map it is clear, as in the case of lava flows, that
 798 evacuation routes are located in moderate-to-high probability areas.

5.4. Hazard map

799 Finally, we obtained a qualitative hazard map with four levels of haz- 800
 801 ard (Fig. 12): very low, low, moderate and high. We established these 802
 803 levels on the basis of a combination of simulations for an area invaded 804
 805 by lava flows, lahars, and PDCs. The map shows that in the interior of 806
 807 the caldera there is mostly a moderate-to-high risk of being affected 808
 809 by one of the hazard scenarios considered. The highest hazard level is 810
 811 confined to the north-eastern flanks of Mt. Kirkwood, Pendulum Cove 812
 813 and the south-eastern slopes of Telefon Ridge (Fig. 12). The few areas 814
 815 with only a very low hazard level are mainly limited to Baily Head and 816
 817 Entrance Point (Fig. 12). From the hazard map it is clear that the two 818
 819 scientific stations on the island are both located in moderate-to-high 819
 820 hazard zones. Moreover, some of the evacuation routes run through 820
 821 areas possessing very high hazard level.

6. Discussion

814 Deception Island is the most active volcanic complex in the South 814
 815 Shetland Islands. Despite the important continuous research activity 815
 816 and the increasing number of tourists per year, no detailed hazard 816
 817 assessment has ever been conducted for the island. Two previous 817
 818 attempts have been made: Roobol (1982) mainly focused on assessing 818
 819 the zones threatened by lahars and constructed a model using topo- 819
 820 graphic data and the extent of the ice cap, while Smellie (2002a) 820



basically used observations of the extent of the products from the most recent historical eruptions in 1842, 1967, 1969 and 1970. 821

It is clear that hazard assessment on Deception Island may be limited by the lack of a complete geological record (e.g. chronological and stratigraphic data). Nonetheless, the threat evaluation and the spatio-temporal analysis presented here do provide a comprehensive hazard assessment for the island. Despite the intrinsic limitations of the methodology (partially due to the scarcity of data), we believe that this first analysis – albeit subject to improvement by new data – represents an important tool in management planning and in preparation for possible evacuations. 822–831

Even by assuming conservative values for some of the evaluated factors, the threat score obtained using the NVEWS test (Ewert et al., 2005) gives a range of 107.2–180, which places Deception Island in the category of a volcano with a high-to-very-high threat, comparable to Crater Lake, St. Helens, Novarupta and Katmai in the USA (Ewert et al., 2005). According to Ewert et al. (2005), these high-threat volcanoes should be closely monitored in real-time. In more detail, the monitoring network must be able to track changes occurring in the system as they happen and to apply models to the on-going and expected activity. On Deception Island, Spanish seismologists monitor the island with five seismometers and one array during the austral summer (Carmona et al., 2012). During some campaigns other scientific groups also measure ground deformation and temperature (e.g. Prates et al., 2013; Peci et al., 2014). In light of the NVEWS recommendations, the volcano-monitoring network on Deception Island should be improved, especially considering the important tourist and scientific activity occurring during the Antarctic summer. 832–848

The present hazard assessment is relevant as an analysis of the adequacy of the current evacuation routes and locations of the active scientific stations. From Fig. 12, it is clear that both *Base Deception* and *Gabriel de Castilla* station are located in areas of moderate to high hazard. Previous work dealing with hazard assessment on Deception Island has already advised against the construction of permanent buildings on the shores of Port Foster (Roobol, 1982; Smellie, 2002a). Baker et al. (1975) highlighted that it would be “evidently unwise” to construct any new stations or any other kind of installation on the island. Roobol (1982) proposed that the safest place would be along Kendall Terrace outside the ring-fault zone (Fig. 5a) and argued that, if two different constructions were installed there, it seemed extremely unlikely that one would not survive the other in case of an eruption. Fig. 12 demonstrates that the destroyed Chilean and British stations were, indeed, located in areas with high hazard level. 849–863

As is clearly suggested by the range of volcanic hazards identified on Deception Island, and given the increasing number of tourists and scientific expeditions visiting the island and its surroundings, it is important to identify escape routes in case of a sudden volcanic eruption. The escape strategy provided by the Spanish military staff is illustrated in Fig. 12. However, the evacuation routes from both scientific stations run through zones with high hazard level. Indeed, as Smellie (2002a) remarks, all possible escape routes from the inner bay to the outer coast are demanding since they include climbing up on to the steep caldera walls. So, because the routes are physically arduous, even fit persons may end exhausted. It should be added that it is almost impossible to use ground vehicles to transport people and, if possible, considerable skill and local knowledge of the routes are required (cf. Smellie, 2002a). 864–877

All routes to the outer coast would take hours to complete – a minimum of 2 h for the easiest route (Fig. 12, label 1) and over 3 or 4 h (or more) for the most difficult ones (Fig. 12, label 2). According to Smellie (2002a), there are no recommended safe routes over snow and ice because the inherent difficulties of travelling over glaciers (e.g. crevasses, whiteout, slippery surfaces). So, glacier travel should 878–882

Fig. 11. Lava flow (a), PDC (b) and lahar (c) simulation probability maps. Evacuation routes provided by the Spanish military staff are indicated by dotted lines.

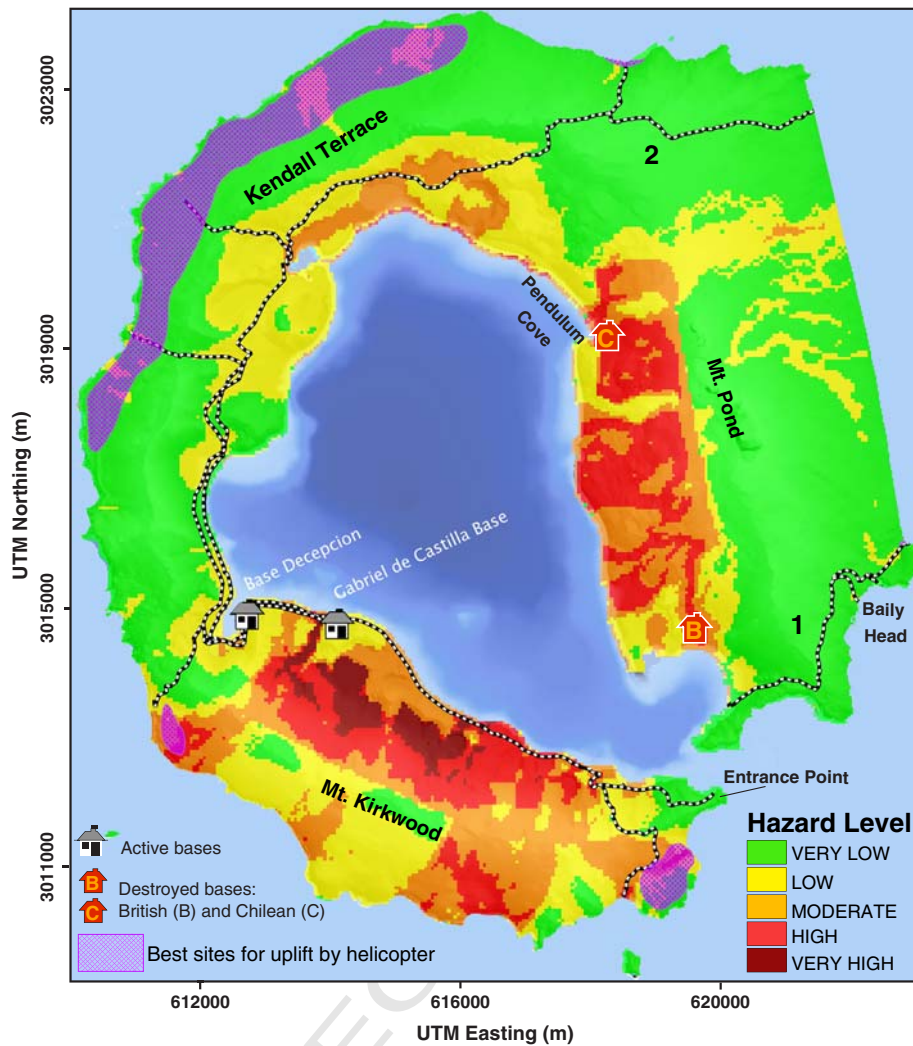


Fig. 12. Qualitative hazard map for Deception Island. The evacuation routes provided by the Spanish military staff and the best sites for helicopter uplift according to Smellie (2002a) are also indicated.

887 be avoided unless with trained guides using suitable equipment,
 888 although this is unlikely to be readily available in an emergency
 889 (cf. Smellie, 2002a). It should be added that the existing evacuation
 890 routes shown in Fig. 12 were defined without any accurate hazard
 891 assessment and taking into account only logistical considerations.
 892 Thus, the results presented here should encourage a revision of the
 893 distribution and course of the evacuation routes.

894 The evacuation of the island would be difficult for a number of other
 895 reasons. First, it is possible that the entrance to Port Foster would be
 896 blocked or difficult to sail through due to the eruption, a tsunami or
 897 any other hazards outlined here. Thus, all ships present within the bay
 898 when an eruption begins should set sail immediately, preferably after
 899 uplifting all people on the ground (Smellie, 2002a). Vessels should
 900 also avoid sailing too close to Cathedral Crags given the possibility of
 901 rock falls from these unstable cliffs.

902 Another aspect to be taken into account is that all rescue ships
 903 and helicopters should avoid passing through or under the eruption
 904 ash cloud due to the possibility of damage to machinery caused by
 905 ash particles. This is an important difficulty during rescue operations
 906 given that the hazard assessment developed in this study and, above
 907 all, the eruptive simulations reveal the possibility that Neptune's
 908 Bellows will be affected by ash fall. This would hamper any rescue
 909 operation and navigation routes, as well as activity on other islands.
 910 On the other hand, PDCs and lava flows are more constrained to the

area around the vents, but these could still affect the research stations
 and create a problem for the existing evacuation routes.

7. Conclusions

914 Here we present a long-term volcanic hazard assessment of Deception
 915 Island that takes into account both temporal and spatial probabilities.
 916 The computation of the latter probabilities for the different eruptive
 917 scenarios is important in the evaluation of the hazard level on different
 918 parts of the island. These values can be easily updated and improved
 919 with the incorporation of new information such as a more complete
 920 volcanic stratigraphy and geochronological data.

921 The hazard probability map shows that the research stations could
 922 be affected by PDCs and that a large area of the island could be covered
 923 by ash fallout. Furthermore, the opening of new fissures in the glacier
 924 zones could generate lahars that would reach the research stations
 925 and affect evacuation routes. These results are useful for planning and
 926 choosing suitable routes for evacuating the island during a volcanic
 927 crisis in the Antarctic summer when the island is populated.

928 Finally, it is worth mentioning that this long-term assessment may
 929 help decision makers when faced with difficult situations such as the
 930 allocation of resources for hazard prevention and evacuation whose ob-
 931 jective is to reduce the loss of life due to the potential impact of volcanic
 932 hazards.

Acknowledgements

This work was supported by the European Commission (FP7 Theme: ENV.2011.1.3.3-1; Grant 282759: VUELCO) and the MICINN grant CTM2011-13578-E. AG is grateful for her Juan de la Cierva Grant (JCI-2010-06092) and Ramón y Cajal contract (RYC-2012-11024). We would like to thank all the military staff from the Spanish Antarctic Base *Gabriel de Castilla* for their constant help and for the logistic support, without which this research would have been impossible. We would also like to thank Manuel Bañón for his help with the meteorological information. The authors are grateful to two anonymous reviewers for their insightful comments and review of the manuscript, which has helped us improve this work. We also thank the Editor Lionel Wilson for handling this paper. The English text was corrected by Michael Lockwood.

Appendix A. Supplementary data

Supplementary data to this article can be found online at <http://dx.doi.org/10.1016/j.jvolgeores.2014.08.009>.

References

- Aristarain, A.J., Delmas, R.J., 1998. Ice record of a large eruption of Deception Island Volcano (Antarctica) in the XVIIIth century. *J. Volcanol. Geotherm. Res.* 80, 17–25.
- Aspinall, W.P., 2006. Structured elicitation of expert judgment for probabilistic hazard and risk assessment in volcanic eruptions. In: Mader, H.M., Coles, S.G., Connor, C.B., Connor, L.J. (Eds.), *Statistics in Volcanology: Special Publication of IAVCEI*, 1. Geol. Soc. London, pp. 15–30.
- Aspinall, W.P., Woo, G., 1994. An impartial decision-making procedure using expert judgment to assess volcanic hazards. *Large Explosive Eruptions. Accad. Naz. dei Lincei, Rome. Atti Conv. Lincei.* 112, pp. 211–220.
- Baker, P.E., McReath, I., Harvey, M.R., Roobol, M.J., Davies, T.G., 1975. The geology of the South Shetland Islands: V. Volcanic evolution of Deception Island. *Br. Antarct. Surv. Sci. Rep.* 78–81.
- Bartolini, S., Cappello, A., Martí, J., Del Negro, C., 2013. QVAST: a new Quantum GIS plugin for estimating volcanic susceptibility. *Nat. Hazards Earth Syst. Sci.* 13, 3031–3042.
- Becerril, L., Cappello, A., Galindo, I., Neri, M., Del Negro, C., 2013. Spatial probability distribution of future volcanic eruptions at El Hierro Island (Canary Islands, Spain). *J. Volcanol. Geotherm. Res.* 257, 21–30.
- Becerril, L., Bartolini, S., Sobradelo, R., Martí, J., Morales, J.M., Galindo, I., 2014. Long-term volcanic hazard assessment on El Hierro (Canary Islands). *Nat. Hazards Earth Syst. Sci.* 14, 1853–1870.
- Birkenmajer, K., 1991. Lichenometric dating of a mid-19th century lava eruption at Deception Island (West Antarctica). *Bull. Pol. Acad. Sci. Earth Sci.* 39, 1–9.
- Björck, S., Sandgren, P., Zale, R., 1991. Late Holocene tephrochronology of the Northern Antarctic Peninsula. *Quat. Res.* 36, 322–328.
- Cappello, A., Neri, M., Acoella, V., Gallo, G., Vicari, A., Del Negro, C., 2012. Spatial vent opening probability map of Etna volcano (Sicily, Italy). *Bull. Volcanol.* 74, 2083–2094.
- Cappello, A., Bilotta, G., Neri, M., Del Negro, C., 2013. Probabilistic modeling of future volcanic eruptions at Mount Etna. *J. Geophys. Res. Solid Earth* 118, 1–11.
- Carmona, E., Almendros, J., Martín, R., Cortés, G., Alguacil, G., Moreno, J., Martín, B., Martos, A., Serrano, I., Stich, D., Ibañez, J.M., 2013. Avances y mejoras en el monitoreo sísmico de Isla Decepción (Antártida). *Proceedings de la 7ª Asamblea Hispano-Portuguesa de Geodesia y Geofísica*, pp. 267–271.
- Caselli, A.T., Augusto, M.R., 2004. Recent hydrovolcanic deposits with evidence of magmatic immiscibility on Deception Island, Antarctica (Depósitos hidrovolcánicos recientes con indicios de inmiscibilidad magmática en la isla Decepción (Antártida)). *Rev. Asoc. Geol. Argent.* 59 (3), 495–500.
- Connor, C.B., Hill, B.E., 1995. Three nonhomogenous Poisson models for the probability of basaltic volcanism: application to the Yucca Mountain region, Nevada. *J. Geophys. Res.* 100 (B6), 107–110.
- Connor, L.J., Connor, C.B., Meliksetian, K., Savov, I., 2012. Probabilistic approach to modeling lava flow inundation: a lava flow hazard assessment for a nuclear facility in Armenia. *J. Appl. Volcanol.* 1 (3), 1–19.
- Delmas, R.J., 1992. Environmental information from ice cores. *Rev. Geophys.* 30, 1–21.
- Diggle, P.J., 1985. A kernel method for smoothing point process data. *Applied Statistics. J. R. Stat. Soc. Ser. C* 34, 138–147.
- Ewert, J., Guffanti, M., Murray, T., 2005. An assessment of volcanic threat and monitoring capabilities in the United States: framework for a National Volcanic Early Warning System. *NVEWS. US Geol. Surv. Open-File Rep.* 1164, pp. 1–62.
- Felpeo, A., Martí, J., Ortiz, R., 2007. Automatic GIS-based system for volcanic hazard assessment. *J. Volcanol. Geotherm. Res.* 166, 106–116.
- Fernández-Ibañez, F., Perez-Lopez, R., Martínez-Díaz, J.J., Paredes, C., Giner-Robles, J.L., Caselli, A.T., Ibañez, J.M., 2005. Costa Recta beach, Deception Island, West Antarctica: a retreated scarp of a submarine fault. *Antarct. Sci.* 17, 418–426.
- Folch, A., Felpeo, A., 2005. A coupled model for dispersal of tephra during sustained explosive eruptions. *J. Volcanol. Geotherm. Res.* 145, 337–349.
- Fretzdorff, S., Smellie, J.L., 2002. Electron microprobe characterization of ash layers in sediments from the central Bransfield basin (Antarctic Peninsula): evidence for at least two volcanic sources. *Antarct. Sci.* 14 (4), 412–421.
- González-Ferrán, O., 1985. Volcanic and tectonic evolution of the northern Antarctic Peninsula – Late Cenozoic to Recent. In: Husebye, E.S., Johnson, G.L., Kristoffersen, Y. (Eds.), *Geophysics of the Polar Regions. Tectonophysics.* 114, pp. 389–409.
- González-Ferrán, O., Munizaga, F., Moreno, H., 1971. Síntesis de la evolución volcánica de la isla Decepción y la erupción de 1970. *Inst. Antártico Chil. Ser. Cient.* 2 (1), 1–14.
- Gottsmann, J., Folch, A., Rymer, H., 2006. Unrest at Campi Flegrei: a contribution to the magmatic versus hydrothermal debate from inverse and finite element modelling. *J. Geophys. Res.* 111, B07203.
- Gottsmann, J., Carniel, R., Coppo, N., Wooller, L., Hautman, S., Rymer, H., 2007. Oscillations in hydrothermal systems as a source of periodic unrest at caldera volcanoes: multiparameter insights from Nisyros, Greece. *Geophys. Res. Lett.* 34, L07307.
- Grad, M., Guterch, A., Sroda, P., 1992. Upper crustal structure of Deception Island area, Bransfield Strait, West Antarctica. *Antarct. Sci.* 4, 469–476.
- Hawkes, D.D., 1961. The geology of the South Shetland Islands: II. The Geology and Petrology of Deception Island. *Falkland Islands Dependencies Survey Scientific Reports* 27, 43.
- Hoblitt, R.P., Walder, J.S., Driedger, C.L., Scott, K.M., Pringle, J.T., Vallance, J.W., 1995. Volcano hazards from Mount Rainier, Washington. *U.S. Geological Survey Open-File Report* 95-273, p. 10.
- Hodgson, A.D., Dyson, C.L., Jones, V.J., Smellie, J.L., 1998. Tephra analysis of sediments from Midge Lake (South Shetland Islands) and Sombre Lake (South Orkney Islands), Antarctica. *Antarct. Sci.* 10, 13–20.
- Ibañez, J., Almendros, J., Carmona, E., Martínez-Arévalo, C., Abril, M., 2003. The recent seismo-volcanic activity at Deception Island volcano. *Deep-Sea Res.* II 50, 1611–1629.
- Keller, R.A., Fisk, M.R., White, W.M., Birkenmajer, K., 1992. Isotopic and trace element constraints on mixing and melting models of marginal basin volcanism, Bransfield Strait, Antarctica. *Earth Planet. Sci. Lett.* 111, 287–303.
- Kendall, E.N., 1831. An account of the Island of Deception, one of the New Shetland Isles. Extracted from the private journal of Lieutenant Kendall, R.N., embarked on board his Majesty's sloop *Cjunticier*, Captain Foster, on a scientific voyage; and communicated by John Barrow, Esq., F.R.S. *J. Roy. Geogr. Soc.* 1, 62–66.
- Kinvis, H.S., Winson, A., Gottsmann, J., 2010. Analysis of volcanic threat from Nisyros Island, Greece, with implications for aviation and population exposure. *Nat. Hazards Earth Syst. Sci.* 10, 1101–1113.
- López-Martínez, J., Serrano, E., Rey, J., Smellie, J.L., 2000. Geomorphological map of Deception Island. *BAS GEOMAP Series, Sheet* 6-B, 1:25,000. *Br. Antarct. Surv., Cambridge.*
- Lutz, T.M., Gutmann, J.T., 1995. An improved method for determining and characterizing alignments of point-like features and its implications for the Pinacate volcanic field, Sonoran, Mexico. *J. Geophys. Res.* 100, 17659–17670.
- Maestro, A., Somoza, L., Rey, J., Martínez-Frías, J., López-Martínez, J., 2007. Active tectonics, fault patterns, and stress field of Deception Island: a response to oblique convergence between the Pacific and Antarctic plates. *J. S. Am. Earth Sci.* 23, 256–268.
- Malin, M.C., Sheridan, M.F., 1982. Computer-assisted mapping of pyroclastic surges. *Science* 217, 637–640.
- Martí, J., Felpeo, A., 2010. Methodology for the computation of volcanic susceptibility: application to Tenerife Island (Canary Islands). *J. Volcanol. Geotherm. Res.* 195, 69–77.
- Martí, J., Aspinall, W., Sobradelo, R., Felpeo, A., Geyer, A., Ortiz, R., Baxter, P., Cole, P., Pacheco, J., Blanco, M., Lopez, C., 2008. A long-term volcanic hazard event tree for Teide-Pico Viejo stratovolcanoes (Tenerife, Canary Islands). *J. Volcanol. Geotherm. Res.* 178 (3), 543–552.
- Martí, J., Sobradelo, R., Felpeo, A., García, O., 2012. Eruptive scenarios of phonolitic volcanism at Teide-Pico Viejo volcanic complex (Tenerife, Canary Islands). *Bull. Volcanol.* 74, 767–782.
- Martí, J., Geyer, A., Aguirre-Díaz, G., 2013. Origin and evolution of the Deception Island caldera (South Shetland Islands, Antarctica). *Bull. Volcanol.* 75, 732.
- Martin, A.J., Umeda, K., Connor, C.B., Weller, J.N., Zhao, D., Takahashi, M., 2004. Modeling long-term volcanic hazards through Bayesian inference: an example from the Tohoku volcanic arc Japan. *J. Geophys. Res.* 109, B10208.
- Marzocchi, W., Sandri, L., Selva, J., 2008. BET EF: a probabilistic tool for long- and short-term eruption forecasting. *Bull. Volcanol.* 70 (5), 623–632.
- Marzocchi, W., Sandri, L., Selva, J., 2010. BET VH: a probabilistic tool for long-term volcanic hazard assessment. *Bull. Volcanol.* 72, 705–716.
- Mathies, D., Mäusbacher, R., Storz, D., 1990. Deception Island tephra: a stratigraphical marker for limnic and marine sediments in Bransfield Strait area, Antarctica. *Zentralbl. Geol. Palaeontol.* Teil (1–2), 153–165.
- Moreton, S.C., 1999. Quaternary tephrochronology of the Scotia Sea and Bellingshausen Sea, Antarctica. Ph.D. thesis, Cheltenham and Gloucester College of Higher Education, pp. 164, unpublished.
- Moreton, S.G., Smellie, J.L., 1998. Identification and correlation of distal tephra layer; in deep-sea sediment cores, Scotia Sea, Antarctica. *Ann. Glaciol.* 27, 285–289.
- Neri, A., Aspinall, W.P., Cioni, R., Bertagnini, A., Baxter, P.J., Zuccaro, G., Andronico, D., Barsotti, S., Cole, P.D., Esposti Ongaro, T., Hincks, T.K., Macedonio, G., Papale, P., Rosi, M., Santacroce, R., Woo, G., 2008. Developing an event tree for probabilistic hazard and risk assessment at Vesuvius. *J. Volcanol. Geotherm. Res.* 178 (3), 397–415.
- Newhall, C.G., Hoblitt, R.P., 2002. Constructing event trees for volcanic crisis. *Bull. Volcanol.* 64, 3–20.
- Orheim, O., 1972. A 200-year Record of Glacier Mass Balance at Deception Island, South-west Atlantic Ocean, and Its Bearing on Models of Global Climate Change. *Institute of Polar Studies, Ohio State University*, p. 118.
- Ortiz, R., Araña, V., Vila, J., Viramonte, J.G., Mazzuoli, R., 1987. Mecanismos de erupción de la reciente actividad volcánica en Decepción. *Actas II Simposio Español de Estudios Antárticos. CSIC*, pp. 217–227.

- 1092 Palais, J.M., Kirchner, S., Delmas, R., 1989. Identification and correlation of volcanic
1093 eruption horizons in a 1000 year ice-core record from the South Pole. *Antarct. J. US*
1094 *Rev.* 24, 101–104.
- 1095 Pallàs, R., Smellie, J.L., Casas, J.M., Calvet, J., 2001. Using tephrochronology to date temper-
1096 ate ice: correlation between ice tephros on Livingston Island and eruptive units on
1097 Deception Island volcano (South Shetland Islands, Antarctica). *The Holocene* 11 (2),
1098 149–160.
- 1099 Patrick, M., Smellie, J.L., 2013. Synthesis. A spaceborne inventory of volcanic activity in
1100 Antarctica and southern oceans, 2000–10. *Antarct. Sci.* 25 (4), 475–500.
- 1101 Peccerillo, A., Tripodo, A., Villari, L., Currier, S., Zimbalaiti, E., 1991. Genesis and evolution
1102 of volcanism in back-arc areas. A case history, the Island of Deception (Western
1103 Antarctica). *Period. Mineralog.* 60, 29–44.
- 1104 Peci, L.M., Berrocoso, M., Fernández-Ros, A., García, A., Marrero, J.M., Ortiz, R., 2014.
1105 Embedded ARM system for volcano monitoring in remote areas: application to the
1106 active volcano on Deception Island (Antarctica). *Sensors* 14, 672–690.
- 1107 **Q12** Pedrazzi, D., Aguirre Díaz, G., Bartolini, S., Martí, J., Geyer, A., 2014. The 1970 eruption on
1108 Deception Island (Antarctica): eruptive dynamics and implications for volcanic haz-
1109 ards. *J. Geol. Soc. Lond.* (in press).
- 1110 Prates, G., Berrocoso, M., Fernández-Ros, A., García, A., 2013. Enhancement of sub-daily
1111 positioning solutions for surface deformation monitoring at Deception volcano
1112 (South Shetland Islands, Antarctica). *Bull. Volcanol.* 75 (2), 1–10.
- 1113 Ramos, M., Ortiz, R., Diez-Gil, J.L., Viramonte, J., 1989. Anomalías térmicas y balance de
1114 flujo energético sobre el suelo del volcán Decepción, Isla Decepción (Shetland del
1115 Sur). *Actas del III Simposium Español de Estudios Antárticos. CSIC*, pp. 203–219.
- 1116 Rey, J., Somoza, L., Martínez-Frías, J., 1995. Tectonic, volcanic, and hydrothermal event
1117 sequence on Deception Island (Antarctica). *Geo-Mar. Lett.* 15, 1–8.
- 1118 Roach, P.J., 1978. The nature of back-arc extension in Bransfield Basin. *Geophys. J. Roy.*
1119 *Astron. Soc.* 53, 165.
- 1120 Roobol, M.J., 1973. Historic volcanic activity at Deception Island. *Br. Antarct. Surv. Bull.* 32,
1121 23–30.
- 1122 (for 1979) Roobol, M.J., 1980. A model for the eruptive mechanism of Deception Island
1123 from 1820 to 1970. *Br. Antarct. Surv. Bull.* 49, 137–156.
- 1124 Roobol, M.J., 1982. The volcanic hazard at Deception Island, South Shetland Islands. *Br.*
1125 *Antarct. Surv. Bull.* 51, 237–245.
- 1126 Schilling, S.P., 1998. LAHARZ: GIS program for automated mapping of lahar-inundation
1127 hazard zones. U.S. Geological Survey Open-File Report, pp. 98–638.
- 1128 Sheridan, M.F., Malin, M.C., 1983. Application of computer-assisted mapping to volcanic
1129 hazard evaluation of surge eruption: Vulcano, Lipari, Vesuvius, explosive volcanism.
1130 *J. Volcanol. Geotherm. Res.* 17, 187–202.
- 1131 Shultz, C.H., 1972. Eruption at Deception Island, Antarctica, August 1970. *Geol. Soc. Am.*
1132 *Bull.* 83 (9), 2837–2842.
- 1133 Smellie, J.L., 1988. Recent observations on the volcanic history of Deception Island, South
1134 Shetland Islands. *Br. Antarct. Surv. Bull.* 81, 83–85.
- 1135 Smellie, J.L., 1999. The upper Cenozoic tephra record in the south polar region: a review.
1136 *Glob. Planet. Chang.* 21, 51–70.
- 1137 Smellie, J.L., 2001. Lithostratigraphy and volcanic evolution of Deception Island, South
1138 Shetland Islands. *Antarct. Sci.* 13, 188–209.
- Smellie, J.L., 2002a. Volcanic hazard. In: López-Martínez, J., Smellie, J.L., Thomson, J.W.,
Thomson, M.R.A. (Eds.), *Geology and Geomorphology of Deception Island*. Br. Antarct.
Surv., Natural Environmental Research Council, Cambridge, pp. 47–53. 1139–1141
- Smellie, J.L., 2002b. The 1969 subglacial eruption on Deception Island (Antarctica): events
and processes during an eruption beneath a thin glacier and implications for volcanic
hazards. *Volcano–Ice Interactions on Earth and Mars*. *Geol. Soc. Lond. Spec. Publ.* 202,
59–79. 1142–1145
- Smellie, J.L., López-Martínez, J., 2002a. Introduction. In: López-Martínez, J., Smellie, J.L.,
Thomson, J.W., Thomson, M.R.A. (Eds.), *Geology and Geomorphology of Deception Is-
land*. British Antarctic Survey, Natural Environmental Research Council, Cambridge,
pp. 1–6. 1146–1147
- Smellie, J.L., López-Martínez, J., and others, 2002. Geology and geomorphology of Decep-
tion Island. BAS GEOMAP series, Sheets G-A and G-B, 1:25 000. Cambridge, Br. Antarct.
Surv., Cambridge, pp. 78. 1148–1152
- Smith Jr., K.L., Baldwin, R.J., Glatts, R.C., Chereskin, T.K., Ruhla, H., Lagunc, V., 2003. **Q13**
Weather, ice, and snow conditions at Deception Island, Antarctica: long time-series
photographic monitoring. *Deep-Sea Res.* II 50, 1649–1664. 1154–1155
- Sobradelo, R., Martí, J., 2010. Bayesian event tree for long-term volcanic hazard assess-
ment: application to Teide-Pico Viejo stratovolcanoes, Tenerife, Canary Islands. *J.*
Geophys. Res. 115, B05206. 1156–1157
- Sobradelo, R., Bartolini, S., Martí, J., 2014. HASSET: a probability event tree tool to valueate
future volcanic scenarios using Bayesian inference presented as a plugin for QGIS.
Bull. Volcanol. 76, 770. 1158–1159
- Suzuki, T., 1983. A theoretical model for dispersion of tephra. In: Shimozuru, D.,
Yokoyama, I. (Eds.), *Arc Volcanism, Physics and Tectonics*. Terra Scientific Publishing
Company, Tokyo. 1160–1162
- Torrecillas, C., Berrocoso, M., García-García, A., 2006. The Multidisciplinary Scientific
Information Support System (SIMAC) for Deception Island. In: Fütterer, D.,
Damaske, D., Kleinschmidt, G., Miller, H., Tessensohn, F. (Eds.), *Antarctica*. Springer,
Berlin Heidelberg, pp. 397–402. 1163–1166
- Toyos, G.P., Cole, P.D., Felpeto, A., Martí, J., 2007. A GIS-based methodology for hazard
mapping of small pyroclastic density currents. *Nat. Hazards* 41, 99–112. 1167–1170
- Turner, J., Pendlebury, S., 2004. *The International Antarctic Weather Forecasting Hand-
book*. Br. Antarct. Surv., Cambridge. 1171–1172
- Valencio, A., Mendía, E., Vilas, J., 1979. Palaeomagnetism and K–Ar age of Mesozoic and
Cenozoic igneous rocks from Antarctica. *Earth Planet. Sci. Lett.* 45, 61–68. 1173–1174
- Valenzuela, E., Chávez, L., Munizaga, F., 1970. Actividad volcánica en isla Decepción,
Antártica, 1967. *Inst. Antártico Chil. Ser.* 1, 5–16. 1175–1176
- Wilkes, C., 1845. American Exploring Expedition: Narrative of the United States Exploring
Expedition During the Years 1838–1842 I–V. Lea and Blanchard, Philadelphia. 1177–1178
- Woo, G., 1999. *The Mathematics of Natural Catastrophes*. Imperial College Press, London. 1179
- Zandomenighi, D., Barclay, A., Almendros, J., Ibáñez, J.M., Wilcock, W.S.D., Ben-Zvi, T.,
2009. The crustal structure of Deception Island Volcano from P wave seismic tomog-
raphy: tectonic and volcanic implications. *J. Geophys. Res.* 11, B06310.

Appendix 6

Hazard assessment at the Quaternary La Garrotxa Volcanic Field (NE Iberia)



**Hazard assessment at the Quaternary La Garrotxa
Volcanic Field (NE Iberia)**

Journal:	<i>Journal of Quaternary Science</i>
Manuscript ID:	JQS-14-0200.R1
Wiley - Manuscript type:	Research Article
Date Submitted by the Author:	n/a
Complete List of Authors:	Bartolini, Stefania; CSIC, ICTJA Bolós, Xavier; CSIC, ICTJA Martí, Joan; CSIC, ICTJA Riera Pedra, Elisabeth; CSIC, ICTJA Planagumà, Llorenç; Tosca S.A. Serveis d'Educació Ambiental
Keywords:	Garrotxa Volcanic Field, Volcanic hazard, Volcanic susceptibility, Recurrence rate, European Cenozoic Rifts System

SCHOLARONE™
Manuscripts

Hazard assessment at the Quaternary La Garrotxa Volcanic Field (NE Iberia)

Stefania Bartolini^{a*}, Xavier Bolós^a, Joan Martí^a, Elisabeth Riera Pedra^a, Llorenç Planagumà^b

^a *Institute of Earth Sciences Jaume Almera, ICTJA-CSIC, Group of Volcanology, SIMGEO (UB-CSIC), Lluís Solé i Sabarís s/n, 08028 Barcelona, Spain.*

^b *Tosca, Environment Services of Education. Casal dels Volcans, Av. Santa Coloma, 17800 Olot, Spain.*

Corresponding author: tel.: +34 934095410; *E-mail address:* sbartolini.1984@gmail.com (S. Bartolini).

Submitted to: Journal of Quaternary Science

1 **Abstract**

2 La Garrotxa Volcanic Field (GVF), located in NE Iberian Peninsula, is
3 one of the Quaternary alkaline volcanic provinces of the European Cenozoic
4 Rifts System. This volcanic zone has been active during the last 12 Ma, being
5 the last dated eruption of early Holocene age. The volcanic activity varies from
6 Hawaiian to Violent Strombolian, showing numerous episodes of
7 phreatomagmatic activity, and has been controlled by the main regional normal
8 faults generated during the Neogene extension that affected the area. Despite
9 the potentiality for future eruptions and the fact that this is a densely populated
10 and industrialised area, volcanic hazard assessment has not been conducted
11 yet. In this work, we present the first comprehensive evaluation of volcanic
12 hazard at La Garrotxa Volcanic Field, through (1) an evaluation of the volcanic
13 susceptibility, (2) a temporal recurrence rate analysis, (3) a simulation of
14 different eruptive scenarios, such as lava flow, pyroclastic density current
15 (PDC), and ash fall, and (4) the elaboration of a qualitative hazard map. The
16 final hazard map shows La Garrotxa volcanic field subdivided into five different
17 levels of hazards and aims to become useful for land use management planning
18 and elaboration of emergency plans.

19

20

21

22 **Keywords** Garrotxa Volcanic Field · Volcanic hazard · Volcanic susceptibility ·
23 Recurrence rate · European Cenozoic Rifts System

24

25

26

27

28

29

30

31

32

33

34

35 **Introduction**

36 The impact of a natural event, as a volcanic eruption, can significantly
37 affect human life. Long periods of quiescence are quite common in many
38 volcanic areas and this often leads to a reduction of the alert level. The
39 consequence is not being prepared to deal with a volcanic crisis. For this
40 reason it is necessary to evaluate the possible hazards that could affect the
41 studied area and develop volcanic hazard and risk maps. Volcanic hazard
42 assessment is part of the scientific task to be achieved in an active volcanic
43 area where population could be affected by an eruptive episode. Possible future
44 volcanic activity can be understood and predicted by analysing the past eruptive
45 behaviour, through the study of the geological record.

46 Most of the hazard assessment studies conducted during last years refer
47 to composite or stratovolcanoes located close to populated areas, for which
48 volcanic threat is always present (e.g.: Somma-Vesuvio, Italy (Lirer *et al.*, 2001);
49 Campi Flegrei and Somma-Vesuvio (Alberico *et al.*, 2011); Teide-Pico Viejo,
50 Canary Islands (Martí *et al.*, 2008); Popocatepetl, Mexico (Siebe and Macías,
51 2006); Mt. Cameroon, Africa (Favalli *et al.*, 2012); Etna, Italy (Cappello *et al.*,
52 2011)). However, monogenetic volcanic fields are commonly not regarded as
53 potentially dangerous and only a few studies concerning hazard assessment
54 have been conducted in such environments (e.g.: Auckland volcanic field, New
55 Zealand (Bebbington and Cronin, 2011), El Hierro, Canary Islands (Becerril *et al.*,
56 2014); Tohoku volcanic arc, Japan (Martin *et al.*, 2004)). This is probably
57 due to the relative small size of their eruptions and their episodic recurrence,
58 sometimes separated by inter-eruptive periods of thousands to ten thousands
59 years. Nevertheless, numerous Quaternary monogenetic volcanic fields exist
60 around the World, covering periods of activity from several millions of years to
61 present, sometimes with high potentiality to erupt in the near future (Wood,
62 1980; Cas and Wright, 1987; Kereszturi and Németh, 2012). Examples of
63 monogenetic eruptions occurred in recent times after long periods of
64 quiescence are not uncommon (e.g.: Jorullo, Mexico (Guilbaud *et al.*, 2011),
65 Paricutin, Mexico (Scandone, 1979), El Hierro, Canary Islands (Becerril *et al.*,
66 2014)). All this tells us that undertaking hazard assessment in Quaternary
67 monogenetic fields is also necessary as a precautionary measure to reduce
68 volcanic risk, even if no signals of volcanic activity are now present.

69 La Garrotxa Volcanic Field (GVF) has been active from 0.7 Ma to early
70 Holocene (Araña *et al.*, 1983; Bolós *et al.*, 2014a). Since 2013, this volcanic
71 field is considered as an active volcanic area jointly to other Spanish volcanic
72 zones, such as the Canary Islands (see Spanish for Official Bulletin of the State
73 (B.O.E) of February 11th of 2013). In addition, this area is highly populated with
74 urban, agricultural, industrial and communication infrastructure including an
75 international airport. However, no studies have addressed the assessment of
76 volcanic hazard and risk, essential task that should enable local authorities to
77 apply more rational territorial planning and to design more adequate emergency
78 plans in order to face future volcanic crises.

79 The aim of this study is to obtain a qualitative long-term volcanic hazard
80 map of the GVF, taking into account that an important part of this zone lies
81 underneath the city of Olot (almost 40,000 inhabitants). This is a highly
82 industrialised and urbanised area covering about 30 km². Recent studies (Bolós
83 *et al.*, 2014a), (Bolós *et al.*, 2014b), (Bolós *et al.*, 2014c), have permitted to
84 obtain a detailed picture of the stratigraphic evolution and structural controls of
85 this volcanic zone, filling the gap of an incomplete knowledge due to urban and
86 industrial construction, and due to a dense carpet of vegetation covering most
87 of volcanic deposits.

88 Taking advantage of this new geological and volcanological knowledge of
89 the area, we conduct its hazard assessment assuming that the future eruptive
90 behaviour will be similar to the last eruptive activity, thus taking as the main
91 reference for a potential future eruption the eruption of Croscat, the last dated
92 (11-13 ka) of the GVF (Fig. 1a and Fig. 2). We first describe the main
93 geological, stratigraphic, structural, and volcanological features of the area.
94 Then we compute the volcanic susceptibility by identifying those zones with a
95 higher probability of hosting a new vent. This information is then used to
96 compute different simulations of eruptive scenarios. Finally, we obtain a
97 qualitative hazard map that allows us to identify different levels of hazard in the
98 study area.

99

100 **General features of the GVF**

101 GVF is the youngest part of the Catalan Volcanic Zone (CVZ), situated in
102 the NE part of Iberian Peninsula (Fig. 1b). This basaltic monogenetic field is one

103 of the Quaternary alkaline volcanic provinces belonging to the European
104 Cenozoic Rift System (Martí *et al.*, 1992; Dèzes *et al.*, 2004). The CVZ ranges
105 in age from >12 Ma to early Holocene and it is mainly represented by alkaline
106 basalts and basanites (Martí *et al.*, 1992; Cebriá *et al.*, 2000). GVF is
107 characterised by small-sized cinder cones formed along widely dispersed
108 fissure zones during monogenetic, short-lived eruptions. Hydromagmatic events
109 were also common. Each eruption was caused by an individual batch of magma
110 that was transported rapidly from the source region, each batch representing
111 the products of an individual partial melting event (Martí *et al.*, 1992; Bolós *et al.*
112 *et al.*, 2014c). The magma ascent rates indicate that only a relatively short time
113 was required for magma to reach the surface (Bolós *et al.*, 2014c). The
114 intermittent character of this volcanism (Martí *et al.*, 1992) indicates that each
115 eruptive episode corresponds to an intermittent reactivation of the main fault
116 system every 5,000 – 20,000 years. These tectonic reactivations would permit
117 the ascent of deep magma and the opening of subordinate fractures in the
118 uppermost crust, which would erupt on the surface each time in a different
119 location in the volcanic field (Bolós *et al.*, 2014c).

120 The GVF embraces two geographically distinct zones, the larger one
121 located in the north in the area of La Garrotxa and a southerly area that
122 contains fewer but larger and more complex volcanic edifices (Martí *et al.*, 2011;
123 Bolos *et al.*, 2014a) (Fig. 1a). Although both corresponding to tectonically
124 controlled depressions, the northern sector has a substrate of thick layers of
125 Tertiary affected by Alpine reverse faults and Quaternary sediments.
126 Geophysical data and volcano-structural analysis show that the previous Alpine
127 tectonic structures played no apparent role in controlling the loci of this
128 volcanism (Bolós *et al.*, 2014c). In the southern sector is floored by
129 unconsolidated Quaternary sediments in combination with the Palaeozoic
130 basement.

131 GVF is formed by more than 50 well preserved monogenetic volcanic
132 cones, distributed along the fracture system of NNW-SSE direction (Barde-
133 Cabusson *et al.*, 2014), corresponding to the Neogene extensional faults
134 system, associated to the main transtensional faults that constrain this volcanic
135 field (Bolós *et al.*, 2014c).

136 The total volume of extruded magma in each eruption is typical of the
137 monogenetic volcanism (0.01–0.2 km³ Dense-Rock Equivalent (DRE))
138 (Cimarelli *et al.*, 2013; Bolós *et al.*, 2014a), suggesting that the magma
139 available to feed each eruption was also very limited. Strombolian and
140 phreatomagmatic episodes alternated in most of these eruptions giving rise to
141 complex stratigraphic successions composed of a wide range of pyroclastic
142 deposits (Martí and Mallarach, 1987; Martí *et al.*, 2011).

143 Most volcanoes show different phases during the same eruptive event.
144 The activity varies from Hawaiian to Violent Strombolian, whereby we found
145 alternate deposits of phreatic phases produced by vapour explosions that only
146 erupted lithic clasts from the substrate, with typical phreatomagmatic phases
147 that generated a wide diversity of pyroclastic density currents and fallout
148 deposits, with typically Strombolian phases including explosive and effusive
149 episodes (Martí *et al.*, 2011).

150

151 **Methods**

152 Long-term volcanic hazard assessment is defined as the evaluation of
153 the eruption recurrence and the possible nature of a forthcoming eruption,
154 based on the past history of the volcano and information from the geological
155 record (Marzocchi *et al.*, 2006; Becerril *et al.*, 2014; Bartolini *et al.*, 2014). To
156 evaluate the long-term volcanic hazard, different steps need to be followed
157 sequentially (see Alcorn *et al.*, 2013; Becerril *et al.*, 2014; Bartolini *et al.*, 2014).
158 In this study, we carried out both temporal and spatial analyses: the former
159 evaluates the recurrence rate of the volcanic activity in the studied area, while
160 the latter uses simulation models to predict the most probable eruptive
161 scenarios and which areas could be affected by a future eruptive event. Since
162 the results from these temporal and spatial analyses are highly dependent on
163 the data used, the selection of the data source is one of the most important
164 steps to be undertaken during the hazard evaluation.

165 The susceptibility analysis is the first step and enables us to identify
166 which areas have the greatest likelihood of hosting new vents (Martí and
167 Felpeto, 2010). Once the susceptibility analysis has been estimated, the next
168 step consists of computing several eruptive scenarios as a means of evaluating
169 the potential extent of the main expected volcanic and associated hazards. The

170 evaluation of volcanic susceptibility and eruptive scenarios are based on the
171 use of simulation models and Geographical Information Systems (GIS) that
172 allow volcanic hazards to be modelled. Volcanic susceptibility was calculated
173 using QVAST tool (Bartolini *et al.*, 2013), and modelling of eruptive scenarios,
174 which include lava flows, pyroclastic density currents (PDCs), and fallout, used
175 the VORIS 2.0.1 tool (Felpeto *et al.*, 2007). For detailed information regarding
176 each specific tool, readers are referred to the original papers.

177

178 **Characterisation of past eruptive activity**

179 To forecast the future behaviour of the volcanic area under study we
180 need to know its past eruptive history. So, we need to characterise the past
181 volcanic activity through the determination of eruptive parameters derived from
182 the study of the erupted products. The last dated and well-studied eruptive
183 episode of La Garrotxa corresponds to the Croscat volcano, one of the most
184 representative edifices of the N sector of the studied area (Fig. 1a and Fig. 2),
185 so that we take it as the past eruption example to be used to define future
186 eruptive scenarios. This volcano is approximately 160 meters high and has a
187 base diameter of 950 meters and it has been dated in $11,500 \pm 1,500$ years
188 (Martí *et al.*, 2011; Puiguriquer, 2012; Bolós *et al.*, 2014a).

189 Recent studies show as Croscat has a complicated eruptive sequence
190 (Martí *et al.*, 2011; Bolos *et al.*, 2014a). The Croscat volcano corresponds to the
191 cone building phase of a more complex eruption that occurred along the longest
192 eruptive fissure identified in this volcanic field (Fig. 2). This eruption also
193 created the Santa Margarida and La Pomareda vent sites at both end of the
194 fissure with the Croscat volcano in the middle of it. For the purpose of this study
195 we only consider the Croscat cone building phase. The Croscat activity
196 generated three main scoria fallout units (Di Traglia *et al.*, 2009; Martí *et al.*,
197 2011) (Fig. 2). The lower one corresponds to a spatter deposit formed during a
198 Hawaiian phase that generated also the spatter deposit of La Pomareda at the
199 northern end of the eruptive fissure (Martí *et al.*, 2011; Bolós *et al.*, 2014a). The
200 middle unit conformably overlies the basal spatter and is formed by a several
201 metres thick, poorly stratified Strombolian coarse lapilli size scoria deposit with
202 several scoria bomb beds. The upper unit constitutes the main volume of the
203 Croscat cone and is formed by a well stratified to thinly laminated, medium to

204 fine lapilli size scoria deposit, more than ten metres thick that contains sparse
205 scoria bombs and blocks and that forms most of the intermediate to distal
206 outcrops towards the east of the volcano, that can be recognised at distances
207 farther than 5 km. It also covers the Pomareda spatter and the
208 phreatomagmatic deposits and the explosion crater of Santa Margarida. The
209 topmost unit of the Croscat pyroclastic succession corresponds to a few metres
210 thick, lithic-rich, thinly laminated pyroclastic surge deposit, thus indicating the
211 return to phreatomagmatic activity towards the end of the eruption. This deposit
212 extends for several kilometres to the east, covering area of 8.4 km².

213 The last eruptive phase of Croscat corresponds to a lava flow that
214 covered an area of 5 km² and flowed more than 10 km west, with an average
215 thickness of 10 m of the emplacement, which emplacement caused the
216 breaching of the western flank of the cone. The total volume of magma (DRE)
217 emitted during the Croscat eruption is of the order of 0.2 km³.

218

219 **Volcanic susceptibility**

220 The first step to undertake hazard assessment is to determine the
221 location of possible new eruptive vents, i.e. the susceptibility analysis (Felpeto
222 *et al.*, 2007; Martí and Felpeto, 2010). In monogenetic volcanism volcanic
223 susceptibility contains a high degree of randomness caused by the changes in
224 regional and/or local stress fields originated by tectonic or lithological contrasts
225 (Martí *et al.*, 2013). So, to reduce the uncertainty in the spatial forecasting, the
226 calculation of the probability of the opening of new emission centres should take
227 into account all available volcano-structural parameters (fractures, faults,
228 location of vents, eruptive fissures, etc...). In the case of the GVF, the input
229 parameters we used were the location of past recognisable eruptive vents and
230 fissures, but also structural elements related to this volcanism such as fractures
231 and faults identified in previous geological and geophysical studies (Barde-
232 Cabusson *et al.*, 2014; Bolós *et al.*, 2014b), (Bolós *et al.*, 2014c).

233 Once all the input parameters are obtained, the next step is to apply
234 different statistical methods in order to obtain the corresponding probability
235 density functions (PDFs) required to obtain the final susceptibility map (Martin *et*
236 *al.*, 2004; Felpeto *et al.*, 2007; Connor and Connor, 2009; Martí and Felpeto,
237 2010; Cappello *et al.*, 2012; Becerril *et al.*, 2013; Bartolini *et al.*, 2013). The

238 PDFs for the GVF were obtained through the application of the QVAST tool
239 (Bartolini *et al.*, 2013). The most important factor is the smoothing coefficient h
240 that determines the shape and, consequently, the resulting PDF. It depends on
241 a combination of different factors such as the size of the volcanic field and the
242 degree of clustering or density of the volcano-structural data (Cappello *et al.*,
243 2012; Becerril *et al.*, 2013; Bartolini *et al.*, 2013). The smoothing factor values
244 we used were: (a) 1568 m for Holocene and Upper Pleistocene volcanism vents
245 and fissures, (b) 1900 m for Middle Pleistocene volcanism vents and fissures,
246 (c) 363 m for normal and transtensional Neogen faults, and (d) 5856 m for
247 inferred faults. The PDFs obtained are shown in Figure 3.

248 Once the PDF is obtained for each type of structural data, we need to
249 combine them in a Non-Homogeneous Poisson Process (NHPP) to obtain the
250 final susceptibility map. These weights were assigned using expert elicitation
251 judgment (see Aspinall, 2006; Neri *et al.*, 2008) by members from the Group of
252 Volcanology of Barcelona on the basis of structural criteria (see Martí and
253 Felpeto, 2010), which provide initial indicative probability distributions
254 associated with each PDF. We obtained the following values: 0.5 for the
255 Holocene and Upper Pleistocene volcanism (vents and alignments), 0.25 for the
256 Middle Pleistocene craters and lineaments, 0.15 for normal and transtensional
257 Neogen faults, and 0.07 for inferred faults.

258 The final susceptibility map obtained is shown in Figure 4. The map
259 represents those areas with more or less probability to host a new vent and is
260 important as input parameter in the eruptive scenarios simulation to localise the
261 starting point for simulating lava flows, PDCs, and ash fall.

262

263 **Temporal recurrence rate**

264 Temporal analysis to determine the recurrence rate of the volcanic
265 activity is an important issue in hazard assessment, as it allows to calculate the
266 temporal probability of occurrence of a new event.

267 The approach that we used to calculate the temporal recurrence rate λ_t is
268 based on the repose-time method (Ho *et al.*, 1991; Connor and Conway, 2000).
269 In this method, the average recurrence rates of volcanic events depend only on
270 the measure of the relative activity of the Garrotxa volcanic field (for details of
271 volcanic events in the GVF see Table 2 in Bolós *et al.*, 2014a). Average

272 recurrence rates of volcanic events are a simple measure of the relative activity
273 in volcanic fields, defined using a maximum likelihood estimator that averages
274 events over a specific period of volcanic activity (Connor and Conway, 2000):
275

$$276 \quad \lambda_r = \frac{N-1}{t_0 - t_y} \quad (1)$$

277 where N is the total number of eruptions or vents, t_0 is the age of the oldest
278 event and t_y is the age of the youngest event. For the GVF we obtain a long-
279 term average recurrence rate of $7.7 \cdot 10^{-5}$ volcanic events per year (v/yr).
280

281 **Eruptive scenarios**

282 Eruptive scenarios were computed using a VORIS 2.0.1 tool (Felpeto *et*
283 *al.*, 2007; available at <http://www.gvb-csic.es/GVB/VORIS/VORIS.htm>),
284 developed in a GIS framework (ArcGis®), which enables to elaborate volcanic
285 hazard maps and eruptive scenarios based on geological record information.
286 The VORIS 2.0.1 tool generates quantitative hazard maps for lava flows and
287 PDCs and simulates fallout deposits for a single vent. A 50 m resolution digital
288 elevation model (DEM) was used for topography during the lava flow and PDC
289 simulations. The DEM was generated by the Institut Cartogràfic i Geològic de
290 Catalunya (ICGC, <http://www.icc.cat>).

291 In the following subsections we present the input parameters for the
292 models based on the eruptive behaviour of the Croscat volcano described
293 before.

294

295 *Lava flow*

296 Lava flow model is a probabilistic model based on the assumption that
297 the topography and flow thickness play major roles in determining the path
298 followed by the lava flow (Felpeto *et al.*, 2007 and references therein). Input
299 data for the simulation are a Digital Elevation Model (DEM), the maximum flow
300 lengths and height correction (i.e. average thickness of the flow). The Croscat
301 lava flow flowed for more than 10 km, which is a distance in accordance to other
302 lava flows of the same area (Martí *et al.*, 2011). Thus, we assumed maximum
303 flow lengths in our simulation of the order of 12 km. The thickness used as input

304 data for the models was 10 m, corresponding to the average value of individual
305 flows (Crosca and others) measured in the field. We ran simulations for all cells
306 in the DEM and the sum of the 5,000 iterations provided a map with the
307 probability for any particular cell of being covered by a lava flow.

308 The result of the simulation in the GVF is shown in Figure 5. It consists of
309 a lava flow simulation probability map, which shows that there is a moderate-to-
310 high probability that the municipalities of Olot and Girona, two populated areas,
311 will be affected by lava flows.

312

313 *Pyroclastic density current*

314 Numerical simulation for PDCs is based on the concept of the energy
315 cone model (Malin and Sheridan, 1982; Felpeto *et al.*, 2007; Toyos *et al.*, 2007),
316 constrained by the topography, collapse equivalent height of the column, and
317 friction parameter, known as the collapse equivalent angle. The output of the
318 model is the maximum potential extent that can be affected by the PDC.

319 The eruptive constraints of the PDC simulation were estimated from the
320 extent of Crosca eruption, one of the best examples of a PDC from the GVF.
321 The runout length was considered equivalent to the most distal exposure of
322 Crosca uppermost phreatomagmatic pyroclastic density current deposit, which
323 lies about 5 km from the crater towards the southeast. To reproduce a PDC
324 deposit similar to that from Crosca, collapse equivalent heights of 400 m above
325 the vent were chosen together with an angle of 6°. The result shows that a PDC
326 could reach with high probability a large area (about 8 km diameter) around the
327 municipality of Olot (Fig. 6).

328

329 *Ash fall*

330 The numerical model for the simulation of ash fall is an advection-
331 diffusion model where the vertical distribution of mass is calculated using the
332 Suzuki approach (Suzuki, 1983; Felpeto *et al.*, 2007). The main input
333 parameters are the volume emitted during the eruption, the height of the
334 column, the particles grain-size characteristics, and the wind data. The result of
335 the ash fall simulation is the thickness of the ash deposit in the analysed area.

336 The eruptive style considered in this study was a violent Strombolian
337 eruption, which coincides with the main magmatic phase of the Crosca

338 eruption. The corresponding input data were obtained from distribution of the
339 fallout deposits, considering that the total volume of magma (DRE) emitted was
340 of the order of 0.2 km^3 (Martí *et al.*, 2011). We assumed a volume of about 0.05
341 km^3 for the fallout phase and an eruptive column about 8 km high, considering
342 that the tephra deposits from this volcanic episode had reached Banyoles Lake
343 25 km towards the East (Höbig *et al.*, 2012). Westerly and southwesterly winds
344 prevail in general throughout the year at intervals of about 1500 m up to an
345 altitude of 9,000 m (Farnell and Llasat, 2013). Up to five different wind direction
346 inputs and intensities at different vertical heights can be set with the VORIS
347 2.0.1 tool. Data on particle size were obtained from field studies and grain-size
348 analysis of selected samples sieved in the laboratory.

349 The result shows that a fallout with the characteristics described above
350 and with W-SW predominant winds could affect a large area of the
351 northwesterly sector of the GVF around the municipality of Olot (Fig. 7),
352 according to the ash deposits found in Banyoles lake (Höbig *et al.*, 2012).

353

354 **Discussion and conclusions**

355 The long-term hazard assessment is a necessary task to be undertaken
356 at Quaternary monogenetic volcanic fields, even if eruptive activity has not been
357 recorded in recent (historical or pre-historical) times. Most of these volcanic
358 regions show very long recurrence periods, so that they are frequently regarded
359 as non-active. However, the fact that volcanic activity has been present a long
360 time ago, normally for several millions of years, and the fact that the same
361 geodynamic conditions that gave rise to these volcanisms in most cases still
362 prevail, constitute sufficient evidence to consider these areas with the
363 necessary caution to assume that future eruptions may have a low probability
364 but are not impossible. The demographic expansion of most of these areas
365 recommends undertaking hazard assessment as a precaution measure in order
366 to reduce the potential risk that could affect them.

367 The GVF is a typical monogenetic field in which the lack of data and the
368 absence of recent eruptions could lead us to assume that volcanic hazard and,
369 consequently, risk is inexistent. On the contrary, all geological indicators
370 suggest that the area is subjected to the same geodynamic conditions that
371 favoured the initiation and continuation of this volcanism, so that we must

372 consider this volcanic area as potentially active. In fact the important socio-
373 economic development of the area and the high number of infrastructures,
374 including an international airport, requires to evaluate the potential hazard of the
375 zone and to identify those areas that could be affected by an eruption of the
376 same type than the ones occurred more recently.

377 Based on a susceptibility analysis and the identification of the most
378 common eruptive types and products from the geological record, we have
379 applied the available tools, such as QVAST (Bartolini *et al.*, 2013) and VORIS
380 2.0.1 (Felpeto *et al.*, 2007), designed to undertake volcanic hazard assessment
381 and to update the results whenever new information becomes available. These
382 tools allowed us to simulate different eruptive scenarios and to develop a long-
383 term qualitative hazard map of the area.

384 The volcanic hazard map of the GVF (Fig. 8) has been obtained using a
385 combination of the lava flow, PDC, and fallout eruptive scenario simulations,
386 and represents how the area could be affected by future eruptive events. This
387 first hazard map also takes into account the results of ash fall simulations
388 strictly dependent on the average of the wind directions and velocities, which
389 means that it will be updated if new data were available based on the
390 meteorological predictions. We have considered five different levels of hazard,
391 from very low to very high, thus indicating the relative probability for the area of
392 being affected by any of the hazards considered in this work. The final
393 qualitative hazard map (Fig. 8) will be useful to minimise the impact of future
394 volcanic eruptions in the area, allowing local authorities to use it as a reference
395 for land-use planning and for the elaboration of an emergency plan for the GVF.

396

397 **Acknowledgements**

398 This research has been partially funded by the European Commission
399 (FP7 Theme: ENV.2011.1.3.3-1; Grant 282759: VUELCO). We would like to
400 thank Jordi Zapata of the Museu dels Volcans d'Olot for his help with the
401 meteorological information.

402

403

404

405

406

407 **References**

408 Alberico I, Petrosino P, Lirer L. 2011. Volcanic hazard and risk
409 assessment in a multi-source volcanic area: the example of Napoli city
410 (Southern Italy). *Natural Hazards and Earth System Science* **11**: 1-14.

411 Alcorn R, Panter KS, Gorsevski PV. 2013. A GIS-based volcanic hazard
412 and risk assessment of eruptions sourced within Valles Caldera, New Mexico.
413 *Journal of Volcanology and Geothermal Research* **267**: 1-14.

414 Araña V, Aparicio A, Martín Escorza C, García Cacho L, Ortiz R, Vaquer
415 R, Barberi F, Ferrara G, Albert J, Gassiot X. 1983. Neogene-Quaternary
416 volcanism of Catalunya: structural, petrological, and geodynamic
417 characteristics. *Acta Geologica Hispanica* **18**: 1-17.

418 Aspinall WP. 2006. Structured elicitation of expert judgment for
419 probabilistic hazard and risk assessment in volcanic eruptions. In *Statistics in*
420 *Volcanology*, Mader HM, Coles SG, Connor CB, Connor LJ (eds). Geological
421 Society of London: Special Publication of IAVCEI 1; 15–30.

422 Barde-Cabusson S, Gottsman J, Martí J, Bolós X, Camacho AG, Geyer
423 A, Planagumà LI, Ronchin E, Sanchez A. 2014. Structural control of
424 monogenetic volcanism in the Garrotxa volcanic field (Northeastern Spain) from
425 gravity and self-potential measurements. *Bulletin of Volcanology* **76**: 788.

426 Bartolini S, Cappello A, Martí J, Del Negro C. 2013. QVAST: a new
427 Quantum GIS plugin for estimating volcanic susceptibility. *Natural Hazards and*
428 *Earth System Science* **13**: 3031–3042.

429 Bartolini S, Geyer A, Martí J, Pedrazzi D, Aguirre-Díaz G. 2014. Volcanic
430 hazard on Deception Island (South Shetland Islands, Antarctica). *Journal of*
431 *Volcanology and Geothermal Research*, 10.1016/j.jvolgeores.2014.08.009.

432 Bebbington MS, Cronin SJ. 2011. Spatio-temporal hazard estimation in
433 the Auckland Volcanic Field, New Zealand, with a new event-order model.
434 *Bulletin of Volcanology* **73**: 55–72.

435 Becerril L, Bartolini S, Sobradelo R, Martí J, Morales JM, Galindo I. 2014.
436 Long-term volcanic hazard assessment on El Hierro (Canary Islands). *Natural*
437 *Hazards and Earth System Science* **14**: 1853-1870.

- 438 Bolós X, Planagumà L, Martí J. 2014a. Volcanic stratigraphy and
439 evolution of the Quaternary monogenetic volcanism in the Catalan Volcanic
440 Zone (NE Spain). *Journal of Quaternary Science* **29(6)**: 547–560.
- 441 Bolós X, Barde-Cabusson S, Pedrazzi D, Martí J, Casas A, Lovera R,
442 Nadal-Sala D. 2014b. Geophysical exploration on the subsurface geology in the
443 monogenetic La Garrotxa Volcanic Field (NE Iberian Peninsula). *International*
444 *Journal of Earth Science*, <http://dx.doi.org/10.1007/s00531-014-1044-3>.
- 445 Cappello A, Vicari A, Del Negro C. 2011. Assessment and modeling of
446 lava flow hazard on Etna volcano. *Bollettino di Geofisica Teorica ed Applicata*
447 **52(2)**: 299-308.
- 448 Cappello A, Neri M, Acocella V, Gallo G, Vicari A, Del Negro C. 2012.
449 Spatial vent opening probability map of Mt Etna volcano (Sicily, Italy). *Bulletin of*
450 *Volcanology* **74(9)**: 2083-2094.
- 451 Cas RAF, Wright JV. 1987. *Volcanic successions (modern and ancient).*
452 *A geological approach to processes products and successions*. Allen and
453 Unwin: London.
- 454 Cebrià JM, López-Ruiz J, Doblás M, Oyarzun R, Hertogen J, Benito R.
455 2000. Geochemistry of the Quaternary alkali basalts of Garrotxa (NE Volcanic
456 Province, Spain): a case of double enrichment of the mantle lithosphere.
457 *Journal of Volcanology and Geothermal Research* **102**: 217-235.
- 458 Cimarelli C, Di Traglia F, de Rita D, Gimeno Torrente D, Fernandez Turiel
459 JL. 2013. Space–time evolution of monogenetic volcanism in the mafic Garrotxa
460 Volcanic Field (NE Iberian Peninsula). *Bulletin of Volcanology* **75**: 758.
- 461 Connor CB, Conway FM. 2000. Basaltic Volcanic Fields. In *Encyclopedia*
462 *of Volcanology*. Academic Press; 331-343.
- 463 Connor CB, Connor LJ. 2009. Estimating spatial density with kernel
464 methods. In *Volcanic and Tectonic Hazard Assessment for Nuclear Facilities*,
465 Connor CB, Chapman NA, Connor LJ (eds). Cambridge University Press; 346–
466 368.
- 467 Dèzes P, Schmid SM, Ziegler PA. 2004. Evolution of the European
468 Cenozoic Rift System: interaction of the Alpine and Pyrenean orogens with their
469 foreland lithosphere. *Tectonophysics* **389**: 1–33.
- 470 Di Traglia F, Cimarelli C, de Rita D, Gimeno Torrente, D. 2009. Changing
471 eruptive styles in basaltic explosive volcanism: examples from Croscat complex

472 scoria cone, Garrotxa Volcanic Field (NE Iberian Peninsula). *Journal of*
473 *Volcanology and Geothermal Research* **180**: 89–109.

474 Farnell C, Llasat MC. 2013. Proposal of three thermodynamic variables
475 to discriminate between storms associated with hail and storms with intense
476 rainfall in Catalonia. *Tethys* **10**: 25–34.

477 Favalli M, Tarquini S, Papale P, Fornaciai A, Boschi E. 2012. Lava flow
478 hazard and risk maps at Mount Cameroon volcano. *Bulletin of Volcanology* **74**:
479 423–439.

480 Felpeto A, Martí J, Ortiz R. 2007. Automatic GIS-based system for
481 volcanic hazard assessment. *Journal of Volcanology and Geothermal Research*
482 **166**: 106–116.

483 Guilbaud MN, Siebe C, Layer P, Salinas S, Castro-Govea R, Garduño
484 Monroy VH, Le Corvec N. 2011. Geology, geochronology, and tectonic
485 setting of the Jorullo volcano region, Michoacán, México. *Journal of*
486 *Volcanology and Geothermal Research* **201**: 97–112.

487 Ho CH, Smith EI, Feuerbach DL, Naumann TR. 1991. Eruptive
488 calculation for the Yucca Mountain site, USA: statistical estimation of recurrence
489 rates. *Bulletin of Volcanology* **54**: 50–56.

490 Höbig N, Weber ME, Kehl M, Weniger GC, Julià R, Melles M, Fülöp RH,
491 Vogel H, Reicherter K. 2012. Lake Banyoles (northeastern Spain): A Last
492 Glacial to Holocene multi-proxy study with regard to environmental variability
493 and human occupation. *Quaternary International* **274**: 205–218.

494 Lirer L, Petrosino P, Alberico I. 2001. Volcanic hazard assessment at
495 volcanic fields: the Campi Flegrei case history. *Journal of Volcanology and*
496 *Geothermal Research* **101(1–4)**: 55–75.

497 Malin MC, Sheridan MF. 1982. Computer-assisted mapping of pyroclastic
498 surges. *Science* **217**: 637–640.

499 Martí J, Mallarach JM. 1987. Erupciones hidromagmáticas en el
500 volcanismo cuaternario de Olot. *Estudios Geológicos* **43**: 31–40.

501 Martí J, Mitjavila J, Roca E, Aparicio A. 1992. Cenozoic magmatism of
502 the Valencia trough (western Mediterranean): relationship between structural
503 evolution and volcanism. *Tectonophysics* **203**: 145–165.

504 Martí J, Aspinall W, Sobradelo R, Felpeto A, Geyer A, Folch A, Teixidó F,
505 Ortiz R, Baxter P, Cole P, Pacheco J, Blanco MJ, Lopez C. 2008. A long-term

506 volcanic hazard event tree for Teide-Pico Viejo stratovolcanoes (Tenerife,
507 Canary Islands). *Journal of Volcanology and Geothermal Research* **178**: 543–
508 552.

509 Martí J, Felpeto A. 2010. Methodology for the computation of volcanic
510 susceptibility. An example for mafic and felsic eruptions on Tenerife (Canary
511 Islands). *Journal of Volcanology and Geothermal Research* **195**: 69–77.

512 Martí J, Planagumà L, Geyer A, Canal E, Pedrazzi D. 2011. Complex
513 interaction between Strombolian and phreatomagmatic eruptions in the
514 Quaternary monogenetic volcanism of the Catalan Volcanic Zone (NE of Spain).
515 *Journal of Volcanology and Geothermal Research* **201**: 178-193.

516 Martí J, Pinel V, López C, Geyer A, Abella R, Tárraga M, Blanco MJ,
517 Castro A, Rodríguez C. 2013. Causes and mechanisms of the 2011-2012 El
518 Hierro (Canary Islands) submarine eruption. *Journal of Geophysical Research:*
519 *Solid Earth* **118**: 823–839.

520 Martin AJ, Umeda K, Connor CB, Weller JN, Zhao D, Takahashi M.
521 2004. Modeling long-term volcanic hazards through Bayesian inference: an
522 example from the Tohoku volcanic arc Japan. *Journal of Geophysical Research*
523 **109**: B10208.

524 Marzocchi W, Sandri L, Furlan C. 2006. A quantitative model for volcanic
525 hazard assessment. In *Statistics in Volcanology*, Mader HM, Coles SG, Connor
526 CB, Connor LJ (eds). Geological Society of London: Special Publication of
527 IAVCEI 1; 15–30.

528 Neri A, Aspinall WP, Cioni R, Bertagnini A, Baxter PJ, Zuccaro G,
529 Andronico D, Barsotti S, Cole PD, Esposti Ongaro T, Hincks TK, Macedonio G,
530 Papale P, Rosi M, Santacroce R, Woo G. 2008. Developing an event tree for
531 probabilistic hazard and risk assessment at Vesuvius. *Journal of Volcanology*
532 *and Geothermal Research* **178(3)**: 397-415.

533 Puiguriquer M, Alcalde G, Bassols E, Burjachs F, Expósito I, Planagumà
534 LI, Saña M, Yll E. 2012. ¹⁴C dating of the last Croscat volcano eruption
535 (Garrotxa Region, NE Iberian Peninsula). *Geologica Acta* **10(1)**: 43-47.

536 Scandone R. 1979. Effusion rate and energy balance of Parícutin
537 eruption (1943-1952), Michoacan, Mexico. *Journal of Volcanology and*
538 *Geothermal Research* **6**: 49-59.

539 Siebe C, Macías JL. 2006. Volcanic hazards in the Mexico City
540 metropolitan area from eruptions at Popocatepetl, Nevado de Toluca, and
541 Jocotitlán stratovolcanoes and monogenetic scoria cones in the Sierra
542 Chichinautzin Volcanic Field. *Special Papers, Geological Society of America*
543 **402**: 253.

544 Suzuki T. 1983. A theoretical model for dispersion of tephra. In *Arc*
545 *Volcanism: Physics and Tectonics*, Shimosuru D, Yokoyama I (eds). Terra
546 Scientific Publishing Company (TERRAPUB), Tokyo; 93 – 113.

547 Toyos GP, Cole PD, Felpeto A, Martí J. 2007. A GIS-based methodology
548 for hazard map- ping of small pyroclastic density currents. *Natural Hazards* **41**:
549 99–112.

550 Kereszturi G, Németh K. 2012. Monogenetic Basaltic Volcanoes: Genetic
551 Classification, Growth, Geomorphology and Degradation. In *Updates in*
552 *Volcanology - New Advances in Understanding Volcanic Systems*, Németh K
553 (ed). Jeddah, Kingdom of Saudi Arabia.

554 Wood CA. 1980. Morphometric evolution of cinder cones. *Journal of*
555 *Volcanology and Geothermal Research* **7**: 387–413.

556

557

558

559

560

561

562

563

564

565

566

567

568

569

570

571

572

573 **Figure captions**

574

575 **Figure 1:** a) Simplified geological map of the GVF modified from Bolós et al.
576 (2014c). The sites of the historical volcanic vents, divided into Holcene-Upper
577 Pleistocene and Middle Pleistocene, fissures, normal and transtentional Neogen
578 faults, inferred faults, and reverse Alpine faults. b) Location of the study area.

579

580 **Figure 2:** Croscat volcano: 3D view with the main volcanic deposits (modified
581 from Bolós et al. (2014a) and a panoramic view of an outcrop showing the main
582 deposits.

583

584 **Figure 3:** PDFs of the five different layers (a–e) considered for the susceptibility
585 analysis: (a) Holocene and Upper Pleistocene volcanism vents (dots) and
586 fissures (lines); (b) Middle Pleistocene volcanism vents (dots) and fissures
587 (lines); (c) Normal and transtentional Neogen faults; and (d) Inferred faults.

588

589 **Figure 4:** Susceptibility map of future eruptions on GVF calculated with QVAST
590 (Bartolini et al., 2013).

591

592 **Figure 5:** Lava flow simulation probability map.

593

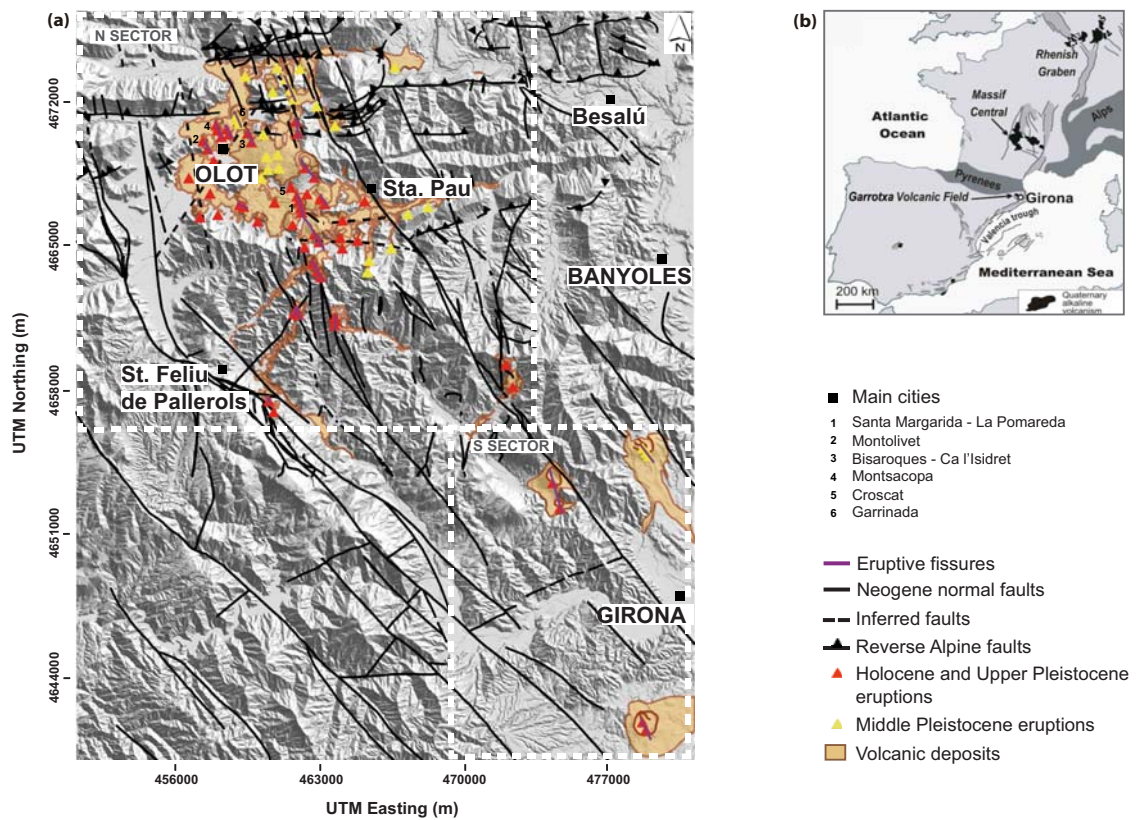
594 **Figure 6:** PDC simulation probability map.

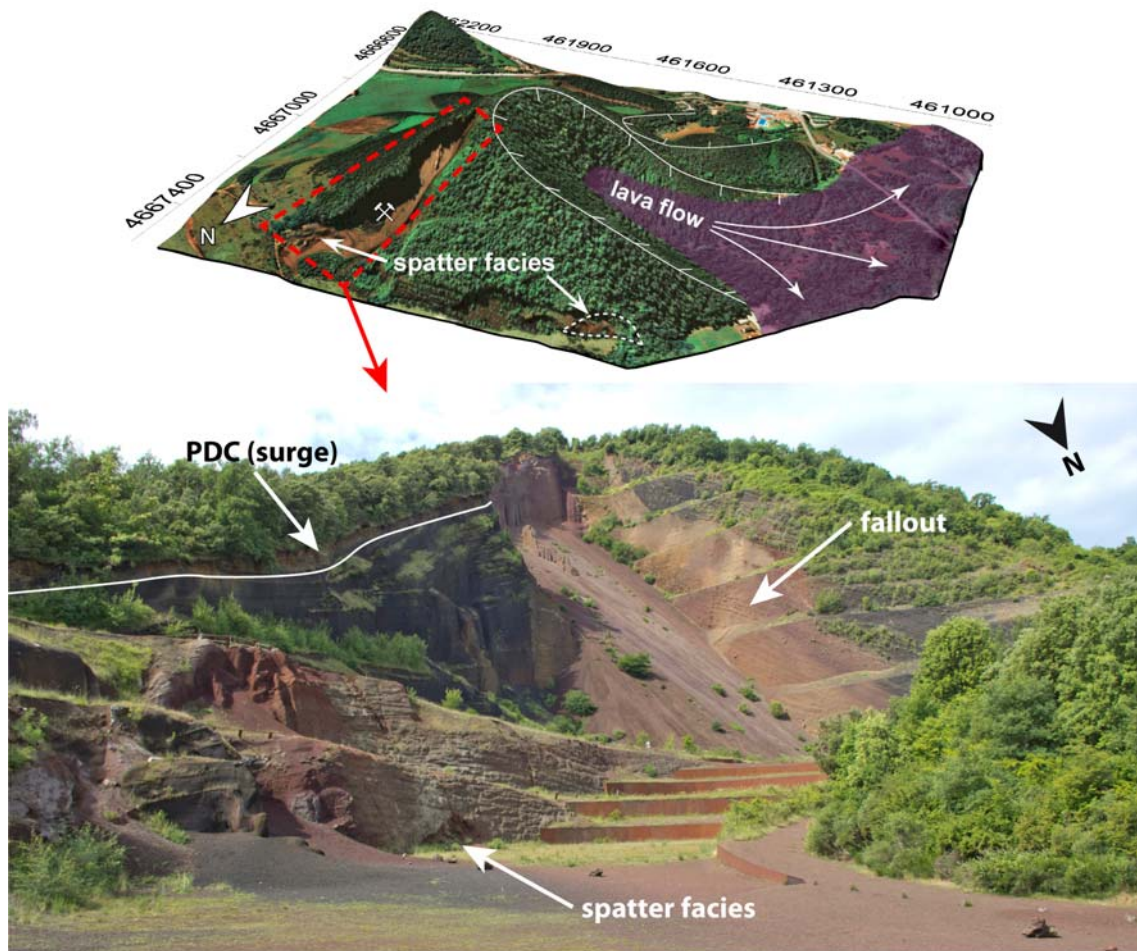
595

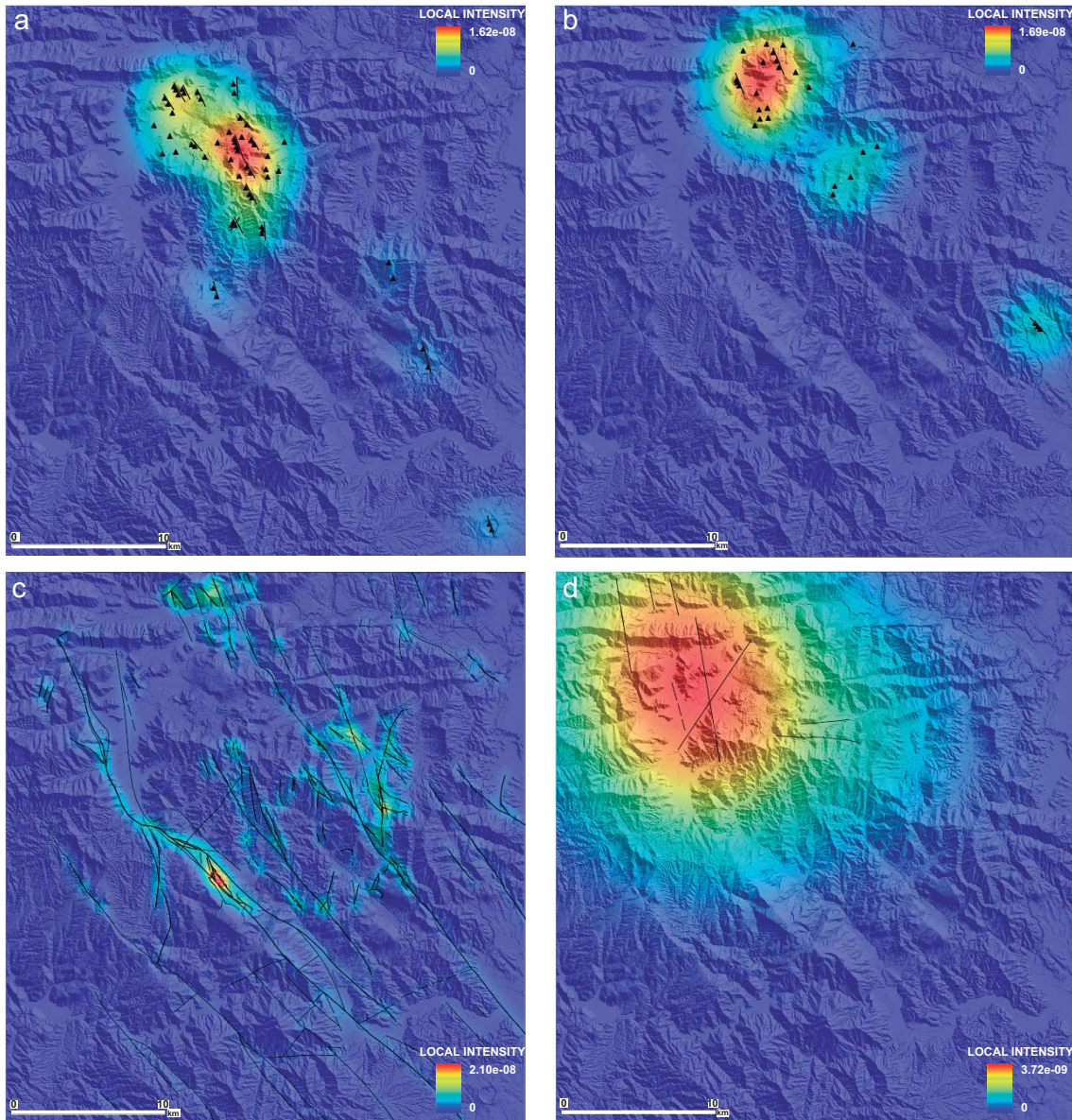
596 **Figure7:** Ash fallout simulations with a 8-km column height and volume of 0.05
597 km³.

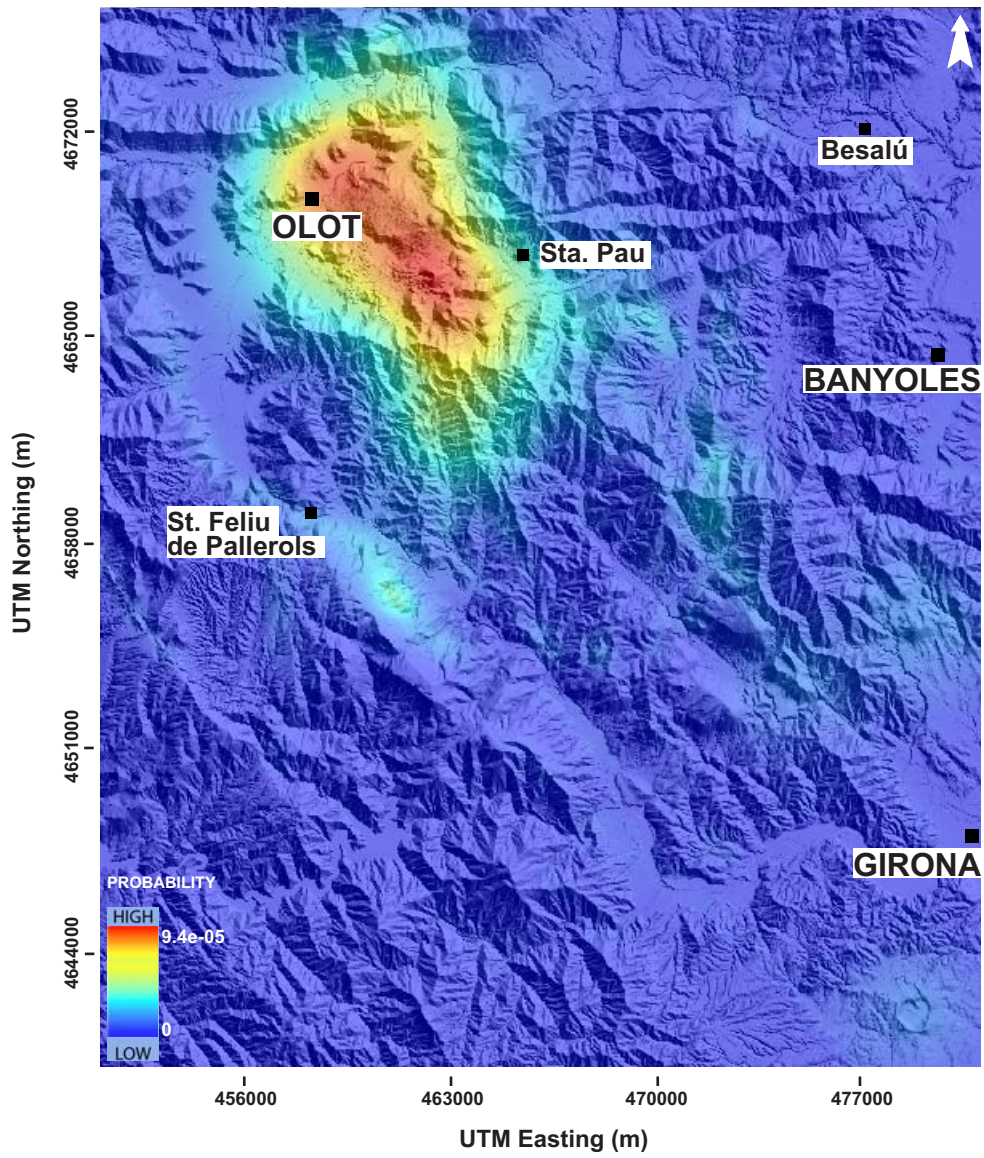
598

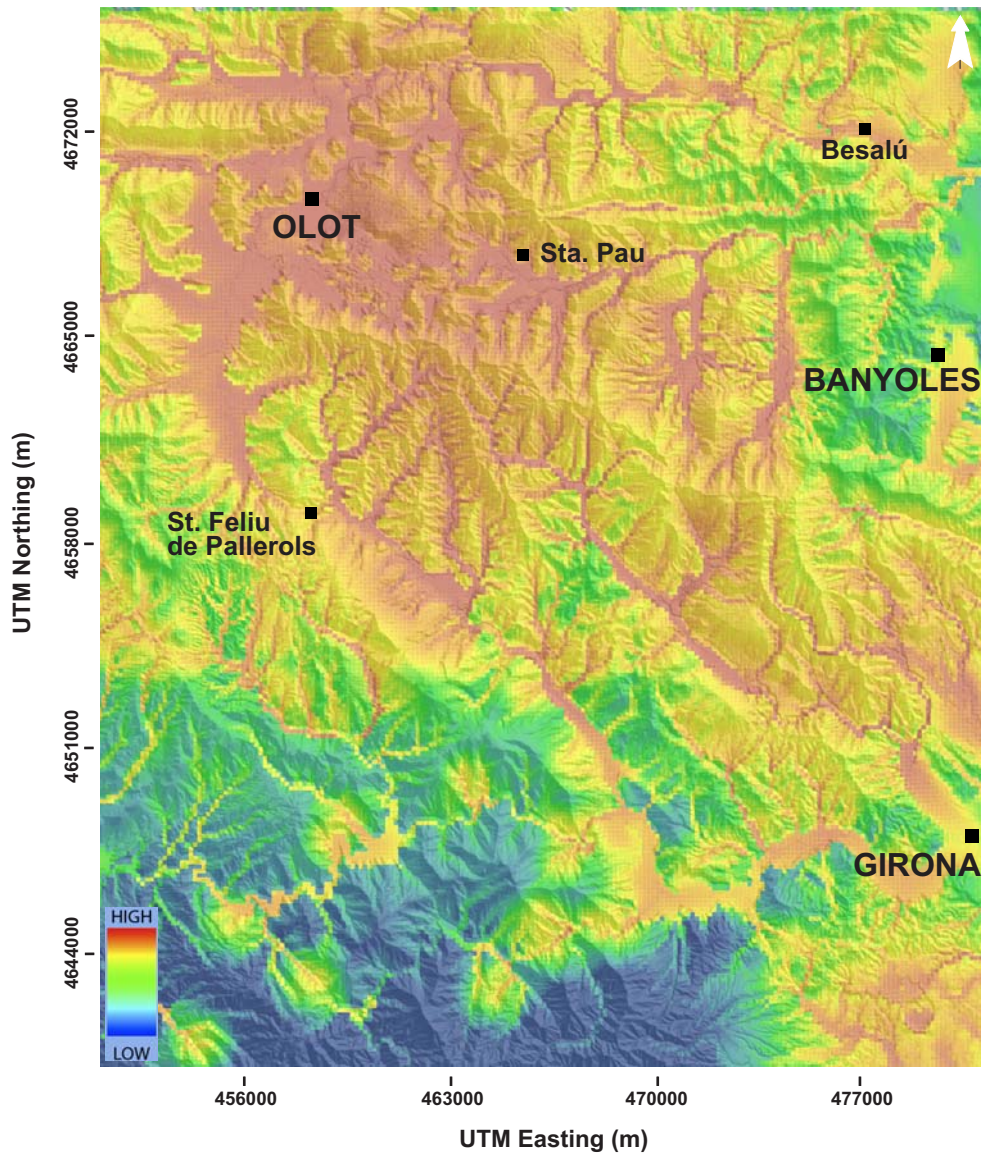
599 **Figure 8:** Qualitative hazard map for GVF.

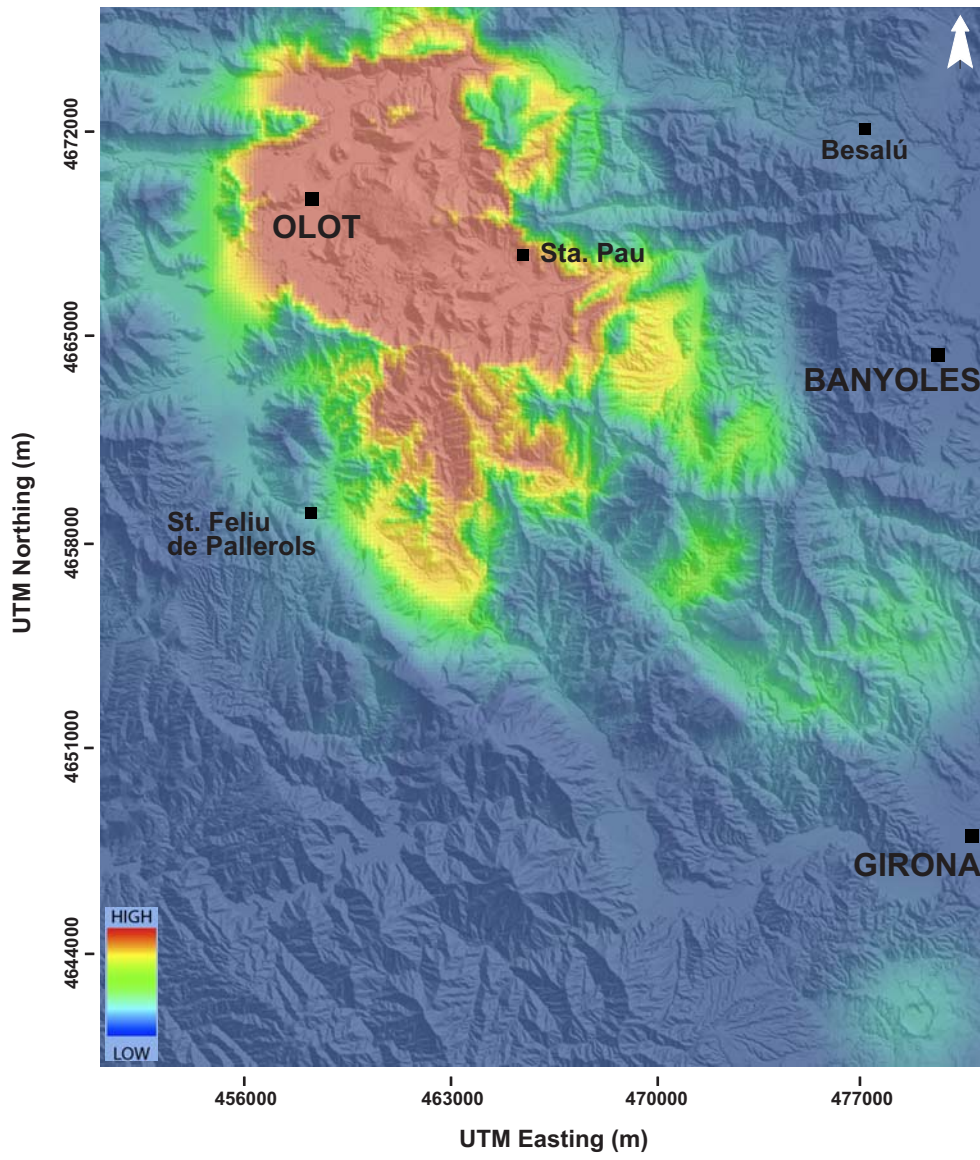


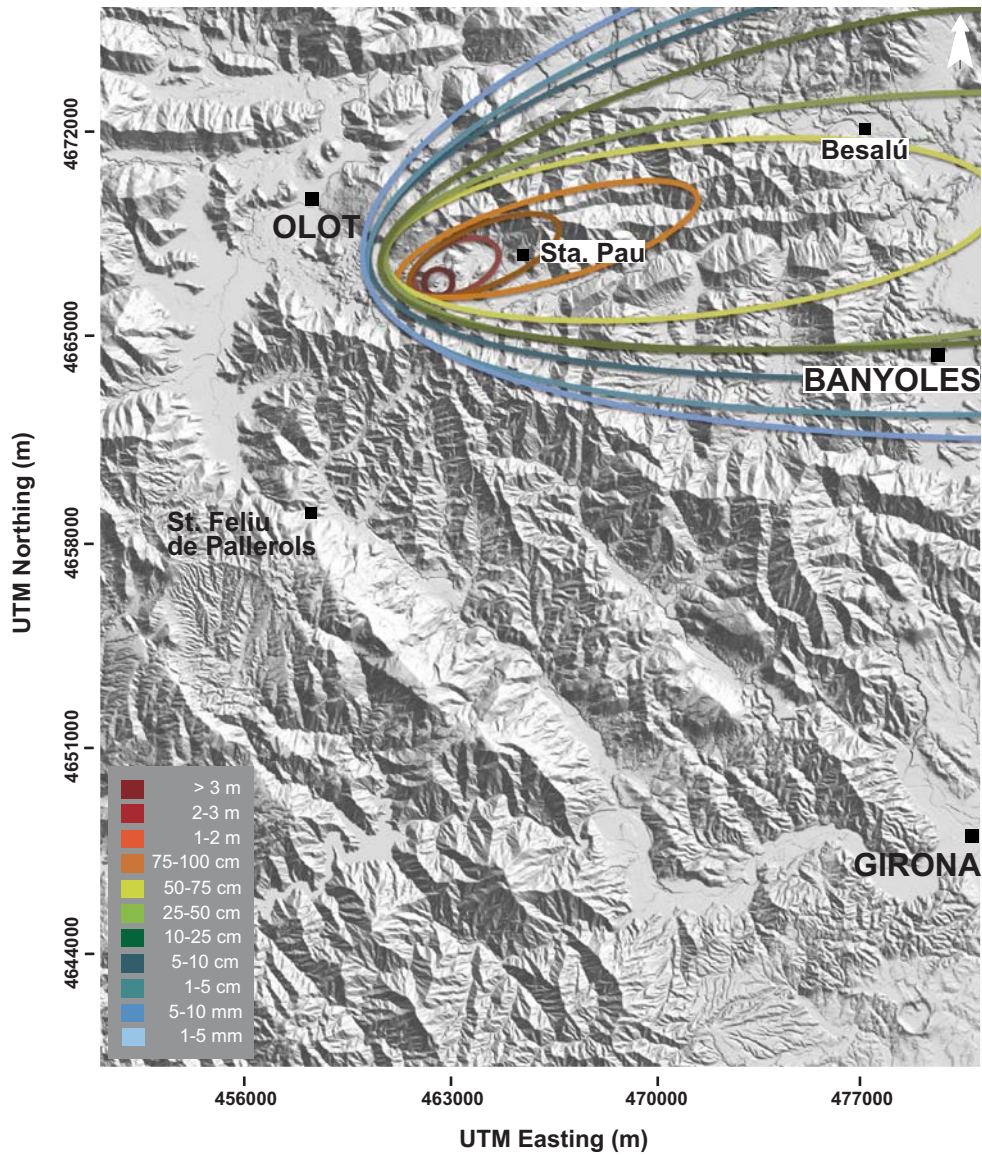


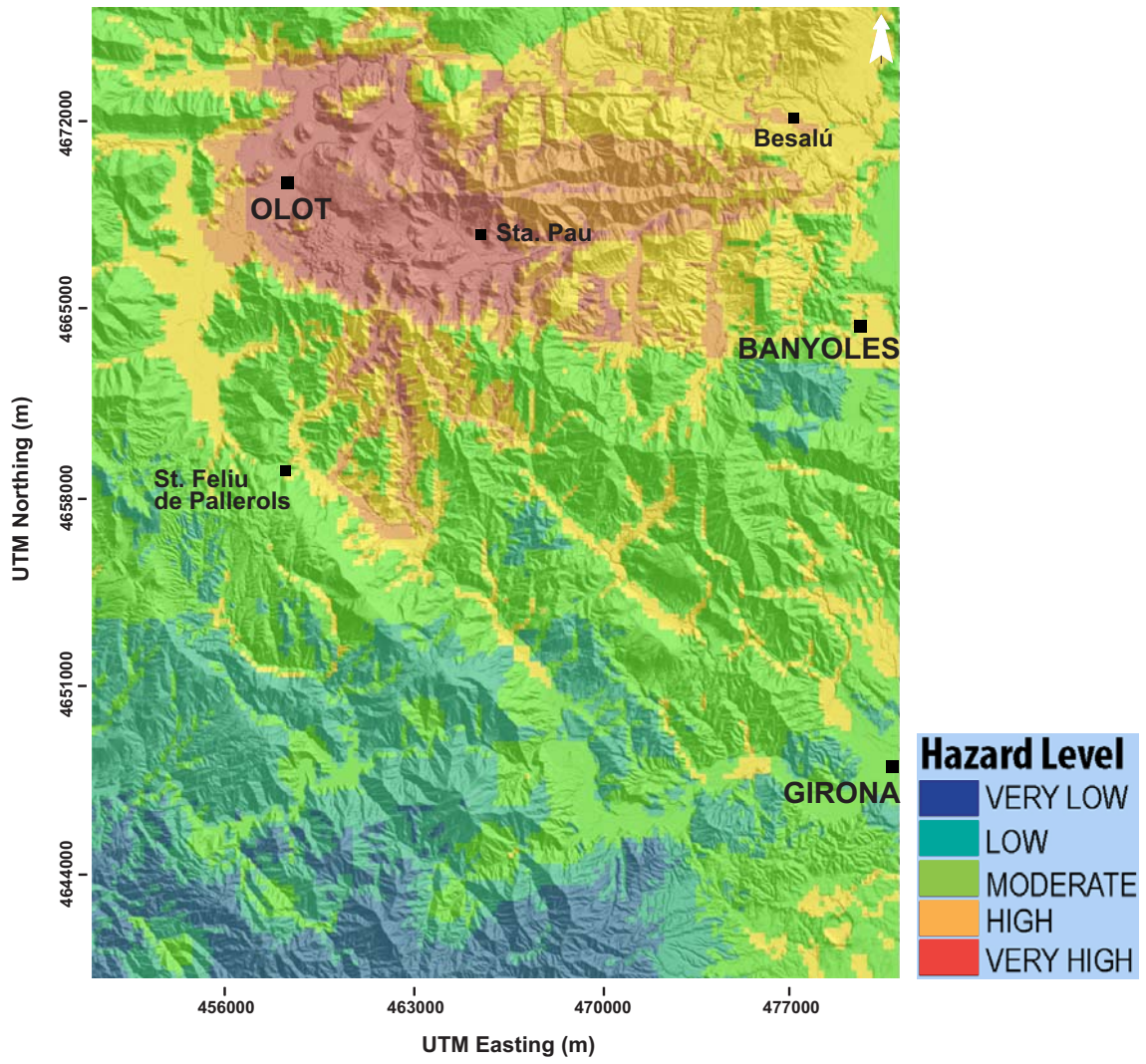












Appendix 7

VERDI: a new Volcanic managEment Risk Database desIgn

VERDI: a new Volcanic manEgement Risk Database desIgn

S. Bartolini^{a*}, L. Becerril^a, J. Martí^a

^a *Group of Volcanology. SIMGEO (UB-CSIC) Institute of Earth Sciences Jaume Almera, ICTJA-CSIC, Lluís Solé i Sabarís s/n, 08028 Barcelona, Spain*

* Corresponding author. Tel.: +34 934095410; *E-mail address*: sbartolini@ictja.csic.es (S. Bartolini).

1 **Abstract:**

2 One of the most important issues in modern volcanology is the assessment of
3 volcanic risk, which will depend – amongst other factors – on both the quantity and
4 quality of the available volcanic data and an optimum storage mechanism. This will
5 require the design of purpose-built databases that take into account data format and
6 availability and afford easy data storage and sharing, and will provide for a more
7 complete risk assessment that combines different analyses but avoids any duplication of
8 information. Data contained in any such database should facilitate spatial and temporal
9 analysis that will (1) produce probabilistic hazard models for future vent opening, (2)
10 simulate volcanic hazards and (3) assess their socio-economic impact. We describe the
11 design of a new spatial database structure, VERDI (Volcanic manEgement Risk
12 Database desIgn), which allows different types of data, including geological,
13 volcanological, meteorological, monitoring and socio-economic information, to be
14 manipulated, organized and managed. The root of the question is to ensure that VERDI
15 will serve as a tool for connecting different kinds of data sources, GIS platforms and
16 modelling applications. We present an overview of the database design, its components
17 and the attributes that play an important role in the database model. The potential of the
18 VERDI structure is here shown through its application on El Hierro (Canary Islands)
19 and the possibilities it offers in regard to data organization. The VERDI database will in
20 coming years provide scientists and decision makers with a useful tool that will assist in
21 volcanic risk assessment and hazard prioritization.

22

23 *Keywords*: database design, volcanic risk, decision making, El Hierro

24

25 **1. Introduction**

26

27 Volcanic risk assessment and management are complex issues due largely to the
28 nature, variety and availability of the data they handle (De la Cruz-Reyna, 1996). The
29 quality of the data will determine the evaluation of the volcanic risk, which is an
30 essential part of risk-based decision making in land-use planning and emergency
31 management. The first step in the evaluation of volcanic risk consists of obtaining and
32 organizing all pertinent data derived from disciplines such as geology, volcanology,
33 geochemistry, petrology and seismology, as well as vulnerability and socio-economic
34 information relating to the elements that are potentially at risk. Some of the most
35 relevant issues include how and where to store the data, in which format should it be
36 made available, and how to facilitate its use and exchange. Thus, it is essential to design
37 an appropriate database that is specifically adapted to the task of evaluating and
38 managing volcanic risk.

39 The design of an appropriate database for risk assessment and management
40 should aim to organize all the available and necessary information on volcanic risk
41 assessment in a standardized way that is easy to consult and exchange.

42 As in any other field, the first step in designing a database for volcanic risk
43 assessment and management is the definition of its architecture. This must allow for
44 effective interaction between the different information fields and offer users a clear
45 vision of its internal organization and rapid access to its contents. Nevertheless, it will
46 be the quantity and quality of the information contained in the database that will
47 determine the reliability and validity of the final risk analysis. Subsequent steps will
48 consist of the creation, maintenance and updating of all data related to volcanic risk. It
49 is important to ensure that the database will be able to evolve freely from a simple to a
50 more complex structure and be updated when new data are available.

51 To facilitate its operability and the visualisation of the data the database must be
52 integrated into a GIS (Geographical Information System). A GIS is an organized
53 integration of software, hardware and geographic data designed to capture, store,
54 manipulate, analyze and represent georeferenced information (Longley et al., 2005). In
55 recent years, the use of GIS and the improvement of the modelling of volcanic
56 processes have become useful tools in volcanic hazard and risk assessment. In fact,
57 susceptibility, hazard, vulnerability and risk maps have been generated using GIS tools

58 (Pareschi et al., 2000; Felpeto et al., 2007; Barreca et al., 2013) and can be represented
59 in a GIS environment as a support for spatial decision making (Cova, 1999).

60 Furthermore, thematic volcanic risk maps can facilitate land-use planning and
61 appropriate actions required during emergencies. In fact, hazard and risk maps are key
62 tools in emergency management: the former depicts the hazard at any particular
63 location, while the latter shows the spatial variation of both hazard and vulnerability
64 (Lirer et al., 2001).

65 To date, the databases used in volcanology have been created to store and
66 analyze different types of information and have been employed to analyze, for example,
67 (1) the impacts of volcanic phenomena on people (Witham, 2005); (2) potentially active
68 volcanoes situated in regions of high geodynamic unrest (Gogu et al., 2006); (3)
69 collapse calderas (Geyer and Martí, 2008); (4) volcano monitoring data that include
70 instrumentally and visually recorded changes in seismicity, ground deformation, gas
71 emission and other parameters (WOVOdat (Venezky and Newhall, 2007)); (5) global
72 volcanic unrest (Phillipson et al., 2013); and (6) active faults on Mt. Etna (Barreca et al.,
73 2013). In particular, efforts have been made to construct a Global Volcanic Risk
74 database of large magnitude explosive volcanic eruptions (LaMEVE (Crosweller et al.,
75 2012)). However, none of the existing databases is based on a simple architecture that
76 contains all the necessary information for volcanic risk analysis and management.

77 Here we present *Volcanic managEment Risk Database desIgn* (VERDI), the
78 architecture for a geodatabase for volcanic risk assessment and management. The
79 rationale behind constructing this database is the need to create a comprehensive
80 structure including all known or identified fields that might contribute to the assessment
81 of volcanic risk. The database also aims to make the task of volcanic risk management
82 easier for decision makers. Currently, relevant data are stored in a variety of different
83 formats and are not always easily accessible. Thus, this new way of compiling extensive
84 data aims to provide an accessible and useful structure that will facilitate information
85 sharing and risk assessment. This new database has been designed to work in a GIS
86 environment.

87 The ultimate aim of VERDI is to create a platform for expanding, updating and
88 sharing information that is open to the incorporation of new data. In the future, a web
89 site could be set up to make it a truly user-friendly application.

90 In this paper, we also present an example of the applicability of VERDI, taking
91 as example the island of El Hierro (Canary Islands, Spain). We show how all the

92 available data necessary for conducting a preliminary risk assessment can be integrated
93 and discuss the limitations of existing data and the inherent advantages in storing data in
94 the proposed form.

95

96 **2. VERDI architecture**

97 A simplified version of the VERDI database design structure is shown in Figure
98 1. The full version of the VERDI structure and the user manual will be published online
99 on the website of the CSIC Barcelona Volcanology Group (<http://www.GVB-csic.es/>).

100 The design of the database has taken into account the type of data required and
101 possible inter-relationships in order to avoid duplication.

102 The first steps in the creation of the database model were the collection of
103 metadata, the analysis of the required features and the calculation of the expected output
104 responses. This phase included the creation of information groups and the definition of
105 the table fields and the relationships between tables.

106 In order to optimize the accurate evaluation of volcanic risk, VERDI contains 12
107 information groups regarding past and current volcanic activity and the associated
108 hazards and the potential vulnerability of the elements that may be affected by such
109 hazards. The information included in each group is recorded in individual tables.
110 Additionally, VERDI includes spatial features that can be visualized with a GIS
111 application. The rationale behind the VERDI architecture is based on the principle that
112 all the information concerning the evaluation of volcanic risk should be comparable,
113 consistent and available for future comparisons and data analyses.

114 In the following subsections we offer a brief description of each information
115 group and the type of data included therein.

116

117 *2.1. GroupCore*

118

119 *GroupCore* is the central group of VERDI and represents the metadata
120 information of all the actions that could be incorporated into the database as new data.
121 This group governs the recorded information added to each group of the database,
122 thereby controlling the insertion of new data.

123 The tables contained in this group are ACTION, ACTION_TYPE, PROJECT,

124 REPORT and SUPPORT (Fig. 2): ACTION and ACTION_TYPE correspond to actions
125 and the type of actions, respectively, that generate new data (volcanic event, fieldwork,
126 bibliography, etc.); PROJECT is a reference to a project undertaken by a institution such
127 as a ministry or an institute; the REPORT table describes the action and includes
128 information about the project related to the action; and SUPPORT adds information
129 about the entity that is managing or funding the project. Table 1 shows the structure and
130 field details of each table contained in this group.

131

132 *2.2. GroupVolcano*

133

134 This group contains information about the volcano or the studied volcanic area
135 and includes data on the volcanic event itself, the characteristics of the type of
136 volcanism and the magnitude of the event (Fig. 3).

137 The table VOLCANO provides general information about the location of the
138 volcano and volcanic area, which will normally be associated with spatial information
139 included in a shapefile of polygons or in raster images. Spatial features contain a folder
140 with additional information such as Digital Elevation Models (DEM), hillshades and
141 orthophotos.

142 VOLCANO_TYPE completes the information about the volcano and identifies
143 different types and features of volcanoes (stratovolcano, shield volcano, etc...)
144 ERUPTIVE_EVENT provides information about eruptive events including date and
145 location and enables the volcano-stratigraphy of the volcano and the study area to be
146 obtained. ACTIVITY_TYPE characterizes the eruptive behaviour of the volcano thus:
147 Hawaiian, Strombolian, Vulcanian, Peléan/Plinian, Plinian, Ultra-plinian and/or
148 Caldera. The size and magnitude of the eruption is contained in the VEI_MAGNITUDE
149 table, which includes parameters such as volume, column height, fragmentation index,
150 dispersion index, Dense-Rock Equivalent (DRE), magnitude (Pyle, 2000) and the
151 Volcanic Explosivity Index (VEI) according to Newhall and Self's (1982) classification
152 (Newhall and Self, 1982).

153

154 *2.3. GroupSusceptibility*

155

156 Volcanic susceptibility (i.e. the probability of vent opening) represents an
157 important step in simulating eruptive scenarios and developing hazard maps (Martí and

158 Felpeto, 2010). Thus, *GroupSusceptibility* contains information on all structural
159 elements such as vents, dykes, faults, fractures and eruptive fissure-alignments obtained
160 from both geological and geophysical studies. The location of gas emissions or water
161 springs, as well as thermal anomalies related to the volcanic activity, are also included
162 in this group. All of these elements enable susceptibility maps in long-term analyses to
163 be generated. During volcanic unrest episodes, real-time monitoring information – in
164 particular regarding the location of the volcano-tectonic seismicity and surface
165 deformation – can be added to permit the susceptibility to be re-evaluated. This group
166 also contains a GEOPHYSICS subgroup with information on structural geophysics that
167 includes data derived from structural studies using different geophysical techniques
168 such as self-potential, tomography, magnetometry, magnetotelluric and gravimetry. This
169 type of geophysical data is useful in susceptibility analyses and in both short- and long-
170 term hazard evaluation. In addition, it is useful for studying dispersed volcanic fields
171 and their relation to local tectonics (Barde-Cabusson et al., 2014) and can thus facilitate
172 a complete analysis of the probability of future activity in monogenetic fields and
173 improve understanding of the internal structure of composite volcanoes (Rout et al.,
174 1993; Blakely et al., 1997; Connor et al., 2000; Kiyosugi et al., 2010).

175 Moreover, in both short- and long-term hazard assessment the monitoring and
176 interpretation of geophysical parameters such as temporal gravity changes, seismicity
177 and ground deformation can benefit from integration with structural geophysical data.
178 Figure 4 shows the organization of this group.

179

180 2.4. *GroupHazard*

181

182 *GroupHazard* contains basic data for computing volcanic hazards to be
183 employed in simulation models that take susceptibility information into account. This
184 group constitutes the information on which territorial and emergency plans should be
185 based and has been divided into LONG TERM and SHORT TERM subgroups (see Fig.
186 5).

187 The tables of the LONG TERM hazard subgroup contain mainly data regarding
188 the products generated during the past activity of the volcano. The information required
189 comes mainly from geological and historical records and laboratory analyses. This
190 subgroup includes the following information split into different tables: magma and
191 volcanic products (lava flows, pyroclastic deposits, etc.); petrological and geochemical

192 data from volcanic rock samples; granulometry classification of pyroclasts based on
193 sieved samples; and morphometry.

194 The SHORT TERM hazard subgroup tables contain monitoring data collected
195 during an unrest episode. These data are useful for short-term hazard assessments. The
196 information is usually organized in terms of volcanic monitoring networks (seismicity,
197 deformation, gas, thermal, groundwater, remote sensing images, etc.).

198

199 *2.5. GroupMeteorology*

200

201 *GroupMeteorology* includes the information required for the analysis of wind
202 profiles, atmospheric parameters and precipitation data (see Fig. 6). These parameters
203 are very important as inputs for ash-fall simulations. Other important parameters
204 included in this group are related to the atmospheric diffusion coefficient, the eruption
205 style and the grain-size classification. Ash-fall simulations are very useful in volcanic
206 risk assessment and consider the impact of volcanic ash not only on the population and
207 infrastructures but also on aircraft safety (Johnson et al., 2012).

208

209 *2.6. GroupLaboratory*

210

211 *GroupLaboratory* contains information supplementing the *GroupSusceptibility*
212 and *GroupHazard* groups that relates to the laboratories in which sample analyses are
213 conducted. This group specifies the kind of samples used, the analytical tests applied
214 and the results obtained (see Fig. 7). This group is important for controlling the quality
215 of data used to characterise the expected type of eruption (e.g. lava composition) by
216 means of the analysis of past products.

217

218 *2.7. GroupDevice*

219

220 *GroupDevice* provides information about the measurement devices in tables
221 such as PETROLOGY, SELF_POTENTIAL, MONITORING, and WIND. A large
222 amount of information in the database is obtained through the use of instruments such
223 as seismographs and microscopes and the DEVICE table (Fig. 8) contains the names,
224 models, types and functions of these devices.

225

226 2.8. *GroupVulnerability*

227

228 This group includes all the elements that could be affected by a destructive
229 volcanic event.

230 Vulnerability is the potential of exposed elements to be directly or indirectly
231 damaged by a given hazard (Scaini et al., 2014). There are many types of vulnerability –
232 physical, infrastructural, social and economic – and in combination they constitute the
233 vulnerability of the system (Menoni et al., 2011). Physical vulnerability due to volcanic
234 activity has been widely observed and studied, in particular in recent decades (Blong
235 and McKee, 1995; Annen and Wagner, 2003; Spence, 2004; Baxter et al., 2005; Spence
236 et al., 2005; Gomes et al., 2006; Martí et al., 2008; Zuccaro et al., 2008; Scaini et al.,
237 2014).

238 Thus, the VERDI database includes administrative divisions, infrastructure
239 networks (TRANSPORT, ELECTRICITY, and WATER_SYSTEM tables), as well as a
240 socio-economic table that includes POPULATION information, FACILITY, BUILDING
241 and LANDUSE (Fig. 9). A LAND_USE classification is included because correct land-
242 use planning is fundamental in minimising both loss of life and damage to property
243 (Pareschi et al., 2000). The information contained in this part of the database is very
244 important in the organization of evacuation plans, the reduction of potential losses
245 caused by the impact of volcanic and associated hazards, the design of land-planning
246 measures, and the evaluation of potential economic losses.

247

248 2.9. *GroupCosts*

249

250 *GroupCosts* (Figure 10) represents the huge economic losses (human life,
251 infrastructure, property, productivity, etc.) that volcanic activity can cause. Estimating
252 the economic costs associated with volcanic eruptions is very difficult due to their
253 duration and the variety of the types of impacts (Annen and Wagner, 2003). However,
254 the quantitative estimation of economic losses is of primary importance when providing
255 mitigation recommendations aimed at reducing damage (Spence et al., 2005).

256 The ECONOMIC_LOSSES and VOLCANO_IMPACT tables refer to the
257 economic and human losses evaluated after a volcanic crisis and the economic impact
258 for a specific volcanic event. The third table, SCENARIO_IMPACT, represents a
259 support table that allows a cost evaluation to be added when a volcanic hazard scenario

260 is computed and enables the human losses expected during a volcanic crisis to be
261 calculated.

262

263 *2.10. GroupManagement*

264

265 *GroupManagement* (Figure 11) is a useful group for decision makers and risk
266 managers that should include ideally all types of emergency services (e.g. police, fire
267 department, Red Cross, NGOs, etc.), although in most cases Civil Protection bodies will
268 take responsibility during a volcanic crisis. Volcanic crises require continuous close
269 collaboration between civil protection bodies and scientists in order to best analyse
270 observational and monitoring data, to evaluate short-term hazards, to draw up plans for
271 optimizing existing monitoring networks, to install new instruments and to provide
272 advice in decision making (Bertolaso et al., 2009).

273

274 *2.11. GroupReferences*

275

276 *GroupReferences* contains contact information for key people and institutions, as
277 well as bibliographic references (see Figure 12) related to the data contained in the
278 database. This group is important for obtaining the reference for any input into the
279 VERDI database and thus enables the origin of the data to be known; in this way, if
280 necessary, the person or team in question can be contacted if there is any explanation
281 needed for the data introduced.

282

283 *2.12. GroupModels*

284

285 *GroupModels* contains examples of hazard-modelling tools. It includes the most
286 relevant available software and a summary of both the required main input parameters
287 and the output formats.

288 In recent years, new tools have been developed for generating hazard and risk
289 maps, evaluating long- and short-term hazards, simulating different eruptive scenarios
290 and designing evacuation plans. Examples of these tools include QVAST (Bartolini et
291 al., 2013), VORIS (Felpeto et al., 2007), a model for lava flow simulation (Connor et
292 al., 2012), HASSET (Sobradelo et al., 2014), BET_EF (Marzocchi et al., 2008),
293 BET_VH (Marzocchi et al., 2010), HAZMAP (Bonadonna et al., 2002; Macedonio et

294 al., 2005), FALL3D (Costa et al., 2006; Folch et al., 2009), TEPHRA2 (Connor et al.,
295 2001), PUFFIN (Patra et al., 2013), VOLCFLOW (Kelfoun and Druitt, 2005),
296 TITAN2D (Sheridan et al., 2005) and EJECT (Mastin, 2001).

297 Simplified schematic tables are given in the Supplementary Material with the
298 main input parameters required for the above-listed tools.

299

300 **3. VERDI usefulness: case study of El Hierro**

301

302 One of the main obstacles when attempting to develop a robust database is the
303 lack of quality, well-gathered data. This issue can be made simpler and easier in part by
304 selecting small areas in which to test the operability database. With this aim in mind, a
305 pilot project to check the feasibility of VERDI was set up with information available
306 from the island of El Hierro (Canary Island, Spain).

307 The last eruption on El Hierro occurred in 2011–2012 (López et al., 2012; Martí
308 et al., 2013) and demonstrated the importance of reliable data and tools that can enable
309 scientific advisors and decision-makers to consider possible future eruptive scenarios.
310 Furthermore, this was the first ever eruption in the Canary Islands to tracked in real-
311 time (López et al., 2012).

312 Most of eruptions occurring on El Hierro are similar in type and in size, and
313 consist of the emission of mafic lava flows, the ballistic projection of pyroclasts and
314 proximal fallout from low fire-fountains. Its simple volcanic history, relative
315 homogeneous petrology and the new data collected during the last eruption, among
316 other factors, prompted us to select El Hierro as a case study for testing the
317 methodology proposed here.

318 In order to show the functionality of the VERDI database, we describe here two
319 hypothetical phases in the volcanic risk assessment on El Hierro. We analyze the most
320 representative and necessary information in each of the two periods: (1) the pre-eruption
321 or emergency planning phase of the volcanic process and (2) the unrest episode itself. In
322 these examples we try to summarize the information required to complete a qualitative
323 volcanic risk analysis for the island, show how to find and to store data, and outline the
324 advantages of organizing the available data.

325 Indeed, we believe that the availability of a well-organized database at the
326 beginning of an unrest phase could become a very useful tool for decision-makers and
327 for the scientists that have to provide assessment.

328

329 *3.1. Emergency planning phase*

330

331 The emergency planning phase is a moment of relative calm during the volcanic
332 activity in which long-term volcanic hazard and risk assessment become feasible.

333 During this phase, the research, compilation and interpretation of different types
334 of data should be carried out. Furthermore, available information should be organized
335 and stored in the database and completed by further fieldwork, library searches and
336 monitoring wherever data is lacking.

337 Once uploaded, the data must be filtered before being used as inputs for spatial
338 and temporal analysis and for defining eruptive scenarios. The results obtained from the
339 aforementioned analysis will become a useful tool for institutions such as Civil
340 Protection when developing their emergency plans.

341 We assume that the Canary Islands Civil Protection Organization needs to know
342 what impact the most likely eruption scenarios on El Hierro will have on the population
343 and the other exposed elements (property, infrastructures, communication networks,
344 etc.). For this analysis different data layers will have to be superimposed in order to
345 reach a final risk assessment. Figure 13 shows the different data and steps to be
346 performed in a GIS environment.

347 The first step is to obtain the Digital Elevation Model (DEM) of El Hierro and
348 general information about the volcanic area and the eruptive event (see GroupVolcano).
349 The DEM of this area can be freely obtained from the website of Spanish Instituto
350 Geográfico Nacional (IGN,
351 <http://centrodedescargas.cnig.es/CentroDescargas/index.jsp>).

352 The second step involves the collection of volcano-structural data via new
353 fieldwork measurements and bathymetric information, as well as the analysis of
354 geological maps, orthophotos and aerial photographs (Becerril et al., 2013). Once the
355 whole volcano-structural elements have been assembled, they can be geo-referenced on
356 the DEM.

357 The susceptibility map, i.e. the spatial distribution of new vent openings, is
358 based on the analysis of the aforementioned volcano-structural data. One of the tools
359 that facilitates this type of analysis is QVAST (Bartolini et al., 2013) (the main input
360 parameters required are specified in the Supplementary Material).

361 All necessary data for conducting the susceptibility analysis is contained in

362 *GroupSusceptibility*. In our example, we need to collect as much data as possible to
363 improve the accuracy of the spatial probability of a new vent opening. In the case of El
364 Hierro, data referring to past vent locations, dykes, eruptive fissures and faults are used.
365 To compile information related to vents, we refer to the table VENT in VERDI that
366 contains information about all known emission centres on the island. This table is linked
367 to a point shapefile that permits us to visualize the vents and use them in QVAST to
368 obtain probability density functions. This procedure can also be carried out with the
369 other volcano-structural elements.

370 The result will be a raster file (map) in which each pixel has a value that
371 represents the probability that it will host a new emission centre. In the specific case of
372 El Hierro, this map has already been published by Becerril et al. (2013).

373 Once the susceptibility map has been drawn up, eruptive scenarios for hazard
374 assessment can be computed. In Becerril et al. (2014), different eruptive scenarios such
375 as lava flow, ash fall and pyroclastic density currents (PDC) were considered and
376 enabled a qualitative volcanic hazard map to be generated.

377 VORIS (Felpeto et al., 2007), which requires different types of input data
378 parameters that are presented and organized in VERDI, was used to produce this map
379 (see Supplementary Material). All the information obtained during fieldwork, be it from
380 the bibliography or from devices (i.e. meteorological data), is vital in determining these
381 parameters.

382 Once the distribution of the eruptive scenarios has been developed, Civil
383 Protection is then able to evaluate the most likely eruption scenarios for the island and
384 their impact on the population and other exposed features. For this, relevant data on
385 elements such as population and transport networks must be obtained for analysis. For
386 example, Population data for El Hierro can be downloaded from the website of the
387 Spanish Instituto Nacional de Estadística (INE, <http://www.ine.es/>). Data on transport
388 networks can be obtained from the IGN website and OpenStreetMap
389 (<http://downloads.cloudmade.com/>), the latter a tool used by public administrations,
390 NGOs and even Civil Protection bodies to manage in the aftermath of disasters such as
391 the Haiti earthquake.

392 The acquisition of this information allows evacuation routes and even a
393 preliminary evaluation of general losses due to volcanic hazards such as lava flows to be
394 calculated.

395

396 3.2. *Unrest phase*

397

398 Entry into the unrest phase means that the volcanic system has reawakened.
399 During this phase, monitoring data plays an important role and is essential as a support
400 for decision making. For this reason, the VERDI database contains monitoring
401 information distributed in different groups and tables. *GroupHazard* contains precursor
402 data such as deformation, seismic activity and groundwater monitoring for short-term
403 hazard assessment; the MONITORING table summarizes all the monitoring networks
404 within a volcanic area.

405 The 2011–2012 eruption on El Hierro was preceded by three months of unrest.
406 From July 2011 onwards a dense multi-parametric monitoring network including
407 seismic and magnetic stations and GPS recorders were deployed throughout the island
408 by the Instituto Geográfico Nacional (IGN). Data recorded during this unrest episode
409 contributed to the understanding of the reawakening of the volcanic activity on the
410 island. In general, this monitoring network assisted authorities in emergency
411 management (López et al., 2012) and prepared them for the eruption that finally started
412 on 10 October 2011, 2 km off the southern coast.

413 During an unrest phase, the updating of the possible eruptive scenarios
414 computed during the emergency planning is necessary, mainly because the arrival of
415 new data such as seismic information can change previous susceptibility analysis and,
416 consequently, eruption forecasts. This may involve a change in the direction taken by
417 the crisis management.

418 During an unrest phase economic losses may be estimated by using information
419 derived from spatial and temporal analysis.

420 It is imperative that data regarding possible costs, along with an *a priori* analysis of
421 losses, are stored right from the beginning of the process (Baxter et al., 2005). In
422 VERDI, we have added a support table (Table 2) for cost evaluation when a hazard
423 volcanic scenario is computed.

424 At the end of this phase, all the data obtained are uploaded to the database to
425 facilitate future risk evaluations.

426

427 **4. Conclusions and final remarks**

428

429 VERDI is a new design for a database for risk assessment. Its logical structure
430 has been conceived in order to facilitate the interaction between data sets and to
431 guarantee the maintenance and evolution of the system. It is essential that the database
432 structure permits the exchange of standardized information and the updating of data in
433 order to prevent redundancy and repetitiveness. The VERDI database design aims to
434 make scientific research easier and to promote information-sharing for volcanic
435 surveillance, susceptibility, hazard and vulnerability. Its structure is linked to a spatial
436 database in a GIS environment, which is used to create susceptibility, hazard,
437 vulnerability, and risk maps.

438 VERDI has been conceived to be used as a source for modelling software
439 packages such as QVAST (Bartolini et al., 2013), HASSET (Sobradelo et al., 2014) and
440 VORIS (Felpeto et al., 2007). New geological hazard models related to volcanic
441 systems such as landslides, lahars and tsunamis could be included in order to complete
442 geo-risk databases. VERDI also helps to identify the basic information required to
443 conduct hazard and risk assessment. We thus suggest that all the information included in
444 VERDI should be available for each volcanic area. We also believe that it is important
445 that information is stored in the same structure and format.

446 A future role for VERDI will be the publication of an interactive web site that
447 will enable registered users to access and share the information in the database, thereby
448 allowing VERDI to become more dynamic and to continue to develop. However, we
449 cannot ignore the inherent limitations of available data and the effect that this may have
450 on the interpretation of the compiled information. It is therefore vital to acknowledge
451 that both data and interpretations are dynamic, that is, they have to be subject to
452 continuous revision and updating. For this reason, VERDI needs to be freely available
453 to all scientists interested in volcanic risk assessment since only contributions from all
454 will allow VERDI to grow and evolve into the useful tool we envisage.

455

456

457 **Acknowledgements**

458

459 This research has been partially funded by the European Commission (FP7
460 Theme: ENV.2011.1.3.3-1; Grant 282759: VUELCO) and the MINECO grant

461 CGL2011-16144-E. We thank Xavier Castelltort for their suggestions and Jorge Pedro
462 Galve for thorough and helpful views.

References

- Annen, C., Wagner, J.J., 2003. The Impact of Volcanic Eruptions During the 1990s. *Nat. Hazards Rev.* 4(4), 169-175.
- Barde-Cabusson, S., Gottsmann, J., Martí, J., Bolós, X., Camacho, A.G., Geyer, A., Planagumà, Ll., Ronchin, E., Sánchez, A., 2014. Structural control of monogenetic volcanism in the Garrotxa volcanic field (Northeastern Spain) from gravity and self-potential measurements. *Bull. Volcanol.* 76, 788.
- Barreca, G., Bonforte, A., Neri, M., 2013. A pilot GIS database of active faults of Mt. Etna (Sicily): A tool for integrated hazard evaluation. *J. Volcanol. Geotherm. Res.* 251, 170-186.
- Bartolini, S., Cappello, A., Martí, J., Del Negro, C., 2013. QVAST: A new Quantum GIS plugin for estimating volcanic susceptibility. *Nat. Hazards Earth Syst. Sci.* 13(11), 3031-3042.
- Baxter, P., Cole, P., Spence, R., Neri, A., Zuccaro, G., Boyle, R., 2005. The Impacts of Pyroclastic Surges on Buildings at the Eruption of the Soufriere Hills Volcano, Montserrat. *Bull. Volcanol.* 67, 292-313.
- Becerril, L., Cappello, A., Galindo, I., Neri, M., Del Negro, C., 2013. Spatial probability distribution of future volcanic eruptions at El Hierro Island (Canary Islands, Spain). *J. Volcanol. Geoth. Res.* 257, 21-30.
- Becerril, L., Bartolini, S., Sobradelo, R., Martí, J., Morales, J.M., Galindo, I., 2014. Long-term volcanic hazard assessment on El Hierro (Canary Islands). *Nat. Hazards Earth Syst. Sci. Discuss.* 2, 1799-1835.
- Bertolaso, G., De Bernardinis, B., Bosi, V., Cardaci, C., Ciolli, S., Colozza, R., Cristiani, C., Mangione, D., Ricciardi, A., Rosi, M., Scalzo, A., Soddu, P., 2009. Civil protection preparedness and response to the 2007 eruptive crisis of Stromboli volcano, Italy. *J. Volcanol. Geotherm. Res.* 182, 269-277.
- Blakely, R.J., Christiansen, R.L., Guffanti, M., Wells, R.E., Donnelly-Nolan, J.M., Muffler, L.J.P., Clynne, M.A., Smith, J.G., 1997. Gravity anomalies, Quaternary vents, and Quaternary faults in the southern Cascade Range, Oregon and California: implications for arc and backarc evolution. *J. Geophys. Res.* 102(B10), 22513–22527.

Blong, R., McKee, C., 1995. The Rabaul eruption 1994. Destruction of a town, National Hazards Research Centre, Mcquarie University, Sydney.

Bonadonna, C., Macedonio, G., Sparks, R.S.J., 2002. Numerical modelling of tephra fallout associated with dome collapses and Vulcanian explosions: application to hazard assessment in Montserrat. In: Druitt, T.H., Kokelaar, B.P. (Eds.). The eruption of Soufrière Hills Volcano, Montserrat, from 1995 to 1999. Geological Society of London, Memoir, London, pp. 517-537.

Connor, C.B., Stamatakos, J.A., Ferrill, D.A., Hill, B.E., Ofoegbu, G.I., Conway, F.M., Sagar, B., Trapp, J., 2000. Geologic factors controlling patterns of small-volume basaltic volcanism: application to a volcanic hazards assessment at Yucca Mountain, Nevada. *J. Geophys. Res.* 105, 417–432.

Connor, C.B., Hill, B.E., Winfrey, B., Franklin, N.M., LaFemina, P.C., 2001. Estimation of volcanic hazards from tephra fallout. *Nat. Hazards Rev.* 2, 33-42.

Connor, L.J., Connor, C.B., Meliksetian, K., Savov, I., 2012. Probabilistic approach to modeling lava flow inundation: a lava flow hazard assessment for a nuclear facility in Armenia. *J. Appl. Volcanol.* 1(3), 1-19.

Costa, A., Macedonio, G., Folch, A., 2006. A three-dimensional Eulerian model for transport and deposition of volcanic ashes. *Earth Planet Sci. Lett.* 241, 634-647.

Cova, T.J., 1999. GIS in emergency management. In: Longley, P.A., Goodchild, M.F., Maguire, D.J., Rhind, D.W. (Eds.), *Geographical Information Systems: Principles, Techniques, Applications, and Management*. John Wiley and Sons Ltd, New York, pp. 845-858.

Croweller, H.S., Arora, B., Brown, S.K., Cottrell, E., Deligne, N.I., Ortiz, N., Hobbs, L.K., Kiyosugi, K., Loughlin, S.C., Lowndes, J., Nayembil, M., Siebert, L., Sparks, R.S.J., Takarada, S., Venzke, E., 2012. Global database on large magnitude explosive volcanic eruptions (LaMEVE). *J. Appl. Volcanol.* 1.

De la Cruz-Reyna, S., 1996. Long-term probabilistic analysis of future explosive eruptions. In: Scarpa, R., Tilling, R.I. (Eds.), *Monitoring and mitigation of volcanic hazards*. Springer-Verlag, Berlin, pp. 599-629.

Felpeto, A., Martí, J., Ortiz, R., 2007. Automatic GIS-based system for volcanic hazard assessment. *J. Volcanol. Geotherm. Res.* 166, 106116.

Folch, A., Costa, A., Macedonio, G., 2009. FALL3D: A computational model for transport and deposition of volcanic ash. *Comput. Geosci.* 35, 1334-1342.

Geyer, A., Martí, J., 2008. The new worldwide collapse caldera database (CCDB): A tool for studying and understanding caldera processes. *J. Volcanol. Geotherm. Res.* 175, 334-354.

Gogu, R.C., Dietrich, V.J., Bernhard, J., Schwandner, F.M., Hurni, L., 2006. A geo-spatial data management system for potentially active volcanoes-GEOWARN project. *Comput. Geosci.* 32, 29-41.

Gomes, A., Gaspar, J.L., Queiroz, G., 2006. Seismic vulnerability of dwellings at Sete Cidades Volcano (S. Miguel Island, Azores). *Nat. Hazards Earth Syst. Sci.* 6, 4148.

Johnson, B., Turnbull, K., Brown, P., Burgess, R., Dorsey, J., Baran, A.J., Webster, H., Haywood, J., Cotton, R., Ulanowski, Z., Hesse, E., Woolley, A., Rosenberg, P., 2012. In-situ observations of volcanic ash clouds from the FAAM aircraft during the eruption of Eyjafjallajökull in 2010. *J. Geophys. Res.* 117, D00U24.

Kelfoun, K., Druitt, T.H., 2005. Numerical modeling of the emplacement of Socoma rock avalanche, Chile. *J. Geophys. Res.: Solid Earth* (19782012), 110(B12).

Kiyosugi, K., Connor, C.B., Zhao, D., Connor, L.J., Tanaka, K., 2010. Relationships between volcano distribution, crustal structure, and P-wave tomography: an example from the Abu Monogenetic Volcano Group, SW Japan. *Bull. Volcanol.* 72, 331–340.

Lirer, L., Petrosino, P., Alberico, I., Postiglione, I., 2001. Long-term volcanic hazard forecasts based on Somma-Vesuvio past eruptive activity. *Bull. Volcanol.* 63, 45-60.

López, C., Blanco, M.J., Abella, R., Brenes, B., Cabrera-Rodríguez, V.M., Casas, B., Domínguez-Cerdeña, I., Felpeto, A., Fernández de Villalta, M., Del Fresno, C., García, O., García-Arias, M.J., García-Canada, L., Gomis-Moreno, A., González-Alonso, E., Guzmán-Pérez, J., Iribarren, I., López-Díaz, R., Luengo-Oroz, N., Meletlidis, S., Moreno, M., Moure, D., Pereda de Pablo, J., Rodero, C., Romero, E., Sainz-Maza, S., Sentre-Domingo, M.A., Torres, P.A., Trigo, P., Villasante-Marcos, M., 2012. Monitoring the unrest of El Hierro (Canary Islands) before the onset of the 2011 Submarine Eruption. *Geophys. Res. Lett.* 39.

Macedonio, G., Costa, A., Longo, A., 2005. A computer model for volcanic ash fallout and assessment of subsequent hazard. *Comput. Geosci.* 31(7), 837-845.

Martí, J., Spence, R.J.S., Calogero, E., Ordonez, A., Felpeto, A., Baxter, P., 2008. Estimating building exposure and impact to volcanic hazards in Icod de los Vinos, Tenerife (Canary Islands). *J. Volcanol. Geotherm. Res.* 178(3), 553-561.

Martí, J., Felpeto, A., 2010. Methodology for the computation of volcanic susceptibility: Application to Tenerife Island (Canary Islands). *J. Volcanol. Geotherm. Res.* 195, 69-77.

Martí, J., Pinel, V., López, C., Geyer, A., Abella, R., Tárraga, M., Blanco, M.J., Castro, A., Rodríguez, C., 2013. Causes and mechanisms of the 2011-2012 El Hierro (Canary Islands) submarine eruption. *J. Geophys. Res: Solid Earth* 118(3), 823-839.

Marzocchi, W., Sandri, L., Selva, J., 2008. BET EF: a probabilistic tool for long- and short-term eruption forecasting. *Bull. Volcanol.* 70, 623-632.

Marzocchi, W., Sandri, L., Selva, J., 2010. BET VH: a probabilistic tool for long-term volcanic hazard assessment. *Bull. Volcanol.* 72, 705-716.

Mastin, L.G., 2001. A simple calculator of ballistic trajectories for blocks ejected during volcanic eruptions. U.S. Geological Survey Open-File Report 01-45, pp. 16.

Menoni, S., Costa, L., Galderisi, A., Margottini, C., 2011. Methodological framework for an Integrated multi-scale vulnerability and resilience assessment. ENSURE, Del 4.1.1. ENSURE project, WP4, deliverable 4.1.1, pp. 96.

Newhall, C.G., Self, S., 1982. The volcanic explosivity index (VEI): an estimate of the explosive magnitude for historical eruptions. *J. Geophys. Res.* 87, 1231-1238.

Longley, P.A., Goodchild, M.F., Maguire, D.J., Rhind, D.W., 2005. *Geographic Information Systems and Science*. 2nd ed. John Wiley and Sons Ltd, England, pp. 517.

Pareschi, M.T., Cavarra, L., Favalli, F., Gianni, F., Meriggi, A., 2000. GIS and volcanic risk management. *Nat. Hazards* 21, 361-379.

Patra, A.K., Bursik, M., Dehne, J., Jones, M., Madankana, R., Mortone, D., Pavolonis, M., Pitman, E.B., Pouget, S., Singha, T., Singla, P., Stefanescu, E.R., Webley, P., 2013. Challenges in Developing DDDAS Based Methodology for Volcanic Ash Hazard Analysis Effect of Numerical Weather Prediction Variability and Parameter

Estimation. *Procedia Computer Science* 18, 1871-1880.

Phillipson, G., Sobradelo, R., Gottsmann, J., 2013. Global volcanic unrest in the 21st century: An analysis of the first decade. *J. Volcanol. Geotherm. Res.* 264, 183-196.

Pyle, D.M., 2000. Sizes of volcanic eruptions. In: Sigurdsson, H. (Ed.), *Encyclopedia of Volcanoes*. Academic, San Diego (California), 263-269.

Rout, D.J., Cassidy, J., Locke, C.A., Smith, I.E., 1993. Geophysical evidence for temporal and structural relationships within the monogenetic basalt volcanoes of the Auckland volcanic field, northern New Zealand. *J. Volcanol. Geotherm. Res.* 57(1), 71–83.

Scaini, C., Felpeto, A., Martí, J., Carniel, R., 2014. A GIS-based methodology for the estimation of potential volcanic damage and its application to Tenerife Island, Spain. *J. Volcanol. Geotherm Res.* 278-279, 40-58.

Sheridan, M.F., Stinton, A.J., Patra, A., Pitman, E.B., Bauer, A., Nichita, C.C., 2005. Evaluating Titan2D mass-flow model using the 1963 Little Tahoma Peak avalanches, Mount Rainier, Washington. *J. Volcanol. Geophys. Res.* 139, 89-102.

Sobradelo, R., Bartolini, S., and Martí, J., 2014. HASSET: a probability event tree tool to evaluate future volcanic scenarios using Bayesian inference presented as a plugin for QGIS. *Bull. Volcanol.* 76, 770.

Spence, R.J.S., 2004. Risk and regulation: can improved government action reduce the impacts of natural disasters?. *Building Research and Information* 32(5), 391-402.

Spence, R.J.S., Kelman, I., Calogero, E., Toyos, G., Baxter, P., Komorowski, J.C., 2005. Modelling expected physical impacts and human casualties from explosive volcanic eruptions. *Nat. Hazards Earth Syst. Sci.* 5, 1003-1015.

Venezky, D.Y., Newhall, C.G., 2007. WOVOdat design document: The schema, table descriptions, and create table statements for the database of worldwide volcanic unrest (WOVOdat version 1.0). US Geological Survey Open-File Report 2007-1117, pp.184.

Witham, C., 2005. Volcanic disasters and incidents: a new database. *J. Volcanol. Geotherm. Res.* 148, 191-233.

Zuccaro, G., Cacace, F., Spence, R., Baxter, P., 2008. Impact of explosive eruption scenarios at Vesuvius. *J. Volcanol. Geotherm. Res.* 178(3), 416-453.

Figure captions

Figure 1: VERDI database design structure.

Figure 2: *GroupCore* structure.

Figure 3: *GroupVolcano* structure.

Figure 4: *GroupSusceptibility* structure.

Figure 5: *GroupHazard* structure.

Figure 6: *GroupMeteorology* structure.

Figure7: *GroupLaboratory* structure.

Figure 8: *GroupDevice* structure.

Figure 9: *GroupVulnerability* structure.

Figure 10: *GroupCosts* structure.

Figure 11: *GroupManagement* structure.

Figure 12: *GroupReferences* structure.

Figure 13: Data layers in a GIS environment.

Table captions

Table 1: *GroupCore* tables.

Table 2: *GroupCosts*: SCENARIO_IMPACT table.

TABLE 1

Table	Field	Info	Type
ACTION	action_id	primary key	AutoNumber
	action_date	date of the data entry	dd/mm/yyyy
	actionT_cd	type of the new data entry (foreign key ACTION_TYPE table)	Integer
	report_cd	report reference (foreign key REPORT table)	Integer
	project_cd	project reference (foreign key PROJECT table)	Integer
	support_cd	who funds the action (foreign key SUPPORT table)	Integer
	contact_cd	contact reference (foreign key CONTACT table)	Integer
ACTION_TYPE	actionT_id	primary key	AutoNumber
	actionT_info	different types of data entry (Volcanic Event, Fieldwork, ...)	Text
PROJECT	project_id	primary key	AutoNumber
	project_ref	code of the project reference	Text
	project_name	name of the project	Text
	project_start	date when project starts	dd/mm/yyyy
	project_end	date when project finishes	dd/mm/yyyy
REPORT	report_id	primary key	AutoNumber
	report_name	name of the report	Text
	report_start	date when report starts	dd/mm/yyyy
	report_end	date when report finishes	dd/mm/yyyy
	report_info	info report	Text
SUPPORT	support_id	primary key	AutoNumber
	support_info	info about the entity that manages or funds the project	Text

TABLE 2

Table	Field	Info	Type
SCENARIO_IMPACT	scenarioImpact_id	primary key	AutoNumber
	scenarioImpact_type	type of scenario simulation (lava, pdc, ashfall, ...)	Text
	scenarioImpact_pop	population affected by eruptive scenario	Integer
	scenarioImpact_facility	facility affected by eruptive scenario	Integer
	scenarioImpact_building	building affected by eruptive scenario	Integer
	scenarioImpact_landUse	land use affected by eruptive scenario	Integer
	scenarioImpact_transport	transport affected by eruptive scenario	Integer
	scenarioImpact_electricity	electricity network affected by eruptive scenario	Integer
	scenarioImpact_waterSystem	water system affected by eruptive scenario	Integer
	population_cd	foreign key POPULATION table	Integer
volcano_cd	foreign key VOLCANO table	Integer	

Figure 1
[Click here to download Figure1.pdf](#)

VERDI

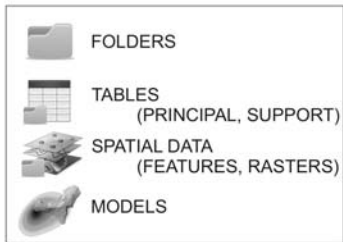
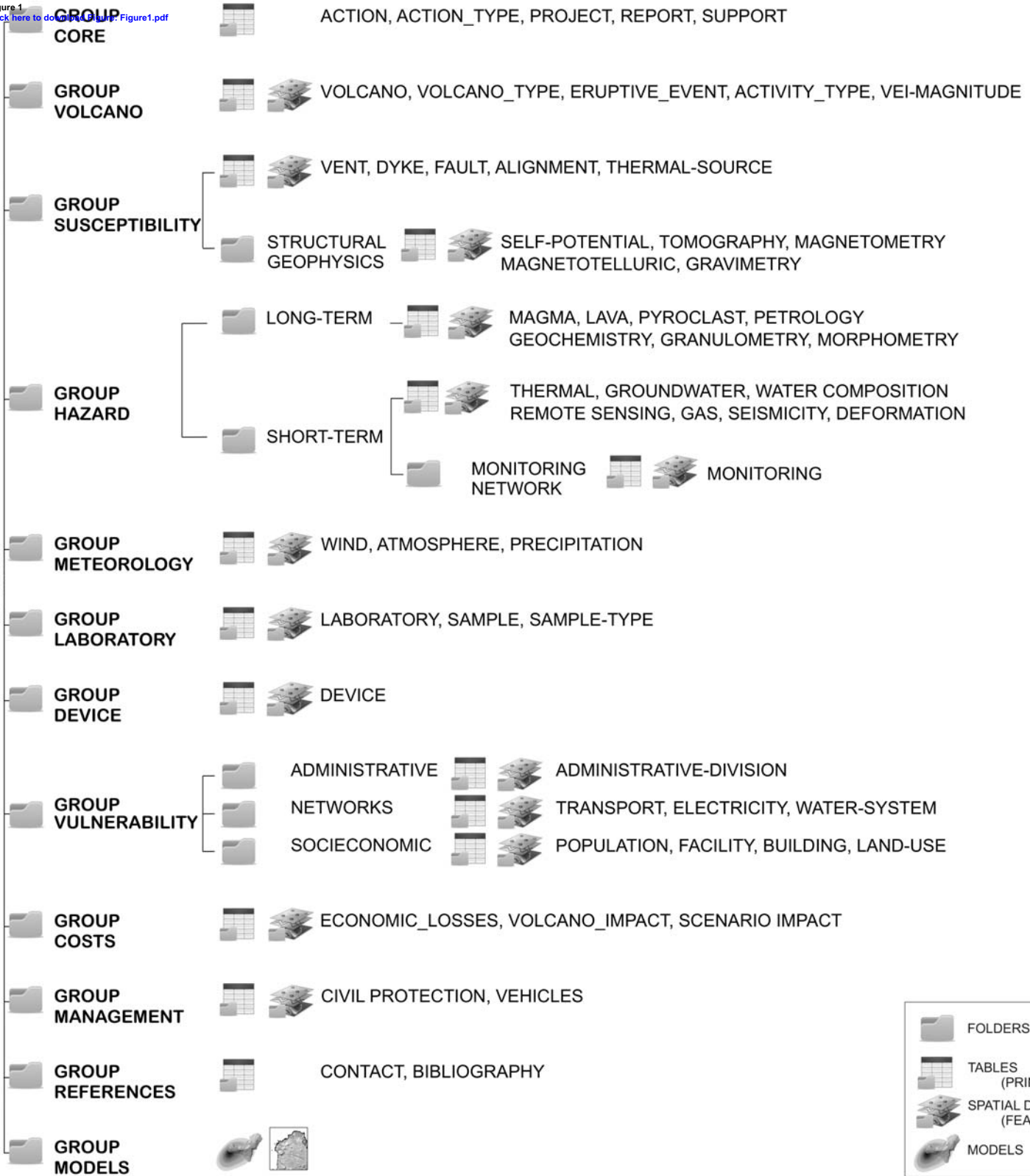


Figure 2

[Click here to download Figure: Figure2.pdf](#)

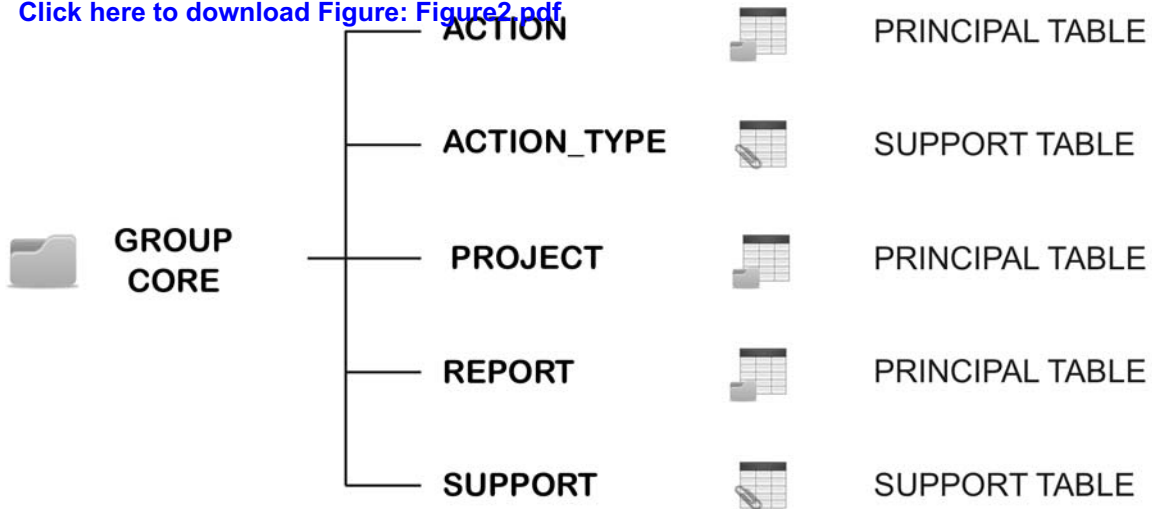


Figure 3

[Click here to download Figure: Figure3.pdf](#)

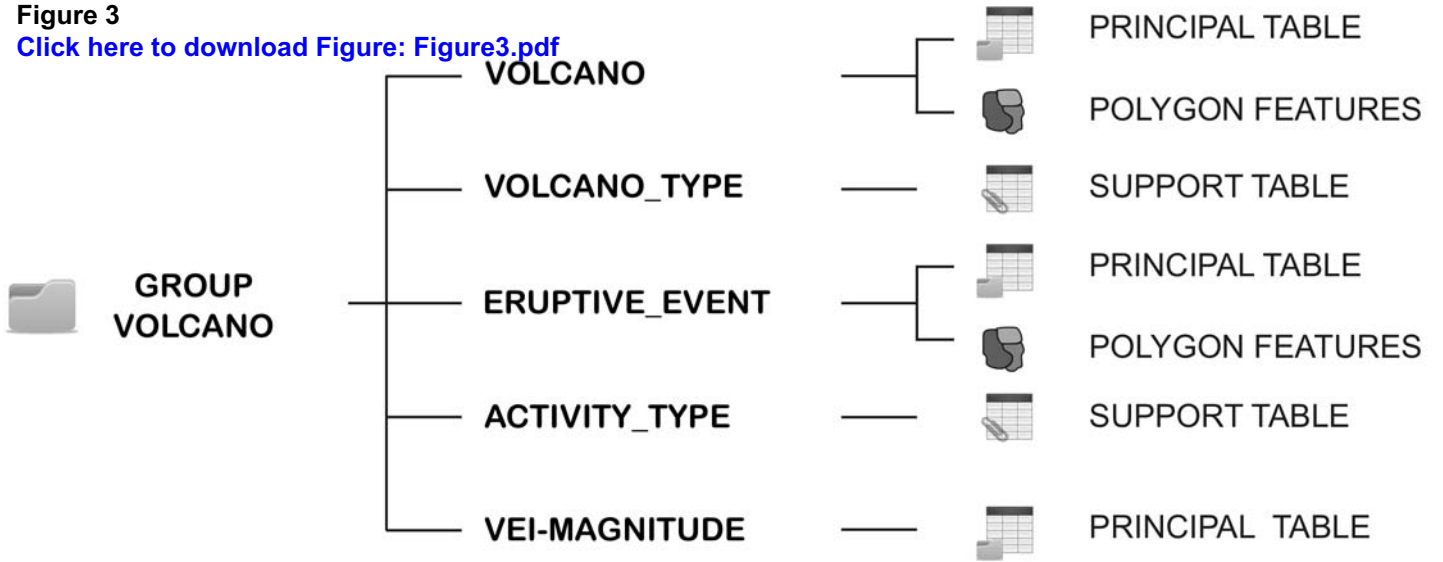


Figure 4
[Click here to download Figure: Figure4.pdf](#)

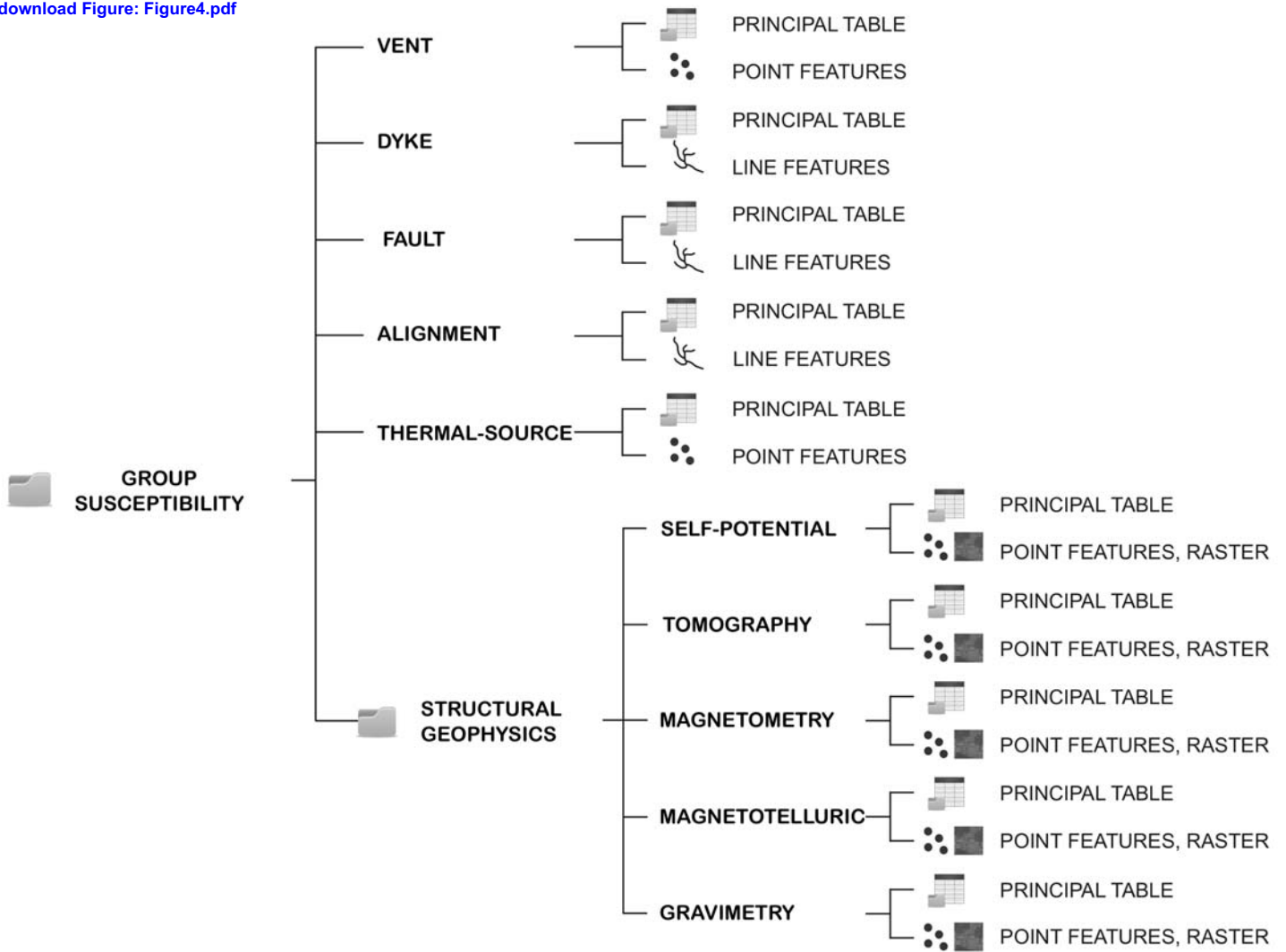


Figure 5
[Click here to download Figure: Figure5.pdf](#)

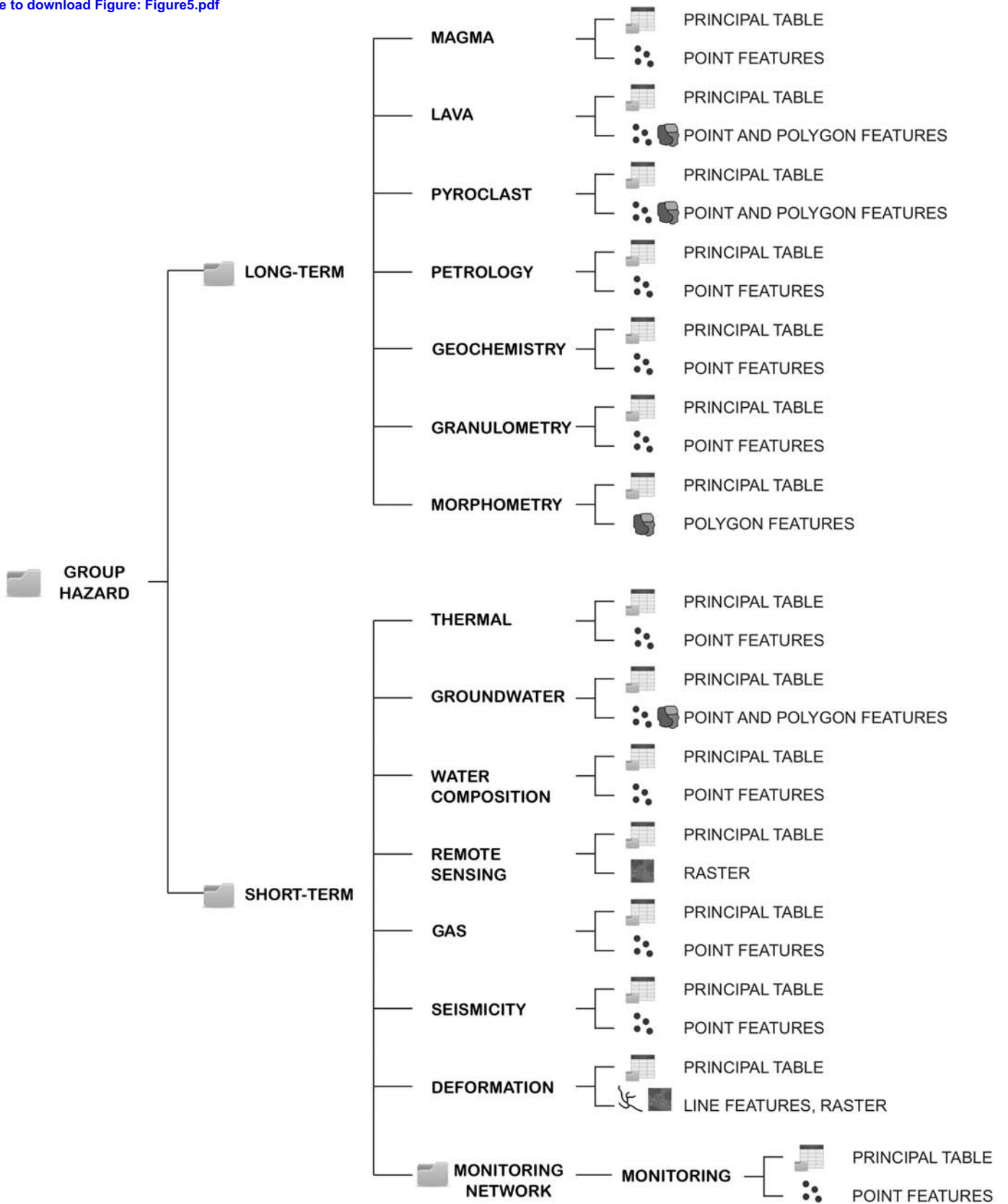


Figure 6

[Click here to download Figure: Figure6.pdf](#)

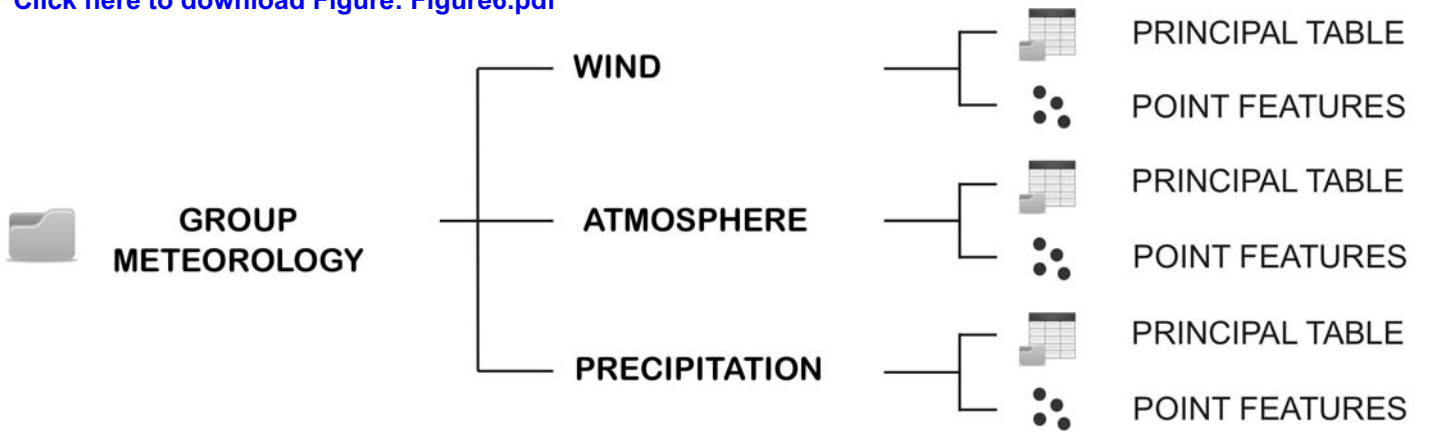


Figure 7

[Click here to download Figure: Figure7.pdf](#)

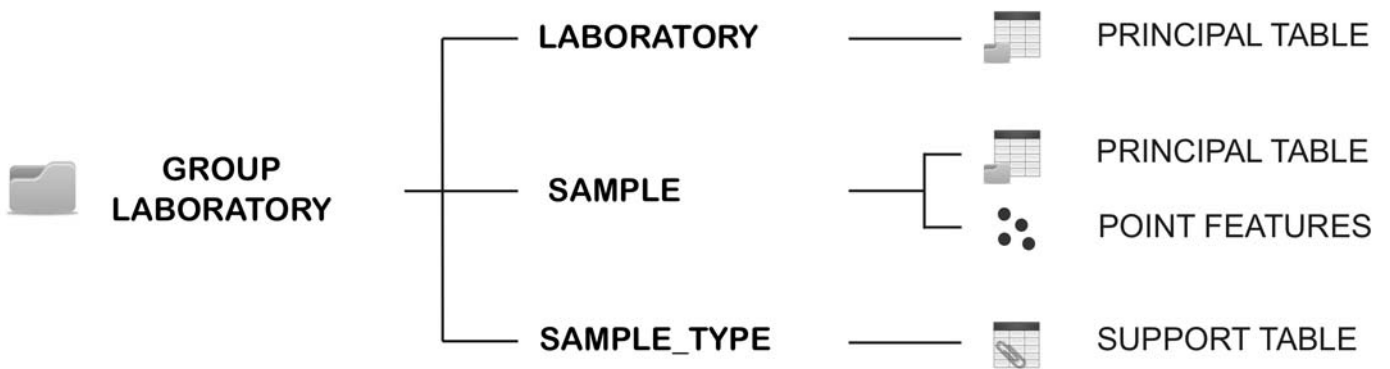


Figure 8

[Click here to download Figure: Figure8.pdf](#)

 **GROUP
DEVICE**

———— **DEVICE**



 **PRINCIPAL TABLE**
 **POINT FEATURES**

Figure 9
[Click here to download Figure: Figure9.pdf](#)

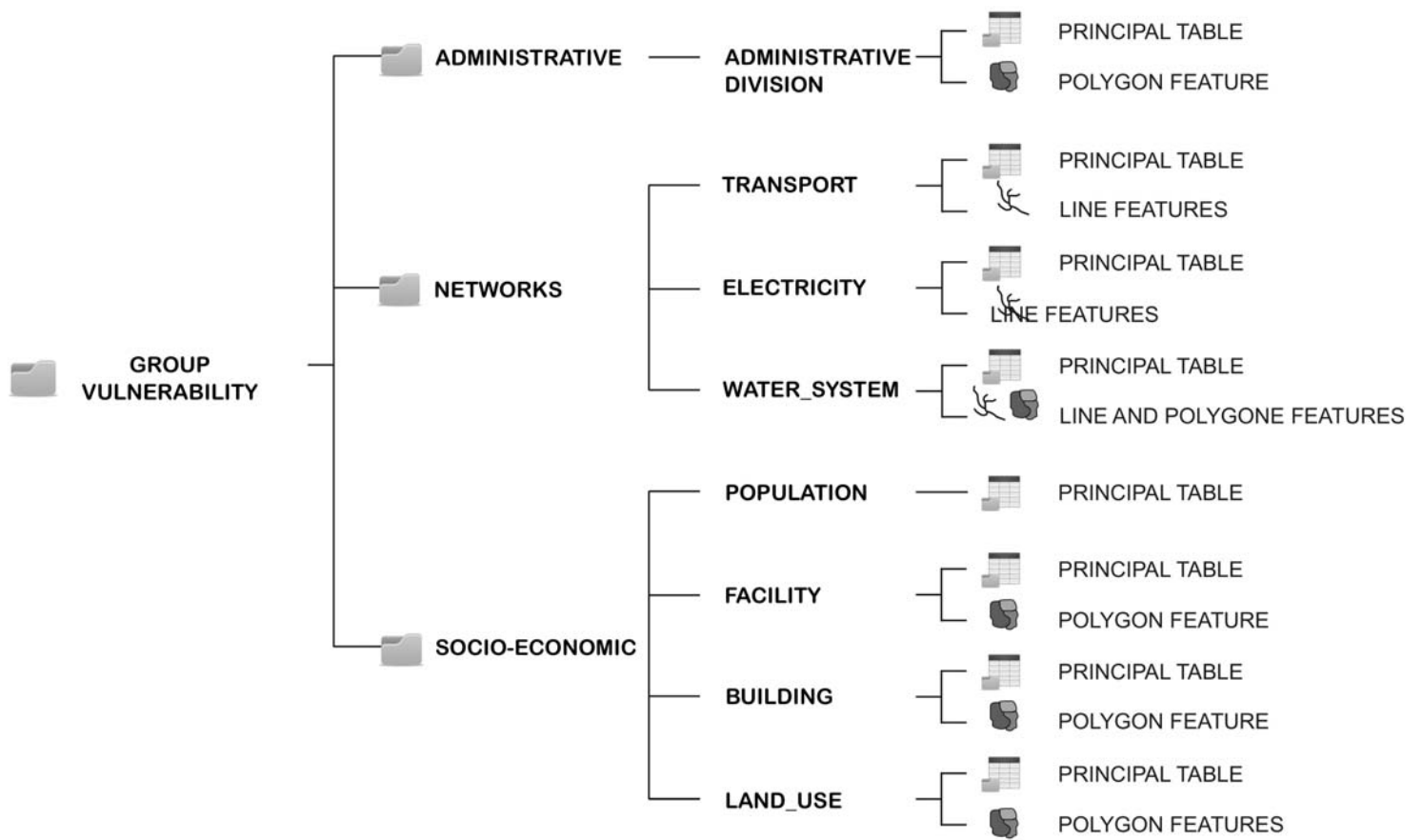


Figure 10

[Click here to download Figure: Figure10.pdf](#)

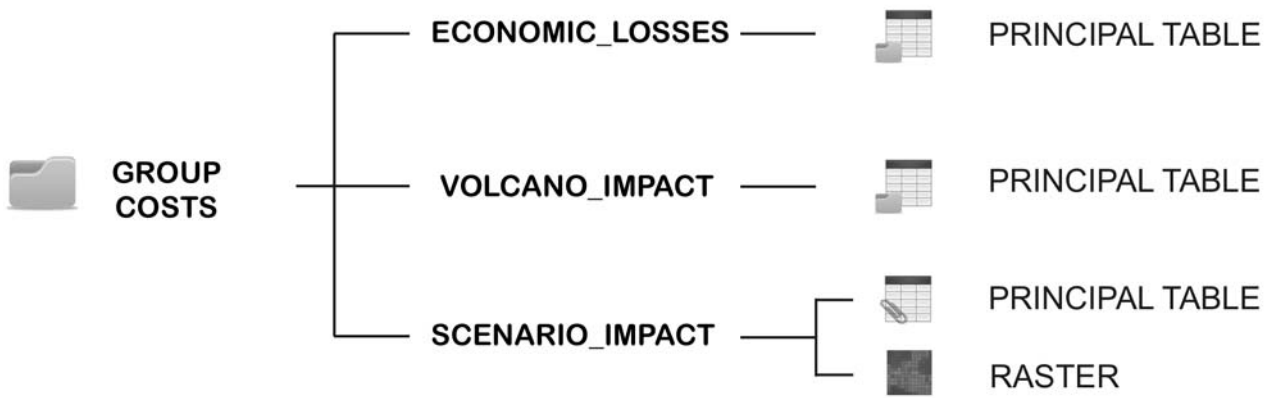


Figure 11
[Click here to download Figure: Figure11.pdf](#)

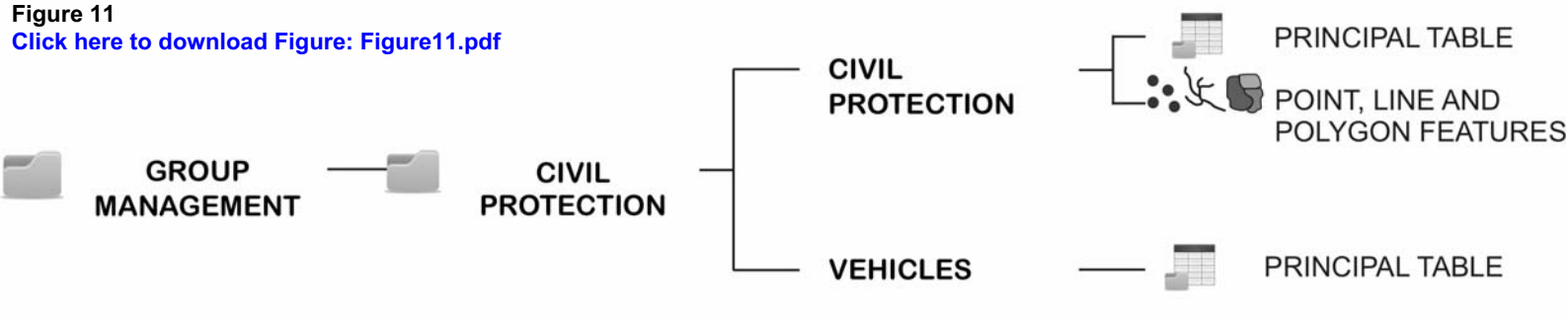


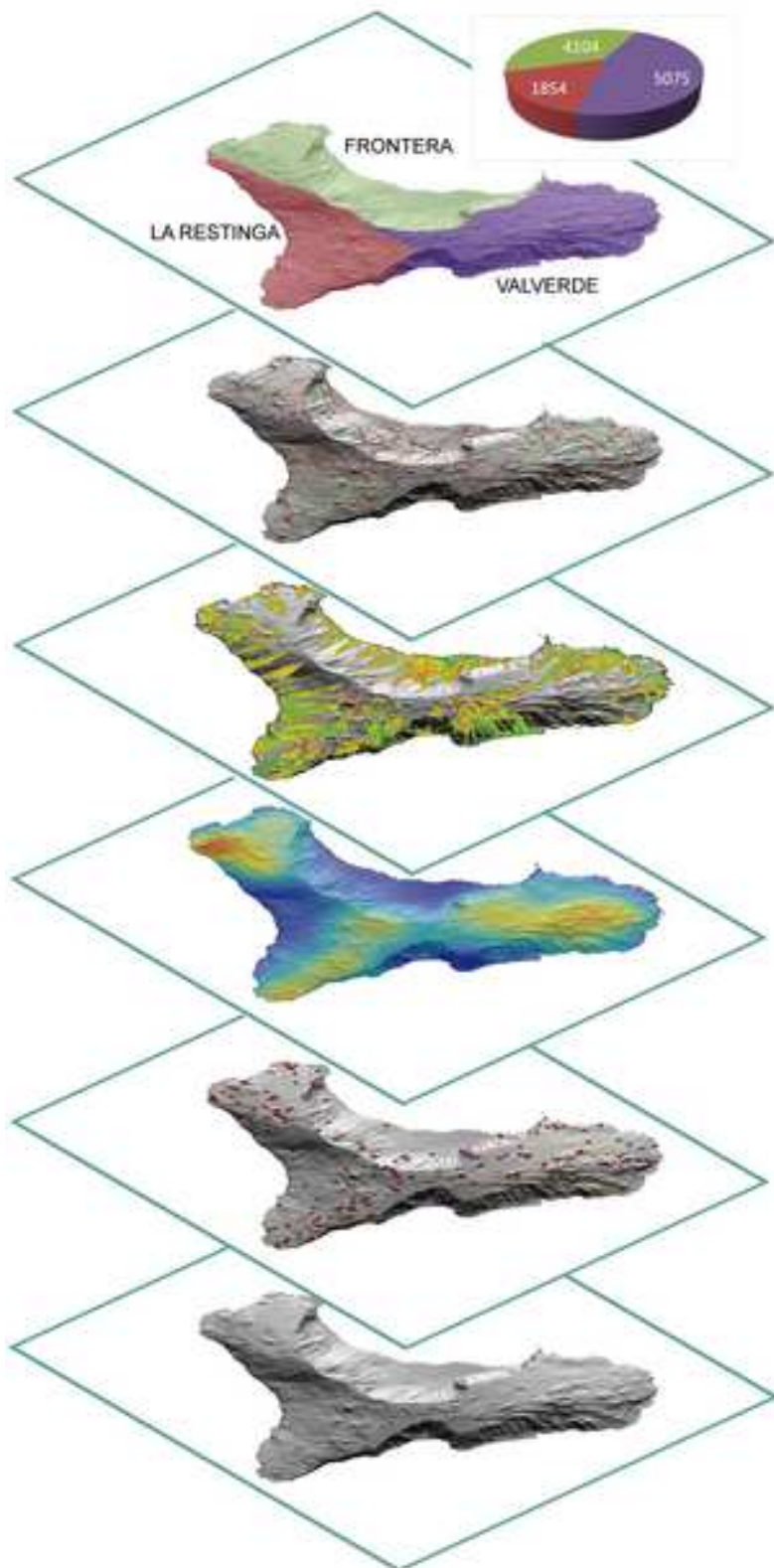
Figure 12

[Click here to download Figure: Figure12.pdf](#)



Figure 13
[Click here to download high resolution image](#)

DATA LAYERS



DATA SOURCES

POPULATION x municipality

NETWORKS (roads)

ERUPTIVE SCENARIOS

SUSCEPTIBILITY

STRUCTURAL DATA

DEM - HILLSHADE



9.1 Submission decision

Submissions Needing Revision for Author Stefania Bartolini, Ph.D.

A submission has been returned to you for revision. To revise the submission, click 'File Inventory' in the Actions menu to download any files requiring revision. When you are ready to submit the revised files, click 'Revise Submission' and then 'OK' to begin the submission process.

For more information, click [here](#), or view this short [tutorial](#) on submitting a revision.

If you do not want to submit a revised version, click 'Decline to Revise' and then 'OK'. Your submission will be moved to the Declined Revisions folder.

Page: 1 of 1 (1 total submissions)

Display results per page.

Action ▲	Manuscript Number ▲▼	Title ▲▼	Initial Date Submitted ▲▼	Date Revision Due ▲▼	Status Date ▲▼	Current Status ▲▼	View Decision ▲▼
Action Links	VOLGEO4376	VERDI: a new Volcanic managEment Risk Database desIgn	16 May 2014	20 Oct 2014	21 Aug 2014	Revise	Moderate revision

Page: 1 of 1 (1 total submissions)

Display results per page.

View Letter

[Close](#)

Date: 21 Aug 2014
To: "Stefania Bartolini" sbartolini@ictja.csic.es
From: "J. Volcanology Geothermal Research" volgeo-eo@elsevier.com
Subject: VOLGEO4376 - Editor decision - revise

Dear Dr. Bartolini,

I can now inform you that the reviewers and editor have evaluated the manuscript "VERDI: a new Volcanic management Risk Database design" (Dr. Stefania Bartolini). As you will see from the comments below and on <http://ees.elsevier.com/volgeo/>, moderate revision has been requested.

Please consider the reviews to see if revision would be feasible. Should you wish to resubmit you should explain how and where each point of the reviewers' comments has been incorporated. For this, use submission item "Revision Notes" when uploading your revision. Also, indicate the changes in an annotated version of the revised manuscript (submission item "Revision, changes marked"). Should you disagree with any part of the reviews, please explain why. To facilitate further review, add line numbers in the text of your manuscript.

Please strictly follow the formatting requirements as presented in the Guide for Authors.

Given that the requested revisions are moderate the new version is required within six weeks.

To submit a revision, go to <http://ees.elsevier.com/volgeo/> and log in as an Author. You will find your submission record under Submission(s) Needing Revision.

When resubmitting, please present any figures, tables etc. as separate files. See the Artwork Guidelines on the home page right menu for further file naming conventions, referencing and format issues.

I hope that you will find the comments to be of use to you and am looking forward with interest to receiving your revision.

PLEASE NOTE: The journal would like to enrich online articles by visualising and providing geographical details described in Journal of Volcanology and geothermal Research articles. For this purpose, corresponding KML (GoogleMaps) files can be uploaded in our online submission system. Submitted KML files will be published with your online article on ScienceDirect. Elsevier will generate maps from the KML files and include them in the online article.

When submitting your revised paper, we ask that you include the following items:

Response to Reviewers (mandatory)

This should be a separate file labeled "Response to Reviewers" that carefully addresses, point-by-point, the issues raised in the comments appended below. You should also include a suitable rebuttal to any specific request for change that you have not made. Mention the page, paragraph, and line number of any revisions that are made.

Manuscript and Figure Source Files (mandatory)

We cannot accommodate PDF manuscript files for production purposes. We also ask that when submitting your revision you follow the journal formatting guidelines. Figures and tables may be embedded within the source file for the submission as long as they are of sufficient resolution for Production. For any figure that cannot be embedded within the source file (such as *.PSD Photoshop files), the original figure needs to be uploaded separately. Refer to the Guide for Authors for additional information.

<http://www.elsevier.com/journals/journal-of-volcanology-and-geothermal-research/0377-0273/guide-for-authors>

Highlights (mandatory)

Highlights consist of a short collection of bullet points that convey the core findings of the article and should be submitted in a separate file in the online submission system. Please use 'Highlights' in the file name and include 3 to 5 bullet points (maximum 85 characters, including spaces, per bullet point). See the following website for more information

<http://www.elsevier.com/highlights>

Graphical Abstract (optional)

Graphical Abstracts should summarize the contents of the article in a concise, pictorial form designed to capture the attention of a wide readership online. Refer to the following website for more information:

<http://www.elsevier.com/graphicalabstracts>

Please note that this journal offers a new, free service called AudioSlides: brief, webcast-style presentations that are shown next to published articles on ScienceDirect (see also <http://www.elsevier.com/audioslides>). If your paper is accepted for publication, you will automatically receive an invitation to create an AudioSlides presentation.

Please note that we allow 60 days for the first author revision and 30 days for any additional author revisions that are required.

Thank you for submitting your work to this journal.

Kind regards,

Prof. Lionel Wilson
Editor
Journal of Volcanology and Geothermal Research

.....
Important note: If a reviewer has provided a review or other materials as attachments, those items will not be in this letter. Please ensure therefore that you log on to the journal site and check if any attachments have been provided.

COMMENTS FROM EDITORS AND REVIEWERS

Editor: both reviewers of your paper have raised the issue of whether this work would be better presented in a more applied Journal. I have no problem with this paper appearing in JVGR, so please do not worry about this issue. The other issue mentioned by both reviewers is that your paper would be more appealing to JVGR readers if it gave somewhat more detail about the application to the El Hierro eruption. This is probably true, so please keep this in mind while you are responding to the other comments. As to the issues about the structure of the paper, perhaps some material could be moved to an Appendix to streamline the text? I leave this for you to judge.

Reviewer #1: This is a useful paper addressing core database issues involved in promoting coherent volcano risk assessment.

It would be more insightful and instructive to the reader, (who is not a VERDI user), if this paper focused rather more on the El Hierro application, to make clear and explicit the advantages and efficacy of the database design chosen. In particular, this application might be specifically named in the title of the paper. Only a few pages are given to an outline of this application. The integration of the various component packages is key to a successful implementation, but there is no indication given on how the complex software interfaces and compatibility were handled. Hazard and loss estimation packages are diverse in origin and challenging to coordinate for real-time risk management. In particular, there are often multiple alternative models with contrasting assumptions for a given segment of the risk analysis. It is unclear how choices are made between alternatives, and how the associated uncertainties are treated.

These issues should emerge in a fuller account of the El Hierro application.

A formal verbal description of the database logic and design can never be convincing in its own right as a practical software tool, recognizing that an actual website demonstration is really not just desirable but necessary. Publication in a technical journal of database design or geoscience software might be more appropriate for some of the material in the paper.

Reviewer #2: Review of the manuscript: "VERDI: a new Volcanic management Risk Database design" by S. Bartolini, L. Becerril and J. Martí.

The manuscript proposes a new GIS-integrated geo-database designed to organize and store a great variety of data as input to volcanic risk evaluation. Database tables are listed and their attributes synthetically described. Finally, authors described a simple case study applied to El Hierro volcano, on the basis of some available data and results published within the same working group of the authors.

In my opinion, such tools can provide a very important support in modern volcanology (as well as in any other scientific branch) and I agree with the authors about the importance of developing a well-defined database to organize and handle the increasing amount of available data for multi-disciplinary topics as volcanic hazard and risk.

However, I would like to express my doubts about the aim of the manuscript with respect to the scope of the journal. The manuscript could match point (6) in aim and scope: "volcano hazard and risk research: hazard zonation methodology, development of forecasting tools; assessment techniques for vulnerability and impact". But, if I understood well, VERDI is a well structured container of raw input data and it does not contain any method to analyze, assess or perform hazard or risk analyses. Neither new data are presented or analyzed, since in the example at El Hierro is shown how to visualize results coming from raw input data or from other tools (as HASSET or QVAST).

My feeling is that the topic of this manuscript is more suited to other kind of journals, as, for example, the Journal of Applied Volcanology or Computers and Geosciences. Nevertheless, I'm not an usual reviewer for JVGR, so I prefer to let this decision to the Editor.

Independently on this possible mismatch with respect to the goal of the journal, I wrote here below some points that, in my opinion, need to be addressed in order to improve the manuscript.

Major comments:

1) In its current form, the manuscript is more similar to a technical report than a research paper. Abstract and introduction are well written, but I think that the overall structure needs some changes. Section 2 is just a list of all the tables defined in the database and their attributes. I think that 11 figures (over a total of 13) of each table are really too much. This is more appropriate for a user guide, but for a research paper I suggest to reduce this section as short as possible, pointing out only the very important features/advantages of the DB architecture and connections/compatibilities, if any, with existing volcanological DB (as WOVODAT). On the other hand, I also suggest to expand the case study at El Hierro, describing (with some figures), for example, how VERDI can be used in the frame of a GIS environment (I guess with QGIS, since both QVAST and HASSET have been developed for this free GIS tool) and integrated with the already mentioned existing tools QVAST, HASSET, etc. It could be also of interest to describe better, through the El Hierro examples, how the visualization can help stakeholders. Risk evaluation is not so straightforward by just stating that all available data will be stored and visualized through GIS layers. By looking figure 13 only, it seems quite difficult to understand how these six layers can synthesize all data in rapid decisions for stakeholders. This is even more important during the unrest phase that is, instead, too rapidly described: no examples of visualization are provided and described for this phase.

2) In conclusions (lines 432-433) it is stated: "It is essential that the database structure permits the exchange of standardized information and the updating of data in order to prevent redundancy and repetitiveness". Exchange data formats are not mentioned. How data can be insert into VERDI? I'm not asking to describe all the standards available for each field of volcanology, but if (and possibly how) in VERDI has been faced the issue of handling standard data format to populate the database. Are there guidelines about this point for users? or tools included in VERDI which support data exchanges?

3) I found strange that a database for volcanic risk do not contains any table to store and visualize values of calculated risk or to visualize risk maps/plots/tables.

Minor comments:

1) I like the idea of publishing a web interface of VERDI as it is stated in the manuscript. The existence of this interface could be a surplus value. Is such a tool in development?

2) The second part of the manuscript contains more English grammatical errors and the composition seems less well-finished than the first part.

